hiRESILIENT RESPONSE AND PERFORMANCE OF BITUMEN STABILIZED MATERIALS WITH FOAM INCORPORATING RECLAIMED ASPHALT

by
Matteo Dal Ben

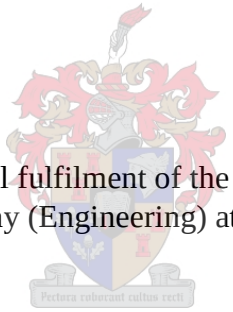

Thesis presented in partial fulfilment of the requirements for the degree of Doctor of Philosophy (Engineering) at Stellenbosch University

Supervisor: Professor Kim J. JENKINS
SANRAL Chair of Pavement Engineering
Faculty of Engineering
Department of Civil Engineering

January 2014

Declaration

By submitting this dissertation electronically, I declare that the entirety of the work contained therein is my own, original work, that I am the sole author thereof (save to the extent explicitly otherwise stated), that reproduction and publication thereof by Stellenbosch University will not infringe any third party rights and that I have not previously in its entirety or in part submitted it for obtaining any qualification.

Signature:

Name: M. Dal Ben

Date:

"Imagination is more important than knowledge. For knowledge is limited to all we now know and understand, while imagination embraces the entire world, and all there ever will be to know and understand."

Albert Einstein

SUMMARY

The increased use of reclaimed asphalt (RA) in Bitumen Stabilised Materials (BSMs), shortcomings in the existing design guidelines and manuals and ongoing developments in the concepts and understanding of these materials require further research into the fundamental properties and behaviour of BSMs. The state-of-the-art of foamed bitumen techniques is reviewed in the literature study. Current best practices in the design of BSMs and pavements incorporating such materials are also included in this literature study. Shortcomings and areas for further improvement of the design practice have been identified. With new environmental legislation, the importance of BSM technology including RA as an environmentally-friendlier and more sustainable construction technique is set to increase in the coming years.

Changes in the behaviour of materials and failure mechanisms of BSM mixes are long-term phenomena. This implies that the study of the physico-chemical and mechanical properties of the mixes with increasing amount of RA is vital. Therefore, fundamental understandings of moisture damage and thermo-physical characteristics, which are related to material properties, are required. The main objective of this study is to advance BSM technology by assessing the influence of the selected materials on durability behaviour, temperature distribution and long-term performance in all phases of application (i.e. mix design, construction, and in-service condition).

This study begins with a comprehensive literature review of research dealing with the interactions between RA and mineral aggregates. The properties of RA and mineral aggregates were reviewed. This was followed by a review into the mechanical properties of BSM-foam mixes with high percentage of RA and its durability performance. Factors influencing the temperature gradient of BSMs were then identified. Achieving a better understanding of the fundamental performance properties and temperature influence on the behaviour of BSMs with high percentage of RA is one of the key factors of this research, with a view to using the extended knowledge for improvements to current mix design and structural design practices. Finally, the fundamental theories on thermo-conductivity and the mechanical properties of the BSM were used to create a relationship between temperature and mechanical properties in a pavement section.

A laboratory testing programme was set up to study the properties and behaviour of BSMs and to establish links with the compositional factors, i.e. the type of binder used, the percentage of RA in the mix and the addition of a small amount of cement as active filler. BSMs were blended in three different proportions of RA and good quality crushed stone materials: 100% RA (with 2 % bitumen content), 50% RA and 50% G2 Hornfels crushed stone (with 2.1% bitumen content) and 100% G2 (with 2.3 % bitumen content). Tri-axial testing was carried out to determine shear parameters, resilient modulus and permanent deformation behaviour, while brushing testing was carried out to determine the possible durability performance of the BSMs. The mixture durability in terms of moisture damage was investigated.

Temperature data were collected and a model to accurately simulate the temperature distribution in the BSMs was identified and proposed for further investigation and validation. It was found from the laboratory temperature data collected in this study that the temperature gradient varied according to the depth of the BSMs. A considerable part of the efforts of this

study were dedicated to characterise and model the temperature distribution in a pavement section, taking into account the mechanical properties and performance of the BSMs at different temperature layers.

The study provides an insight into fundamental mechanical performance, material durability properties, and the thermal capacity and conductivity of the BSM-foam mixes with high percentage of RA. This will assist in improving the current procedure for selection, combining and formulation of the mix matrices for BSMs. In addition, the study provides guidelines that will enable practitioners to confidently understand the relationship between temperature gradient and mechanical behaviours of BSM-foam pavement section. The specific durability-related issues addressed in this study are substance for future research.

OPSOMMING

Die toenemende gebruik van herwonne asfalt (Engels: reclaimed asphalt (RA)) in bitumen gestabiliseerde materiaal (Engels: Bitumen Stabilised Materials (BSMs)), tekortkominge in die bestaande ontwerpriglyne- en handleidings en deurlopende verbeteringe in die konsepte en begrip van hierdie material vereis verdere navorsing oor die fundamentele eienskappe en gedrag van BSM. In die literatuurstudie word die huidige stand van kennis van die ontwerp van skuimbitumentegnieke ondersoek. Die literatuurstudie dek ook die huidige beste praktyke in die ontwerp van BSM en plaveisels wat hierdie materiale insluit. Tekortkominge en areas van verdere verbetering in die ontwerppraktyke is geïdentifiseer. Onlangse omgewingswetgewing verhoog die belangrikheid van BSM tegnologie, insluitend RA, as ‘n meer omgewingsvriendelike en volhoubare konstruksie-tegniek. Hierdie faktor sal in die toekoms al hoe belangriker word.

Die verandering in die gedrag van materiaal en die falingsmeganismes van BSM mengsels is langtermynverskynsels. Dit impliseer dat die studie van die fisio-chemiese en meganiese eienskappe van mengsels met toenemende verhoudings van RA van kardinale belang is’n Fundamentele begrip van die vogskade en temo-fisiese eienskappe, wat verwant is aan die materiale se eienskappe, word vereis. Die primêre doelwit van die studie is die bevordering van BSM tegnologie deur die invloed van die geselekteerde materiale op duursaamheid, temperatuurverspreiding en langtermyn gedrag in al die fases van toepassing (mengselontwerp, konstruksie en in-dienstoestand) te bepaal.

Die verhandeling begin met ‘n omvattende literatuuroorsig van navorsing oor die interaksie tussen RA en mineraalaggregate. Die eienskappe van RA en die mineraalaggregate word bespreek. Dit word gevolg deur ‘n oorsig van die meganiese eienskappe van die BSM-skuimbitumenmengsels met ‘n hoë persentasie RA en die duursaamheidgedrag daarvan. Faktore wat die temperatuurgradient van BSM beïnvloed word dan aangetoon.

‘n Beter begrip van die fundamentele gedragseienskappe en die invloed van temperatuur op die gedrag van BSM met ‘n hoë persentasie RA is een van die sleutelfaktore van hierdie navorsing. Dit het ten doel om die uitgebreide kennis te gebruik om huidige mengselontwerp en strukturele ontwerppraktyke te verbeter. Laastens is die fundamentele teorie van termogeleiding en die meganiese eienskappe van BSM gebruik om ‘n verhouding tussen temperature en meganiese eienskappe in ‘n plaveiselsnit te ontwikkel.

‘n Laboratoriumtoetsprogram is opgestel om die eienskappe en gedrag van BSM te bestudeer en om verwantskappe tussen samestellende faktore soos die tipe bindmiddel gebruik, die persentasie RA in die mengsel en die toediening van klein hoeveelhede sement as aktiewe vuller te bepaal. BSM is in drie verskillende verhoudings van RA en goeie gehalte gebreekte klipmateriaal vermeng: 100% RA met 2 % bitumen, 50% RA en 50 % G2 Hornfels gebreekte klip met 2.1 % bitumen en 100% G2 met 2.3 % bitumen. Drie-assige druktoetse is gebruik om skuifsterkteparameters, elastiese modulus en permanente vervormingsgedrag te bepaal. Borseltoetse is gebruik om die duursaamheidgedrag van BSM te bepaal. Die mengsels se duursaamheid is ook in terme van vogskade ondersoek.

ACKNOWLEDGMENTS

Despite the fact that the page that I am about to complete is the last of my research, it was the first that I wanted to write, since the beginning of my studies at the University of Stellenbosch. Sitting at my desk, occupied in the latest writing of this thesis, it is still unreal to me that I have reached the end of this important final project, which occupied me over the past four years. Looking back I realize that many things in my life and inside of me have changed my way of thinking, how to deal with people, different cultures, and my way of relating with others. Maybe I grew up, but I hope to remain that humble person that I have always been.

Thinking back to the route that I took four years ago, I cannot forget how many people and different situations I have found on the side of this incredible road. It is similar to the situation as when a cyclist, pushing every single fibre of his being to win the peak that separates him from the finish line, finds strength from the support of the crowd along the way.

The idea of this thesis was born from the desire to meet new realities and to increase my knowledge of new and different road construction technologies. As an international student I was lucky enough to be able to enter into a working group, at one of the most prestigious universities for Road Pavement Engineering namely the University of Stellenbosch, represented by the Faculty of Civil Engineering, Department Road and Transportation. It is difficult in a few lines to remember all the people who, in various ways, have helped to make "better" these past years here in South Africa.

From the point of view of the thesis I wish to thank Professor Kim J. Jenkins, who gave me the chance to become part of a new and exciting working group at the University of Stellenbosch, and for giving me the opportunity to complete this important work. He breathed in this thesis with me, from the first moment in which I arrived in Stellenbosch. Professor Jenkins has established with me an equal relationship, not a professor and hearing care, but two men who interacted all together. I will never forget, also, the vivid exchange of views and experiences, just like two friends. All this is topped by a desire of reaching the same goal. Without his support, my efforts would have been in vain. I cannot emphasise enough how important I feel because of his sincere assistance during my stay here at Stellenbosch. Probably, it is an investment for a long-term working relationship. Thank you Professor Jenkins, I will always keep you in my heart for all the support in the future.

I would like to especially thank Professor M.F.C. van de Ven for valuable lessons during the last part of my degree at the University of Stellenbosch and for the many hours which he dedicated to me and my technical questions. I wish to thank Prof. Erik Schlagen from the TUDelft in the Netherlands for this important support and guidance in the use of the MLS FEMMASSE simulation program and Prof KD Palmer for his help to write a MATLAB program for my research.

I would like to express my gratitude to Mr. Johan Muller and Mr. Nic Van Der Westhuizen. Their selfless time and creative thinking has made possible the research work being presented in this dissertation. Their creative ideas on the design of the infrared light system and the brushing machine device are greatly appreciated.

Design and manufacturing go hand in hand. In that respect, I wish to thank Mr. Dion Viljoen and Johan van der Merwe from the Civil Engineering workshop for their manufacturing of these important devices and always assisting on day-to-day maintenance of equipment. They have been maintaining the MTS equipment and foam-plant, which were at the core of my research.

Special thanks also go to Dave Ventura and Alan Crawford at the CSIR Laboratory in Pretoria for their comments and for sharing their knowledge on the different laboratory procedures and test setup. Your continual co-operation is very much appreciated.

This research could not have been completed without the generous support of the external laboratory, in particular MUCH Asphalt central laboratory in Eersterivier. I want to thank Alec Rippenaar and Henry for providing access to the facilities and the use of the installed rotary recovery device. Your allocation of laboratory staff, particularly Jonathan, in assisting the extraction and recovery was very much appreciated. I would also like to express my gratitude for the support and help that I received from the laboratory at the Department of Chemistry and Polymer Science at the University of Stellenbosch.

Special thanks to Chevron and La Farge for the supply of the bitumen and aggregates used in the project.

The performing of intensive laboratory experiments would not have been possible without the help of the Laboratory assistants. My great appreciation goes to Colin Isaacs and Gaven Williams. Without their help this thesis would not have seen the light. I owe a lot of gratitude to Colin for not only helping me on laboratory work but also facilitating the procurement of various materials, as well as assisting me.

Administratively, my studies would not have gone smoothly without the assistance and facilitation of the following: Janine Myburgh, Dr. Marius de Wet, Alett Slabbert, Amanda de Wet, and Rodney Davidse. My special thanks go to Janine. Your quick response to all my requests and facilitation of research was greatly appreciated. I would further like to acknowledge the individuals and institutions whose support impacted significantly on my career. Prof. Fred Hugo, I thank you very much for giving me the opportunity to undertake prestigious managerial training as a CMP delegate. Thank you for understanding the objective of us being in Stellenbosch and cheering me all along to be able to meet the deadlines.

I would also like to thank all those people with whom I started my studies and met along the way, with which I exchanged ideas and experiences. In many ways they helped me to believe in myself and aroused new interests in me. I cannot forget to mention all the friends at the University. Thanks to all my Italian friends in Stellenbosch who were with me along this long way, with whom I shared my personal experience which will mark the rest of my life.

My special thoughts go to all my friends in Italy and for their friendship during these years despite the distance between Italy and South Africa.

I wish to thank my parents with great affection for the great help and support they have given me, economic support, for all the love (very much), and for having been close to me all the time during these years of study. Special thanks also to my grandparents always present in my life.

Finally I want to express my deep gratefulness to Cristina, my fiancée, for her love, endless patience and strong support. No words can express my thanks to her.

Thanks also to me that in the end I came to the end of this journey!

TABLE OF CONTENTS

LIST OF TABLES

LIST OF FIGURES

LIST OF ABBREVIATIONS AND SYMBOLS

Abbreviations

AASHTO	Highway and Transportation Officials
ASTM	American Society for Testing and Materials
BRD	Bulk relative density
BSM-emulsion	Bitumen stabilised materials-with bitumen emulsion as a binder.
BSM-foam	Bitumen stabilised material- with foamed bitumen as binder
BSMs	Bitumen stabilised materials
CBR	Californian Bearing Ratio
CIPR	Cold In-Place Recycling
CSIR	Council for Scientific and Industrial Research; based in Pretoria, South Africa
CTMs	Cement treated materials
FTIR	Fourier transformation infra-red
HMA	Hot mix asphalt
ITS	Indirect tensile strength
LVDT	Linear variable displacement transducer
MC	Moisture Content
MDD	Maximum Dry Density
MIST	Moisture induction simulation test
MTS	Material testing system
OMC	Optimum moisture content
PI	Plasticity index
RA	Reclaimed asphalt
RC	Retained cohesion
RDm	Relative maximum theoretical density
RM	Residual Modulus
SAMDM	South African Mechanistic (pavement) Design Method
SHRP	Strategic Highway Research Programme
TG2	Technical Guideline, published by the Asphalt Academy (2009)
TRH	Transport research highway
TSR	Tensile strength retained
UCS	Unconfined compression strength
UTM	Universal Testing Machine (UTM®)
VdB %	Percent of the Bulk Volume of the entire water, bitumen and solid aggregate components in a mastic occupied by the compacted filler

American
Association of

Symbols

Σ	
ε	Normal stress
E	Strain
μ	Elastic stiffness
V	Friction
P	Velocity/speed
n	Density
C	Viscosity
φ	Cohesion
Δ	Angle of internal friction
τ	Small increment
T	Shear stress
K	Time
Q	Coefficient
Θ	Rate
L	Angle
S	Liquid
V	Solid
O	Volume, Vapour/gas
H	Oxygen
C	Hydrogen
S_r	Carbon
M_r	Saturation
T	Resilient modulus
N	Temperature
$\sigma_{1,f}$	Amount or number of load repetitions
σ_1, σ_2, σ_3	Major principal stress at failure
$\sigma_{a,f}$	Major, intermediate and minor principal stress
σ_d	Applied stress at failure
σ_{dw}	Deviator stress = σ_1-σ_3
σ	Dead weight pressure
ε_f	Normal Stress
ε_p	Strain at failure
θ	Permanent strain
ρ_b	Bulk stress = σ_1+ σ_2+ σ_3
ρ_d	Bulk density
	Dry density

Symbols for temperature distribution

A	Solar absorptivity
ε	Emissivity
Δε	Emissivity correction
Ω	Hour angle
A	Ambient air
D_p	Dew point
L_w	Long wave
P	Pressure
S	Surface or solar
W	Wind
Z	Zenith
C_f	Friction coefficient
H	Conventional heat transfer coefficient
I	Solar radiation
Q	Heat flux

CHAPTER 1

INTRODUCTION

1.1 Background

In large parts of the world there has been an increase in infrastructure development as well as an increased global network of communication. In both developing and developed countries, in order to ensure sustained economic growth, the quest for optimal performance of roads is an extremely high priority. Worldwide, road networks are deteriorating rapidly and traffic on road systems is increasing exponentially especially in developing countries. Road maintenance, rehabilitation and upgrading have become very important for the community of pavement engineers.

The upgrading and construction of road infrastructure is regarded as the forerunner to this development. In many areas however, conventional road building materials are not readily available. In such instances the use/reuse of locally available material must be considered against the environmental issue of opening a new rock source (if available) or the financial cost of hauling suitable material over great distances on low volume roads.

The level of service of a pavement structure is characterized by the lifetime for which the network has been designed, as well as a number of factors such as the increase in heavy traffic on the road system, environmental conditions, the quality of materials used in the project and the properties of the sub-base. In particular, the progressive deterioration of a pavement is largely due to:

- environmental factors responsible for the formation of cracks in the surface layer, which enable infiltration of rainwater with consequent reduction of the load-bearing capacity;
- effects of traffic load, responsible for the accumulation of permanent deformation and fatigue damage;
- choice of unsuitable materials, especially the type of bitumen and stone aggregates. This choice seen in the context of an overall project, is really important to avoid future failures of the pavement structure and its consequent deterioration of level of service. In order to restore the functionality of the road package is indispensable a maintenance intervention that, in most cases, involve the removal of part or all the entire thickness of the structural package. The intervention of maintenance must be designed by choosing the more appropriate solution from the technical, economic, logistic as well as production point of view. The recycling of existing road infrastructure and the reuse of materials coming from the old pavement is part of the rehabilitation of existing pavements.

There are many arguments in support of recycling existing road materials, namely

- reduced use of virgin materials;

- reduction of the areas to be used as waste dump sites;
- reduction of the causes of environmental pollution;
- energy saving, and
- saving of costs

In most European countries, the USA and Japan the production and management of material from recycling operations (commonly known as milled) are heavily regulated with the main objective to reduce the waste of materials. A wide variety of stabilising agents are currently in use in the road construction industry around the world. These include chemical compounds, polymers and petroleum products, cement stabilisers, petroleum resins, modified waxes and bitumen. All these products aim to achieve:

- the same objective of binding the individual aggregate particles together to increase strength and durability;
- improved workability, and
- reduced possible deformation and fatigue damages.

Clearly, some are more effective than others on specific materials, while others have clear cost advantages, but all have a place in the road construction industry.

New technologies and research in new materials in the last decades have been a fundamental part of developing new guidelines and use of Bitumen Stabilised Materials (BSMs). A global increase in the use of foamed bitumen and bitumen emulsion as a solution to roads maintenance, rehabilitation and upgrading, has become important to pavement engineers. This has created a need for practitioners to understand the mechanisms that influence the durability and long-term performance of these materials. In particular, bitumen stabilisation is increasingly being used to rehabilitate base layers of pavements incorporating thick asphalt layers (300 mm), resulting in higher percentages of RA (reclaimed asphalt) in the mixes.

The basic premise of pavement design is to generate a profile of material layers that both protect the sub-grade from strains that will induce permanent deformation, and to generate independent pavement layer properties that provide appropriate stiffness and durability for the position in the pavement system. Foamed bitumen is typically utilised for the base course (or upper pavement) layer – which is typically protected from traffic stresses only by a sprayed seal or thin asphalt surfacing. Although (BSMs) require higher initial material costs than cement or lime stabilization, they offer the advantages of being free from transverse shrinkage cracking and being a quick technique that minimizes traffic delays.

BSM-foam and emulsion stabilisation is a road construction technique which is suitable to both construction of new road networks and to pavement rehabilitation. On the other hand hot bitumen is used to bind the granular material to produce flexible bound pavement layers, in particular for road rehabilitation. Road pavements built with BSMs are more environmentally sustainable and cost effective than rehabilitation with cement or other chemical composites. Bitumen stabilisation produces a relatively flexible layer compared to the same material treated with cement. A variety of *in situ* pavement materials have been successfully treated with bitumen emulsion and foam for over thirty years, proving that such treatment is a cost-effective

way of improving the strength, as well as reducing the detrimental effects of water and permanent deformation. In addition, a pavement layer constructed from a BSM is relatively flexible compared to using cement to stabilise the same material. In South Africa, several pavements with Bitumen Stabilised Materials have provided service lives in excess of 20 years and are still performing well today (Long and Jooste 2007).

1.2 What is foamed bitumen stabilisation?

Foamed bitumen (also known as foamed asphalt, foam bitumen or expanded asphalt) is a mixture of air, water and bitumen. When injected with a small quantity of cold water, the hot bitumen expands explosively to about fifteen times its original volume and forms a fine mist or foam. In this foamed state, the bitumen has a very large surface area and an extremely low viscosity. The expanded bitumen mist is incorporated into the mixing drum where the bitumen droplets are attracted to and coat the finer particles of pavement material, thus forming a mastic that effectively binds the mixture together.

Foaming increases the surface area of the bitumen and considerably reduces its viscosity, making it well suited for mixing with cold and moist aggregates. Foamed bitumen can be used with a variety of materials, ranging from conventional high-quality graded materials and recycled asphalt to marginal materials such as those having a high plasticity index. Binder contents are based on the mix design, and are determined as percentage (by weight) required for the mix to have optimum properties. A foamed bitumen stabilised pavement can be produced either in situ or by using a central plant through a pugmill-paver operation.

1.2.1 Introduction to foamed bitumen

Recycling with foamed bitumen is emerging as a proven technique for new road design as well as pavement rehabilitation with secondary materials i.e. re-use in asphalt layers. The technology behind the method, based on adding foamed bitumen to the aggregate materials, is already well established and highway authorities are increasingly latching onto the economic and environmental benefits. Many countries in the world use the process as a tool to help maintain the integrity of their transportation infrastructure.

The performance of BSM-foam has the potential to be as good as mixes containing aggregates, so BSM-foam can more confidently be used as an option for construction and maintenance of roads carrying heavy traffic loads. Some countries like South Africa have already used foamed asphalt with success. However, general information about the successful use of foamed asphalt with recycled asphalt (RA) is not widely known for South African applications.

Only in the last few years more attention has been given to the new possibilities offered by RA. Due to the increasing demand of more “green solutions” in all parts of the world and a consequent decrease of the production cost for the rehabilitation of existing roads, the use of RA is becoming a possible answer to all these tasks. However, the knowledge regarding the application of different percentages of RA is not completely understood, especially because BSM technology can be considered a recent method of pavement construction.

In order to ensure reliable application of these technologies, research activities on the design and use of cold bituminous treated materials should be given more emphasis to give sound guidelines to the road practitioner on the use of foamed bitumen associated with different amounts of recycled materials. Like conventional hot mix asphalt (HMA) and cement treated materials (CTMs), the use of BSMs for road construction, rehabilitation and upgrading needs proper design. The mix design procedures for BSMs have advanced and this has opened an avenue for understanding the behavioural and failure characteristics of BSM mixes. The research on BSMs, however, has been limited to permanent deformation, bearing strength, shear strength and fatigue failure (Jenkins, 2000; Ebels, 2008; Twagira, 2010) and little is known about durability properties. Therefore, there is potential for the development of new or improved mechanisms of failure that influence long-term performance of BSMs.

Globally the use of RA materials in pavement construction is increasing. Similarly, the South African Environmental and Resource conservation Act of 2004 limits exploitation of new borrow pits for road construction and rehabilitation. Currently in South Africa, the use of RA in pavement rehabilitation is less than 30% (National Department of Transport, 2009). In the European countries the reuse of old pavement surface is reaching higher percentages: Germany and the Netherlands are utilising almost 80% and 90% of their reclaimed asphalt, where the Mediterranean countries are at 40% or 50%. In the USA the amount of RA is reaching values close to 70%, while in China it is less than 50%. Most of these percentages of RA are inserted in new HMA road pavements and only a small portion in BSM rehabilitation projects. Using RA in new mixtures can reduce the amount of new material that has to be added, saving money and natural resources. In addition, hot-mix asphalt mixtures with RA can perform as well as mixtures made with all new material. Due to these advantages of using RA, many highway agencies are moving toward rising the percentages of RA in their hot-mix asphalt pavements and in BSM rehabilitation projects. However, the challenge is to understand the long-term performance and durability properties of BSM mixes incorporating the higher percentages of RA materials. The lack of knowledge of the mechanical properties and durability characteristics of the materials, which compose the structure of a road network, is one of the most important limitations to the design of a flexible pavement. In this regard the scientific community has taken many benefits from the development of new information technologies that today characterize many test equipment and standard procedures.

In an engineering context, durability is defined as ability to maintain the initial performance properties through time above a certain threshold level. Durability is achieved by resisting stresses and strains or withstanding destructive agents (air, water, solar irradiation, temperature and chemicals) with which the materials come in contact. It's becoming very clear that durability is a time-related issue and that durability has multidimensional parameters and is not a single property. There are very few single measurements of durability of pavement materials. For BSMs, the durability has commonly been referred to only as the measure of moisture resistance (Twagira 2010). In fact, moisture damage often manifests in a BSM's life. However, in long-term performance, other factors, such as temperature and traffic loading can influence a BSM's durability. In comparison to other pavement materials, durability of HMA is measured as resistance of binders to stripping, ageing and degeneration of modifiers in specific application, knowing that parent aggregates in HMA are adequately durable (Shell Bitumen, 2003). The fact that BSM is applicable in a wide range of aggregates (including RA at different percentages) and varying bitumen contents, its durability is based on material durability, as well as mixture durability. Although moisture damage is considered a major factor influencing durability of BSMs, the durability of parent aggregates and bitumen are found to play a significant role (Jenkins, 2000; Paige-Green and Ventura 2004).

The material's durability, mechanism of moisture failure, binder ageing, critical mechanical properties and thermo conductivity that influence durability of BSMs require clarification. This will enable reliable and cost-effective construction of pavement structures. The parent mineral aggregates and binders used in BSMs are natural and found in different sources. Since the utilisation of locally available materials must be efficient and cost-effective, the selection of materials for BSMs should focus on their durability properties. Durability properties influence other mechanical performances under different environmental and traffic conditions. This is applicable to both new construction and road rehabilitation works, with the latter placing emphasis on in-place or in-plant recycling of existing pavement materials.

This study therefore, focuses on the understanding of durability properties of BSM-foam with the aim of providing a better decision in all stages of application, i.e. mix design, construction and in-service condition.

1.2.2 Stabilising with foamed bitumen

Due largely to technological advances and the benefits that accrue, the use of bitumen as a stabilising agent has become increasingly popular. There are many forms of bitumen but only two are used for stabilising: bitumen emulsion and bitumen foam. Foam generally is a substance that is formed by trapping many gas bubbles in a liquid or solid. Foamed bitumen is a type of foam that is produced by adding a small amount of water (approximately 2 to 3 % by weight of bitumen) to hot bitumen (150 – 160 °C) in a special expansion chamber. When injected into the hot bitumen, the water evaporates abruptly thus causing explosive foaming of the bitumen in the saturated stream. The bitumen therefore, expands between 10 to 15 times its original volume (Jenkins, 2000). The bitumen used for this process is ordinary penetration grade bitumen which is used for standard hot mix asphalt road construction applications.

In this foamed state, which is a temporary state of low viscosity, bitumen is workable at ambient temperatures and in-situ moisture conditions and can easily be mixed with aggregates. The foaming process of bitumen is dependent on the water changing state from liquid to vapour. When water particles come into contact with hot bitumen, heat energy from the bitumen is transferred to the water. Almost immediately the water temperature reaches boiling point and changes state, thereby creating a thin-filmed bitumen bubble filled with water vapour.

The potential of using foamed bitumen as a stabilising agent was first realised over fifty years ago by Prof. Ladis Csanyi at the Engineering Experiment Station of the Iowa State University (Csanyi, 1957; 1959). Several decades later in the mid-1990s, Wirtgen developed a system which injects both air and water in an expansion chamber, as shown in Figure 1.1. It can be seen that the nozzle includes an expansion chamber to accommodate the foaming of the bitumen before it is released into the mixing chamber.

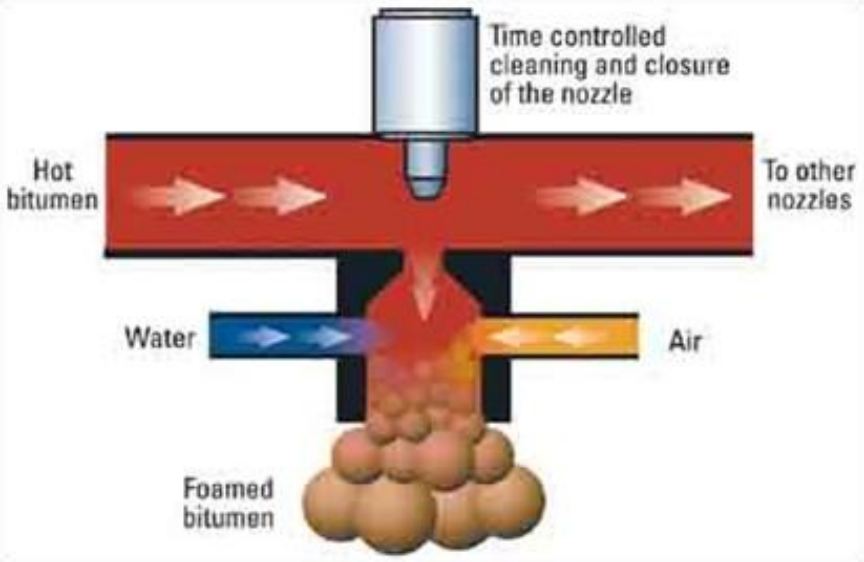

Figure 1.1: Foamed Bitumen Production in Expansion Chamber (Asphalt Academy, 2009).

1.2.3 Characterisation of foamed bitumen

A significant amount of variability is inherent in the foamed bitumen treatment process, which in turn influences the mechanical properties of mixes. Ideally one would want to produce foamed bitumen with properties that will give the mix desirable mechanical properties and a low enough viscosity during the mixing and compaction process. The quality of foam produced is a major contributor to the variability.

Foamed bitumen is characterised by two primary parameters, namely expansion ratio which is a measure of viscosity of the foam and will determine how well it will disperse in the mix and half-life which is a measure of the stability of the foam and provides an indication of the rate of collapse of the foam. Half-life is calculated as the time taken in seconds for the foam to collapse to half of its maximum volume (Figure 1.2).

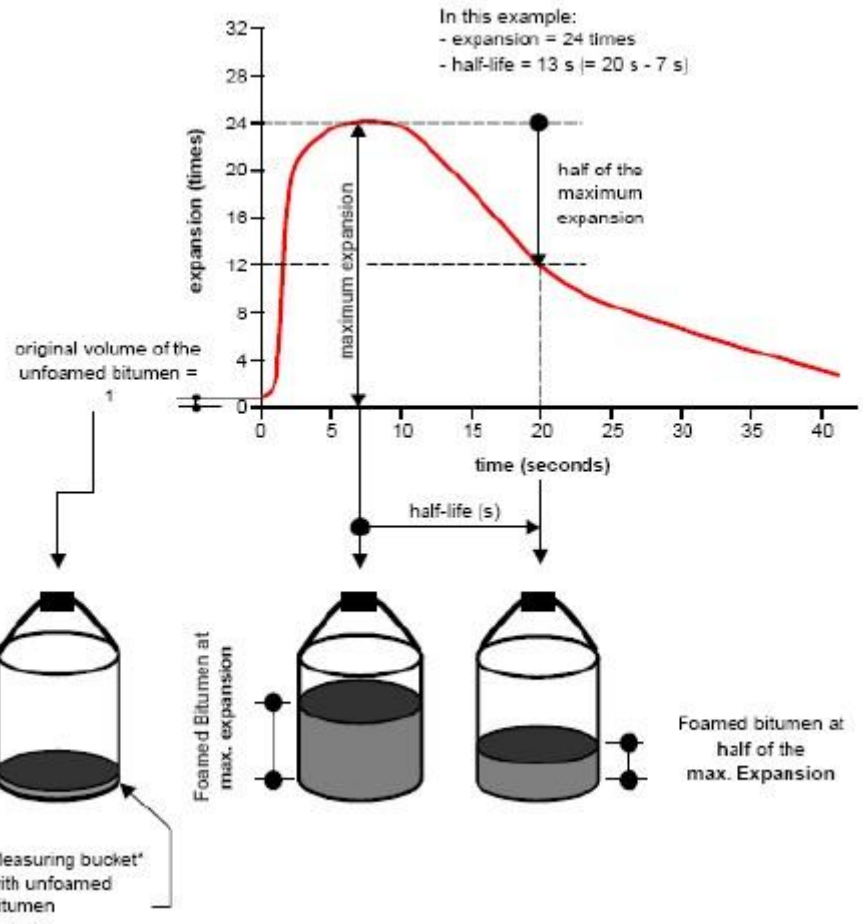

Figure 1.2: Explanation of expansion and half-life (Wirtgen, 2010).

The two foam properties are influenced by several factors described below. However, the best foam is generally considered to be the one that optimises both expansion and half-life.

1.2.4 Advantages of using BSM-foam

BSM-foam is different from all other pavement materials, primarily due to the "spotty" nature of the bitumen dispersion that creates a non-continuously bound material. The following summarises the main features of these materials:

- since the individual bitumen droplets are not connected and the coarser aggregate particles remain uncoated, the treated material reflects the granular characteristics of the untreated material. It is therefore stress dependent and not prone to cracking when subjected to tensile stresses (induced by applied or thermal forces);
- the foamed bitumen is applied in a heated state to cold, damp aggregate, thus negating the necessity to preheat the aggregate which consumes the majority of heat needed in conventional processes (conservation of energy);

- since the bitumen is dispersed only amongst the finer aggregate particles, they are encapsulated and immobilised. Such materials are not prone to pumping when load is applied under saturated conditions (Paige-Green and Ventura 2004; Collings and Jenkins 2008);
- the material acquires significant flexural strength as a result of the visco-elastic properties of the dispersed bitumen (Jenkins, 2000);
- materials can be treated at ambient temperatures (Jenkins, 2000);
- the ability to open the rehabilitated road to traffic soon after construction;
- marginal aggregates can be effectively used in pavement layers when treated with foamed bitumen or bituminous emulsion (Ebels, 2008; Twagira, 2010);
- another major advantage of the foamed bitumen stabilization process is that it does not have any particular adverse environmental impacts. The stabilization process does not involve the emission of volatiles, such as in cutback stabilisation or corrosive dust when using lime or cement stabilization, which is particularly important in urban areas;
- foam bitumen increases the shear strength of a granular pavement (Jenkins, Long, and Ebels, 2007);
- the effective stiffness of a layer of BSM in a pavement structure and its behaviour under load is a function of the parent material, the density of the material in the layer, the amount of bitumen added (and how well it is dispersed), active filler, temperature, moisture content and support characteristics (Asphalt Academy, 2009; Long and Jooste, 2007);
- BSM can be carried out *in situ* or in a plant and it's quicker than other types of stabilisation;
- construction time is shorter than for emulsion treatment. A long "break time" is needed for emulsion to enable proper mixing and compaction and moisture control is imperative (Jenkins, 2000);
- no heating of aggregates is necessary. Energy is however required to heat the bitumen to 160 °C, and
- BSM-foam has a balance of strength and flexibility versus cement or emulsion treated material and does not break down to the original strength properties of the parent material as quickly as cement treated material.

BSMs are used for the construction of base or sub-base layers. They are therefore always surfaced and protected from the direct effects of environmental and traffic forces. Under such conditions the bitumen droplets are protected from UV rays and the ageing effects of oxidation and high temperature. They can therefore be expected to retain their elastic properties for extended periods, especially the droplets located in the lower portion of thick layers where tensile stresses develop when the pavement structure is loaded.

The behaviour of BSMs, relative to other pavement materials is illustrated in Figure 1.3.

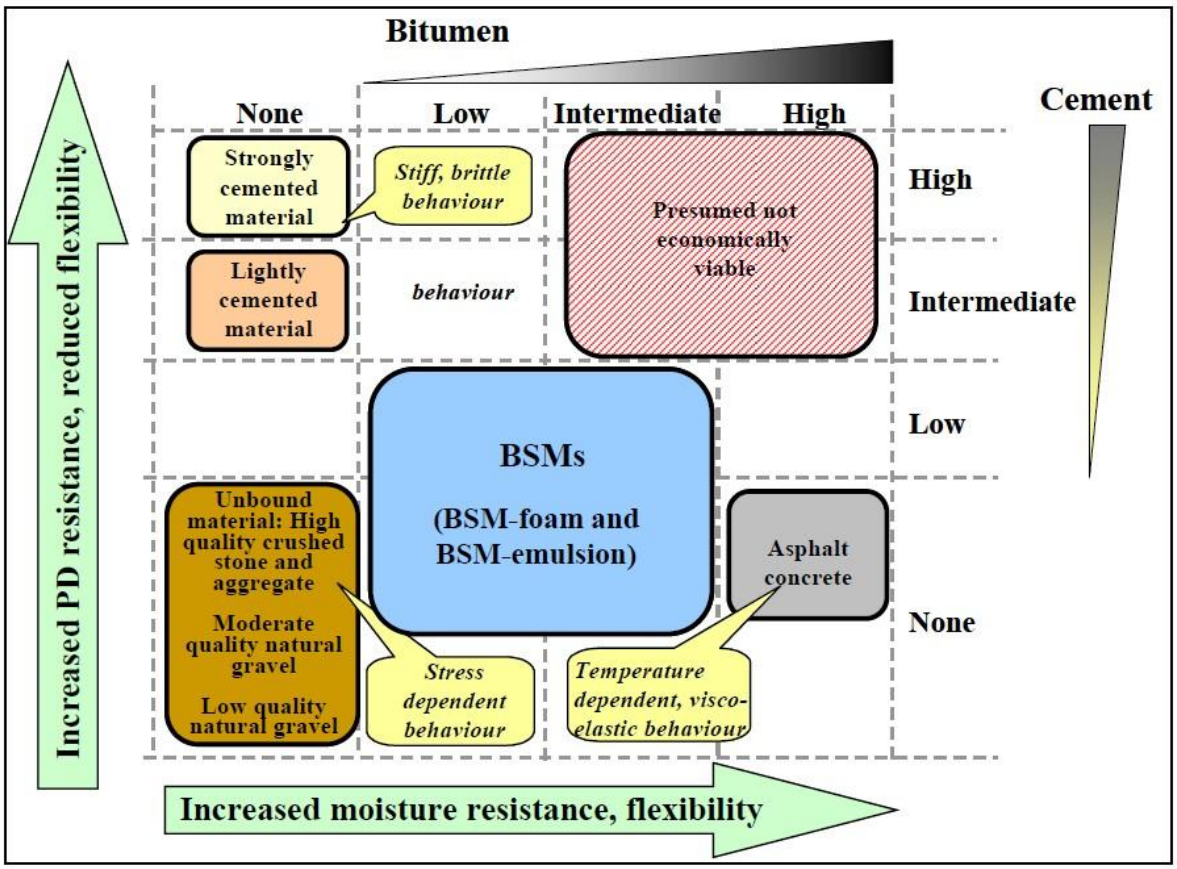

Figure 1.3: Matrix of bituminous and mineral binder influence on BSMs behaviour (Asphalt Academy, 2002).

1.2.5 Disadvantages of using BSM-foam

There are also various disadvantages to the use of BSMs. According to Jenkins (2000) as well as the CSIR (Theyse, 2004), disadvantages include:

- the mix design and manufacturing process of foamed bitumen mixes require an advanced level of skill and experience. This is necessary to produce a product of satisfactory quality;
- mix design methods for foamed bitumen are not as well formulated as for HMA. This makes the process of acquiring experience in mix production and mix specification difficult;
- anti-foaming agents added to some bitumen in the refining process rule out their suitability for use in foamed bitumen without the addition of foaming agents. This adds to the cost of the bitumen;
- no transfer functions have as yet been developed for the design of foamed bitumen layers in a pavement. This makes accurate design of pavement structures difficult;

- not suitable for all pavement types (requires a full particle size distribution). BSM-foam requires strict adherence to grading requirements, especially the fraction < 0.075mm (Jenkins, 2000), and

- the process requires hot bitumen (160°C) for the foaming action to be successful and thus there is the risk of burning.

The advantages and disadvantages of foamed bitumen are factors that should be taken into account, when deciding whether or not to stabilise with foamed bitumen.

1.2.6 Advantages of cold recycling in the bitumen stabilised technology

One of the advantages of stabilising with foam bitumen is its suitability for treating a wide range of materials, from sands, weathered gravels to crushed stone and Reclaimed Asphalt (RA). Mineral aggregates constitute the largest part (both in mass and volume) of BSMs. Crushed stone, natural gravel, RA and natural sand are amongst the mineral aggregates used to produce BSMs. When *in situ* recycling is applied, the selection of aggregates is limited and one has to work with the materials present in the pavement. Weinert (1980) states that materials placed in the pavement layers normally have specific properties at the time of testing or construction that need to be retained over the service life of the layer; hence, mineral aggregates need to be durable. Durable aggregates are able to resist deterioration or disintegration and so retain their original grading, shape and physico-chemical properties during the service life of the pavement.

The main advantages of cold *in situ* recycling are (Asphalt Recycling and Reclaiming Association, 1992):

- *Precise control of layer thickness*
  Once set, the depth cut of the milling drum is controlled by sensors, ensuring an accurate layer of thickness;

- *Consistent mixing*
  Good mixing of *in situ* materials with new aggregates and stabilising agents is assured. Addition of water and stabilising agents is electronically controlled and sprayed across the full width of the milling drum though a series of nozzles;

- *Shorter construction period*
  This is possible due to the new technologies implemented in the new recycling machines;

- *Greatly reduced traffic disruption and improved safety*
  The entire process can be carried out on one half of the road width, leaving the other half open to traffic;

- *Less reliance on fine weather conditions*
  The process offers the distinct advantage of being able to continue working during a period of uncertain weather. When rain threatens the work can be temporally stopped and then restarted again as soon as the rain has passed;

- *Cost effectiveness*

The construction industry is not exempted and several studies have been undertaken to estimate the amount of energy being consumed, particularly in the construction of roads where large machinery is employed and the quantities of material either consumed or moved is high. BSMs offer a lower whole-of-life cost through lower maintenance and other interventions required to achieve an acceptable level of service over the design life of the pavement, as well as the cost of rehabilitation when the terminal condition is reached. The above benefits all combine to make cold recycling a most attractive process for pavement rehabilitation in terms of cost effectiveness.

1.3 Objective and scope of this dissertation

The increased use of bitumen stabilised materials (BSMs), shortcoming in the existing design guidelines (Technical Guideline 2 , Asphalt Academy, 2009) and manuals (Wirtgen, 2010) and ongoing developments in the concepts and understanding of BSM-foam requires further research into the fundamental properties and the behaviour of this materials.

In this research the mechanical behaviour and durability properties of bitumen stabilized material (BSM) produced using high percentages of recycled asphalt pavement (RA) shall be investigated.

- The primary objective of this study is to contribute to the development of resilient response and damage models for stabilised materials, in particular BSM-foam with high percentage of RA. Mechanical properties of BSM-foam mixes with different percentage of RA will be investigated in more depth with extensive laboratory tests. It is essential to understand the mechanical properties of BSMs with the increasing amount of RA. The objective of this research is to investigate mechanisms that influence durability properties and long term performance through tri-axial tests including advanced parameters such as haversine wave loading and different temperatures on specific selected mixes.

- Improve the knowledge about the mechanical characteristic of recycled materials blended with different percentage of virgin materials.

- In terms of structural pavement design, the characteristics of bitumen stabilised material need to be defined for the initial condition of the pavement but also especially for the long-term behaviour. Several tests in the laboratory will show some critical parameters, like temperature grading and resilient modulus that influence the mechanical and rheological properties of BSM-foam mixes with the high presence of recycled asphalt pavement material (RA).

- Developing a fundamental understanding of mechanisms that govern durability behaviour of BSMs, with emphasis on moisture damage. Current understanding of BSMs moisture sensitivity is limited and based on empirical relationships and on a developed laboratory device (Moisture Induced Simulation Test, MIST). The identification of a relevant method that simulates field conditions and the development of a laboratory brushing device to effectively understand the moisture damage in the BSM mixes is an objective of this study.

- Identification of the influence of temperature and voids distribution in the BSM mixes particularly in field conditions. Temperature distribution in pavement layers plays a significant role in both the ultimate gains of mix engineering properties and the exhibition of premature distress. Void content distribution in the mix influences moisture transport into the BSM layer as well as enhancing age hardening of the binder. The objective of this research is to identify temperature distribution behaviour in the different layers of a BSM pavement and its magnitude in the BSMs layer under environmental conditions. The temperature distribution can be linked to void content characteristics in the mix to provide a better understanding of the influence of curing or evaporation of moisture from the BSM layer.

- Demonstration of temperature vs. mechanical properties and its influence on pavement performance. This leads to laboratory test results with the performance of the BSM pavement layer with respect to the different temperature in a BSM layer. The mechanisms that influence the long term behaviour in BSMs should preferably be measurable through mix design and utilised in pavement design by incorporating the relevant mix properties. This important part of the research will move from the last considerations developed by the SHRP Program (Kennedy et al.,1994) and Viljoen (2001) to new more exhaustive tests and results. The objective of this part of the research is to demonstrate the relevance of pavement models to sufficiently represent the temperature gradient in the BSM as determined in the laboratory.

- One of the main goals of this thesis will be to develop a model of the thermo conductivity properties of BSM-foam with different percentages of RA. Studying the gradient of temperature in a BSM pavement at different depths will contribute to understand the mechanical properties and long term performance of the BSM. Select appropriate existing material models (FEMMASE MLS) to describe the observed temperature properties of the BSM-foam mixes, to determine the model parameters and to compare these model parameters with those coming from real temperature measurements. The ultimate goal of the study is to lay the groundwork for the development of methods and procedures to determine temperature profiles in BSM pavements and to provide pavement engineers with computational tools that increase the prediction accuracy of temperatures in BSM pavements for reliable pavement design.

Finally, significant conclusions are highlighted and recommendations for future studies are provided.

Figure 1.4 illustrates the general overview of the research approach.

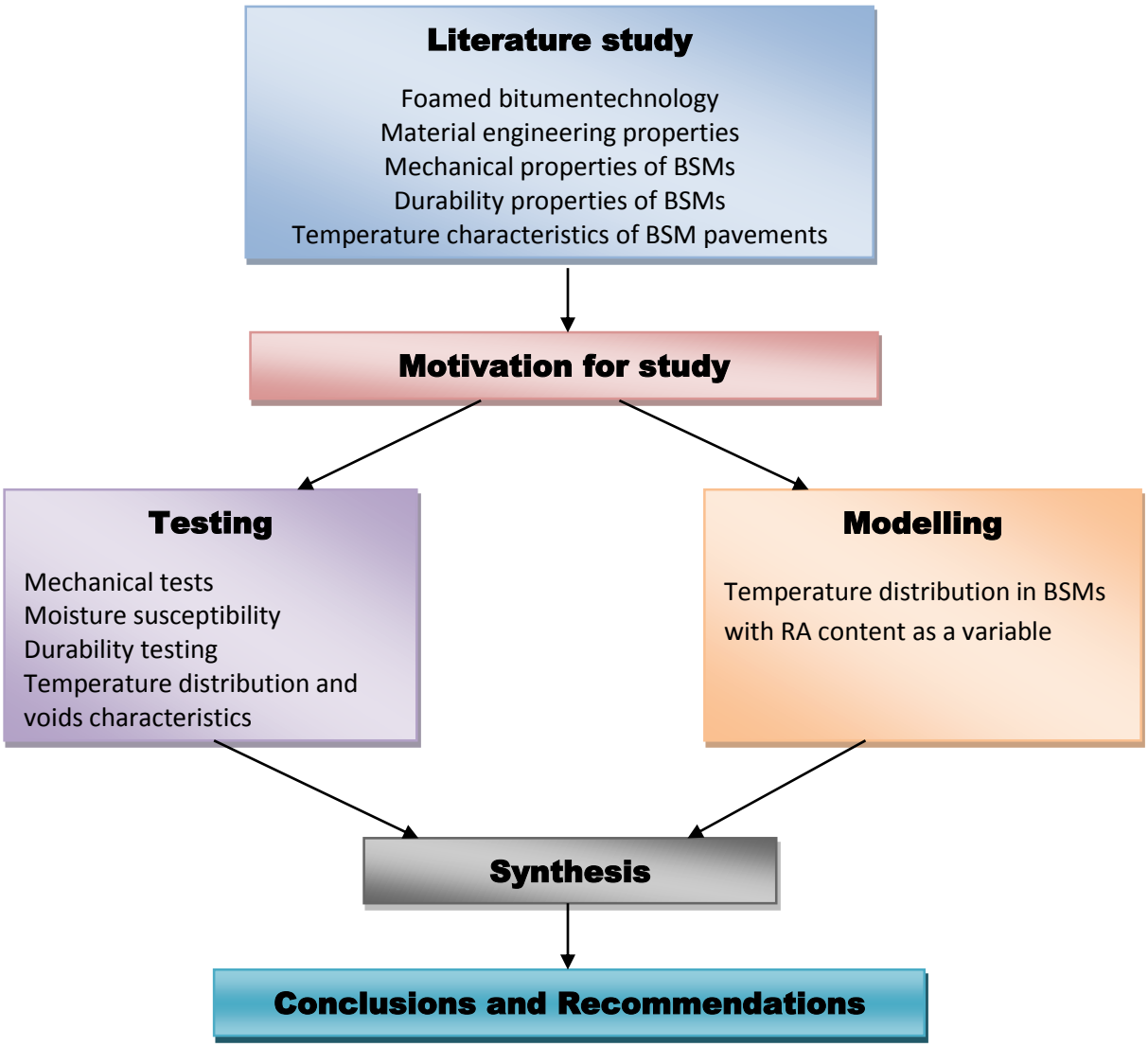

Figure 1.4: Reading guide – structure of dissertation.

1.3.1 The need to understand the temperature distribution of BSM-foam pavement

Pavement engineers clearly understand that pavement materials are predominantly natural and variable. Therefore, the area of application influences their variability, suitability and the behaviour of the composite materials. Pavement materials are often a combination of numerous ingredients formulated, combined, and processed to provide a composite product for a specific purpose. In order to produce construction materials with the necessary quality and consistency to fulfil their intended function, adequate mix design procedures need to be established. This will assist in identifying temperature and mechanical properties for optimal formulation, blending, and production of BSM-foam pavement materials with a high percentage of RA.

Temperature properties are particularly pertinent for the lifetime of a BSM-foam pavement. The temperature distribution in a pavement can be measured by means of a nonintrusive method to retrieve the topmost pavement temperature values. By utilizing the latest infrared (IR)

technology, it is possible to retrieve additional information concerning both road temperatures and road conditions. Nonintrusive measurement of the road temperature is able to provide an increase in relation to the knowledge about both the road temperature and the road condition. Studies by SHRP program (1994) and Viljoen (2001) have indicated that the temperature distribution in a road package requires consideration during mix design. In particular, temperature effects on mechanical properties of BSM-foam need to be characterized in terms of its suitability prior to its application. Although mechanical properties correlate with the temperature distribution are the prime factors in addressing the long-term performance of BSMs mixes.

1.4 Layout of dissertation

In Chapter 2 a comprehensive background is provided for the use of RA in BSMs. Considerations are given to engineering properties and structural design of pavements incorporating RA in the BSM-foam mixes and certain shortcomings have been identified. The chapter provides a literature overview of the available models to describe material properties and behaviour. These models form the basis for the interpretation and evaluation of the test results in the later chapters. The chapter provides a review and analysis of mixture durability in the BSM-foam mixtures. The chapter closes with a discussion on the importance of understanding the temperature in a BSM-foam pavement section.

Chapter 3 presents the experimental design and methodology employed in this thesis. This part of the thesis includes the experimental matrix. The test protocols followed and the test conditions are described in this chapter.

The materials and mixes tested in this study are described in detail in Chapter 4. The laboratory testing in this part of the thesis focuses on ITS tests and tri-axial testing. The results of materials testing are showed in the form of tables and graphs.

Chapter 5 describes the durability properties of BSM-foam mixes with an increasing amount of RA. Permeability tests, wet-dry durability tests and Moisture Induction Simulations Tests (MIST) are presented and discussed in this chapter.

In Chapter 6 the influence of temperature in BSM-foam sections are analysed at different depths. The second part of the chapter focuses on the modelling of thermal transfer in the BSM sections. Some comparisons are drawn with the SHRP program (1994) and Viljoen research (2001) and a consistent analysis through the FEMMASSE Heat-MLS computer program is presented and discussed at the end of the chapter.

In Chapter 7 a synthesis of the study results is provided. The importance of the thermal characteristics of a pavement section with different BSM-foam mixes is discussed. The performance of the different mixes and the influence of the temperature distribution in the BSM-foam sections are compared over the full range of laboratory tests carried out.

In the last chapter the conclusion and recommendations that follow out of this study are presented. These conclusions and recommendations are broad and aimed at providing an overview of the overall performance of BSMs and with a view that the results of this study may contribute towards improving current design practice.

1.5 Expected outcomes of the research programme

The role of recycled material inside a new BSM-foam mix is not completely understood. The research would try to explain through indirect tensile strength (ITS) tests, monotonic tri-axial tests, resilient modulus cyclic tri-axial tests and tests on the energy gradient and temperature in a road package, the mechanical properties that influence BSM-foam mixes with different percentages of RA.

The research will investigate the Resilient Modulus (Mr) of the BSM-foam mixes through intensive laboratory tests and will explain its relevance. In fact, the Resilient Modulus in a BSM-foam mix is very difficult to measure, but it's really important for the correct study of the load spreading ability and mechanical properties of BSM mixes. The method of testing influences the values of Mr, making reconciliation between laboratory and field measurements very difficult. In this study, the results of the previous tests shall be compared with the temperature study. The goal of this part of the research would try to explain the relevant significance and the impact that the Resilient Modulus could have on the BSM-foam mixes through the temperature distribution.

The influence of different percentages of RA on BSM-foam mixes could be better investigated with tests, which will simulate the behaviour of a pavement, subjected to intensive road traffic through long term repeated dynamic tri-axial tests. Temperature and curing phase are important parameters for all the tests on BSM-foam mixes. The research will consider the possible influence of the temperature and curing on the bitumen stabilized material (BSM-foam) with higher percentage of RA, with particular attention to the monotonic tri-axial tests and resilient modulus cyclic tri-axial tests. Temperature distribution in a pavement plays a significant role in both the ultimate gains of mix engineering properties and the exhibition of premature and permanent distress. Void content distribution in the mix influences moisture transport into the BSM-foam layers as well as enhancing age hardening of the binder. The temperature distribution can be linked to void content characteristics in the mixture to provide a better understanding of the influence of performance of the BSM-foam pavement.

The influence of durability properties on the mix design of stabilized material is not completely understood, especially with the presence of recycled materials. However, there are potential reasons that durability and mechanical properties affect the performances of the materials. These mechanisms need to be investigated and reliably simulated using laboratory testing results. The identification of a relevant method that simulates field conditions and the development of a laboratory brushing device should be structured to suit the needs of the road construction industry.

This research will aim to give a complete and detailed study on the possibility to use different percentage of recycled materials in new BSM-foam pavements through a clear programme of laboratory tests results and simulations.

1.6 Limitations of the research

This research was limited to two granular material types due to the extensive range of tests performed in the laboratory: G2 Hornfels crushed stone (good quality material) from the Tygerberg Quarry (LaFarge) and RA made at the Asphalt and Geotechnical Laboratory at the University of Stellenbosch. The typical mixes in this research had a range of different RA contents and G2 material, for example 100% RA and 0% G2, 50% RA and 50% G2, 0% RA and 100%G2. The bituminous binder content for all this researc ranged between 2% and 2.3% for all the mixtures in order to get a comparison of mechanical and durability properties. One type of bitumen (80/100) was used for foamed bitumen, one grading for each aggregate, one compaction method, standard curing, and mechanical testing i.e. tri-axial testing and ITS test. In addition limited ITS test in dry conditions and tri-axial tests were performed for advanced classification of BSMs. Dynamic tri-axial tests were widely carried out in this research but only with a haversine wave form at different temperatures and one frequency. Permanent deformation tests were limited to only three temperatures (25˚C, 40˚C and 50˚C) for the BSM-foam mix with 50%RA. The other two mixes with 100%RA and 100%G2 were tested at one temperature (40˚C). The modelling of the material behaviour in this study was limited to using existing material and behavioural models. The temperature distribution in the BSM-foam mixes was limited to the diurnal effects of the temperature on the surface of the pavement. The experimental investigations are restricted to laboratory testing and no field testing or field performance monitoring were carried out during this study due the large number of tests performed in the laboratory and time constraints.

REFERENCES

Asphalt Academy. 2002. The design and use of foamed bitumen treated materials. Interim Technical Guideline No. 2, Pretoria, South Africa.

Asphalt Academy. 2009. A guideline for the design and construction of bitumen emulsion and foamed bitumen stabilised materials. 2nd edition technical guideline. Pretoria, South Africa. (TG2).

Asphalt Recycling and Reclaiming Association. 1992. Guidelines for Cold In-Place Recycling, Annapolis, MD.

Collings, D.C. and Jenkins, K.J. 2008. Characteristics of Materials Stabilised with Foamed Bitumen. Eurobitume Conference, Copenhagen, Denmark.

Csanyi, L. H. 1957. Foamed Asphalt in Bituminous Paving Mixtures, Bulletin No. 160, Vol. 10, Highway Research Board, Washington D.C., USA, 1957.

Csanyi, L. H. 1959. Foamed Asphalt, Technical Bulletin Vol. 240, American Road Builders Association, USA.

Ebels, L.J. 2008. Characterisation of Material Properties and Behaviour of Cold Bituminous Mixtures for Road Pavements. PhD Dissertation, Department of Civil Engineering, Faculty of Engineering, University of Stellenbosch, South Africa.

Jenkins, K.J., Long, F.M., and Ebels, L.J. 2007. Foamed Bitumen Mixes Shear Performance International Journal of Pavement Engineering. Volume 8 Number 2.

Jenkins, K.J. 2000. Mix Design Considerations for Cold and Half-Warm Bituminous mixes with the emphasis on foamed bitumen. PhD Dissertation. University of Stellenbosch.

Kennedy, T.W., Huber, G.A., Harringan, E.T., Cominsky, R.J., Hughes, C.S., Von Quintis, H., Moultrop, J.S. 1994. Superior Performing Asphalt Pavements (SUPERPAVE): The product of the SHRP asphalt research program, Report no: SHRP-A-410, Strategic Highway Research Program, Washington.

Long, F.M. and Jooste, F.J. 2007. Summary of LTPP Emulsion and Foamed Bitumen Treated Sections. Technical memorandum compiled on behalf of SABITA and GDPTRW. Modelling and Analysis Systems, Cullinan, South Africa. (Gautrans report: CSIR/BE/ER/2007/0006/B).

National Department of Transport. 2009. Technical Recommendations for Highways : TRH 21 Hot Mix Recycled Asphalt. Pretoria, South Africa.

Paige-Green, P. and Ventura, D. 2004. Durability of Foamed Bitumen Treated Basalt Base Courses. Council for Scientific and Industrial Research, Transportek Division. Contract Report: CR-2004/08, Pretoria, South Africa.

Shell Bitumen, 2003. Shell Bitumen Handbook. Shell Bitumen UK.

Theyse, HL. 2004. Restricted CSIR Contract Report CR-2004/38, The Compaction Potential of Foamed and Emulsified Bitumen Treated Material, Pretoria, South Africa.

Twagira, E.M. 2010. Influence of durability properties on performance of bitumen stabilised materials, PhD Dissertation, Department of Civil Engineering, Faculty of Engineering, University of Stellenbosch, South Africa.

Viljoen, A. W. 2001. Estimating Asphalt temperatures from air temperatures and basic sky parameters. Internal report, Transportek, CSIR, Pretoria. South Africa.

Weinert, H.H. 1980. The Natural Road Construction Materials of Southern Africa. Academia. Cape Town, South Africa.

Wirtgen GmbH. 2010. Cold Recycling Manual, 3rd edition published by Wirtgen GmbH, Windhagen, Germany.

CHAPTER 2

LITERATURE REVIEW

2.1 Introduction

This chapter presents a literature review which is focused on reclaimed asphalt materials (RA), mechanical performance of BSM-foam mixes, influence of temperature distribution on BSM-foam pavement layers and durability characterization of BSM-foam with high percentage of RA. This will include a discussion about material properties and mixture design for foamed asphalt materials. An understanding of what road pavement materials are and how to characterise them is required in order to provide a correct understanding of BSM-foam mixtures as a road material. The full review on characterization of BSM-foam mixes and properties of RA is designed to support the summary and problem statement given in the previous chapter.

Material properties and durability play a prominent role during the selection of combined and processed BSMs for mix design. The mix design for BSM-foam pavement should maintain its initial performance properties through time, above a certain level of service by resisting stresses, strains, climate and temperature effects. Failure mechanism in BSM-foam layers cannot be determined through mechanical evaluation alone like in the past years, but further studies at high and low levels of mineral aggregate interaction, durability and temperature behaviour need to be analysed. The restrictions and constraints in terms of use of RA in BSM-foam mixes need to be scientifically understood. Durability properties and temperature behaviour of BSM-foam mixtures with high percentage of RA should help to explain the performance and mechanical characterizations of these mixes better. In this way the mix design can be optimised by addressing specific investigations that ensure that the collected data are appropriate and important enough to result in the correct decision in the application of BSM-foam mixes with an increasing amount of RA.

In this research a clear distinction is made between mechanical performance and mixture composition requirements for the durability properties, temperature behaviour and long-term performance of BSM-foam mixes. This chapter reviews the key factors that influence the performance and behaviour of BSM-foam mixes with high percentage of RA through a detailed analysis of the mechanical performance of the mixes, the durability properties, the temperature gradient distribution inside BSM pavement layers and long-term performance of BSMs. The review provides a substantial understanding of the mechanisms related to the use of RA in BSM-foam mixes and compiles the research to investigate some of the more important, but less understood variables, with a marked emphasis on:

- characterising the behaviour and durability properties of RA in BSM-foam mixes in terms of mechanical properties of aggregates and mixtures. These aspects put emphasis on the use of consistent amounts of RA in BSM-foam mixes to determine the technical performance and relationship between RA and mineral aggregates properties and bonding;
- analysing the effect of the temperature gradient on different BSM-foam pavement layers with different amount of RA through the use of a system of infrared lights; and the possible implications and influences on the mechanical properties of the BSMs.

2.2 Purpose for characterisation of materials

There are several reasons why laboratory characterisation of materials is undertaken. These include:

- to optimise material performance and to ensure the material meets minimum service requirements;
- to provide material parameters for the thickness design method;
- to minimise costs and to save non-renewable resources by optimising use of materials and additives;
- to ensure the pavement when constructed according to the specification lasts a minimum design period, and
- research to determine fundamental pavement properties, to refine design methods and to generally extend knowledge that may be applied to pavements in material selection, material performance, pavement performance, application of pavement processes in various climatic conditions, and the effect of different axle loads and configurations on pavements.

For all but the first point above, a laboratory method and mix design procedure needs to meet the following criteria:

- cost-effective;
- relatively quick;
- repeatable;
- reproducible by any competent technician;
- provide realistic design inputs that match field performance, and
- ensure that the material and binders perform for the design period and withstand the traffic load applied.

Another important factor is that generally pavements are not uniform, there are often significant variations within a pavement section, and during construction, there will be variations in moisture content, compaction input and mixing. In selecting densities for preparation of laboratory test specimens, consideration should be given to the minimum specified relative compaction levels and the variation in field compaction with depth below the surface. In some cases in urban areas, the presence of sensitive services such as old water mains and gas mains, and proximity to structures, mean that vibratory compaction may not always be possible and this may affect the level of compaction achieved. In addition, the action of mechanical stabilisers on softer aggregate may change the particle size distribution during construction, and laboratory mixing may not reflect this change.

It is therefore important that any mix design process:

- recognises construction limitations;
- considers variations in grading, and
- recognises that pavements are rarely consistent.

It is essential to recognise that laboratory mix design should be used as a guide (Asphalt Academy, 2009). As with all bituminous mixes, it is essential to have a proper mix design procedure for foamed asphalt mixes in order to optimize the usage of available materials and to optimize mix properties.

2.3 Reclaimed asphalt (RA) characteristics

With the introduction of the cost-efficient cold recycling process for the rehabilitation of damaged roads, a technology has earned itself worldwide renown which has ecological as well as economic benefits. The reuse of part of the existing road structure which, when treated with binding agents, becomes the foundation of a new road, is the basis for a recycling method that has become a pillar of economical road rehabilitation worldwide.

Recycling hot mix asphalt (HMA) material results in a reusable mixture of aggregate and asphalt binder known as reclaimed asphalt (RA). Recycling of asphalt pavements is a valuable approach for technical, economical, and environmental reasons (Kennedy et al., 1998). Using RA has been favoured over virgin materials in the light of the increasing cost of asphalt, the scarcity of quality aggregates, and the pressuring need to preserve the environment. Many countries in the northern hemisphere, in particular the USA, have also reported significant savings when RA is used (Page and Murphy, 1987). Considering material and construction costs, Kandhal and Mallick (1997) estimated that using RA provides a saving ranging from 14 to 34% for a RA content varying between 20 to 50%.

The use of RA also decreases the amount of waste produced and helps to resolve the disposal problems of highway construction materials and rehabilitations, especially in large urban areas. Use of pavement recycling as an alternative to the conventional pavement rehabilitation methods started on a small scale in the 1930s and gained much of its popularity in the 1970s due to the energy crisis that hit the globe in 1973 (Van Wijk and Wood, 1984). The resulting fuel-associated rise in construction costs sparked a research interest into the viability of pavement recycling starting in Europe, Australia, the United States and South Africa. In 1996, it was estimated that about 33% of all asphalt pavement in the United States was recycled into new road pavements (Sullivan, 1996). Laboratory models and field trial sections were constructed and monitored over time to ascertain the engineering properties of the recycled asphalts and to devise ways of improving their performance to match those of conventional rehabilitation materials. To facilitate incorporating RA in the design of new pavements, many countries have relied on blending charts developed in the late 1980s (Asphalt Institute 1989). Most countries have also established limits on the maximum percentage of RA that can be used, ranging typically between 10 to 90%. High percentages of RA are quite commonly used in practice. RA has been used in hot mix asphalt pavements in various percentages that reached in some cases up to 80% (EPA and FHWA, 1993), and typically from 20 to 50% (Kim, 2007; Solaimanian, 1996; Lynn, 1992). In the Netherlands almost all the RA is used in the mix design

and rehabilitation projects of existing road networks (Dutch environmental policy concerning the use of secondary materials, 2011). In South Africa the percentage of RA that is usually added back in new road project, is up to 30% (National Department of Transport, 2009).

Stabilization of RA material with foamed asphalt has been tried in South Africa and abroad. Roberts *et al.* (1984) compared the performance of stabilized RA material with BSM-foam with those treated with cut-back asphalt and asphalt emulsion in the laboratory. Maccarone (1994), Lancaster (1994) and Ramanujam (1997) reported successful stabilization with foamed asphalt of RA material, both in-plant and *in situ*, in Australia. The first attempts in the USA were carried out by Van Wijk and Wood (1983) and then in recent years by Romanoshi *et al*. (2003), Appea *et al*. (2009) *,* Caravalho *et al*. (2010) and Musselman (2009) . In Europe most projects use BSM technology to stabilise base and subbase courses for roads and highways (Loizos and Papavasiliou, 2007; Whiteoak, 2000; Zoorob *et al*., 2002; Montepara and Giuliani, 2002; Santangata *et al*., 2009) . Stabilization of RA is now an accepted road rehabilitation process and it can be used to improve various road pavements ranging from low volume unsurfaced roads to main highways carrying heavy traffic (Moore, 2004; Cross, 1999; Mallick *et al*., 2002; Karlsson and Isacsson, 2006). In South America several road projects started to use RA in recent years (Walter J. *et al*. 2008; Bonfim, 2008) .Van der Walt *et al*. (1999), Jenkins (2000), Ebels (2008) and Twagira (2010) have reported the use of increasing quantities of BSMs stabilized with RA materials in South Africa.

Using RA in new mixtures can reduce the amount of new material that has to be added, saving money and natural resources. In addition, BSM mixtures with RA can perform as well as mixtures made with all new material (Twagira, 2010). Some countries in South America, in the Middle East and in Indonesia are taking a more aggressive approach by considering increasing the allowable percentages of RA in BSMs to take full advantage of this promising technology. In 2000, for example, approximately 100 000 t of various aggregates were treated with foamed bitumen alone in the Netherlands. In Brazil, more than 2.5 million m^2 of road surface have been rehabilitated with foamed bitumen since 1998. In Norway, approximately 3.0 million m^2 of road surface has been recycled with foamed bitumen since 1983 (Wirtgen, 2002). This is sufficient proof of the reliability rightly attributed to this innovative technology. Today, this technology is successfully employed worldwide. In Europe, particularly in Norway and the Netherlands, but also in Eastern European countries, such as Russia and the Baltic Republics, the use of foamed bitumen in cold recycling, as an alternative to conventional binding agents, gains more and more acceptance. In addition, numerous projects are being carried out in North and South America. Foamed bitumen technology is being successfully employed even in countries with extreme climatic conditions, such as Saudi Arabia or Iran, and African states like Lybia, Malawi, Nigeria or South Africa (Wirtgen, 2002). On the Asian and Australian continents, too, traffic routes have been economically rehabilitated within extremely short periods of time by using the cold recycling process with foamed bitumen.

However, ensuring confidence in the design procedure and the success of using RA would require addressing many durability concerns related to the interaction between virgin and recycled materials and their use in BSM-foam mixes. Well-graded material with a satisfactory distribution from fine to large grained aggregates is required for treatment with foamed bitumen. The sieve analysis will aid to draw conclusions as to whether additional aggregates will have to be added. If the mineral aggregates are deficient in fines (minimum 5% passing the 0.075 mm sieve) as most of RA coming from rehabilitation projects, crushed sand with a high filler content or active fillers can, for example, be added (Wirtgen, 2010). When using foamed bitumen as a binding agent, the content of fines in the mineral aggregates is very important.

The foaming process results in a surface expansion of the bitumen and a simultaneous reduction of its viscosity. The dispersing properties thus improved ensure that the fines in the mineral aggregates are coated. The filler and the foamed bitumen together produce a mortar binding the coarse aggregates.

When RA is reused in a new mixture, it is necessary to properly account for the old material in the new design. The aggregate from the RA has to be included with the new aggregate, and that blend of aggregate has to meet certain physical properties. The experience with RA in Twagira (2010) mixtures has shown that properly designed and constructed RA mixes can perform as well as, or even better than, mixtures made with all new materials. The mixtures with RA designed by Ebels (2008) and Jenkins (2000) have also shown good performance. It is apparent from the mentioned studies that the influence of high percentage RA was investigated only recently. However, further research is required to better understand the behaviour of BSM-foam mixes with increasing amounts of RA and the effects of durability and temperature behaviour on this type of mixes. The durability and the temperature aspects are probably the principal component of the total system affecting the mechanical performance and long-term lifetime of BSMs.

One major factor that is still unclear is the level of interaction between aged binder and virgin bitumen binders. If RA acts like a black rock, the aged and virgin binders will not interact. Hence, it would be assumed that RA does not significantly change the virgin binder properties. However, it is usually assumed that RA does not act as a black rock and that the aged asphalt blends with the virgin binder during mixing. In fact, many design procedures assumes that all the aged binder would effectively contribute to the blend. This means that the amount of virgin asphalt binder can be reduced by the full amount of asphalt binder in the RA for the percentage specified.

When HMA reaches the end of its service life, milled materials still maintain considerable value. Most of the recycled RA comprises aggregates of good quality e.g. crushed stone from Hornfels, Granite and Quartzite rock type. The milled materials, RA, can be reused in virgin BSM-foam mixes to reduce the amount of new material and bitumen that needs to be used. However, it is necessary to account for old materials in the BSM design process. During service, the blend of aggregates and binders undergoes various physical and rheological changes that have to be considered in the design process to ensure that the BSMs mixtures with RA perform as well as the original pavement produced with virgin materials (Ebels, 2008 and Twagira, 2010).

The current South African guidelines i.e. Guideline for road construction materials (TRH14, 1985) and South African Mechanistic Pavement Design Method (Theyse *et al*., 1996) provide quality and durability of mineral aggregate requirements for the HMA, and granular layers. No cognisance of quality and durability is indicated for the recycled composite materials for BSMs. Therefore, classification of recycled materials based on quality and durability requirements for BSMs is an area which needs more investigation.

2.3.1 RA binder properties

In general, asphalt binder demonstrates two stages of ageing: short-term and long-term. During construction (short-term), asphalt binder is exposed to hot air at temperatures ranging from 140 to 160°C, resulting in a significant increase in viscosity and changes in the associated

rheological and physiochemical properties such as complex shear modulus and adhesion. During service (long-term), asphalt binder also progressively ages and hardens through various mechanisms. Age hardening during construction and service has been associated with six major mechanisms (Roberts et al., 1996; Tyrion, 2000; Karlsson and Isacsson, 2006):

- Oxidation through diffusive reaction between the binder and oxygen in the air;
- Volatilization through evaporation of the lighter components especially during construction;
- Polymerization through chemical reaction of molecular components;
- Thixotropy due to the formation of a structure within the asphalt binder over a long period of time;
- Syneresis due to the exudation of thin oily components, and
- Separation through the removal of oily constituents, resins, and asphaltenes by absorptive aggregates.

The level of ageing that asphalt binder experiences during production and service also depends on the void content of the HMA. Recovered binder from porous HMA has shown significantly greater stiffness than regular HMA (Kemp and Predoehl, 1981). In addition, properties of aged binder depend on the level of damage to the recycled asphalt (Smiljanic *et al*. 1993). The greater the damage to the pavement prior to recycling, the greater the changes in the properties of the binder. This is illustrated by the reduced oxidation susceptibility in pavements that are better preserved. Stockpiling also accelerates binder ageing as the material is more prone to air exposure and oxidation (McMillan and Palsat, 1985). As asphalt binder reacts and loses some of its components during the ageing process, its rheological behaviour will naturally differ from virgin materials. This suggests the importance of controlling the blending process between recycled and virgin binders. If the old binder is too stiff, the blend of old and virgin binders may not perform as expected. At small percentages (up to 30%), an aged binder does not significantly affect the properties of the blend of virgin and RA binder (Twagira, 2010). However, when used at intermediate to higher percentages, an aged binder can significantly influence the properties of the blend and may affect the resultant mechanical properties.

The properties of aged binder are also affected by the level of moisture damage on the existing pavement prior to recycling. However, when a small percentage of RA is used (15 to 20%) other researchers have reported that RA materials might in fact provide stronger moisture resistance than virgin material since the aggregates are already covered and protected with binder (Ebels, 2008, Twagira, 2010).

2.3.2 Performance of RA in BSM-foam mixture

The current guidelines i.e. Wirtgen (2010) and TG2 (2009) provide quality of mineral aggregate requirements for the BSMs layers but no durability is indicated for the recycled composite materials for BSMs. Therefore, classification of recycled materials needs more study.

According to TRH 14, the performance classification of different mineral aggregates in newly constructed layers is G1, G2, G3, etc. However, this type of classification becomes more complex if these materials have been in service for some time. If the plasticity index (PI) of mineral aggregates, G1 changes and conforms to G4, while the grading or CBR conforms say to G3, then what could be the new class?

Based on the complexity of the classification of recycled materials for pavement rehabilitation, Jooste (2007) introduces a classification system called "design equivalent materials". This classification indicates that: "when a design equivalent class is assigned to a material, it implies that the materials exhibit *in situ* shear strength, stiffness and flexibility properties similar to newly constructed materials of the same class as in TRH14". It is apparent from a newly proposed classification that additional information on the aggregate properties are required to ensure consistent application of recycled materials for the BSM mix design. Apart from strength properties of the mineral aggregates indicated above, surface characteristics also need to be evaluated and included in the classification as they play a significant role in the bitumen-aggregate-water interaction (bonding).

2.3.3 Ageing

Significant ageing takes place during short-term ageing where the binder is subjected to high temperature during production of the asphalt mixture. During the short-term ageing of the bitumen, both oxidation and volatilization processes take place. The hardening of the binder during the service period of the pavement (long-term ageing) is mainly due to oxidation. The long-term ageing process of an asphalt pavement depends on the prevailing environmental conditions and the type and origin of the binder. The ageing process is influenced by the type of asphalt mixture (Kandhal and Chakraborty, 1996).

In a study conducted by Choquet (1991 from Franken *et al*. 1997) the effect of ageing over the entire thickness of a porous asphalt pavement layer was observed, indicating the severity of ageing in highly porous mixtures. The reason is attributed to the high amount of voids in porous asphalt that allows access to oxygen and water, resulting in changes in the binder property over the whole thickness within a relatively short period of time. As a result, substantial rheological changes take place such as a decrease in penetration, an increase in 'softening point', and an increase in viscosity of the binder due to age hardening. According to Franken *et al*. (1997) practical experimental studies on a number of asphalt sites indicate that the original 80/100 bitumen displayed penetration of less than 30 dm and a softening point (ring and ball temperature) higher than 60ºC after 3 years of service, which could contribute to brittle behaviour of the binder and sensitivity to ravelling.

Figure 2.1 shows a general trend of the effect of ageing during production (short-term) and service period (long-term) on the viscosity ratio (ratio of the aged to un-aged binder viscosity). The change in viscosity ratio shown in Figure 2.1 is typical for ageing of dense asphalt mixtures.

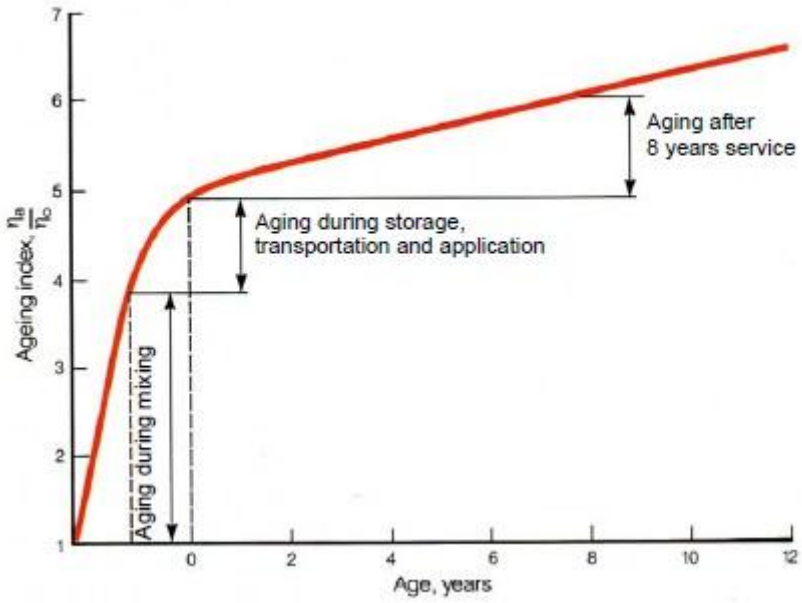

Figure 2.1: Effect of short and long term ageing of the binder on viscosity ratio with ageing period (Shell Bitumen, 1993).

It is important to note that these indices of ageing vary with the pavement structure, location, and mixture type, which is the reflection of the effect of environment, binder source and asphalt mixture type.

Durability of a wearing course is affected by binder age hardening both during the construction phase and service period; therefore, simulation of ageing needs to take into account these effects. In order to accelerate the ageing process in the laboratory in a realistic way, understanding the mechanism of ageing in the field is essential. Ageing is predominantly caused by oxidative ageing, which is an irreversible process, where oxygen from the environment has to diffuse physically into the binder before it reacts chemically with the binder components resulting in hardening. High temperature serves two purposes during the ageing process:

- it softens the bitumen and increases the diffusion rate;
- it accelerates the chemical reaction.

Based on the ageing process, two alternative mechanisms are therefore used to accelerate ageing:

- reducing the film thickness;
- accelerating the diffusion of air/oxygen into the binder film under pressure (Anderson *et al*. 1994).

After short-term ageing, bituminous binders are subject to field (natural) ageing during their service life under the prevailing climatic conditions of the road location. This second stage ageing process is a very important factor in the long-term behaviour of bituminous mixtures and in the development of their performance characteristics (Francken *et al*., 1997). Long-term ageing occurs primarily due to the oxidation of an asphalt mixture in service. Long-term ageing

is defined as a slow oxidation (ageing) process that the binder undergoes as a result of interaction with the environment or air. A laboratory test which was carried out to simulate long-term ageing, i.e. ageing occurring during in service, is discussed later in this research.

Binder oxidation causes formation of functional groups which are characterized by the growth in the infra-red carbonyl and sulfoxide peaks. The infra-red absorption at 1700 cm^{-1} represents carbonyl formation (C=O) and at 1030 cm^{-1} represents sulfoxide formation (S=O), which are characteristic of chemical bonds formed by the oxidation process (Figure 2.2). It should be noted, however, that the increase of carbonyl and sulfoxide formation represents only the major portion of the spectral change during oxidation (Domke *et al*. 1997). The increase in the area under the carbonyl (ketone) and sulfoxide peaks are usually used to describe the degree of binder ageing. Because ketones and sulfoxides are the major oxidation products, their sum indicates the relative degree of oxidation in binders.

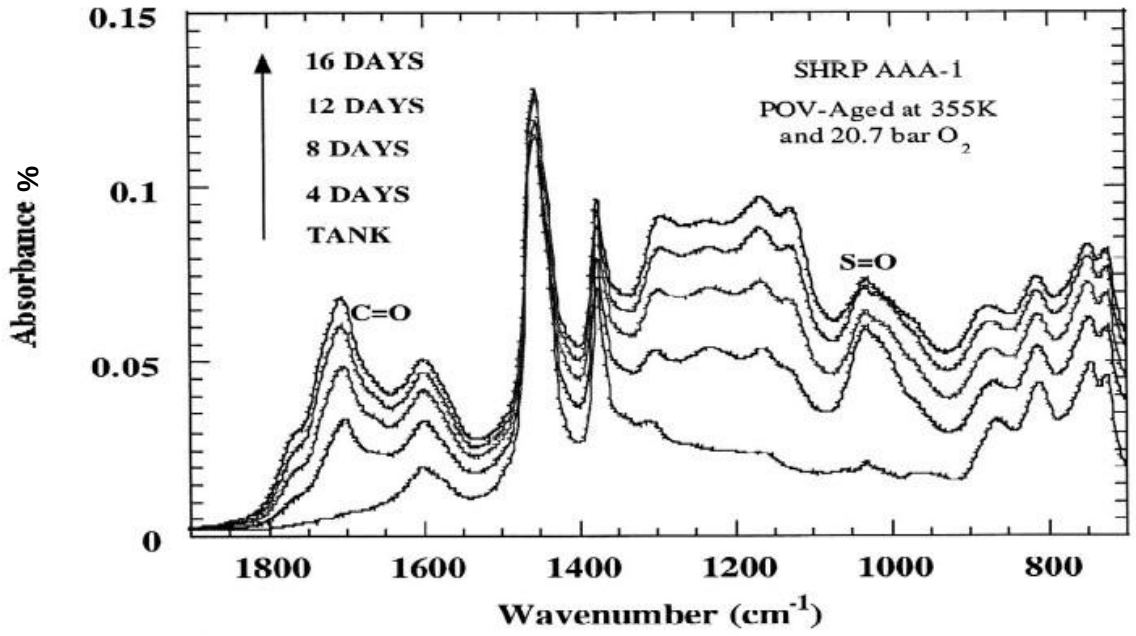

Figure 2.2: FTIR spectrum showing increase in carbonyl/ketone (1700 cm^{-1}) and Sulfoxide (1030 cm^{-1}) formation with ageing (Domke and et al., 1997).

Sensitivity to oxidation is generally related to the sulphur content present. The rate of ketone formation decreases and sulfoxide formation increases for binders with a higher sulphur content. Ketone concentration due to oxidation is strongly related to the increase in viscosity of the binder. A higher amount of ketones appear to be formed at the expense of sulfoxides at higher temperatures and ketone formation rate decreases with increasing viscosity (Peterson and Harnsberger, 1998). The formation of ketones and sulfoxides increases as a function of the ageing period and the sum of area under the FTIR peaks can be used as an indication for relative sensitivity of binders to oxidative ageing.

2.4 Engineering properties of BSMs

The engineering properties of BSMs have extensively been studied in the past. As a result, numerous tests have been utilised to characterise the properties of the BSM mix durability. However, testing procedures for BSMs have undergone major transformation in recent times,

with a shift from ITS, UCS and dynamic creep to tri-axial testing (i.e. resilient modulus, permanent deformation, and shear property), fatigue testing.

The Indirect Tensile Strength (ITS) and tri-axial tests are normally performed in numerous mix designs. An overview on the background and fundamentals of standard ITS tests and tri-axial testing is presented in this section.

The ITS, originally designed for testing the moisture susceptibility, is an accepted method for evaluating BSM-foam mixtures for mix design purposes. It is a relatively quick test to obtain strength characteristics of BSMs in soaked and unsoaked conditions. Design guides such as the South African TG2 (Asphalt Academy, 2009) and Wirtgen Cold Recycling Manual (Wirtgen, 2010) both employ strength tests in dry conditions for mix design optimization purposes and advise a minimum requirement for moisture susceptibility. However, the ITS test is considered to be a 'simple test' (because it can be performed in a relative easy manner). The interpretations of the results are very complex since internal stress distribution in the test is extremely complicated (Jenkins and Ebels, 2007).

A tri-axial test is a recognised method used to measure the mechanical properties such as shear, resilient and plastic behaviour of many deformable granular materials. The use of tri-axial testing has its origin in geotechnical engineering. However, for pavement engineering the use of tri-axial testing is less common. It is mostly limited to research projects.

The monotonic failure tri-axial test can be used to determine the shear parameters cohesion (C) and angle of internal friction (φ) while elastic resilient stiffness behaviour (Resilient Modulus, Mr) and permanent deformation can determined by short duration dynamic loading and long duration dynamic loading tri-axial tests respectively. These parameters can be used for pavement design in combination with mechanistic-empirical design methods, linear-elastic multi layer pavement design software and finite element software.

The fundamental objectives of the literature study (Jenkins, 2000, Ebels 2008) on tri-axial testing are to illustrate:

- the general theory and principles of tri-axial testing;
- the role that tri-axial testing fulfil in material classification, mechanistic-empirical design and modelling of pavements, and
- the appropriateness of the tri-axial test in quality control/assurance and performance prediction of flexible pavement materials.

Testing procedures for BSMs have undergone major transformation in recent years, with a shift from ITS to the fundamental tests such as tri-axial testing (i.e. resilient modulus, permanent deformation,...), and fatigue testing (Ebels, 2008, Twagira, 2010). The limiting values of these tests on BSMs are still uncertain, as the mechanisms of failure are not yet clearly defined especially for BSMs with a high percentage of reclaimed asphalt (RA).

2.4.1 Indirect Tensile Strength test

As mentioned in the introduction to this chapter, the most commonly used mechanical properties are derived from a standard tension test. Originally the ITS test was used to measure rupture strain in concrete (Blakey and Beresford, 1955); it was thereafter adapted to determine

the elastic properties (E and ν) of concrete (Wright, 1955; Hondros, 1959). Kennedy and Hudson (1968) first suggested the use of the test for stabilized materials, while Schmidt (1972) used the test to determine the resilient modulus of HMA. Since then, ITS has become the main setup selected by most engineers for evaluation of tensile strength in the BSM-foam mixes (Jenkins, 2000).

The ITS is measured by loading the specimen at a constant strain rate until it fails by splitting along the diametral axis. The horizontal tensile stress at the centre of the test specimen is calculated using Equation 2.1; the tensile strain is calculated using Equation 2.2:

$$\text{Horizontal Tensile Stress} = \sigma_{xy} = \frac{2P}{\pi Dt} \qquad [2.1]$$

where
D = diameter of the specimen,
P = the applied load, and
t = the thickness of the test specimen or core

and

$$\text{Horizontal Tensile Strain} = \varepsilon_{xy} = \delta_{xy} = \left(\frac{2(1+3\mu)}{d(a+b\mu)\pi}\right) \qquad [2.2]$$

where
δ_{xy} = horizontal strain across the test specimen,
μ = Poisson's ratio, and
a, b and d = integration constants that are specimen geometry dependent.

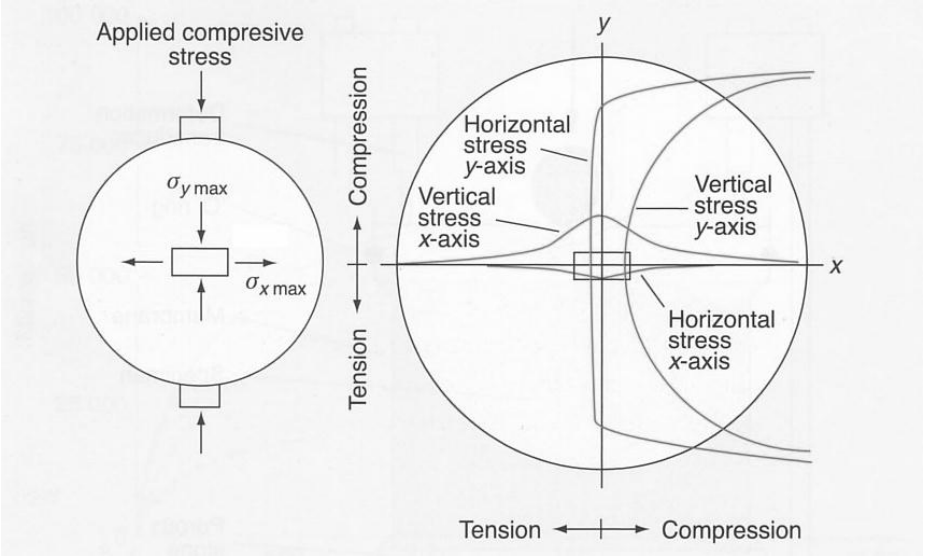

Figure 2.3: Stress distribution in a cylindrical sample (Witczak and Mirza, 1999).

The only unknowns in the previous equation are Poisson's ratio and the integration constants. The integration constants are dependent on the geometry of the test specimen. The determination of Poisson's ratio requires both horizontal and vertical deformation measurements made on the specimen, or it can be calculated from the regression equation developed by Witczak and Mirza (1999), as shown below:

$$\mu = 0.15 + \frac{0.35}{1+exp(3.1849-0.04233\ x\ Temp)} \quad [2.3]$$

Temperature in Equation 2.3 is expressed in degrees Celsius.

In the ITS test, the specimen is radially loaded, as shown in Figure 2.3, resulting in non-uniform stresses in the specimen. As indicated with the shaded area in this figure, the vertical stress σ_v varies along the V-axis of the specimen, while the horizontal stress σ_u remains constant except near the edges of the specimen. The horizontal (tensile) in-plane (V-U plane) stress at the centre of the specimen with diameter "d" and thickness "t," which is the height of the specimen measured in the out-of-plane direction, is induced by the applied vertical load (P) on the cylindrical specimen, while the out-of-plane horizontal stresses are zero.

Under conditions of a line load, the specimen would be expected to fail near the load points due to compressive stresses and not in the center portion of the specimen due to tensile stress. It has been shown, however, that these compressive stresses are greatly reduced by distributing the load through a loading strip (Witczak and Mirza, 1999).

Parameters from the indirect tensile test that have been correlated to actual cracking values include indirect tensile strength (S_t), horizontal strain at failure (ε_f) and total fracture energy (Γ_f). These indirect tensile strength parameters are defined below:

1. The maximum horizontal tensile stress at the centre of the specimen and the horizontal tensile strain are calculated from the plot shown in the following figure. The ITS is the maximum stress developed at the centre of the specimen in the radial direction during the loading operation for a fixed geometry.
2. The fracture energy is calculated as the area under the load-vertical deformation curve as shown in Figure 2.4.
3. The energy until failure is calculated from the results of this test as shown in Figure 2.4.

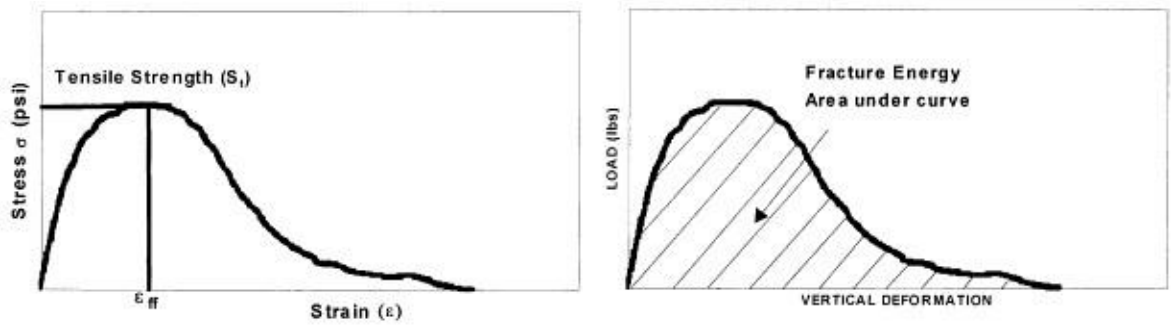

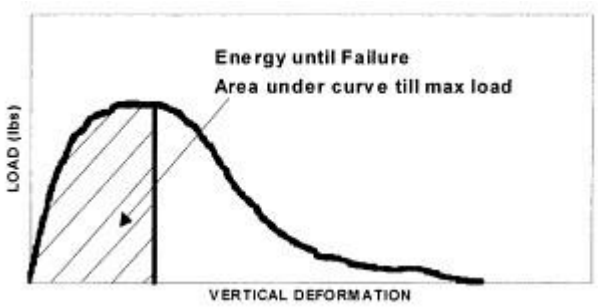

Figure 2.4: Determination of the indirect tensile strength, determination of the total fracture energy and determination of energy to peak load (Witczak et al., 2002).

The ITS of BSMs is conducted by loading a cylindrical specimen across its vertical diametral plane at 50 mm/min deformation rate and 25°C test temperature. The peak load at failure is recorded and used to calculate the tensile strength of the specimen.

The ITS is considered an indicator for the initial mix design of BSMs, TG2 (Asphalt Academy, 2009). Past studies (Jenkins and Ebels, 2007) have investigated the ITS test and posed the question whether the ITS (splitting) test is an appropriate test to determine the flexibility of BSMs.

2.4.2 Dynamic tri-axial tests

The load spreading ability of granular layers is a function of the stiffness of the layer. This stiffness or resilient modulus under dynamic loading of a granular material is not a single discrete value because this material is stress dependent. In addition, the behaviour of granular materials is non-linear elastic, but rather elasto-plastic (see Figure 2.5). Tri-axial testing using dynamic loading at applied vertical different stress levels and at different deviator stresses, can be used to determine the resilient modulus of granular material.

The short-duration dynamic tri-axial test is well suited to determine the resilient stiffness of pavement materials. It is also capable of determining the stress dependency of this material property. It is however a test that is typically carried out in a research environment. As such it has been used extensively by many researchers around the world. From research carried out during the 1960's, Hicks and Monismith (1971) summarised that the resilient response of granular materials under short-duration dynamic loading is significantly influenced by:

- Stress levels (confining pressures);
- Degree of saturation;
- Dry density;
- Fines content (percentage passing 0.075mm sieve); and
- Aggregate properties (density, type, particle angularity, particle texture)

The resilient response of untreated granular materials is most significantly affected by the stress level and can therefore be related to the confining pressure, σ_3, or to the bulk stress, $\theta = \sigma_1 + \sigma_2 + \sigma_3$, as follows, for as long as shear failure does not occur (Jenkins, 2000):

$$Mr = k_1\sigma_3^{k2} \qquad [2.4]$$

Or

$$Mr = k_3\theta^{k4} \qquad [2.5]$$

where
M_r = Resilient modulus (MPa)
σ_3 = Confinement pressure (kPa)
θ = Bulk stress = $\sigma_1 + \sigma_2 + \sigma_3$ (kPa)
k_1, k_3 = model coefficients
k_2, k_4 = model coefficients

The results of dynamic tri-axial tests can best be analysed by plotting resilient modulus versus the total stress, both on a logarithmic scale. (Figure 2.5)

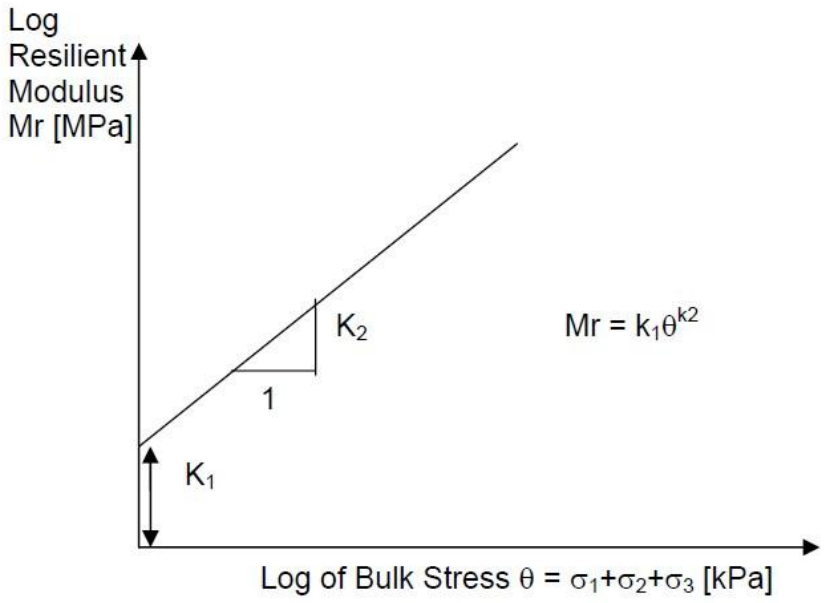

Figure 2.5: Mr-θ Model of Resilient Modulus for granular coarse material (NCHRP 1-37A, 2004).

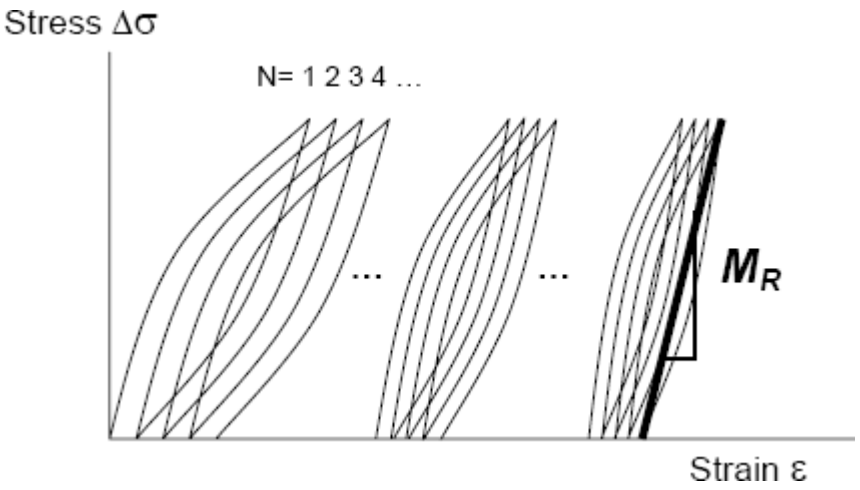

Figure 2.6: Resilient modulus test (NCHRP 1-37A, 2004).

The model shown in Equation 2.4 is the model used for fine-grained soils, while the model shown in Equation 2.5 has been widely accepted to describe the stress-dependent behaviour of a granular material, amongst others for its simplicity. The latter is often referred to as the Mr-θ model. On a log-log scale this model represents a linear function, whereby the k_1-value is a measure of the intersection with the y-axis, while the k_2 value indicates the slope of the line. Jenkins (2000) modified these equations to use the deviator stress ratio ($\sigma_d/\sigma_{d,f}$) as opposed to the principal stress ratio ($\sigma_1/\sigma_{1,f}$) to account for the damage that occurs in a granular or cold mix material that is stressed relatively close to the failure stress. This accounted more accurately for the relative stress conditions i.e. deviator stress that is applied to the material divided by the maximum deviator stress that the material can withstand (Figure 2.7).

The Mr-θ model as shown in Equation 2.5 is used to analyse the stiffness of BSMs and will be used for analysis of resilient modulus test results in this study.

In this test the load signal is a haversine load with a pre-load of 20% of the confining pressure or 5kPa is applied at a frequency of 1 Hz (load pulse of 0.1s followed by 0.9s rest period).

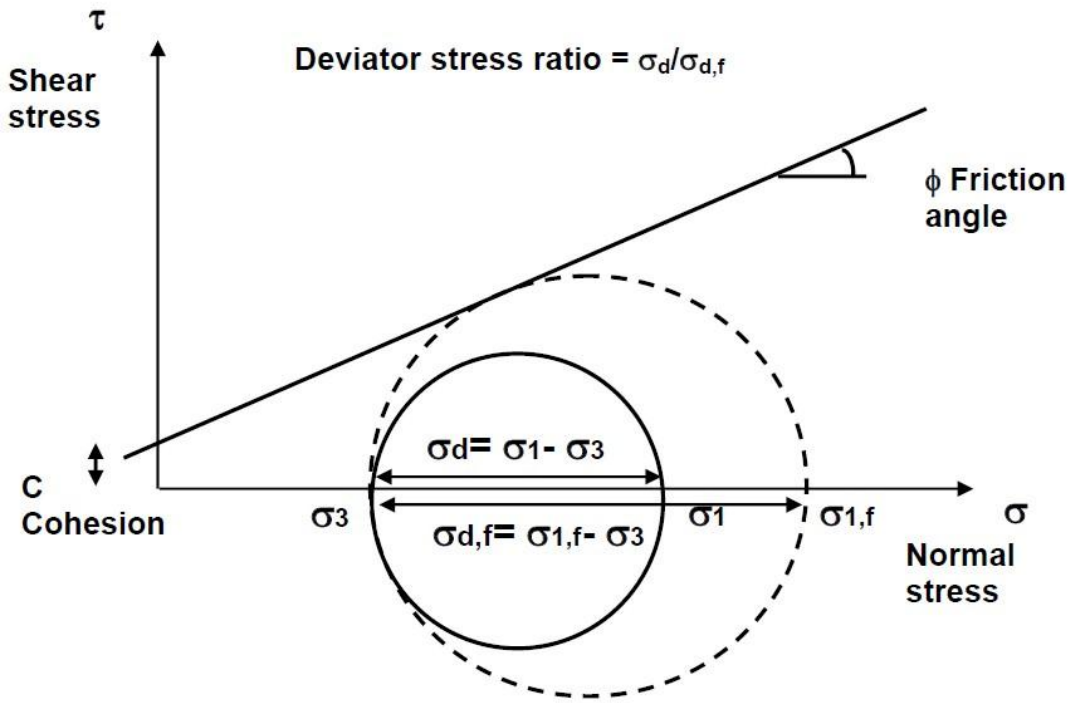

Figure 2.7: Concept of Deviator Stress Ratio (Jenkins, 2008).

A formula that is important in the determination of the stress ratio, is provided below (Equation 2.6). It is apparent that the cohesion and friction angle are important parameters in determining this ratio.

$$\sigma_{1,f} = \frac{(1+\sin\varphi)\sigma_3+2C\cos\varphi}{(1-\sin\varphi)} \qquad [2.6]$$

where,
C = cohesion;
σ_3 = minor principal stress (kPa);
φ = angle of internal friction.

BSM materials do not respond to dynamic loading in the same manner as granular coarse materials. The BSMs materials can experience alignment of particles or platelets, loss of shear strength and reduction in resilient modulus at higher stresses, as shown in Figure 2.8.

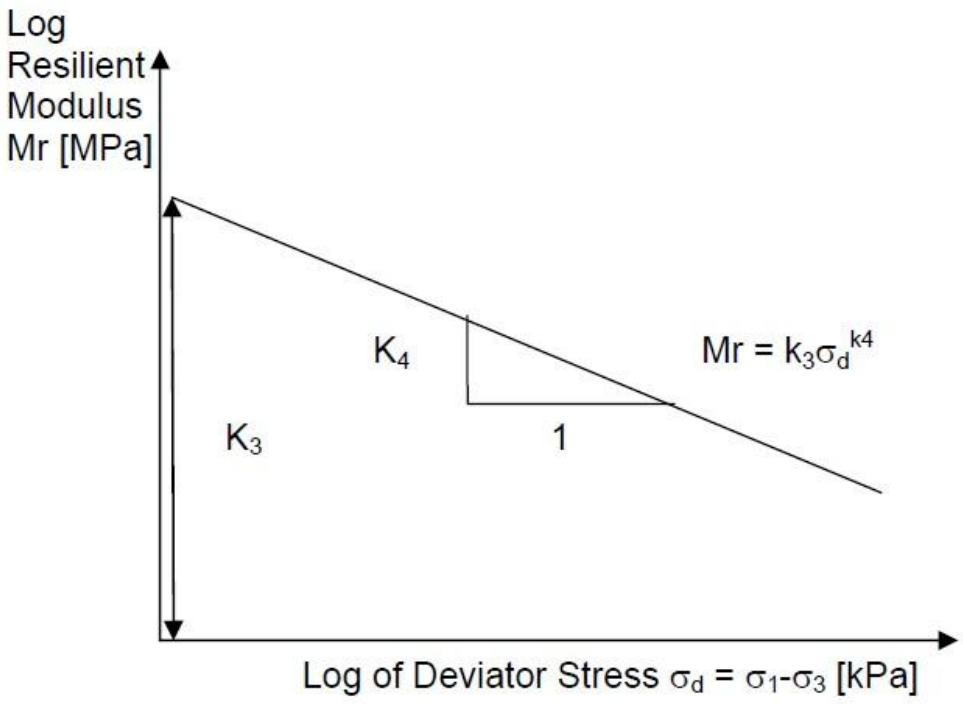

Figure 2.8: Mr-σ_d Model of Resilient Modulus for BSMs materials (Jenkins, 2008).

2.4.3 Permanent deformation

Another important application of the tri-axial test is in the modelling of granular materials for permanent deformation. In this type of test the dynamic tri-axial test is carried out on several separate specimens at different applied deviator stress levels. At sufficiently low deviator stress ratios, the permanent deformation or plastic strain ε_p stabilises with a large number of load repetitions. This occurs because the material densifies during loading and becomes more resilient. However, when a critical deviator stress ratio is exceeded, the steady state of plastic strain ε_p becomes unstable and accelerated deformation occurs. South African research (Maree and Freeme, 1981) indicated that in order to limit the permanent deformation in BSMs, the applied stresses should remain below some 60 to 70% of the stress at failure i.e. the critical stress ratio. The permanent deformation experienced by the specimen is monitored over an extended period, sometimes to more than 500 thousand load repetitions.

Francken (1977) plotted the permanent axial strain against the loading time on a log scale and found that the permanent deformation behaviour of HMA mixes could be adequately described by a loading time dependent creep curve as follows:

$$\varepsilon_p(t) = At^B + C(e^{Dt} - 1) \qquad [2.7]$$

where
$\varepsilon_p(t)$ = permanent deformation (axial strain)
t = loading time
A, B, C, D = model parameters

In the Francken model above the permanent deformation can be related to the number of applied load cycles by substituting the loading time variable with the number of applied load cycles taking into account the loading frequency.

$$N = \frac{\omega t}{2\pi} \quad [2.8]$$

$$\sigma_v = \sigma_0 + \sigma_1 \sin\omega t \quad [2.9]$$

where
N = number of applied load cycles
ω = angular frequency (rad)
σ_v = applied vertical stress
σ_0 = static component of vertical stress
σ_1= amplitude (dynamic component) of vertical stress

As did Barksdale (1972), Francken (1977) identified threshold stress combinations (σ_v , σ_3) below which the creep curve is nearly linear and the relationship between permanent axial strain and loading time is reduced to (coefficient C = 0):

$$\varepsilon_p(t) = A\, t^B \quad [2.10]$$

When the stress (σ_v , σ_3) exceeds certain limits the rate of strain (dε/dt or dε/dN) increases in the final part of the test. The second term in Equation 2.7 appears in this case (C ≠ 0). The exponential shape is characteristic of an irrecoverable failure of the material in the tertiary flow phase.

Huurman (1997) researched the development of permanent strain in typical Dutch sands (eight different types) and granular base course material (four different types) used in concrete block pavements using the repeated load tri-axial test. Huurman used two different specimen sizes, i.e. 200 mm high, 101.6 mm in diameter and 800 mm high, 400 mm in diameter. The permanent deformation tests were continued up to 1,000,000 load repetitions or 10% permanent axial strain, whichever came first.

The loading was applied in the form of a half-sine shaped wave with a frequency of 1 Hz (0.5 sec load pulse, 0.5 sec rest period). Only the applied deviator stress levels were varied (four different levels) during the permanent deformation study.

Huurman found that the reduced Francken model (C = 0) for permanent deformation of HMA mixes also applies to the permanent deformation behaviour of sand. When analysing the behaviour of granular base course materials, it was found that for certain applied stress conditions C ≠ 0 and tertiary flow occurs. However, Huurman substituted the loading time in Equation 2.7 with the number of applied load cycles as described above, following which Equation 2.7 can be re-written as:

$$\varepsilon_p = A\left(\frac{N}{1000}\right)^B + C\left(e^{D\frac{N}{1000}} - 1\right) \quad [2.11]$$

Huurman (1997) stated that the model parameters A, B, C and D are a function of the applied stresses and that this stress dependency can be described by:

$$A = a_1\left(\frac{\sigma_1}{\sigma_{1,f}}\right)^{a2} \qquad B = b_1\left(\frac{\sigma_1}{\sigma_{1,f}}\right)^{b2}$$

$$C = c_1\left(\frac{\sigma_1}{\sigma_{1,f}}\right)^{c2} \qquad D = d_1\left(\frac{\sigma_1}{\sigma_{1,f}}\right)^{d2} \qquad [2.12]$$

where
σ_1 = major principal stress
$\sigma_{1,f}$ = major principal stress at failure
$a_1, a_2, \ldots, d_2$ = model coefficients

The model coefficients a_1, a_2, …, d_2 as determined by Huurman can be used in the prediction of permanent strain in a pavement structure modelled using finite element methods. Huurman developed a rutting performance model to this extent.

The fundamental mechanical behaviour of unbound and lightly bound base and subbase materials (mixed granulate) as commonly used in the Netherlands was further investigated by Van Niekerk (2002). The repeated load tri-axial test was used to investigate the behaviour of the mix granulate in a very similar fashion as Huurman (1997) did. The specimens tested by Van Niekerk were 600 mm high and 300 mm in diameter. Each type of mix material was tested at four different applied stress levels, all with a constant confinement pressure of 12kPa. The tests were continued to 1,000,000 load repetitions or 10% permanent axial strain, whichever came first. The continuous haversine load (no rest period) was applied at 5 Hz. Van Niekerk used a similar model to describe the permanent deformation as Huurman (1997) did, save for the fact he replaced the principal stress ratio ($\sigma_1/\sigma_{1,f}$) as used in Equation 2.12 with a deviator stress ratio ($\sigma_d/\sigma_{d,f}$). The advantage hereof is that the deviator stress ratio is not influenced by the confinement pressure levels, while the principal stress ratio is. At decreasing friction angles φ, this difference becomes more evident (Jenkins, 2000).

A material subjected to two different stress levels can have a significantly different principal stress ratio, but relative to its shear capacity be in a similar stress state. In such a scenario the deviator stress ratio of the two different stress levels would be the same. During his research, Van Niekerk (2002) tested the permanent deformation behaviour of mixed granulate whereby he varied the grading and relative density of the specimens.

A limited investigation was also performed on a mix granulate that was hydraulically bound with 10% blast furnace slag. For these mixes he determined the model coefficients a_1, a_2, …, d_2 as used in Equation 2.12. Van Niekerk (2002) showed that these model coefficients can be used in the prediction of rutting in a pavement structure analysed with a finite element program.

In his study of foamed bitumen stabilised material Jenkins (2000) also investigated the permanent deformation behaviour using the repeated load tri-axial test (Figure 2.9).

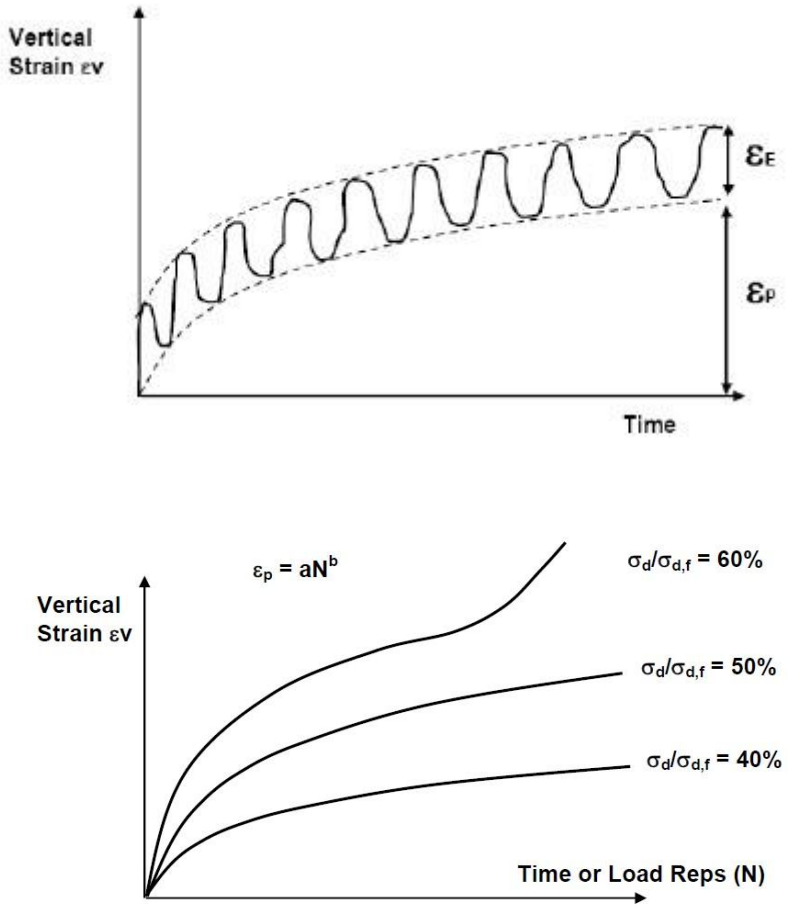

Figure 2.9: Typical permanent deformation tri-axial test (Jenkins, 2008).

Jenkins tested approximately 250 mm high, 150 mm diameter specimens as well as 600 mm high, 300 mm diameter specimens. The latter were tested in the same set-up and under the same conditions as described for the work done by Van Niekerk (2002). The smaller specimens were loaded with a haversine wave (no rest period) with a frequency of 2 Hz and a constant confinement pressure of 50 kPa. The tests were continued to 1,000,000 load repetitions or 4% permanent axial strain (10% in case of the larger specimens). Jenkins (2000) determined the model coefficients a_1, a_2, …, d_2 as used in Equation 2.12. He showed that these model coefficients can be used in the prediction of rutting in a pavement structure analysed with a finite element program.

It is recognised that materials that yield the same failure test parameters can differ significantly in a repeated load test at a lower stress level. The same applies to the resilient modulus. Tri-axial tests have indicated that there can be a significant difference between two materials with the same resilient modulus in their permanent deformation behaviour. In addition, moisture content and the number of load repetitions (because of the difference in permanent deformation development with load repetitions) are of paramount importance (Jenkins *et al.* 2007).

A general formula for permanent deformation is provided by Huurman (1997), Jenkins (2000) and Van Niekerk (2002):

$$\varepsilon_p = A\, N^B \qquad [2.13]$$

where
N = number of load repetitions
A, B = material constants

The formula can be graphically represented on a log scale (Figure 2.10):

$$\log\varepsilon_p = \log A + B \log N \qquad [2.14]$$

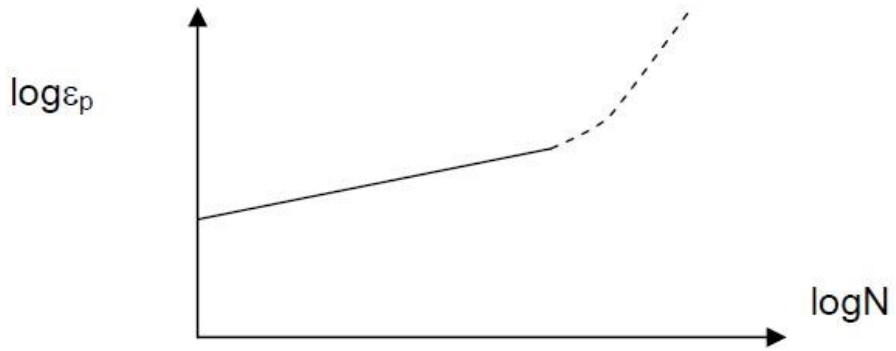

Figure 2.10: N-ε_p Permanent Deformation Model (Jenkins, 2008).

The granular type behaviour of BSM mixes is apparent when analysing the resilient response to loading at different stress level before failure (Jenkins 2000). The values of Mr are seen to increase with increasing of σ_3. In addition, as σ_1 increases, the resilient modulus increases further until a critical value is reached and thereafter the Mr decreases.

The advantage of using deviator stress ratio over principal stress ratio is that the deviator stress ratio is not influenced by the confining pressure levels, while the principal stress ratio is. At decreasing friction angles φ, this difference becomes more evident (Jenkins, 2000). In such a scenario the deviator stress ratio of the two different stress levels would be the same. Stress ratio is also useful in predicting the development of permanent deformation as a function of the number of load repetitions, stress conditions and material characteristics. It is apparent in that cohesion and friction angle are important parameters in determining this ratio. Tri-axial testing using dynamic loading at different vertical stress levels and at different deviator stresses, can be used to determine the resilient modulus of granular material. The results of dynamic tri-axial tests can best be analysed by plotting resilient modulus versus the total stress, both on a logarithmic scale.

Various researchers (Loizos and Papavasiliou, 2007, Ebels, 2007) and amongst others Jenkins (2000) and Van Niekerk (2002) have shown that the resilient modulus models developed for granular material can also be used to describe the stress-dependency of BSM mixes.

2.4.4 Influence of RA in the mechanical properties of BSM

The field investigation on BSM foam using high percentages of RA indicates that stiffness of the foamed bitumen layer increases with time. Loizos and Papavasiliou (2007) indicate that fatigue behaviour in BSMs is not a dominant failure mechanism. This behaviour is contrary to the fatigue failure mechanism known for HMA. Jenkins (2000) comments that foamed bitumen with relatively high binder content (> 3.5%) can be considered to have a performance similar to HMA. Twagira (2010) tested fatigue behaviour of BSMs at varying binder content from 2.4% to 3.6% and varying percentage of RA content. Their results show that fatigue stiffness behaviour is time and temperature dependent (i.e. if loading rate increases, stiffness increases and if testing temperature increases, stiffness reduces). This trend is typical for HMA; however because BSMs have much lower temperature susceptibility compared to HMA, the stiffness results were relatively small compared with HMA as indicated in Figure 2.11.

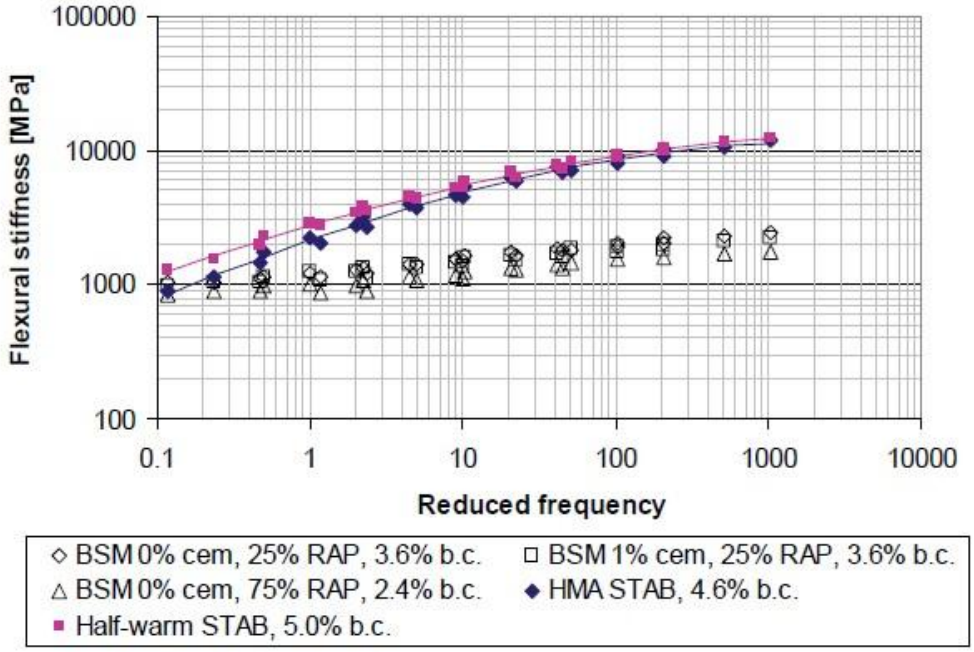

Figure 2.11: Master curves of BSM (foam), Half-Warm and HMA (Tref = 20ºC) (Ebels, 2008).

From the graph it can also be seen that time-temperature superimposition for BSMs is much lower than for HMA, particularly at a higher loading rate. This is in part due to the lower binder content as well as stiffening behaviour of the mastics in the BSM mixture.

Further analysis shows that flexural stiffness is influenced by the percentage of RA in the mix, the addition of active filler and the type of binder. Twagira (2010) reports that BSM emulsion with higher RA content (B-75M-0%) without cement has a relatively lower fatigue life compared to the same mix treated with foamed bitumen (C-75M-0%) as indicated in Figure 2.12.

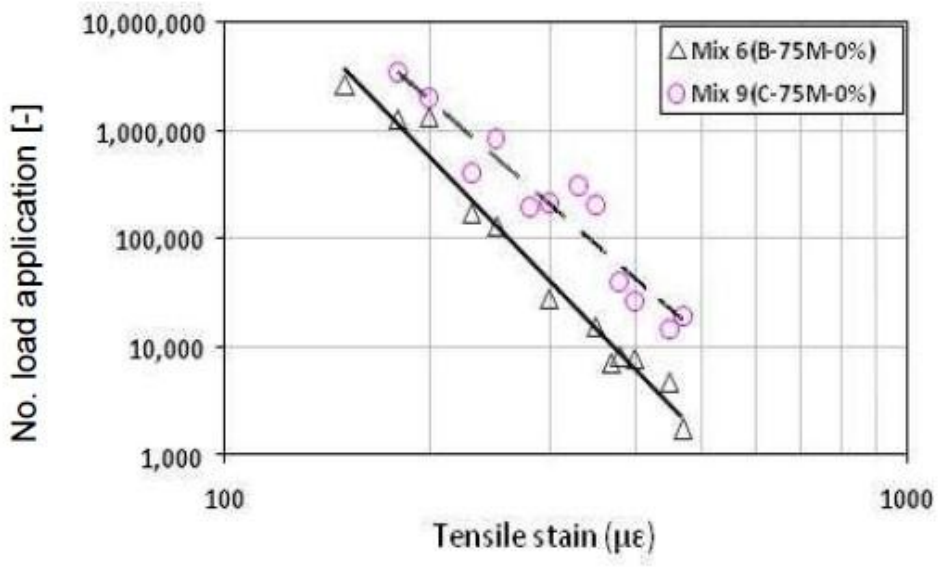

Figure 2.12: Fatigue behaviour of BSM-emulsion and BSM-foam with higher percentage of RA materials (Twagira, 2010).

Jenkins (2000) indicates that the rate of heat transfer from foamed bubbles to the aggregate surface, even at lower temperatures of aggregate, may contribute to comparative performance of the foamed bitumen. This is because the heat transfer dissipated from the bubble might soften the old bitumen (both in the filler and in coarse fraction) and enhance adhesion of new bitumen. While, because emulsion is applied at ambient temperature, the old coated bitumen in mineral aggregates is inactive, reactivity and adhesion of new bitumen will be retarded. However, depending on the type of bitumen, BSM-foam might behave differently in adhesion and cohesion with a higher addition of RA content in a mix.

Recent research on permanent axial strain due to the effect of moisture on BSM-foam, was carried out by Fu *et al*. (2009). Their objective was to determine the influence of cement on different curing conditions and shear strength development. Permanent deformation tri-axial testing was performed on different mixes with different moisture contents. Ebels (2008) indicates that the critical stress ratio's for the BSMs range from 0.4 to 0.6 for tertiary flow to occur. More interesting to note from Ebels' results, is that an increase in the RA content of the mix stabilised with foamed bitumen has better initial permanent strain accumulation even with higher stress ratio's compared to similar mix stabilised with bitumen emulsion. The reason for the better performance of foam with RA is the same as the one given in fatigue behaviour. Ebels reported that the resistance to permanent deformation is a function of the binder content and the degree of saturation (% voids filled with water by volume) of BSM. The ratio of axial strain to peak axial strain (ε_{axial} / $\varepsilon_{peak\ axial}$) decreases with the increase in binder content and degree of saturation.

The temperature test of 40°C was selected for all the permanent deformation tests. From previous studies conducted by Twagira in 2010 it was evident that the critical temperature of BSM mixes lies between 40°C and 50°C (Figure 2.13). Therefore, in this case it is effective to use a temperature of 40°C to evaluate the permanent deformation of the BSM-foam mix. However, the critical temperature is influenced by binder content, percentage of RA and

addition of active filler. It must be emphasized that the temperature at 40°C influences strongly the states of stress and strain caused by traffic loading (i.e. pavement rutting).

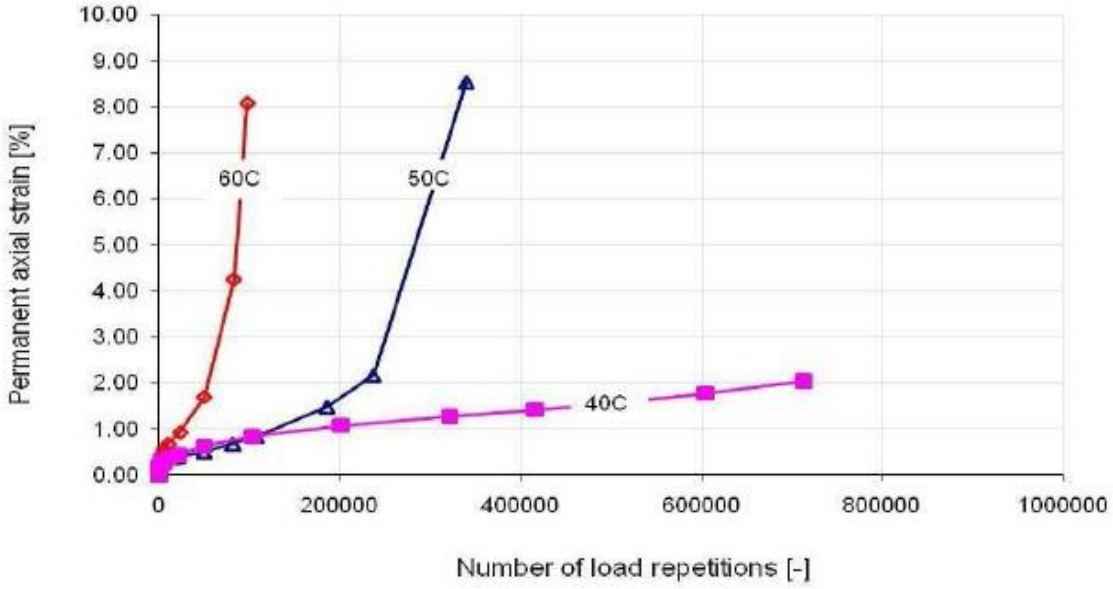

Figure 2.13: Example of permanent axial strain of field extracted cores (BSM-foam) with 100% RA from Twagira 2010, tested at different temperatures of 40°C, 50°C and 60°C.

Jenkins (2000) studied the stiffening behaviour of mastics with water and foamed bitumen or bitumen emulsion with a variety of filler types. His study revealed that the percentage of bulk volume for the mastic is a primary factor influencing the stiffening of foam or emulsion mix. Using a softening point temperature approach, mastics produced by 150/200 pen-grade foamed bitumen with different filler types at different percentages of bulk volume were tested and compared with HMA as indicated in Figure 2.14.

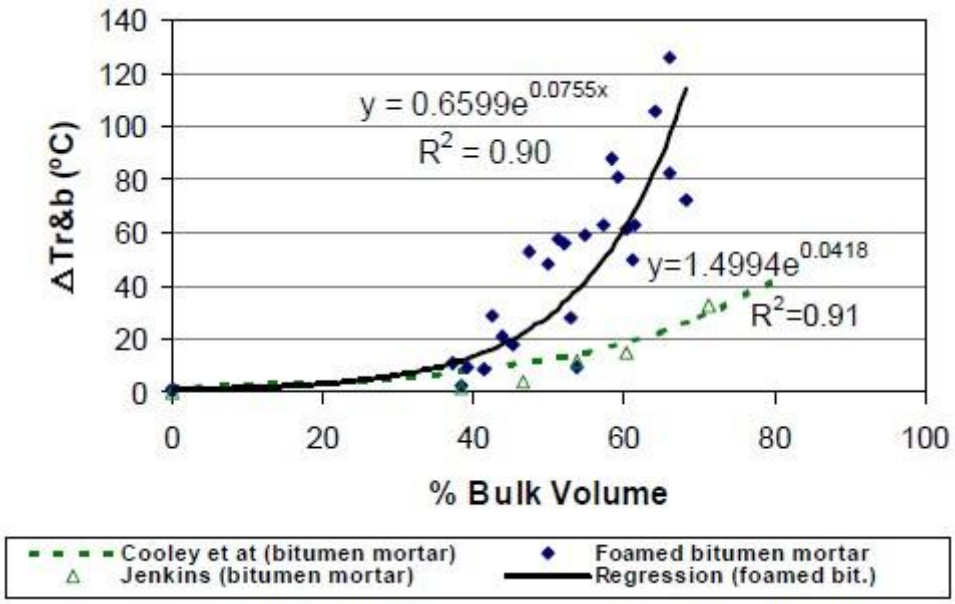

Figure 2.14: Comparison of stiffening potential versus percentage bulk volume of mastic for the BSM- foam and HMA (Jenkins, 2000).

It is evident from Figure 2.14 that foamed bitumen stiffens at a lower percentage of the bulk volume of the entire water, bitumen and solid aggregate components in a mastic occupied by the compacted filler (%Vdb) (40%) and stiffens more rapidly as %Vdb increases, compared to HMA. The best explanation for the stiffening behaviour of a mastic is the physico-chemical properties of filler-binder interaction. The high reactivity of filler fraction to the polar and non-polar molecules of the dispersed foamed bubbles influences the faster stiffening potential compared to the interaction of thick film dispersed in the HMA.

2.4.5 Data analysis methods for dynamic tests

The data analysis methods described by Ebels and Jenkins (2007) and proposed in the revision of the South African Pavement Design Method (CSIR, 2011) are presented here:

1- Monotonic tri-axial tests

For each specimen, the applied maximum load and the corresponding deformation were determined for the calculation of the failure stress and unit strain.
Failure stress was calculated as follows:

$$\sigma_{af} = \frac{P_{af}}{A} \qquad [2.15]$$

where P_{af} is the applied failure load (N) and A is the initial end area of the cylindrical specimen (m^2). Major principal stress at failure is the sum of the axial stress at failure and the confining pressure shall be calculated as follows:

$$\sigma_{1f} = \sigma_{af} + \sigma_3 \qquad [2.16]$$

Shear strength parameters (φ and C) are calculated as follows:

First determine the relationship between σ_{1f} and σ_3,

$$\sigma_{1f} = A\sigma_3 + B \qquad [2.17]$$

where

$$A = \frac{1+\sin\varphi}{1-\sin\varphi} \quad \text{and} \quad B = \frac{2\cos\varphi}{1-\sin\varphi} \qquad [2.18]$$

A linear regression analysis is then performed, on the three combinations of σ_{1f} and σ_3 per treatment in the case of stabilised materials, to determine the values of A and B:

$$\varphi = sin^{-1}\left(\frac{A-1}{A+1}\right) \quad [2.19]$$

$$C = \frac{B(1-\sin\varphi)}{2\cos\varphi} \quad [2.20]$$

2- Resilient modulus test

For every applied stress level and at every confining pressure level the following was determined for each of each of the cycles (N) sampled:

Resilient axial strain: first, the minimum deformation reading $LVDT_{min}$ and the maximum deformation reading $LVDT_{max}$ for each of the three on specimen LVDTs j was determined to calculate the average axial deformation $\Delta\delta_{a(N)}$ of the specimen per cycle (N).

$$\Delta\delta_{a(N)} = \frac{\sum_{j=1}^{j=3} LVDT_{j,max} - LVDT_{j,min}}{3} \quad [2.21]$$

Resilient axial strain $\varepsilon_{a(N)}$ per load cycle (N) is given by:

$$\varepsilon_{a(N)} = \frac{\Delta\delta_{a(N)}}{L_g} \quad [2.22]$$

where L_g is the gauge length.

Resilient modulus calculation: first the cyclic stress for each cycle (N) was determined:

$$\sigma_{cyclic(N)} = \sigma_{d(N)} = \left(\sigma_{\max(N)} - \sigma_{contact(N)}\right) \quad [2.23]$$

where
$\sigma_{max(N)}$ is the axial stress (ratio of maximum applied load to the area of specimen) applied to the specimen; it consists of the seating/contact stress ($\sigma_{contact}$) and the cyclic stress (σ_{cyclic}).
$\sigma_{contact(N)}$ is the axial contact or seating stress applied to the specimen to maintain a positive contact between the loading ram and the specimen top cap. Units are in kilopascal (kPa).

Resilient modulus M_r at the N_{th} cycle was determined by:

$$M_r = \frac{\sigma_{cyclic(N)}}{\varepsilon_{a(N)}} \quad [2.24]$$

The average of the last five cycles in a loading sequence was reported:

$$M_r = \frac{\sum_{i=1}^{i=l} M_{r,j}}{l} \quad [2.25]$$

where l is the number of full load cycles sampled, equal to 5.

3- Permanent deformation test

For every applied stress level and at every confining pressure level the following was determined for the (N) cycles sampled in a given sampling window.

Where on-specimen LVDTs have been used, first, the minimum deformation reading $LVDT_{min}$ and the maximum deformation reading $LVDT_{max}$ for each of the three on-specimen LVDTs j were determined to calculate the average axial deformation reading for a sampling window n, whereby n is the number of load repetitions at which the sampling window was taken.

$$\Delta\delta_{a(n)} = \frac{\sum_{i=1}^{i=3}\left(\frac{\sum_{j=1}^{j=3} LVDT_{j,max} - LVDT_{j,min}}{6}\right)}{3} \quad [2.26]$$

The average displacement reading of the sampling window after 20 load repetitions, $\delta_{a(n)}$, was taken as the zero reading. The relative axial deformation of the specimen for each subsequent sampling window n was then calculated:

$$\Delta\delta_{a(n)} = \delta_{a(n)} - \delta_{a(20)} \quad [2.27]$$

The cumulative axial permanent strain (ε_{ap}) for each sampling window was given by:

$$\varepsilon_{ap(n)} = \frac{\delta_{a(n)}}{L_{sg}} \quad [2.28]$$

where L_{sg} is the gauge length over which the deformation is measured, when on-specimen LVDTs are used or the distance between top cap and bottom seating platen, when LVDTs on top of specimens are used.

The average resilient modulus per sampling window, $M_{r(n)}$ was then calculated according to:

$$M_{r(n)} = \frac{\sum_{i=1}^{i=l} M_{r,j}}{l} \quad [2.29]$$

where l is the number of full load cycles sampled.

2.5 Mixture durability

The central role of the mixture compositional design and performance in BSMs is becoming a key factor in the performance of the long-term BSMs pavements. For HMA, durability is measured as resistance of binders to stripping, ageing and degeneration of modifiers in specific application, knowing that parent aggregates in HMA are adequately durable (Shell Bitumen, 2003). The fact that BSM is applicable in a wide range of aggregates (including RA) and varying bitumen contents, its durability is based on material durability, as well as mixture durability. Although moisture damage is considered a major factor influencing durability of BSMs, the durability of parent aggregates and bitumen are found to play a significant role (Øverby *et al*., 2004; Jenkins, 2000; Paige-Green, 2004).

A more detailed approach to mixture compositional durability is indispensable to understand the relationship between binder and mineral aggregate durability. Based on physico-chemical interaction between binder (foam) and mineral aggregates mixture composition durability requires more investigation. Due to the unique nature of dispersion of foam, mastic behaviour and the manner in which it combines with the larger aggregates require special attention in the mixture composition durability studies.

The adhesion and cohesion bonding between binder and aggregates in BSM mixtures is one of the most important bonds that differentiate BSMs from granular materials. However, it is also one of the least understood bonds, partly due to the complexity of the binder characteristics and partly due to the variety of surfaces of aggregates with which the binder comes into contact. Most researchers attempt to describe cohesion and adhesion in the binder-aggregates system in BSMs using mechanical means. But in the HMA, the work of adhesion and cohesion using thermodynamic theory has extensively been studied by measuring the surface free energy of the asphalt and aggregates with four advantages (Elphingstone, 1997):

- the mechanical work required to crack an asphalt-aggregate interface is related to the free energy of the adhesion, and cohesion in a certain limiting case;
- crack propagation models have shown to be a function of the surface free energy of materials. By measuring the surface free energy of the asphalt and aggregates the cracking parameters can be calculated,
- the asphalt-aggregate system can be evaluated for the propensity to be water susceptible (stripping potential), and
- ability to relate asphalt healing after cracking to the surface free energy of the asphalt and aggregates.

Moisture transport mechanisms, coupled with adverse environmental conditions and dynamic loading, have been found to influence moisture damage mechanisms of BSMs (Twagira, 2010). Therefore, there is a need to use new moisture conditioning procedures, which accurately simulate field moisture infiltration conditions and consequently to perform a mechanical test peculiar to BSM properties such as shear and stiffness. In Chapter 5, a device, called moisture induction simulation test (MIST), which simulates more realistic pulsing of water pressured into mix matrix to determine the consequential adhesion and cohesion deterioration, is used.

2.5.1 Influence of compaction

The compaction method and level of BSMs play a significant role, in both the laboratory prepared specimens and in the field construction, to achieve the intended durability properties. The dispersion of foam bubbles and breaking of emulsion droplets favourably coat the filler fraction and partly coat the coarse fraction. During mixing, the mineral aggregates are in a conglomerate state which means the binder-aggregate interaction is incomplete. It is therefore through compaction that the following advantages might occur:

- improvement in adhesion and cohesion of mastic and mineral aggregates;
- compression of bitumen or mastic (spot glue) between large fractions;
- moisture squeezes out of the mineral aggregates and mastic to the surface, and
- enhanced parking of mineral aggregates.

The compaction method of BSMs in a laboratory-prepared specimen is a primary factor in producing mix designs which simulate durability behaviour in field conditions. Previous research on compaction methods of BSMs conducted by Weston *et al*., (2002) uses Marshall, Hugo, Kango, Superpave Gyratory and pedestrian roller. The research indicates that the modified Kango Hammer® could be a useful tool in the compaction of BSMs. The advantages of the Kango Hammer® is that it requires low compaction energy to obtain equivalent levels of compaction compared to other method. Additionally, it is relatively cheap, easy to use and simulates field compaction.

Current research in Stellenbosch develops a more robust compaction method for the BSMs using a BOSCH® vibratory hammer (Kelfkens, 2008). This device was extensively used in preparing laboratory specimens designed in this study, for the reasons indicated above.

2.5.2 Influence of curing

Curing of BSMs is the main influential process for the development of bonding between binder and mineral aggregate interfaces and consequently the building of durability properties. It has been indicated in the literature (Serfass *et al*., 2008) that failure manifestation in these mixes might occur at an early age of service life due to insufficient curing.

Curing of BSMs is a process which depends on the mechanism of moisture evaporation. Literature reviews have indicated that in field conditions the evaporation process is linked to the temperature gradient in the layer, wind speed, relative humidity and boundary conditions surrounding BSMs. During mixing and compaction this moisture content is near the optimum moisture content for compaction. In the field curing continues typically up to 6 – 18 months. With the reduction of moisture in the mix the strength and stiffness increase. The field curing times are too long for laboratory mix design purposes. When specimens are to be tested at equilibrium field moisture content, the laboratory curing process needs to be accelerated.

Jenkins, Ebels and Twagira (2006) described the factors which can cause materials to cure. These are scientific mechanisms which invariably influence the rate of curing and moisture behaviour within the mix.

High pore water pressures

Both laboratory and field compaction of BSMs are generally the cause of development of high pore water pressures in the compacted mix. In the field, areas with high water tables generally lead to the development of high pore water pressures during compaction. The build-up of such high pore water pressure regions often causes water to migrate to the surface of the recycled layer.

Taking a closer look at laboratory compaction for instance, pore water pressure developed during compaction cannot fully dissipate because of confinement by steel moulds. The accumulation of pore water pressure as function of compaction time is common laboratory science, and in some instances of high moisture contents during compaction, water tends to seep through the bottom of the steel mould.

The interaction of higher pore water pressure in the compacted material leads to water seeping out through voids in the mix during interaction with the surrounding environment. This interaction often forces water to escape due to differences in outside atmospheric pressure and internal pore water pressure. The migration of water from higher pore water pressure regions in the mix to lower atmospheric pressure zones towards the surface of the compacted material leads to surface curing.

Water expulsion

Water expulsion is the physical release of compacted water from the mix during compaction. Furthermore, water expulsion is a consequence of high pore water pressure developing in the compacted material due to high compaction forces or energy.

Compaction of BSMs reduces the volume of air voids in the mixture through the application of external forces. The expulsion of air and consequently compaction water enables the mix to occupy less volume, thereby increasing the density of the mass. This occurrence is often accomplished by high energy compactors which provide the necessary external forces. The expulsion of water through air void channels in the compacted mix continues even after compaction due to migration of high pore water pressure as discussed above. Water expulsion is one of the additional factors driving curing of BSMs.

Evaporation

Evaporation is the process by which molecules in a liquid state spontaneously become gaseous or transform into water vapour. Consequently, evaporation guides the curing of bitumen stabilized materials due to moisture behaviour in the compacted mix as influenced by pore water pressure and water expulsion characteristics.

In South Africa a climatic index called Weinert N-value can be used to estimate mean annual evaporation of regions under analysis. Weinert N-value is a climatic index on

evaporation which is based on the warmest month of the year and annual rainfall. In South Africa, three main climatic zones were defined by Weinert (1980), these zones include Wet (Weinert N<2), Moderate (Weinert N=2 to 5) and Dry (Weinert N>5).

During the initial stages of curing, water evaporates from the exposed surface of the compacted mix, leading to surface interaction with the surrounding environment. Depending on evaporation characteristics of the surrounding environment, curing of BSMs will take place at faster or slower rates.

Evaporation also contributes to moisture behaviour in compacted pavements over both the short and long-term analysis. Malubila (2005) investigated the effects of environmental evaporation on field equilibrium moisture contents (EMC) of foam mixes. Malubila (2005) derived models to predict field EMC given the material's OMC, binder content and Weinert's N-value of the region under investigation. Malubila's findings supported evaporation as a fundamental factor towards determining residual moisture contents in the field over the long term.

Currently, the curing process in laboratory conditions is focused on achieving equilibrium moisture content (i.e. 40–50% OMC). This process stems from the model established by Jenkins (2000). The Jenkins model is a modification of a model developed by Emery (1988) who studied equilibrium moisture content of granular base layers in South Africa using the Weinert Climatic Index. Malubila (2005) indicates that the model developed by Jenkins is not sufficient to encounter or predict the actual moisture content measured in field conditions. During Malubila's studies, he further extends Jenkins model by including constant parameters established from the acquired field data. However, these extended constant parameters still do not address the fundamental environmentally related conditions occurring in the pavement layers in field environmental conditions. The study on the curing mechanism of BSMs by Jenkins *et al*. (2008) tries to focus on the fundamental environmental conditions occurring in the pavement layer during the curing process.

2.5.3 Moisture damage

Moisture damage contributes significantly to the premature deterioration of pavement materials, HMA, BSMs or granular. The deterioration process is the degradation of the mechanical properties of the materials due to the infiltration of excess moisture into the microstructure.

Microstructure moisture damage is a complex phenomenon that involves thermodynamic, chemical, physical and mechanical processes. Unlike HMA where the effect of the infiltration of water at the binder-aggregate interface and consequential damage has extensively been studied, little has been reported about moisture damage, particularly in BSMs (Long *et al*. 2003; Fu *et al*., 2009; Gonzalez, 2009; Twagira, 2010). The research presented in the following chapters would like to explore the context in which the developed adhesive and cohesive bond in the mix might be affected by infiltrated excess moisture in the microstructure of BSMs and hence influence the durability behaviour.

Damage mechanism is a process that leads to change in the internal or external conditions of a system producing a new state or condition (Caro *et al*., 2008). When the final state of the system

represents a reduction in its original integrity, the process is considered a damaged mechanism. Moisture damage mechanism consists of the following steps:

- moisture transport: the process by which moisture or vapour infiltrates the pavement materials and reach binder and aggregate interface;
- the response of the system: change in the microstructure properties that lead to a loss of engineering properties.

The materials and mixture composition that influence moisture transportation comprise the following:

- the binder in BSMs does not completely cover the larger particles of aggregate;
- binder contents utilised in the mix are generally lower than equivalent HMA, which lives more isolated and interconnects void in the mix;
- the mineral aggregate is moist at the time of mixing which reduces adhesion, and
- the air void content of the mix is higher than HMA.

The possible moisture mechanisms described above are probably duo:

- high percentage of air void with low connectivity. This allows development of pore pressure in a saturated flow condition and can cause erosion upon dynamic loading causing mechanical failure.
- infiltrated excessive moisture can also diffuse through the mastic and displace the binder from the aggregate surface resulting in poor adhesive bond strength at the interface.

Moisture damage is a process that leads to a change in the internal structure of a mixture by a reduction in adhesion and cohesion. The damaging mechanisms consist of moisture transport, which largely depends on the voids structure. Localised voids are prone to severe damage because the residing moisture generates higher pore pressure during dynamic loading, whilst interconnected voids might result in severe erosion under high dynamic loading. The BSM mix matrix is generally characterised by large localised voids and few interconnected voids. Therefore, pore pressure is characteristic of moisture damage mechanisms in BSMs.

Pore pressure and erosion result in disintegration, which progressively degrade the physical integrity of cohesion and adhesion in the mixture. Reduction in adhesion and cohesion (i.e. ravelling or stripping of mastic) in BSMs is a failure pattern which undoubtedly relates to a combined action of mechanical failure and moisture infiltration. Weakening of the interlocking bonds of the mineral aggregates promotes a cohesive failure, while weakening of the binder-aggregates leads to a pronounced adhesive failure.

Past research (Caro *et al*., 2008, Twagira, 2010) indicates that the common moisture damage mechanisms are related to ravelling-distress manifestation due to dislodgement of aggregate particles in the mixture from the surface and hydraulic erosion of saturated surface due to dynamic action of tyre in the presence of water. It is certain that adverse environmental conditions play a significant role: high relative humidity in the material, intense rainfall periods and temperature variation in the materials increase the damaging potential. Other factors that

influence moisture damage are intense traffic loading. However, the quantification of these damages is not completely understood and described.

2.5.4 Wet and Dry Brush Test

A good BSM stabilisation design should produce a material that will provide the required stiffness over the design life of the road. Jenkins *et al*. in 2006 executed research on improving mix design for BSMs, with the focus on moisture susceptibility as a prime factor in addressing durability requirements of BSMs. However, the core issue was to outline the mix composition including binder and aggregate durability. Natural aggregate durability has been addressed by many researchers including Sampson and Netterberg (1989) and Sampson and Paige-Green (1990).

Problems of moisture susceptibility on BSMs have been identified in various studies (Jenkins, 2000; Long *et al*., 2004; Liebenberg, 2002; Paige-Green and Ventura, 2004, Twagira 2010). Its complexity has made it difficult to find a unique test or analytical method to comprehensively quantify damage and accurately predict the material performance in the field.

Paige-Green and Ventura (2004) say that bitumen stabilisation with the addition of an active filler changes the physico-chemical properties of mineral aggregates. They recommend that it is appropriate to quantify the effect on long-term durability by looking at the binder-aggregate system and not only at aggregates or bitumen materials. The conventional test applicable for assessing the durability of cement or lime-treated materials is the wet/dry test or erosion test. The wet/dry test is commonly performed to identify the susceptibility of cement or lime stabilised materials to degradation (disintegration) in the presence of adverse conditions of cyclical wetting and drying and carbonation.

The mechanical brushing test measures the loss of materials from the specimen surface resulting from soaking, drying and carbonation. The loss of materials is a result of chemical alteration (decomposition) or physical weakening (disintegration) of cemented bonds developed during cement hydration. Disintegration of BSMs has not been studied extensively; therefore, this type of distress and failure is likely to occur depending on binder content and type of materials coupled with environmental conditions.

As well as ensuring that an adequate strength and stiffness has been achieved by the stabilisation process, it is also necessary to ensure that this strength is maintained over the design life of the pavement. It should be noted that the ITS tests in equilibrium conditions do not actually measure the durability of the stabilised material. This can be determined by durability testing which could take the form of either a soaked ITS test or a wet/dry brushing test (Sampson, 1988). In more temperate climates this test may also be appropriate. A revision of the South African wet/dry brush test has been recommended by Paige-Green (1998), who proposed that the mechanical wet/dry brush test should be used as it removes some of the operator variability that was apparently present with the previous test.

The standard prescribed durability testing in South Africa is the wet/dry brushing test. This is based on the original PCA test (Portland Cement Association, 1971) (also specified as ASTM D559-03 and AASHTO T 135-97(2005)) but has been modified to more closely simulate the compaction levels utilised in South Africa. The variability in the original test caused by hand

brushing has been eliminated by using a mechanical brushing technique (Sampson, 1988). The current qualitative method to assess moisture damage in BSMs is the related test method designed for cement-treated material. This test is similar to the mechanical brushing test method and is conducted on compacted and cured specimens. The assessment of the quality of adhesion and cohesion with the influence of moisture is done by determining the loss of surface material. After this testing has been carried out, if any doubt remains about the durability of the material, then a further moisture induction simulation test (MIST) test could be carried out (Twagira, 2010).

2.6 Influence of temperature distribution in BSM-foam layers

In a pavement structure, BSMs are incorporated as a base layer particularly in *in situ* recycling technology. Therefore, understanding the thermal properties of BSMs requires a good knowledge of the thermal properties of the surface layer (i.e. AC or seals). From literature surveys, it is clear that the thermal properties of HMA has been extensively studied.

Highter and Wall (1984) studied the thermal conductivity of different limestone mixes in HMA with different asphalt contents (i.e. 3.5 to 6.5%). They found that the thermal conductivity of the mix increases as binder content increases. This is due to the fact that an increase in binder content replaces the air in the voids in the mix and because the conductivity of bitumen is higher than air this results in higher mix conductivity. The general conclusion shows that the dominant mechanism for thermal conductivity depends on the asphalt content and mix properties such as percentage coarse fraction, gradation and the specific surface of the mix (percentage of filler content).

Solaimanian and Kennedy (1993) extend the work of Barber (1957) on heat diffusion theory. They propose the mathematical method for predicting maximum pavement surface temperature using maximum air temperature and hourly solar radiation. Their method was developed based on heat transfer theory and takes into account the effect of latitude on solar radiation. Jia and Sun (2007) improved this work by indicating that the method focuses on calculating maximum higher temperature, while assuming wind speed remains constant; this is different from actual field conditions. Therefore, Jia and Sun incorporated the effect of wind speed and develop a numerical temperature prediction model for the thermal properties of asphalt pavement applicable to Chinese weather conditions. Burger (2005) indicates that most of the existing simplified numerical models that predict pavement temperature are in part based on equations that do not adequately describe actual heat transfer rates in the pavement layer.

Starting from the deficiencies in the SHRP model reported by Solaimanian and Kennedy (1993), Burger further improves the temperature distribution and prediction model for HMA. The sensitivity test in the model was based on South African environmental conditions. Although the model was designed for HMA, its applicability, and usefulness can be extended to BSMs. BSMs are generally less susceptible to temperature variations (Jenkins, 2000; Loizos and Papavasiliou, 2007). However, depending on mix composition, e.g. higher BC and RA content, temperature distribution in the layer may adversely influence the performance of BSMs. The heat transfer coefficient of the surface layer, i.e. thin AC or seal, and its mix composition contribute to temperature distribution in BSMs. Jenkins and Twagira (2008) investigated the excess deformation that occurred in full-depth *in situ* recycled BSM-foam constructed in Saudi Arabia (Shedgum Road Project). The site inspection on the distressed area

shows that during summer months the temperature distribution in the pavement layer was as is indicated in Figure 2.15.

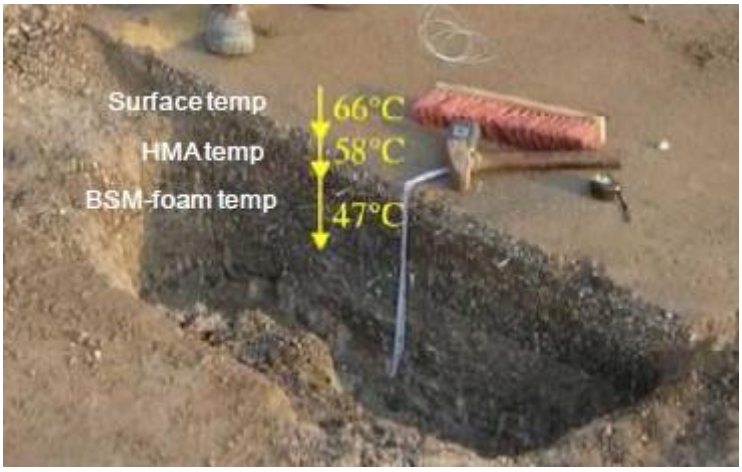

Figure 2.15: Temperature distribution of distressed pavement structure including BSM-foam as a base layer (Jenkins and Twagira, 2008).

The advantages of predicting temperature distribution in the BSMs layer from local environmental conditions are:

- the ability to understand the mechanism of binder ageing and mastic stiffening during curing process of the compacted mix;
- the ability to predict water evaporation from the material during the curing period. This is an important aspect for the contractor/designer to be able to predict the early opening of the BSMs layer for traffic.

Thermal environmental conditions, to which pavements continuously are exposed in the construction and repair phases, as well as in use, determine the temperature profile in BSMs sections. Fluctuations in ambient air temperatures diurnal and seasonal, intensity of solar radiation, pavement materials and geometry, convective surface conditions, and precipitation significantly impact pavement stability and therefore the long term success of pavement design. Accurate prediction of the temperature profile in pavements could greatly aid pavement engineers, specifically in the assessment of pavement deflection, in back calculations of pavement modulus values, in estimations of deformations, in calculations of the heating rates in BSMs layers, and in the assessment of diurnal and seasonal heating and cooling effects.

Temperature can contribute to certain common types of BSMs pavement distresses such as permanent deformation or rutting (typically associated with high temperature environments). The top pavement layer normally is exposed to greater temperature fluctuations than the layers below it. Because of this, detailed knowledge of the temperature distribution in BSMs layers could also allow for a more sophisticated specification of BSMs for lower lifts through specification of less expensive BSMs applications, and thus it could provide an economical solution to rising pavement construction costs. An assessment of the impact of pavement temperature variations on various pavement materials, such as BSMs with low and high percentage of reclaimed asphalt (RA), shall be possible with a higher degree of accuracy.

Therefore, depending on the RA contents in the mix, durability and long-term performance of BSMs will be affected. Twagira (2010) and Ebels (2008) indicate that BSMs with a higher percentage of RA show inferior performance in terms of mechanical properties (such as shear, stiffness and fatigue) compared to virgin aggregates or mixes with a lower percentage of RA aggregates.

Design temperature is an important parameter in the selection of BSMs. Many methods dealing with prediction of temperature gradients in pavements are based on statistical and probabilistic methods developed based on weather and pavement data collected through the Superpave program (SHRP) by Kennedy *et al*. (1994) and Viljoen (2001) research are validated against new laboratory data. The algorithms provide acceptable estimates of the actual pavement temperatures for HMA. However, such statistical and probabilistic methods display shortcomings in that they tend to either underestimate high pavement temperatures or overestimate low pavement temperatures raising questions about their accuracy and reliability. The uncertainties associated with the Superpave algorithms call for computationally fast tools that can accurately and reliably predict BSMs pavement temperatures at different pavement depths based on local environmental conditions. Various studies have been carried out that included experimentation with the curing temperature and moisture to investigate the influence of these factors on the behaviour of BSM mixes (Twagira 2010, Moloto, 2010; Serfass *et al*., 2003) but without consideration of the temperature distribution in the BSM layer under controlled conditions.

Understanding the temperature distribution and heat transfer of BSMs gives insight for simulation of BSMs pavement design procedure more accurately. Temperature in BSMs is known to influence the following:

- evaporation of moisture present in the mixes, enhancing adhesion of the binder to the mineral aggregates (Jenkins, 2000);
- stiffening of the mastic, which in turn affects stiffness, shear properties, and ultimate strength of the mixes;
- equilibrium moisture content in the mixes, and
- ultimate durability behaviour of the mixes and long-term performance.

Depending on mix composition, e.g. higher binder content, air voids and percentage of reclaimed asphalt, temperature distribution in the layer may adversely influence the performance of BSMs.

The temperature distribution observed in the pavement structure gives an insight into the performance of the BSM-foam layer. The higher temperature in the BSM layers, coupled with the void content in the mixtures and high percentage of reclaimed asphalt, result in deformation under heavy traffic loading. It is apparent from these observations that the determination of the temperature distribution in the BSM layer is playing a key factor in the design, in the mechanical and durability properties in a pavement structure.

Temperature, voids distribution, binder content, increasing percentage of reclaimed asphalt, coupled with environmental conditions have found to influence gain in mix engineering properties, whilst adverse environmental conditions coupled with dynamic loading, have found to initiate the premature distress of the BSMs. Loizos and Papavasiliou (2007) reported that the

stiffness modulus gain of foam mix in the field tends to occur within weeks of construction. Jenkins and Twagira (2008) found that premature distress of permanent deformation occurred in full-depth *in situ* recycled (FDR) of BSM-foam was a result of higher temperature distribution in BSMs-foam layer coupled with excessive loading. Fu *et al*., (2007) reported failure on FDR of BSM-foam due to infiltration/suction of subgrade moisture through capillary action resulted from higher percentage of voids distribution in the mix. These findings emphasize the importance of predicting the temperature distribution and its influence on the durability and performance when choosing different BSMs mixes.

The temperature profile in a pavement structure is normally affected directly by the thermal environmental conditions to which it is exposed.

The primary modes of heat transfer are incident solar radiation, thermal and long-wave radiation between the pavement surface and the sky, convection due to heat transfer between the pavement surface and the fluid (air or water) that is in contact with the surface, and conduction inside the pavement as shown in Figure 2.16.

The intensity of solar radiation (direct and diffuse) is dependent on diurnal cycles, the location of the sun in the sky and the incident angle between the surface and sun's rays. The solar radiation results in direct and diffuse heat gain on the pavement through absorption of solar energy by the pavement. The convection heat flux is a function of fluid velocity and direction, and it is affected primarily by wind velocity and direction on the surface. As the convection heat transfer coefficient increases due to higher velocities and opportune wind directions, the convective heat flux also increases. Thus, at relatively high wind velocities a convective cooling of the surface occurs when the temperature of the wind is lower than the temperature of the pavement surface. The direction of the heat transfer due to thermal and long-wave radiation is away from the pavement since deep sky temperatures typically are significantly lower than pavement surface temperatures (Burger and Kröger, 2006).

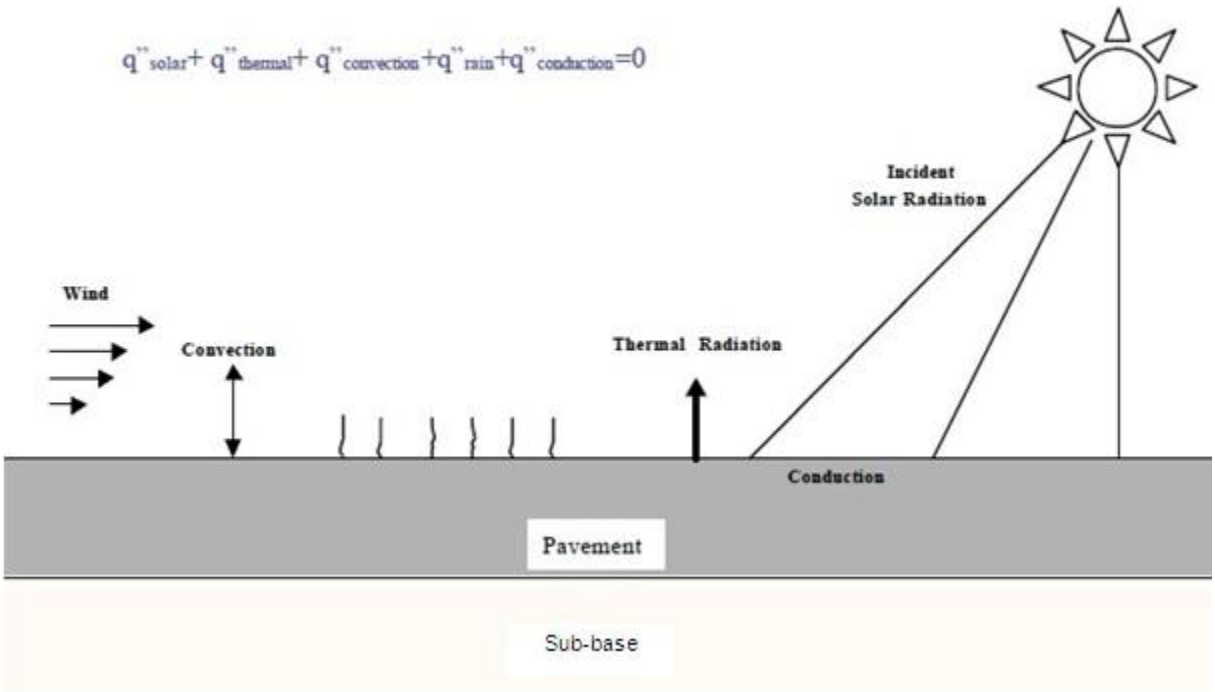

Figure 2.16: Energy balance in a pavement structure.

The surface energy balance on a pavement requires that the sum of all heat gains through the surface of the pavement must be equal to the heat conducted in the pavement. The direction of the heat flux due to convection and thermal radiation is a function of the temperature difference between the pavement surface and the bulk fluid/sky temperatures. In cases where the sky temperature and the bulk fluid temperature are lower than the pavement surface temperature, a cooling of the surface occurs while the surface might simultaneously be heated through incident solar radiation. Thus, depending on the magnitudes of individual heat fluxes, a heating or a cooling of the pavement takes place. An adiabatic bottom surface can be assumed for sufficiently thick pavements stipulating no heat transfer between the pavement and sub-grade layers. Similarly, side surfaces of the pavement (pavement edges) are considered to be adiabatic for sufficiently large horizontal expansions since spatial temperature changes in the vertical direction will be much greater than horizontal changes at pavement edges, and any heat transfer through pavement edge surfaces can be neglected (Jia and Sun, 2007).

In this study, a pavement of three different BSM-foam mixes with an increasing amount of RA (from 0% to 100%) was built in the lab. Every BSM-foam mixture had a pavement structure of 1.2m width, a length of 1m and a thickness of 400mm. A thick layer of good quality crush stone was placed at the bottom of the BSMs layer, simulating a possible road section.

2.7 Conclusions

In this section, the conclusions on the literature review are summarised. The findings on use of RA in BSM-foam mixes, durability behaviour, temperature distribution in BSMs layers and engineering aspects of BSMs are presented. The knowledge gained from the comprehensive literature review provides an insight into the mechanical, temperature distribution and durability properties of BSMs, creating a platform from which new developments were established.

Use of RA in BSM-foam mixes

Recycling HMA material results in a reusable mixture of aggregate and asphalt binder known as RA. Recycling of asphalt pavements is a valuable approach for technical, economical, and environmental reasons. Using RA has been favoured over virgin materials in the light of the increasing cost of paving, the scarcity of quality aggregates, and the pressuring need to preserve the environment. It appears that the use of RA will not only be a beneficial alternative in the future but will also become a necessity to ensure economic competitiveness of flexible pavement construction.

A BSM-foam mix with 100% G2 material (no RA) is considered as a reference for the research in the following chapter. In evaluating the results of the mixes with high and low percentages of RA it needs to be kept in mind that the bitumen contents of these mixes differ. It is therefore difficult to conclude with confidence if the difference in performance is the effect of the percentage of RA or the bitumen content. Aggregate gradation concerns become significant at higher RA percentages, principally due to low fines content.

The stiffness of a mixture can be impacted by the aggregate and gradation, but the most significant factor is the bond between the new virgin materials and the recycled aggregates. Because the mixture properties are so highly dependent on the amount of RA, further laboratory testing is necessary to determine the mechanistic design properties of a BSM-foam mixture with high RA content.

Mechanical tests at different temperatures and study on durability performance of BSM-foam mixes with an increasing amount of RA are necessary to understand the behaviour of these particular BSM mixes. This research has been supported by the findings of previous studies conducted by Jenkins (2000), Ebels (2008) Twagira (2010) and other South African researchers.

Engineering properties

The engineering properties of BSMs have extensively been studied in the past. As a result, numerous tests have been utilised to classify the properties of BSM mix durability. However, in recent times there has been a shift from ITS, UCS and dynamic creep to more fundamental tests related to principle material behaviour in BSM-foam mixes.

A summarised comparison of different tri-axial tests common in Pavement Engineering and ITS tests has been included in Table 2.1. It compares features including common apparatus used, test conditions, loading conditions, test results, models used in analysis and parameters of materials determined.

Table 2.1: Summary of comparison of different tests conducted at the University of Stellenbosch.

Feature	**Types of tests**			
	Indirect Tensile Test (ITS)	Monotonic Tri-axial test	Dynamic Tri-axial test (short duration)	Dynamic Tri-axial test (long duration)
Apparatus	Loading plates Testing System • Actuator • Control panel in the computer software • Data acquisition Measuring Devices • Load cell • Actuator displacement transducer • Computer program recorder • Temperature sensor	Tri-axial Cell Testing System • Actuator • Reaction frame • Control panel • Data acquisition Measuring Devices • Load cell • Actuator displacement transducer • Pressure gauge • Analogue data unit recorder (SPIDER 8) • Temperature sensor	Tri-axial Cell Testing System • Actuator • Reaction frame • Control panel • Data acquisition Measuring Devices • Load cell • Actuator displacement transducer • Pressure gauge • 3 external LVDTs • 2 circumferential LVDTs gauges • Analogue data unit recorder (SPIDER 8) • Temperature sensor	Tri-axial Cell Testing System • Actuator • Reaction frame • Control panel • Data acquisition Measuring Devices • Load cell • Actuator displacement transducer • Pressure gauge • 3 external LVDTs • Analogue data unit recorder (SPIDER 8) • Temperature sensor

Test conditions	Varying temperature -10, 0, 10, 25, 40°C	Temperature 25°C Varying confinement pressure, σ_3 = 50, 100, 200 kPa	Varying temperature 10, 25, 40°C Varying confinement pressure, σ_3 = 50, 100, 200 kPa	Temperature 40°C Constant confinement pressure, σ_3
Loading	Static load applied at a 50 mm/minute	Static or Ramp load applied at a 2.1% mm/min displacement	Dynamic or Cyclic haversine load with preload of 20% of the confining pressure or minimum of 5kPa applied at 1 Hz frequency	Dynamic or Cyclic haversine load with preload of 20% of the confining pressure or minimum of 5kPa applied at 1 Hz frequency
Test Results	Load (Stress) vs. Displacement (Strain)	Load (Stress) vs. Displacement (Strain)	Load (stress) vs. Time and Displacement (Strain) vs Time	Permanent Axial Strain vs. No. of Load Repetitions or Time
Models Used	$\sigma_{xy} = 2P/\pi Dt$	$\tau_f = c + \sigma \tan \varphi$	$M r = k_1 . \theta^k 2$	$\varepsilon_p = A*N^B$
Parameters determined	The indirect tensile strength σ_{xy}	Shear strength of material (cohesion, C and angle of internal friction φ)	Resilient stiffness behaviour of a material, M_r	Permanent deformation behaviour of a material, ε_p
Name of apparatus	Universal Testing machine 25KN - IPC	Material Testing System (MTS)	Material Testing System (MTS)	Material Testing System (MTS)

In order to make reliable designs that accurately estimate the performance of the pavement, it is necessary to have the following information on the mechanical properties of the pavement materials used:

- Indirect Tensile Strength (kPa);
- Shear strength (C and φ)
- Resilient modulus (Mr);
- Permanent deformation (N-εp)

Different mechanisms are involved in saturating BSMs. One of the causes of moisture induction to the BSMs in a pavement layer is traffic related. Typical flexible pavement components in South Africa consist of a surface layer, base layer (granular or BSM), subbase (granular or CTM) and subgrade (natural or selected materials). Surface design consists of the selection of two types of wearing course, either thin asphalt concrete or surface seals. With the modern trend of increased traffic loading and contact stresses, seal performance criteria have been designed to avoid certain failure parameters (Milne, 2004). These are: 1) permanent deformation (punching, rotation of stone, reducing void), 2) early rutting or ponding, 3) fatigue cracking, 4) moisture damage and 5) adhesive failure. Seal design has extensively been studied in New Zealand, South Africa and Australia. The research conducted by Land Transport New Zealand (2005) confirms that at high vehicle speed, surface water can be forced through the cheap seal that does not show signs of cracking. The water which penetrated to the base layer may in turn result in detrimental moisture damage. Ball *et al*. (1999) report a similar behaviour. They studied the effect of water on the flushing process in cheap seal and observed that under tyre pressure water can penetrate through the cheap seal. The study involved tyre deformation and the surrounding fluid in the pavement is referred to as hydroplaning phenomenon. From the mechanism of hydrodynamic pressure, it can be seen that at high speed, generation of

hydrodynamic pressures increases and when the contact pressure (loading condition) at the leading edge, exceeds the hydrodynamic pressure, the water film which penetrated into the contact patch is forced through the pavement layer. However, the water infiltration depth depends on: 1) tread pattern of the tyre, 2) velocity of the tyre, 3) size of the tyre, 4) inflation pressure, 5) loading of the tyre and 6) surface condition between the tyre and the road.

Nikajima *et al*. (2000) modelled the water flow under a tyre as it went through a 10mm deep water film. Their results show that the contact pressure on the pavement with and without water is different in the area noted as rolling, and the difference between these pressures is considered hydrodynamic uplift force caused by water not being removed from under the tyre.
The finding on hydrodynamic pressure between tyre-road interactions is considered an avenue for hydrodynamic simulation of moisture susceptibility of the underlying surface layer. The variables determined in hydrodynamic studies were used by Twagira (2010) in his research to develop new conditioning system for BSM moisture susceptibility (MIST device). The research in New Zealand (2005) on multiple seals shows that the measurable flow rate under the surface course was a pressure of around 100kPa, with potholing observed to appear where water had ponded. That means rutting and stagnant water on pavement surfaces may result in high hydrodynamic pressure under dynamic loading.

This puts the tri-axial test at the centre stage of any mechanistic approach to pavement design.

Durability of BSM-foam mixes

The study of mixture composition structure at micro and macro levels develop a fundamental understanding of durability properties. The use of material performance models can be used to explain material behaviour and assist in the prediction of long-term performance of BSMs.
The adhesion and cohesion bonding between binder and aggregates in BSMs is one of the most important bonds that differentiate BSMs and granular material. However, it is one of the least understood bonds. This is partly due to the complexity of the binder characteristics and partly due to the variety of surfaces of aggregates with which the binder comes into contact.

Curing of mixture composition in BSMs remains an influential process for bond development within the mix matrix. However, the curing process is entirely dependent on the mechanisms of moisture evaporation. The review shows that the evaporation process is linked to the temperature gradient in the layer, wind speed, relative humidity and boundary conditions surrounding the BSMs pavement. The model that sufficiently addresses these parameters has not been studied. In the following chapters, a proposed model for BSM-foam mixes is presented. It is believed that further investigation into the model will accurately predict the temperature distribution, particularly under the field conditions, by encompassing all evaporation parameters.

Moisture damage contributes significantly to the premature deterioration of pavement materials. Moisture transport mechanisms, coupled with adverse environmental conditions and dynamic loading, have been found to influence moisture damage mechanisms of BSMs. A wide approach for quantification of moisture damage is derived by testing dry or soaked specimens and moisture-conditioned specimens using the same variable parameters. Although the methods provide an empirical measure of moisture damage, they also provide both variable and

unreliable results. Therefore, there is a need to develop a new moisture conditioning procedure through the use of a mechanical brushing tester.

Temperature behaviour in the BSM – foam layers

Temperature distribution and void characteristics in a pavement layer play a significant role in both the ultimate gain in mix engineering properties and the exhibition of premature distress in field conditions. The importance of predicting field temperature and void distribution and its influence on the durability and performance when adjudicating mix selection are indispensable for understanding the effect of strength development for BSMs. The magnitude of this test temperature coupled with material properties can significantly influence the durability behaviour and long-term performance of BSM layers.

The temperature across the pavement section of BSM-foam mixes with a high percentage of RA has not been not completely studied over the layers. The temperature gradient in the layers may be used to determine its influence on moisture evaporation and mechanical response. That means, understanding of the temperature distribution in BSM-layers is important for judging the appropriate mechanical and durability properties of BSM-foam mixes. The key factors that have been indicated to influence temperature distribution and voids characteristics in BSMs are heat transfer and void structure. The heat transfer in the BSM-layers depends on local environmental factors such as solar radiation, wind speed as well as material properties. Therefore, modelling of these factors is required for proper prediction of strength gain in the layers. Therefore, the linkage of temperature distribution with mechanical properties in BSM-foam mixes with high percentage of RA requires further investigation.

The findings in the literature review have defined the pertinent mechanical, durability and temperature distribution issues to be researched on BSM-foam mixes with higher percentage of RA.

REFERENCES

AASHTO T 135-97. 2005. Standard Method of Test for Wetting-and-Drying Test of Compacted Soil-Cement Mixtures.

Anderson, D. A., Christensen, D. W., Bahia, H. U., Dongre, R., Sharma, M. G., and Antle, C. E. 1994. Binder characterization and evaluation: Volume 3 Physical characterization. Rep. No. SHRP-A-369, National Research Council, Washington DC.

Appea A. K., Rorrer T.and Clark T. 2009. Case Studies on Processes Involved in the Production and Placement of High RAP Asphalt Concrete Mixes in 2007 on Selected Routes in Virginia. In Transportation Research Board 88th Annual Meeting. CD-ROM. Washington, D.C.

Asphalt Academy. 2009. A guideline for the design and construction of bitumen emulsion and foamed bitumen stabilised materials. 2nd edition technical guideline. Pretoria, South Africa. (TG2).

Asphalt Institute, 1989. Hot-Mix Recycling, The Asphalt Handbook MS-4.

Ball G.F.A, Logan T.C, and Patrick J.E. 1999. Flushing process in chip-seals: Effects of water. Transfund NZ research report, no. 156.

Barber E.S. 1957. Calculation of maximum pavement temperature from weather report. TRB no.168, pg. 1-8.

Barksdale, R. D. 1972. Laboratory Evaluation of Rutting in Base Course Materials, 3rd International Conference on the Structural Design of Asphalt Pavements, London, England.

Blakey, F.A., and Beresford, F.D. 1955. Tensile Strain in Concrete II. C.S.I.R.O. Div. Build. Res. Rep. No. C2. 2-2, 15.

Bonfim V. 2008 . Cold Milling of Asphalt Pavements, Sao Paulo. Brazil.

Burger M. 2005. Prediction of the temperature distribution in asphalt pavement samples. Master thesis, Department of mechanical engineering, Stellenbosch University, South Africa.

Burger, M. and Kröger D.G. 2006. Experimental convection heat transfer coefficient between a horizontal surface and the natural environment, proceedings of the 17th International congress of chemical and process engineering, Prague, Czech Rep. pp. 1523 – 1524.

Caravalho, R.L., Shirazi, H., Ayres, M. Jr. and Selezneva, O. 2010. Performance of Recycled Hot-Mix Asphalt Overlays in Rehabilitation of Flexible Pavements. In Transportation Research Record: Journal of the Transportation Research Board, No. 2155, (pp. 55-62) Transportation Research Board of the National Academics, Washington, D.C.

Caro, S., Masad, E., Bhasin, A. and Little, D. N. 2008. Moisture susceptibility of asphalt mixtures, Part 1: mechanisms, Part 2: Characterisation and modelling. International Journal of Pavement Engineering. Vol. 9, No. 2, pg81–98.

Cross, S.A. 1999. Experimental Cold In-Place Recycling with Hydrated Lime, Transportation Research Record, No. 1819, Transportation Research Board, National Research Council, Washington, D.C., USA , pp.186-193.

CSIR. 2011. Revision of the South African Pavement Design Method, Proposed Protocol for Resilient Modulus and Permanent Deformation Characteristics of Unbound and Bound Granualr Materials. CSIR, Pretoria, South Africa.

Domke, C. H., Liu, M., Davison, R. R., Bullin, J. A. and Glover, C. J. 1997. Study of Strategic Highway Research Program pressure ageing vessel procedure using low-temperature ageing experiments and asphalt kinetics. Transportation Research Record, (no. 1586), pp. 10-15.

Dutch (environmental) policy concerning the use of secondary materials. 2011. Reuse and recycling of waste materials in the Netherlands, Road and Hydraulic Engineering Division, Directorate-General for Public Works and Water Management, Ministry of Transport, Public Works and Water management, The Netherlands.

Ebels, L. J. and Jenkins, K. 2007. Determination of Shear Parameters, Resilient Modulus and Permanent Deformation Behaviour of Unbound and Bound Granular Materials Using Tri- Axial Testing on 150mm Ø x 300mm High Specimens. Technical Memorandum, Pave Eng cc. Stellenbosch.

Ebels L.J. 2008. Characterisation of Material Properties and Behaviour of Cold Bituminous Mixtures for Road Pavements. PhD Dissertation, Department of Civil Engineering, Faculty of Engineering, University of Stellenbosch, South Africa.

Elphingstone, G.M. 1997. Adhesion and cohesion in asphalt-aggregate systems. PhD dissertation, Texas A&M University, College station, Texas.

Emery, S.J. 1988.The prediction of moisture content in untreated pavement layers and an application to design in Southern Africa. CSIR research report no.644. Division of Roads and Transport Technology. DRTT Bulletin 20. Pretoria

Environmental Protection Agency and Federal Highway Administration. 1993. Recycling of Asphalt Pavements Using at Least 80 Percent Recycled Asphalt Pavement Engineering and Environmental Aspects of Recycled Materials for Highway Construction, Report No. FHWA-RD-93-088.

Francken, L.1977. Permanent Deformation Law of Bituminous Road Mixes in Repeated Tri-axial Compression, 4th International Conference on the Structural Design of Asphalt Pavements, Ann Arbor, Michigan, USA.

Francken, L., Vanelstraete, A. and Verhasselt, A. 1997. Long-term ageing of pure and modified bitumen: Influence on the rheological properties and relation with the mechanical performance of asphalt mixtures. pp. 1259-1278.

Fu P., Harvey J.T., Jones D. and Chao Y.C. 2007. Understanding internal structure characteristics of foamed asphalt mixes with fracture face image analysis. Journal of transportation research board. TRB. Washington DC.

Fu P., Jones D., Hervey J.T, Asce M. and Halles F. A. 2009. An investigation of the curing of foamed asphalt mixes based on micromechanics principles. Journal of materials in civil engineering.

Gonzalez, A. 2009. An experimental study on deformational characteristic and performance of foam bitumen pavements. PhD dissertation. University of Canterbury. New Zealand.

Hicks, R. G. and Monismith, C. L. 1971. Factors influencing the resilient response of granular materials, Highway Research Record No. 345, Highway Research Board, Washington DC, USA.

Highter, W.H. and Wall D.J. 1984. Thermal properties of some asphaltic concrete mixes. TRB no. 969 pg. 38-45.

Hondros, G. 1959. The Evaluation of Poisson's Ratio and the Modulus of Materials of a Low Tensile Resistance by the Brazilian (Indirect Tensile) Test with Particular Reference to Concrete, Australian Journal of Applied Science, Vol. 10, No. 3, p. 243-268.

Huurman, M., 1997. Permanent Deformation in Concrete Block Pavements. PhD Dissertation. Delft University of Technology, Netherlands.

Jenkins, K.J. 2000. Mix Design Considerations for Cold and Half-Warm Bituminous mixes with the emphasis on foamed bitumen. PhD Dissertation. University of Stellenbosch.

Jenkins, K.J., Ebels, L.J. and Twagira, M.E. 2006. Updating bituminous stabilised materials guideline: Mix design inception study. First draft. Pav. Eng.cc, Stellenbosch, South Africa.

Jenkins, K.J., Long, F.M. and Ebels, L.J., 2007. Foamed Bitumen Mixes Shear Performance International Journal of Pavement Engineering. Volume 8 Number 2.

Jenkins, K.J. 2008. Lecture Notes on Hitchhiker's Guide to Pavement Engineering. Flexible Pavement Design Course University of Stellenbosch.

Jenkins, K.J. Ebels, L.J. Twagira, M.E. Kelfkens, R.W. Moloto, P. and Mulusa, W.K. 2008. Updating bituminous stabilised materials guideline: Mix design report, phase II. Research report, prepared for SABITA and Gautrans, Pretoria. South Africa.

Jenkins, K.J. and Twagira, M.E. 2008. Failure mechanism of in-situ recycling with foamed bitumen stabilisation. Technical report on the investigation of distress on Shedgum Road in Saudi Arabia. Loudon International.

Jia, L. and Sun, L. 2007. Numerical prediction model and thermal properties for asphalt pavement. Journal of advanced characterisation of pavement and soil engineering materials. Taylor and Francis Group. London.

Jooste, F.J., Long, F.M. and Hefer, A. 2007. A Method for Consistent Classification of Materials for Pavement Rehabilitation Design, Technical Memorandum compiled on behalf of Sabita and GDPTRW. Modelling and Analysis Systems, Cullinan, South Africa.

Kandhal, P. S. and Chakraborty, S. 1996. Effect of Asphalt Film Thickness on Short and Long-Term Aging of Asphalt Paving Mixtures. Transportation Research Record, (TRR No. 1535, pp. 83).

Kandhal, P. S. and Mallick, R. B. 1997. Pavement Recycling Guidelines for State and Local Governments – Participant's Reference Book, Report No. FHWA-SA-98-042, National Center for Asphalt Technology, Auburn, AL.

Karlsson, R. and Isaacsson, U. 2006. Material-Related Aspects of Asphalt Recycling — State of the Art, Journal of Materials in Civil Engineering, American Society of Civil Engineers, Vol. 18, No. 1, 2006, pp. 81-92.

Kelfkens, R.W.C. 2008. Vibratory hammer compaction of bitumen stabilised materials. MSc. Thesis. University of Stellenbosch. South Africa.

Kemp, G. R. and Predoehl, N. H. 1981. A Comparison of Field and Laboratory Environments on Asphalt Durability, Proceedings of the Association of Asphalt Paving Technologists, Vol. 50, 1981, pp. 492-537.

Kennedy, T. W. and Hudson, W.R. 1968. Application of the Indirect Tensile Test to Stabilized Materials. Highway Research Record N^0. 235, Highway Research Board, pp 36-48.

Kennedy, T. W., Tam, W. O. and Solaimanian, M. 1998. Optimizing Use of Reclaimed Asphalt Pavement with the SuperPave System, Journal of the Association of Asphalt Paving Technologists, Vol. 67, pp. 311-333.

Kennedy, T.W., Huber, G.A., Harringan, E.T., Cominsky, R.J., Hughes, C.S., Von Quintis, H. and Moultrop, J.S. 1994. Superior Performing Asphalt Pavements (SUPERPAVE): The product

of the SHRP asphalt research program, Report no: SHRP-A-410, Strategic Highway Research Program, Washington.

Kim, S., Byron, T., Sholar, G. A. and Kim, J. 2007. "Evaluation of Use of High Percentage of Reclaimed Asphalt Pavement (RAP) for Superpave Mixtures" Research Report FL/DOT/SMO/07-507, Florida, USA.

Lancaster, J., McArthur, L. and Warwick, R. 1994. VICROADS experience with foamed bitumen stabilisation. In the Proceedings of the 17th ARRB Conference, Gold Coast, Queensland, Volume 17, Part 3, pp 193-211.

Land Transport New Zealand. 2005. The waterproofness of first coat chipseals. Research Report Style Guide (Report). (p. 35). Auckland, New Zealand: Land Transport New Zealand.

Liebenberg, J.J.E. 2002. The Influence of Various Emulsion and Cement Contents on an Emulsion Treated Ferricrete from the HVS Test Sections on Road P243/1.

Loizos, A. and Papavasiliou, V. 2007. Assessment of in-situ cold in-place recycling performance using the foam asphalt technique. Workshop on pavement recycling. Athens, Greece.

Long, F. Theyse, H. and Ventura, D.F.C. 2004. Characterisation of foamed bitumen treated materials from HVS test sections, Pretoria, South Africa.

Long, F. and Ventura, D.F.C. 2003. Laboratory testing for the HVS, Test Sections on the N7, Pretoria, South Africa.

Lynn, L. 1992. Three States OK More RAP in Recycling Specs: Asphalt Recycling and Reclaiming, Roads and Bridges.

Maccarone, S., Holleran, G., Leonard, D.J., and Hey, S. 1994. Pavement Recycling using Foamed Bitumen. In the Proceedings of the 17th ARRB Conference, Gold Coast, Queensland, Volume 17, Part 3, pp 349-365.

Mallick, R. B., Bonner, D.S., Bradbury, R.L., Andrews, J.O., Kandhal, P.S. and Kearney, E.J. 2002. Evaluation of Performance of Full-Depth Reclamation Mixes, Transportation Research Record No. 1809, Transportation Research Board, National Research Council Washington, D.C., USA , pp.199-208.

Malubila, S.M. 2005. Curing of foamed bitumen mixes. Master's thesis. University of Stellenbosch. South Africa.

Maree, J. H. and Freeme, C. R. 1981. The mechanistic design method used to evaluate the pavement structures in the catalogue of the draft TRH4 1980, Technical Report RP/2/81, National Institute for Transport and Road Research, CSIR, Pretoria, South Africa.

McMillan, C. and Palsat, D. 1985. Alberta's Experience in Asphalt Recycling, Proceedings of the Canadian Technical Asphalt Association, Vol. 30, 1985, pp. 148-167.

Milne, T. I. 2004. Towards a Performance Related Seal Design Method for Bitumen and Modified Bitumen Seal Binders. PhD Thesis, University of Stellenbosch. South Africa.

Moloto, P. 2010. Curing protocol for the Bitumen Stabilised Materials (BSMs) Improving and Validation. Master's thesis. Stellenbosch University, South Africa.

Montepara, A. and Giuliani, F. 2002. A Study on Design and performance of Recycled Pavement Cold Stabilized with Cement and Bituminous Emulsion. Proceeding of 4th European Symposium on Performance of Bituminous and Hydraulic Materials in Pavement, BITMAT 4, University of Nottingham, UK, 11-12 April 2002, A.A. Balkema Publishers, Netherlands, pp 213-217.

Moore, K.D. 2004. Foamed Asphalt Gains New Attention in Cold In-Place Recycling, Better Road, July 2004.

Musselman, J. 2009. High RAP Performance in Florida, HMA Recycling Expert Task Group, Department of Transportation, Washington, DC.

National Department of Transport. 2009. Technical Recommendations for Highways : TRH 21 Hot Mix Recycled Asphalt. Pretoria, RSA.

NCHRP 1-37A. 2004. Mechanistic-Empirical Design of New and Rehabilitated Pavement Structures, Final Report, NCHRP Project 1-37A, Transportation Research Board, National Research Council, Washington, D.C.

Nikajima, Y., Seta, E., Kamegawa, T. and Ogawa, H. 2000. Hydroplaning analysis by FEM and FVM: Effect of the rolling and tire pattern on hydroplaning. International journal of automotive technology, Vol. 1 no.1 pp. 26-34.

Øverby, C., Johanson, R. and Mataka, M. 2004. Bitumen foaming: An innovative technique used on a large scale for pavement rehabilitation in Africa. Case study: Same-Himo monitored pilot project. Proceedings of the 8th Conference on Asphalt Pavements for Southern Africa (CAPSA'04). Sun City, South Africa.

Page, G. C. and Murphy, K. H. 1987. Hot-Mix Recycling Saves Florida DOT $38 Million, Asphalt, Vol. 1, No.1.

Paige-Green, P. 1998. Recent Developments in Soil Stabilization. p121-135, Proceedings: 19th ARRB Conference, Sydney, Australia, Dec 1998.

Paige-Green, P. and Ventura, D.F.C. 2004. Durability of foamed bitumen treated basalt base course. CSIR report CR 2004/8. Pretoria.

Portland Cement Association (PCA). 1971. Soil cement laboratory handbook. PCA, Skokie.

Peterson, J. C. and Harnsberger, P. M. 1998. Asphalt Ageing: Dual Oxidation Mechanism and its Relationship with Asphalt Composition and Oxidative Age Hardening. Transportation Research Record, (TRR No. 1638). National Academy Press.

Ramanujam, J.M. and Fernando, D.P. 1997. Foam Bitumen Trial at Gladfield-Cunningham Highway. In the Proceedings of the Southern Region Symposium, Australia.

Roberts, F.L., Engelbrecht J.C. and Kennedy T.W. 1984. Evaluation of Recycled Mixtures Using Foamed Asphalt. In Transportation Research Record No. 968, Washington, DC, Transportation Research Board, pp. 78-85.

Roberts, F. L., Kandhal, P. S., Brown, E. R., Lee, D. and Kennedy, T. W. 1996. Hot Mix Asphalt Materials, Mixture Design, and Construction, 2nd Edition, Napa Education Foundation, Lanham, MD.

Romanoschi, S.A., Heitzman, M. and Gisi, A.J. 2003. Foamed Asphalt Stabilized Reclaimed Asphalt: A Promising Technology for Mid-Western Roads. Proceedings of the August 2003 Mid-Continent Transportation Research Symposium, Ames, Iowa.

Santangata, F. A., Bocci, M., Grilli, A. and Cardone, F. 2009. Rehabilitation of an Italian Highway by Cold In-Place Recycling Techniques. Advanced Testing and Characterization of Bituminous Materials, (eds Loizos, A., Partl, Scarpas, T. and Al-Qadi, I. L.), Taylor and Francis Group, London.

Sampson, L.R. 1988. Development of the mechanical wet/dry brushing test for the durability testing of stabilized materials. Report V/DPVT/3.1, CSIR, Pretoria.

Sampson, L.R. and Paige-Green, P. 1990. Recommendation for suitable durability limits for lime and cement stabilized materials. Research Report DPVT 130, CSIR, Pretoria.

Sampson, L.S. and Netterberg, F. 1989. The durability mill: A new performance related test for base course aggregates. The civil engineer in South Africa, pg. 287-294.

Schmidt, R. J. 1972. Practical Method for Measuring the Resilient Modulus of Asphalt-Treated Mixes. Highway Research Record n°404, pg. 22-29.

Serfass, J. P., Poirier, J. E., Henrat, J. P. and Carbonneau, X. 2003. Influence of Curing on Cold Mix Mechanical Performance. Performance Testing and Evaluation of Bituminous Materials PTEBM'03, 6th International Rilem Symposium, Zurich, Switzerland.

Serfass, J. P., Carbonneau, X., Delfosse, F., Triquigneaux, J.P. and Verhee, F. 2008. Mix Design Method and Field Performance of Emulsion Cold Mixes. 4th Eurobitume and Eurasphalt Congress, Copenhagen.

Shell Bitumen U.K., 1993. The Shell Bitumen Handbook, United Kingdom.

Smiljanic, M., Stefanovic, J. Neumann, H.-J. Rahimaian, I. and Jovanovic, J. 1993. "Ageing of Asphalt on Paved Roads — Characterization of Asphalt Extracted from the Wearing Courses of the Belgrade-Nis Highway," Journal of Erdol and Kohl, Vol. 46, No. 6, Hamburg, Germany.

Solaimanian, M. and Kennedy, T.W. 1993. Predicting maximum pavement surface temperature using maximum air temperature and hourly solar radiation. TRB no. 1417 pg. 1-11.

Solaimanian, M. and Tahmoressi, M. 1996. Variability Analysis of Hot-mixed Asphalt Concrete Containing High Percent Reclaimed Asphalt Pavements, Presented at the 75th Annual Meeting of Transportation Research Board, Transportation Research Record, No.1543, National Research Council, Washington, D.C., 89-96.

Sullivan, J. 1996. Pavement Recycling Executive Summary and Report, FHWA-SA-95-060, Federal Highway Administration, Washington, D.C.

Theyse, H. L., De Beer, M. and Rust, F. C. 1996. Overview of the South African Mechanistic Pavement Design Method. Transportation Research Record 1539. Transportation Research Board, Washington D. C.

Theyse, H. L. 2000. Laboratory design models for materials suited for labour-intensive construction, Contract Report CR-99/038 Volume I: Report, Transportek, CSIR, Pretoria, South Africa.

TRH14. 1985. Guideline for road construction materials Department of Transport–Technical recommendations for highways. Pretoria. South Africa.

Twagira, E.M. 2010. Influence of durability properties on performance of bitumen stabilised materials, PhD Dissertation, Department of Civil Engineering, Faculty of Engineering, University of Stellenbosch, South Africa.

Tyrion, F. C. 2000. Asphalt Oxidation, Asphaltenes and Asphalts, Development in Petroleum Science, Vol. 40B, Elsevier, NY.

Van der Walt, N., Botha, P., Semmelink, C., Engelbrecht, F. and Salminen, N. 1999. The Use of Foamed Bitumen in Full-depth In-place Recycling of Pavement Layers Illustrating the Basic Concept of Water Saturation in the Foam Process. Proceedings of the Seventh Conference on Asphalt Pavements for South Africa, Pretoria, South Africa.

Van Niekerk, A.A. 2002. Mechanical Behaviour and Performance of Granular Bases and Subbases. PhD Dissertation. Delft University of Technology. Delft.

Van Wijk, A.J. and Wood, L.E. 1984. Construction of Cold Recycled Pavements Using Emulsion as a Binder. Proceedings of the Fourth Conference on Asphalt Pavements for Southern Africa. Cape Town, South Africa.

Van Wijk, A. and Wood, L.E.. 1993. Use of Foamed Asphalt in Recycling of an Asphalt Pavement. In Transportation Research Record No. 911, Transportation Research Board. Washington, DC, pp. 96-103.

Viljoen, A. W. 2001. Estimating Asphalt temperatures from air temperatures and basic sky parameters. Internal report, Transportek, CSIR, Pretoria.

Walter, J., Attané, P., Kalaaji, A. and Lancaster, I. 2008. Regeneración del betún en el proceso de reciclado en frío (Bitumen regeneration in cold recycling processes). Carreteras, número 158/Mar-Abr 08, pp 27-35.

Weinert, H.H. 1980. The natural road construction materials of Southern Africa. Academia. Cape Town.

Weston, C., Van Amsterdam and Jenkins, K. 2002. A Study into the Mechanical Properties of Foamed Bitumen Stabilised Materials. 21st Annual South Africa Transportation Conference.

Whiteoak, D. 2000. Specialist Surface Treatments, Bituminous Mixture in Road Construction, Hunter, R. N., ed., Thomas Telford, London, pp. 465-509.

Wirtgen GmbH. 2002. Foamed Bitumen – The Innovative Binding Agent for Road Construction, published by Wirtgen GmbH, Windhagen, Germany.

Wirtgen GmbH. 2010. Cold Recycling Manual, 3rd edition published by Wirtgen GmbH, Windhagen, Germany.

Witczak, M. W., Andrei, D. and Mirza, M. W. 1999. Development of Revised Predictive Model for the Dynamic (Complex) Modulus of Asphalt Mixtures. Interim technical report, NCHRP Project 1-37A, University of Maryland.

Witczak, M.W., Kaloush, K., Pellinen, T. and El-Basyouny, M. 2002. Simple Performance Test for Superpave Mix Design, NCHRP Report 465, Transportation Research Board, Washington, DC

Wright, P.J.F. 1955. Comments on an indirect tensile test for concrete Mag. Conc. Res. 20: 87-96.

Zoorob, S. E. and Thanaya, I.N.A. 2002. Improving the Performance of Cold Bituminous Emulsion Mixtures (CBEMs) Incorporating Waste Materials. Proceeding of 4th European Symposium on Performance of Bituminous and Hydraulic Materials in Pavement, BITMAT 4, University of Nottingham, UK, 11-12 April 2002, A.A. Balkema Publishers, Netherlands, pp. 237-249.

CHAPTER 3

EXPERIMENTAL DESIGN AND METHODOLOGY

3.1 Introduction

In this chapter the key design parameters and the methodology followed in this research are presented and discussed. The chapter begins with a discussion of the materials used to produce the BSM mixes, providing some background on the material properties and characteristics. This is followed by a description of the type and number of mixes tested (Figure 3.1). The materials used in this study along with their characteristics and specific roles in foamed asphalt stabilization process are explained. Where appropriate, relevant findings from previous studies are also provided. Although most detail on the procedures followed to produce the mixes and the specimens is provided along this chapter and the following one, this chapter includes a summary of the most pertinent issues relating to the mix and specimen preparation.

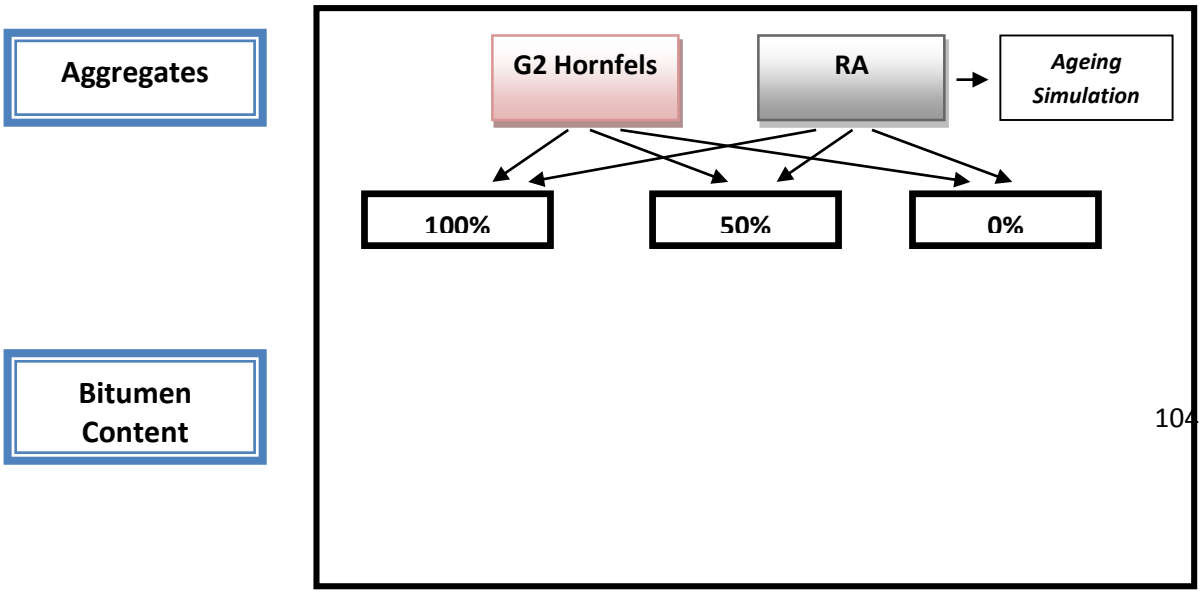

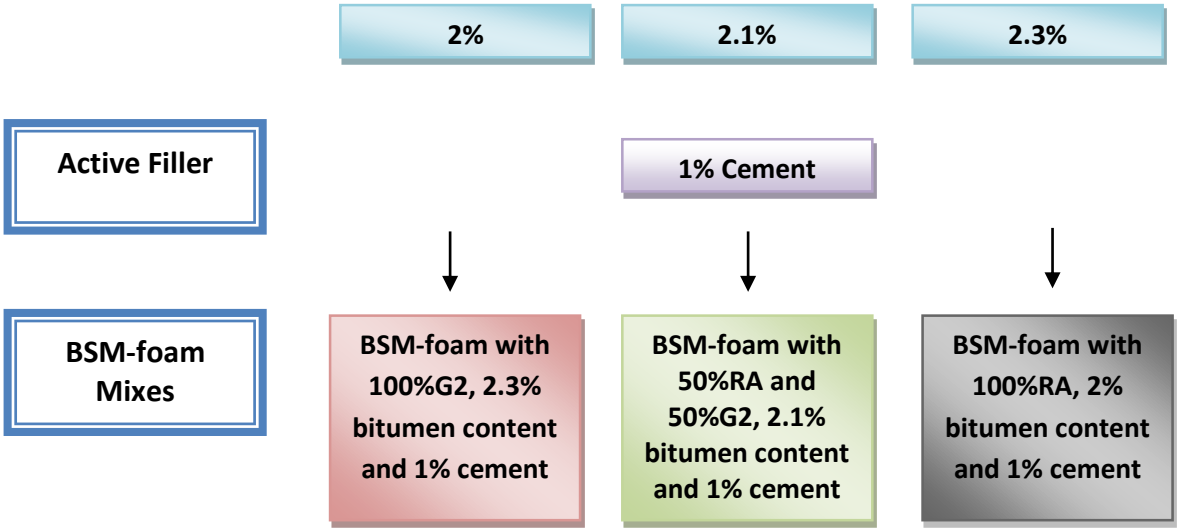

Figure 3.1: Experimental design matrix conducted in this thesis.

The experimental testing described in this study is mainly focussed on three types of testing (Figure 3.2): mechanical tests, durability tests and temperature tests. The types of mechanical tests, durability tests used during the study are briefly discussed in this chapter. The most important aspects relating to test conditions and methods are also provided.

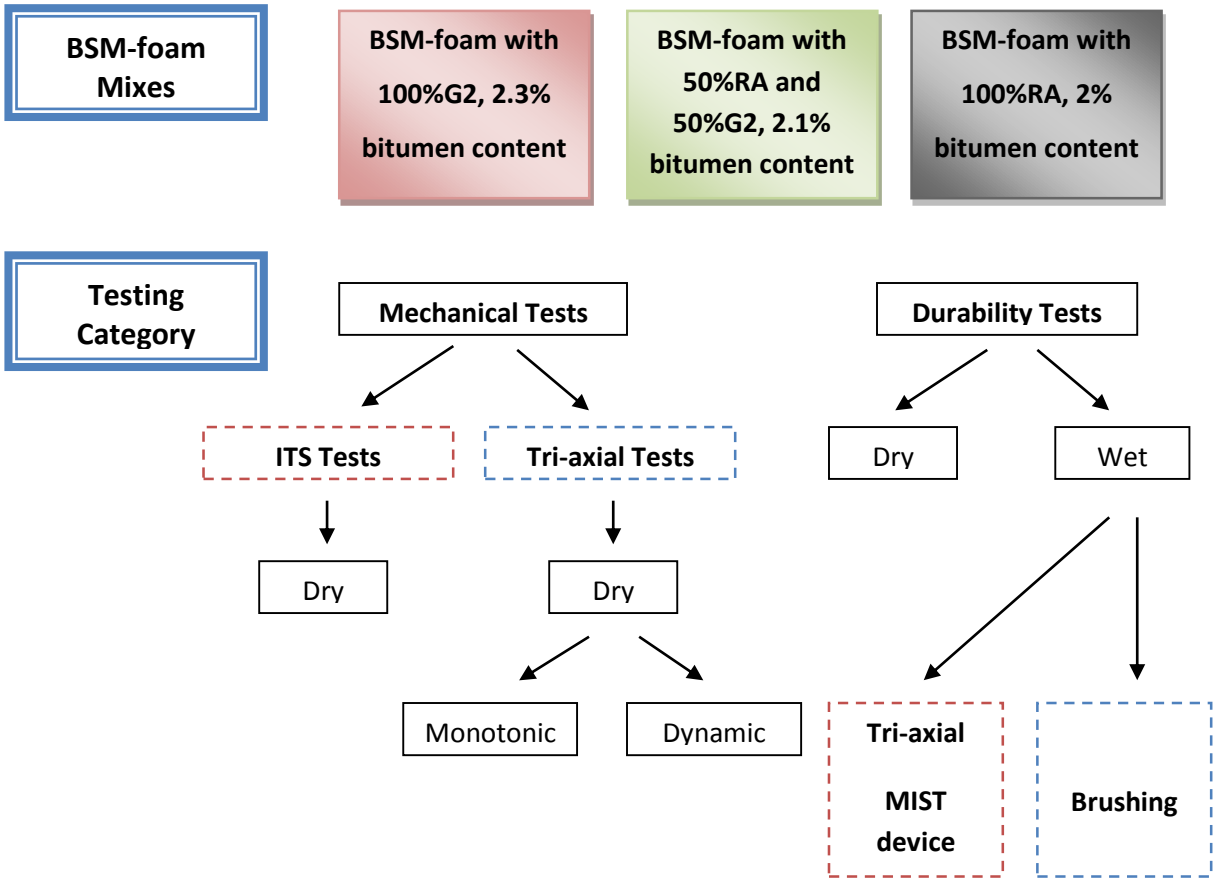

Figure 3.2: Experimental testing matrix conducted in this thesis.

Additional temperature tests were carried out in order to investigate the appropriate temperature distribution for the testing of BSMs (Figure 3.3). A final chapter will include a major synthesis of all of these tests conducted in the Laboratory at the University of Stellenbosch.

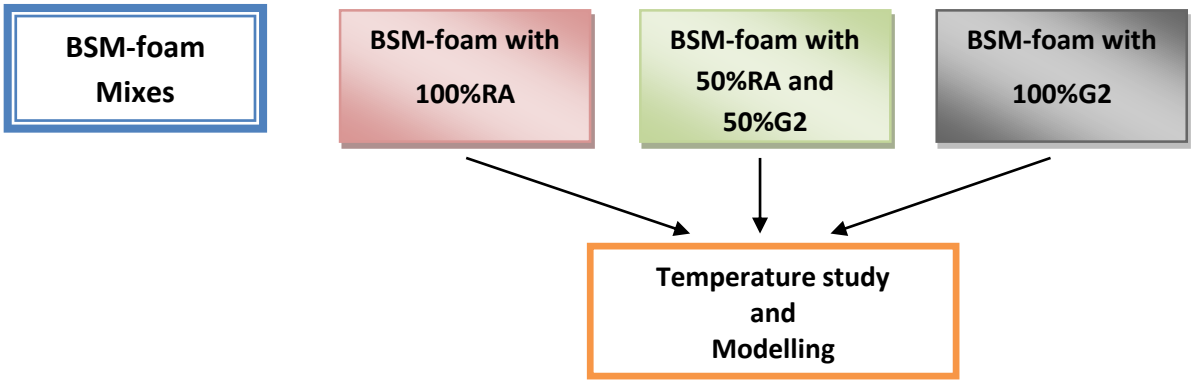

Figure 3.3: Temperature study conducted in this thesis.

3.2 Materials

3.2.1 Aggregate properties

Recycling old pavements requires the reuse of high percentage of Reclaimed Asphalt (RA) before blending with other materials. In this case, the influence of the aggregate (RA) composition has to be carefully considered in the mix design, especially for road networks with a high level of traffic.

The bitumen stabilised material (BSM) mixes that are the subject of this study were produced using two main sources of mineral aggregates:

- Hornfels, good quality crushed stone (G2)
- Reclaimed Asphalt (RA) produced in the laboratory

Three different mixes have been used in this research with three different percentage of RA blended with G2 material (crushed Hornfels): 100%RA; 50%RA and 50%G2; and 100%G2. Continuously graded aggregates have been selected for a focussed investigation into performance of bitumen stabilised materials BSM-foam. 1% of Portland cement (strength class 32.5) has been included in all the mixtures.

Paragraph 3.2.2 describes the technique adopted to recreate RA in the laboratory at the University of Stellenbosch. The decision to use RA from the laboratory and not from the industry was due to the high variability (RA coming from different sites and mixed) and contamination of RA directly at the source. A visual inspection indicated that the RA was contaminated by rubbish from the roads such as broken glass, tree roots, small pieces of wood and plastic as shown in Figure 3.4.

Figure 3.4: RA sample from the industry.

The RA produced artificially was subsequently used for this research on BSM-foam described in subsequent paragraphs of this thesis.

3.2.2 Ageing simulation

The standard simulation of ageing in the laboratory is performed under the influence of temperature and air which doesn't differ too much from the ageing conditions in reality in the field.

The most common ageing indicators for binders are the extent of age hardening of fresh bitumen materials which can be quantified in terms of penetration (% Retained Penetration), change in softening point, mass loss (STA, short-term ageing), or viscosity (Ageing Index) (Roberts *et al*. 1996). It is important to note that these indices of ageing vary with the pavement structure, location, and mixture type, which is the reflection of the effect of environment, binder source and mixture type. Apart from empirical methods, fundamental properties such as stiffness are also used to describe the effect of binder ageing over a wider spectrum of temperatures including low temperatures corresponding to cracking temperatures (Anderson *et al*. 1994). Ageing of binders is also related to the change in binder chemical composition. The ageing process can also be explained by the changes in fundamental rheological properties of bitumen, such as complex modulus and phase angle as a function of frequency.

Standard laboratory protocols for long-term ageing of asphalt mixtures have been developed during the Link BITUTEST and SHRP programmes in the UK and USA respectively (Bell, 1989 and Scholz, 1995). Long-term laboratory ageing under these protocols was conducted at 85°C over five days, and the assumption is that this is representative of 15 years or more of ageing of pavements in service in temperate regions of the world (Bell 1989; and Scholz, 1995).

However, these standard laboratory ageing protocols use compacted specimens (Airey, 2003) and require long laboratory ageing times in order to produce the desired properties. This is understandable as such protocols were not designed for the harsh conditions considered in this work. Ageing loose samples at higher temperatures (100°C and 125°C) than standard will generate more homogeneous (De la Roche *et al*, 2009) severely aged RA in a practical time but risks unduly degrading the binder in the mix. Researchers have suggested that this degradation

would normally affect the physico-chemical and rheological properties of the binder in the mix (Airey, 2003 and Wu *et al*, 2007).

It was considered important to conduct this investigation and come up with an ageing protocol that can be as quick as possible without compromising the integrity of the residual binder or introducing any significant changes to its properties when compared to a standard ageing protocol.

Reclaimed asphalt pavement (RA) with maximum aggregate size of 19 mm was used with grading. The RA was made locally at the laboratory of the University of Stellenbosch from an original base course aggregate (G2) obtained from Lafarge Tygerberg Quarry. The RA was obtained in the laboratory, by mixing a gradation of G2 material with 5% of bitumen with a 60/70 penetration grade (Chevron refinery plant in Cape Town). The decision to make RA directly in the laboratory was dictated by the presence of high variability in the RA stockpiles. Recreating RA in the laboratory allows controlling the quality and condition of the RA produced.

The investigation required verifying and comparing viscoelastic response and temperature susceptibility (penetration and softening point) of recovered binder from mixture immediately after 1) mixing and compaction (representing short-term ageing) and 2) subsequent ageing at 100°C (representing long-term ageing) over 20hrs in the forced draft oven prior to compaction with the condition that they be stirred and turned along the process. These materials were placed in oven trays such that the thickness of the loose materials in the tray was not more than 40mm. This allowed for homogeneous ageing. As ageing progressed in the forced draft oven irrespective of the ageing temperature used in this work, the bituminous binder melted and once again bound (although slightly) most of the aggregates together forming lumps. This was not a major issue for the binder recovery tests, but it became obvious at the mass production level that, running them through the Jaw Crusher was unavoidable. Apart from facilitating the production of a more homogeneous final product (artificial RA), using the Jaw Crusher grossly reduced handling time of the materials.

The RA made in the laboratory was found to represent 15 years in service for dense mixtures. The results were compared to real values coming from the analysis of old RA presented in the area of the Western Cape (Much Asphalt plant in Eersteriver) and showed in paragraph 3.2.6. A summary of commonly used ageing indicators for both binders and asphalt mixtures is given in Table 3.1.

Table 3.1: Summary of Ageing Indicators Used to Describe Changes in Binder Property

	Ageing Indicators

Binders	*Rheology:* 1. Retained Penetration (%) 2. Change in Softening Point (ΔTRB = TRB - TRB) 3. Ageing Index / Viscosity Ratio (AI) 4. Mass loss (short term ageing) 5. Complex modulus, G* and phase angle, δ as a function of frequency *Mechanical*: 6. Tensile/Creep strength (stiffness) *Chemical:* 7. Increment in carbony + sulfoxide area (Infra-red Spectroscopy test) 8. Change in molecular weight distribution (GPC test)
Asphalt Pavement Mixture	1. Resilient modulus ratio 2. Ductility Index (DI) 3. Cantabro Test: Change in mass loss

3.2.3 Infra-red spectroscopy (FTIR)

Fourier Transform Infra-red Spectroscopy (FTIR) is an advanced technique aimed at classifying the organic chemical compounds found in various organic substances. This technology is based on the principle that a beam of infrared light is comprised of multiple wavelengths and that specific organic chemical compounds will absorb only one range of wavelengths. This allows the instrument to send a beam of infra-red light through a sample mounted on a substrate and, using a detector on the other side of the sample, read the wavelengths that pass freely though the sample. Calibrating these results with pure, known substances, the wavelengths that are absorbed can be correlated with specific organic bonds (functional groups). One advantage to FTIR analysis is that the user is provided with both qualitative and quantities results. This will not only identify the different functional groups present in the sample, but it will also give some measure of the percentage contained.

When asphalt binder is analysed with FTIR testing, a number of functional groups can be observed within the binder. Table 3.2 contains a comprehensive list of the common groups within asphalt binder (Ouyang *et al*. 2006a; Shakirullah *et al*. 2007; Zhang and Yu 2009; Zhang *et al*. 2011). Since both asphalt and engine oil are hydrocarbons, most of the samples mainly comprise of aromatic and saturated hydrocarbons. The two compounds of most interest are the sulfoxides and carbonyls which peak at 1030 cm^{-1} and 1700 cm^{-1} respectively. These two compounds are commonly used as an indication of the amount of ageing asphalt binder has undergone. As the amount of sulfoxides and carbonyls increase, the binder is shown to age (Ouyang *et al*. 2006b; Wu *et al*. 2009). The increase in either of these two compounds corresponds to an increase in polar compounds of higher molecular size (Cortizo *et al*. 2004).

Table: 3.2: FTIR Compounds and Functional Groups (Ouyang et al. 2006a; Shakirullah et al. 2007; Zhang and Yu; Zhang et al. 2011).

Compound Name	Functional Groups	Spectrum Range (cm^{-1})
Alkanes	C-H	650-910
Butadiene	HC=CH	965
Sulfoxide	S=O	1030
Aromatic Hydrocarbons	C-H, CH_2 and CH_3	1375-1530
Aromatics	C=C	1600
Carbonyl	C=O	1700
Saturated Hydrocarbons	C-H	2850-3000

One reason FTIR testing is useful is because it can provide insight as to the relative levels of maltenes contained in the asphalt samples. Asphaltenes are much larger and more polar then their maltene counterpart (Lins *et al*. 2008). When there is an increase in either the carbonyl or sulfoxide index, there is an increase in the amount of large polar molecules, or asphaltenes, contained inside the binder. As maltenes oxidize, they will tend to form into asphaltenes. This means the FTIR test can be used to quantify the change in the molecular structure inside the asphalt binder from maltenes into asphaltenes.

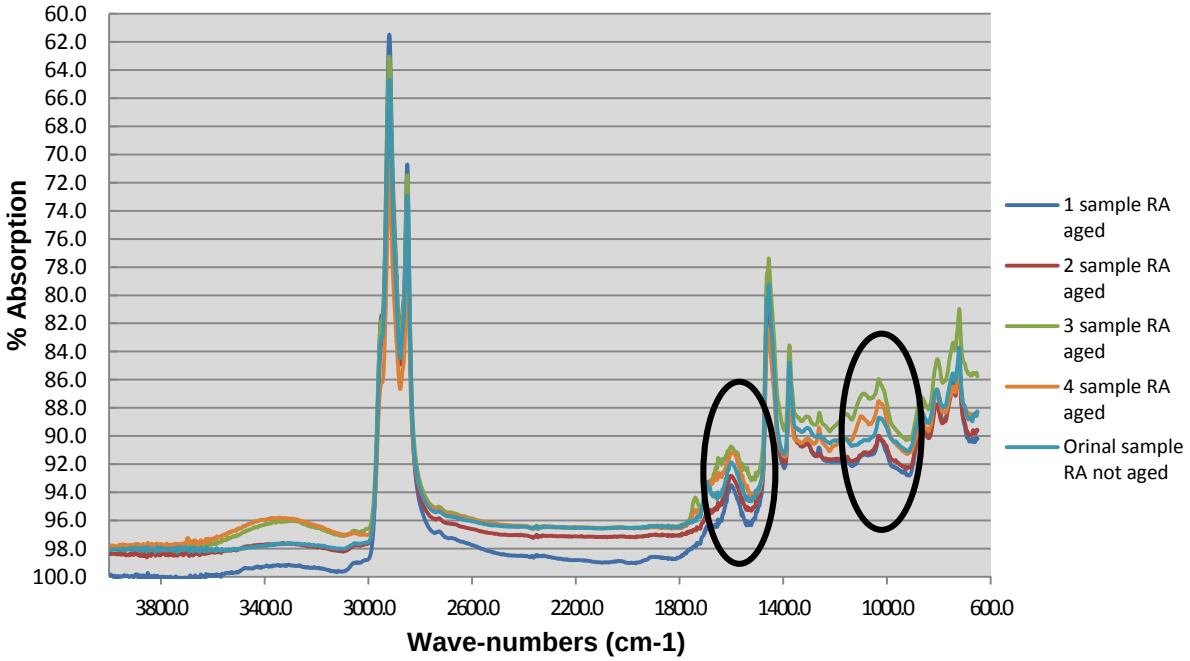

Figure 3.5: FTIR spectrum showing increase in carbonyl/ketone (1700 cm^{-1}) and sulfoxide (1030 cm^{-1}) formation with ageing.

The Fourier Transform Infra-red Spectroscopy (FTIR) can give an idea of the behaviour of a RA mix that has been subject to a period of ageing. The peaks in the circles show how marked the difference in absorption of (C=O) and (S=O) is. The tests were performed at the Department of Chemistry and Polymer Science at the University of Stellenbosch.

Ageing of the RA causes changes in the binder property resulting in hardening of the material. Stiffening of the binder might be desirable but at some critical stage the binder starts to behave in a brittle mode and subjects the asphalt mixture to wear due to its sensitivity to traffic loading and other influences such as water damage (Ouyang *et al*. 2006b; Wu *et al*. 2009).

Oxidation is an irreversible chemical process that changes the molecular composition of binders increasing the binder hardness or stiffness. Compositional change due to oxidative ageing results in the transformation of components from non-polar to more polar fractions. The formation of polar products alters the state of dispersion of the binder's chemical components which also change the chemical reactivity because of change in the mobility of the molecules. Ketones also known as carbonyl (C = O) and sulfoxides (S = O) are the two major functional groups formed during oxidative ageing; they characteristically peak at 1700 cm^{-1} and 1030 cm^{-1} wave number in the FTIR spectrum respectively. The formation of ketones and sulfoxides shows an increase as a function of ageing time and the sum of the area under the characteristic IR peaks can be used as an indicator for rating the degree of sensitivity of binders to oxidative ageing (Wu *et al*. 2009; Zhang and Yu, 2009).

3.2.4 Bitumen recovery and extraction of the binder

The binder characteristics in the mixture cannot be examined easily without full separation of bitumen from aggregates. Full extraction therefore, has to be performed to recover the bitumen from the mix or RA to enable examination of its rheological properties. Full extraction implies the use of a particular solvent, and equipment to separate bitumen from aggregates. In preparation for the recovery of bitumen from RA mixtures, the following activities were performed:

- the RA was crushed into a loose mixture, and
- the material was split into small portions of 3.5 kg and soaked with extraction solvent. In this study, trichloroethylene was used to dissolve and wash the binder from the mineral aggregates.

The extraction and recovery process was conducted in the Much Asphalt central laboratory located in Eersterivier, Western Cape. At Much Asphalt, the rotary vapour method is used after cold centrifuge. The extraction and recovery procedure can be aggressive and they could possibly lead to the following effects:

- the filler part is not completely separated from the bitumen;
- some trace of solvent can remain in the bitumen resulting in softer bitumen;
- possible oxidation effects in the bitumen.

Therefore, additional measures were taken to minimise the speculated causes by carrying out the following procedures:

- A small dry mass of 3.5 kg was dissolved in the trichloroethylene solvent and left soaking for 1–2 hours to ensure that all the binder adhered to the filler was dissolved before extraction;

- Several cycles of capturing filler from the centrifuge were performed to ensure all filler has been separated from the binder. The weight of the empty cup and the cup with filler was taken after every cycle and dried in the oven and the filler weight was determined. It was realised that six to seven cycles were needed to reduce filler from the bitumen liquid (bitumen and solvent) to 0.5% - 1.5%; a cycle means one time desiccation of filler from 3.5 kg of material.

The recovery of bitumen from the liquid phase was achieved through the evaporation method (DIN EN 126997-3). The recovered binder content for the RA mixed in the laboratory ranged between 4.9 % and 5.2 %.

3.2.5 Penetration, softening point and viscosity test methods

Penetration, softening point (ring and ball temperature test) and dynamic viscosity are common test methods used to characterise bitumen properties. The age hardening of bitumen can be described from the change in the values obtained from these tests.

The penetration test provides one measure of the consistency and hardness of asphalt binder. The test for asphalt (ASTM D-5, IP 49) is a commonly used consistency test. One set of tests was done per sample of recovered bitumen. The softening point test was performed according to ASTM D36. The dynamic viscosity test was done according to ASTM D4402 using a Brookfield Model. Viscosity is also termed to be a measure of deformation of fluid due to shear stress or tensile stress, and is a fundamental parameter in the investigation of the rheological properties of bitumen.

Table 3.3 shows the average rheological properties of the RA created in the laboratory at the University of Stellenbosch.

Table 3.3: Rheological properties of the bitumen extracted from the RA mixed in the laboratory before and after ageing procedure.

Properties	**RA properties before ageing procedure**	**RA properties after ageing procedure**
Penetration 25°C (dmm) ***(ASTM D5)***	61	33
Brookfield Viscosity at 60°C (Pa·s) ***(ASTM D4402)***	295.0	251.8
Brookfield Viscosity at 135°C (Pa·s) ***(ASTM D4402)***	0.503	0.379

Softening Point (°C)	58.5	52.2

3.2.6 Mineral aggregates

The mineral aggregates that were used in this study (crushed stone G2 and RA) were subjected to sieve analysis according to TMH1 method B4 (1986).

The technical characteristics of the RA mix, obtained in the laboratory, were compared with the field data obtained from the Central Laboratory of the Much Asphalt facilities in Eersterivier (Western Cape). Tables 3.4 and 3.5 show similar data between the two sources.

The RA was obtained in the laboratory, by mixing a gradation of G2 material with 5% of bitumen with a 60/70 penetration grade. The G2 material used to make the RA was using the same grading characteristics of the 100% G2 material. No additional filler was inserted in the mix. After the ageing procedure implemented in the laboratory, the RA was left cool down. The materials were subsequently crushed using the jaw crusher and then sieved, recreating a realistic grading, which can be found on field applications.

Table 3.4: Comparison of the rheological properties of the bitumen extracted from the RA mixed in the laboratory and the RA from a field source (Much Asphalt).

Properties	**RA from field source (mean value)**	**RA from the US laboratory (mean value)**
Penetration 25°C (dmm) ***(ASTM D5)***	28	33
Brookfield Viscosity at 60°C (Pa·s) ***(ASTM D4402)***	233.2	251.8
Brookfield Viscosity at 135°C (Pa·s) ***(ASTM D4402)***	0.358	0.379
Softening Point (°C)	58.9	52.2

Table 3.5: Comparison of the RA grading sources between US and Much Asphalt.

Sieve size (mm)	100% RA from US	100% RA from Much Asphalt
	Percentage passing (%)	Percentage passing (%)
37.5	100.0	100.00
26.5	99.8	100.00
19.0	95.4	98
13.2	86.0	96
9.5	75.7	85
6.7	65.8	73
4.75	55.0	63
2.36	34.7	46
1.18	19.2	30
0.6	10.4	18
0.425	7.6	11
0.3	5.5	7
0.15	3.0	4.5
0.075	1.5	2.0

For the RA material the fraction larger than 19.0 mm was in the order of approximately 10 % (oversize material). The washed grading curves of the crushed stone G2 and RA are provided in Table 3.6. Figure 3.6 shows the gradation of the aggregates. The gradation was monitored during the mix design and testing process to ensure uniformity. Scalping material off has the disadvantage that the grading used for the laboratory testing is not the same as the grading in the field. However, consistency of results took priority over representative of field mixes.

The minimum amount of filler that can be expected in 100% RA mix is 1% passing the 0.075mm sieve. The use of 100% RA in BSMs is an extreme case in South Africa (lower percentages of RA are normally used) but it was included in the testing matrix here to study the effect of high percentages of RA in BSMs. High percentages of RA are commonly used in rehabilitation projects especially in Europe and United States while in South Africa it is in the order of 30% or lower. When recycling with high percentages of RA, consideration should also be given to other economical and sustainability aspects, which may favour the re-use of RA in an HMA instead of in a BSM application. Fines are necessary for better BSM-foam dispersion

in the mixture. However, excess fines reduce the permeability and drainage capacity, which is another important criterion for a base course (G2). Table 3.4 shows a comparison of the RA grading between the Stellenbosch University and the data obtained from the field and processed at the Much Asphalt laboratory facilities. The percentages of RA retained at the different sieve sizes at the US are close to the values obtained from the field, especially at the lower sieve size.

Table 3.6: Aggregate type and grading of Hornfels-RA and G2 crushed stone.

Sieve size (mm)	**100% RA**	**50% RA + 50% G2**	**100% G2**
	Percentage passing (%)	**Percentage passing (%)**	**Percentage passing (%)**
37.5	100.0	100.00	100.00
26.5	99.8	99.69	99.54
19.0	95.4	92.04	88.69
13.2	86.0	82.15	78.28
9.5	75.7	72.19	68.68
6.7	65.8	61.67	57.57
4.75	55.0	52.28	49.57
2.36	34.7	37.74	40.77
1.18	19.2	26.13	31.76
0.6	10.4	19.52	25.03
0.425	7.6	17.11	22.22
0.3	5.5	14.85	19.69
0.15	3.0	9.90	12.79
0.075	1.5	5.25	6.99

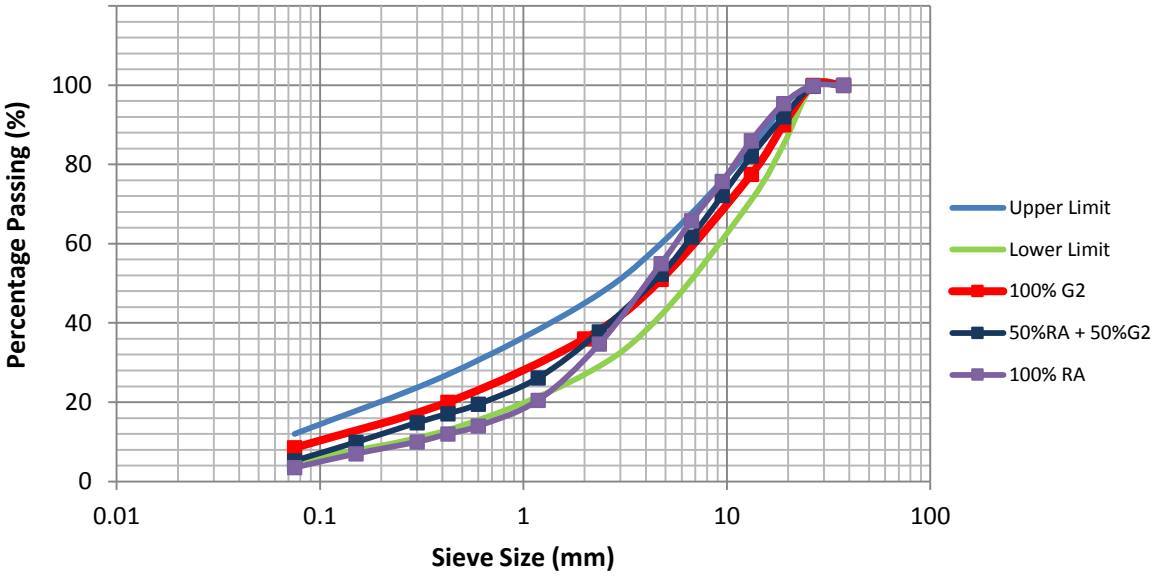

Figure 3.6: Grading curves of Hornfels-RA and G2 crushed stone.

It can be seen in Figure 3.6 that the 100% RA has a big difference in the amount of fine fractions compared with the 100% G2. The grading with 100% RA changes slightly (mainly the percentages under the passing 1.18 mm sieve) from 100% G2 Hornfels crushed stone. This is typically normal in a mix with 100%RA where the percentage of fine is always less than in virgin aggregates. The 100%RA was left to cool down before it was crushed, recreating a grading curve similar to a real RA source coming from Much Asphalt. A small part of fine material was observed to be glued by the old bitumen with the coarser RA gradation. Althought, this glueing effect didn't create any particular problem during the mixing phase, because the fine material remained sticked to the biggest particles. Base-course aggregate (G2) material with maximum aggregate size of 26.5 mm was obtained from the quarry. A comparative grading analysis was performed to investigate any discrepancies on a selected sample in comparison with the grading analysis obtained with the material from Lafarge Tygerberg Quarry. The blend with 50%RA and 50%G2 material was made up of an equal contribution of aggregates from the two different sources. The mixes were constituted according to mass percentages from the fractions discussed above. This ensured that the grading of the mixes and specimens was consistent throughout the study.

Figure 3.7: Crushed stone G2 and Hornfels RA.

Figure 3.7 represents the virgin crushed stone G2 material coming from the Lafarge Tygerberg Quarry and the RA mixed in the laboratory.

3.2.7 Maximum dry density and optimum moisture content

The optimum moisture content (OMC) and maximum dry density (MDD) for the three different mixes were determined by Modified AASHTO compaction. Details on the composition of all three mixtures are listed in Table 3.7. The hygroscopic moisture in the mineral aggregates were 0.7% for the virgin G2 crushed stone material, 0.9% for the 50%RA and 50%G2 and 0.65% for the 100%RA obtained in the laboratory. The MDD obtained by Modified AASHTO compaction is presented in Table 3.7 for all three mixes and it contains the hygroscopic moisture in the mineral aggregates. The correct proportions of fraction were then weighed off to reconstitute a sample thus ensuring a consistent grading across all samples.

Table 3.7: Summary of maximum dry densities (MDD) and optimum moisture contents (OMC).

Mix	**100%RA**	**50%RA 50%G2**	**100%G2**
Optimum Moisture Content (%)	4.05	5.7	5.7
MDD (kg/m^3)	2 006	2 195	2 335

The Modified AASHTO curve for the 100%RA mix indicates a well defined optimum at 4.05% moisture with a maximum dry density of 2006 kg/m^3. The optimum moisture content for the 50%RA and 50%G2 mix is determined at 5.7% of moisture as well as the 100%G2 blend. The density for these two last mixes is really close to each other due to the high presence of more fine material in the G2 than in the 100%RA. The high density (MDD) in the 100%G2 is more explicable with a particular observation that was made during the phase of preparation and compaction of the specimens. This is a general behaviour for granular materials. It was visually established that at all high moisture contents the materials appeared wet and were over the optimum moisture content.

Water has three specific roles in BSM-foam mixes.

- First, when introduced to the hot asphalt, water induces foaming. Foaming water content is the 2-3% water mass/mass to binder needed for foaming of the bitumen binder.
- Second, the optimum moisture content (OMC) is the water needed to act as a dispersion agent during mixing. The mixing water also works as a carrier for the foam droplets within the aggregate. The OMC is needed for adequate dispersion of BSM-foam in the aggregate (Fu *et al*., 2009).
- Third, the optimum moisture content (OMC) provides workability and compactibility for the BSM-foam mixture. Similar to any granular material, compactibility of BSM materials is governed by their conventional moisture – density behaviour i.e. the water

alone provides lubrication. The maximum dry density (MDD) is achieved at optimum moisture content (OMC).

The OMC and MDD were determined without the presence of BSM-foam and cement in the mix. Adding the BSM-foam in the mixtures moves the OMC to slightly higher values (1% more), which is necessary to hydrate the cement in the mixes. Additional moisture influences the dispersed energy of the bubbles of the BSM-foam to the moist surface for better spread and coating on the filler.

The maximum dry density for the 100%RA mixture was quite low due to the grading properties of the RA, where the amount of fine particles is averaging on low percentages. Most of the original fine material, mixed during the preparation of the RA, was found to be glued to the coarser RA particles.

Appendix H shows the Mod AASHTO compaction test results obtained for the three BSM-foam mixes with an increasing amount of RA.

3.3 Bituminous binder

Bitumen from the Chevron refinery, 80/100 pen grade, was used for the foaming process in the mix design to determine a suitable compaction binder content for the candidate materials. The rheological properties of the bitumen are presented in Table 3.8. A decision was made to use only the one penetration grade bitumen in the mix design using the assumption that the volumetric and ITS strength values would be the same as investigated by other previous extensive research programs at the University of Stellenbosch (Ebels, 2008; Moloto, 2010; Twagira, 2010).

Table 3.8: Bitumen properties (80/100 pen grade) used in the BSM-foam mixes (Chevron, South Africa).

Inspection	Test Method	Limits
Ductility (cm)	ASTM D113	100 min
Flash Point, (°C)	ASTM D92	225 min
Loss of Heating (% mass)	ASTM D6	0.5 max
Penetration (0.1mm)	ASTM D5	80 to 100
Penetration of residue after loss on heating (% of original)	ASTM D6	80 min
Softening Point (°C)	ASTM D36	45.0 – 52.0
Solubility in trichloroethylene (% mass)	ASTM D2042	99 min
Specific Gravity @ 25/25°C	ASTM D70	1.00 to 1.05

Viscosity at 60°C (Pa.s)	ASTM D4402	75-150
Viscosity at 135°C (Pa.s)	ASTM D4402	0.15 – 0.4

3.4 Mixing Process

2% residual binder content of foam bitumen was applied for stabilisation of the 100%RA mix. 2.1% of foam was used in the mixing of the 50%RA and 50%G2 blend and 2.3% of foam bitumen for the 100%G2 crushed aggregates. All three blends were previously mixed with 1% of cement and 75% of their optimum moisture content. Figure 3.8 shows the mixing process carried out in the laboratory.

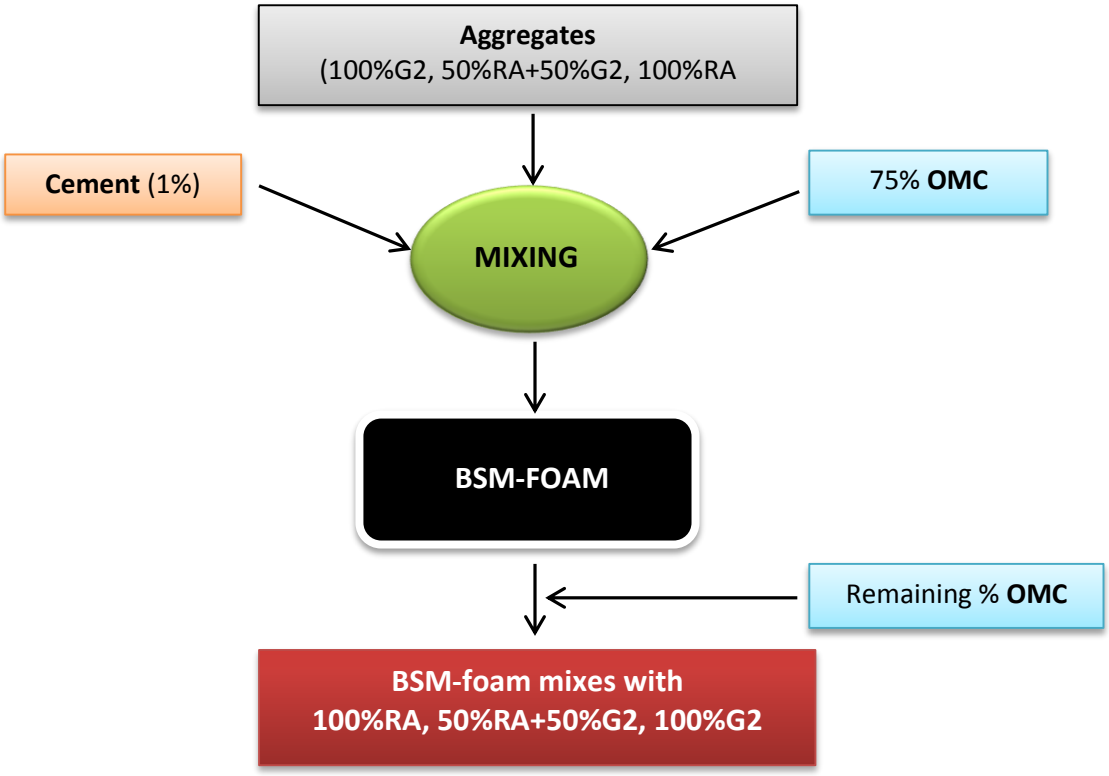

Figure 3.8: Mixing process.

The lower binder content for the mix with a high percentage of RA was chosen because of the difference in grading of the other two blends through the mix design. The fact that the RA particles already have a film of old bitumen also plays a role. The old bitumen film may perhaps not have a "glueing" effect, but it reduces absorption of fresh bitumen and results in a greater affinity between the fresh bitumen and the RA particles than what would be the case for virgin crushed stone materials. This resulted in a total of three different aggregate blends combined with three different binders. At the end of the foam treatment, the remaining water percentage was added to the mix with the scope to achieve the OMC of every single mix.

The BSM-foam was produced in a Wirtgen® laboratory foamed bitumen dispenser (WLB 10 S) as shown in Figure 3.9. This mobile foam plant has been developed to produce small quantities of foam bitumen under laboratory conditions (Wirtgen, 2010). The foamed asphalt was mixed together with aggregates (100%RA, 50%RA and 50%G2, 100%G2) in the laboratory-scale twin-shaft pug-mill mixer WLM 30 (Figure 3.9). This mixer has the capacity of 30 kg.

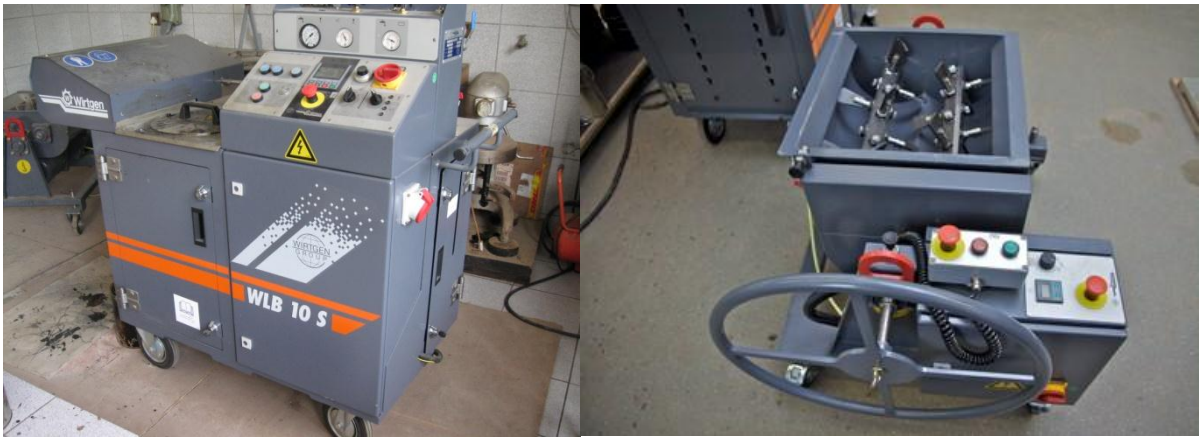

Figure 3.9: Laboratory scale foam bitumen plant WLB 10S and pug-mill mixer WLM 30.

Before production of foam bitumen, the foaming properties of bitumen viscosity (expansion ratio) and stability (half-life) are determined using 2% foamant water, by mass percentage of the bitumen. The bitumen was found to have an expansion ratio of 13 times and a half-life of 15 seconds (Figure 3.10). The short half-life of foamed bitumen can negatively influence the durability properties of BSM mix (Twagira 2010). In fact the dispersion and wettability potential during mixing is influenced by the foam properties. Short half-life reduces dispersion, resulting in balling on collapsed bubbles, in turn resulting in no coating. Foaming of the bitumen took place at temperatures between 155 and 160°C.

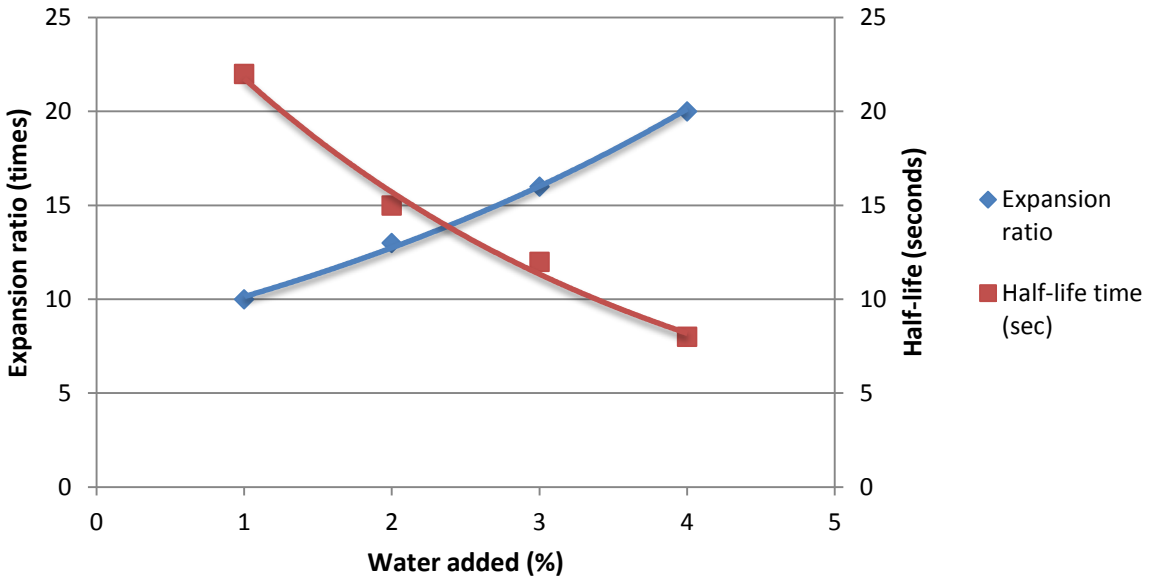

Figure 3.10: Foaming properties of bitumen 80/100.

3.5 Compaction

The compaction of BSM-foam was carried out using a vibratory BOSCH® compactor. The advantages of using a vibratory hammer are discussed in detail in the literature review (Chapter 2). The conclusion drawn was that the modified BOSCH® compactor is a useful tool for the compaction of BSMs. It has higher point energy, which requires low compaction effort to obtain an equivalent level of compaction compared to other methods. Secondly, the higher point energy significantly influences the wettability (coating) of the binder (mastic) into the aggregate surface. Lastly, it is relatively easy to use and simulates field compaction. The complete compaction protocol is reported in TG2 Asphalt Academy (2009) and Kelfkens (2008). The prepared tri-axial specimens were compacted in five layers of 50 mm thick, each layer compacted to target density. The target density was achieved by measuring the amount of material required to achieve 100% of the Modified AASHTO compaction (TMH 1, 1986).

3.6 Curing

The samples were cured under accelerated curing conditions at 30°C for 20 hours unsealed and two days sealed at 40°C as specified by the TG2 manual (Asphalt Academy, 2009). The accelerated curing process simulates in-field curing and is deemed appropriate to simulate the realistic strength gain for BSM-foam. After curing, the samples were securely placed within a sealed plastic bag, and kept intact until testing. The oven cured samples were tested within two days after curing was completed. Efforts were made to ensure that the period between curing and testing remained constant in all cases. Before testing, all the specimens cured and sealed in a bag were placed in a controlled temperature envinroment at the temperature of 25°C. Moisture contents were tested for each sample before and after compaction.

Figure 3.11: ITS and Tri-axial specimens at the end of their curing period.

3.7 Indirect Tensile Strength Configuration

The Indirect Tensile Strength test (ITS) is used to determine the tensile strength of BSMs materials. Cylindrical specimens are loaded in the diametral plane as shown in Figure 3.12.

Figure 3.12: ITS test set-up.

The ITS test is a displacement-controlled test in which a monotonic load is applied to specimens. Figure 3.13 shows a typical ITS curve.

Test conditions are as follows:

- loading rate 50 mm/minute;
- temperature 25°C.

The mechanical testing was undertaken in the servo-hydraulic UTM-25 (Universal Testing Machine - IPC®) at the University of Stellenbosch. The UTM-25 consists of a hydraulic system, being able to provide a maximum compressive load of 25kN. The UTM-25 is formed by a climate chamber containing a thermal load cell, a set the frames for testing, a monitoring system connected to a computer, and a unit for air conditioning (range -15°C to 60°C).

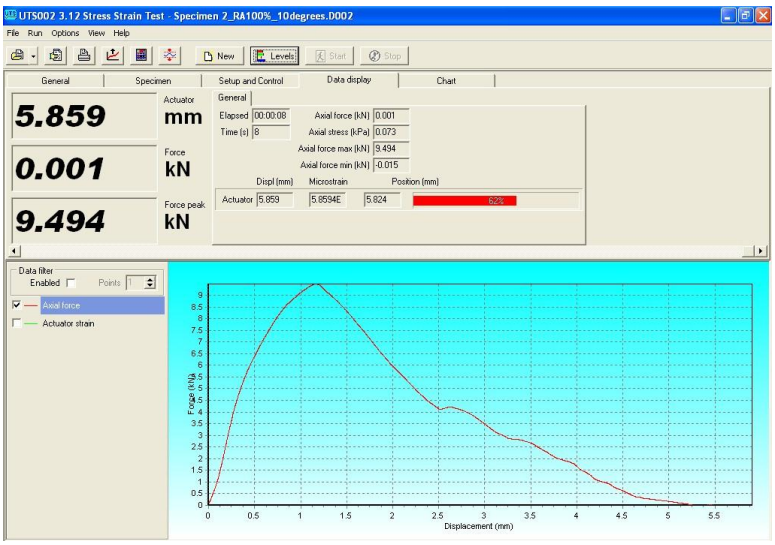

Figure 3.13: Typical ITS curve showing load and displacement (IPC® software).

To determine the maximum strength, the actuator of the UTM-25 contains an LVDT which is able to measure the loading curve directly through a computer. The loading is applied through a hydraulic piston which is able to move from the top down. Figure 3.14 shows the UTM-25 machine with temperature chamber and computers.

Figure 3.14: Universal Testing Machine 25KN - IPC®.

3.8 Tri-axial testing

The tri-axial testing was carried out on a hydraulic testing system (MTS). This testing system is a closed loop servo-hydraulic testing press system. The system uses a hydraulic power unit with a high pressure supply. The loading capacity of the MTS is 10 metric tons or 98.1kN with an actuator of 80 mm stroke (up and down). The MTS is operated and controlled by an MTS Controller 407. The measuring range of the load cell and MTS in-built LVDT can be adjusted to suit the testing range. This is done by increasing or decreasing the gain for either of the measuring devices. Increasing the gain results in a smaller measuring range and therefore a higher level of accuracy is achieved. The loading and displacement test data of the load cell, MTS actuator (in-built LVDT) and external LVDTs are captured by a Spider 8 device, an amplifier that converts analogue voltage data to digital using a 12-bit A/D converter and displays the data in real-time on a computer. Data from the tests (load cell and MTS LVDT) can be captured on computer while the tests are in progress in a Microsoft® Excel format. Figure 3.15 presents the MTS in a climate chamber (a), the tri-axial cell used in all the tests (b), the MTS controller (c) and the Spider 8 unit to capture all the data live (d). The measuring range of the load cell and the MTS LVDT can be adjusted to suit the testing range. This is done by increasing or decreasing the gain for either of the measuring devices. Increasing the gain results in a smaller measuring range and therefore a higher accuracy.

For the monotonic tri-axial testing the load cell gain was set to measure over the full capacity (98.1 kN), while the LVDT gain was set to measure over 50 % of the full range (80 mm).

(a) (b)

(c) (d)

Figure 3.15: MTS loading system set-up and tri-axial cell.

To measure the dynamic displacements during testing, three LDVTs with a range of +/- 2.0 mm were fitted to the specimens, and equally distributed around the circumference, to measure the displacements over the middle 100 mm of the specimen only (Figure 3.16). By doing so, attempts were made to exclude side effects, such a displacement / movement of the loading plates, internal displacements of the tri-axial cell and edge effects of the specimens were tried to be included from the measured displacements through the use of two circumferential LVDTs gauges with a range of +/- 5.0 mm. The manner in which the on-specimen LVDTs were fitted to the specimens is discussed in Appendix C.

During permanent deformation tests, the same set-up of gauges used in the resilient modulus tests were applied to the specimens.

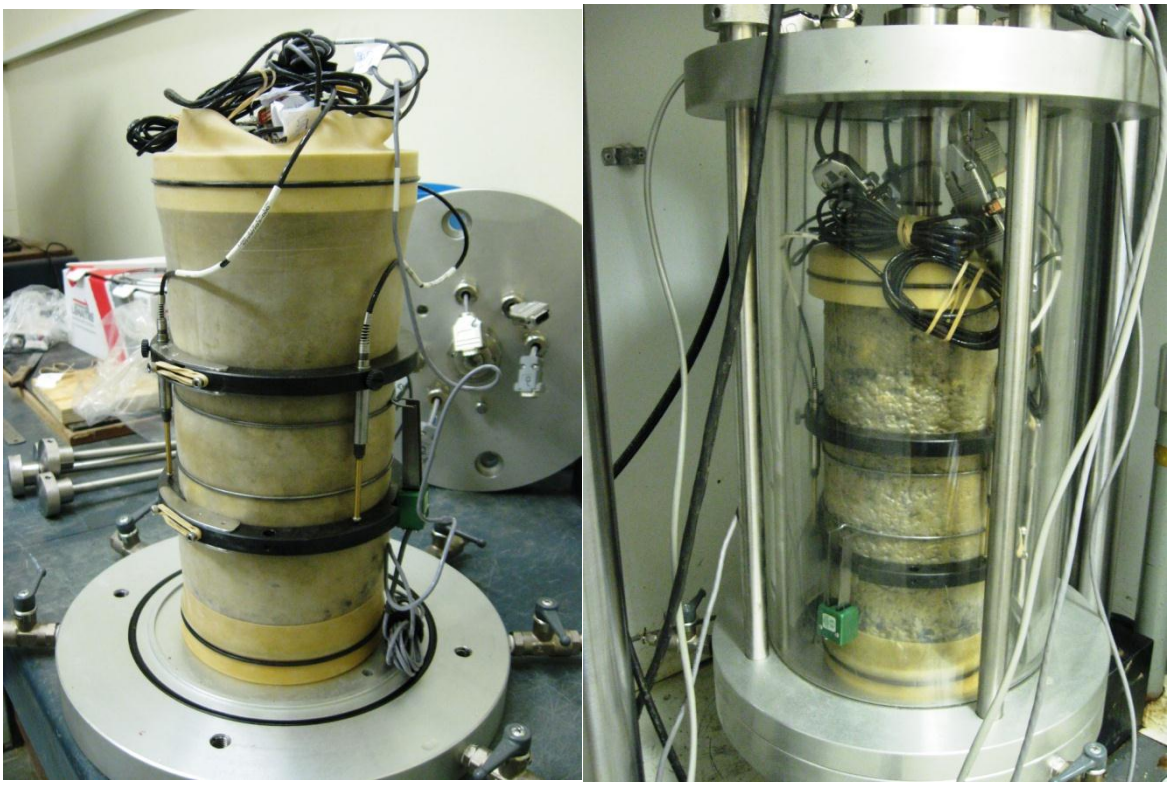

Figure 3.16: Vertical and circumferential LVDTs for resilient modulus tests.

The circumferential LVDTs were not fitted around the specimens due to the high risk to get permanent damage for the high load rating application.

The tri-axial cell used in this research has a maximum rating pressure of 1700 kPa. A sample with a maximum diameter of 150 mm and a height of 300 mm can be accommodated in the cell. The MTS is situated in a climate chamber, where temperature can be controlled between 0°C and 60°C. The temperature variable in this study was between 10°C and 40°C. These temperatures were found to be common in the BSM base layers. Twagira (2010) presented in his thesis a case study related to real temperature measurements conducted on the N7 expressway near Cape Town. The temperature data recorded in a full cycle of different seasons (i.e. from winter to summer and winter) showed a maximum measured temperature of 49.6°C in the BSM layer during the summer season and a minimum temperature of 9.6°C during the winter period.

No friction reduction between the specimen and the loading plates was applied in this study due to the granular nature of the specimens. The friction between the specimen and loading plate was however kept as constant as possible by thoroughly cleaning the loading plates after each test and ensuring the same conditions at the start of every new test.

The measuring scale setting of the load cell and MTS LVDT for the three types of tri-axial testing are summarised in Table 3.9.

Table 3.9: Scale settings of load cell and MTS LVDT for tri-axial testing.

Testing Mode	**Range settings**	
	Load cell MTS	*LVDT*
Monotonic testing to failure	100% = +/- 98.1 kN	50% = +/- 40 mm
Short duration repeated load testing	20% = +/- 19.6 kN	3 external LVDTs placed around the specimen in the middle third
Long duration repeated load testing	20% = +/- 19.6 kN	3 external LVDTs placed around the specimen in the middle third

3.8.1 Monotonic tri-axial test method

Monotonic tri-axial tests were carried out at 25°C and the specimens were conditioned at this temperature overnight. All the specimens were tested in unsoaked conditions. The test is performed with a controlled constant strain rate of 2.1% per minute. For a typical height of 300 mm this results in 6.3 mm per minute. This strain rate has in the past been used for numerous monotonic tri-axial tests in South Africa (Jenkins, 2000; Ebels, 2008; Twagira, 2010) and in order to eliminate any possible variables in the comparison of the results of this study with that of other studies, the same strain rate was adopted here. Confinement pressure was provided by regulating the air pressure in the tri-axial cell. A set of three monotonic tri-axial tests for every BSM-foam mix were carried out over a range of confinement pressures. The confinement pressures at which the tests were carried out were:

- 50 kPa;
- 100 kPa, and
- 200 kPa.

Immediately after completion of a set of monotonic tests (one series with three different confinement pressures) the tested specimens were broken up and a sample for the determination of the moisture content was taken from the middle of the specimens. Figure 3.17 shows the set-up configuration of a monotonic tri-axial test.

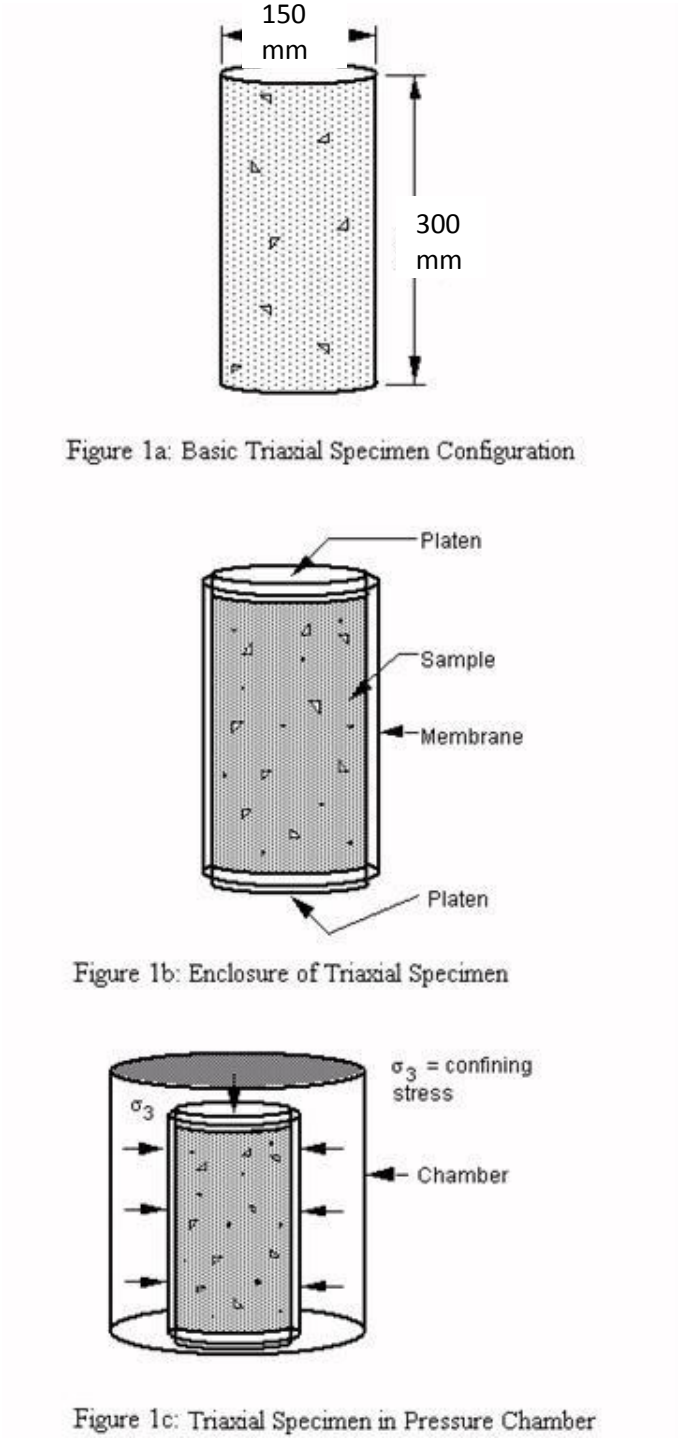

Figure 3.17: Set-up configuration during a monotonic tri-axial test (Fu, P., Jones, D., Harvey, J.T., and Bukhari, S.A. 2009).

3.8.2 Repeated load tri-axial test for the determination of resilient modulus

Dynamic tri-axial tests were performed for each of the three BSM-foam mixtures. Due to the nature of the test preparation, these tests have to be prepared accurately, fixing all the external LVDTs and gauges in the proper manner. They were therefore performed at different temperatures and different confinements. The dynamic tri-axial tests were carried out at 10, 25 and 40ºC. The confinement pressures were the same three of the previous monotonic tri-axial tests. The deformation in the specimen was measured by an external system of on-specimen LVDTs and circumferential gauges. The loading consisted of a continuous haversine load with a pre-load of 20% of the confining pressure was applied with frequency of 1 Hz. The decision to use only one frequency was taken due to the guidelines presented in the "Proposed Protocol for Resilient Modulus and Permanent Deformation Characteristics of Unbound and Bound Granular Materials" (CSIR 2011). 1 000 conditioning repetitions were applied using a haversine shaped load pulse consisting of 0.1 second followed by 0.9 second rest period. The haversine load pulse is proposed for conducting the test since it simulates the stress state under a dynamic wheel loading better. In the AASHTO T307 and in the NCHRP 1-28A procedure, a haversine load pulse with 0.1 second loading and 0.9 second rest period is generally applied on the specimens. The use of a rest period attempts to simulate the pauses in between wheel loads and because some delayed elastic recovery can be expected in BSMs due to the presence of bitumen in the mix.

The selection of stress levels for the resilient modulus test was related to the type of BSM-foam tested in the monotonic tri-axial tests. The cyclic stress has to be specified as a ratio to the average failure deviator stress ($\sigma_{d,f}$) obtained from a monotonic tri-axial test, performed on replica specimens at a similar confining pressure and prepared in the same way as those for the resilient modulus test, i.e $\sigma_{cyclic} = 0.3\sigma_{d,f}$.

The initial stage, called the conditioning stage, consisted of 1 000 cycles of loading and unloading. This was followed by specific stress regimes. For the subsequent loading stages after the conditioning, 100 cycles of loading and unloading were applied to the specimens, using a haversine shaped load pulse consisting of 0.1s followed by 0.9s rest period. The actual confining pressure and deviator stress were according to the three different BSM-foam mixes. If at any time the total permanent strain of the specimen exceeded 5%, the test was stopped and the results reported. At the end of every 100 cycles the average recovered deformation for each LVDT for the last five cycles were recorded. The data were sampled at a rate of 200Hz.

During all these tests the data were recorded in a Spider 8 analogue data acquisition system and the tests were performed using a MATLAB® program developed locally at the University of Stellenbosch. The program was able to set-up different haversine load pulses with different loading and unloading times. In all the tests the same configuration of 0.1s loading and 0.9s rest period was carried out.

Tentative to record radial expansion have been carried on all the specimens but without good success. Strain gauges of +/-5mm were mounted around the specimens in the middle third surface area. The data were always recorded through the Spider 8 as well as the three vertical LVDTs displacements.

After testing, the external gauges and the membrane were removed from all the specimens. The entire specimen was then broken and used for moisture content determination.

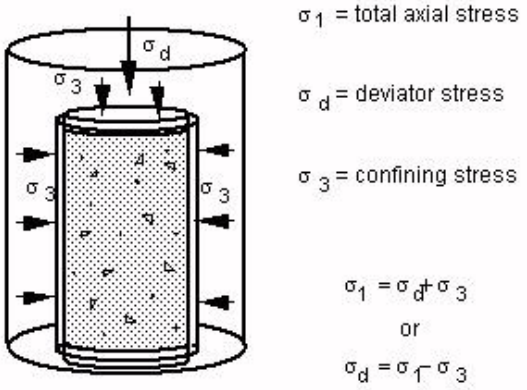

Figure 2a: Stresses Acting on Triaxial Specimen

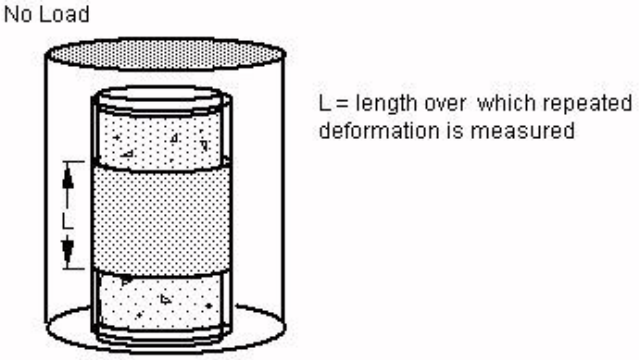

Figure 2b: Gage Length for Measurement of Strain on Triaxial Specimen

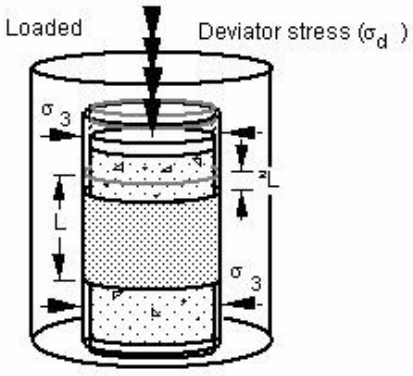

Figure 2c: Deformation of Triaxial Specimen Under Load

Figure 3.18: Setup configuration during a dynamic tri-axial test (Fu, P., Jones, D., Harvey, J.T., and Bukhari, S.A. 2009).

During the dynamic tri-axial tests the response of the specimen to different levels of loading at a range of confinement pressures were measured. These confinement pressures are the same as

used during the monotonic testing. The load level during the dynamic tri-axial test is described by the deviator stress ratio. This is the ratio between the applied deviator stress and the deviator stress at failure:

$$Deviator\ stress\ ratio = \frac{\sigma_{d,a}}{\sigma_{d,f}} \quad [3.1]$$

where:
$\sigma_{d,a}$ = applied deviator stress = $\sigma_1 - \sigma_3$ [kPa]
$\sigma_{d,f}$ = deviator stress at failure = $\sigma_{1,f} - \sigma_3$ [kPa]

$\sigma_{d,f}$ is derived from the cohesion and friction angle as determined by the monotonic tri-axial testing. The confinement pressures and deviator stress ratios at which the resilient moduli were determined are summarised in Table 3.10.

Wave Form: Haversine with rest period

Load pulse: 0.1 s
Rest period: 0.9 s

Temperature: 10, 25 and 40 °C

Table 3.10: Example of loading schedule for the resilient modulus test on BSM-foam mixes

Loading Sequence	Confining pressure (kPa)	Contact Stress (kPa)	Contact Load (kN)	Stress Ratio (%)	Cyclic Stress (kPa)	Cyclic Load (kN)	Load Repetitions
Conditioning	100	10	0.18	30	312.99	5.53	1000
1.1	200	20	0.35	50	528.30	9.34	100
1.2	200	20	0.35	40	422.64	7.47	100
1.3	200	20	0.35	30	316.98	5.60	100
1.4	200	20	0.35	25	264.15	4.67	100
1.5	200	20	0.35	15	158.49	2.80	100
2.1	100	10	0.18	40	417.32	7.37	100
2.2	100	10	0.18	35	365.16	6.45	100
2.3	100	10	0.18	30	312.99	5.53	100
2.4	100	10	0.18	25	260.83	4.61	100
2.5	100	10	0.18	20	208.66	3.69	100
2.6	100	10	0.18	15	156.50	2.77	100
3.1	50	5	0.09	35	350.70	6.20	100
3.2	50	5	0.09	30	300.60	5.31	100
3.3	50	5	0.09	25	250.50	4.43	100
3.4	50	5	0.09	20	200.40	3.54	100
3.5	50	5	0.09	15	150.30	2.66	100

Care was taken not to overstress the specimens at the lower confinement pressures and therefore the resilient modulus testing at the 50 kPa confinement pressure was limited to deviator stress

ratios of up to 35%. Only when the permanent deformation in the specimen was limited, resilient moduli data could be sampled at the high deviator stress ratios of 50% 200 kPa confinement pressure.

The following definitions are used throughout this research:

- Haversine Shaped Load Form: the required load pulse form for the resilient modulus test. The load pulse is of the form [(1 – cosθ)/2], and the cyclic load (P_{cyclic}) is varied from a seating load ($P_{contact}$) to the maximum load (P_{max}), as shown in Figure 3.19.

- Maximum Applied Load (P_{max}): the maximum total load applied to the sample, including the contact and cyclic loads.

$$P_{max} = P_{contact} + P_{cyclic} \quad [3.2]$$

- Contact Load ($P_{contact}$): the vertical load placed on the specimen in order to maintain contact between the loading strip and the specimen.

- Cyclic Load (Resilient Load, P_{cyclic}): load applied to a test specimen which is used to calculate the resilient modulus.

$$P_{cyclic} = P_{max} - P_{contact} \quad [3.3]$$

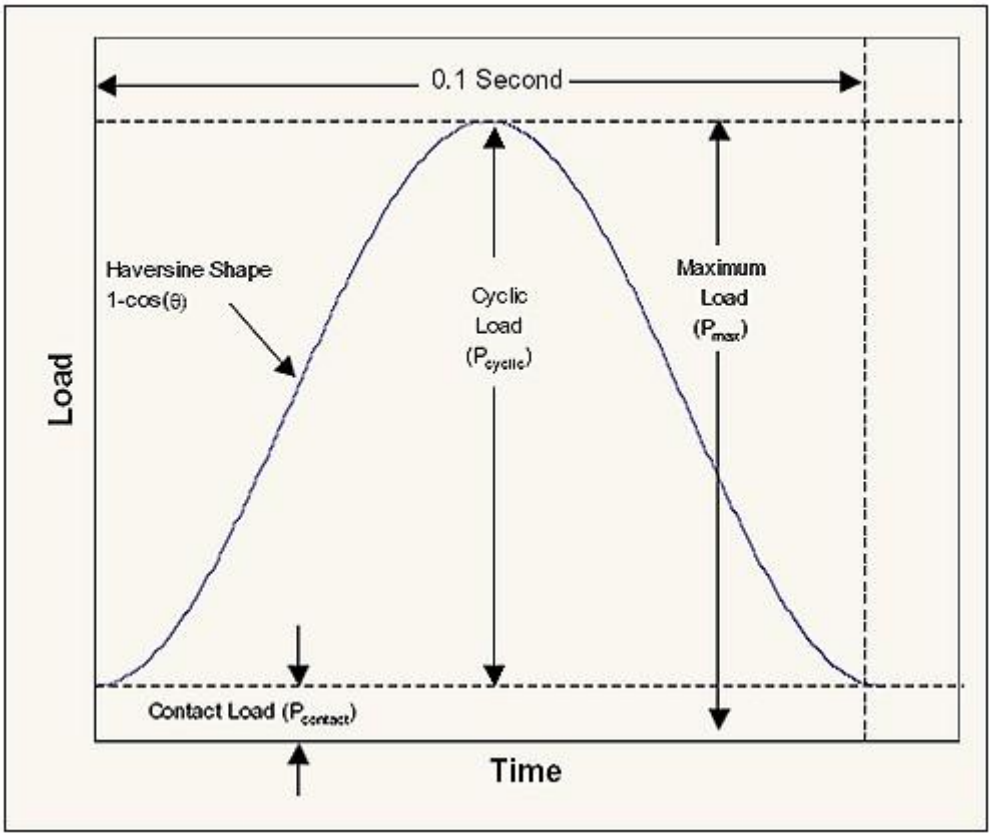

Figure 3.19: Definition of load pulse terms.

- Instantaneous Resilient Modulus: determined from the deformation-time plots (both horizontal and vertical) using the instantaneous resilient deformation, obtained in the manner indicated in Figure 3.20 and described herein. For each cycle, two regression lines are used to determine the instantaneous and total deformations. The range for regression line 1 starts at the 5th point after the maximum deformation value and ends at the 17th point after the maximum deformation (13 points total). The range for regression line 2 includes the last 299 points of the cycle and the first point from the following cycle. For each cycle, the instantaneous deformation is calculated by subtracting the deformation value at the intersection of regression lines 1 and 2 from the maximum deformation. A typical deformation versus time graph for resilient modulus testing is shown in Figure 3.21.

- Total Resilient Modulus: determined from the deformation-time plots using the total resilient deformation, obtained in the manner indicated in Figure 3.20 and described herein. For each cycle, the total deformation is calculated by the deformation value of regression line 2 at the first point of the next cycle from the maximum deformation. This value includes both the instantaneous recoverable deformation and the time -dependent continuing recoverable deformation during the rest-period portion of one cycle.

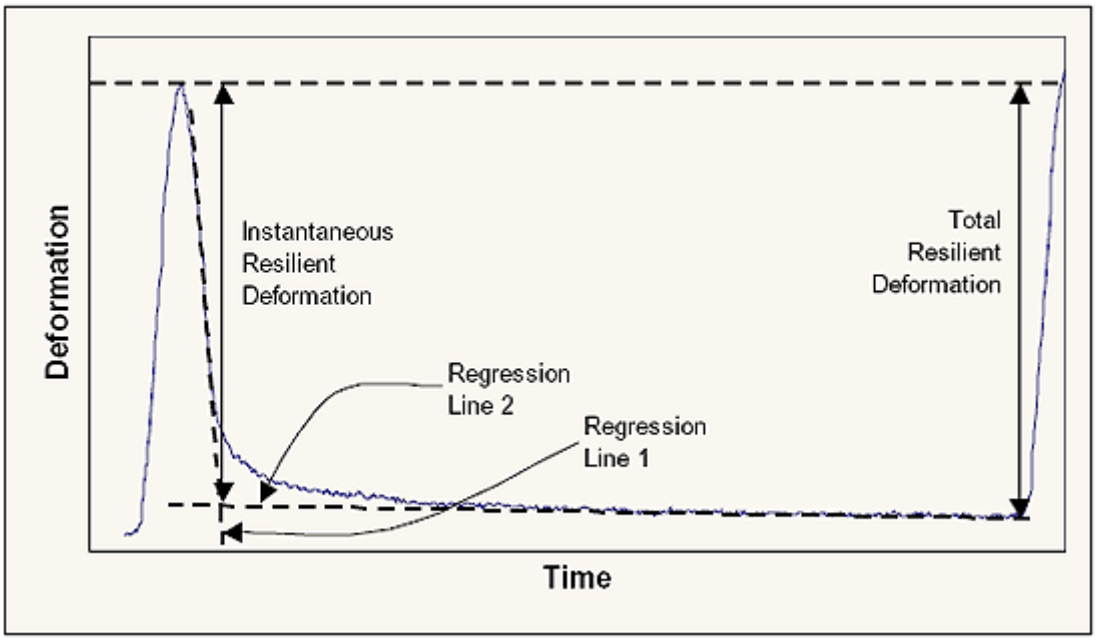

Figure 3.20: Instantaneous and total resilient deformations.

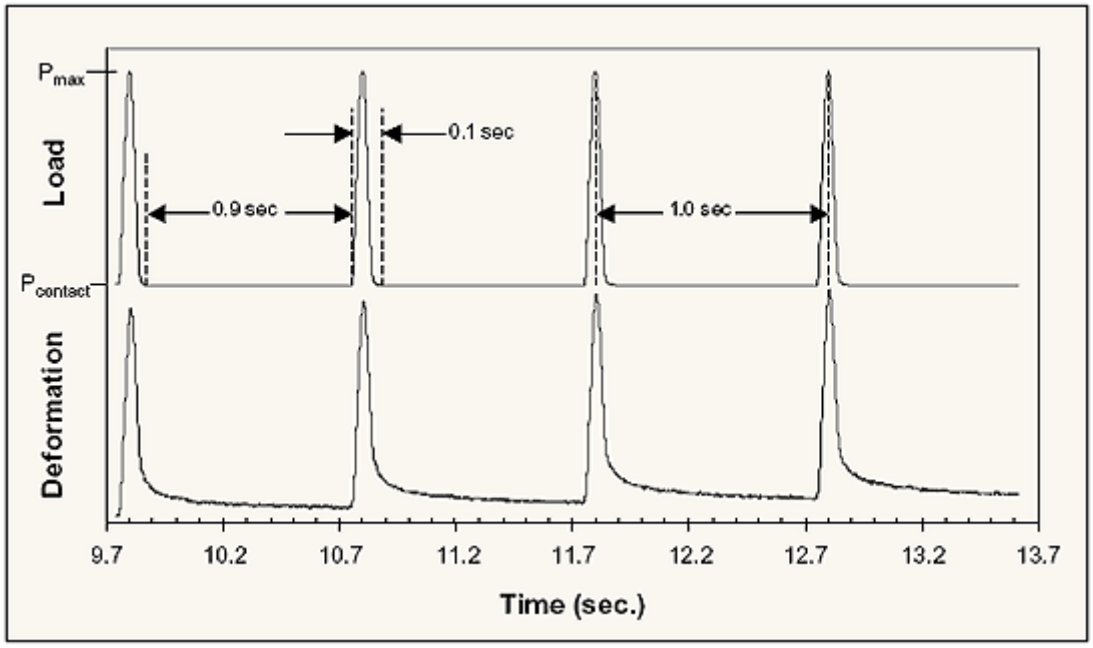

Figure 3.21: Typical resilient modulus test at the temperature of 25°C.

A pure elastic material can be characterised by a spring with a spring stiffness and which obeys Hooke's Law:

$$\sigma = E\varepsilon \qquad [3.4]$$

where
σ = stress
ε = strain
E = Modulus of Elasticity or Young's Modulus

A pure viscous material is characterised by a dashpot with a certain viscosity and obeys Newton's Law:

$$\sigma = \lambda\,(\partial\varepsilon/\partial t) \qquad [3.5]$$

where
λ = viscosity
t = time

Several material models, consisting of combinations of springs and dashpots, have been developed to describe visco-elastic behaviour of a material. Burgers Model (2005) is a combination of Maxwell and Kelvin-Voigt (delayed elastic model) models in series. The Burgers Model consists of three parts, *i.e.* an instantaneous elastic part, a viscous part and a delayed elastic part. The Burgers Model represents the behaviour of a visco-elastic material well. However, it is quantitatively not sufficient to cover the long period of time over which retarded strain takes place. For this a number of Kelvin-Voigt Models in series may be required, which is called the Generalised Model (Huang, 1993). The models listed above are shown in Figure 3.22.

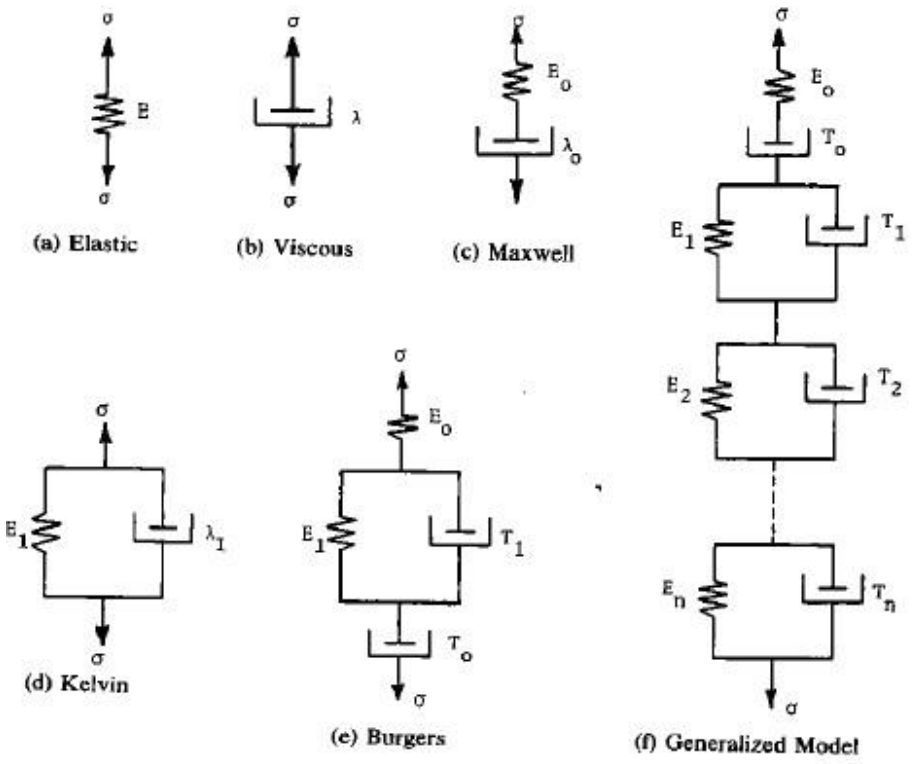

Figure 3.22: Mechanical models for visco-elastic materials (Huang, 1993).

– Tensile Strength: the strength shown by a specimen subjected to tension, as distinct from torsion, compression, or shear. A typical load versus deformation plot for indirect tensile strength testing is shown in Figure 3.23.

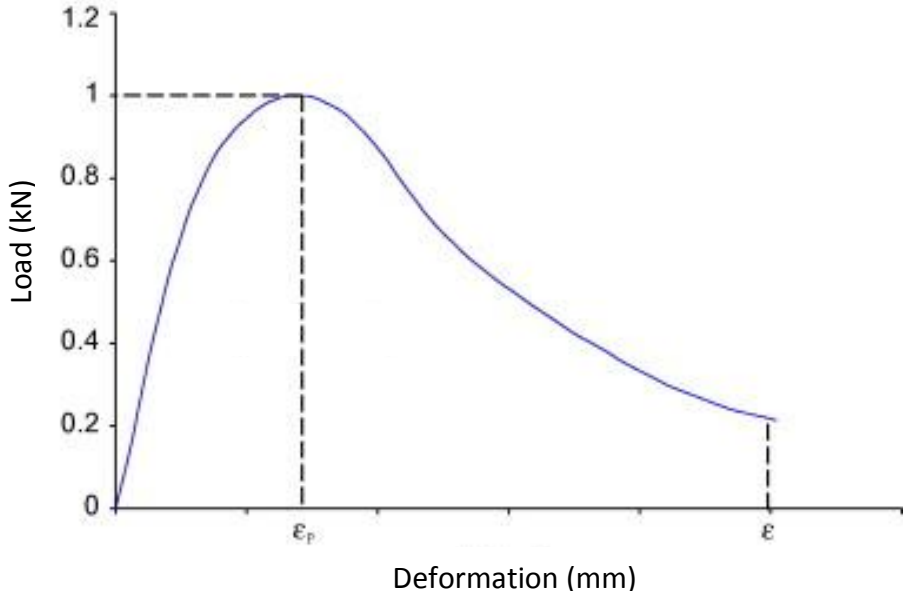

Figure 3.23: Typical indirect tensile test.

3.8.3 Repeated load tri-axial test for the determination of permanent deformation

The test consists of applying a large number of repeated axial loading cycles on the same specimen. The objective of the test procedure is to determine the permanent deformation behaviour of the BSM-foam mixes as a function of the number of repeated loading cycles at different stress levels for the purpose of examining the stress-dependent permanent strain characteristics of the tested material. This method uses the single stage procedure in which one single stress path is repeatedly applied on the same specimen. The number of tests to perform depends on the type of material. These tri-axial tests have a long duration. Depending on the performance of the specimen, a test can last up to 500 000 load repetitions or 6 days. The permanent deformation test runs continuously around the clock until failure of the specimen occurs.

Tests were carried out on dry specimens at different deviator stress ratios but the same confining pressure. In that way, it was possible to understand the plastic-strain behaviour of the mix. The quantification of permanent strain was aimed at investigating this behaviour with the same loading waveform and temperature.
The variables, which were selected, are:

- Loading waveform = haversine with rest period
- Haversine load with a duration of 0.1s followed by a rest period of 0.9s
- Temperature = 40°C
- Mix type =BSM-foam 50%RA and 50%G2
- Deviator stress ratio = different stress ratios (range from 30% to 50%)
- Confining pressure = 100kPa

The failure criteria for the permanent deformation test were limited to total axial stain of 4% or 500 000 load repetitions, whichever came first. In order to determine the distinguishable failure behaviour under dry conditions, step-up of deviator stresses criteria were applied. In a multi-stage permanent deformation test, a different stress ratio was selected starting from 30% then increased at intervals of 5% from 30% to 50%. The change in stress level was measured after each 500 000 load applications. The test was performed by applying load repetitions using a haversine shaped load pulse consisting of 0.1s load followed by a 0.9s rest period. A preload equal to 20% of the confining pressure was applied during all load applications. This loading waveform is deemed to simulate the passing of an axle over a pavement section. It is applicable to base and subbase layers.

During all the tests, load and displacement were recorded in sampling windows consisting of three full load cycles at a minimum sample rate of 200Hz. The recommended intervals between sampling windows is given in Table 3.11.

Table 3.11: Example of data sampling interval for permanent deformation test.

Cumulative number of cycles	Data sampling window
1 to 100	100 cycles
101 to 3000	Every 1000 cycles (three full cycles)
3001 to 20000	Every 5000 cycles (three full cycles)
20001 to 50000	Every 10000 cycles (three full cycles)
50001 to 500000	Every 20000 cycles (three full cycles)

Due to limitation in the tri-axial set-up, testing at a higher frequency was not possible. The reason is that the loading piston in the MTS equipment is fixed and the tri-axial cell is moving up and down from bottom against the fixed loading piston. The pressure confinement σ_3 of 100kPa was consistent through all the tests and it was kept constant for all the tests due to limitations in the time of this study. During testing, the total plastic strain was recorded electronically by the Spider 8 unit analogue system. All the input data for every test were controlled by a second computer through a MATLAB® program developed at the University of Stellenbosch. The axial deformation was measured over the middle third height of the specimen by three vertical external LVDTs. Due to possible problems of permanent deformation of the specimens, radial expansion was not measured during the tri-axial testing. Therefore, the effect of dilatation could not be accounted for.

For the three BSM-foam mixes permanent deformation tests were performed at a different deviator stress ratio. The deviator stress ratios at which the tests were carried out were determined as the series of tests progressed. The objective of the testing was to determine which deviator stress ratio is the critical stress ratio. Specimens subjected to a stress ratio higher than the critical stress ratio will show an accelerated rate of plastic strain accumulation towards the end of the test. Specimens subjected to a stress ratio lower than the critical stress ratio typically shows an ever decreasing rate of plastic strain accumulation until a stable condition is reached the end of the test (500 000 load repetitions). Typically, the applied stress ratios were chosen to first obtain a test result at a stress ratio well above and one well below the critical stress ratio. The stress ratios for the three remaining tests were chosen approximately around the critical stress ratio.

The temperature test of 40°C was selected for all the permanent deformation tests. From previous studies conducted by Twagira (2010) it was evident that the critical temperature of BSM mixes lies between 40°C and 50°C as reported in pararagraph 3.8.

Wave Form: Haversine with Rest period

Load pulse: 0.1 s
Rest period: 0.9 s

Temperature: 40 °C

Table 3.12: Example of loading sequence for permanent deformation test.

Loading Sequence	Confining pressure (kPa)	Contact Stress (kPa)	Contact Load (kN)	Stress Ratio (%)	Cyclic Stress (kPa)	Cyclic Load (kN)	Load Repetitions
Conditioning	100	10	0.18	30	501	5.53	1000
2.2	100	10	0.18	50	835.00	14.76	100
2.2	100	10	0.18	45	751.50	13.28	100
2.1	100	10	0.18	42.5	709.75	12.54	100
2.3	100	10	0.18	40	668.00	11.80	100
2.4	100	10	0.18	30	501.00	8.85	100

3.9 Effect of the preconditioning time – temperature in the mechanical tests

This research presents the important role played by the time-temperature variable on BSM-foam mixes before mechanical tests at high and low temperatures are to be carried out. BSMs are generally less susceptible to temperature variations (Jenkins, 2000; Loizos and Papavasiliou, 2007). However, depending on mix composition, e.g. higher binder content and RA content, temperature distribution in the specimens can adversely influence the performance of BSMs. This research was conducted before performing the mechanical tests on the BSM-foam mixes at the University of Stellenbosch. An accurate measure of the time-temperature conditioning is vital for a successful series of laboratory tests.

3.9.1 Test configuration

A set of six specimens representing the three BSM-foam mixes (two per mix) were analysed in this research. To simulate as much as possible the conditions of the tri-axial tests a latex membrane was inserted around the specimen with the scope of creating the same configuration for a possible monotonic or dynamic tri-axial test and reduce the influence of air voids present in the BSM-foam mixes.

Representative specimens for tri-axial tests with dimensions of 150 mm diameter and 300 mm height were placed in a controlled temperature cabinet and then they were drilled in the middle of the surface until reaching the centre of the specimen. A latex membrane was positioned around each specimen and two metallic plates were positioned on the top and at the bottom of the specimen. Thereafter, a thermocouple was positioned inside a hole (several mm) in the membrane and attached to the inner part of the specimen (75 mm deep). After the thermocouple was inserted in the specimen the small hole was sealed with an epoxy resin, ensuring that no air was able to pass through. The thermocouple was then connected to an analogue gauge. The monitoring of the temperature in the BSM specimen was conducted through the use of a MicroDAQ data acquisition system (Eagle® technology) and a laptop.

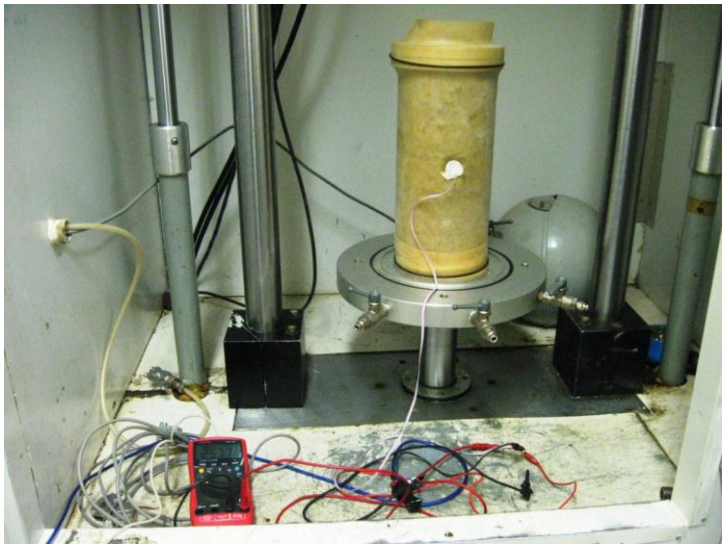

Figure 3.24: Temperature test set-up on a BSM-foam specimen.

The thermocouple was previously calibrated in a water bath at low temperature (15°C) and at high temperature (80°C) and was able to measure the temperature gradient inside the specimenevery 10 seconds.

Two levels of temperature profiles were conducted:

- the temperature in the climate chamber was increased to 40°C;
- the temperature in the cell was decreased to 10°C.

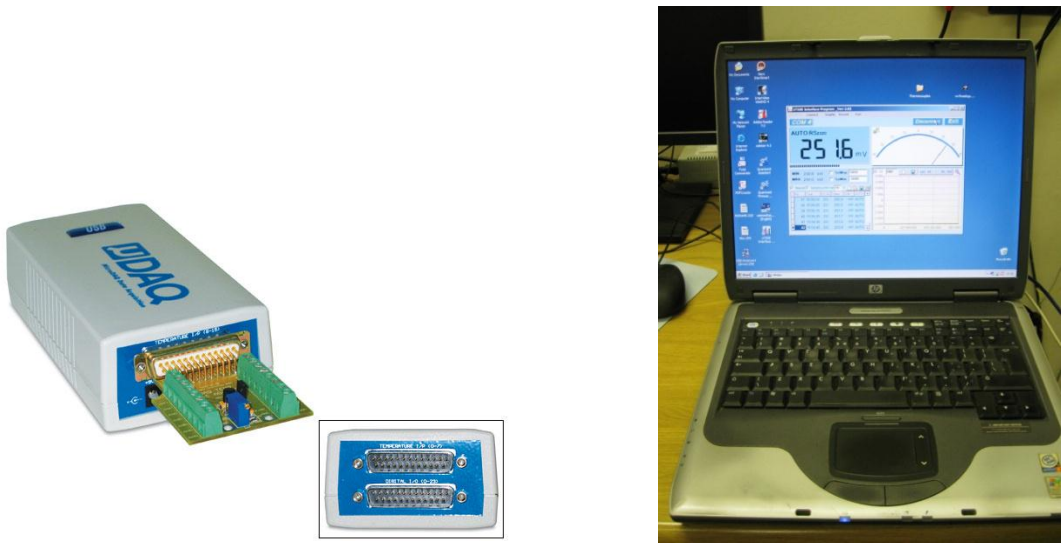

(a) (b)

Figure 3.25: Instrumentation used during the temperature test: (a) MicroDAQ data acquisition system (Eagle® technology); (b) laptop used to record the data.

All the tests started at the environmental temperature of 25°C. A thermometer placed inside the temperature cabinet helped to monitor the temperature during all the phases of the tests. The stored data was exported after every test into an Excel spreadsheet for analysis. The measured data is presented and discussed in the following section.

During conditioning, the specimens were sealed with a latex membrane to maintain the equilibrium moisture content prior to testing and to simulate the configuration of a possible tri-axial test.

3.9.2 Test results

The results are an indication of the importance of the preconditioning time to allow the specimens to reach different level of test temperature. BSM-foam mix with 100% RA and the mix with 50% RA and 50% G2 reached 40°C in almost 2 hours and 3 hours respectively, while a BSM-foam with 100% G2 material took almost 5 hours. The analysis shows how the percentage of RA is important for the preconditioning time-temperature. In fact, as the percentage of RA increases, the specimen is able to reach a high temperature quicker than a

BSM-foam mixture with low percentage of RA. The tests carried out at a low temperature demonstrated that the BSM-foam with 100%RA reaches low temperatures quicker than the BSM-foam mix with 100%G2. The influence of the percentage of RA is visible through the graph, but it is not as evident as in the previous series of tests at high temperature. At a temperature of 13°C the BSM-foam mixes are not able to completely reach the target value for temperature (10°C) probably due to the presence of the latex membrane. This one could be considered a sort of barrier to the external reduction of the temperature.

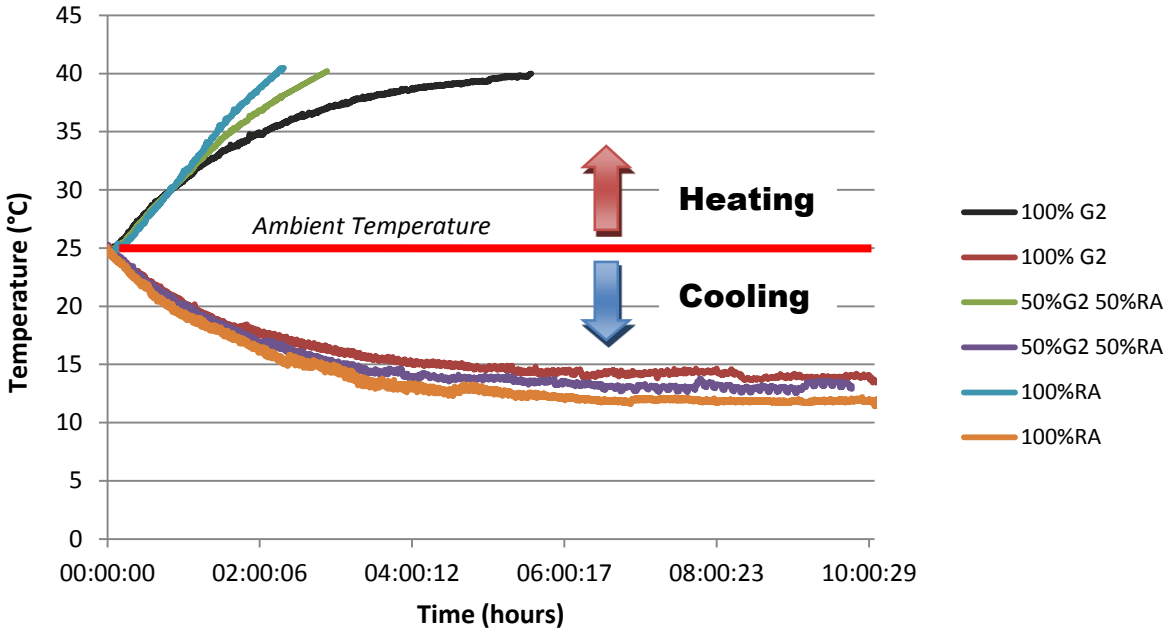

Figure 3.26: Time – temperature relationship for BSM-foam mixes.

Temperature in BSM-foam mixes is known to influence the following:

- evaporation of moisture present in the mix;
- development of bonding between the binder and mineral aggregate surfaces (Jenkin, 2000);
- stiffening of the mastic, which in turn affects stiffness, shear properties, and ultimate strength of the mix (Jenkins, 2000 and Ebels, 2008);
- equilibrium moisture content in the mix, and
- ultimate durability behaviour of the mix and long-term performance (Twagira 2010).

It is apparent from these observations that the determination of the temperature distribution in the BSM specimen is vital for future tests in a temperature controlled environment. Temperature is regarded as a powerful factor which can strongly influence the mechanical test characteristics of BSMs.

An extensive number of studies have been done on hot mix asphalt in the past, but only a few researches focused on the possible relationship between temperature and behaviour of BSMs (Twagira, 2010). During this research more detailed tests and studies on the gradient of

temperature and the possible interaction and behaviour of BSMs materials will be provided and analysed.

3.10 Brushing test

The environment in which each road is built, has a greater influence on its durability behaviour and long-term performance than is often realised. The road environment has to be accepted as it is and the design and method of construction must be suitably adapted. The climatic influence on the quality of mineral aggregate durability, as well as the general performance of roads, has been studied. Weinert (1980) indicates that the climatic effects are more pronounced in well territorially large countries where climate variation regionally and seasonally is wide, e.g. South Africa. As aggregates and binder age and are exposed to the cycles of varying temperature, humidity and dynamic loading, their physico-chemical properties might change. This in turn influences bonding characteristics or durability behaviour.

To potentially evaluate if the quantity of stabiliser added is adequate to ensure the long-term durability of the BSM-foam mixes with greater reliability than ITS_{dry} and ITS_{wet} tests, the wet/dry brushing test was investigated in this study. The results are compared with the more sophisticated MIST (Moisture Induced Simulation Test). The wet/dry brushing test, illustrated in Figure 3.27, assesses the effect of wetting and drying on the surface of BSM-foam specimens. The test takes into account the effect of carbonation and soaking of the cemented treated specimen surface as some degree of carbonation occurs during the drying cycle (Paige-Green and Ventura, 2004).

The test was carried out on the three BSM-foam mixes with different percentage of RA. The brushing was applied on the specimens after each wet/dry cycle by mechanical brushing. The CSIR and University of Stellenbosch are developing a mechanised brushing system and a new protocol which considers the force applied when using the manual brushing method. The test method for the mechanised test on BSMs materials is currently under review and this research is a product of an experimentation of possible different protocols.

The Appendix A reports all the details for these tests and the most suitable procedure for this research.

Figure 3.27: Mechanical brushing device at the University of Stellenbosch.

The mechanical brushing test was initially designed for cement-treated material. During the last few years more attention has been given to the possible use of this apparatus on different kinds of material like BSMs. The test works on a series of 12 cycles of brushing on a specimen that has a diameter of 150mm and a height of 150mm. The wire brush used in this study is a standard wire brush. It is made of 40mm x 1.8 mm x 0.5 mm spring steel bristles randomly assembled in 180 groups of 6 bristles and mounted on a 200mm x 60mm wooden block. The wire brush is loaded with the same load of 2.25 kg during every cycle. This load can be adjusted through a small weight on the arm that connects the brush to the rest of the machine. Two electronic counters are built in to control the number of revolutions per minute and the total number of revolutions for every cycle.

The CSIR (Test Method No CA 15, 2004) suggests in its procedure for granular and cemented material to adopt 50 revolutions per cycle (12 in total) and a speed of 60 revolutions per minute for each cycle. The preparation and the accelerated curing procedure of the BSM-foam specimens for the three different mixes with RA followed the same method used in previous studies and presented in earlier chapters and in the TG2 technical guideline (Asphalt Academy 2009).

The wet-dry brushing test is an empirical test if compared with the the Moisture Induction Simulation Test (MIST) or the MMLS tests. However, it has the possibility to give an assessment of the quality of adhesion and cohesion bonding between the aggregates and the dropplets of binder content in the BSM-foam mixes with the influence of moisture.

3.10.1 Calibration of the procedure for wet-dry brushing tests

After curing, the preliminary procedure proposes to submerge the specimens in a water bath at room temperature for 5 hours and then place them in a draft oven at 71°C for 42 hours (CSIR, 2004). After this period the specimens can be clamped in the brushing apparatus and the test can start. The procedure described so far represents only one cycle (48 hours) of the wet/dry durability test. The specimens are then submerged in water and the method repeated for other 11 cycles.

Unfortunately, this scheme is not suitable for BSMs materials. BSMs have a big component of water and bitumen in their own matrix. Leaving a specimen in a draft oven for 42 hours at 71°C after curing can introduce problems of ageing, redistribution of the bitumen inside the specimens (above the bitumen softening point ageing), high evaporation of the moisture and a consequent alteration of the degree of density. To overcome this problem, the procedure adopted through this study didn't use a draft oven during the 12 wet/dry cycles.

3.11 Conclusions

Mix design procedures that are available for BSMs are well formulated especially for BSM-foam (Asphalt Academy, 2009). Almost all existing mix design procedures for BSMs use ITS and tri-axial tests to evaluate the strength of BSMs. As an alternative road material, the

properties of foamed asphalt mixture, either under field conditions or at laboratory scale, assumes a central point for the international scientist community.

Some guidance and specifications related to the increasing use of RA in BSMs and product performance have been introduced. All these contribute to the improvement of BSM application. However, BSM-foam characteristics are not yet fully understood in correlation with mixture properties, especially with an increasing amount of RA.

Shearing resistance of BSM (influenced by gradation, moisture, density, fines, particle geometry and confining pressure) is used to develop a load distributing quality that reduces the stresses transmitted to the underlying layers. Therefore, as discussed in the next chapter, ITS and monotonic tri-axial tests are going to be well suited for characterising BSMs and a more suited test such as Dynamic tri-axial tests that can simulate the stress scenario under which BSMs function more accurately and which has long been recognised by the road construction industry.

The wet/dry test is commonly performed to identify the susceptibility of cement/lime stabilised materials to degradation (disintegration or decomposition) in the presence of adverse conditions of cyclical wetting and drying. The erosion of BSM-foam materials used in pavements and which are subject to service conditions in the pavement, have not been studied extensively. This thesis focuses on the wet-dry durability performance of the three BSM-foam mixes with an increasing amount of RA, developing a new possible evaluation method for long-term durability.

Some limits could be expected during the brushing test. Firstly, it might be harsh on the adhesive bond due to the dispersion nature of the bitumen into the mix (spot welding of the foam to the coarse aggregates). Secondly, its applicability does not simulate the mode of moisture failure (erodability or mass loss) that BSMs experience in field conditions. ITS_{wet} tests have not been taken into account in this research due to the limits of time and material.

Temperature studies have been carried out to analyse the temperature gradient only on a small scale. More careful attention will be given to the temperature distribution and modelling in three BSM-foam mixes in the following chapters. Therefore, understanding of this behaviour is important for predicting the heat transfer in pavement structure and the mechanical properties of the BSM.

REFERENCES

AASHTO T307, 2005. Standard Method of Test for determining the resilient modulus of soil and aggregate materials.

Airey, G.D. 2003. State of the Art Report on Ageing Test Methods for Bituminous Pavement Materials. The International Journal of Pavement Engineering, Vol. 4 (3) September, pp165-176.

Anderson, D. A., Christensen, D. W., Bahia, H. U., Dongre, R., Sharma, M. G. and Antle, C. E. 1994. Binder characterization and evaluation: Volume 3 Physical characterization. Rep. No. SHRP-A-369, National Research Council, Washington DC.

Asphalt Academy. 2009. A guideline for the design and construction of bitumen emulsion and foamed bitumen stabilised materials. 2nd edition technical guideline. Pretoria, South Africa. (TG2).

Bell, C.A. 1989. Summary Report on Ageing of Asphalt-Aggregate Systems. SHR-A/IR-89-004, Strategic Highway Report Research program, National Research Council.

Burger, M. 2005. Prediction of the temperature distribution in asphalt pavement samples. Master thesis, Department of mechanical engineering, Stellenbosch University, South Africa.

Cortizo, M.S., Larsen, D.O., Bianchetto, H. and Alessandrini, J.L. 2004. Effect of the thermal degradation of SBS copolymers during the ageing of modified asphalts. Polymer Degradation and Stability 86(2):275-282.

CSIR, 2004. Test Method No CA 15, The Wet-Dry Brush Test For Cemented Treated Materials Using The Mechanical Brushing Machine. CSIR, Pretoria, South Africa.

CSIR, 2011. Revision of the South African Pavement Design Method, Proposed Protocol for Resilient Modulus and Permanent Deformation Characteristics of Unbound and Bound Granular Materials. CSIR, Pretoria, South Africa.

De la Roche, C., Van de Ven, M., Van den Bergh, W., Gabet, T., Dubois, V. and Grenfell, J. 2009. Development of a laboratory bituminous mixtures ageing protocol. Advanced Testing and Characterization of Bituminous Materials, (eds Loizos, d. Q., Partl, M., Scarpas, T. and Al-Qadi, I.), Taylor and Francis Group, London.

Fu, P., Jones, D., Harvey, J.T. and Bukhari, S.A. 2009. Laboratory Testing Methods for Foamed Asphalt Mix Resilient Modulus. Road Materials and Pavement Design, 10(1): 187-212.

Huang, Y. H. 1993. Pavement Analysis and Design, published by Prentice Hall, Englewood Cliff, New Jersey, USA.

Jenkins, K. 2000. Mix Design Considerations for Cold and Half-Warm Bituminous mixes with the emphasis on foamed bitumen. PhD Dissertation. University of Stellenbosch.

Lins, V.F.C., Araujo, M.F.A.S., Yoshida, M.I., Ferraz, V.P., Andrada, D.M. and Lameiras F.S. 2008. Photodegradation of hot-mix asphalt. Fuel 87(15-16):3254-3261.

Loizos, A. and Papavasiliou, V. 2007. Assessment of in-situ cold in-place recycling performance using the foam asphalt technique. Workshop on pavement recycling. Athens, Greece.

NCHRP 1-28A. 2004. Recommended standard method for routine resilient modulus testing of unbound granular base/subbase materials and subgrade soils. NCHRP Research Results Digest No 285, Laboratory determination of resilient modulus for flexible pavement. January 2004

Ouyang, C., Wang, S., Zhang, Y. and Zhang, Y. 2006a. Improving the ageing resistance of styrene-butadiene-styrene tri-block copolymer modified asphalt by addition of antioxidants. Polymer Degradation and Stability 91(4):795-804.

Ouyang, C., Wang, S., Zhang, Y. and Zhang, Y. 2006b. Improving the ageing resistance of asphalt by addition of Zinc dialkyldithiophosphate. Fuel 85(7-8):1060-1066.

Paige-Green, P. and Ventura, D.F.C.2004. Durability of foamed bitumen treated basalt base course. CSIR report CR 2004/8. Pretoria. South Africa.

Roberts, F.L., Kandhal, P.S., Ray, B.E., Lee, D.Y. and Kennedy, T.W. 1996. Hot mix asphalt materials, mixture design and construction. NAPA, Research and Education Foundation, Lanham, Maryland.

Shakirullah, M., Ahamd, I., Ishaq, M., Shah, A.A., Kahn, M.A., Rehman, H.U. and Kahn, H. 2007. FTIR Analysis of the Whole Asphalt and Some Crackates. Journal of the Chemical Society of Pakistan.

Software and data acquisition system http://www.eagledaq.com/

Scholz, T.V. 1995. Durability of Bituminous Paving Mixtures. PhD Thesis, School of Civil Engineering, University of Nottingham.

TMH 1 (Technical Methods for Highways). 1986. Standard methods of testing road construction materials. (TMH 1). National Institute for Transport and Road Research, Pretoria.

Twagira, E.M. 2010. Influence of durability properties on performance of bitumen stabilised materials, PhD Dissertation, Department of Civil Engineering, Faculty of Engineering, University of Stellenbosch, South Africa.

Weinert, H.H. 1980. The natural road construction materials of Southern Africa. Academia, Cape Town.

Wirtgen GmbH. 2010. Cold Recycling Manual, 3rd edition published by Wirtgen GmbH, Windhagen, Germany, 2010.

Wu, J., Lepercq, E. and Airey, G. D. 2007. Ageing of bitumen in bulk versus the ageing in asphalt mixture. Advanced Testing and Characterization of Soil Engineering Material, (eds Lois, d. Q., Partl, M., Scarpas, T. and Al-Qadi, I.), Taylor and Francis Group, London.

Zhang, F. and Yu, J. 2009. The research for high-performance SBR compound modified asphalt. Construction and Building Materials 24(3):410-418.

Zhang, F., Yu, J. and Han, J. 2011. Effects of thermal oxidative ageing on dynamic viscosity, TG/DTG, DTA and FTIR of SBS- and SBS/sulphur-modified asphalts. Construction and Building Materials 25(1):129-137.

CHAPTER 4

MECHANICAL PROPERTIES OF BSM-FOAM MIXES

4.1 Introduction

This chapter focuses on the mechanical properties of the three different mixtures evaluated at the University of Stellenbosch:

- BSM-foam with 100% reclaimed asphalt (RA), 1% of cement and 2% bitumen content;
- BSM-foam with 50%RA and 50% graded crushed stone G2 Hornfels, 1% of cement and 2.1% bitumen content;
- BSM-foam with 100% graded crushed stone G2 Hornfels, 1% of cement and 2.3% bitumen content.

Four main parameters have been evaluated for an exhaustive investigation of the cold recycling mixtures. The test programme included the following test procedures:

- Indirect Tensile Strength Tests (ITS) on 75-150 mm diameter cylindrical specimens, performed at different temperatures;
- Monotonic tri-axial tests on 300 mm height and 150 mm diameter cylindrical specimens, tested at environmental temperature (25°C);
- Dynamic tri-axial tests (short duration) on 300 mm height and 150 mm diameter cylindrical specimens, tested at different temperatures (10, 25 and 40°C) and different confining pressures (50, 100 and 200kPa);
- Dynamic tri-axial tests (long duration) on 300 mm height and 150 mm diameter cylindrical specimens of:
  - BSM-foam with 100%RA tested at 40°C, with a confining pressure of 100kPa;
  - BSM-foam with 50%RA and 50%G2 tested at 25°C, 40°C and 50°C, with a confining pressure of 100kPa;
  - BSM-foam with 100%G2 tested at 40°C with a confining pressure of 100kPa;

All the tests on the three BSM-foam mixtures were carried out at Stellenbosch University. The tests focused mainly on the strength, resilient modulus and permanent deformation behaviour of three different BSM-foam mixes with different amounts of reclaimed asphalt (RA).

The flow diagram below illustrates the testing method and selected parameters applied during tri-axial testing and ITS tests (Figure 4.1).

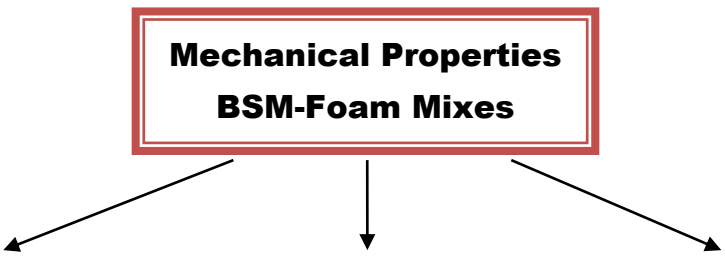

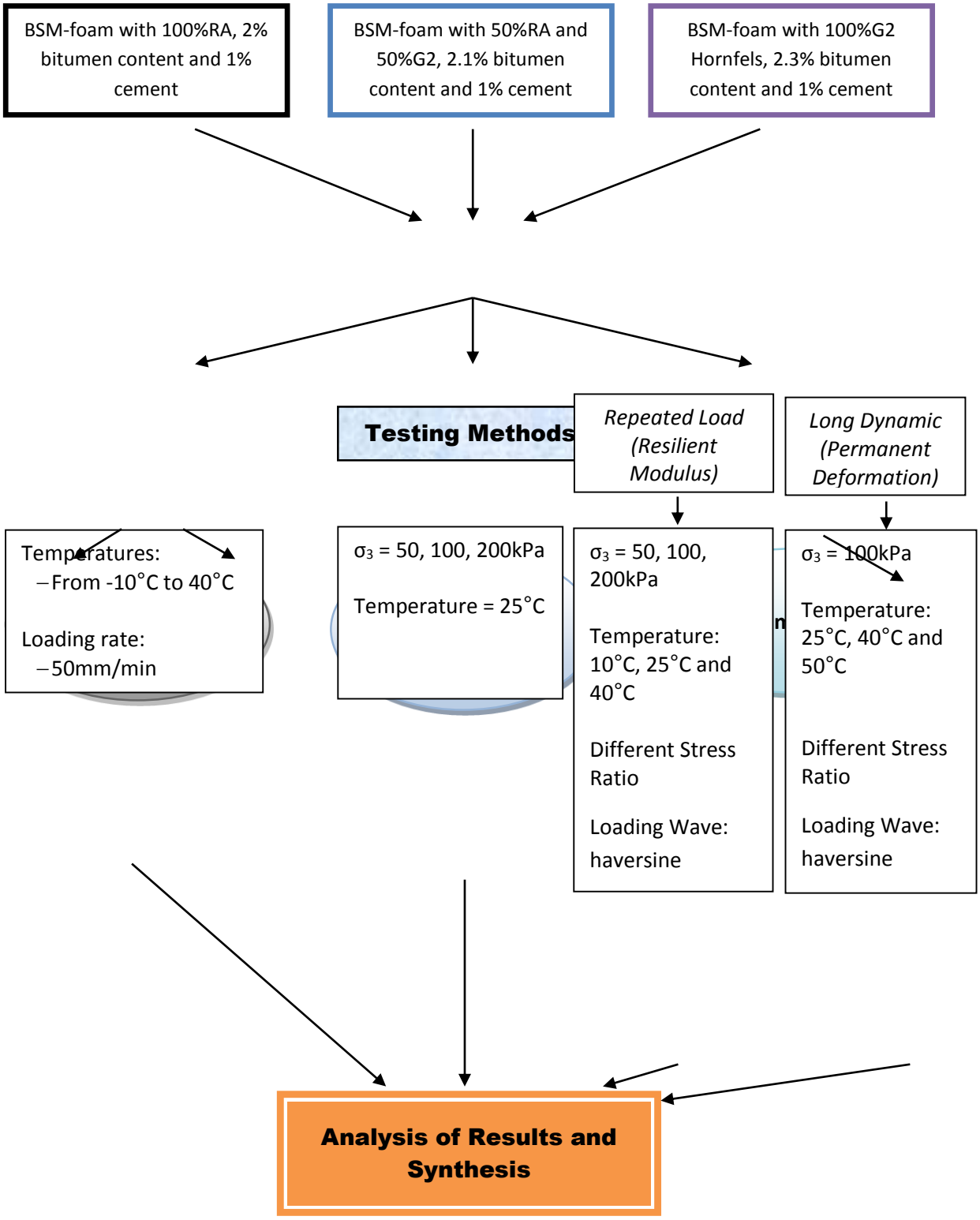

Figure 4.1: Flow diagram illustrating the tri-axial and ITS testing methods.

4.2 Selection of mixes

All three BSM mixes have been obtained mixing foam bitumen 80/100 in the laboratory at the environmental temperature (close to 25°C). Every batch of material was placed in an oven for two hours, maintaining the temperature at 25°C. For purposes of mixing and compaction,

characterization of the natural materials is necessary before treatment with foamed bitumen can be carried out. Details on the composition of all the three mixtures are listed in Table 4.1.

Table 4.1: Details of BSM – foamed mixes.

Mix	100%RA	50%RA 50%G2	100%G2
Cement (%)	1	1	1
Optimum Moisture Content (%)	4.05	5.7	5.7
BSM-foam content (%)	2	2.1	2.3
Average voids in the mix (%)	16.49	15.48	13.46
Density (kg/m^3)	2006	2195	2335

The test specimens were compacted using a vibratory Bosch® hammer (Kelfkens, 2008). The specimen is compacted in one layer (ITS specimens, 75 mm height and 150 mm diameter) or in five layers (tri-axial specimens, 300 mm height and 150 mm diameter). This method is fast (less than one minute per layer) and produces homogeneous densities through the entire specimen.

Different percentages of RA are expected to yield different air void contents in the mixes, but the same compaction energy produced yields to the same relative density (Modified AASHTO compaction).

The benefits of compaction are the following: 1) squeezing water out of the mastic and mineral aggregates to the surface. The exposed surface water can easily be evaporated in a conducive environment; 2) compaction energy significantly influences the wettability of the mastic to the coarse fraction surface, thus squeezing the bitumen polar fraction to react (interact) with the mineral aggregate surface charges; 3) packing of mineral aggregates during compaction results in an increase in cohesion and a reduction in the voids content or the conduit of water infiltration back to the cured mix matrices. There is a limit to the ultimate density after which no further compaction will take place without “damaging” particles or de-densifying the material.
The specimens were compacted and then subjected to a period of curing of three days, at 30°C unsealed for 20 hours and then sealed at 40°C for other 48 hours. The aim is to simulate the long term behaviour and moisture conditions of the material in service. After compaction, the water content of three mixes was close to the values reported in Table 4.1. The specimens have been tested at these moisture contents (unsaturated).

More details regarding the mix design, compaction and curing procedures were presented in Chapter 3.

4.3 Indirect Tensile Strength Test (ITS)

Indirect Tensile Strength is a parameter used as an indicator in defining the cracking resistance of BSM-foam mix. Nevertheless, testing at 25ºC results in shear and compression damage occurring in the ITS, thus providing a composite response to loading .The ITS test is one of the more frequently used tests for BSMs mixture characterization in evaluating pavement structures. The indirect tensile test has been extensively used in structural design research for flexible pavements and it is performed by loading a cylindrical specimen with a single compressive load, which acts parallel to and along the vertical diametric plane. This loading configuration develops a relatively uniform tensile stress perpendicular to the direction of the applied load and along the vertical diametric plane, which ultimately causes the specimen to fail by splitting along the vertical diameter.

In this study the ITS has been used to evaluate the tensile properties of the three BSM-foam mixtures at different temperatures. All the ITS tests were carried out in equilibrium conditions due to the extensive test program. The results are an average of three repeat tests per temperature and mix. Table 4.2 shows the average results between temperature and tensile strength. Six different temperatures (-10,-5, 0, 10, 25, 40°C) are used. Standard deviation and covariance are presented in all the different average test results.

Table 4.2: ITS_{equil} results of BSM – foam mixes.

BSM-foam mixes	**Indirect Tensile Strength (kPa)**					
	-10°C	*-5°C*	*0°C*	*10°C*	*25°C*	*40°C*
100%RA	815 819 816	813 811 809	805 796 801	647 656 651	438 439 443	341 339 340
50%RA 50%G2	1068 1071 1071	921 926 924	818 822 820	668 670 671	497 499 501	320 320 321
100%G2	1218 1222 1220	1000 1001 1000	849 849 851	591 588 591	450 450 449	328 332 331

Figure 4.2 gives a detailed comparison of the three BSM-foam mixes at high and low temperatures. Eighteen specimens in groups of three were tested at each temperature.

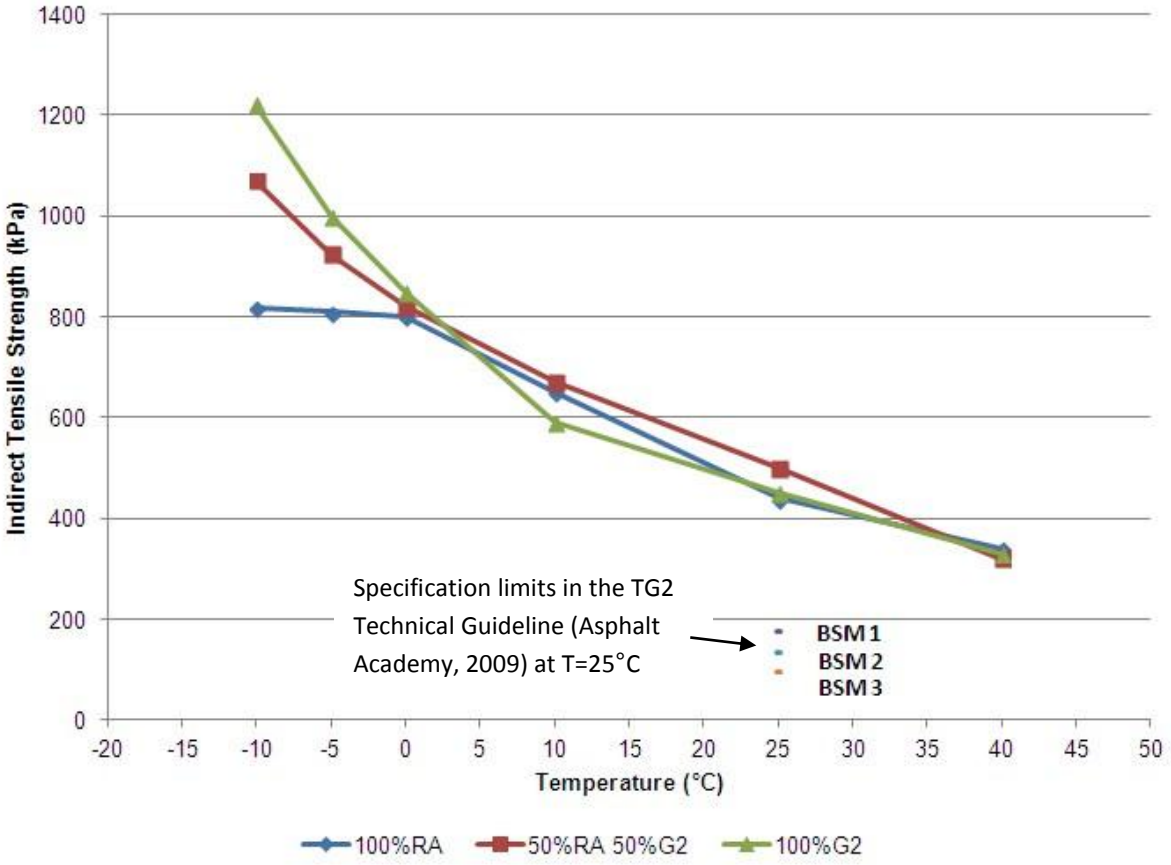

Figure 4.2: ITS_{equil} values as a function of %RA and test temperature.

The investigation yields a curvilinear relationship between all three mixtures: the strength constantly increases for all three BSM-foam mixtures from a temperature of 40°C to a temperature of 0°C. Below 0°C the relationship deviates from the curvilinear. The BSM-foam mix with 100%RA shows a trend of lowest thermal sensitivity. The results indicate the importance of the temperature factor during all the tests. At the same time the quantity of bitumen binder influences the trend line of all the mixtures, in particular in the BSM-foam mix with 100%RA. Generally the tensile strength decreases as the test temperature increases.
The variability of the data recorded during all the tests is very limited. The standard deviation always reaches values not higher than 7.8 and the covariance values vary between 0.7 and 5.7. This is mostly due to the thorough temperature preconditioning period and to a high level of mixing and compaction. All three BSM-foam mixes show a linear behaviour for all the tests conducted at temperatures higher than 10°C. The results for all the three BSM-foam mixes are ranging on the same values due to a combination of factors: density; the percentage of foam which can't guarantee a uniform coated surface on the aggregates; the presence of old binder content in the mixes with an increasing amount of RA. In fact as the temperature raises the visco component of the binder becomes poor and it is not able anymore to distribute and absorb the loading in the specimen. The high percentage of air voids and a low density value in the mix with 100%RA create a sort of a plateau value when the temperature drops under 0°C. These outcomes can be compared to a previous study conducted at the TUDelft in the Netherlands in 2008 and 2009 during previous research on different hot mixes asphalt (Dal Ben, 2009). All the tests were conducted with the same instrumentation and standard used at the University of Stellenbosch. As for the BSM-foam mixes, even in the hot mixes the linear behaviour is presented in the tests at temperature higher than 10°C.

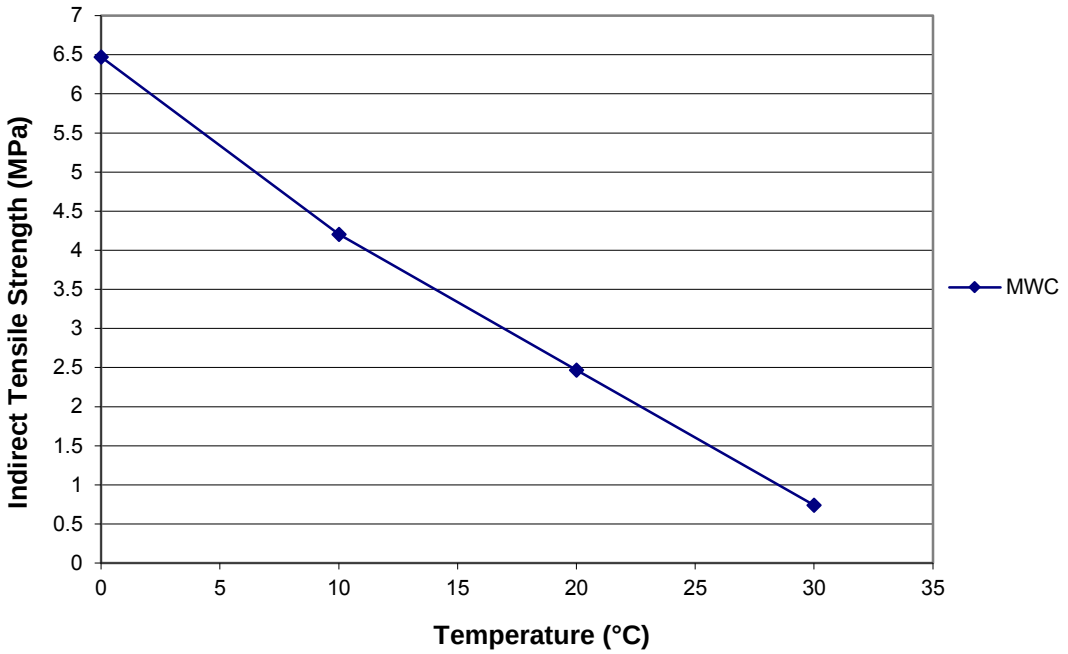

Figure 4.3: ITS values analysed at the TUDelft for modified wearing course (MWC) for Hot Mix Asphalt, 100% limestone, 5.5% bitumen content (Modified Hard Bitumen 2008).

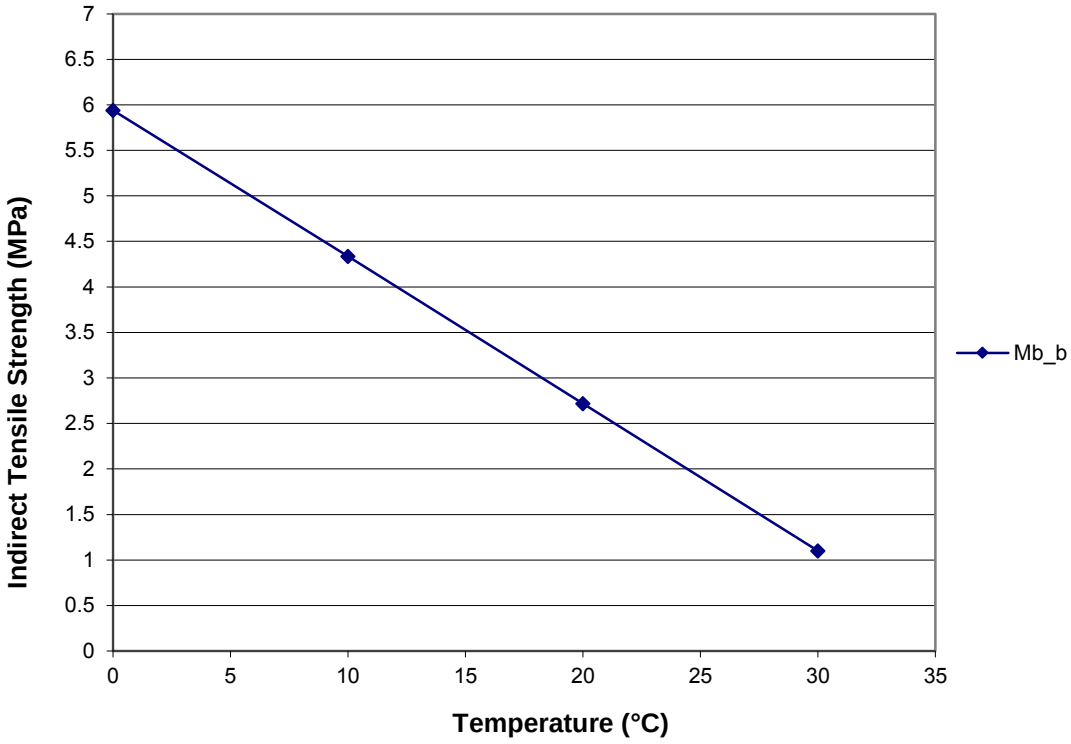

Figure 4.4: ITS values analysed at the TUDelft for modified base binder HMA (Mb_b), 85% limestone, 4.5% bitumen content (Modified Hard Bitumen 2008).

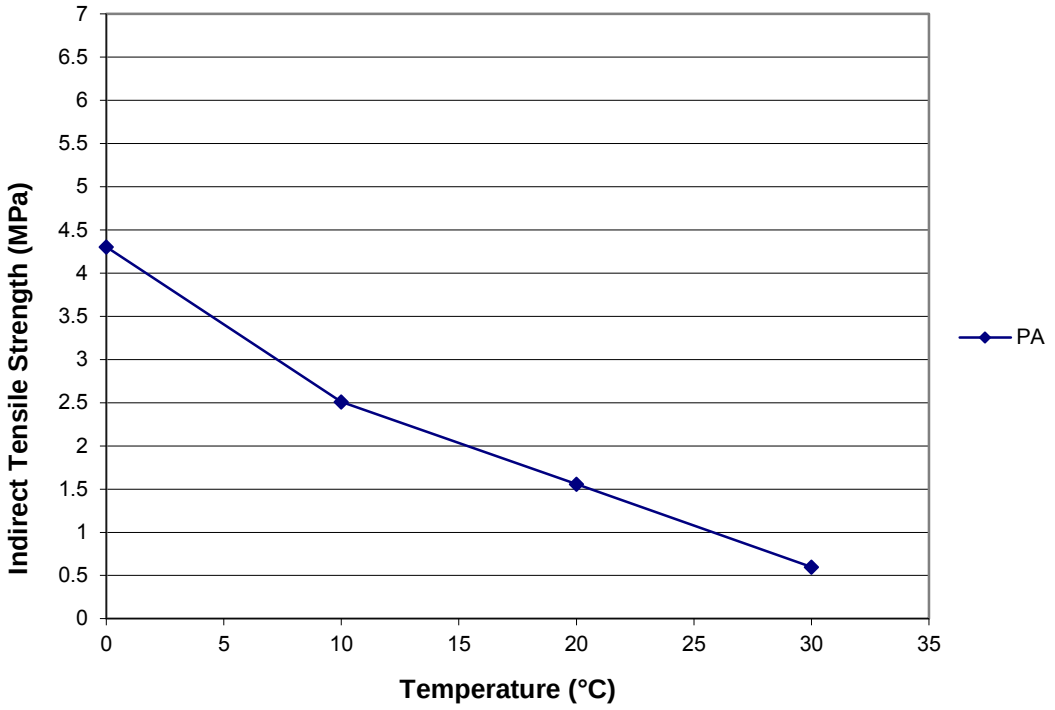

Figure 4.5: ITS values analysed at the TUDelft for porous asphalt (PA), 100% limestone, 5% bitumen content (Modified Hard Bitumen 2008).

Through the results represented in Figures 4.3, 4.4 and 4.5 a valid correlation can be drawn between the hot mixes asphalt and the BSM-foam mixtures. The bitumen, present in the mixes with its property of visco-elasto-plastic material, can influence the ITS results as the temperature changes. The droplets of bitumen in the BSM-foam are strong enough to give a similar behaviour to the 100%RA, 50%RA and 50%G2 and 100%G2 than for hot mixes with high percentage of binder content. Unlike asphalt, BSMs do not have a continuum of bitumen and are seldom homogeneous, especially when recycled material is stabilised. BSMs are non-continuously bound. In fact BSMs have a lower temperature susceptibility compared to HMA. In the previous results the three BSM-foam mixes showed a similar behaviour than the three HMA presented in the graphs above. In BSM-foam, the lack of large aggregate particles completely coated allows friction between aggregate particles whereas with HMA, the bitumen viscosity decreases therefore reducing strength. The distinct difference between mixtures produced using foamed bitumen and HMA is the way in which the bitumen is dispersed through the aggregate. Bitumen in HMA acts as glue and coats the small as well as large aggregates. Ebels (2008) and Twagira (2010) have confirmed the link between shear and tensile strength parameters to the performance of BSM-foam. Mixes with relatively low binder contents exhibit stress dependent behaviour where permanent deformation is a predominant mode of failure.

Table 4.3 highlights some of the differences between BSMs and HMA.

Table 4.3: Summary of comparative materials of different pavement mixtures.

Factors	BSMs	HMA
Aggregate type applicable	Durable	Durable
Binder content	1.5% to 3.5% residual bitumen foam	5% to7% bitumen
Void content	12% to16%	3% to 6%
Strength gain	Slow	Fast
Failure	Permanent deformation, shear properties	Permanent deformation, shear, creep, fatigue, cracks

The South African standard requires only ITS tests at 25°C, which can be compared to the four different classifications of BSMs. The TG2 technical guideline (Asphalt Academy, 2009) suggests four different material classes:

- BSM 1
- BSM 2
- BSM 3
- Unsuitable for treatment with BSMs

The method works by determining for every test result available the certainty that the mix falls into one of each of the four material classes. The certainty that a mixture belongs to a particular class is dependent on how the test results are consistent and on how much of the data falls into that class. The limits for every class are shown in Table 4.4.

Table 4.4: Interpretation of ITS_{equil} tests for classification of BSMs materials for specimen with 75mm height and 150mm diameter.

Test	Material class			
	BSM 1	BSM 2	BSM 3	Not suitable for treatment
ITS (kPa) Equilibrium, 150mm diameter	>175	135 to 175	95 to 135	< 95

Through the analysis of the previous results all three mixtures clearly meet "BSM 1" classification (Asphalt Academy, 2009) at the temperature of 25°C, because they range between the values of 440 kPa (100%RA) and 500 kPa (50%RA and 50%G2). The active filler

of 1% of cement contributes to the strength of the three mixes. The strength recorded during these tests is similar to test results conducted in earlier South African research at the University of Stellenbosch with similar mix compositions (Twagira *et al*. 2006).

The ITS test is considered to be a "simple test", i.e. it can be performed with relative ease. It is generally accepted that the interpretation of the results of "simple tests" is often more complex than the results of "complex tests". The ITS (splitting) tests is a prime example of this, because the internal stress distribution in this test is extremely complicated. Past studies have investigated ITS tests and posed the question whether the ITS test is an appropriate test to determine the flexibility of BSMs. This is due to the complex nature of stress distribution at the centre of the specimen. However, BSMs are stress dependent materials with little tensile strength. Shearing resistance of BSM (influenced by gradation, moisture, density, fines, particle geometry and confining pressure) is used to develop a load distributing quality that reduces the stresses transmitted to the underlying layers. ITS tests are not well suited for characterising BSMs and a more suitable test such as a tri-axial test that can simulate more accurately the stress scenario under which BSMs function has long been recognised by the road construction industry. This is because the ITS test does not accurately represent the failure mode occurring in BSMs. This is due to specimen size and stress distribution at the centre of the specimen and the unconfined nature of the test. The reason for this is that crack formation and development due to tensile stress in the centre of BSM-foam specimens, as well as the unconfined nature of the test, are not typical representations of the failure mechanisms occurring in BSMs during in-service conditions.

The BSM-foam specimens do not only fail in tension but also in shear and compression. This testing configuration increases the surface area between the loading heads and sample, thus reducing the extent of shear-type damage under loading heads and increasing the probability of specimens failing primarily due to tension along the axis of loading. However, flatter ends reduce the tensile stress in the middle of the specimen. Thus, it is important to identify an optimum test geometry that minimizes crushing and failures near the loading heads and at the same time provides sufficient tension in the middle of the specimen for a global tensile failure.

Figure 4.6: Failure in an ITS test.

ITS specimens can fail in a complex way depending on the stress conditions in the specimen as well as the strength characteristics of the material. Because of this failure might initiate at

several locations in an ITS sample and not necessarily in the center. This indeed can complicate the analysis of ITS results.

4.4 Monotonic tri-axial tests

The material properties of BSMs are commonly derived from stress-strain behaviour. Stresses to which materials are subjected in a pavement are overlaying weight, which is constantly vertical and horizontal at any point in the pavement area as well as traffic-induced stresses that are vertical (σ_v), horizontal (σ_h) and shear (τ). This occurs in a pavement as a result of repeated applications of moving wheel loads. The horizontal and shear stresses normally develop as an element of the material is loaded and deformed against neighbouring materials. These stresses are thus a function of the applied vertical stress and of the material's response or behaviour. From the relationship of stress-strain (σ-ε) curves at failure, a distinctive aspect of the mechanical behaviour can be analysed. The σ-ε curves determined under both monotonic demonstrate that the response of BSMs is that of stress-dependent material (Jenkins *et al*., 2007). Stress dependent materials can accurately be modelled using tri-axial testing, as has been shown with tri-axial tests of granular materials (Van Niekerk, 2002).

In a tri-axial test, the applied vertical stress (σ_v) and horizontal confining stress (σ_h) are by definition principal stresses. The monotonic loading test at different horizontal confined stress (σ_3) levels was performed to establish failure behaviour. The failure behaviour is described using the Mohr- Coulomb failure criterion (C and φ). The ratio of stresses within BSMs to the failure stresses have been related closely to the response of the materials in terms of resilient modulus and permanent strain (Jenkins, 2000, Ebels, 2008 and Twagira 2006). The failure envelope as defined in a Mohr-Coulomb diagram is characterised by the cohesion C and the friction angle φ and it represents a straight line.

The monotonic tri-axial tests in this study were conducted at 25°C in a displacement-controlled mode. The applied displacement rate was 6.3 mm/min (strain rate of 2.1% mm/minute at height of 300 mm) and confining air pressure of 50 kPa, 100 kPa and 200 kPa. The results of dry specimens are presented in this section.

Mohr-Coulomb analysis of the results of the monotonic tri-axial tests conducted on the BSM-foam mixtures provides a clear insight into the shear strength of the BSMs (Figures 4.7, 4.8 and 4.9). A linear approximation of the failure model is considered sufficient to define the shear properties, although non-linear behaviour at lower applied stress levels generally occurred (Jenkins *et al*., 2007). The cohesion and angle of internal friction determined according to the methodology discussed in the previous chapter are summarised in Table 4.5.

Table 4.5: Summary of cohesion and angle of internal friction (25ºC.)

BSM-foam mix	Cohesion C (MPa)	Angle of internal friction Φ (°)	Correlation Coefficients (R^2)
100% RA	0.432	8.2	0.98
50%RA 50%G2	0.374	36	0.94
100%G2	0.516	45.5	0.89

In general, good correlation coefficients (R^2 values) were obtained for the linear regression analyses to obtain the Mohr-Coulomb failure envelope lines. This indicates that the ultimate

strength results obtained at the different confinement pressures are in line with each other. All R^2 values are in excess of 0.94, except for the 100%G2 mix, for which an R^2 value of 0.89 was obtained. For two mixes however, where it was observed that one of the four Mohr-Coulomb circles was far from the failure envelope of the other three circles, the failure envelope line is based on those three circles only. These two mixes were 100%G2 and 50%RA + 50%G2.

The BSM-foam mix with 50%RA and 50%G2 showed cohesion lower than the other two mixes. Probably the percentage of air voids and the moisture content reduce this value.

Mohr-circles derived from the measured combinations of $\sigma_{1,f}$ and σ_3, as well as the failure envelope line according to the values of C and φ can be drawn in the Mohr-Coulomb diagram as discussed in the previous chapter. The Mohr-Coulomb diagrams for all mixes are included below.

According to the following graphs, the friction angle φ decreases whilst the cohesion of the mix increases with the inclusion of more reclaimed asphalt RA in a cold mix. This shift in the failure envelope leads to an increase in the maximum principal stress $\sigma_{1,f}$ at low confining stress σ_3 through the addition of reclaimed asphalt. Depending on the confining stress, $\sigma_{1,f}$ can increase through the incorporation of a higher percentage of reclaimed asphalt. The cohesion value increases with a higher RA content. This trend is valid for all the mixes tested using the tri-axial apparatus (MTS). However, with the inclusion of 1% of cement the cold foamed mix results in a marked increase in cohesion with reduction of the value of the internal friction angle (Twagira, 2010). This indicates that stress dependent behaviour i.e. nonlinear mechanical behaviour becomes less applicable to foamed mixes with the addition of cement (unless light cement bonds are broken under traffic loading). The higher friction angle for the BSM-foam 100%G2 can be attributed to the grading of the material, the addition of 1% of cement and a high level of compaction. All the specimens were compacted at 100 - 99% MOD AASHTO.

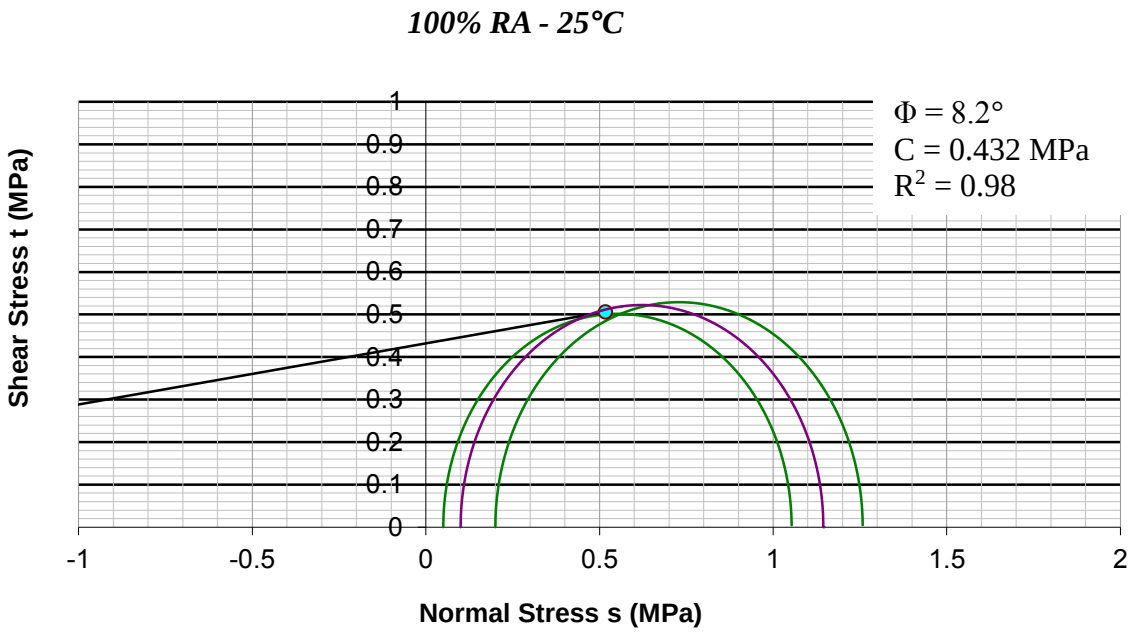

Figure 4.7: Results of monotonic tri-axial tests of BSM-foam with 100%RA, 2% bitumen content and 1% of cement.

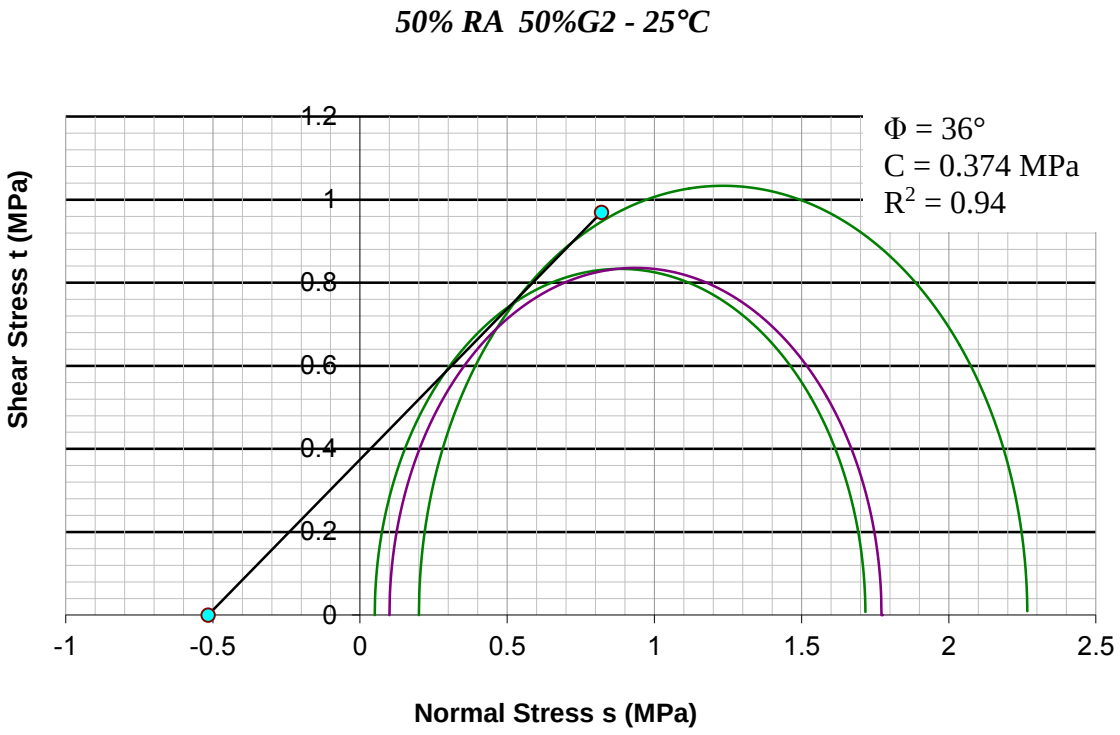

Figure 4.8: Results of monotonic tri-axial tests of BSM-foam with 50%RA + 50%G2, 2.1% bitumen content and 1% of cement.

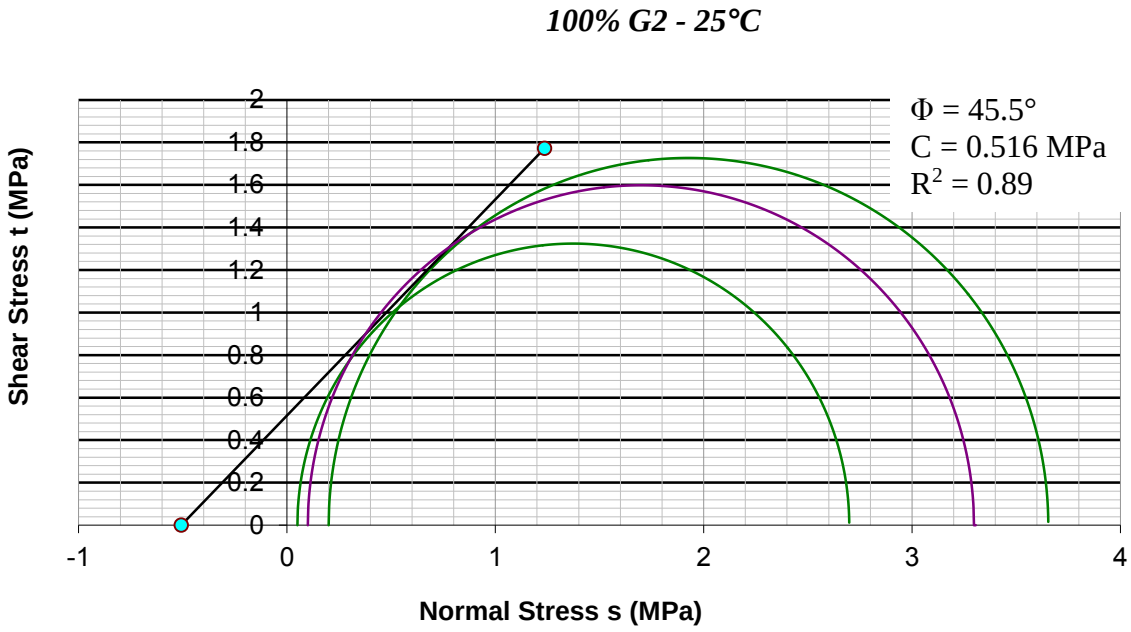

Figure 4.9: Results of monotonic tri-axial tests of BSM-foam with 100%G2, 2.3% bitumen content and 1% of cement.

Long and Ventura (2003) found that:

- an increase in density contributes to higher friction angles and cohesion values, and
- an increase in moisture content appears to have a small effect on the friction angle, but reduces cohesion.

This holds especially for untreated material. However, these effects are reduced for BSM-foamed mixes with active filler contents. The angle of internal friction is believed to be mostly dependent on aggregate properties such as grading and angularity of particles. However, the reduction of the friction angle is quite notable between the mixes with 100%G2 and 100%RA.

The cohesion and friction angle are not entirely independent of each other since there is some sort of a balancing effect where the friction angle reduces when the cohesion increases significantly as a result of chemical stabilisation for the same material. Jenkins (2000) even reported friction angles of as low as $\Phi = 0^o$ for crushed stone foamed bitumen mixes to which 1.5 to 2.0% cement was added. The cohesion in these cases was reported as high as between 0.800 and 1.100 MPa. The low friction angle in the BSM-foam mix with 100%RA is probably due to the ageing process, which created a sensible reduction of the penetration value of the bitumen (Table 3.4).

From the results reported in this paragraph it is possible to conclude that increased density (improved compaction) reduces the risk of shear failure at different load levels. Improved compaction thus increases the pavement life. This is illustrated by the transfer functions for permanent deformation provided in the TG2 Guideline for foamed BSMs, in which the relative density is the most important variable. This transfer function for a 90% reliability level (South African Road Category B) is shown in Equation [4.1]:

$$N_{PD} = \frac{1}{30} \cdot 10^{[-1.95+11.938RD+0.0726PS-1.628SR+0.691\left(\frac{cem}{bit}\right)]} \quad [4.1]$$

where
N_{PD} = Structural capacity (No. of load repetitions)
RD = Relative density (%-Apparent Density)
PS = Plastic strain (%)
SR = Deviator Stress Ratio ($\sigma_1 - \sigma_3/\sigma_{1,f} - \sigma_3$)
cem/bit = ratio of cement and bitumen contents

It is important to control the quality and quantity of RA to prevent lower level of angle of friction and a consequent shear failure. Figure 4.10 summarises the relationship between the friction angle and the cohesion with the increasing amount of RA in the mixes.

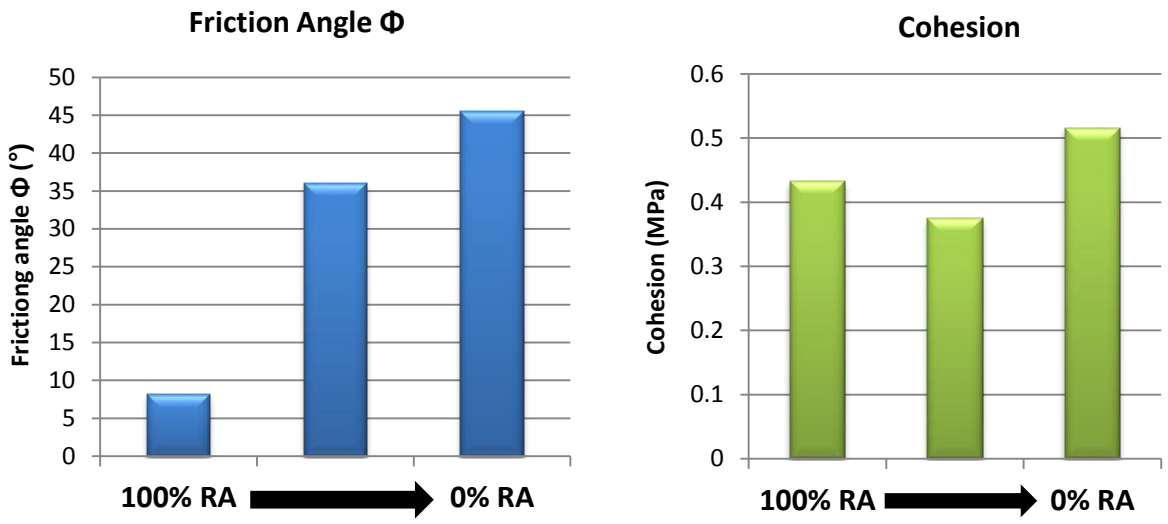

Figure 4.10: Relation between friction angle and cohesion with the percentage of RA.

After the monotonic tri-axial tests the moisture content of the BSM-foam mixed was measured through a draft oven. The average levels of moisture for the three BSM-foam mixtures were 3.8% for the 100%RA, 5.5% for the 50%RA and 50%G2 and 5.5% for the 100%G2. Twagira (2010) showed that mixes with low compaction and high retained moisture content have lower cohesion. In fact, compaction is the factor that influences voids content and the adhesion of the mastic on the coarse fractions, whilst, high saturation indicates poor bond development in the BSM-foam mixtures. Mixes with high density have higher cohesion.

4.5 Resilient modulus tests

The short duration dynamic tri-axial test is well suited to determine the resilient stiffness of granular materials. It is also capable of determining the stress dependency of this material property. It is however a test that is typically carried out in a research environment. As such it has been used extensively by many researchers around the world.

In the resilient modulus dynamic tri-axial test, the resilient modulus is measured over a range of confining and vertical stress levels, to enable the resilient modulus to be determined as a function of the stress condition. The resilient modulus for each of the deviator stress ratios at the three confinement pressures and three different temperatures (10, 25 and 40°C) were determined following the methodology as discussed in Chapter 3. The resilient behaviour of BSMs can be tested in a tri-axial setup by applying relatively low stresses creating low strains so that the elastic range of materials is not exceeded. It is assumed that, within this elastic range, stress history does not affect the material's response. Resilient modulus testing was carried out, guided by the failure parameters obtained in the monotonic tri-axial tests. The dynamic tri-axial tests are used to determine both the resilient modulus and the permanent deformation behaviour of materials.

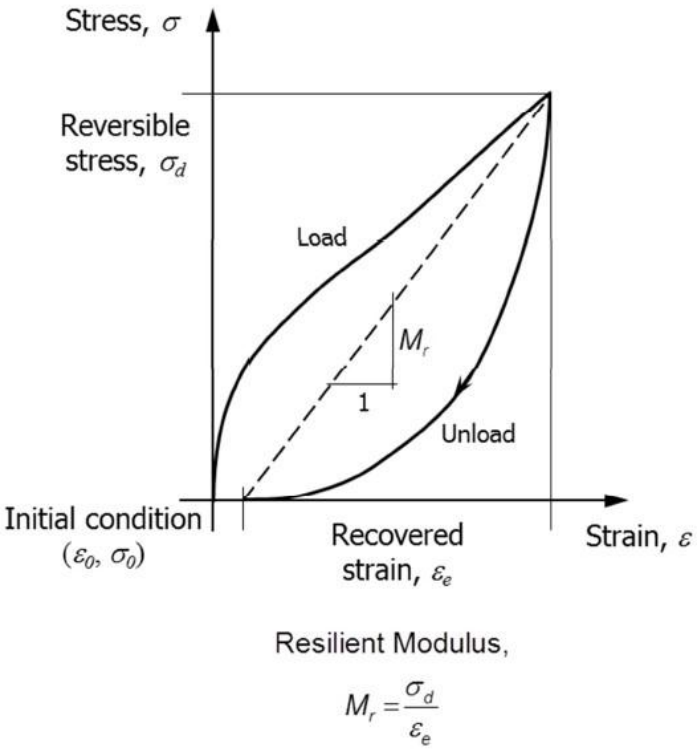

Figure 4.11: Resilient modulus definition and calculation (Jenkins et al., 2007).

The resilient modulus test requires 1000 conditioning load cycles followed by a series of loading sequences that starts at a relatively high confinement pressure of 100 kPa which is then reduced to 50 or increased to 200 kPa for subsequent sequences (Theyse H.L., 2012). The deviator stress was increased during each loading sequence to induce deviator stress ratios ($\sigma_d/\sigma_{d,f}$) of 15 to 50 % of the failure stress at each particular level of confinement pressure. The failure stress model for the particular material was calibrated beforehand from monotonic loading tri-axial tests. A total of 100 load cycles were applied at each confinement pressure – stress ratio combination and the axial load, vertical and radial displacement were recorded for the last five load cycles.

The axial deformations were measured by LVDTs (Linear Variable Differential Transformers) that were fixed around the specimen through plastic brackets. An LVDT can register small displacements very accurately (stroke range ±5 mm, sensitivity 82.7±4 mV/V/mm, test excitation frequency 2.5 kHz, repeatability 0.000004 inch [0.1µm], temp. coefficient of sensitivity [±0.009% per ºC]). Three LVDTs were mounted at equal distances around the specimen. The applied load consisted of a haversine waveform and a pre-load (conditioning phase) of 20% of the confining pressure or a minimum preload of 5 kPa. The confining pressure also works on the top loading plate. The total vertical stress σ_1 is the total of the confining stress σ_3, the seating stress σp and the deviator stress σ_d, i.e., $\sigma_1 = \sigma_3 + \sigma_p + \sigma_d$.

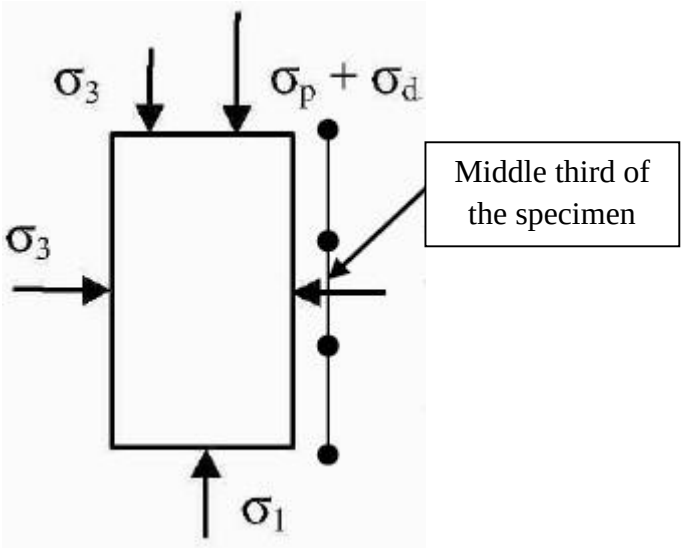

Figure 4.12: Test layout Resilient Modulus Tri-axial Test.

A test frequency of 1Hz with a load pulse of 0.1s followed by 0.9 s rest period was included in the loading. The purpose of a rest period is to simulate the pauses in between wheel loads and because some delayed elastic recovery can be expected in BSMs due to the presence of bitumen in the mix. The rest period allows the complete viscoelastic recovery of the bitumen. The loading level was selected with care so as not to overstress the specimens. The influence of loading wave in determining permanent axial strain accumulation is vital, particularly in urban areas. Pavement in urban areas experiences static as well as dynamic loading. Traffic moving over a pavement structure results in a large number of rapidly applied stress pulses being applied to the material comprising each layer. Typically, these stress pulses last for only a short period of time. The type, magnitude, and duration of the pulse vary with the type of vehicle and its speed, the type and geometry of the pavement structure, and the position of the elements of the material under consideration. The dynamic modulus is measured in the laboratory using a haversine stress pulse as the loading type when testing asphalt concrete specimens. This haversine pulse is assumed to replicate what actually occurs on the pavement in the field. When a truck tire is at a considerable distance away from a point of interest in the pavement, the stress at that point is zero; when the tire is exactly at that point of interest, the stress is maximum. In the 1970s, Barksdale used the finite-element method and elastic theory to calculate the vertical compressive stress pulse (Barksdale, 1971). He concluded that the vehicle speed and the depth beneath the pavement surface are of great importance in selecting the appropriate axial compressive stress pulse time to use in the dynamic testing in the laboratory. He found that the pulse shape varied from approximately the sinusoidal one at the surface to a more nearly triangular one at depths below approximately the middle of the base. The depth of each layer and the change of resilient modulus values of the pavement materials due to changes in the environment were found not to affect the pulse shape and duration.

A number of consistency checks were also done to assess the data quality of individual tests. Different stress ratios were applied to all the three BSM-foam mixes. A conditioning period of 1000 cycles was applied for all the specimens tested.

The axial strain was subjected to 100 cycles prior to the measuring of the stiffness response (Table 4.6). Load and displacement data were sampled using the Spider 8 data acquisition

system at a frequency of 200 Hz. A typical sequence of resilient modulus tests is shown in Table 4.6.

Table 4.6: Typical test parameters used for the determination of the resilient modulus.

Loading Sequence	Confining pressure (kPa)	Contact Stress (kN)	Deviator Stress Ratio (%)	Load Repetitions
Conditioning	100	10	30	1000
1.1	200	20	50	100
1.2	200	20	40	100
1.3	200	20	30	100
1.4	200	20	25	100
1.5	200	20	15	100
2.1	100	10	40	100
2.2	100	10	35	100
2.3	100	10	30	100
2.4	100	10	25	100
2.5	100	10	20	100
2.6	100	10	15	100
3.1	50	5	35	100
3.2	50	5	30	100
3.3	50	5	25	100
3.4	50	5	20	100
3.5	50	5	15	100

During the entire test programme all the vertical LVDTs mounted on the specimens and the two circumferential LVDTs were constantly monitored and recalibrated in the event of a low level of data capturing accuracy. Appendix C describes the complete dynamic test set-up used in this research.

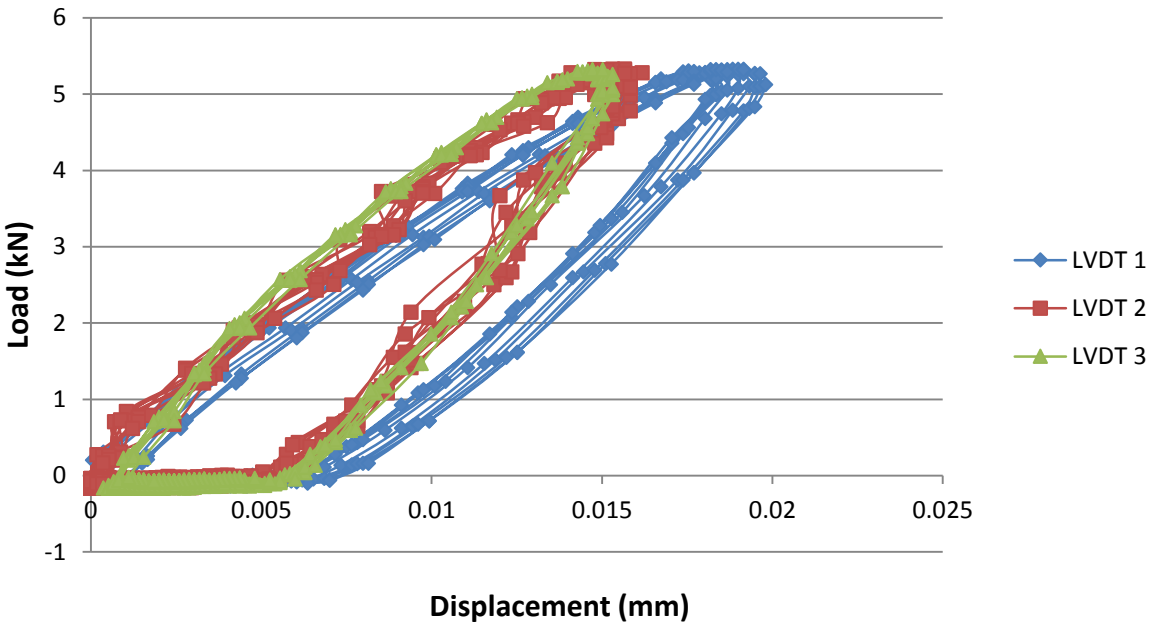

Figure 4.13: Typical relationship between load and displacement in a resilient modulus test.

From Figure 4.13 a good correlation appears between the load recorded through the load cell and the displacement of the three LVDTs. Only the first LVDT shows a small shift compared with the others probably due to a not perfect alignment on the horizontal axis during the phase of mounting.

During all the resilient modulus tests two circumferential LVDTs were mounted around the tri-axial specimens in the middle third. The two gauges were connected to two o-rings situated in the middle third area of the specimen. The two gauges have the capability to measure small amounts of displacement until the maximum displacement of 5mm (stroke range ±5mm, sensitivity 82.7±4 mV/V/mm, test excitation frequency 2.5 kHz, repeatability 0.000004 inch [0.1µm], temperature coefficient of sensitivity [±0.009% per ºC]). Further research needs to be carried out to investigate the possible relations between this recording method and the rest of the other data recorded with the three external LVDTs better.

The justification for stress-dependent behaviour is apparent when considering a typical relationship between resilient modulus and bulk stress, as shown in Figure 4.14. The model shown in this case is Mr-θ-$\sigma_d/\sigma_{d,f}$ and its output is shown relative to the actual results in the figure. The graphs in Figure 4.14 show the importance of the influence of temperature on resilient modulus. The BSM-foam mix with 100%G2 (no RA) achieves higher values than the BSM-foam with 100%RA.The differences could be due to numerous causes such as: cohesion values, percentage of air voids, the amount of filler and foam bitumen.

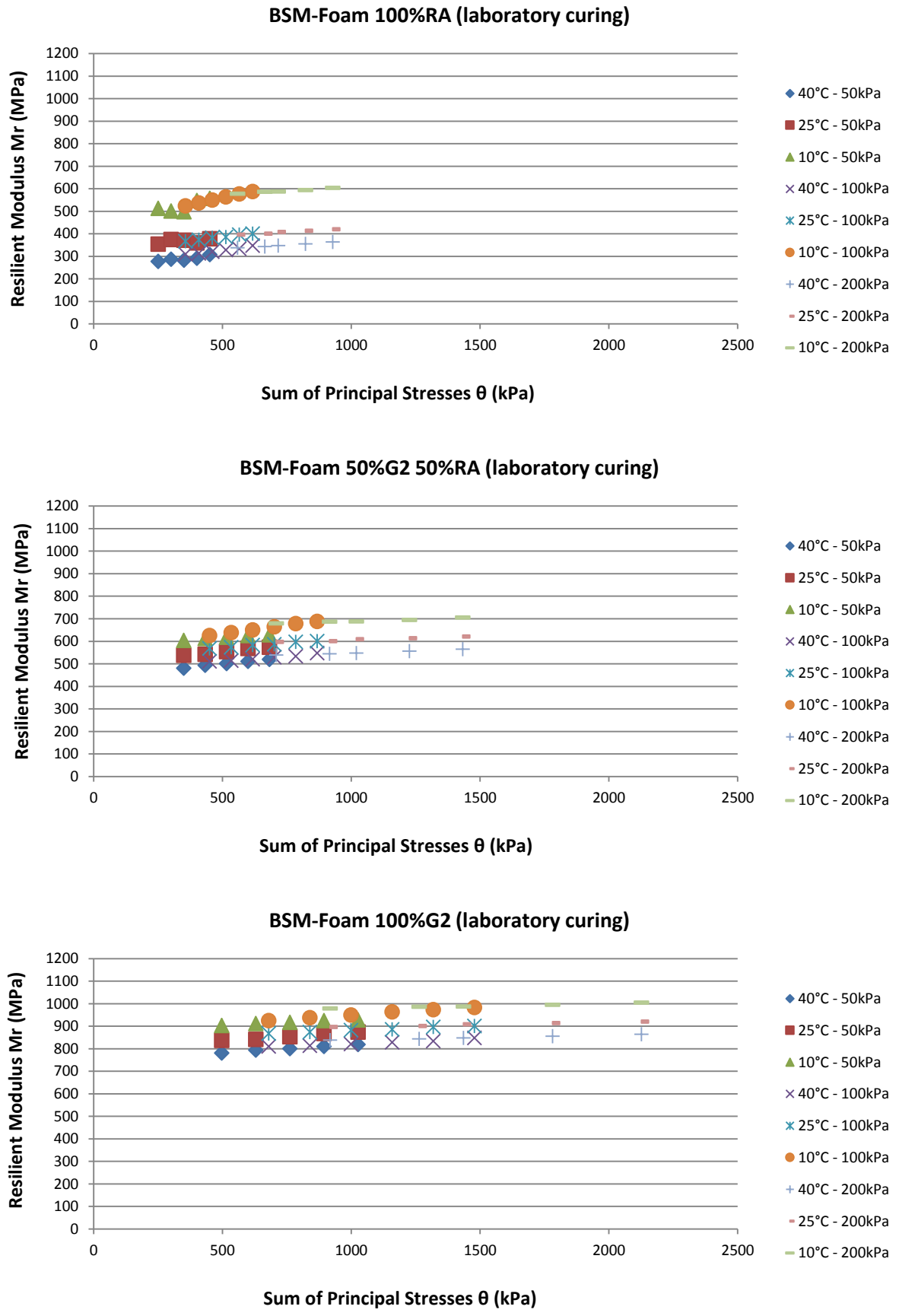

Figure 4.14: Resilient modulus for the three BSM-foam mixtures after laboratory curing (Asphalt Academy, 2009).

Further tests have been conducted to analyse the behaviour of all the mixes after a period of curing of six months better, as shown in Figure 4.15. The resilient modulus increases drastically compared to previous results obtained after a laboratory curing (almost three days). Even in these tests the temperature is an important factor for measuring the resilient modulus. Consistent to resilient modulus results, the mixture containing 100%G2 (no RA) shows the highest resilient modulus.

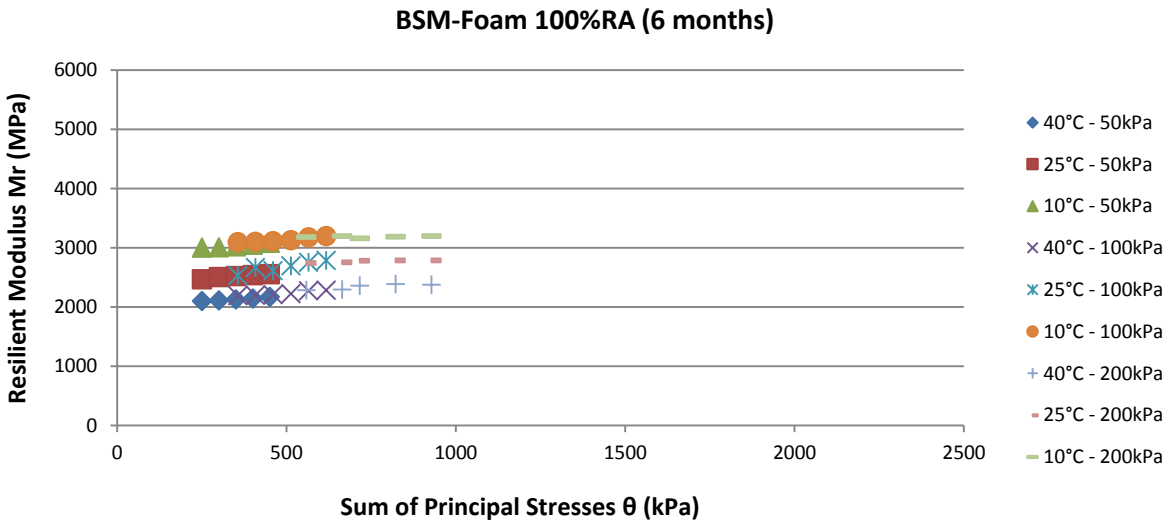

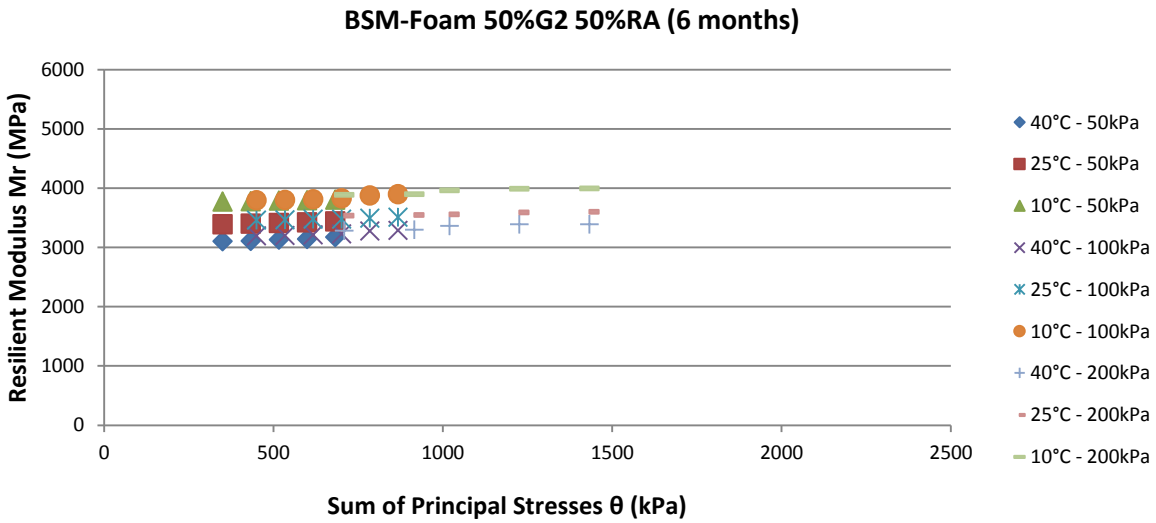

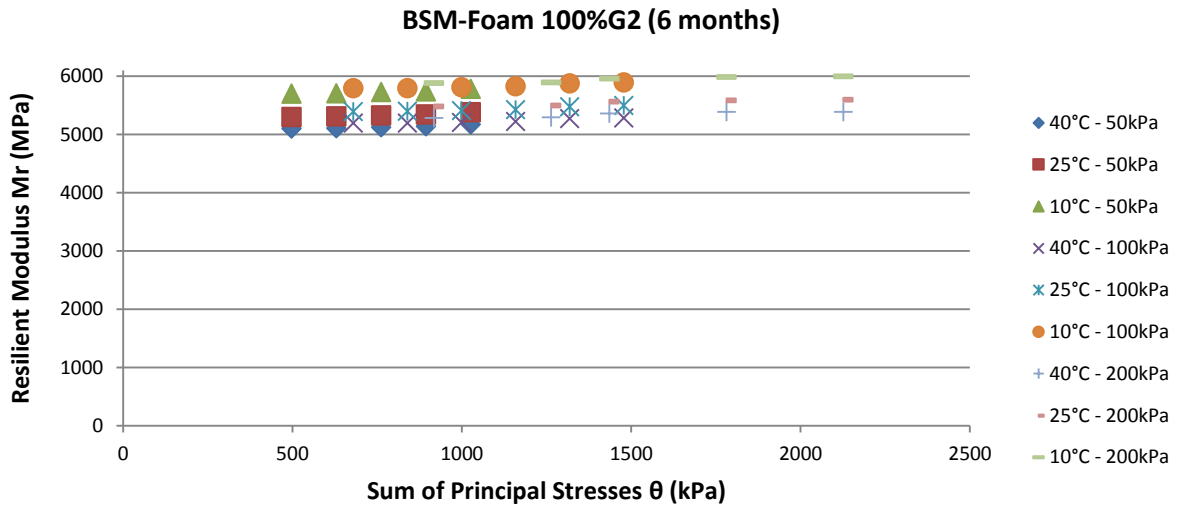

Figure 4.15: Resilient modulus for the three BSM-foam mixtures after a curing period of six months.

The trends in the repeat tests (constant stiffness, stress stiffening or stress softening) are consistent, thus indicating good repeatability of the parameters measured.

The results presented therefore are essentially from laboratory investigations and would require field trials for the validation of the laboratory results.

4.5.1 Modelling Mr

As discussed in Chapter 2, one of the most common models to describe the stress dependent behaviour of a material is the so-called Mr-θ model. Through the analysis of the results showed in the previous paragraph, a new Mr-θ model is presented taking into account two new variables:

- %RA;
- temperature.

To facilitate this study, the three BSM foam mixes with an increasing amount of RA were plotted considering the same confinement pressure σ_3. The same stress situation was selected for all three mixes in all three different figures. This approach was selected to facilitate the regression analysis of Mr with the addition of two new variables.

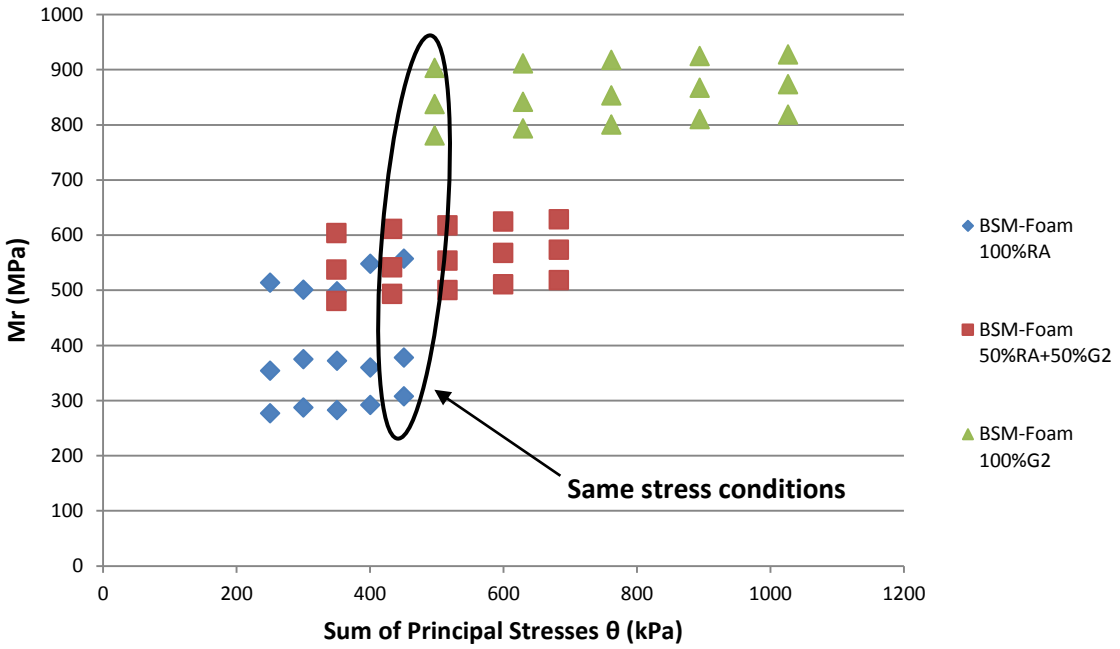

Figure 4.16: Resilient modulus as a function of the total stress from tri-axial tests, at σ_3 constant = 50kPa and different temperatures, for three BSM-foam mixes with an increasing amount of RA.

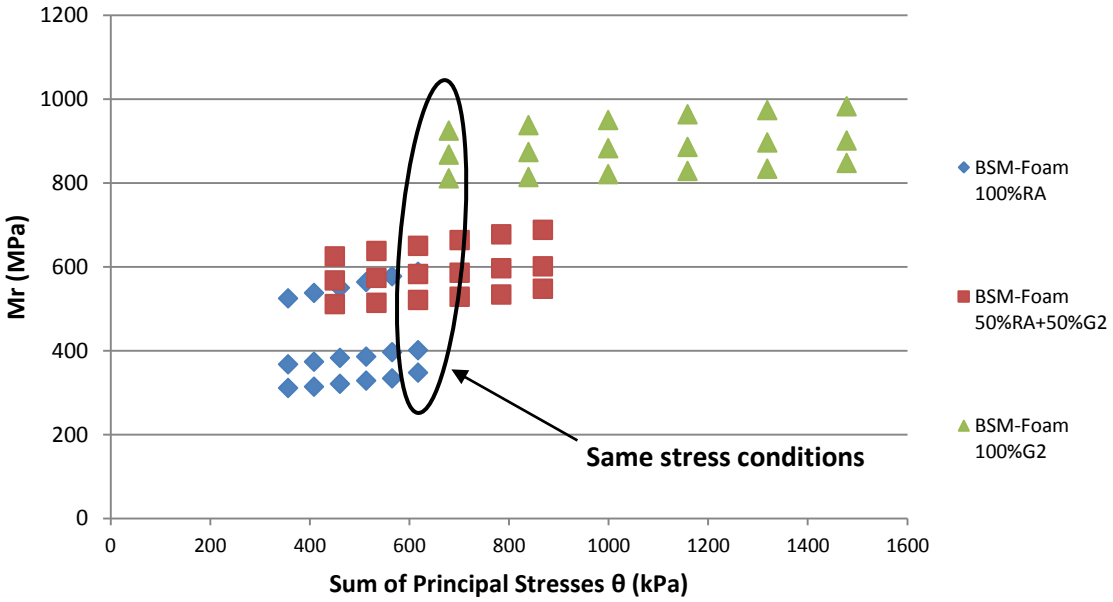

Figure 4.17: Resilient modulus as a function of the total stress from tri-axial tests, at σ_3 constant = 100kPa and different temperatures, for three BSM-foam mixes with an increasing amount of RA.

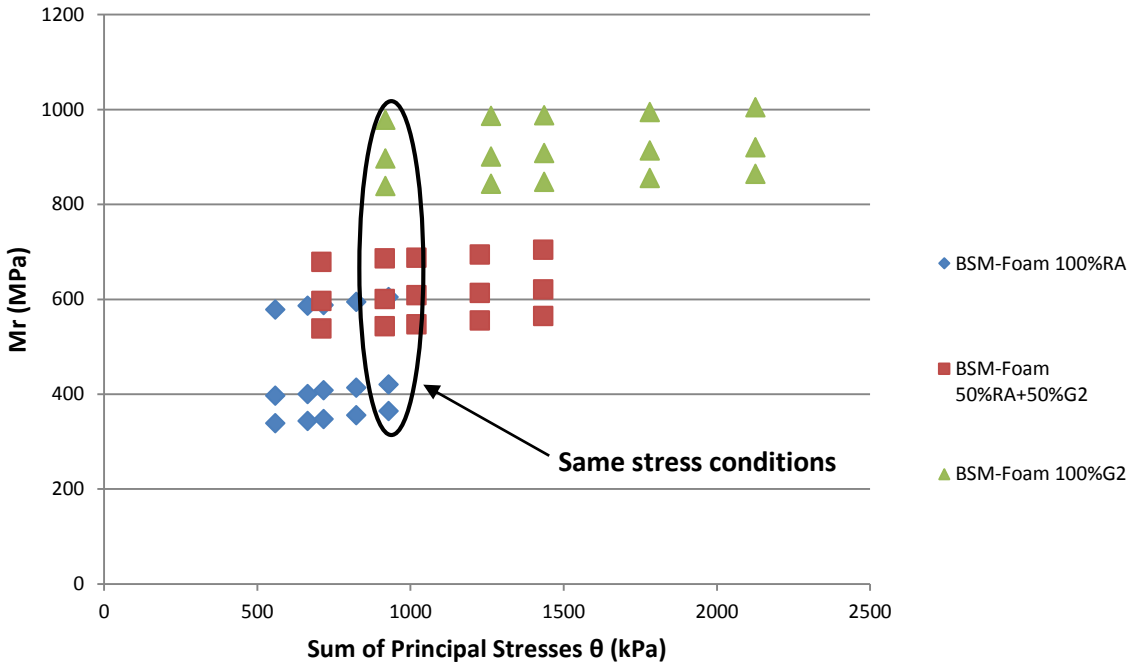

Figure 4.18: Resilient modulus as a function of the total stress from tri-axial tests, at σ_3 constant = 200kPa and different temperatures, for three BSM-foam mixes with an increasing amount of RA.

In all three previous figures (Figures 4.16, 4.17 and 4.18) the Mr values for all the BSM mixes are placed along almost flat lines at different temperatures, which can indicate a low stress dependency.

The Mr values selected at the same stress situation were subsequently plotted against temperature and percentage of RA. An interpolation line was drawn for all three points for each BSM-foam mix at different temperatures and percentage of RA. A similar relationship was discovered between the temperature and the percentage of RA at different confinement pressures. The linear equations for BSM-foam mix with a percentage of RA equal or less than 50% were found to be the best option to fit the three Mr values for each mix at different temperatures and different confinement pressures. An exponential line was preferred to a linear equation for the BSM-foam mix with 100%RA. This choice was due to the different behaviour of the mix, which shows a marked difference of Mr values between low temperatures (10°C) and higher temperatures (25°C and 40°C). Almost the same coefficients were found similar in all the three Mr vs. temperature representations at different confinement pressures (σ_3 = 50kPa, 100kPa, 200kPa).

In the beginning a linear interpolation analysis was tried in the graphs were Mr is plotted against the percentage of RA, but during the modelling, the predicted Mr values did not match the observed values. An exponential line was the best option to interpolate the Mr data in the BSMs even with a percentage of RA less than 50% (Figures from 4.19 to 4.24).

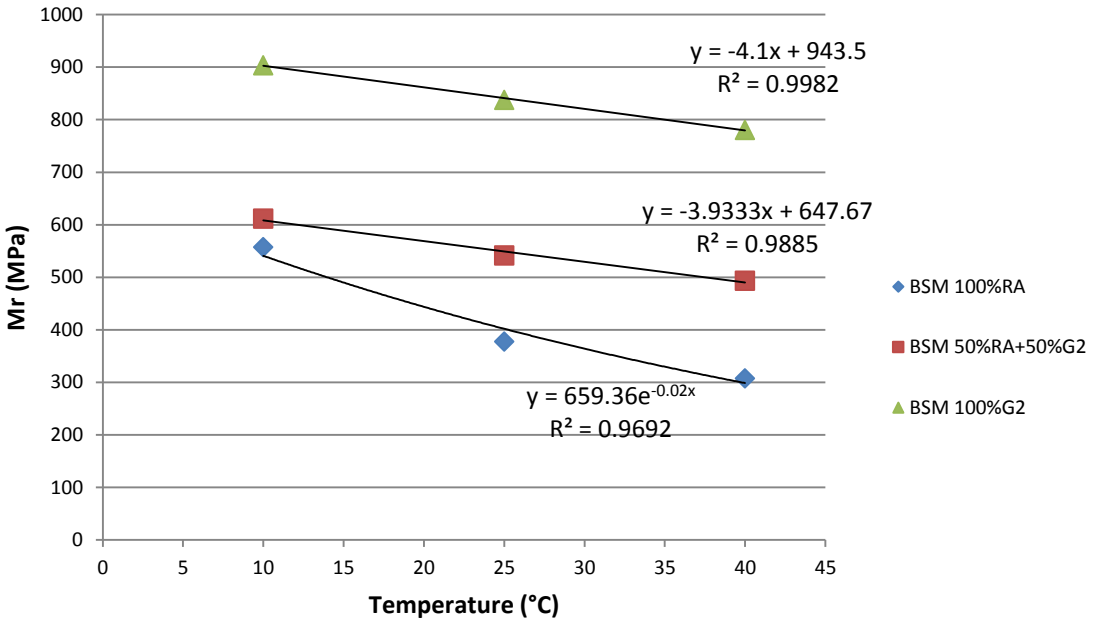

Figure 4.19: Resilient modulus as a function of temperature, at σ_3 constant = 50kPa for three BSM-foam mixes with an increasing amount of RA.

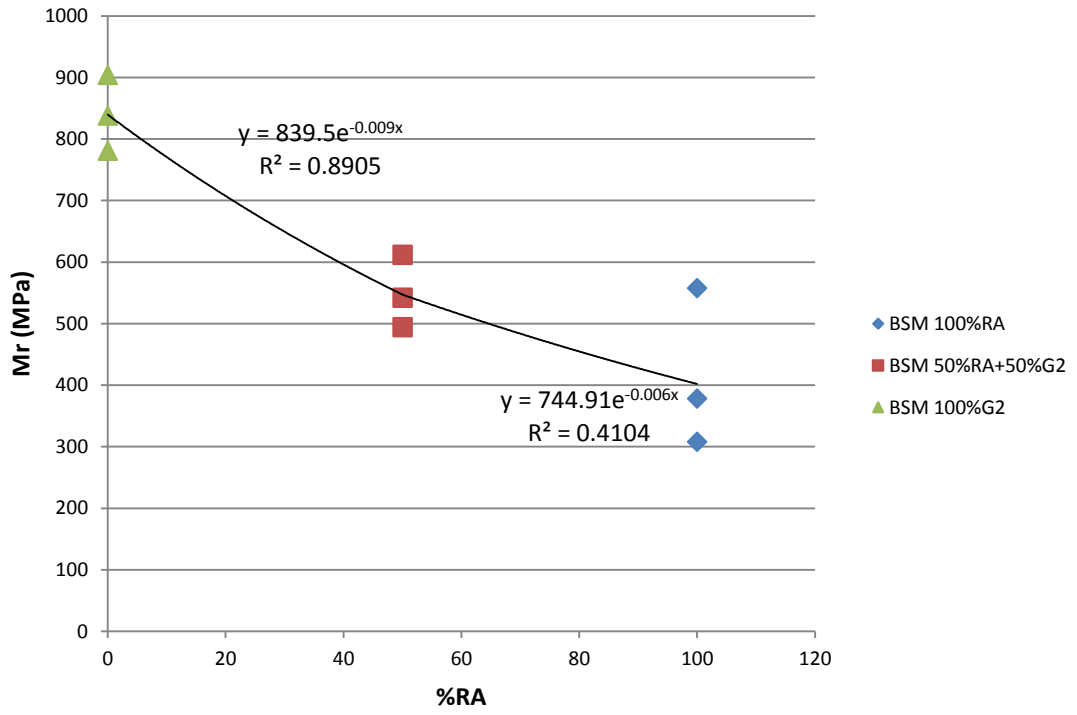

Figure 4.20: Resilient modulus as a function of percentage of RA, at σ_3 constant = 50kPa for three BSM-foam mixes with an increasing amount of RA.

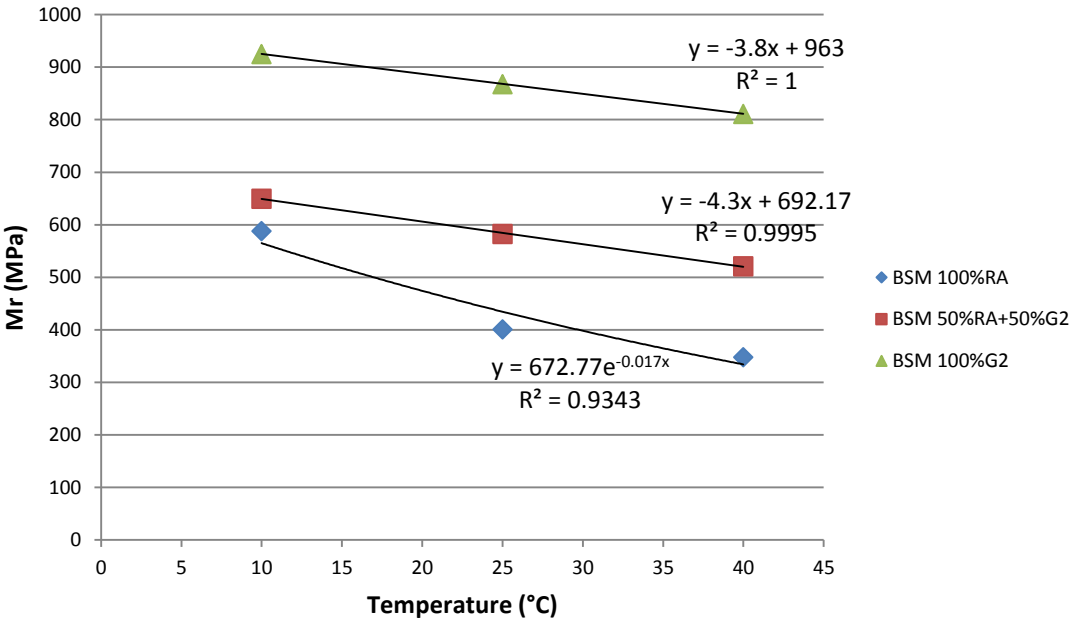

Figure 4.21: Resilient modulus as a function of temperature, at σ_3 constant = 100kPa for three BSM-foam mixes with an increasing amount of RA.

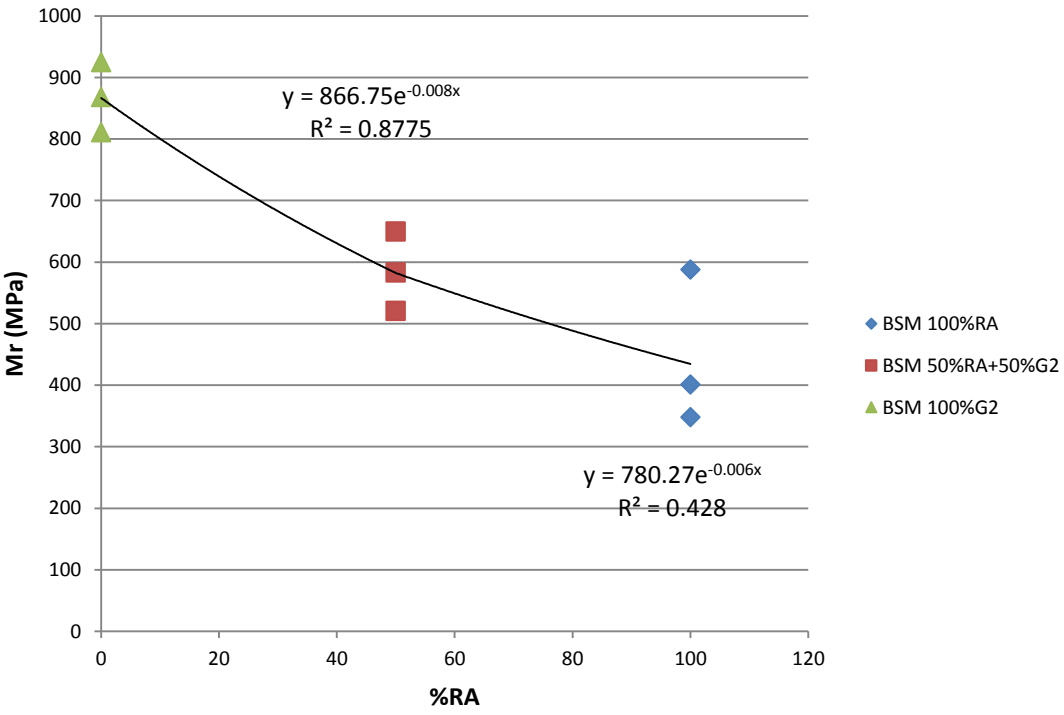

Figure 4.22: Resilient modulus as a function of percentage of RA, at σ_3 constant = 100kPa for three BSM-foam mixes with an increasing amount of RA.

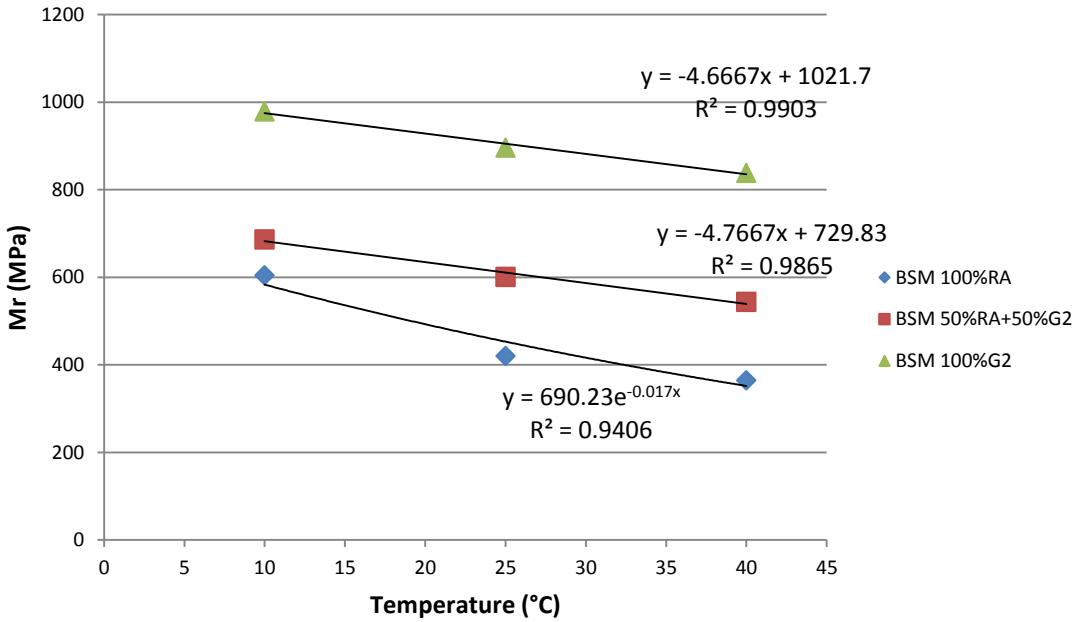

Figure 4.23: Resilient modulus as a function of temperature, at σ_3 constant = 200kPa for three BSM-foam mixes with an increasing amount of RA.

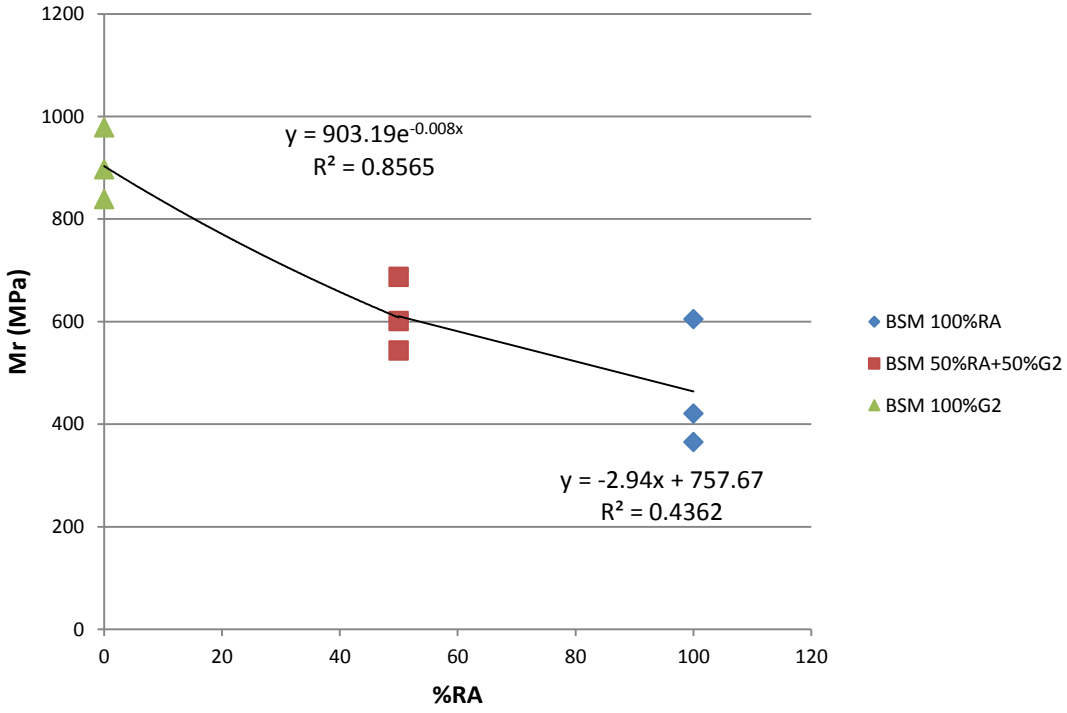

Figure 4.24: Resilient modulus as a function of percentage of RA, at σ_3 constant = 200kPa for three BSM-foam mixes with an increasing amount of RA.

Models used for application to the Mr-θ data depend on the form of the relationship between temperatures and percentage of RA, as exhibited graphically. In the case of the results obtained for the BSM-mix with a percentage of RA less than or equal to 50%, the new model of Mr was applied:

$$Mr = \left(k_2 870 e^{-\left(\frac{\%RA}{100}\right)} + \theta k_1\right) + (-4(T - T_{ref})) \qquad \text{with a \%RA} \leq 50\% \qquad [4.2]$$

where
Mr = Resilient modulus (MPa)
θ = Bulk stress = $\sigma_1 + \sigma_2 + \sigma_3$ (kPa)
T = temperature test (K)
T_{ref} = 298.15K (25°C)
k_1, k_2 = model coefficients

The formula which can describe the Mr values for a BSM-foam mix with higher percentage of RA (>50%) is:

$$Mr = \left(-\left(\frac{T-T_0}{10}\right)\left(\frac{\%RA}{100}\right) + \theta k_1\right) + \left(k_2 e^{\left(\left(\frac{\%RA-50}{100}\right)(-0.034)(T-T_{ref})\right)}\right) \qquad \text{with a \%RA} > 50\% \qquad [4.3]$$

where
Mr = Resilient modulus (MPa)
θ = Bulk stress = $\sigma_1 + \sigma_2 + \sigma_3$ (kPa)
T = temperature test (K)
T_0= 273.15K
T_{ref} = 298.15K (25°C)
k_1, k_2 = model coefficients

Figures 4.25 and 4.26 show the Mr data matching completely the Mr values predicted through the two models for the different BSM-foam mixes with different amount of RA.

The modelling of Mr was designed on a small data population, considering only three mixes with three determined quantity of RA percentage.

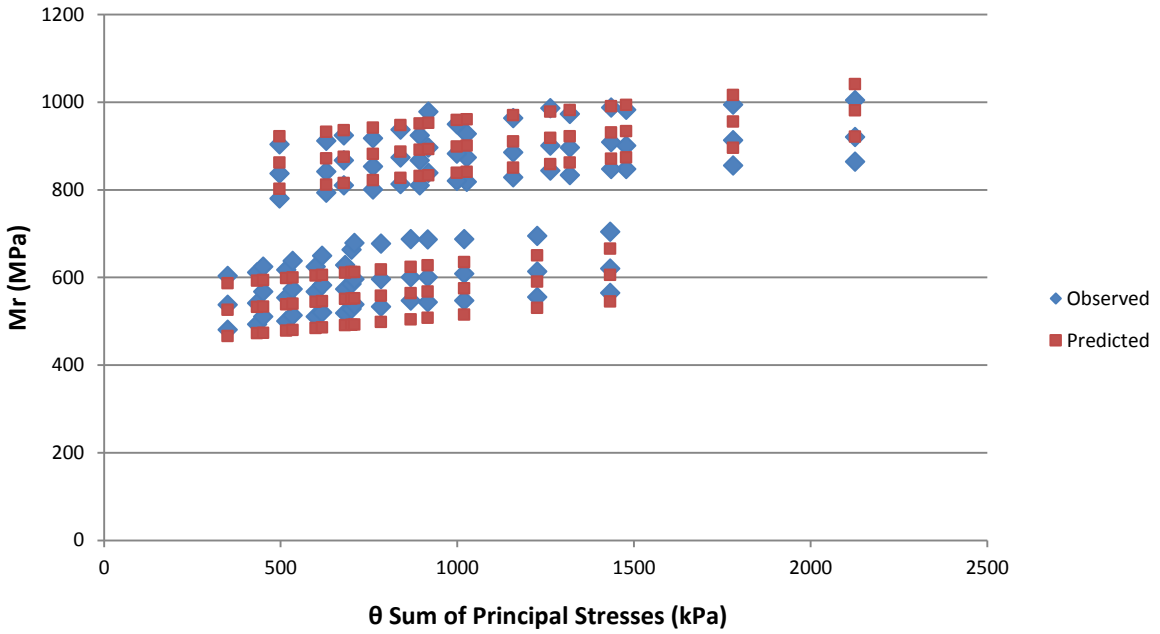

Figure 4.25: Comparison Mr observed and Mr predicted for BSM-foam mixes with a percentage of RA≤50%.

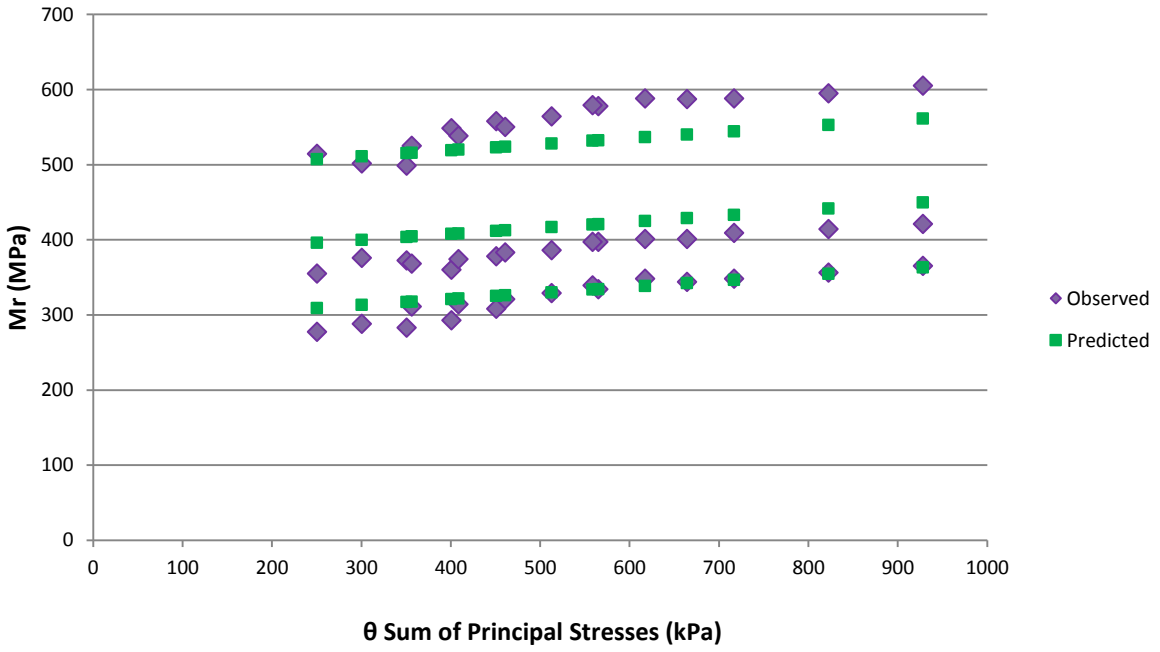

Figure 4.26: Comparison Mr observed and Mr predicted for BSM-foam mixes with a percentage of RA>50%.

Table 4.7 summarises the k_1 and k_2 coefficients for the two models and the R^2 values determined in this study.

Table 4.7: Summary of Mr model coefficients for BSM foam mixes with different percentage of RA.

Mix type	K_1	K_2	R^2
BSM foam mix with RA≤50%	0.073	0.950	0.98
BSM foam mix with R>50%	0.08	378.29	0.96

This modelling didn't include the moisture content (MC) as a factor like in the research conducted in the SAPDM project (Theyse, 2012) and me-PADS (CSIR, 2007) for granular materials. The study was only based on the effective moisture content (EMC) and relative density (RD) prescribed by the specifications for accelerated curing (Asphalt Academy, 2009).

The two models are capable of describing the stress-stiffening up to a certain deviator stress level at different confinement stresses. For the purpose of calculating the resilient modulus (Mr) for the BSM-foam mixes with higher percentage of RA, relationships require establishment for the Mr as a function of the temperature and the percentage of RA. Due to time constrains and availability of material the modelling was only applied to three BSM-foam mixes.

4.6 Permanent deformation tests

Not all mixes were subjected to the same range of temperature. Only the permanent deformation of the BSM-foam mix with 50%RA and 50%G2 was analysed at three different temperatures (25˚C, 40˚C and 50˚C). The other two remaining BSM-foam mixes were tested at only one temperature, namely 40˚C. Tests were conducted in dry conditions.

During the dynamic tri-axial test the response of the specimen to different levels of loading at a range of confinement pressures was measured. These confinement pressures were the same as used during the monotonic testing. The load level during the dynamic tri-axial test was described by the deviator stress ratio. This is the ratio between the applied deviator stress and the deviator stress at failure:

$$\text{Deviator Stress Ratio} = \frac{\sigma_d}{\sigma_{d,f}} \qquad [4.4]$$

where
σ_d = applied deviator stress
$\sigma_{d,f}$ = deviator stress at failure

The latter was derived from the cohesion and friction angle as determined by the monotonic tri-axial testing at different temperatures (25°C and 40°C). The results in terms of $\sigma_{d,f}$ from the monotonic tri-axial test at 50°C for a BSM-foam mix with 50%RA and 50%G2 material were extrapolated from Figure 4.27. The high $\sigma_{d,f}$ recorded for the BSM-foam with 100%G2 material is not completely unusual. Past studies conducted by Twagira (2010) showed values close to $\sigma_{d,f}$ = 3 000 kPa. However, most of the past literature on BSM-foam mixes with 100%G2 presented values closer to 2 500 kPa. The high value recorded in this study can be attributed to the attention given to all the phases of the mix design (grading, compaction,...) and for the presence of 1% of cement in the mix.

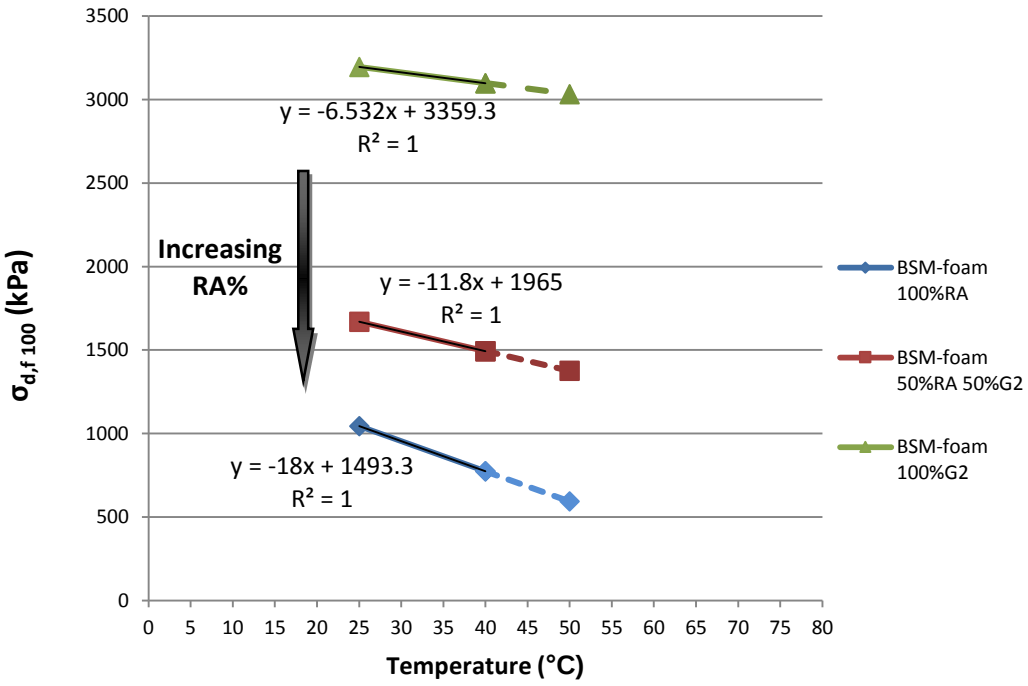

Figure 4.27: Extrapolation of $\sigma_{d,f}$ for BSM-foam mixes with increasing percentage of RA at 50°C.

Each BSM-foam mix showed a different slope, during the interpolation of the different $\sigma_{d,f}$ recorded for monotonic tri-axial tests at 25°C and 40°C. BSMs with high percentage of RA have a higher slope than BSMs with low percentage of RA. A linear extrapolation of the $\sigma_{d,f}$ at 50°C was adopted considering research done by Jenkins (2000). His study revealed that the percentage of bulk volume for the mastic is a primary factor influencing the stiffening of foam or emulsion mix. Foamed bitumen stiffens at lower %Vdb (40%) and stiffens more rapidly as %Vdb increases, compared to HMA. The best explanation for the stiffening behaviour of mastic is the physico-chemical properties of filler-binder interaction. The high reactivity of filler fraction to the polar and non-polar molecules of the dispersed foamed bubbles influences the faster stiffening potential compared to the interaction of thick film dispersed in the HMA.

The confinement pressure, the different temperatures and the deviator stress ratios are summarised in Table 4.8. All the specimens were conditioned in the climate chamber at the 25°C, 40°C and 50°C to achieve a uniform temperature.

Table 4.8: Confinement pressures and deviator stress ratios for different BSM-Foam mixes.

BSM-Foam Mix	Confining Pressure (kPa)	Deviator Stress Ratio	Deviator stress (kPa)	Temperature (°C)
100%G2	100	45	1294.00	40

BSM-Foam Mix	Confining Pressure (kPa)	Deviator Stress Ratio	Deviator stress (kPa)	Temperature (°C)
50%RA + 50%G2	100	40	568.00	25
	100	45	651.50	25
	100	50	735.00	25
	100	30	347.90	40
	100	40	497.20	40
	100	42.5	534.53	40
	100	45	571.85	40
	100	50	646.50	40
	100	40	450.00	50
	100	45	518.75	50

BSM-Foam Mix	Confining Pressure (kPa)	Deviator Stress Ratio	Deviator stress (kPa)	Temperature (°C)
100%RA	100	40	209.32	40
	100	45	247.99	40

Before the actual sampling of test data, the specimens were subjected to 1000 conditioning cycles at the confinement pressure of 100kPa, which is held constant throughout the test to simplify the test control, and at a deviator stress ratio of 0.18. There are indications that the stiffness of previously unloaded BSM-foam specimens reduces during the initial stages of loading and that the stiffness stabilises after a certain number of initial load repetitions. The number of conditioning cycles used in this study was chosen high to ensure that all initial stiffness reduction and settlement had taken place. The number of 1000 may be too high for production testing and could possibly be reduced. This would however require further testing and investigation. Most of the mixes were tested for a limited number of loading cycles; only the BSM-foam with 50%RA and 50%G2 was tested for 500 000 loading cycles at the temperature of 40˚C. The rest of the other permanent deformation tests were carried out at the maximum number of 300 000 loading cycles.

The results of the permanent deformation test for the BSM-foam mixtures with 50%RA and 50%G2 provide a template of deformation at different stress levels and different temperatures. These results can be combined into unified graphs for each specific temperature that exhibit stress dependent behaviour. The plots are shown on a double log scale in Figures 4.28, 4.29 and 4.30.

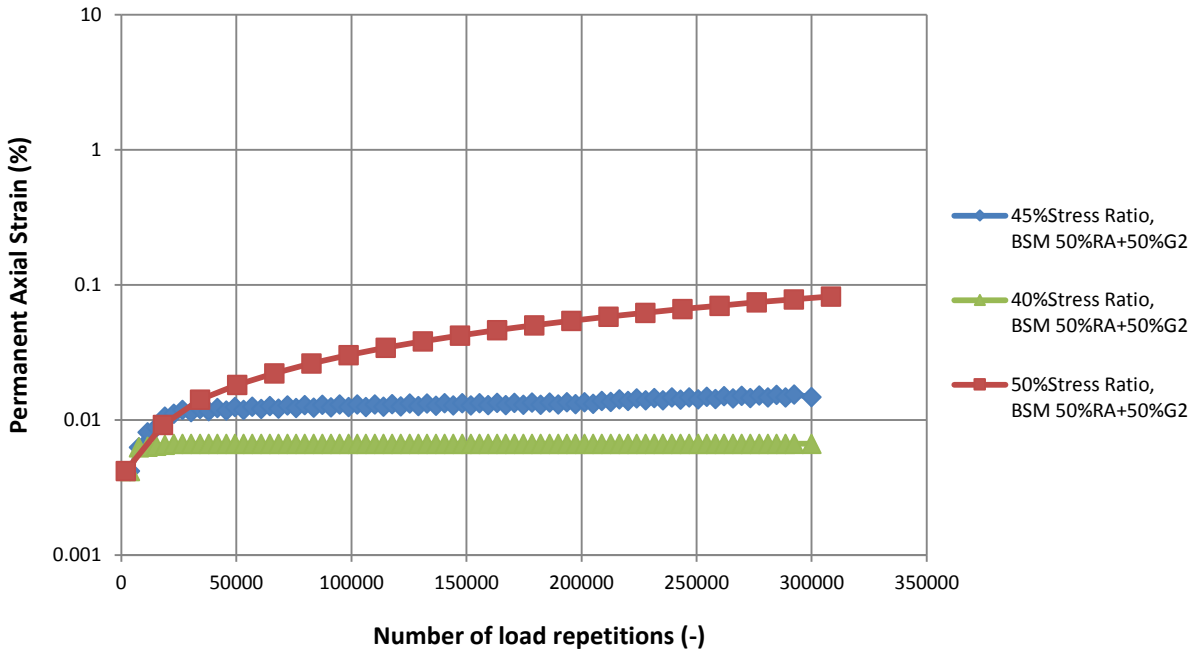

Figure 4.28: Permanent deformation test for BSM-foam mix with 50%RA and 50%G2 at 100kPa of confinement and at 25°C.

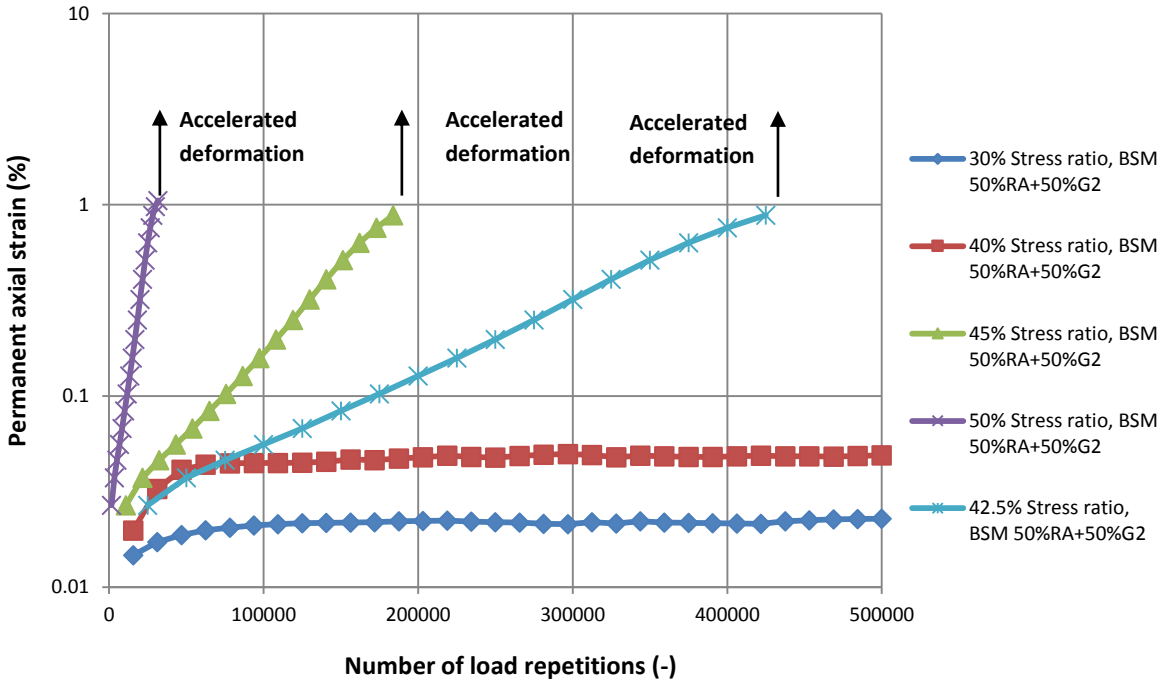

Figure 4.29: Permanent deformation test for BSM-foam mix with 50%RA and 50%G2 at 100kPa of confinement and at 40°C.

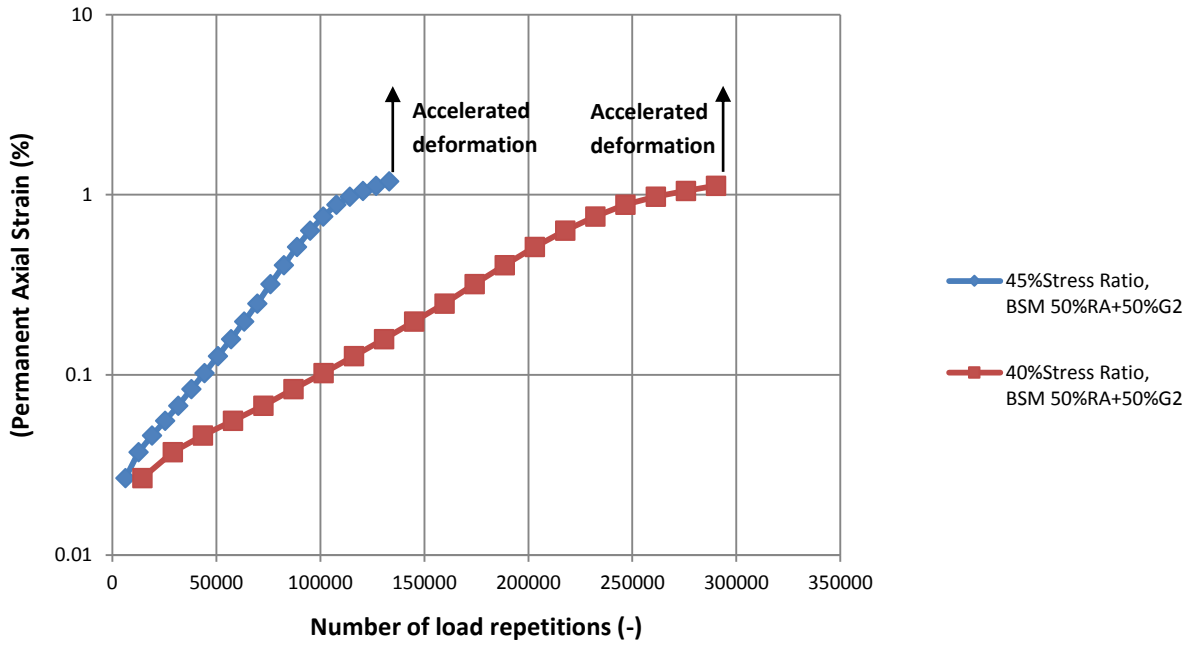

Figure 4.30: Permanent deformation test for BSM-foam mix with 50%RA and 50%G2 at 100kPa of confinement and at 50°C.

Permanent deformation is believed to occur in three phases. During the first phase the accumulation of permanent deformation occurs at a fast rate initially. This can mainly be attributed to bedding-in, seating of the loading plates and initial permanent strain due to densification. The deformation during this initial phase follows a hyperbolic curve. It can be seen that most of the deformation takes place in the first 20,000 load repetitions. Afterwards the rate of deformation starts to reduce. The first phase can last up to 50,000 load repetitions or even more depending on the type of mix and the applied loading. The second phase is characterised by a constant rate of deformation. The accumulation of permanent deformation is more or less linear with respect to load repetitions. The third phase is one of accelerated accumulation of permanent deformation due to tertiary flow. During the third phase the material may be considered to be failing in shear under repeated loading. The third phase starts at the so-called flow-point, which is the number of load repetitions at which the strain accumulation rate is minimal. Up until the flow point the rate of strain accumulation reduces, while after the flow point the rate of strain accumulation accelerates. The number of load repetitions at which the flow point occurs cannot easily be predicted, as tertiary flow may initiate quite unexpectedly.

Previous researchers already identified the existence of a critical stress ratio (Jenkins, 2000, Ebels, 2008 and Twagira, 2010). When a material is repeatedly loaded above this critical deviator stress ratio the permanent deformation behaviour includes a third phase as described above. Repeated loading below this critical stress ratios results in on-going stable second phase behaviour. The critical deviator stress ratios were identified for the mix with 50%RA and 50%G2 at the temperature of 40°C.

As with the stiffness function different deviator stress values σ_d has been used in the calculation of the permanent deformation. According to this research, a ratio of $\sigma_d/\sigma_{d,f} = 42.5\%$ defines this critical boundary for foamed materials with 50%RA and 50%G2 at the temperature of 40˚C. Below a ratio of $\sigma_d/\sigma_{d,f} = 42.5\%$, less than 0.1% permanent axial strain is observed in the BSM-foam material after 500000 load repetitions. This may indicate that mixes with a high percentage of RA have less resistance to permanent deformations. BSM-foam mixes with high percentage of RA are very sensitive to the increasing of the stress ratio. After 40% stress ratio (40˚C) the material is not able to support a continuous level of stress. Just with 2% more the mix is going to fail around 500 000 cycles quickly.

A comparison between the same deviator stress ratio and BSM-foam mix was drawn. Figure 4.31 explains the influence of the temperature on the stress ratio in a mix. The deviator stress ratio of 40% was selected for a BSM-foam mix with 50%RA and 50%G2. Using the same deviator stress ratio, the permanent axial strain increases from 0.008% at 25˚C to values higher than 1% at 50˚C. This change is principally caused by the presence of 50%RA in the mix and the temperature. The softening point is measured around 52°C. This could lead to dispersion of the bitumen inside the specimen, creating premature failure.

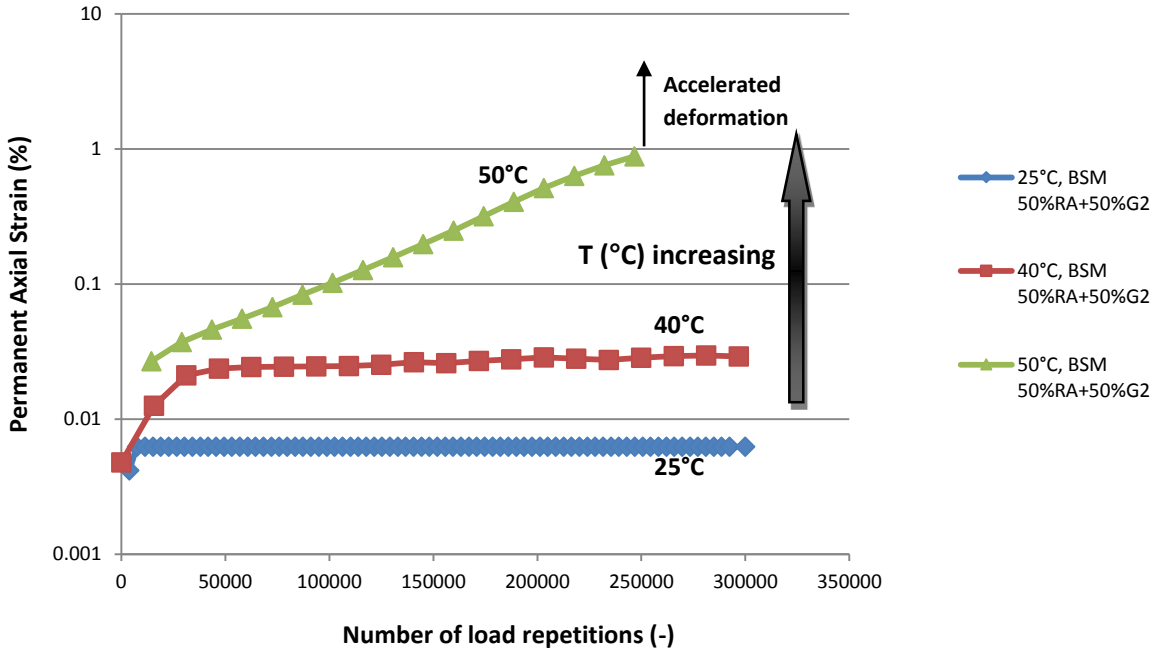

Figure 4.31: Permanent deformation test for BSM-foam mix with 50%RA and 50%G2 at 100kPa of confinement, 40% stress ratio at different temperatures.

The BSM-foam mixes with 100%RA and 100%G2 were tested only at 40˚C. The BSM mix with 100%RA showed high values of permanent deformation already with stress ratios of 40% and 45%. Compared with the BSM-foam mix with 50%RA and 50%G2, the BSM with higher percentage of RA is failing quicker at the same temperature and stress ratio. This is highlighted by the fewer number of cycles and high percentages of axial strain that are already present after 100000 cycles. The BSM with 100%RA reaches permanent deformation with both of the stress ratios of 40% and 45% at 40˚C.

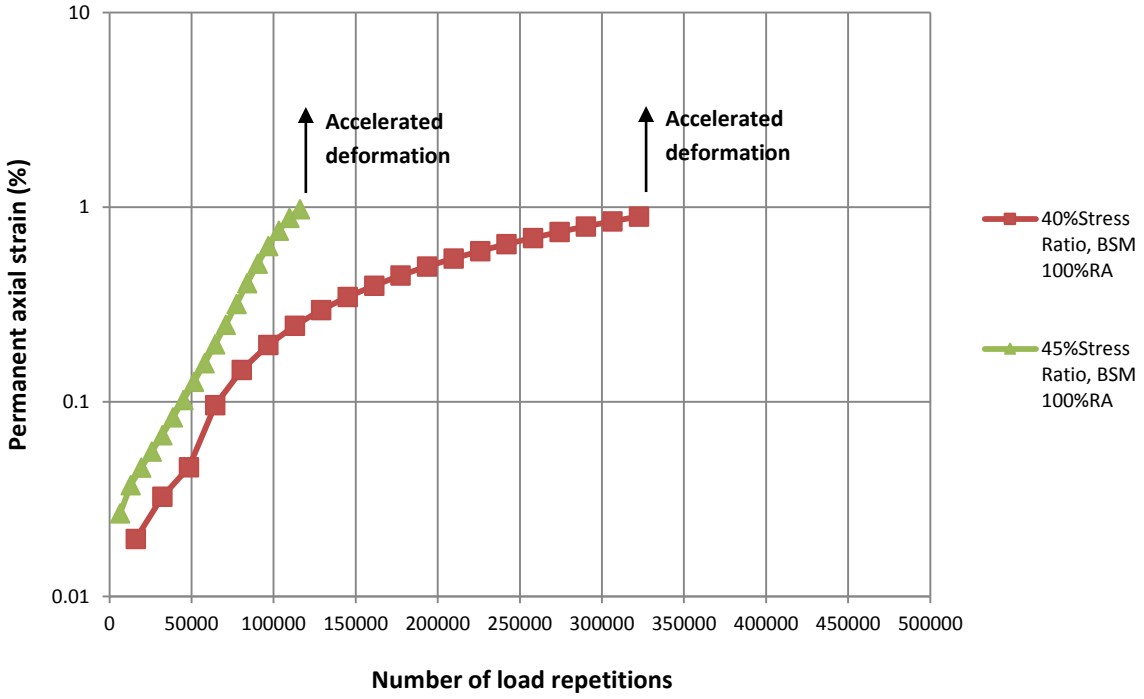

Figure 4.32: Permanent deformation test for BSM-foam mix with 100%RA at 100kPa of confinement and at 40°C.

The BSM-foam mix with 100%G2 crushed stone material was tested at only one temperature (40°C) and only at one deviator stress ratio (45%) (Figure 4.33). From the graph the difference of permanent axial strain between the BSM-foam with 100%G2 and the other two mixes with an increasing amount of RA is clear. The stress ratio of 45% only creates a permanent deformation of 0.15% on the mix. The same stress ratio at the equivalent temperature condition applied to the BSM-foam mix with 50%RA+50%G2 and to the BSM-foam with 100%RA creates a permanent deformation higher than 1% in less than 300 000 cycles.

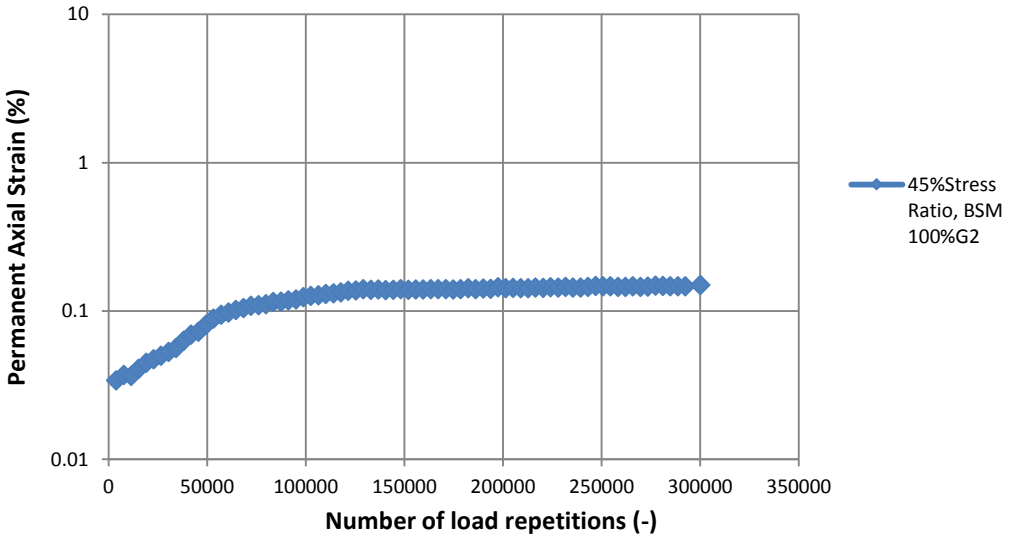

Figure 4.33: Permanent deformation test for BSM-foam mix with 100%G2 at 100kPa of confinement and at 40°C.

The influence of the increasing amount of RA in the BSMs can be analysed through Figure 4.34. The stress ratio of 45% was kept constant as well as the temperature at 40°C. The percentage of RA produces a high level of strain in the mixes as soon the RA becomes predominant in the composition in the mix. The failure in the BSM mixes is reached in fewer amounts of cycles if the percentage of RA is 100%.

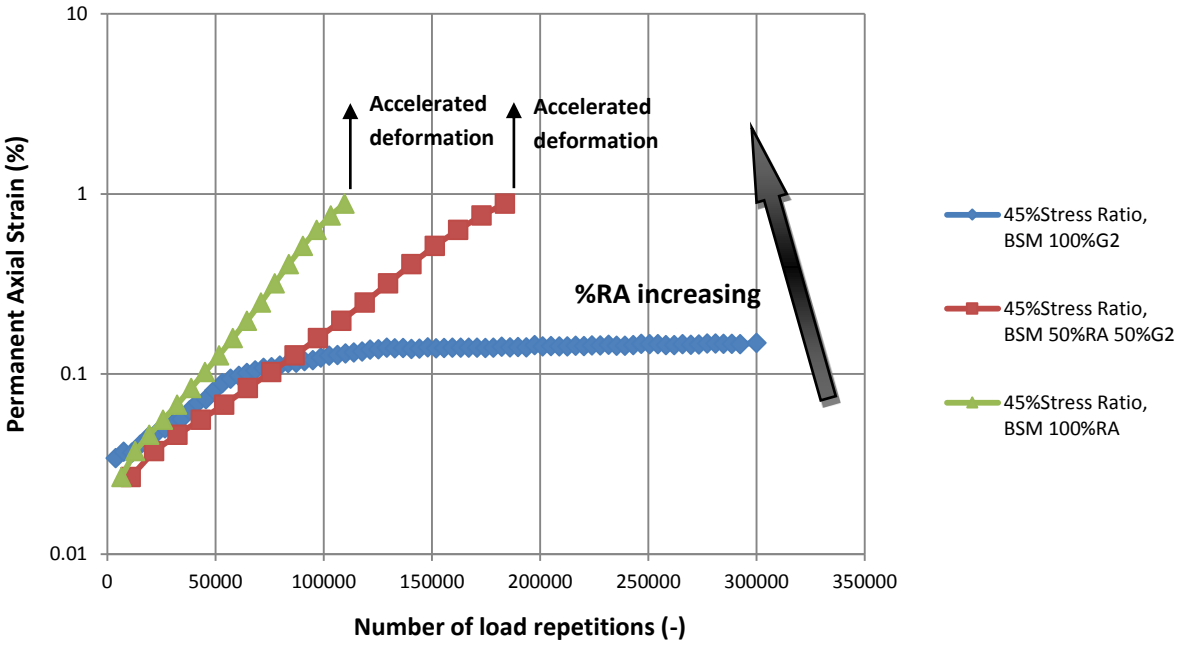

Figure 4.34: Permanent deformation test for BSM-foam mixes with increasing amount of RA, at 100kPa of confinement, 45% stress ratio at 40°C.

Some correlations can be drawn after these tests, even if the database of results is not too wide. Considering the three BSM-foam mixes, the following stress ratio can be represented in the graph at different temperatures (Figure 4.35).

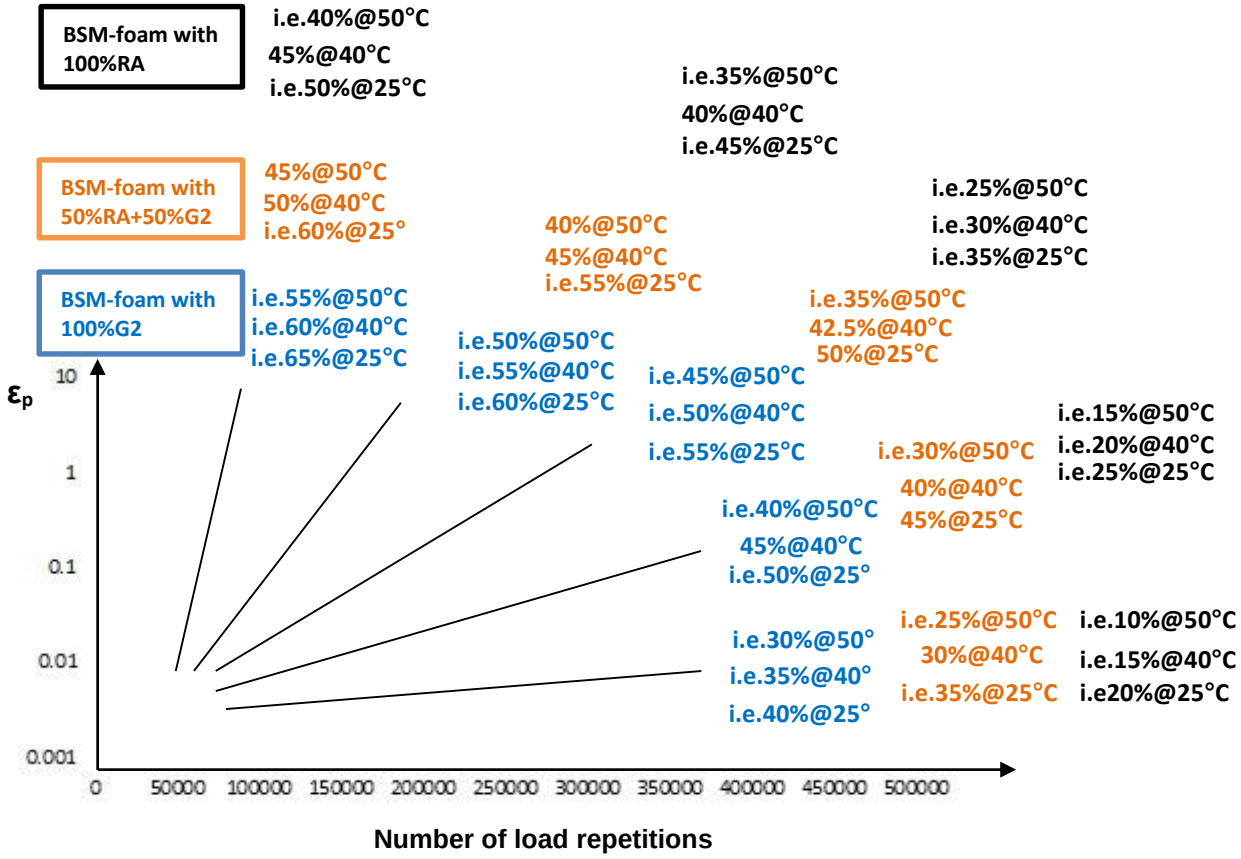

Figure 4.35: Template for permanent deformation modelling for BSM-foam mixes with increasing amount of RA, at σ_3=100kPa and different equivalent temperatures.

From the results presented it can be seen that the plastic strain is influenced by the following three factors (considering a minimum number of load repetitions of 500 000):

- deviator stress ratio;
- percentage of RA, and
- temperature.

This may indicate that mixes with a high percentage of RA have less resistance to permanent deformation as the temperature and the amount of reclaimed asphalt increase. It is evident from the results that the critical temperature of BSM mixes with high percentage of RA lies between 40°C and 50°C. Over 50°C the softening point can influence the resistance to permanent deformation. In fact, the bitumen becomes liquid and it is not able to guarantee the bonds between aggregates any more. The critical temperature is influenced by binder content and the type and percentage of RA.

The previous graph (Figure 4.35) aims to create a relationship between BSM-foam mixes with different percentage of RA, different deviator stress ratio and temperature. The deviator stress

ratios used in the analysis of the three BSM-foam mixes are plotted according to the mix and the temperature with possible estimated deviator stress ratio and temperature.

The extent to which deviator stress ratio, the percentage of RA and the temperature are dependent on each other is difficult to determine, based on the limited number of tests that have been carried out in this study. It is recommended that this dependency and especially the relation between percentage of RA and temperature be studied further.

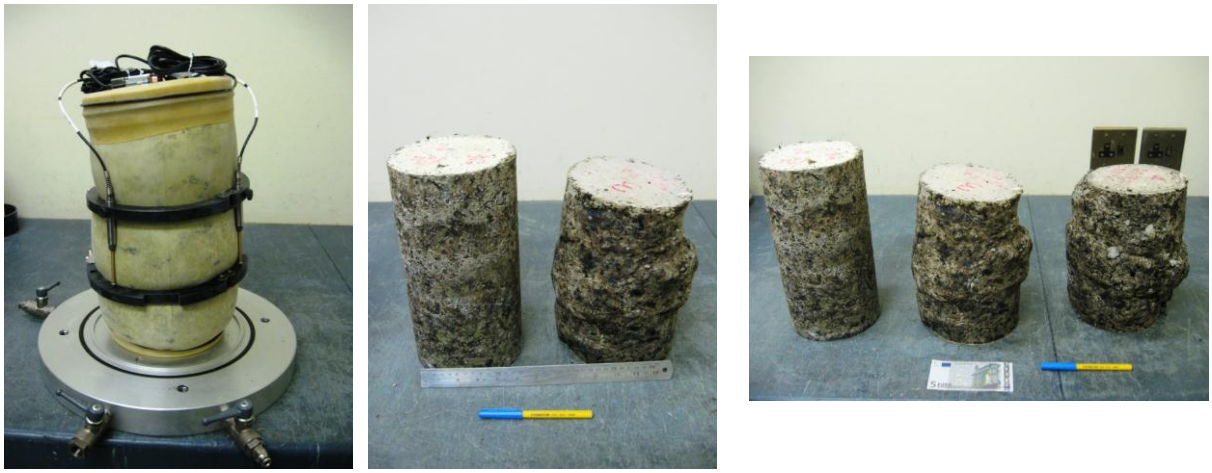

Figure 4.36: Specimens after permanent deformation.

4.7 Conclusions

This chapter presents data and analysis of BSM-foam mixtures with different percentages of reclaimed asphalt (RA) and a constant cement content (1%). Shear strength, resilient behaviour and resistance to permanent deformations were studied. The BSM-foam mixes were investigated at different temperature levels, giving a detailed picture of their mechanical characteristics. The study showed the differences between different mixes with high and low percentage of reclaimed asphalt (RA). The results of this investigation can be summarized in the conclusions set out below.

The dry ITS of BSM-foam materials with different percentage of RA shows a curvilinear behaviour at different temperatures (-10°C to 40°C). Temperature plays a key role in all the tests. The BSM-foam mixes can change their behaviour even with one degree of difference from the initial selected test temperature. The temperature conditioning time results are a key factor to ensure accurate test results.

The use of tri-axial testing can identify mechanical property changes (c and Φ) in BSMs due to the presence of RA. The friction angle reduces with increase in the percentage of reclaimed asphalt. Higher density (BSM-foam 100%G2) results in increased cohesion values and friction angles.

The σ-ε properties determined under both the monotonic and dynamic tri-axial testing demonstrated that the different percentage of RA in BSMs has influence on the reduction of

cohesion and adhesion of the mix matrices. This is more pronounced for mixes with higher percentage of RA stabilised with foamed bitumen, compared to the mixes with low percentage of RA. The shear properties of foamed bitumen mixes with different percentage of RA and different temperatures can provide the basis for models that assist in the prediction of resilient modulus of these mixes under repeated loading. The curing procedure has a high influence on the mechanical properties of the BSM-foam mixtures. The resistance to failure and elastic modulus increase significantly after a long period of curing. Models used for resilient behaviour of BSM-foam mixes with an increasing percentage of RA can accurately simulate the resilient response of mixes tested at different temperatures and at different deviator stress ratios.

The permanent deformation behaviour of a range of BSM-foam mixes has shown that the permanent axial strain determined for a BSM-foam mix, e.g. 50%G2 – 50%RA stabilised with foam and with 1% cement, shows that the axial strain accumulation can be reached quickly with the increasing of even 0.5% stress ratio at the temperature of 40°C and after 500 000 number of load applications. The stress ratio $\sigma_d/\sigma_{d,f}$ is a critical parameter that defines the BSM-foam behaviour with high percentage of reclaimed asphalt. The general law of permanent deformation as originally developed by Francken (1977) for hot-mix asphalt slightly adjusted by Huurman (1997) for granular materials and later by Jenkins (2000) and van Niekerk (2002) for foamed bitumen stabilised material and granular material respectively also applies to the BSMs tested here. In order to accurately determine the permanent deformation behaviour, the testing needs to be of sufficient duration. In this study the test duration of 500 000 load repetitions was adopted. When performing permanent deformation tests in a research environment it is recommended to adopt minimum test duration of 1 million load repetitions (unless failure occurs prior to this).

Depending on the material characteristics (percentage of RA) and temperatures, BSMs can show different deviator stress ratios. The critical stress ratio concept is a relative one. The critical stress ratio must be evaluated together with the stiffness and ultimate strength of the material. Two materials with similar performances in terms of stress ratio can perform substantially different from each other in the pavement structure under similar absolute levels of loading. Considering that the range of BSM-foam mixes that has been investigated is not exhaustive to explain the complete relationship between RA, temperature and deviator stress ratios, more research needs to be carry out.

This research confirms the importance of the cyclic tri-axial test, for determining the mechanical properties of BSM-foam mix with different percentage of RA. The sensitivity to temperature and percentage of RA in BSMs is important, and should be studied more in detail. The work should be continued on the same material, to study the influence of temperature and different percentage of reclaimed asphalt in the BSM-foam mixes on its behaviour in particular.

The results presented therefore are essentially from laboratory investigations and would require field trials for the validation of the laboratory results. Future laboratory studies should similarly be extended to RA obtained from the field.

REFERENCES

Asphalt Academy. 2009. A guideline for the design and construction of bitumen emulsion and foamed bitumen stabilised materials. 2nd edition technical guideline. Pretoria, South Africa. (TG2).

Barksdale, R. D. 1971. "Compressive stress pulse times in flexible pavements for use in dynamic testing." Highway Research Record. 345, Highway Research Board, Washington, D.C., 32–44.

CSIR Built Environment. 2007. Mechanistic-empirical Pavement Analysis and Design Software (mePADS) Version 1.1. Pretoria, South Africa.

Dal Ben, M. 2009. Comparative analysis of experimental protocols developed for the dynamic characterization of asphalt performance. MSc Thesis. University of Padua and TUDelft. Italy, The Netherlands.

Ebels, L.J. 2008. Characterisation of Material Properties and Behaviour of Cold Bituminous Mixtures for Road Pavements. PhD Dissertation, Department of Civil Engineering, Faculty of Engineering, University of Stellenbosch, South Africa.

Francken, L. 1977. Permanent Deformation Law of Bituminous Road Mixes in Repeated Tri-axial Compression, 4th International Conference on the Structural Design of Asphalt Pavements, Ann Arbor, Michigan, USA.

Huurman, M. 1997. Permanent Deformation in Concrete Block Pavements. PhD Dissertation. Delft University of Technology, Netherlands.

Jenkins, K., Long, F. and Ebels, L.J. 2007. Foamed bitumen mixes = shear performance. International Journal of Pavement Engineering, Volume 8, Number 2, pp. 85-98(14). Taylor and Francis Ltd.

Jenkins, K. J. 2000. Mix Design Considerations for Cold and Half-warm Bituminous Mixes with Emphasis on Foamed Bitumen. PhD Dissertation, University of Stellenbosch, South Africa.

Kelfkens, R.W.C. 2008. Vibratory hammer compactor of bitumen stabilised materials. MSc Thesis. University of Stellenbosch. South Africa.

Long, F.M. and Ventura, D.F.C. 2003. Laboratory Testing for the HVS Sections on the N7 (TR11/1), Contract Report CR-2003/56, (CSIR Transportek: Pretoria).

Theyse, H.L. 2012. South African National Roads Agency Limited, March 2012. Stress-dependent Resilient Modulus and Poisson's Ratio Model Formulation for Unbound Granular Material based on Repeated Load Tri-axial Test Results, Version: 2nd Draft. CSIR, Pretoria, South Africa.

Twagira, E.M., Jenkins, K.J. and Ebels, L.J. 2006. Characterisation of Fatigue Performance of Selected Cold Bituminous Mixes. International Conference on Asphalt Pavements ICAP, Quebec, Canada.

Twagira, E.M. 2010. Influence of durability properties on performance of bitumen stabilised materials (PhD (Eng) dissertation). University of Stellenbosch, South Africa.

Van Niekerk, A.A. 2002. Mechanical Behaviour and Performance of Granular Bases and Subbases. PhD Dissertation. Delft University of Technology. Delft.

CHAPTER 5

DURABILITY PROPERTIES of BSM-FOAM MIXES

5.1 Introduction

Despite many years of experience with the use of stabilized materials in road construction and comprehensive specifications based on this experience, a noticeable increase in problems related to road material stabilization is taking place in Southern Africa, resulting in serious cost increases and claims (Netterberg and De Beer, 2012). The distress such as permanent deformations (shear failure) is often aggravated by the detrimental effect of moisture on the internal structure of the pavement materials (Collings and Jenkins, 2011). The durability of mineral aggregates has been a subject of great concern for the performance of HMA, CTB and granular base layers and a number of durability tests have been developed and are in use. Unfortunately, because of the ubiquitous nature of aggregates considered suitable for BSMs and their better performance, the durability of mineral aggregates for both virgin and recycled layers, cannot be overlooked.

Durability is a time-dependent parameter or behaviour. In general terms, it is defined as enduringness, lastingness, persistence, changelessness, or everlasting (Houghton, 2000). Therefore, durability is a measure of the useful life of physical phenomena. In an engineering context, durability is defined as lastingness of structures and materials for the ability to maintain the initial performance properties through time above a certain threshold level. Durability is achieved by resisting stresses and strains or withstanding destructive agents with which the materials come into contact. The destructive agents can include air, water, light, temperature, chemicals and traffic loading over a long period of time. The durability properties of BSMs are related to the intrinsic properties of the mineral aggregates, bitumen binder and mixture and climate conditions (Twagira, 2010), namely

- moisture susceptibility;
- ageing behaviour;
- mineralogical composition and physico-chemical characteristics of the aggregates, and
- interaction between mastic (filler, binder, moisture content) and aggregates surface during adhesion.

In this chapter the durability properties of three different BSM-foam mixes are investigated:

- BSM-foam mix (2.3% bitumen content) with 100%G2 (Hornfels) good quality crushed stones;
- BSM-foam mix (2.1% bitumen content) with 50%RA and 50%G2 materials, and
- BSM-foam mix (2% bitumen content) with 100%RA.

The tests used for assessing the durability of BSM-foam mixes in this research are the mechanical wet/dry test, the permeability test and the moisture induction simulation test (MIST) developed and described in detail by Twagira (2010). The wet/dry test is commonly performed to identify the susceptibility of cement/lime stabilised materials to degradation (disintegration or decomposition) in the presence of adverse conditions of cyclical wetting and drying. The erosion of BSM-foam materials used in pavements and subject to service conditions in the pavement, have not been studied extensively. The permeability of a BSM material is an important construction variable in the long-term durability of paved surfaces. Lower percentages of in-place air voids can result in rutting and shoving, while higher percentages allow water and air to penetrate into a pavement, leading to an increased potential for water damage, oxidation, ravelling, and cracking. Low air voids are generally the result of a mix problem while high voids are generally caused by inadequate compaction (Jenkins *et al*. 2006). The presence of water in the pavement for extended periods of time is directly linked to early deterioration. During mix design, volumetric properties such as air voids and bulk relative density (BRD) are used to evaluate the acceptability of BSMs mixes. Excess moisture in the mix matrix is a major factor contributing to poor adhesion and cohesion in BSMs (Twagira, 2010). One of the aspects of his research was the investigation of moisture damage factors that can influence BSMs mixes. Laboratory simulation through a Moisture Induction Simulation Test (MIST) device can provide a representative replication of the moisture damage mechanisms that are manifested in a BSM layer in service.

5.2 Permeability

In the design characterization of civil engineering projects, one of the most important properties of interest to geotechnical engineers is permeability. One of the primary objectives in structural pavement design for conventional pavements is that the permeability has to be as low as possible in a flexible pavement. The basis for this design approach is to minimize moisture infiltration and thus maintain adequate support from the underlying unbound materials. In recent years, with the implementation of the TG2 technical guideline (Asphalt Academy, 2009), BSMs pavements have been produced widely, especially in South Africa. The permeability (hydraulic conductivity) of BSMs is an important geotechnical property in engineering since many of the problems associated with design and structure require that the permeability of the pavement be determined. Permeability or the hydraulic conductivity of the pavement, defined as the rate of flow of a fluid through a material under a unit head, is usually based on Darcy's Law.

5.2.1 Darcy's Law

Permeability, more properly named hydraulic conductivity or coefficient of permeability, is the rate at which a porous material will transmit water under a hydraulic gradient (Kanitpong *et al*., 2001). BSMs materials are permeable (i.e. water may flow through them) because they consist not only of solid particles (aggregates), but a network of interconnected pores. The degree to which BSMs are permeable depends on a number of factors, such as aggregates type, grain size distribution, water content, degree of compaction and presence of foam bitumen or emulsion. This degree of permeability is characterized by the coefficient of permeability (or hydraulic

conductivity). The coefficient of permeability, k, is a product of Darcy's Law (1856), which establishes the following empirical relationship for flow through saturated porous materials:

$$Q = k \cdot i \cdot A \rightarrow k = \frac{\Delta H}{L} \cdot A \qquad [5.1]$$

where:
Q = flow rate
i = hydraulic gradient
ΔH = the head loss across the specimen;
L = the length of the specimen;
A = cross sectional area of the specimen perpendicular to the direction of flow
k = coefficient of permeability

Flow in unsaturated materials differs significantly from flow in saturated materials. In unsaturated mixes, the pressure head is negative, meaning that it is lower than atmospheric pressure (soil suction). The water content is less than the porosity because some of the void space is filled with gas (air). In saturated porous materials, water can move through the entire cross-sectional area of the pore space. However, as water is replaced by air, it can only move through the reduced cross-sectional area occupied by the remaining water. This has the effect of lowering the hydraulic conductivity. The result is that water content of the porous material is variable and a function of the pressure head and soil suction. The more negative the pressure head (or inversely the higher the suction), the lower the moisture content. The exact relationship depends on the material type. Similarly, the hydraulic conductivity decreases with decreasing water content and increasing suction. The result is that Darcy's Law (presented above) becomes non-linear. Special testing methods therefore were adapted to measure the BSMs permeability.

In the laboratory, permeameters are generally used to perform two common tests to determine the permeability of the materials: the falling head permeability test and the constant head permeability test. Which test is used depends upon the type of material tested. For BSMs and unbound materials of high permeability a constant head test is normally used. In the constant head test, which was used for this research, a constant total head difference is applied to the BSM-foam specimen, and the resulting quantity of seepage can then be measured (Figure 5.1).

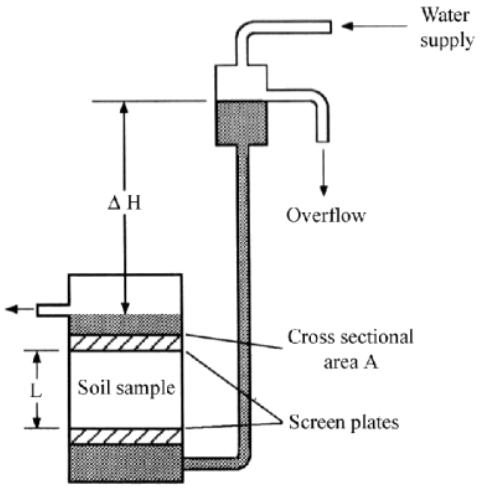

Figure 5.1: Laboratory set-up for a constant head test (Venkatramaiah, 2006)

Factors influencing permeability are compaction level, air voids structure (size and connectivity), mineral aggregates (size, shape and grading), binder content and degree of saturation (Caro *et al*., 2008; Kuvhanganani, 2008).

5.2.2 Laboratory permeability set-up test

The constant head water permeability test was performed at the University of Stellenbosch according to test method ASTM D2434 – 6815. The test method followed was based on the use of the tri-axial cell which is giving the possibility to test a specimen of 300 mm height x 150 mm diameter (Figure 5.2). Confining pressure was applied to the specimen, which was previously fitted by a latex membrane. The specimen was connected through a lead on the top of the specimen to a graduated pipe. After taking the initial height value, the water was left open by means of a valve. Time was taken from the initial height of the water and a low limit fixed on the pipe. The volume of water draining through the specimen was measured as a function of time. The results are given in terms of a coefficient of permeability in centimetres per second (cm/sec). The results of the permeability tests are discussed in the following section.

Figure 5.2: Permeability test in the laboratory at Stellenbosch University.

5.2.3 Permeability tests

Few studies on permeability and its influence on moisture damage have been conducted (Twagira, 2010). Ventura (2001) studied the permeability of foamed bitumen mixes, with different binder contents and percentage of active filler (cement). Twagira investigated the possible relationship between permeability and moisture damages. Twagira's results indicate some possible correlation between density and permeability and moisture damaging. Kanitpong *et al*. (2001) and Twagira (2010) recommend a tri-axial permeability test, where the flow of water through a sample can be maintained under a known pressure. The rate of flow can be measured while the sample is subjected to a known confining stress. The method was found to

produce a more reliable coefficient of permeability than the traditional method which is using an UCS specimen.

An extensive range of permeability tests was conducted at the University of Stellenbosch laboratory. The permeability tests were performed before monotonic tri-axial tests and after dynamic tri-axial tests.

All three BSM mixes have been obtained mixing foam bitumen 80/100 in the laboratory at the environmental temperature (close to 25°C). For purposes of mixing and compaction, characterization of the natural materials is necessary before treatment with foamed bitumen can be carried out. More details about the three BSM-foam mixes have been presented in Chapter 4. The optimum moisture content (OMC) and maximum dry density (MDD) for the three different mixes were determined by Modified AASHTO compaction (constant compaction energy). Details on the composition of all three mixtures are listed in Table 5.1.

Table 5.1: Details of BSM – foamed mixes.

Mix	100%RA	50%RA 50%G2	100%G2
Cement (%)	1	1	1
Optimum Moisture Content (%)	4.05	5.7	5.7
BSM-foam content (%)	2	2.1	2.3
Average voids in the mix (%)	16.49	15.48	13.46
MDD (kg/m^3)	2006	2195	2335

Three tests have been performed for every BSM-foam mixtureat the temperature of 25°C in an environmentally controlled room. The following results represent an average value of all the permeability tests conducted in the laboratory. For every value the standard deviation is reported (Table 5.2).

Table 5.2: Permeability (k) in all three BSM-foam mixes (average values).

Mix	k after compaction and curing [cm/s]	k after Resilient Mod Test [cm/s]	k after Resilient Mod Test (6 months)[cm/s]	Quality of the mixture
BSM-foam 100%RA	8.19*10-3	8.15*10-3	8.07*10-3	Dense (typical BSM)
BSM-foam 50%RA 50%G2	6.7*10-3	6.42*10-3	6.16*10-3	Dense (typical BSM)
BSM-foam 100%G2	4.69*10-3	4.54*10-3	4.34*10-3	Dense (typical BSM)

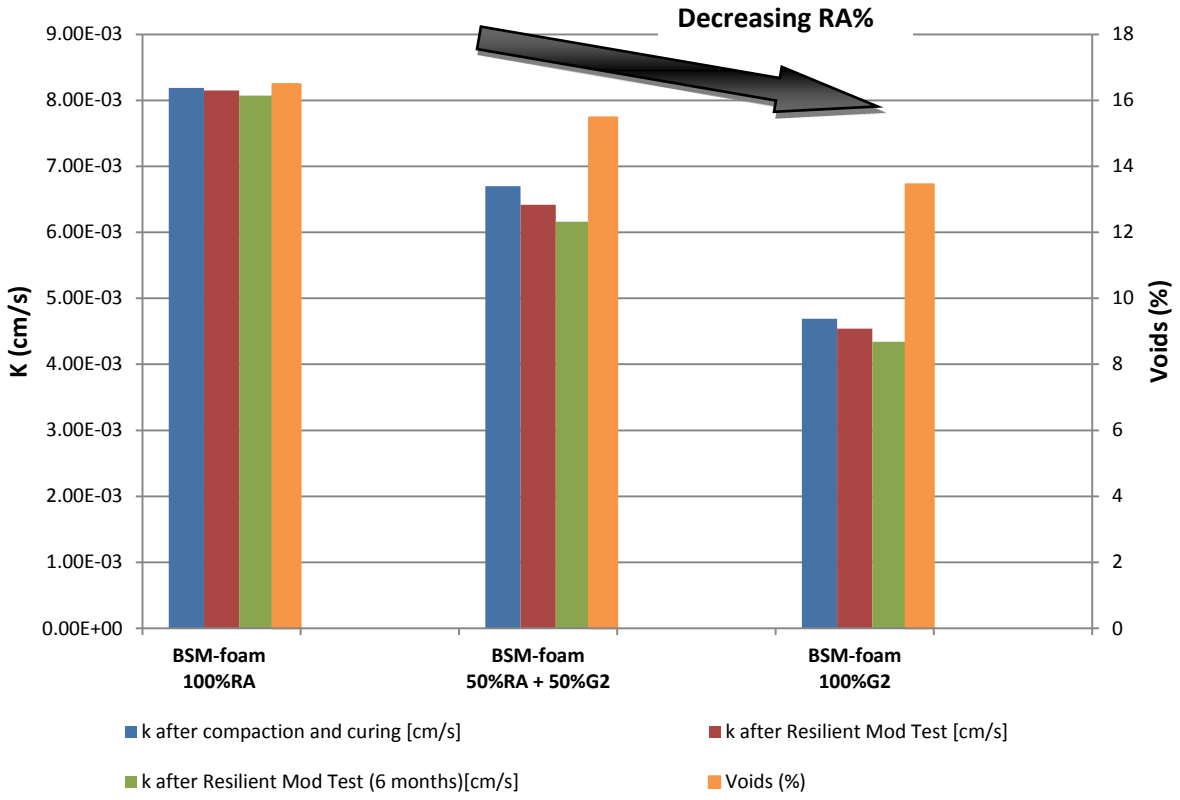

Figure 5.3: Permeability (k) in all three BSM-foam mixes.

The *k* factor changes with an increase in loading. It is possible to see the effect of the distribution of the bitumen and the traffic on the matrix of the specimens (k after resilient modulus test). The permeability decreases due to a continuous but constant loading which simulates the passage of vehicles on the pavement. In the RA mix the permeability has a value higher than the G2 mixture, probably due to the different binder content and a lower level of compaction. The percentage of voids in the RA mix is higher than in the G2 mix. A linear correlation between permeability (*k*) and percentage of RA in the BSMs mixture is evident through the graph presented above. As the percentage of RA decreases, even the permeability is doing the same. This is obviously connected to the percentage of air voids present in the mixtures. In fact the BSM-foam mix with a high percentage of RA has a higher percentage of air voids in the

matrix than the BSM-foam mix with 100%G2 material. The amount of fine material passing the 0.075 mm sieve is considerably higher for the 100%G2 mix than the 100%RA mixture (i.e. 5% difference, but these gradings are representative of real projects). The standard deviation for all three mixes is in a range of small values (Table 5.2). This is an indication of consistent testing procedure and good sampling. The permeability results do not closely match the ranking values suggested by Caro *et al*. (2008) (Table 5.3). This is probably due to the possible correlation between different features that are all related.

Table 5.3: Classification of void in term of permeability (k) Caro et al. (2008).

Void (%)	K [cm/s]	Permeability condition	Void Structure	Mixture
6 or lower	10^{-4} or lower	Impervious	Impervious	Dense (typical HMA)
6 - 16	$10^{-4} – 10^{-2}$	Poor drainage	Semi-effective	Dense (typical BSM)
16 or more	10^{-2} or more	Free drainage	Effective	Porous Asphalt

Several factors were identified that can influence the permeability of a BSM-foam mix and include:

- particle (aggregate) size distribution (grading);
- particle shape;
- molecular composition of BSM;
- air voids (i.e. compaction);
- degree of saturation;
- type of flow, and
- temperature.

The particle size distribution and particle shape have an effect on the size and number of air voids present within a mixture. Figure 5.3 suggests that permeability decreases as the size and number of voids decrease (100%RA has a higher percentage of voids than the 100%G2). The shape of aggregate particles can also influence permeability. Irregularly shaped particles (angular, flat and elongated) can create flow paths which are more tortuous than those created by smooth, rounded aggregates. This can lead to lower flow rates through a BSM mix. High air voids and increasing amounts of RA could reduce the effective service life of the BSM mix.

5.3 Void characteristics in the BSMs mixes

The fundamental influence on moisture damage in BSMs is linked with air void content. The void content characteristics in BSMs play a key role on the volumetric properties of the BSMs.

This was already confirmed from previous research such as Twagira (2010). In this section the degree of void contents is presented for all three BSM-foam mixes analysed in this research. The void content in BSMs is determined from a laboratory compacted specimen which has dimensions of 150 mm diameter and 75 mm height.

The level of air void contents in a BSM-foam mixture strongly depends on the grading of a mix, compaction level and filler/binder ratio. In addition, the physical properties of mineral aggregates, such as size and shape, also play a significant role in minimising the air voids in mixtures. The quantification of void content in the BSM-foam mixes used in this study was essential in order to relate the results with the influence of the moisture damage in a wet and dry durability test. The void content of the mixes was determined after carrying out the test on the bulk relative density (BRD) and maximum theoretical relative density (RICE) according to TMH 1 method C3 and C4 (Technical Methods for Highways, 1986), respectively.

Table 5.4: Average values for bulk density, RICE density and void content in BSMs.

BSM-foam mix	Bulk Density (kg/m^3)	Maximum Theoretical Density, RICE (kg/m^3)	Void content (%)
100% RA	1924.21	2304.19	16.49
50%RA 50%G2	1939.19	2296.34	15.48
100%G2	2094.74	2420.51	13.46

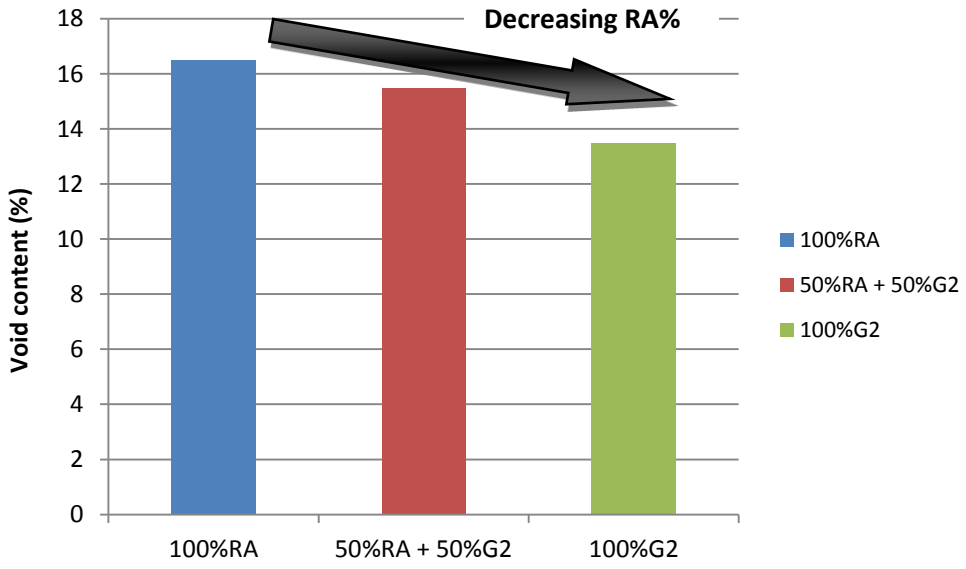

Figure 5.4: Void content (%) in the BSM-foam mixes.

From the void properties results (Figure 5.4), it is evident that BSMs with a high percentage of RA have a higher void content in the mix matrix compared to BSMs with 100%G2 crushed stone. The BSM-foam mix with 100%RA has a level of air voids which could be compared to a relative close UTFC (Ultra Thin Friction Course). The void content determination in the BSM mix matrix is not sufficient to provide a complete answer about a link to mechanisms of moisture transport and its damaging effect in the BSM layer. In this light, a wet and dry durability study through the use of a mechanical brush test needs to be performed to be able to understand the contribution of the voids and failure mechanisms.

5.4 Wet – dry durability test

A good BSM stabilisation design should produce a material that will provide the required stiffness over the design life of the road. Moisture susceptibility and consequent damage manifestation in BSMs is the phenomenon that describes the effect of the presence of excess moisture in the microstructure of the binder and mineral aggregates. Moisture susceptibility is a measure of how prone the mixture's internal system is to weakening i.e loss of adhesion of bitumen to the aggregate, in the presence of moisture. Characterisation of moisture susceptibility is essential to quantify the loss of functionality of the BSM mixture by considering variable parameters, such as shear, strength, stiffness etc. These parameters allow the determination of thresholds that can be used in the form of specification to separate acceptable from unacceptable materials or mixtures in terms of moisture damage resistance. Although problems of moisture susceptibility of BSMs has been identified in various studies (Jenkins, 2000; Long *et al*., 2004; Liebenberg, 2002; Paige-Green and Ventura, 2004), its complexity has made it difficult to find a unique test or analytical method to comprehensively quantify damage and accurately predict the material performance in the field. The actual test method used to assess moisture damage in BSMs is normally ITS soaked tests, but the links to in-service conditions are questionable. The conditioned and unconditioned specimens are then compared in terms of retained strength, e.g. TSR obtained after Indirect Tensile Strength (ITS) or from Unconfined Compressive Strength (UCS). Therefore, tensile cracking in the ITS test do not simulate the failure mechanism of BSMs accurately compared to MIST/triaxial testing. Hence there is a need for a new more reliable durability test.

The possible qualitative method to assess moisture damage in BSMs is the related test method designed for cement-treated material. This test is the mechanical brushing test method and is conducted on compacted and cured specimens with or without loading. The assessment of the quality of adhesion and cohesion with the influence of moisture is done by determining the loss of surface material (Long *et al*., 2004). The goal of the moisture conditioning process is to simulate the detrimental effect of moisture on materials during short periods of time. Moisture conditioning is considered an accelerated damage process.

Figure 5.5: Mechanical brushing apparatus at Stellenbosch University.

5.4.1 Determination of the BSMs losses for different soaking times

The presence of excess pore water in the BSM mix matrix can result in rapid deterioration due to moisture damage. The process typically associated with moisture ingress and damage is a mechanism that occurs over long periods of time under field conditions. Infiltration of moisture to the microstructure can result:

- in pore pressure and erosion due to dynamic loading (Jenkins *et al.*, 2006);
- pore pressure and erosion can result in disintegration, which progressively degrades the physical integrity of adhesion of the bitumen and cohesion of the mixture (Jenkins *et al.*, 2008);
- adhesion and cohesion loss (i.e. ravelling or stripping of mastic) in BSMs is a failure pattern which undoubtedly relates to a combined action of mechanical failure and moisture infiltration (Jenkins *et al.*, 2008);
- weakening of the interlocking bonds of the mineral aggregates promotes a cohesive failure, while weakening of the binder-aggregates promotes a pronounced adhesive failure. Because of weakening of bonds, mixes will slowly lose their strength, hence becoming more prone to cohesive failure (Twagira, 2010).

A method that simulates all of the possible mechanisms of moisture damage is not currently in use for BSM mix evaluation. The mechanical brushing test apparatus aims to measure the loss of materials from the specimen surface resulting from soaking, drying and brushing at 50 revolutions repeated 12 times. The assessment of the quality of adhesion and cohesion with the influence of moisture is done by determining the loss of surface material.

5.4.2 Calibration of the procedure for wet-dry brushing tests

After curing Long *et al*. (2004) propose to submerge the specimens in a water bath at room temperature for 5 hours and then place the specimens in a draft oven at 71°C for 42 hours. After this period the specimens can be clamped in the brushing apparatus and the test can start. The procedure described so far represents only one cycle (48 hours) of the wet/dry durability test. The specimens are then submerged in water and the method repeated for other 11 cycles.

Unfortunately this scheme is not suitable for BSMs materials. BSMs have a significant component of water and bitumen in their own matrix. Leaving a specimen after curing in a oven for 42 hours at 71°C can involve problems of ageing, redistribution of the bitumen inside the specimens, high evaporation of the moisture and a consequent alteration of the degree of density. To overcome this problem, the procedure adopted through this study didn't use a draft oven during the 12 wet/dry cycles. After accelerated curing a BSM-foam mix with 100%G2 material and one BSM-emulsion with 100%G2 material were investigated in the first part of this study. The aim of this first step was to find the best option for soaking and testing with the brush device, without losing too much time and creating a valid test procedure for a possible use in the field. Three specimens for the BSM-foam mixture and two for the BSM-emulsion were soaked in a water bath at 25°C at three different time-schedules (15 specimens in total):

- 4 hours;
- 12 hours, and
- 24 hours

The specimens submerged in the water for 4 hours were tested with the brushing machine in a controlled room at 25 degrees and then left unsealed to dry for one hour. After this procedure the specimens were again placed in the water bath for other 4 hours and then the test was repeated. After this second test, the specimens were sealed in a bag and left in the controlled temperature room until the next day. In this manner it was possible to perform 2 wet-dry cycles every day. At the beginning and at the end of every test, the loss of every specimen was recorded. During the overnight time the water was able to redistribute itself inside the specimen, keeping the moisture at the same level. The mixes soaked for 12 hours were continuously facing direct cycles of wet-dry brushing without exposure to dry conditions. The specimens were placed in the bath for 12 hours and then after measuring the weights, tested with the brushing machine. Subsequently the difference of weight was measured and the specimens were again submerged for other 12 hours. From the beginning this method was considered too difficult to be implemented in the field, but from a research prospective, it was considered valid for the first stage of calibration. The 24 h cycles were processed following the same method described for the 12 hours of soaking.

5.4.3 Influence of soaking

The influence of soaking at different soaking times was documented for all three BSM-foam mixes and is represented in Figure 5.6. After measuring the initial weight, the specimens were placed in the water bath at 25°C. The weight measurement was taken systematically during the first 5 hours and then more randomly.

During the first hour the BSM-foam materials drastically increased their percentage of saturation. The water penetrated easily into the mixes due to the high percentage of void in the mixtures. The 100%G2 material was able to reach 99.7% of saturation in less than one hour. For the other 2 mixes the time was a little bit longer but always less than 4 hours' time. The investigation showed that all the mixes can reach the value of almost 100% of saturation in less than 24 hours.

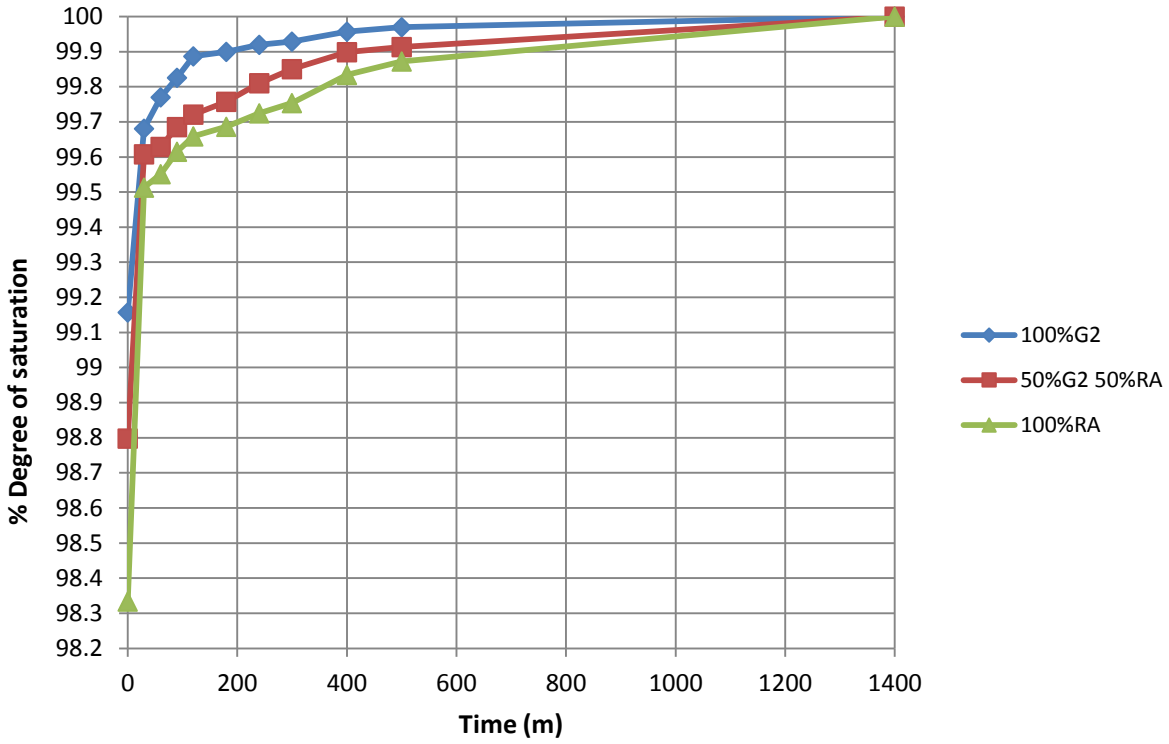

Figure 5.6: Influence of soaking on BSM-foam materials.

A particular investigation was carried out on the soaking cycle of 4 hours. The specimens were tested after having been submerged in the water bath for 4 hours and then left to dry in a temperature controlled room at 25°C for one hour and then placed in water again. The influence of soaking in a test of two wet-dry brushing cycles in one day was measured through the weight of the specimens. The level of saturation increases after 4 hours in the water up to values above 99.6%. Then after the brushing test and exposure to the air for one hour the percentage ranges between 98.5% and 99.2%. The reduction in the percentage is higher for the 100% reclaimed asphalt mix than for the 100%G2 Hornfels-crushed stone. This is mostly due to the larger amount of air voids present in the mix. The level of saturation was again measured after 4 hours. It again ranged around the same values recorded for this cycle. After testing the specimens were sealed in a bag for the night. The percentage of saturation was again measured the following day. It was exactly at the same level of the previous data recorded after one hour in dry conditions.

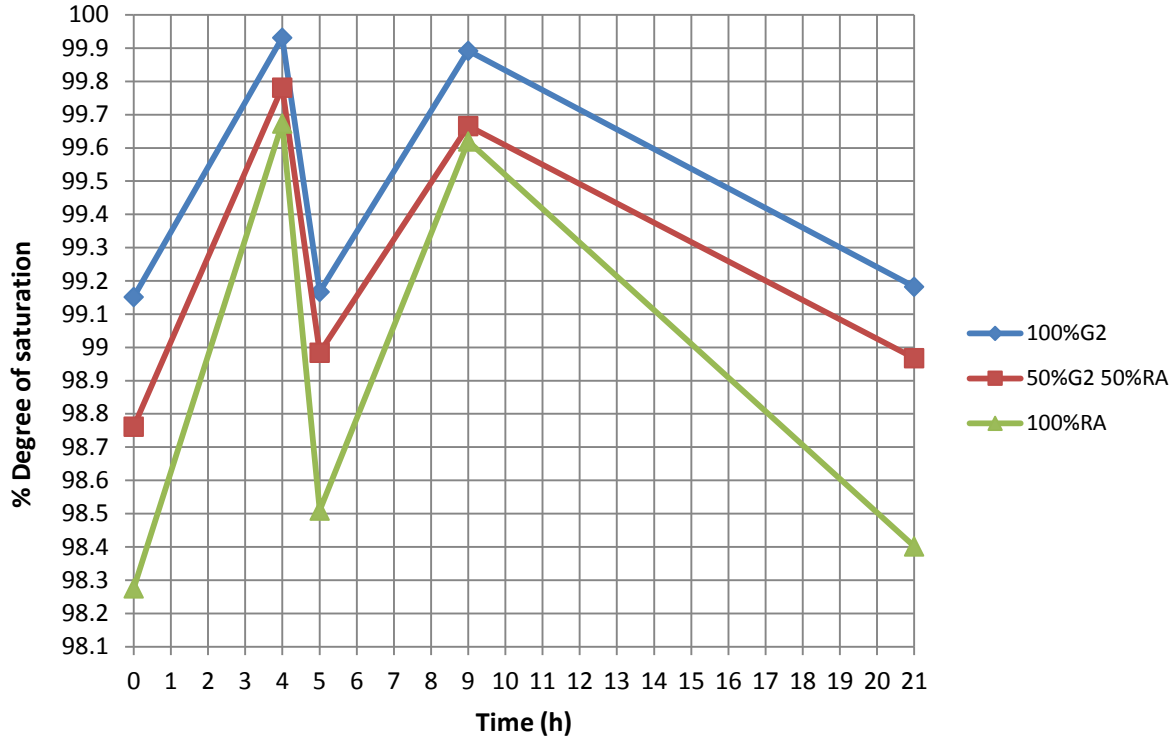

Figure 5.7: Influence of saturation on BSM-foam materials after 4 hours soaking cycles.

The soaking time of 4 hours was judged to be the most repeatable and representative for BSMs materials. A very good level of saturation is reached quickly after 4 hours in a water bath. The test procedure based on 4 hours preconditioning time is more reliable than other possible soaking-time options, because it can give the possibility to test one specimen two times every day, thus enabling two cycles of wet-dry brushing.

5.4.4 Trials of the wet-dry brushing test

This section presents the cumulative percentage of losses for two different BSMs mixes subjected to different cycles of soaking: 4 hours, 12 hours and 24 hours. The BSMs used in this part of the study were:

- BSM-foam (2.3% of bitumen content) with 100%G2 Hornfels crushed-stone and 1% of cement;
- BSM-emulsion (4% emulsion) with 100%G2 Hornfels crushed-stone and 1% of cement.

The decision to test BSM-emulsion specimens was made to create a comparison between the two BSMs (foam and emulsion), using the same wet-brush apparatus. No test on RA was conducted during this part of the research because it didn't have the good quality mechanical characteristics of a BSM with 100% G2.

The cumulative loss, indicated at the top of every column, was measured recording the loss for every single wet-dry brushing cycle. Figures 5.8 and 5.9 represent the influence of the different

soaking times on the brushing test for these two selected mixes. Three specimens for a BSM-foam with 100%G2 material and two specimens for a BSM-emulsion mix with 100%G2 material were tested for each cycle of soaking (4 hours, 12 hours and 24 hours).

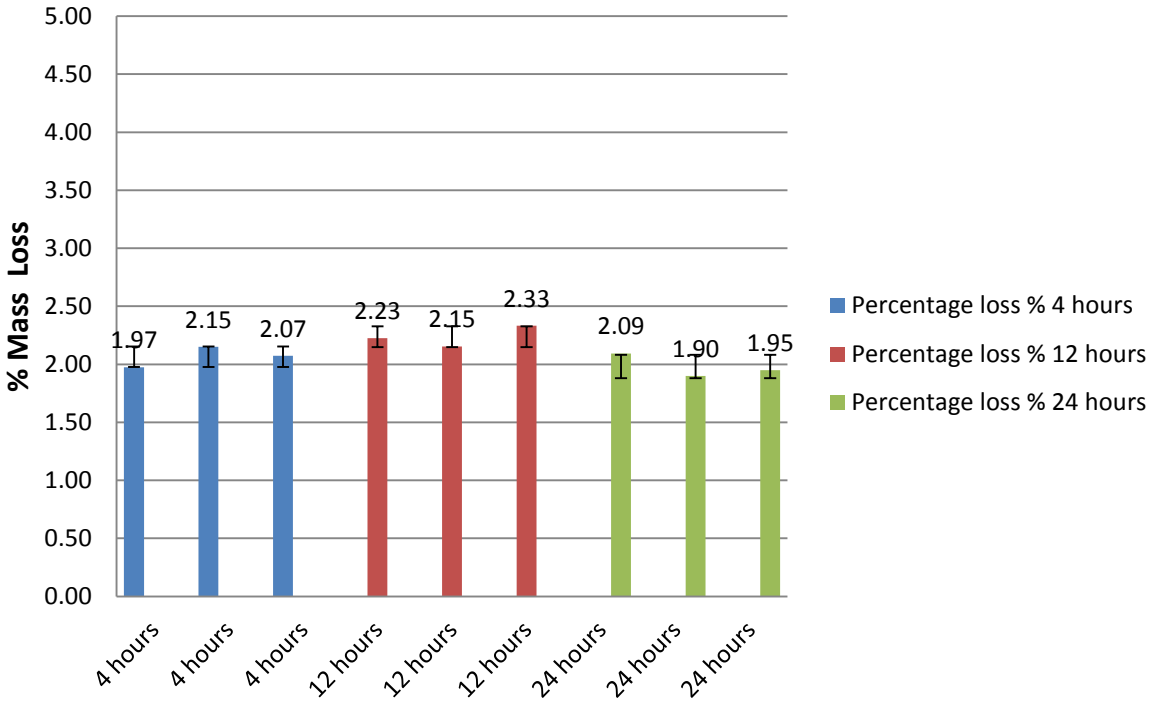

Figure 5.8: Cumulative percentage of loss and influence of different soaking times on BSM-foam with 100%G2 (Hornfels) crushed stone after 12 cycles (3 repetitions).

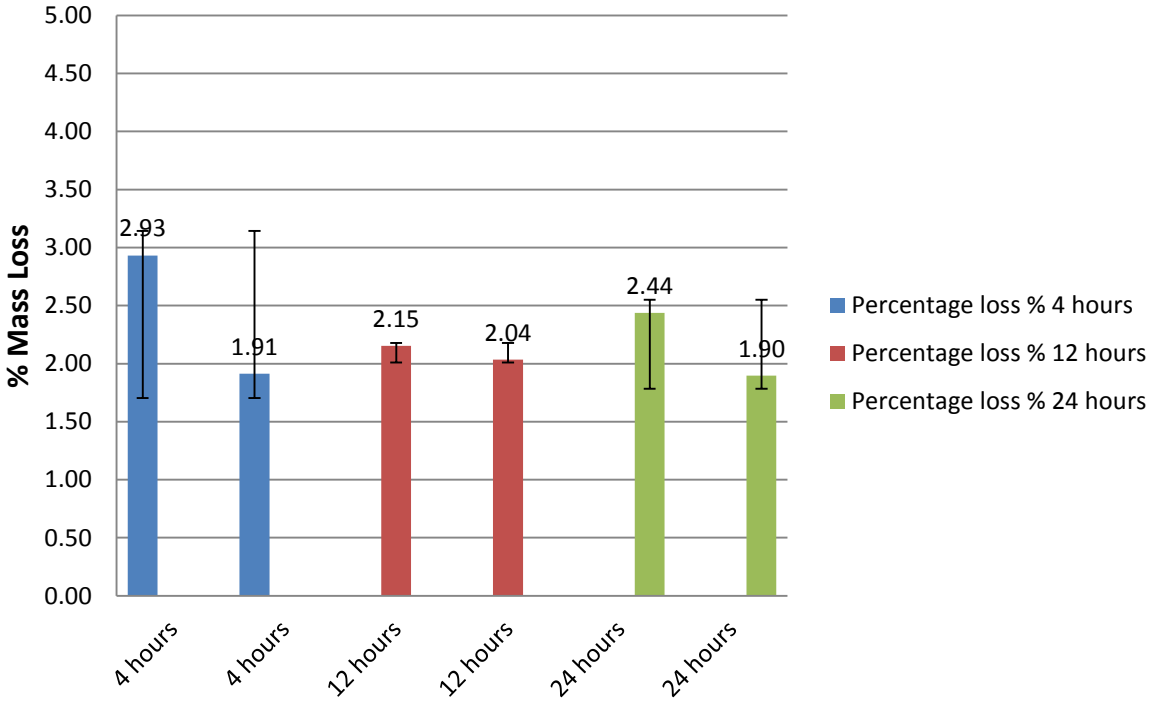

Figure 5.9: Cumulative percentage of loss and influence of different soaking times on BSM-emulsion with 100%G2 (Hornfels) crushed stone after 12 cycles (2 repetitions).

The tests showed similar results after different soaking times and the variability of the results was considered low. A similar cumulative percentage of loss was recorded for both the BSMs. The method to measure the loss of material after every wet-dry brushing cycle is not completely univocal. Long *et al*. (2004) suggest measuring the loss of material at the end of 12 repeated cycles, without considering the loss at the end of every single cycle. The formula for the calculation of the percentage of loss used for every wet-dry brushing cycle is:

$$L = \frac{W-M}{W} \times 100 \qquad [5.2]$$

where
L = mass loss of material (%);
W = original mass of the specimen before testing (g);
M = mass of the specimen after testing (g).

The percentage loss was calculated to the nearest 0.1 percent and it was recorded for every single cycle due to the small amount of material lost after every wet-dry brush cycle. The 4 hours soaking cycles give the possibility to perform two tests every day. This gives the possibility to perform a quick wet-dry brushing test in six days on the field.

Figures 5.10 to 5.15 present the loss of material recorded for every wet-dry brushing cycle. For all soaking cycle options the BSMs show a substantial loss during the first three cycles. After four cycles the percentage reduces and it remains constant until the last wet-dry cycle. The first three graphs (Figures 5.10, 5.11 and 5.12) present the percentage of mass loss for the BSM-foam mix, while the other three graphs (Figures 5.13, 5.14 and 5.15) present the loss for the BSM-emulsion. The percentage of loss in every soaking condition is recorded for nine BSM-foam specimens and for the six BSM-emulsion specimens. An average value was drawn in all the diagrams and reported at the end.

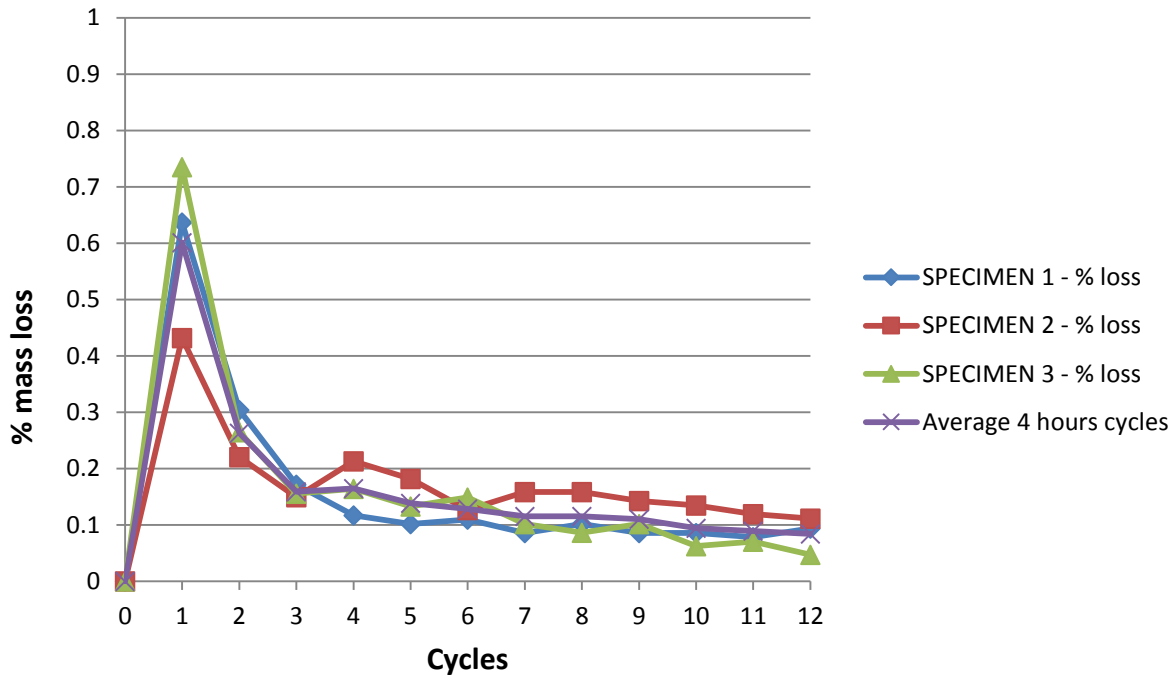

Figure 5.10: Percentage of loss and influence of different soaking times on BSM-foam after 4 hour cycles.

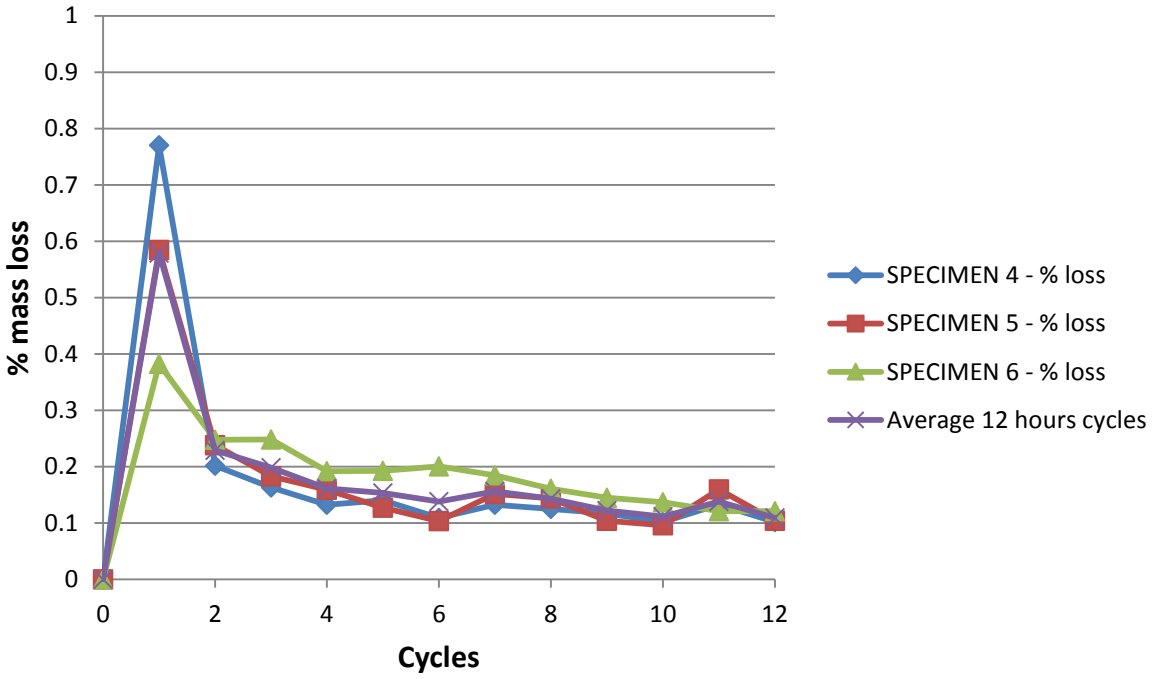

Figure 5.11: Percentage of loss and influence of different soaking times on BSM-foam after 12 hour cycles.

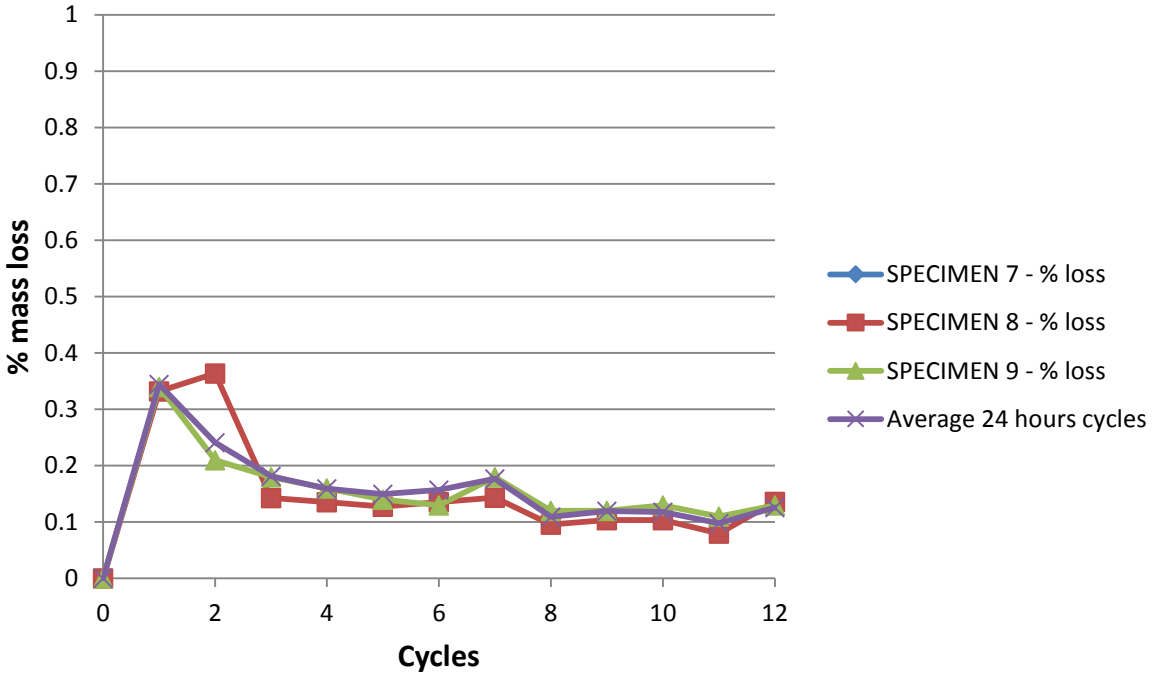

Figure 5.12: Percentage of loss and influence of different soaking times on BSM-foam after 24 hour cycles.

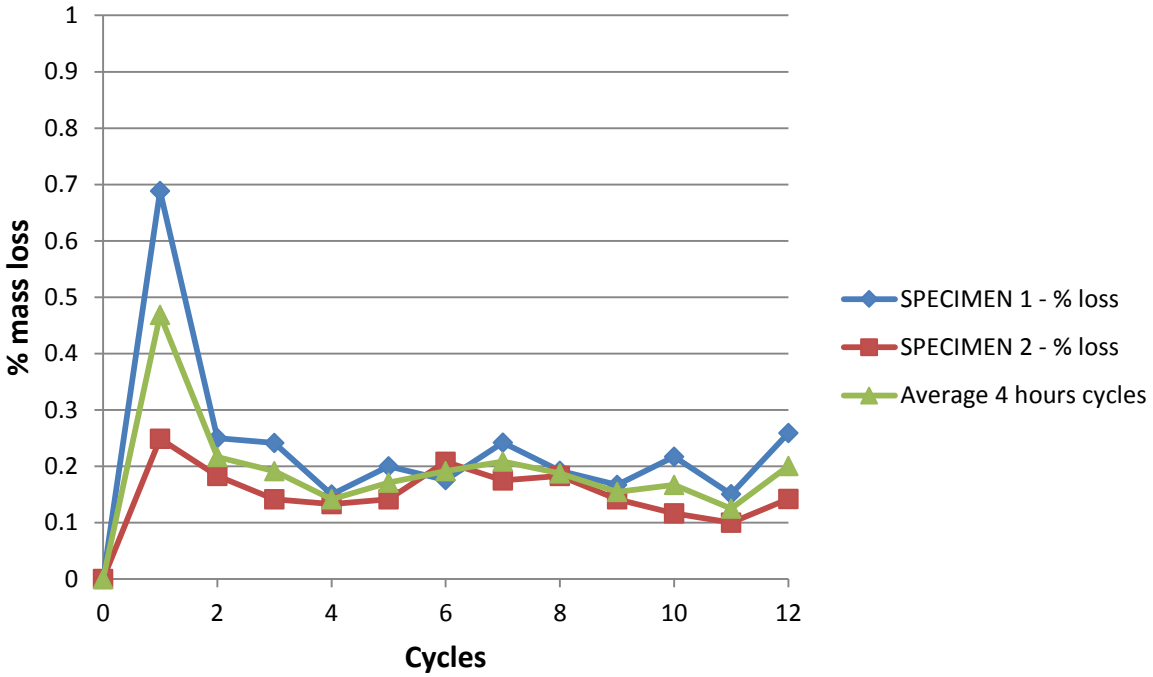

Figure 5.13: Percentage of loss and influence of different soaking times on BSM-emulsion after 4 hour cycles.

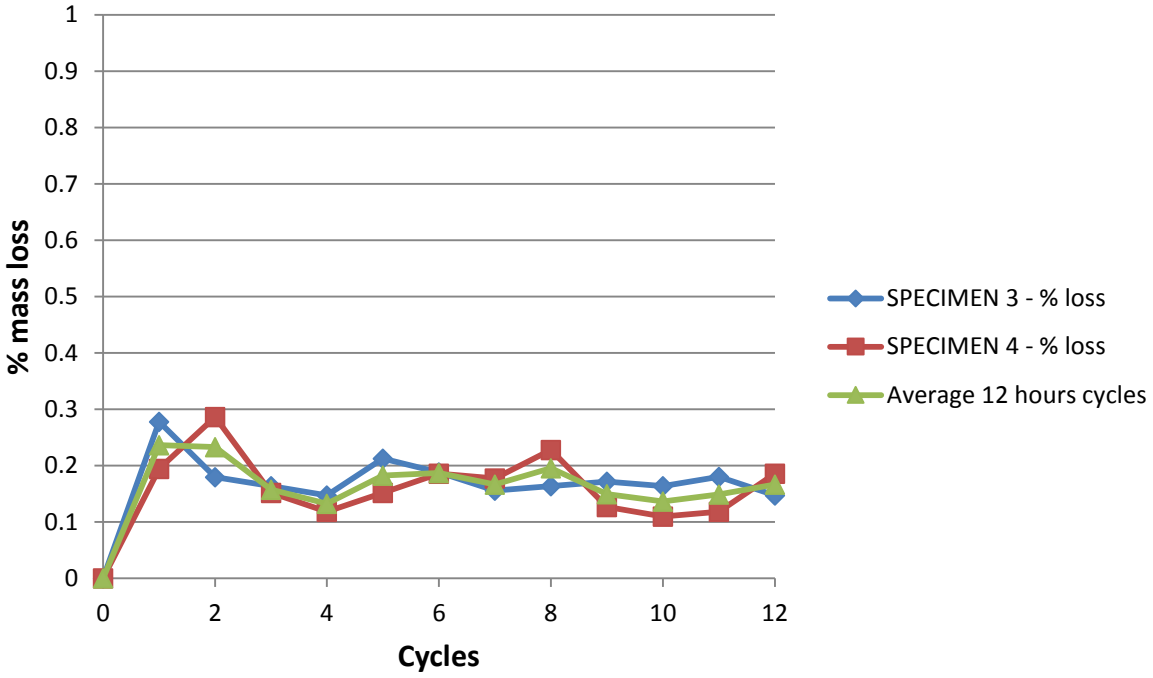

Figure 5.14: Percentage of loss and influence of different soaking times on BSM-emulsion after 12 hour cycles.

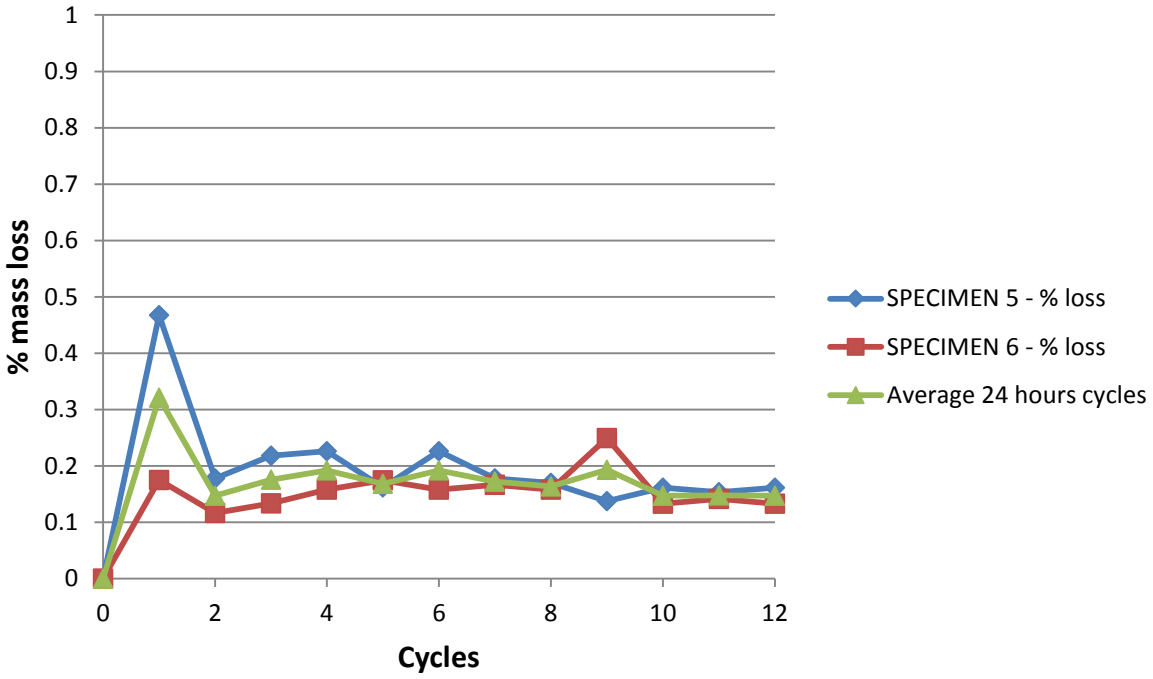

Figure 5.15: Percentage of loss and influence of different soaking times on BSM-emulsion after 24 hour cycles.

Figures 5.16 and 5.17 present a comparison of the average losses for the two BSMs mixes at different soaking times.

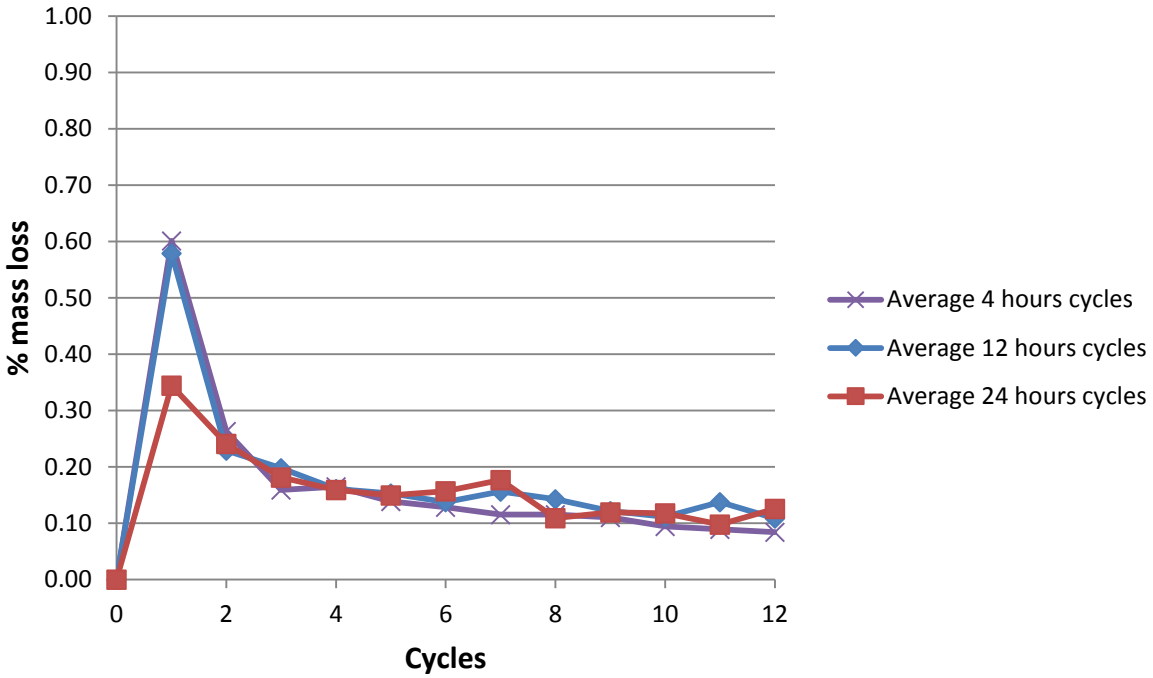

Figure 5.16: Comparison of average percentage of losses and influence of different soaking times on BSM-foam with 100%G2 material.

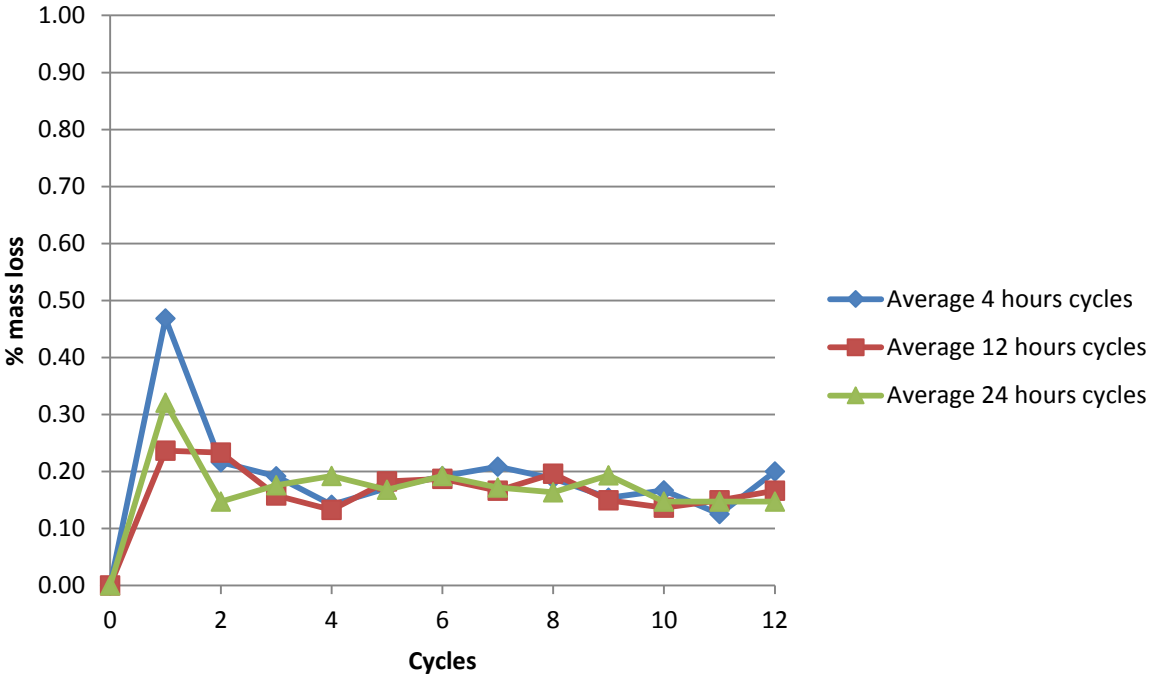

Figure 5.17: Comparison of average percentage of losses and influence of different soaking times on BSM-emulsion with 100%G2 material.

In Figures 5.16 and 5.17 is notable that the biggest percentage of loss occurs during the first four cycles. In the first cycle the loss for every soaking condition is highest compared to the rest of the others. The same range of percentage of loss was recorded during the first cycle for all the soaking time conditioning periods. The percentage of loss after the fifth cycle remains relatively constant and around 0.2% for both of the BSMs mixtures. The higher percentage of loss in the first four-five cycles is probably due to the weakness of the particles and BSM bonds on the surface of the specimens. The percentage of loss was slightly higher in the BSM-foam than in the BSM-emulsion for the first cycle. These findings could explain the necessity to reduce the time cycles from twelve cycles to four cycles for the wet-dry brushing testing. The original protocol developed by Long *et al*. (2004) was designed for only cement treated materials, where the phenomenon of carbonation takes place in the material. In that situation the mechanical brushing test measures the loss of materials from the specimen surface resulting from soaking, drying and carbonation. The loss of materials is a result of chemical alteration (decomposition) or physical weakening (disintegration) of bonds developing during the curing process. The moisture damage in BSMs is a process that leads to change in the internal structure of a mixture by a reduction in adhesion and cohesion and subsequently in the shear strength. The deterioration is linked to void properties (pore pressure), aggregates characteristics and change in moisture state (i.e. degree of saturation). The bond between the foam and emulsion with the aggregates contributes to a reduction in the percentage of loss during the wet-dry brushing cycles. The stiffness developed by the bitumen in the mix can reduce the erosion of the surface especially if the period of curing becomes longer.

5.4.5 Wet/dry brushing test on BSM-foam mixtures

Three BSM-foam mixes with different percentages of reclaimed asphalt were investigated in this study. All the mixes included 1% of cement and were prepared and cured following the TG2 guideline (Asphalt Academy, 2009). After curing, the three specimens per mix were submerged in a bath thermostatically controlled at 25°C for four hours. The specimens were afterwards clamped securely between the pads of the brushing apparatus and they were loaded with a wire brush. After every test the percentage of loss was recorded for every specimen. All the data of losses are presented in the appendix at the end of this research.

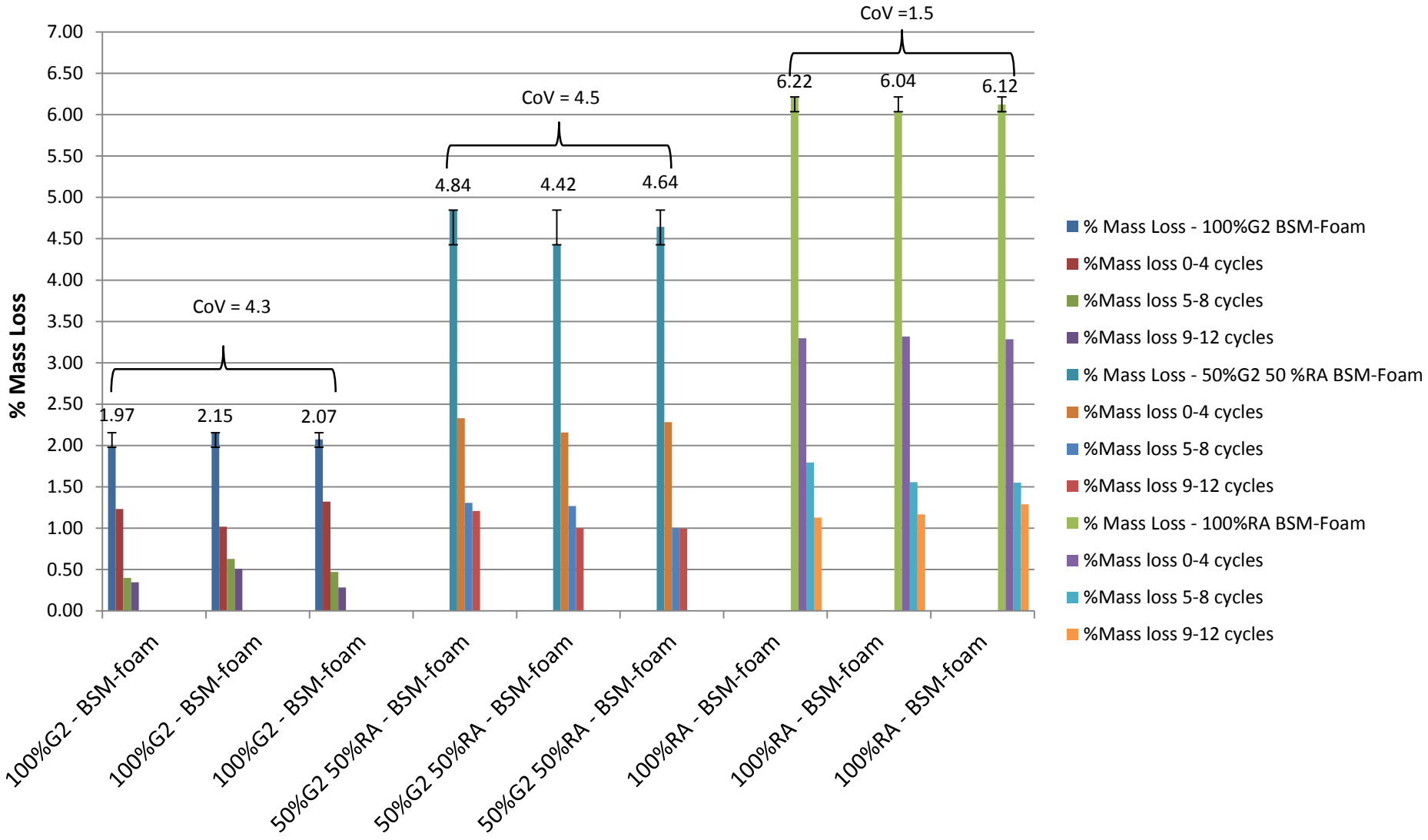

Figure 5.18: Comparison of cumulative mass loss and contribution to the final percentage of loss from groups of cycles.

Figure 5.18 shows at the top of the three highest columns the cumulative percentage of loss for every specimen. The standard deviation and the covariance for the wet-dry brushing test were always low. Next to every cumulative percentage of loss there are three other small columns which represent the contribution to the cumulative percentage of loss from different groups of cycles.

Some findings clearly showed through this research:

- The cumulative percentage of loss ranges in the same value (Sd<0.2) for all three specimens tested with the wet-dry brush apparatus. BSM-foam mixtures with the same composition show the same behaviour.
- The cumulative percentage of loss increases with the percentage of reclaimed asphalt. This is most probably due to the percentage of air voids which increases at the same time. The BSM-foam mix with a high percentage of RA has more air voids than a BSM-foam mix with 100%G2 crushed stone.
- The presence of foam in the mixes contributes to a reduction in the mass loss per cycle. The CSIR performed some study on cement treated materials. The percentage of loss ranged between 3% and 4% (Laboratory testing for the HVS, Test Sections on the N7, Long and Ventura, 2003). The percentage of loss is higher for BSMs than for cement treated material, but not as high as was expected.
- Four hours of soaking is considered the best option for the BSMs preconditioning time for wet-dry brushing tests. Most of the mass loss is measured during the first four cycles. After the fifth cycle the mass loss decreases to lower values and remains constant until the last cycle. The test can be replicated in the field in less than one week (12 cycles).
- The time in the water is balancing the cumulative percentage of loss for the specimens tested. In fact the standard deviation ranges between 0.18 (BSM-foam mixes with a low percentage of RA) to 0.2 (BSM-foam with 100%RA) for the specimens tested in the same conditions.
- The increasing amount of RA in the BSM-foam mix leads to a higher mass loss during the first four cycles compared to BSM-foam with a lower RA percentage. Probably this is due to the gain of air voids in the mix and to the lower maximum dry density (constant compaction energy).

Figure 5.19: Effect of erosion of wet-dry brushing on BSMs mixtures.

5.5 Moisture Induction Simulation Test (MIST)

Twagira (2010) developed and studied the possible mechanism of failure due to moisture infiltration. Through his study, the moisture induction simulation test (MIST) device was developed to assess moisture-induced damage based upon cyclic pulsing of water pressure into a compacted and cured specimen. The MIST device shows the potential to be used as a conditioning device for BSMs, in order to evaluate the reliability of the wet-dry brushing test for moisture damage. The developed and investigated testing protocol for the MIST/tri-axial testing has established threshold values that can be used as ranking criteria for BSMs mix design in relation to moisture damage durability (Twagira, 2010).

This research investigates shear parameters (c and φ) of BSMs before and after a MIST test for all three BSM-foam mixes presented in this research. C and φ are critical parameters for BSMs due to their stress dependent nature. The saturation condition of the MIST test can replicate the field condition of pulsing of cyclic water pressure by dynamic loading. Mechanical tests (monotonic) were applied afterwards on tri-axial specimens for determining the level of moisture damage in the BSM-foam mixes.

This section presents the results of an experiment aimed at determining whether cyclic pulses of water pressure into three different BSM-foam mixes with different percentages of reclaimed asphalt induces sufficient damage to the tri-axial specimen. This enabled a distinction between different levels of resistance to moisture damage in BSMs that are included and classify in the TG technical guideline (Asphalt Academy, 2009). Six tri-axial specimens (150 mm x 270 mm) were prepared for each BSM-foam mix. All the mixes were tested after the moisture damage conditioning in a tri-axial set-up. The tri-axial tests were afterwards compared with the previous tests carried out in dry (equilibrium) conditions without the MIST device.

Table 5.5: Retained cohesion and void content on different BSM mixes after the MIST conditioning.

Mix	Void Content (%)	Cohesion of a dry mix (kPa)	Cohesion of a wet mix (kPa)	Retained Cohesion (%)
BSM-foam 100%RA	16.49	432	242	56
BSM-foam 50%RA 50%G2	15.48	374	346	93
BSM-foam 100%G2	13.46	516	466	90

Mixes with high void contents generally show higher damage due to excess moisture during pulsing time. The differences in the retained cohesion in BSM mixes show ranking of mixes after conditioning using the MIST device. That means ranking of BSM mixes with lower or higher moisture susceptibility can be determined by the pulsing of cyclic water pressure using MIST and tri-axial tests. To this end, the above analysis can establish the MIST threshold values for pulsing cyclic water pressures into the tri-axial cell. The ranking criteria are proposed for BSM mix design in relation to moisture damage (Asphalt Academy, 2009). The classification of three different types of BSMs is consistent with the new guidelines currently being published in South Africa, where BSM1 material is able to withstand the highest levels of traffic patterns in the network (Asphalt Academy, 2009).

The steady-state saturation condition, coupled with the mechanical response of the mixes, is one of the indicators of moisture durability behaviour and long-term performance in field conditions. The difference in MIST pulsing cycles (time) of BSMs relates well with the retained cohesion and retained shear strength determined by tri-axial tests. The results of the retained cohesion (determined from Mohr-Coulomb relationship) indicate that BSMs that withstand higher numbers of pulsing cycles show high retained cohesion while BSM mixes that withstand lower pulsing cycles show lower cohesion values. This is expected due to the fact that cyclic water pressure weakens the cohesion properties of the mixes that are susceptible to moisture damage. It is evident that the progressive loss of cohesion and adhesion in the mix matrix results in reduction in shear strength. Reduction in shear strength may result in a deterioration of the long-term performance of the BSMs, which could lead to deterioration of stiffness properties and permanent deformation. In fact the deviator stress ratio (σ_1-σ_3/$\sigma_{1,f}$-σ_3) is linked directly to the shear strength ($\sigma_{1,f}$).

The corresponding RC of these mixes after MIST conditioning and static tri-axial testing indicates that mixes with 100%G2 material and 50%RA and 50%G2 are more resistant to moisture damage than the 100%RA mix. According to ranking criteria, the first two BSM-foam mixes can be classified as BSM1 (i.e. RC $\geq$ 75%), while mix with 100%RA can be classified as BSM3. The results show that 100%G2 crushed stone and 50%RA and 50%G2 material stabilised with foamed bitumen are less susceptible to moisture damage than a BSM-foam mix with 100%RA. Mixes with high void contents show higher damage due to excess of moisture during pulsing time.

The following monotonic tri-axial tests represent the Mohr-Coulomb results obtained after the wet MIST conditioning and in dry (equilibrium), without the use of the MIST device.

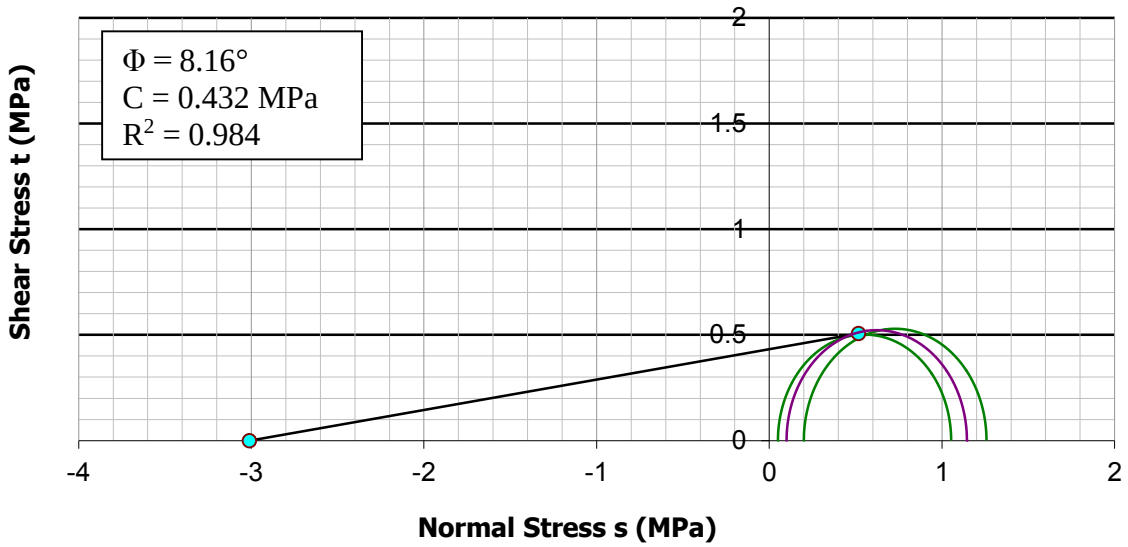

Figure 5.20: Failure envelope of BSM-foam with 100%RA at 25°C without MIST conditioning.

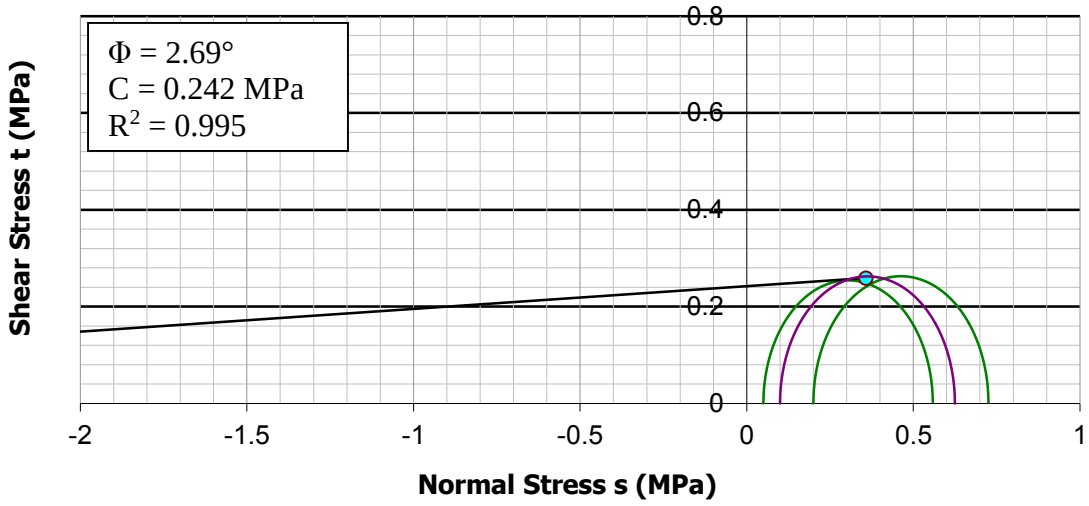

Figure 5.21: Failure envelope of BSM-foam with 100%RA at 25°C after MIST conditioning.

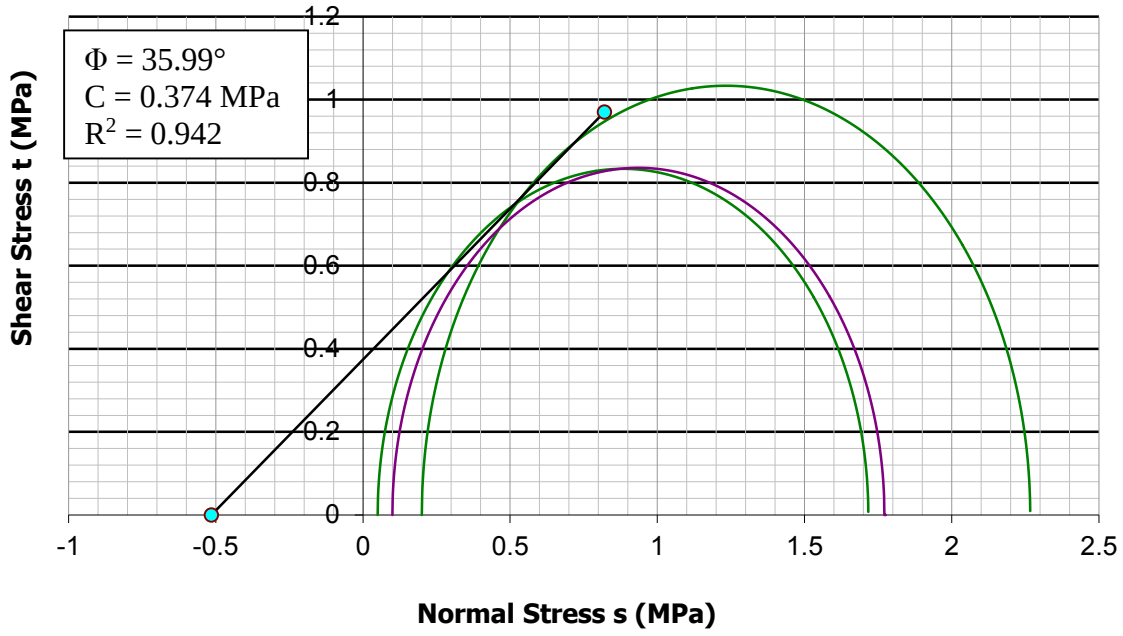

Figure 5.22: Failure envelope of BSM-foam with 50%RA+50%G2 at 25°C without MIST conditioning.

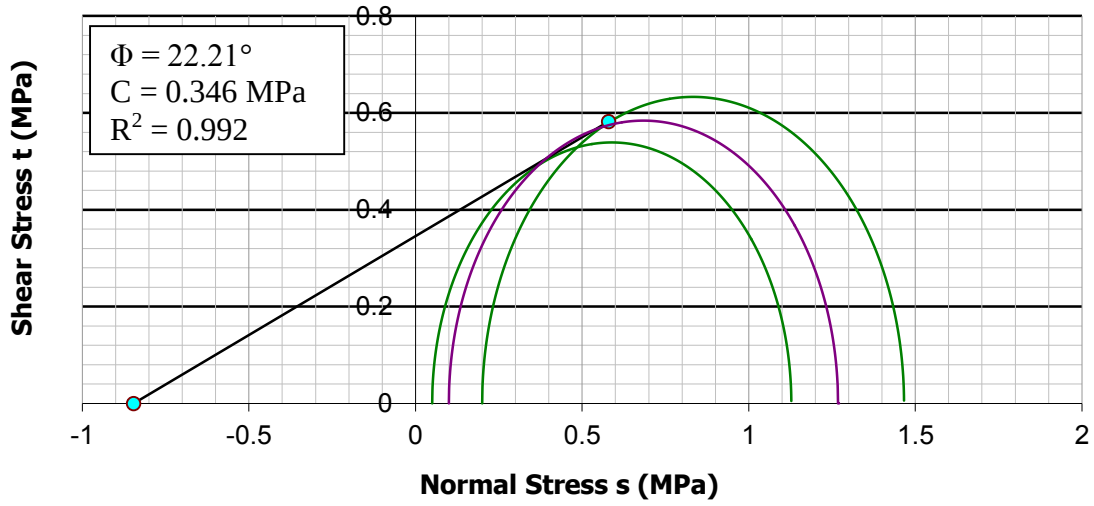

Figure 5.23: Failure envelope of BSM-foam with 50%RA+50%G2 at 25°C after MIST conditioning.

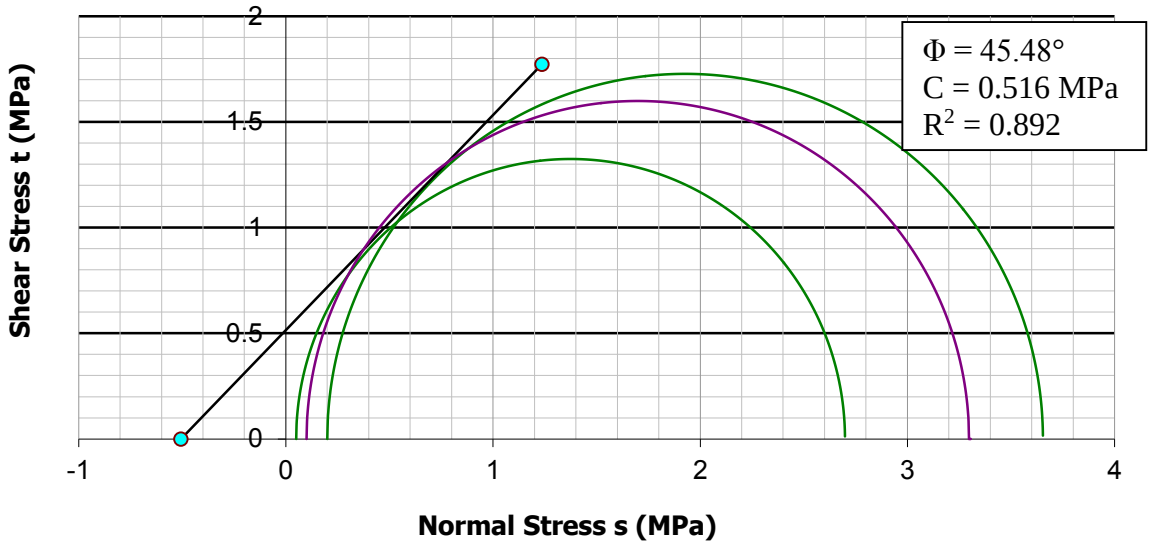

Figure 5.24: Failure envelope of BSM-foam with 100%G2 at 25°C without MIST conditioning.

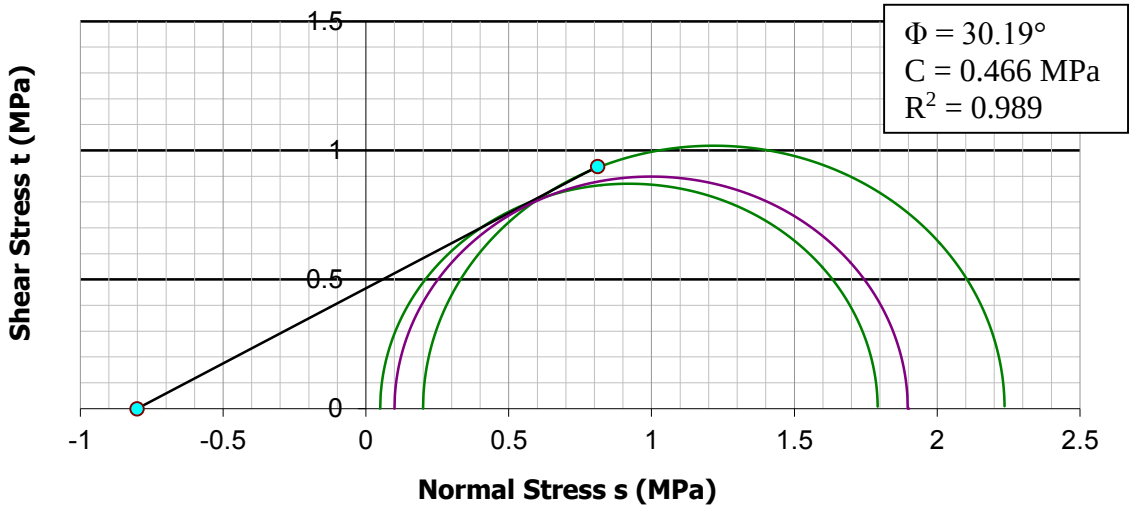

Figure 5.25: Failure envelope of BSM-foam with 100%G2 at 25°C after MIST conditioning.

A summary can be drawn considering the Mohr-Coulomb cycles with the previous use of the MIST device and without it. The cohesion C and the angle of friction φ are represented in Figure 5.26 and related to the percentage of RA included in the BSM-foam mixes.

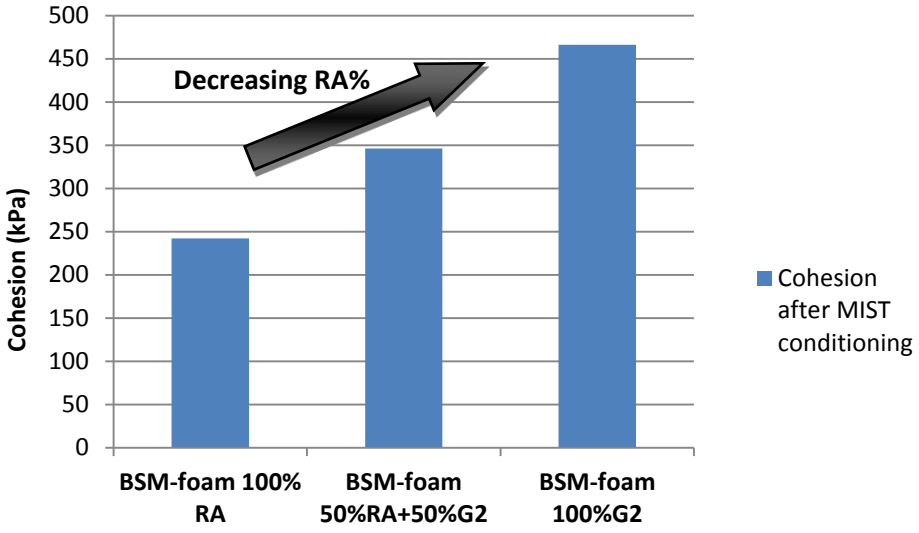

Figure 5.26: Effect of RA on cohesion after MIST conditioning.

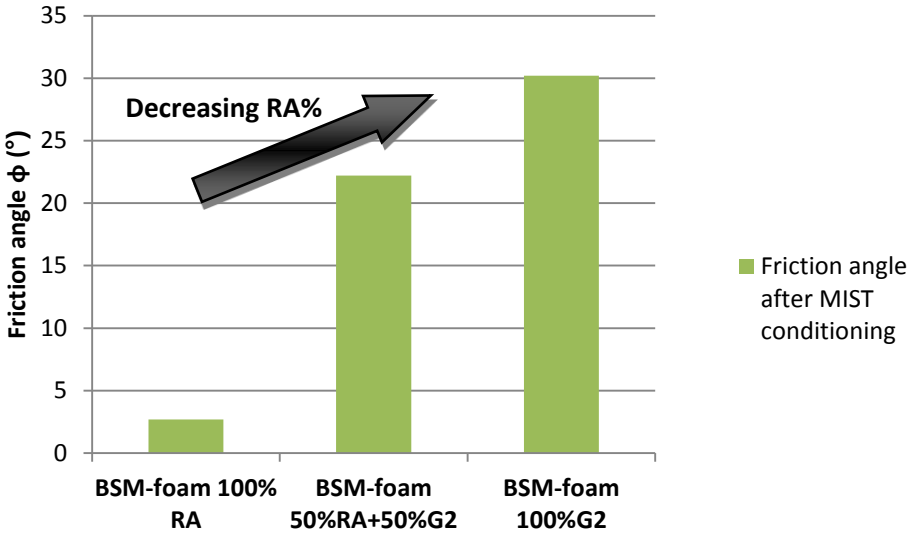

Figure 5.27: Effect of RA on friction angle after MIST conditioning.

As the percentage of RA decreases in the BSM-foam mix, the cohesion and the friction angle increase linearly. The same behaviour was analysed during a cycle of dry (equilibrium) tri-axial tests performed without the use of the MIST device. The following graphs (Figures 5.28 and 5.29) show the same situation for the three BSM-foam mixtures for the angle of friction. The same behaviour discovered for the previous tests is not completely clear during the monotonic tri-axial tests at different confinements but without the use of the MIST device.

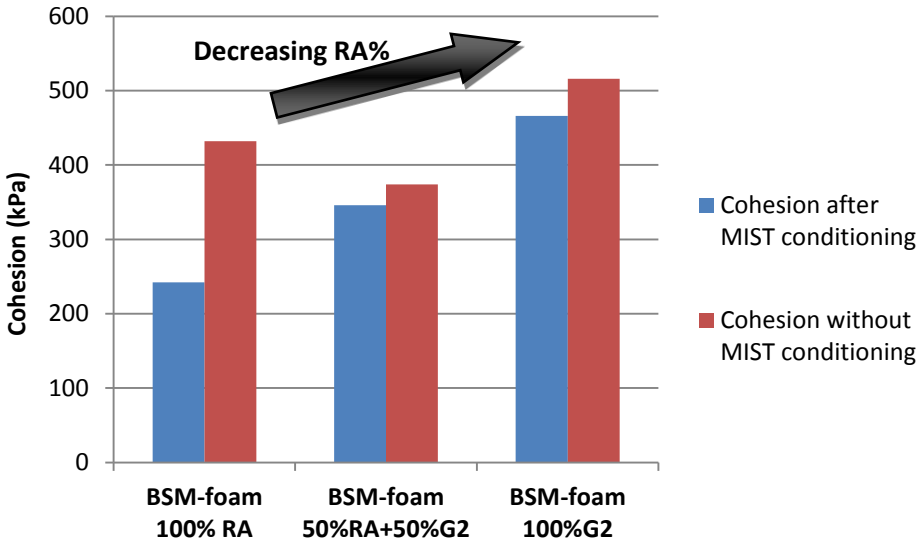

Figure 5.28: Effect of RA on cohesion with and without the MIST conditioning.

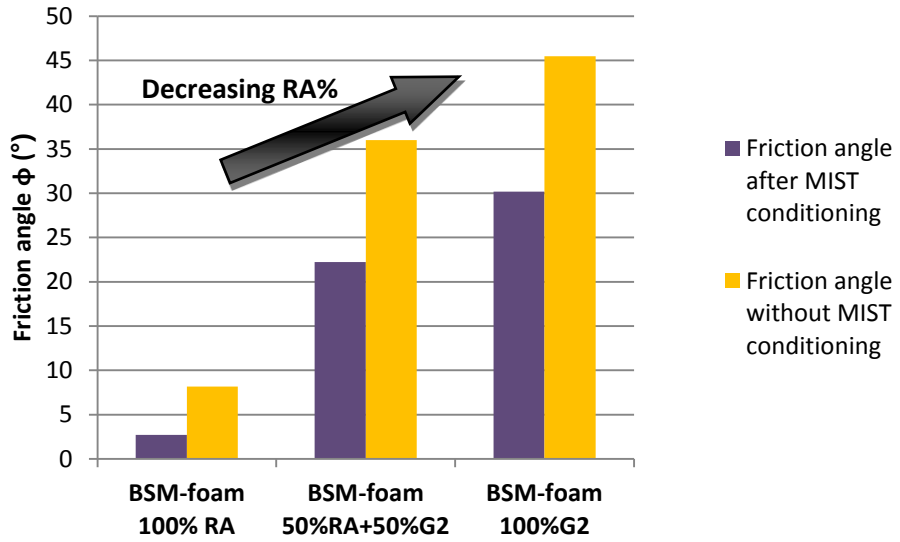

Figure 5.29: Effect of RA on friction angle with and without the MIST conditioning.

The angle of internal friction is almost one third less the original angle of friction in dry conditions. This difference has to be analysed in the light of the influence of mechanisms of moisture damage.

The infiltration of excess moisture is linked to the dynamic loading. The main components of moisture damage mechanisms are identified as:

– change in shear properties (cohesion and friction angle) due to moisture damage mechanisms and cycle of water pumped in the specimens, and

– loss of integrity of the BSMs specimens due to deterioration of the cohesive and adhesive bonding.

The deterioration of the BSM-foam can be linked to void properties, pore pressure and change in moisture state (i.e. degree of saturation). The quantification of voids in the mixes cannot fully describe the performance of BSMs in terms of moisture damage mechanisms. However, understanding the void structure permeability and the wet-dry brush test is important in explaining their relationship to mode of moisture damaging mechanisms.

The study of moisture damage characterisation indicates that BSM-foam with 100% RA were more susceptible to moisture damage than similar materials stabilised (100%G2 Hornfels crushed stone) with foamed bitumen.

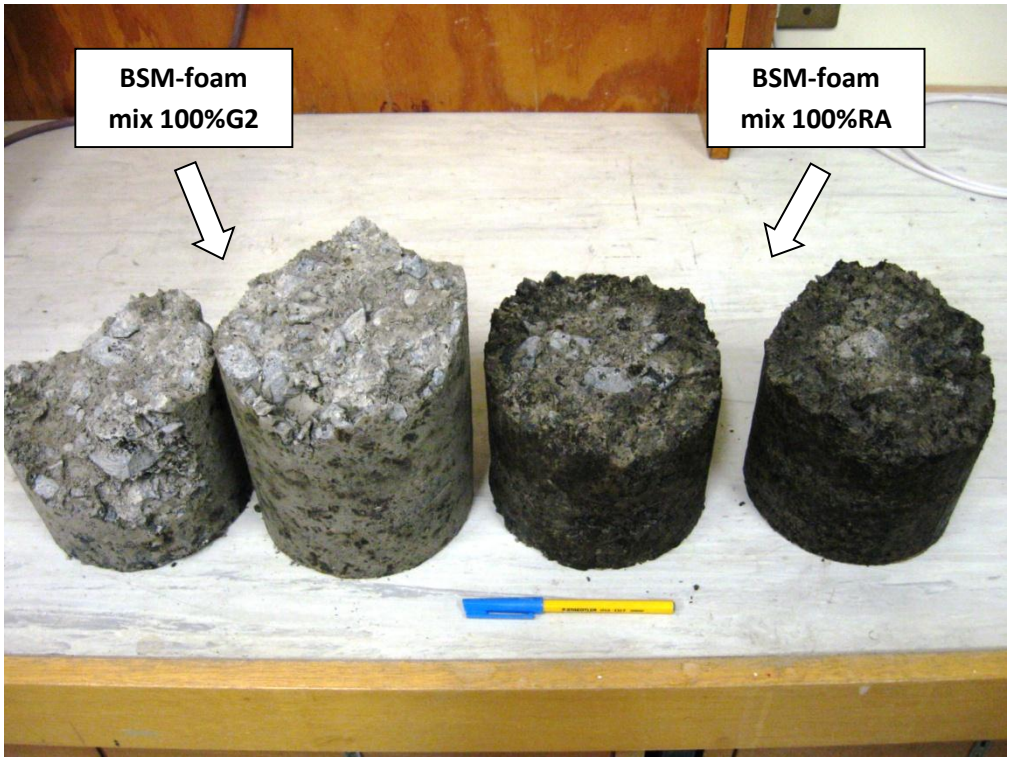

Figure 5.30: BSM-foam specimens after MIST conditioning.

5.6 Possible correlation between air voids, wet – dry brush test and MIST procedure

Disintegration of BSMs during wet trafficking can result from cohesive and adhesive failure. The consequence of this failure is accelerated rutting potential under dynamic loading

confinement. The performance of BSMs is closely dependent not only on mechanical failures but also on other important aspects:

- air voids;
- erosion of the surface;
- behaviour of the material under water, and
- effect of water pumped into the BSMs material at high pressure.

The erosion of the surface of the BSMs material presented in this chapter can draw some possible correlation between the air voids and permeability tests, the wet and dry brushing test and the MIST test. The behaviour of the material is related to from the amount of air voids present in the mix. As the amount of air voids increases, the cumulative percentage of loss measured during the 12 cycles of the wet and dry brushing test rises. At the same time the MIST apparatus preconditions the BSMs specimen, and reduces the angle of friction and cohesion during the monotonic tri-axial tests. The same situation was in part presented by Twagira (2010) in his research focusing on the possible relationship between the MIST device and the ITS test. Visual observation on the surface at the end of every wet-dry brushing cycle showed how the percentage of air voids can affect the percentage of loss. In fact, the air voids constitutes one of the biggest factors that influence the durability of material in the long term. The disintegration during the tests shows that wet preconditioning creates more damage in terms of cohesion loss and angle of friction reduction than dry trafficking. This suggests that cohesion loss accrued under traffic and pore pressures in the presence of water aggravate damage to the pavement.

Wet and dry cycles with the brushing device can simulate the long term problems of moisture damage on the surface of BSMs layers. That means that upon widening of the micro-cracks and surface water infiltration, the hydrodynamic effect on the moisture-susceptible base materials will result in exponential erosion and rutting. This consequently can create a mechanism of failure on the pavement, which can be visible on the road, such as a pothole. The wet dry brushing test can simulate field conditions where moisture damage would occur and accelerates the rate of deterioration into an acceptable time frame.

The wet-dry brush tests can be correlated with the laboratory MIST conditioning and subsequent monotonic tri-axial test results. Wet-dry brushing tests on BSMs specimens submersed in water for cycles of four hours, result in significant distress in terms of cumulative percentage of loss and the increasing amount of air voids in the mixes. This does not occur under dry trafficking conditions, so it simulates wet trafficking. On the other hand, it is apparent that the mixes lose cohesion (and most likely stiffness) due to moisture damage that is activated by dynamic pore pressures through the MIST conditioning. This is related to the amount of air voids that influence the distribution of the material in the mix. The inclusion of active filler and especially cement in BSMs can improve the moisture resistance of the BSMs. The wet-dry brushing test can provide a better understanding of the durability behaviour of BSMs after only four cycles.

In the light of the results obtained through the wet-dry permeability test and the MIST conditioning, a relationship can be drawn between the percentage of mass loss and the cohesion loss after the MIST test. Figure 5.31 shows a direct connection between mass loss, cohesion

loss and percentage of RA. At higher mass loss a higher cohesion loss is directly related especially if the percentage of RA is increased for the BSM-foam mixes. A BSM-foam mix with a percentage of RA lower than 50%, yields a mass loss and cohesion loss three times less than in a mix with 100% RA. In fact the BSM-foam mixes with a lower percentage of RA are less susceptible to moisture damage than the mixes with a higher percentage of RA.

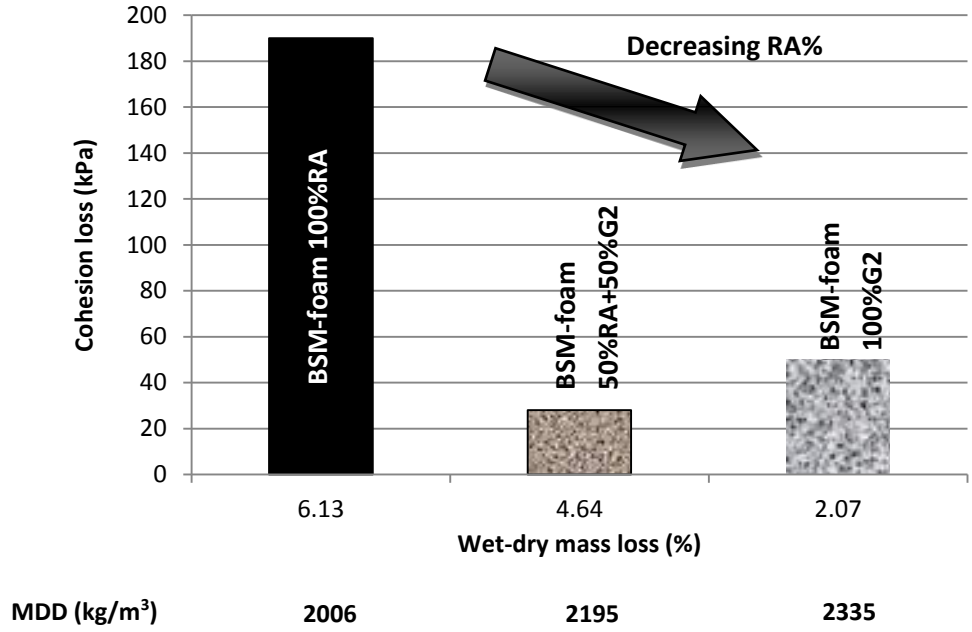

Figure 5.31: Correlation between mass loss and cohesion loss in BSM-foam mixes with a high percentage of RA.

The BSM-foam mix with 50%RA and 50%G2 showed a cohesion loss lower than the other two mixes. Probably this could be explained through a higher fresh bitumen content (2.1% fresh bitumen), higher percentage of fine particles in the mix and an intermediate density (Figure 5.31).

The governing process and bond formation in the BSM mix matrix reveals that adhesion and cohesion between binder and mineral aggregates play a key role during the moisture damage tests (wet-dry durability test and MIST conditioning). The evolution of bonding through the interaction of binder, mineral aggregates and water reflects physico-chemical and mechanical phenomena. These differentiate BSMs from other pavement materials in the evolution of bonding and damaging mechanisms. They should be considered during material selection for mix design.

High temperatures could lead to an increase in wet-dry mass loss and cohesion loss, while low temperatures could lead to a low wet-dry mass loss.

The presence of water in BSMs influences the mechanisms of moisture damage significantly. The infiltration of excess moisture is linked to the environment and dynamic loading. The main components of moisture damage mechanisms can be identified in:

- loss of integrity of the matrix due to deterioration of the cohesive and adhesive bonding and

- change in internal conditions due to moisture transport mechanisms

Moisture damage is linked directly to void properties and contents, aggregates characteristics and quality and change in moisture state (i.e. degree of saturation). The quantification of voids in the mixes can help to describe the performance of BSMs in terms of moisture damage mechanisms. Understanding void structure and distribution is important in explaining their relationship to moisture damage mechanisms.

To support the findings of this paragraph the ITS_{dry} tests, presented in Chapter 4, showed higher tensile strength values for BSMs with a lower percentage of RA. The dominant mode of failure in MIST/tri-axial testing is shear failure and in ITS testing is tensile cracking. In pavement structure, tensile cracking is not a dominant failure of BSMs. Therefore, tensile cracking in the ITS test does not simulate the failure mechanism of BSMs accurately compared to MIST/tri-axial testing. The reason for this is that crack formation and development due to tensile stress in the centre of BSM specimens, as well as the unconfined nature of the test are not typical representations of the failure mechanisms occurring in BSMs during in-service condition.

ITS_{dry} and ITS_{wet} results from the N7 project closed to Cape Town (Sietse Robroch, 2002) showed a reduction of the ITS results from dry to wet conditions. Significant resistance to moisture damage was measured by higher values of retained cohesion (RC) and retained tensile strength (TSR). This is a result of higher degree of field densification and percentage of cement in the mix. However, ranking of these mixes using TSR show some difference. According to TG2 (2009) BSM mix with TSR value $\geq$ 75% is regarded as less susceptible to moisture damage. In this regard, the results presented in the final report on the N7 project (Sietse Robroch, 2002) show that the mixes considered are less susceptible to moisture damage. This might not be realistic, because mixes with ravelling $\leq$ 2mm after 45000 load applications cannot be classified as less resistant or susceptible to moisture damage. Therefore, the use of the TSR in quantifying moisture damage in BSMs is rather an indicator, as it does not simulate the actual failure mechanisms predominant in BSMs. More field tests should be carried out to analyse possible correlations between ITS tests and wet and dry brushing test.

REFERENCES

Asphalt Academy. 2009. A guideline for the design and construction of bitumen emulsion and foamed bitumen stabilised materials. 2nd edition technical guideline. Pretoria, South Africa. (TG2).

Caro, S., Masad, E., Bhasin, A. and Little, D. N. 2008. Moisture susceptibility of asphalt mixtures, Part 1: mechanisms, Part 2: Characterisation and modelling. International Journal of Pavement Engineering. Vol. 9, No. 2, pg81–98.

Collings, D. and Jenkins, K. 2011. The long-term behaviour of bitumen stabilised materials (BSMs). CAPSA 2011.

Houghton Mifflin Company, 2000. Dictionary of English language, 4th edition. Princeton University, USA.

Jenkins, K. 2000. Mix Design Considerations for Cold and Half-Warm Bituminous mixes with the emphasis on foamed bitumen. PhD Dissertation. University of Stellenbosch.

Jenkins, K.J., Ebels, L.J. and Twagira, M.E. 2006. Updating bituminous stabilised materials guideline: Mix design inception study. First draft. Pav. Eng.cc, Stellenbosch, South Africa.

Jenkins, K.J., Ebels, L.J., Twagira, M.E., Kelfkens, R.W., Moloto, P. and Mulusa, W.K. 2008. Updating bituminous stabilised materials guideline: Mix design report, phase II. Research report, prepared for SABITA and Gautrans, Pretoria. South Africa.

Kanitpong, K., Benson, C. H. and Bahia, H. U. 2001, "Hydraulic Conductivity and Permeability of Laboratory Compacted Asphalt Mixtures," Transp. Res. Rec., No. 1767, Paper No.01-2997, pp. 25–32.

Kuvhanganani, L. T. 2008. Moisture sensitivity of selected foamed bitumen-treated Materials. Master's degree in technology, Pavement Engineering. Tshwane University of technology. Pretoria, South Africa.

Liebenberg, J.J.E. 2002. The Influence of Various Emulsion and Cement Contents on an Emulsion Treated Ferricrete from the HVS Test Sections on Road P243/1. Pretoria, South Africa.

Long. F, Theyse, H. and Ventura, D.F.C. 2004. Characterisation of foamed bitumen treated materials from HVS test sections. Pretoria, South Africa.

Long, F. and Ventura, D.F.C. 2003, Laboratory testing for the HVS, Test Sections on the N7, Pretoria, South Africa.

Netterberg, F. and De Beer, M. 2012. Weak interlayers in flexible and semi-flexible road pavements: Part 1. J. S. Afr. Inst. Civ. Eng., vol.54, n.1, pp. 31-42.

Paige-Green, P. and Ventura, D.F.C. 2004. Durability of foamed bitumen treated basalt base course. CSIR report CR 2004/8. Pretoria.

Sietse Robroch, 2002. Laboratory research of foamed bitumen and emulsion mixes (both with cement) for cold mix recycling of N7 near Cape Town. Contract TR 11/1. South Africa.

TMH 1 (Technical Methods for Highways). 1986. Standard methods of testing road construction materials. (TMH 1). National Institute for Transport and Road Research, Pretoria.

Twagira, E.M. 2010. Influence of durability properties on performance of bitumen stabilised materials (PhD). University of Stellenbosch, South Africa.

Venkatramaiah, C. 2006. Geotechnical Engineering. New Age International Pvt Ltd Publishers.

Ventura, D.F.C. 2001. Durability aspects of the ferricrete from the HVS sections on Road P243/1. CSIR Transportek. Pretoria: South Africa. (CR-2001/81).

CHAPTER 6

TEMPERATURE DISTRIBUTION WITHIN BSMs

6.1 Introduction

Bitumen Stabilised Materials (BSMs) pavements form one of the technologies applicable to structural road systems. The response, damage characteristics and structural capacity of the BSMs layers depend on many factors including density, moisture content, bitumen content and temperature, amongst others. Moreover, temperature can be a major contributor to several types of distress. Although temperature is a significant factor in evaluating the performance of a pavement, it is largely overlooked. The objective of this chapter is to present the results of the temperature distribution in a BSM layer measured under laboratory conditions. In addition, a model that can be used in predicting the temperature distribution in a pavement structure at different depths, using direct measurements recorded for three different BSM mixes with an increased percentage of reclaimed asphalt, is presented. The model was developed comparing two past studies on temperature distribution for HMA developed by the Strategic Highway Research Program (SHRP) in the USA (Kennedy *et al*., 1994) and by Viljoen (2001) in South Africa. Lastly, the influence of temperature is investigated through a finite element model, developed to predict the thermal response of the BSM using the MLS software of Femmasse B.V. (2006) The study shows that the numerical simulation is feasible to predict the thermal response of BSMs. Ultimately, the finite element model can provide pavement engineers with an efficient computational tool, which can be a guide for the future research on BSMs and especially for an accurate pavement design method.

6.2 Scope

This chapter has three primary objectives, namely to

- develop a model that can be used to predict the thermal conductivity and temperature fluctuations within a BSM layer, based on temperature data collected during laboratory tests;
- develop relationships between asphalt temperature models (e.g. Kennedy *et al*., 1994; Viljoen, 2001) already consolidated in the research community. The models are to provide the basis for adjusting the temperature in a BSM pavement at different depths; and
- simulate and compare the temperature distribution in a BSM pavement with the existing temperature database through a finite element program developed at the Delft University of Technology in the Netherlands. The model is capable of predicting pavement temperatures at various depths as a function of environmental (thermal) conditions.

6.3 Construction of trial section

To evaluate the temperature distribution in thick BSM layers, three different BSM-foam mixtures were mixed in the laboratory at the University of Stellenbosch. All the BSM-foam mixes were characterized by different percentages of RA and good quality crushed stone (Hornfels). The bitumen used in this research has a penetration value of 80/100 and is produced by the local refinery in Cape Town (Chevron group). The mixes analysed were:

- BSM-foam (2.0 % bitumen content) with 100% RA;
- BSM-foam (2.1 % bitumen content) with 50% RA and 50%G2 Hornfels (good quality crushed stone);
- BSM-foam (2.3 % bitumen content) with 100%G2 Hornfels;

The RA was made inside the lab with 5% of bitumen content (PEN 60/70). More details regarding the mixing phase and the production of the BSM-foam mixtures are presented in the previous chapters. No additional additives were added in the three mixes. The Technical Guideline (Asphalt Academy, 2009) was followed during all the mixing procedures.

Figure 6.1: Sub-base created in the laboratory with a good crushed stone quality material (Hornfels).

In particular, attention was given to quality control during production of the three mixes and compaction.

The optimum moisture content (OMC) and maximum dry density (MDD) for the three different mixes were determined by Modified AASHTO compaction. Details of the composition of all three mixtures are listed in Chapter 4. The hygroscopic moisture contents in the mineral aggregates were 0.7% for the virgin G2 crushed stone material, 0.9% for the 50%RA and 50%G2 and 0.65% for the 100%RA obtained in the laboratory. The BSM-foam was mixed in a twin-shaft pugmill linked to the spraying nozzle of a WLB-10 foam plant. The twin-shaft pugmill is suitable for foamed bitumen dispersion and mixing. After stabilization the mixtures were sealed in a bag, ready to be compacted.

After the mixing phase the BSM-foam mixtures were placed in a wood frame structure and compacted with the help of a vibratory hammer and a reversible plate compactor of 400mm

wide. The primary function of the wood frame was to contain the material inside a determined area and the second one was to avoid possible external interaction between the BSM-foam and other materials. Figures 6.2, 6.3 and 6.4 present the construction of the pavement for all the three BSM-foam mixes in the laboratory step by step.

(a)

(b)

(c)

Figure 6.2: Phase of construction BSMs pavement sections: (a) distribution of the first layer of BSM in the slab; (b) compaction of the BSM layer; (c) a second layer of BSM is added to the previous one.

The density and the moisture content were continuously monitored during the construction of the layers through the use of a nuclear density gauge, as shown in figure 6.3.

(a)

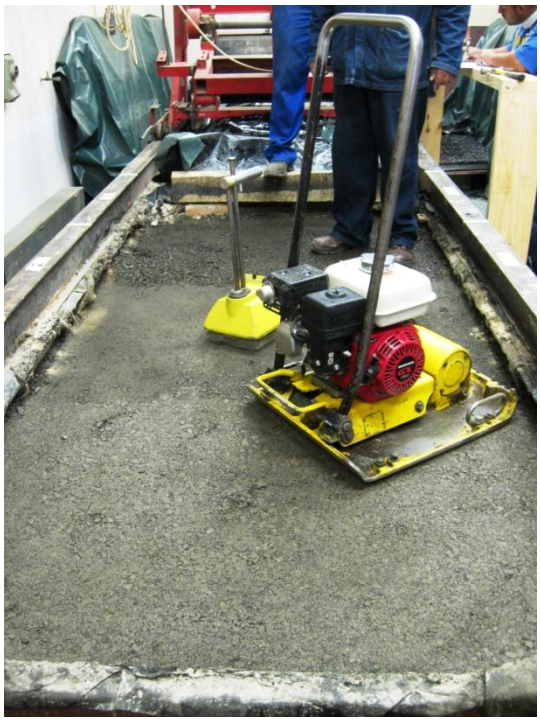

(b)

Figure 6.3: The BSMs layers were compacted through a vibratory hammer compactor and a plate compactor every 100mm depth (b). The density achieved through the compaction was monitored by a nuclear density gauge (a).

For the last layer the compaction was carried out through the use of the roller installed on two special rails on the side of the wood frame. The compaction gave the possibility to achieve almost completely maximum dry density.

Figure 6.4: Final compaction of the three BSM-foam mixtures.

This pavement section was built because the materials used in the BSM-foam mixtures in this project formed the main research component of this thesis. After compaction, the pavement was left in the laboratory for a period of curing of 10 days at 20°C which was regularly controlled.

6.4 Laboratory investigation of temperature distribution

The laboratory investigation of the temperature distribution of the BSM-foam mixes was carried out through the use of a special system of infrared light, specially designed to recreate the same temperature conditions of a pavement in a dry hot region during summer time. A particular effort was dedicated to the design and construction of a frame of infrared lights. All the infrared lights used in this research were Philips® E27 ES and they were able to develop a power of 250W with 30% energy saving. This product was considered more energy efficient than other local infrared lights and able to deliver a constant energy during the test.

Before the creation of this system of infrared lights, some special tests were performed in the laboratory in order to investigate the best distance between the lights. The target of this preliminary study was to create the best light distribution on a surface without having areas with a temperature higher than the rest of the remaining surface. The distance between the lights that was considered most reliable and efficient was 150 mm. The height of the frame from the surface was always kept constant at 300 mm for all the tests. The frame has the possibility to change the height through the use of four special foldable jack stands. Figure 6.5 shows the distribution of the lights on the frame and the spectrum of light. The measuring of the temperature during this first part of the research was conducted with the help of an infrared thermometer temperature gun with a laser sight (range: -32°C to +380°C).

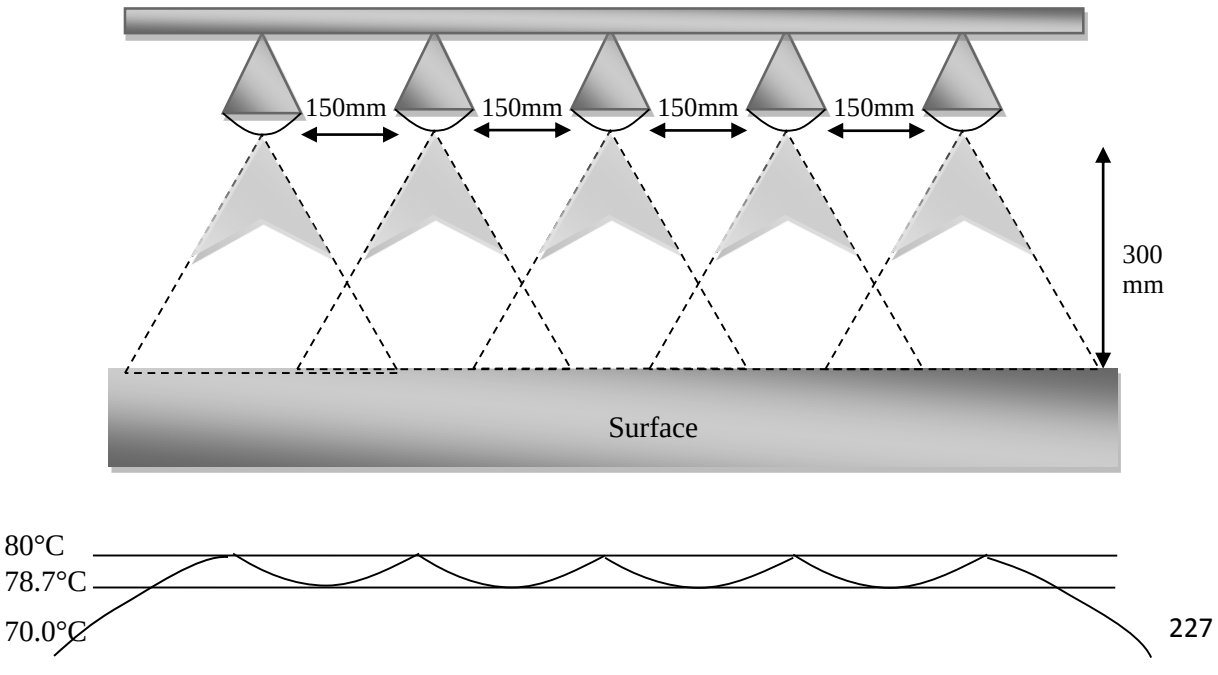

Temperature measured on the surface

Figure 6.5: Set-up of the infrared light system and temperature analysis on the surface.

All the lights were mounted at the same distance of 150 mm from each other on a wooden frame. The basic idea was to create a system unable to conduct the heat across the supporting structure, which would not change the final temperature on the pavement surface (Figure 6.7). The distance between the lights was necessary to guarantee a uniform temperature on the pavement. The lights were all connected to a mobile temperature controller cabinet, which was able to maintain the desired temperature on the surface through the presence of a thermocouple directly inserted on the top of the pavement. A switch mounted on the cabinet was able to switch the lights on or off as soon as the temperature reached the desired target.

The temperature was measured at different depths in all three different BSM-foam mixtures. The frame was moved on the top of each slab of material and well positioned in the middle. The structure with the infrared lights was able to cover the area of each material completely without heating the other BSM-foam mixes. The dimension of the frame was 1000 mm x 900 mm, when every section of BSM was 1200 mm x 1000 mm. The thermocouples were fitted at different depths: 0 mm, 50 mm, 100 mm, 150 mm, 200 mm, 250mm and 300 mm (Figure 6.6). All the thermocouples used in this research where model T (blue colour) and they were calibrated before every test. Figure 6.8 shows the calibration of a series of seven thermocouples. It's possible to see through the graph that all the thermocouples are recording the same temperature at the same time. The average line between all the data recorded shows a linear behaviour from all seven thermocouples. All the thermocouples were measuring the temperature in the centre of every BSM-foam section. After drilling a small hole, the thermocouples were fitted in the BSM-foam mixture at different depths and then sealed with a special epoxy resin to avoid any influence from the external air and temperature. Holes were cleared of loose debris before sensors were inserted. The cable of each thermocouple was surrounded by a small rubber pipe with the aim to limit any interaction with the infrared lights as much as possible.

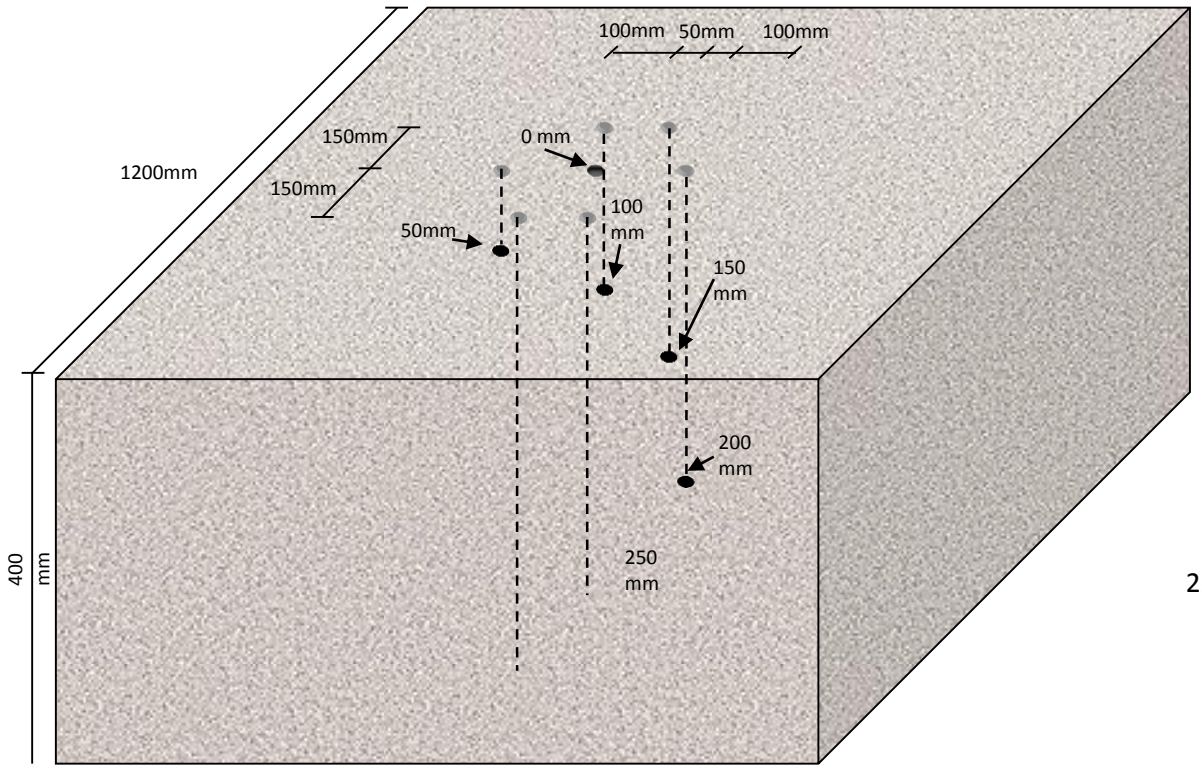

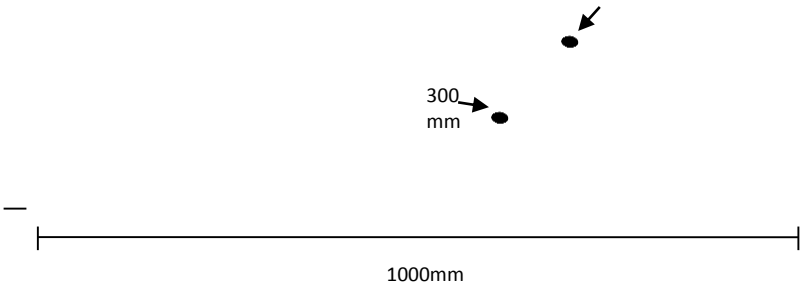

Figure 6.6: Scheme of the installation of thermocouples in the BSMs sections.

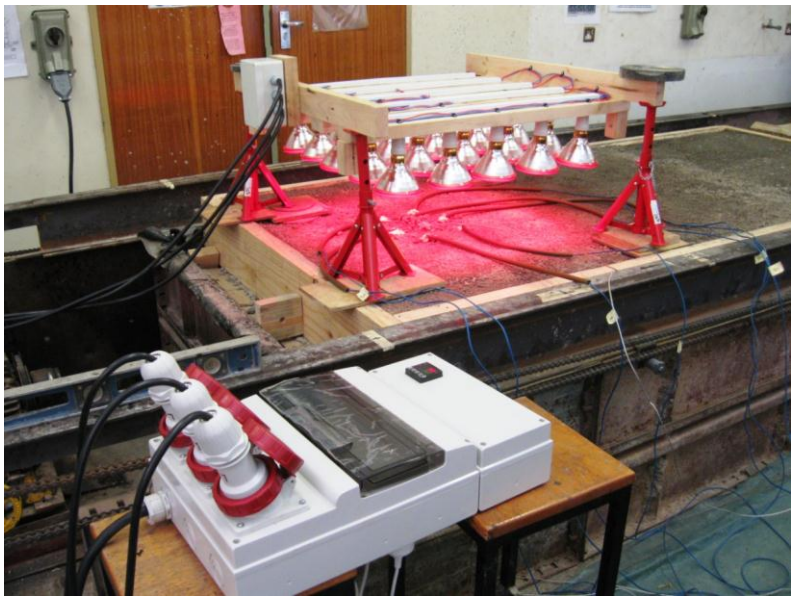

Figure 6.7: Temperature control cabinet and infrared light system mounted on a wooden frame.

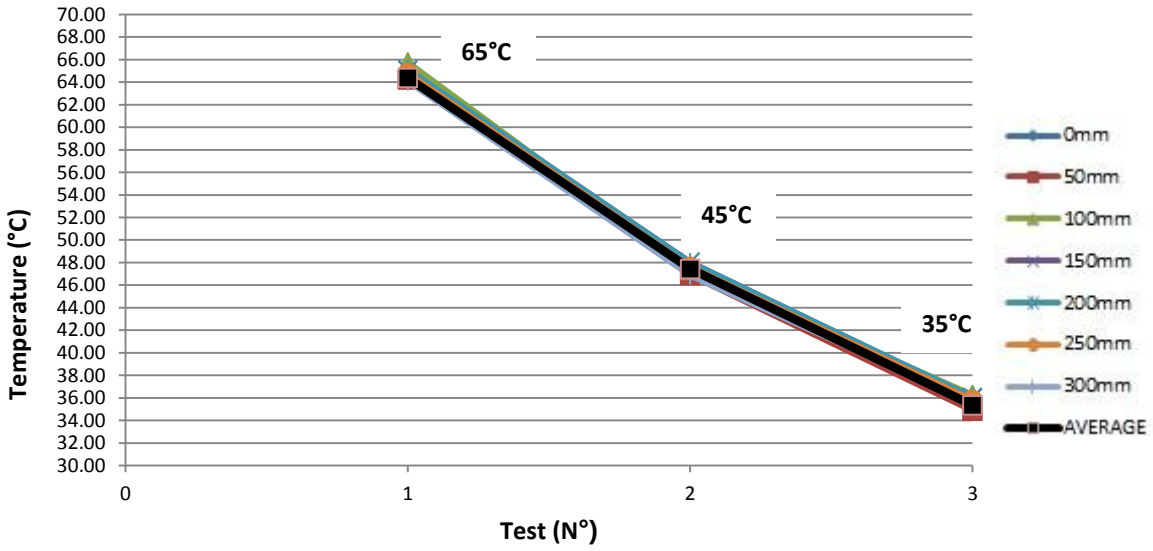

Figure 6.8: Calibration of thermocouples at three different temperatures.

All seven thermocouples were subjected to a previous temperature calibration at three different temperatures: 65°C, 45°C and 35°C. All the thermocouples show the same temperature readings (Figure 6.8). The monitoring of the temperature in the BSM layer was done using a USB DAQ Unit 8/16/32 Channel 14-bit Thermocouple Input Unit, 24 Digital I/O device, purchased from Eagle Technology Ltd. The data logger has eight channels for eight possible thermocouple sensors. The temperatures for every layer were recorded live every 5 minutes and stored in a computer desktop. The stored data was exported into an Excel spreadsheet for analysis. The measured data is presented and discussed in the following section.

6.5 Temperature distribution and data analysis

Previous studies (Jia and Sun, 2007; Burger, 2005 and Twagira, 2010) indicate that the temperature distribution in the pavement layer is influenced by the time of solar radiation and the heat transfer coefficient. This shows that pavement layer conductivity varies in depth during the day and the night. Jia and Sun (2007) indicate that temperature distribution in the pavement layer can be assumed adiabatic at a certain depth (thermally isolated system). That means deeper in the pavement layer, the temperature is constant and the effect on conductivity is negligible. A BSM layer in a South African pavement structure is positioned shallower, at less than 50mm deep.

Therefore, the variation in the temperature distribution in a BSM layer needs to be understood. This involves observing critical temperatures at different depths and the difference between the compositions of the BSM-foam mixtures. Many researches have been conducted on HMA (Kennedy *et al*., 1994; Lukanen *et al*. 2000; Chiasson *et al*. 2008; Wang, 2013), but only few studies have investigated the temperature distribution in a BSM section (Twagira, 2010). The analysis of the temperature in a BSM layer is vital. High temperatures often develop on the surface of the pavement during the summer period. This can create the problem of rutting due to traffic and high temperatures. The infrared light system tried to recreate the same maximum temperatures which can be found on the top surface of a BSM pavement subjected to rutting (Jenkins and Twagira, 2008)

The installed thermocouples recorded the temperature distribution in the BSMs for different periods at the same depths. The first test was carried out on the BSM-foam mix with 100% G2 Hornfels crushed stone and then continued on the BSM-foam mix with 50%RA and 50%G2. Lastly, the test set-up was moved on the top of the BSM-foam section with 100%RA.

During all the test procedures, 12 hours were allowed between one test and the next, enabling the pavement to cool down to 20°C. In this manner every single BSM-foam mixture didn't have any interaction with the earlier test performed on the previous section. The temperature data collected in the computer are presented in the following Figures from 6.9 to 6.17. The temperature distribution shows different variability patterns between the three BSM-foam mixtures with different percentage of RA and different bitumen contents.

Figure 6.9 represents the variation of the temperature during almost 18 hours of continuous heating. The infrared lights were kept on for the duration of the test. The temperature cabinet

control unit was controlling the temperature on the surface ensuring a stable maximum temperature on the surface of the pavement. This was achievable through a relay gauge mounted in the control cabinet which was switching on and off the infrared lights to guarantee the same temperature on the surface. The top layer reached a temperature close to 70°C after 12 hours. It's interesting to note how quickly the temperature rises in the first hour. The temperature rises sharply from 20°C to almost 60°C. The increment of temperature in the other layer during the first hour is more moderate and it's more spread along the remaining hours. The second sensor, positioned at 50mm deep, recorded a maximum value of 55°C. The difference between the top surface and this recording position is approximately 15°C. The temperature in the other layers positioned on the deeper layers of the BSM-foam section registered a difference between each other not bigger than 5°C. The air temperature in the laboratory was kept monitored along the entire test and it was constantly ranging around 20°C.

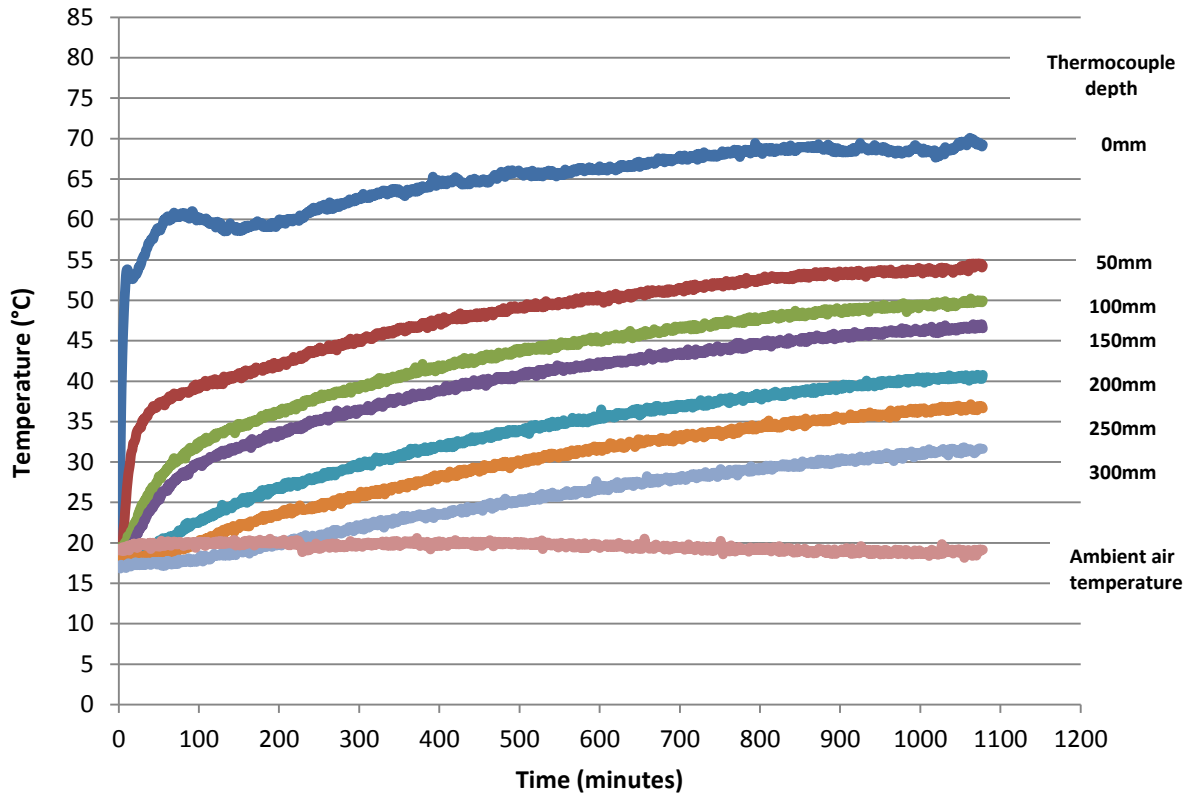

Figure 6.9: Temperature distribution recorded in a BSM-foam section with 100%G2 Hornfels crushed stone (2.3% bitumen content), sustained IR heating.

Figure 6.10 shows the temperature monitored in a BSM-foam mix with 50%RA and 50%G2 material (2.1% bitumen content). The test was conducted with the same set-up of the previous test. The maximum temperature registered by the first thermocouple mounted on the top of the surface was almost 78°C after 11 hours of testing. The surface layer is the layer most sensitive to temperature fluctuations. A similar increase in temperature registered for the BSM-foam with 100%G2 was noted during the first hour of the test. The second layer fixed at 50mm deep

showed a temperature close to 60°C. The difference between the first thermocouple on the surface and this one was even more remarked, namely 18°C. The temperature recorded for all the sections was a little bit higher than in the previous test. This is probably due to the factor that the bitumen content in the mix was a little bit higher due to the presence of a consistent quantity of RA. The binder content used in the production of RA was 5%. The bitumen content plays an important role in this pavement section due to its viscous-elastic nature, because the temperature at 100mm depth is almost 10°C lower than the temperature recorded at 50mm. However, the high percentage of air voids and the different density compared with the other two BSM-foam mixes can contribute to increase the temperature more rapidly (Twagira, 2010). There is a noticeable time lag in the heating between the surface temperature and the deeper pavement temperature. In other words, it takes more time to heat into the BSM than the surface area. The lower levels of the section shows a temperature similar to the BSM-foam with 100%G2. Therefore, further investigation on wide range of mixes is required in the laboratory and in the field to understand the influence of voids distribution and temperature on the performance of BSMs.

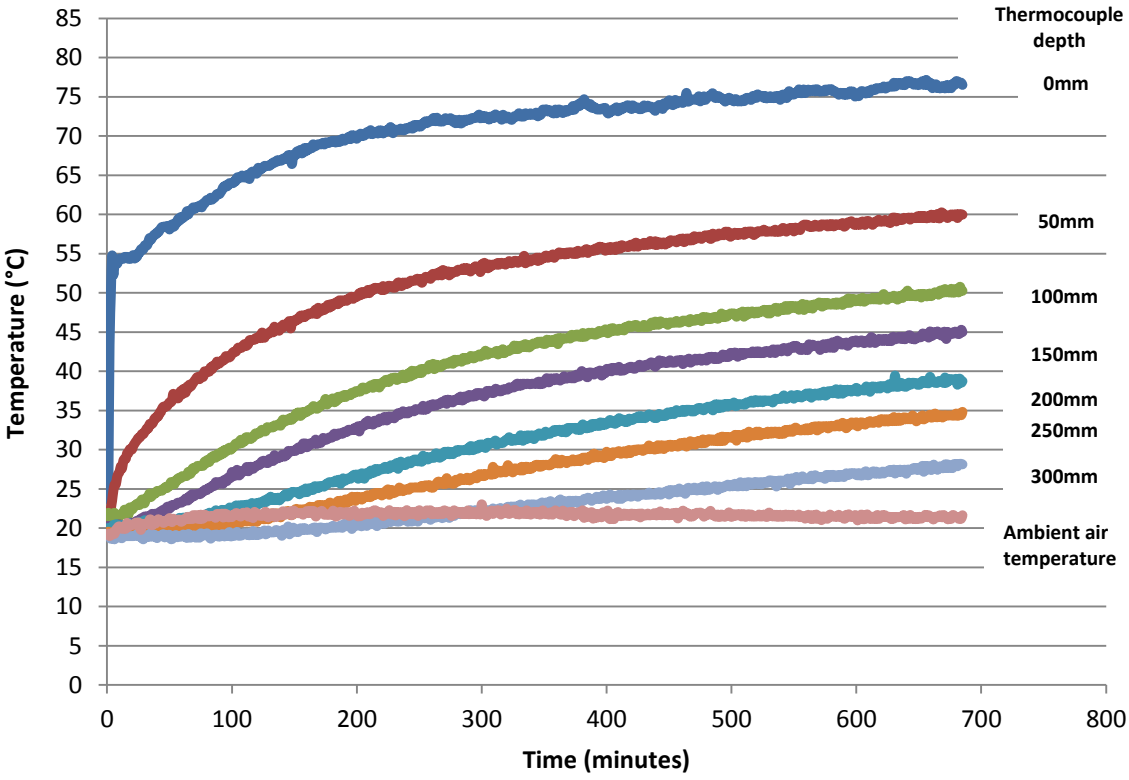

Figure 6.10: Temperature distribution recorded in a BSM-foam section with 50%RA and 50%G2 Hornfels crushed stone (2.1% bitumen content), sustained IR heating.

The temperature monitoring for a BSM-foam section with 100%RA (2.0% bitumen content) shows a value of almost 80°C on the top of the surface after 18 hours. The temperature on the top of the pavement in the first hour rises quickly to 60°C and then increases slowly. The temperature distribution in the lower layers shows higher values compared to the other two BSM-foam sections. The temperature from the top to the 300 mm depth decreases with almost

5-6°C every 50 mm. Compared to the other mixture the BSM-foam with 100%RA has a slow increase in temperature along the entire pavement and it's slower than in the other two BSM-foam mixtures. This is probably due to these important factors:

- quantity of bitumen present in the mix;
- percentage of air voids in the mix, and
- different maximum dry densities.

Therefore, an understanding of the heat transfer coefficient in BSMs is necessary to be able to quantify the temperature variation and its influence on moisture evaporation and other material behaviours affected by temperature variation. It is apparent from the laboratory temperature results that modelling of temperature distribution in a BSM layer is vital for understanding the mechanism of material durability behaviour and long-term performance.

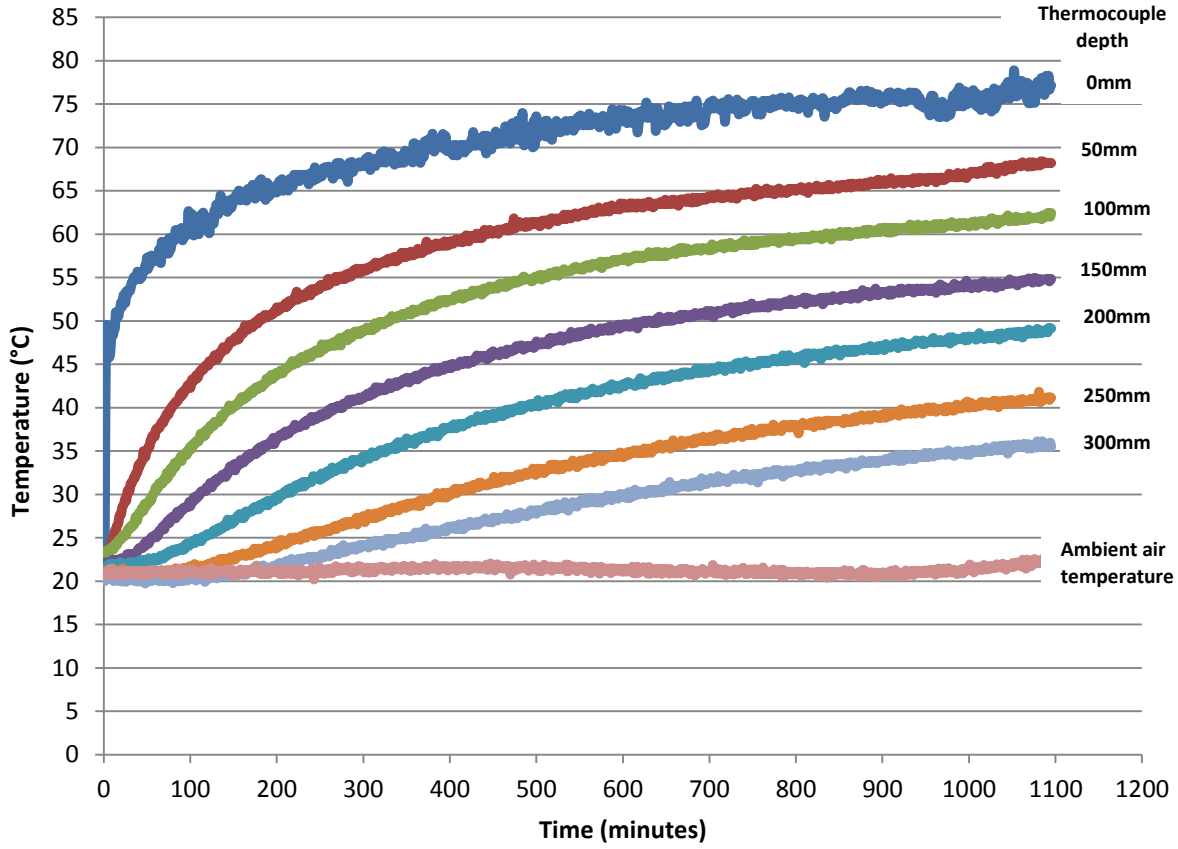

Figure 6.11: Temperature distribution recorded in a BSM-foam section with 100%RA (2% bitumen content), sustained IR heating.

After the description of temperature variation in the BSMs layers, it is important that the temperature gradient in a layer be defined. In practice, BSM construction is carried out during summer time. The temperature distribution recorded during summer is used in the analysis of the temperature gradient in a BSM-foam layer. The temperature gradient due to time of solar radiation can influence the moisture loss, the strength development of the layer over time and

the fatigue performance of the pavement. The temperature results indicated in the previous figures show that solar radiation and heat transfer coefficient of pavement material play significant roles in the temperature gradient in the BSM-foam layer. The temperature gradient varies according to the composition of the mixes. At the top of the BSM-foam layers, the temperature increases rapidly during the first hour and then increases at a lower rate for the rest of the time. The percentage of bitumen can contribute significantly to the temperature distribution, allowing the pavement to heat up more or less homogeneously depending on whether mix characteristics of the BSM. On the other hand, at the bottom of BSM-foam layers, temperature increases very slowly and it always maintains values around 30 – 35°C. All of this is due to the rate of thermal conductivity of the absorbed heat. The top layer heats up at a higher rate compared to the bottom due to the effect the artificial solar radiation created with the infrared light system.

Figures 6.12, 6.13 and 6.14 present the cooling down rate which was measured in all three BSM-foam mixtures.

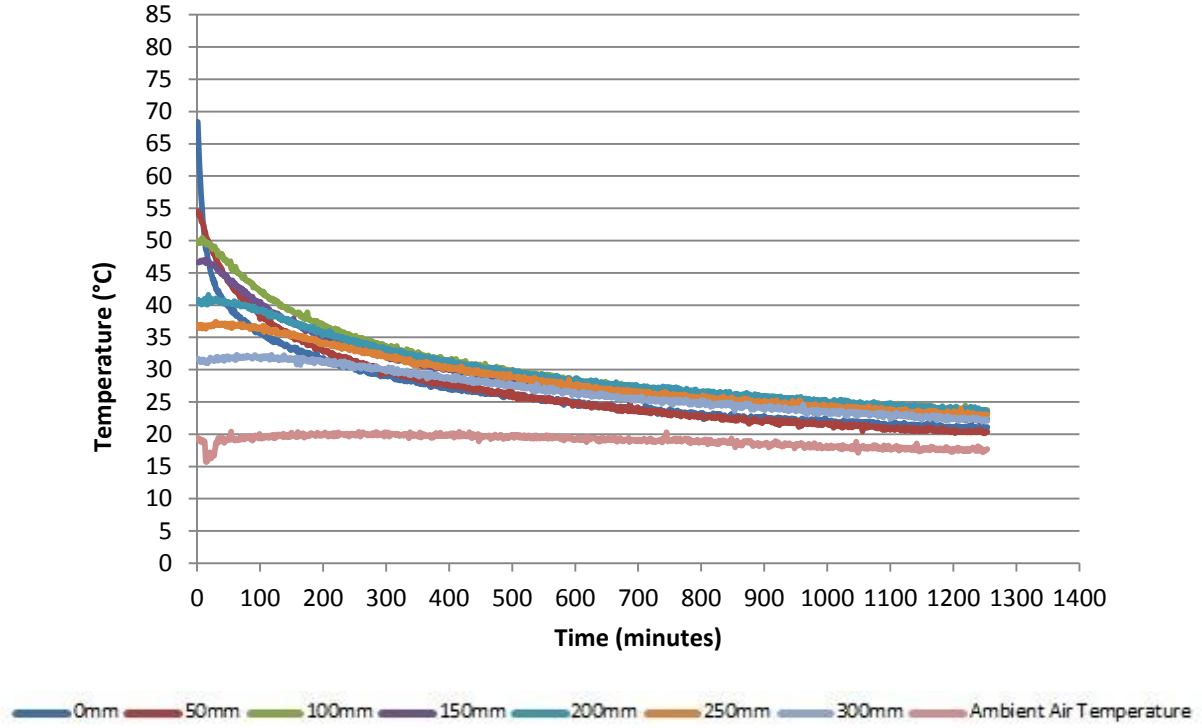

Figure 6.12: Temperature distribution during cooling of BSM-foam (2.3% bitumen content) with 100%G2.

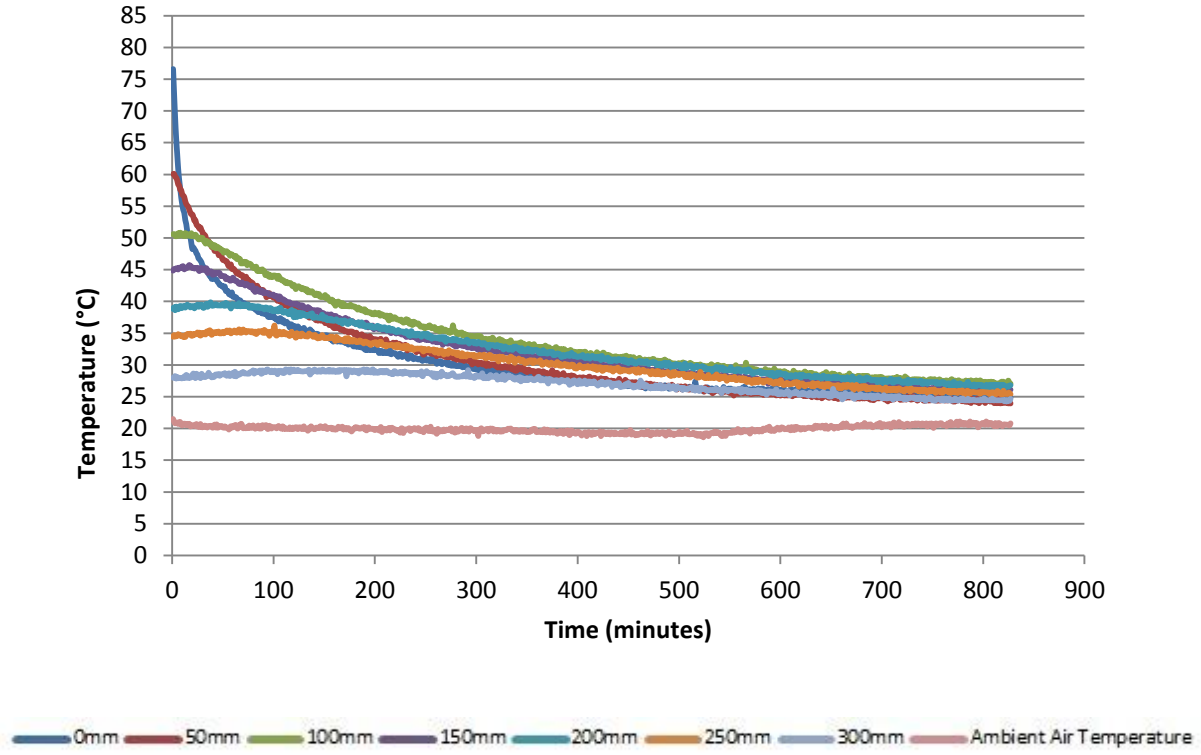

Figure 6.13: Temperature distribution during cooling of BSM-foam (2.1% bitumen content) with 50%RA and 50%G2.

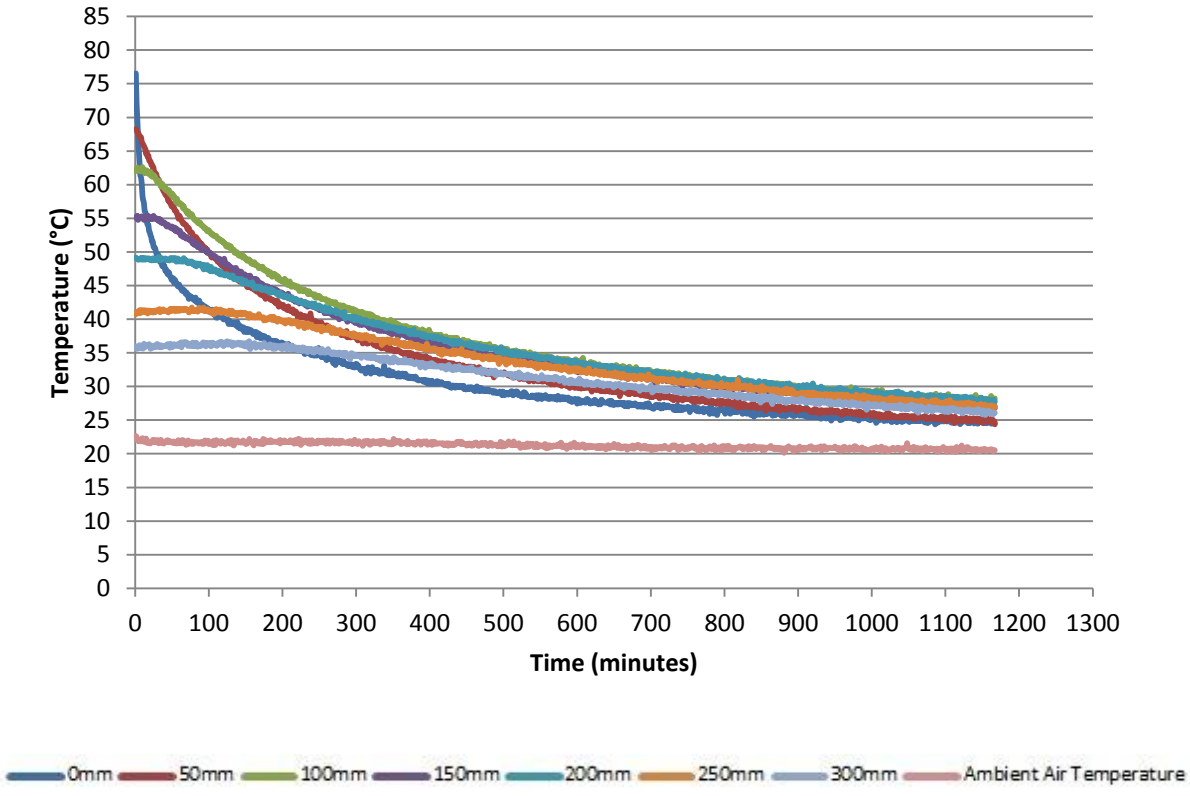

Figure 6.14: Temperature distribution during cooling of BSM-foam (2% bitumen content) with 100%RA.

The initial temperature at the surface of every BSM is high and cools down faster than in the deeper layers. This is more notable in the BSM-foam (2% bitumen content) with 100%RA. In fact, the temperature drops faster than in the other two sections. This is probably due to two important factors: presence of high percentage of RA and the percentage of air voids. All the BSMs register the same temperature after almost 12 hours, in the range of 25-30°C. On the other hand the temperature at the bottom of the three sections drops slower than in the top layers. This is probably due to the immediate response of the surface to the heating, which is completely off during all the phases of this test.

A comparison between the different BSM-foam materials is represented by Figures 6.15, 6.16 and 6.17. The heating and cooling part of every BSM section is plotted for the first three depths: 0 mm, 50 mm and 100 mm. In all three figures the BSM-foam mix with 100%RA showed higher rates for the heating and cooling part compared with the other two mixtures. A marked difference between the three mixes in the highest temperature was observed on the surface. As the depth increased this diversity is maintained and remain constant for all three BSMs.

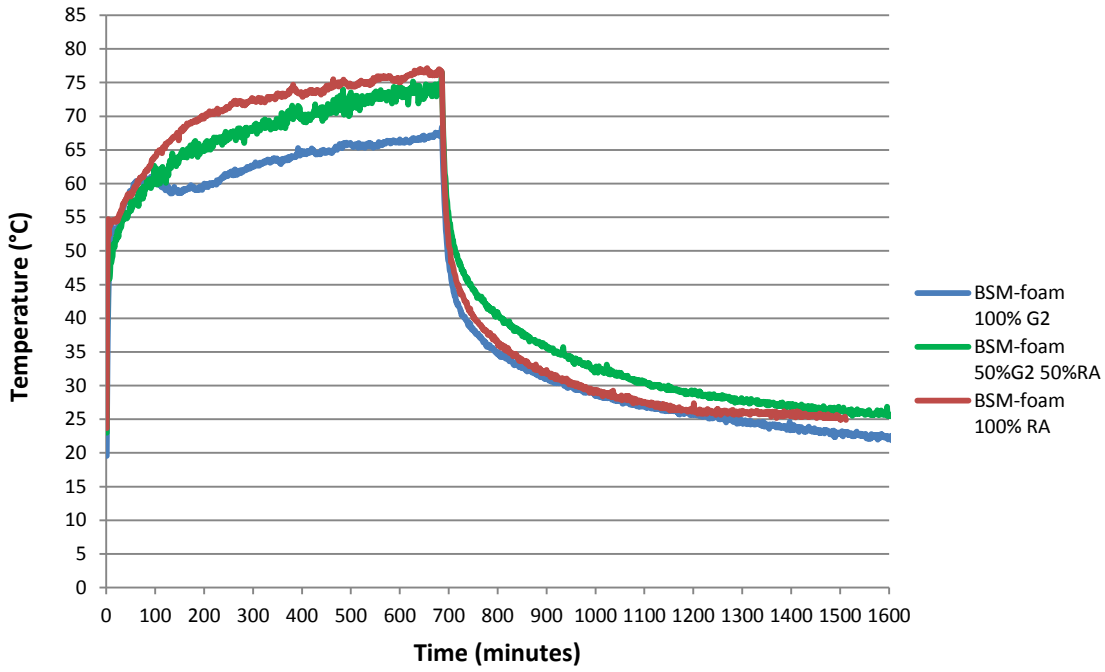

Figure 6.15: Temperature distribution (heating and cooling) at 0 mm depth for 3 BSM mix types.

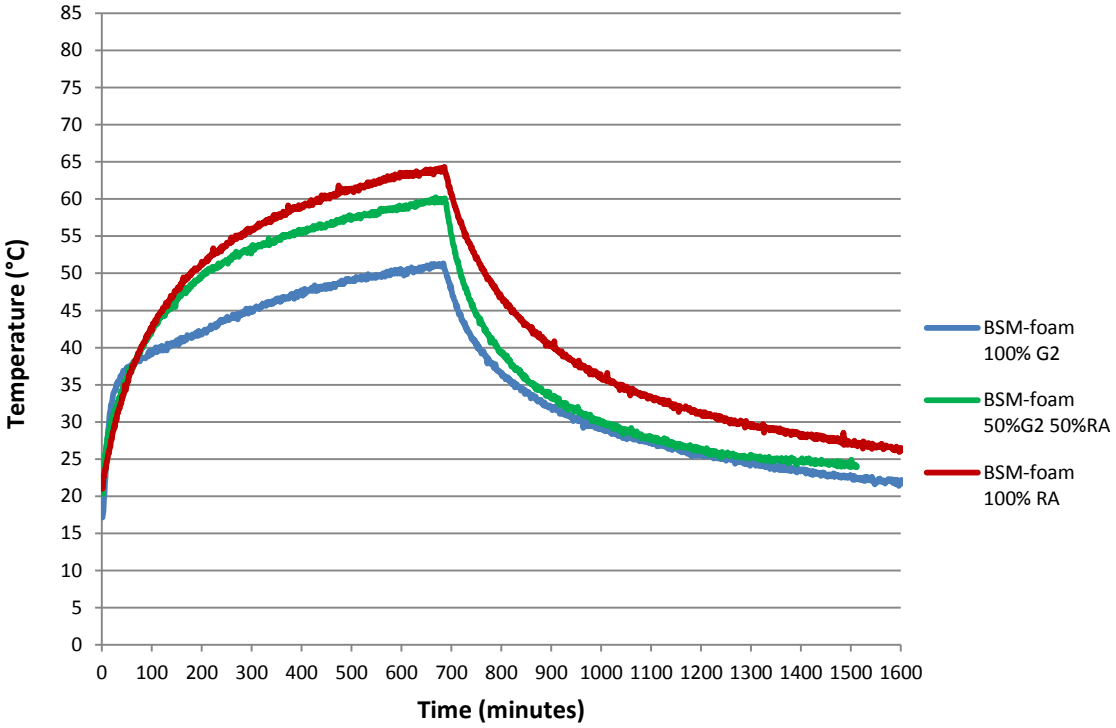

Figure 6.16: Temperature distribution (heating and cooling) at 50 mm depth for 3 BSM mix types.

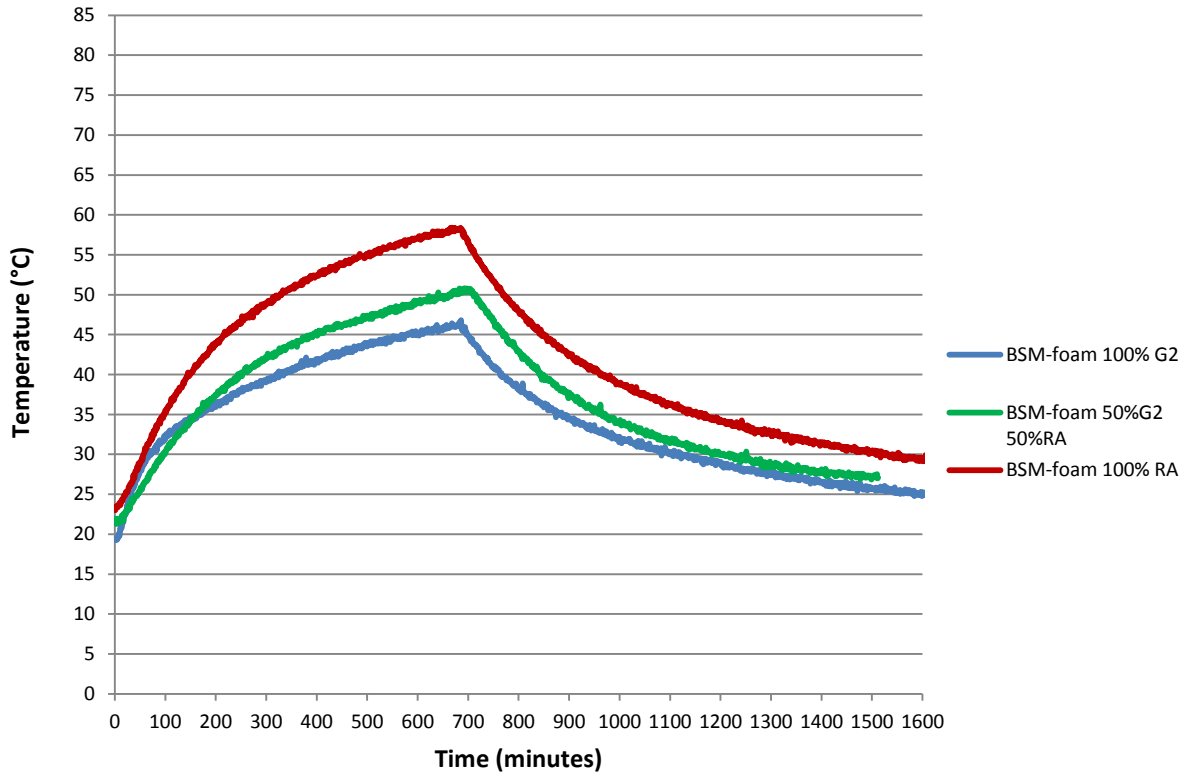

Figure 6.17: Temperature distribution (heating and cooling) at 100 mm depth for 3 BSM mix types.

Therefore, the observed temperature gradient in BSMs needs to be modelled to predict this behaviour accurately. The accurate prediction of the temperature gradient will give a better understanding of the change of material properties under various environmental conditions and during different seasons. From these results, it is evident that understanding the temperature distribution in the BSM layers is important for predicting the long-term material performance based on environmental influences. Temperature distribution in HMA has been extensively studied in the past. In this study, a temperature distribution model developed by Viljoen (2001) and the SHRP model (Kennedy *et al*. 1994) for HMA, which was found to be applicable with the appropriate changes to BSMs, is presented.

6.6 Temperature distribution prediction algorithms

BSMs pavements, a type of temperature-sensitive material, are widely applied on roadways, because of advantages such as a low percentage of binder consumption, good bearing characteristics and possible reuse of existing road materials. BSMs can heat up to high temperature during solar radiation in summer-time because of their excellent heat-absorbing property. Due to the enormous area of BSMs pavements, the thermal energy potential of a BSM

may appear infinite. Therefore, it has become a new research task to understand the temperature distribution in BSM pavements similar to HMA.

The temperature distribution in the pavement layers and its influence on materials performance depend on the existing environmental conditions. In order to accurately predict the engineering properties of the BSMs based on the influence of temperature, the following environmental factors need to be considered:

- air temperature;
- solar radiation;
- wind, and
- relative humidity.

Also other properties have to be considered as input parameters in the model:

- density of materials;
- thermal conductivity, and
- specific heat capacity.

These parameters depend on binder content, mineral aggregates composition and mix composition. For BSMs most of these parameters are not well known and therefore need to be determined experimentally as an input into the model. Whilst the boundary layers such as HMA, granular and cemented these parameters have been documented in the past studies and a considerable literature is available worldwide (i.e. Adams and Curran, 1999; Solaimanian and Kennedy, 1993; Cheng, 2002; Andrew *et al.* 2012). The usefulness of a new temperature distribution model is the introduction of new parameters, which can provide a better understanding of the durability properties and long-term performance under the influence of temperature variation in the BSMs layer. In order to design a temperature distribution model in a BSM pavement, it is necessary to predict the temperature distribution within the BSM-foam pavement section. Understanding the thermal properties of BSMs require good knowledge of the thermal properties. The surface layer transfers the heat to the deeper BSM layers.

The temperature regime to which HMA pavement layers are subjected in South Africa has been the topic of several studies in the past. For BSMs very few and preliminary studies have been done in the past years. In this section the Superpave pavement prediction algorithms, as contained in Kennedy *et al.* (1994), and the algorithms developed for temperature prediction in the South African climate by Viljoen (2001), are presented and compared with the algorithms developed for BSM-foam mixtures at different depths. The algorithms are going to be discussed in detail in the following paragraphs.

6.6.1 Temperature prediction for BSM-foam mixtures

The maximum asphalt surface temperature predictions equations in Superpave (Kennedy *et al*., 1994) and by Viljoen (2001), are based on the energy balance concept, and calibration of the equations involves identifying the best fit of values for the asphalt surface absorptivity, the transmission coefficient of air, the emissivity of air, the emissivity of the asphalt surface, the

asphalt surface heat transfer coefficient and the conductivity of the asphalt material. For the purpose of this research the data recorded for the temperature distribution test, presented in the previous paragraphs are going to be analysed and compared with the Superpave and Viljoen algorithms.

The background of the asphalt surface temperature prediction found by Viljoen (2001) and by Kennedy *et al*. (1994) is showed below. The first equation was found by Viljoen [6.1] and the second one was finalised during the SHRP research [6.2].

$$T_s = 0.89T_{air} + 5.2 \quad [6.1]$$

$$Ts = 0.859T_{air} + 1.7 \quad [6.2]$$

where

T_s = the minimum surface temperature in °C;
T_{air} = minimum air temperature in °C.

The formulas consider the presence of possible wind and the emissivity of the surface which do not affect the BSM base-layers. These two factors were not included in this study. The two algorithms were applied to the BSM-foam mixtures and then plotted in a graph with the real values coming from the past temperature monitoring. Not all the values were considered in the graph, due to the higher amount of data recorded during the test. The collected laboratory data for all three BSMs were compared with the two formulas presented above. A good approximation can be found between all three BSMs and the algorithms presented by Viljoen and Kennedy (SHRP program). In all the BSMs the value range between the two algorithms that belong to Viljoen and to the SHRP program. A small different slope can be visible in the case of a BSM-foam mix with 100%G2 material. The line intercepts the temperature distribution algorithm presented by Viljoen. In the other two study cases the temperature distribution remains far from the Viljoen and SHRP prediction models.

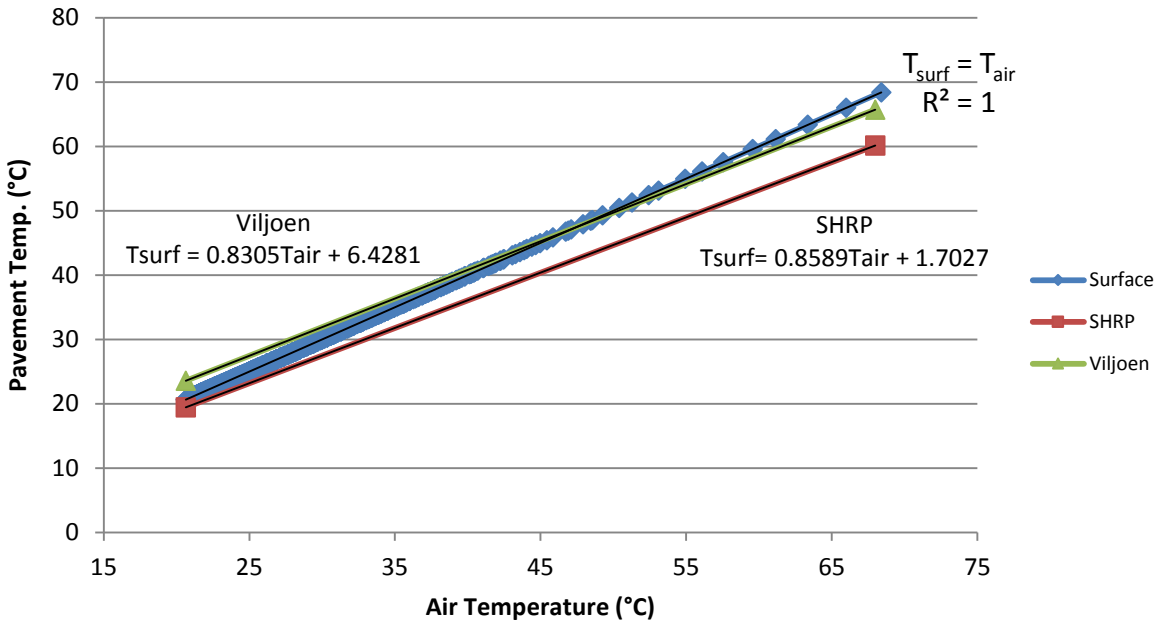

Figure 6.18: Comparison between temperature prediction models at surface for BSM-Foam (2.3% bitumen content) with 100%G2.

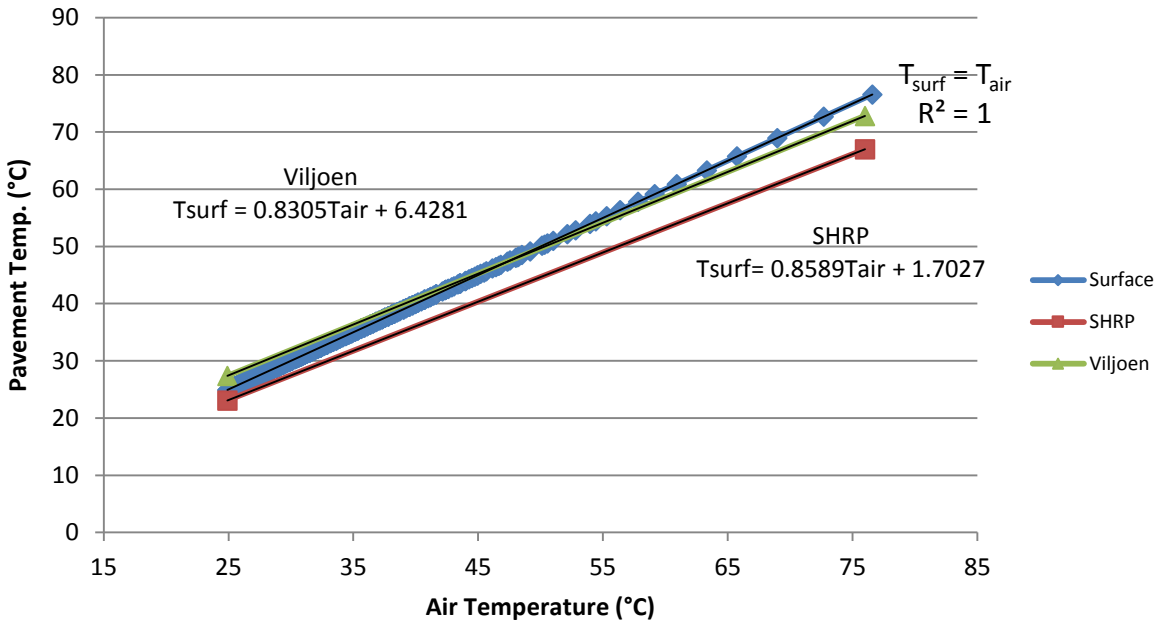

Figure 6.19: Comparison between temperature prediction models at surface for BSM-Foam (2.1% bitumen content) with 50%RA and 50%G2.

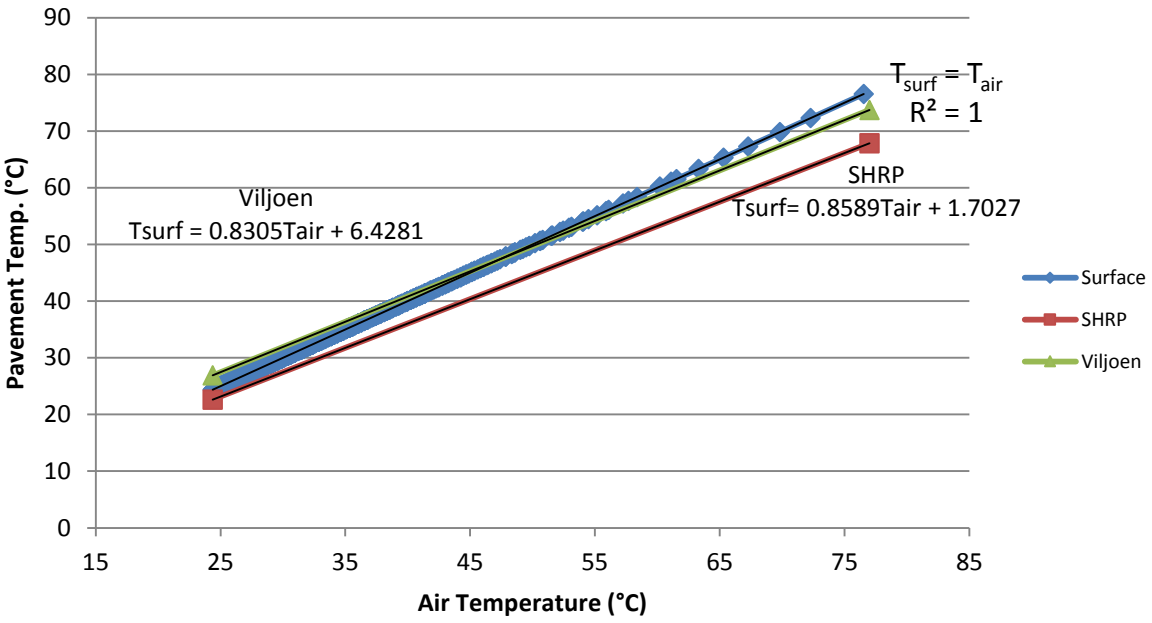

Figure 6.20: Comparison between temperature prediction models at surface for BSM-Foam (2% bitumen content) with 100%RA.

Different algorithms can be used to predict the temperature in the deeper part of a pavement section. The prediction algorithms for pavement temperatures at different depths are given by the following relationships, respectively by Viljoen [6.3] and by the Superpave program [6.4]:

$$T_d = T_s (1 - 4.237 \times 10^{-3} d + 2.95 \times 10^{-5} d^2 - 8.53 \times 10^{-8} d^3) \quad [6.3]$$

where

T_d = maximum asphalt temperature at depth d in °C
T_s = maximum asphalt surface temperature in °C
d = depth in mm

The Superpave algorithm for pavement temperatures at depth is shown in the following equation:

$$T_d = (T_s + 17.8) (1 - 2.48 \times 10^{-3} d + 1.085 \times 10^{-5} d^2 - 2.441 \times 10^{-8} d^3) - 17.8 \quad [6.4]$$

where

T_d = maximum asphalt temperature at depth d in °C
T_s = maximum asphalt surface temperature in °C
d = depth in mm

As outlined, Viljoen and Kennedy developed their algorithms using the data from previous asphalt pavement temperature studies. In Figures 6.21, 6.22 and 6.23 the two formulas are applied to the temperature data recorded in the first part of this chapter. In all cases it was

possible to develop accurate predictions of the temperature deeper into the layers of the three BSM-foam sections. In all the figures a possible algorithm is presented for all three different BSMs and for every layer. All the models developed in this part of the research achieved a R^2 close to values of 0.99. All the models didn't consider the exact contribution of air and solar radiation variables.

Figures 6.21, 6.22 and 6.23 present the analysis of the 100 mm depth for all the BSMs. The study was carried out in two additional layers at 200 mm and 300 mm depth. These results are reported in Appendix D.

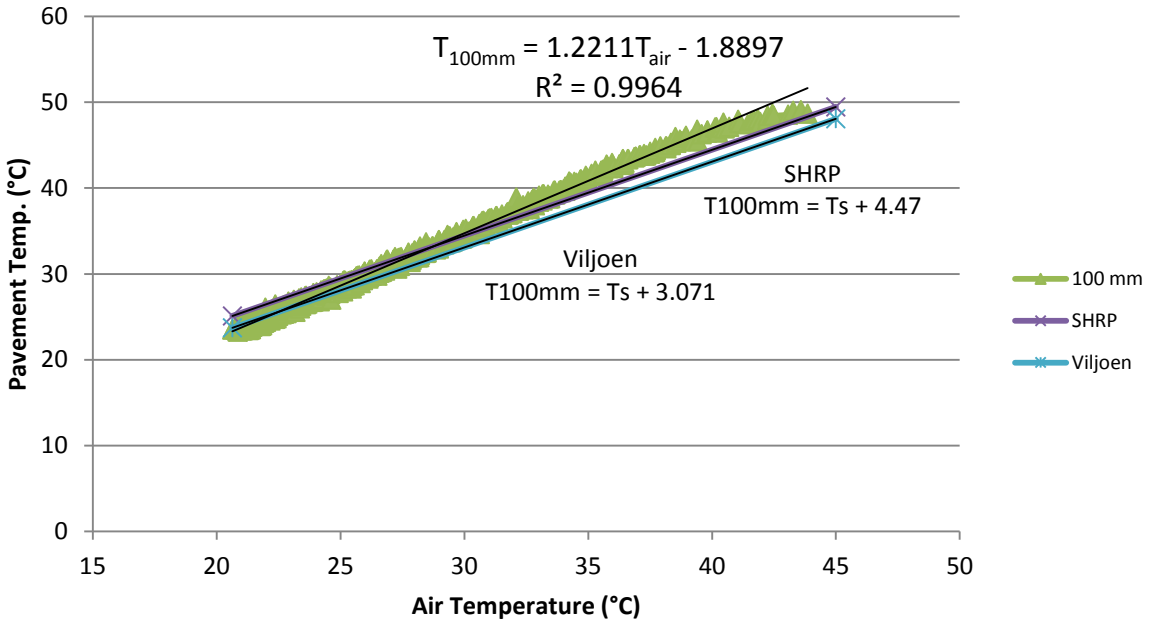

Figure 6.21: Comparison between temperature prediction models at 100mm depth for BSM-Foam (2.3% bitumen content) with 100%G2.

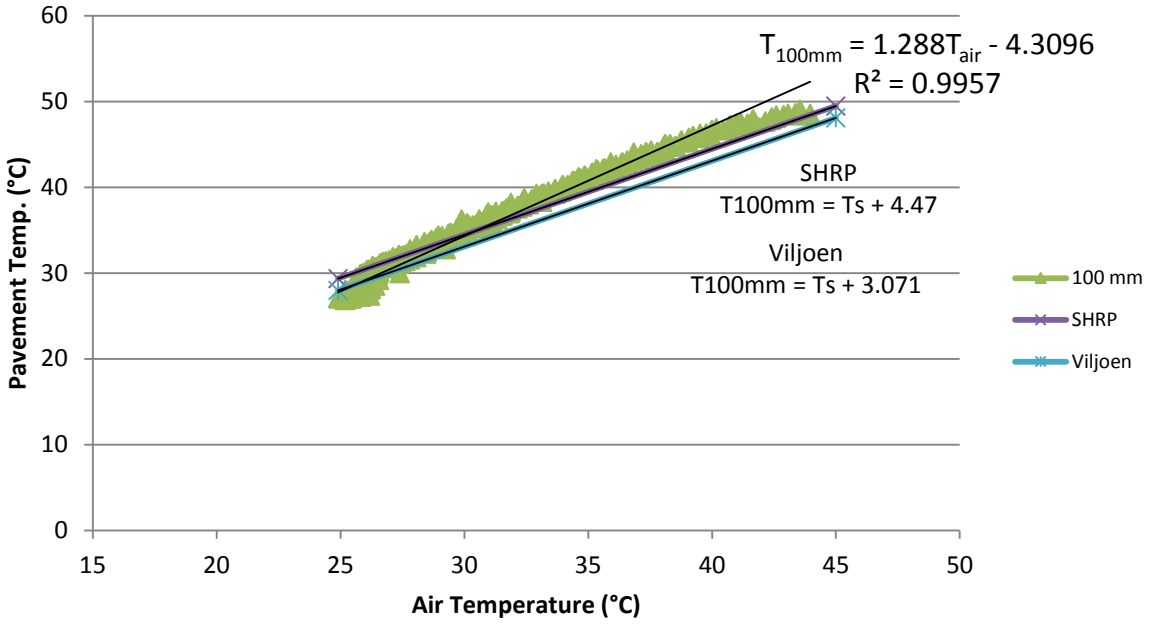

Figure 6.22: Comparison between temperature prediction models at 100mm depth for BSM-Foam (2.1% bitumen content) with 50%RA and 50%G2.

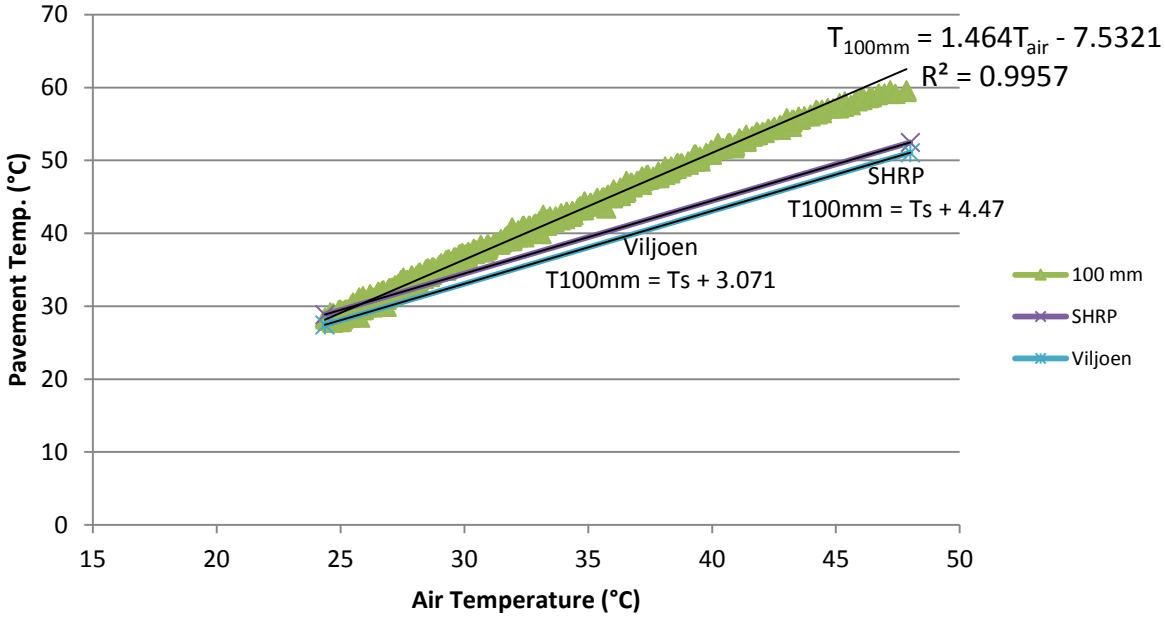

Figure 6.23: Comparison between temperature prediction models at 100mm depth for BSM-Foam (2% bitumen content) with 100%RA.

The Viljoen and SHRP models provide a good approximation of the temperature distribution on the surface of BSM-foam mixtures, but when the depth of the section increases, both models

are not able to estimate the temperature accurately (Appendix D). This difference is consistency for all three BSM-foam mixtures and it can be attributed to the different dispersion of the bitumen in the mix, different percentage of air voids, presence of moisture and different density. Both Viljoen and Superpave algorithms showed an inconsistent trend in the prediction of the temperatures, most likely due to the different composition and rheological properties of the BSMs compared with the HMA.

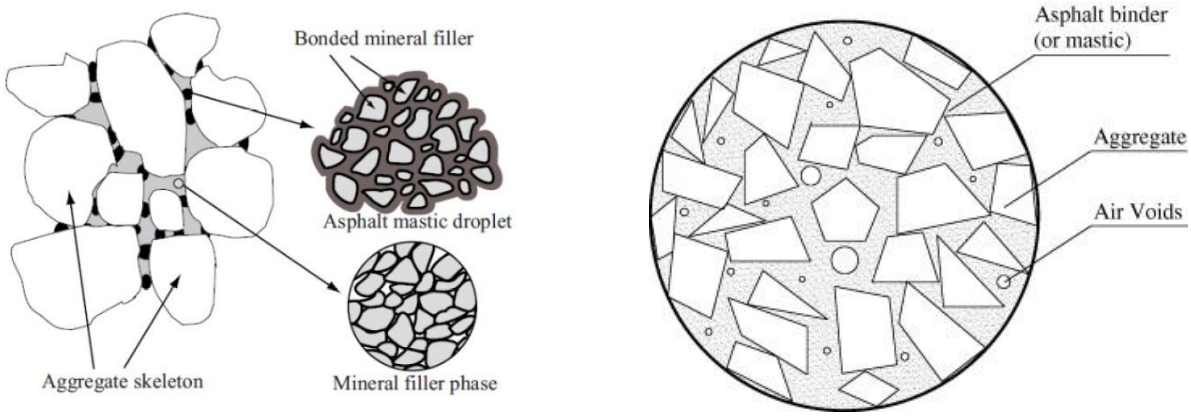

Figure 6.24: Schematic of the microstructure of BSMs (non continuous bitumen) vs. HMA (continuous bitumen).

The suitability of these models developed in the previous graphs for BSMs (Figures 6.21, 6.22 and 6.23) is that they address the temperature distribution in a BSM pavement at different depths quite well, giving the opportunity to estimate the possible implications during the phase of planning, construction of a new pavement, as well a good tool to understand the potential performance and mechanical properties of a BSM surface.

6.7 Modelling of the thermal transfer in BSMs sections after induction heating

Most properties of civil engineering materials are not absolute, but depend on the state of the material. This can be described with parameters such as temperature and moisture content, amongst others. The relation between state parameters and material properties is called the state-parameter concept. This approach is used in the MLS program in order to make realistic analyses. To predict the temperature variations within the BSM-foam pavement after induction heating, a finite element program FEMMASSE HEAT-MLS, which is capable to compute the heat diffusion within a multi layers system, is used in this research. Femmasse is an abbreviation of Finite Element Modules for Materials Science and Structural Engineering (2006). The work on this programme started in the early 1980s at Delft University of Technology in The Netherlands and was continued at the Swiss Federal Institute of Technology (EPFL) in Lausanne, Switzerland.

The flow chart and input parameters of this program are introduced in the following paragraphs. The input parameters such as wind speed, environment temperature and solar radiation can be changed to study their effects on the temperature heating process of the pavement surface.

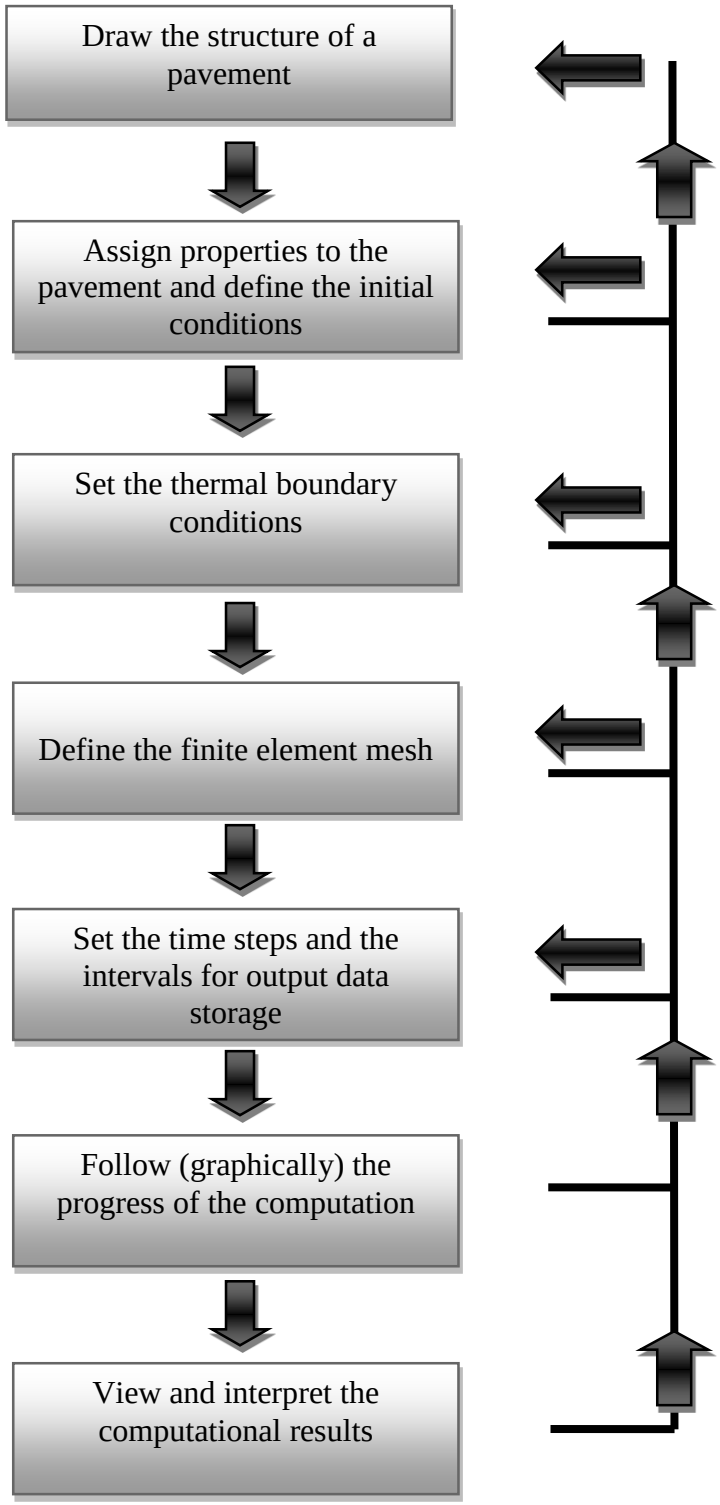

Figure 6.25: Flow chart of the modelling program FEMMASSE HEAT-MLS.

6.7.1 Thermal properties

Thermal properties of asphalt mixtures, such as thermal conductivity, thermal diffusivity and specific heat capacity, have been studied by many authors using traditional thermo-physical tests. The effect of temperature, asphalt content, aggregate gradation, compaction level on these parameters are, for example, proposed by De la Roche, 1990; Highter and Wall, 1984; Luca and Mrawira, 2005, Mrawira and Luca, 2006, Tan *et al*., 1997. Unfortunately information for BSMs materials is not available. However, it is possible to gain some insight by taking into account the individual components.

Thermal properties of the material (i.e. thermal conductivity, specific heat) and the convection heat transfer coefficient are defined as follows:

- Specific heat (C) is the amount of heat per unit mass required to raise the temperature by one degree Celsius.
- Thermal conductivity (k) is the property of material that indicates its ability to conduct heat.

The heat capacity is the ratio of the heat energy absorbed by a substance to its increase in temperature. Heat capacity is also called thermal capacity. The specific heat of a material is related to heat capacity, except that specific heat doesn't depend on an object's mass, though it still depends on the type of material. Specific heat is therefore a property of the material. . The relationship between heat and temperature change is usually expressed in the form shown below where *c* is the specific heat. The relationship does not apply if a phase change is encountered, because the heat added or removed during a phase change does not change the temperature. The specific heat of a material is related to the heat capacity, C_H, of an object made of that material, as follows:

$$c_H = C_H/m \qquad [6.5]$$

where
c_H is the specific heat
m is the mass of the object.

Substituting into the relation above, it's possible to derive a relation between the heat gained or lost by an object, the object's mass, its specific heat, and its change in temperature:

$$\Delta_H = c_H m \Delta T \qquad [6.6]$$

The specific heat or specific heat capacity of a substance is the heat capacity per unit mass, usually measured in joules per kilogram per degree Kelvin.

In physics, thermal conductivity (often denoted k, λ, or κ) is the property of a material to conduct heat. It is evaluated primarily in terms of Fourier's Law for heat conduction. Heat transfer occurs at a higher rate through materials of high thermal conductivity than across materials of low thermal conductivity. Correspondingly materials of high thermal conductivity are widely used in heat sink applications and materials of low thermal conductivity are used as thermal insulation. Thermal conductivity of materials is temperature dependent. The dimension of thermal conductivity is $M^1L^1T^{-3}\Theta^{-1}$. These variables are (M) mass, (L) length, (T) time, and

(Θ) temperature. In SI units, thermal conductivity is measured in watts per meter Kelvin (W/mK).

Heat will flow in the direction of decreasing temperature. In other words, heat flows from hot to cool. To derive the heat equation, the flow of heat through a pavement structure has to be considered. The pavement on one dimension makes it possible to consider the temperature, u(x,t), as one dimensional in x but changing in time, t. The heat flow is proportional to the temperature gradient, i.e (Highter and Wall, 1984).

$$-K = \frac{\partial u}{\partial x} \qquad [6.7]$$

where *K* is a constant of proportionality. Consider a small element of the pavement between the positions x and x + δx. The amount of heat in the element, at time t, is

$$H(t) = \sigma\rho u(x,t)\delta x \qquad [6.8]$$

where σ is the specific heat of the pavement and ρ is the mass per unit length. At time t+δt, the amount of heat is:

$$H(t+\delta t) = \sigma\rho u\,(x,t + \delta t)\,\delta x \qquad [6.9]$$

Thus, the change in heat is simply

$$H(t+\delta t) - H(t) = \sigma\rho(u(x,t + \delta t) - u(x,t))\delta x \qquad [6.10]$$

This change of heat must equal the heat flowing in at x minus the heat flowing out at x+δx during the time interval δt. This may be expressed as:

$$\left[-K\left(\frac{\partial U}{\partial x}\right)_x + K\left(\frac{\partial U}{\partial x}\right)_{x+\delta x}\right]\delta t \qquad [6.11]$$

Equating these expressions and dividing by δx and δt gives,

$$\sigma\rho\,\frac{u(x,t+\delta t) - u(x,t)}{\delta t} = K\,\frac{\left(\frac{\partial U}{\partial x}\right)_{x+\delta x} - \left(\frac{\partial U}{\partial x}\right)_x}{\delta x} \qquad [6.12]$$

Taking the limits of δx and δt as tending to zero, the partial derivatives are possible to be obtained. Hence, the heat equation is:

$$\frac{\partial u}{\partial t} = c^2\,\frac{\partial^2 u}{\partial x^2} \qquad [6.13]$$

where $c^2 = K/\sigma\rho$ is the constant thermal conductivity and $\partial^2 y/\partial x^2$ is the thermal conduction. The heat equation has the same form as the equation describing diffusion. Both processes describe physical phenomena that are being smoothed in time.

The basic law of thermal conduction is *Fourier's Law* which states that the heat flux density q is proportional to the temperature gradient T in an isotropic body:

$$q = -\lambda \text{grad} T \qquad [6.14]$$

The constant of λ is the *thermal conductivity*. The minus sign indicates that the temperature decreases in the direction of heat transport and, hence, the temperature gradient is a negative quantity.

6.7.2 The Finite Element Mesh

The convection heat flux is a function of fluid velocity and direction, and it is affected primarily by wind velocity and direction on the surface. As the convection heat transfer coefficient increases due to higher velocities and opportune wind directions, the convective heat flux also increases. Thus, at relatively high wind velocities a convective cooling of the surface occurs when the temperature of the wind is lower than the temperature of the pavement surface. The direction of the heat transfer due to thermal and long-wave radiation is away from the pavement since deep environmental temperatures typically are significantly lower than pavement surface temperatures. The surface energy balance of a pavement requires that the sum of all heat gains through the surface of the pavement must be equal to the heat conducted in the pavement (Mrawira and Luca, 2006). The direction of the heat flux due to convection and thermal radiation is a function of the temperature difference between the pavement surface and the environmental temperatures. In cases where the environmental temperature is lower than the pavement surface temperature, a cooling of the surface occurs while the surface might simultaneously be heated through incident solar radiation. Thus, depending on the magnitudes of individual heat fluxes, a heating or a cooling of the pavement takes place. An adiabatic bottom surface can be assumed for sufficiently thick pavements stipulating no heat transfer between the pavement and sub-grade layers. Similarly, side surfaces of the pavement (pavement edges) are considered to be adiabatic for sufficiently large horizontal expansions since spatial temperature changes in the vertical direction will be much greater than horizontal changes at pavement edges, and any heat transfer through pavement edge surfaces can be neglected. In this study, a pavement of 1000mm width approximating a lane pavement of 400mm depth and infinitely long length is considered.

Figure 6.26 represents the finite element mesh used in the model. A uniform square nodal spacing of 62.5 mm in x and 50 mm in z-directions has been used. In the *z* direction, the domain corresponds to the top of the pavement and bottom of the pavement or the base of the underlying fill material. A pavement of 1000 mm horizontal surface and 40 mm vertical depth is considered resulting in 128 cells for each of which an energy balance equation is developed.

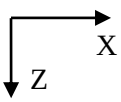

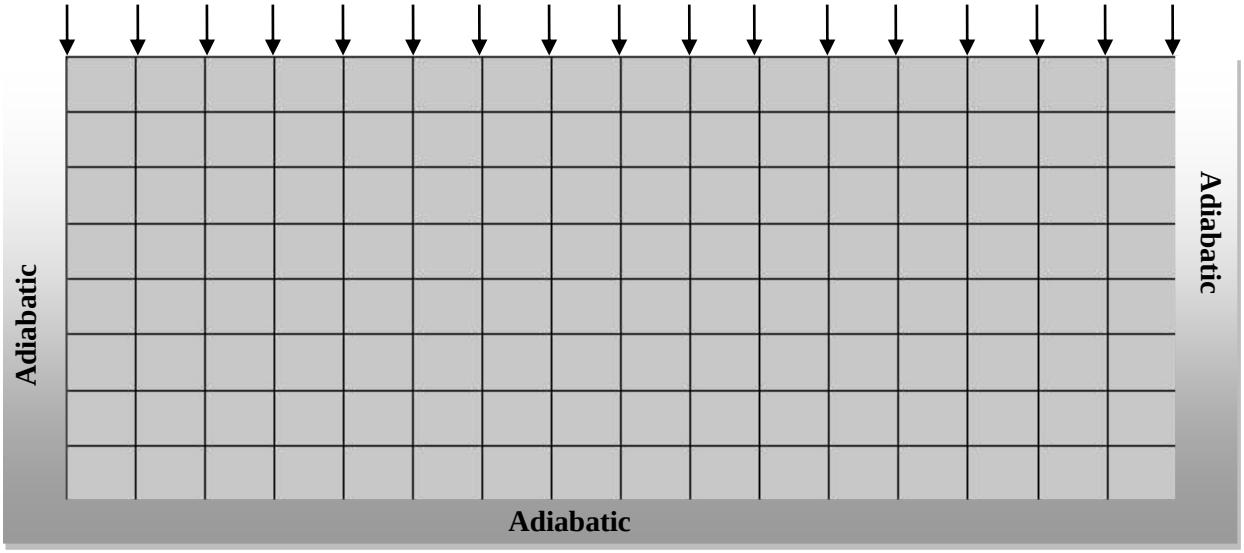

Figure 6.26: Finite Element Mesh of a BSM-foam layer.

6.7.3 Two - dimensional, numerical approach

The time-dependent heat transfer in the pavement is represented in a two-dimensional cross-section using the Cartesian coordinate system. The applicable transient two-dimensional heat transfer equation is expressed as:

$$\frac{\partial^2 T}{\partial x^2} + \frac{\partial^2 T}{\partial z^2} = \frac{1}{\alpha}\frac{\partial T}{\partial t} \qquad [6.15]$$

where α is the thermal diffusivity of the material, T the temperature, x and z are the spatial coordinates and t is the time. The partial differential equation [6.15] is discretized using an explicit finite difference method. The geometry and notation of the finite difference cells in the x-z Cartesian coordinate plane are shown in Figure 6.26.

Using an energy balance approach, the nodal equations are formulated for each cell. The resulting general form of the explicit finite difference equation is:

$$\sum_{i=1}^{4} q^{n(t-\Delta t)} A = V\rho c_p \left(\frac{T^{t}_{(x,z)} - T^{(t-\Delta t)}_{(x,z)}}{\Delta t} \right) \qquad [6.16]$$

where $\Sigma^4_{i=1}\, q^{n(t-\Delta t)}$ is the heat flux across the cell face i at the previous time step, A is the cell face area with a unit depth, V is the cell volume (assuming a unit depth), ρ is the average density of the cell material, cp is the average specific heat capacity of the cell material, $T^{t}_{(x,z)}$ is the nodal temperature at the current time step, $T^{t-\Delta t}_{(x,z)}$ is the nodal temperature at the previous

time step, and Δt is the time step. The heat flux, q^n, for conduction into node (x,z) during a given time step is expressed by Fourier's Law in discrete form as:

$$q^n_{i\rightarrow(x,z)} = k\frac{(T_i - T_{(x,z)})}{l} \quad [6.17]$$

where subscript i denotes a neighboring node, k is the average thermal conductivity of the pavement material between nodes i and (x,z), and l is the distance between nodes i and (x,z). The stability criterion for the explicit method in two-dimensional problems is given through:

$$\frac{\alpha\Delta t}{l^2} \leq 0.25 \quad [6.18]$$

Thus, the stability criterion requires two- minute time intervals for transient progression using typical heat diffusivity values of pavement materials.

6.7.4 Boundary conditions

The boundaries of the model domain are treated as flux-type conditions. The temperature at each boundary node is given by the energy balance equation (Equation 6.16), where q^n_i represents the appropriate external flux and conduction flux from adjacent nodes.

Lines of symmetry on the left- and right-hand boundaries are, by definition, zero-flux conditions. Heat flux at the surface nodes represents convection from the heat transfer fluid. Heat flux at each top surface node ($q^n_{(x,1)}$) is given by:

$$q^n_{(x,1)} = q^n\text{solar} + q^n\text{thermal} + q^n\text{convection} \quad [6.19]$$

where q^nsolar is the solar radiation heat flux, q^nthermal is the thermal radiation heat flux and q^nconvection is the convection heat flux. The bottom surface is treated either as an insulated surface of zero flux condition, or?. Each of the heat flux terms is described in more detail below.

6.7.5 Solar radiation heat flux

Solar radiation heat flux (q^nsolar) is the net solar radiation absorbed by the pavement surface and is given by:

$$q^n\text{solar} = \alpha I \quad [6.20]$$

where I is the solar radiation incident on the pavement surface and α is the absorptivity coefficient for the pavement material. The absorptivity coefficient is corrected for solar

incidence angle (θ) dependence using an empirical correlation given by Duffie and Beckman (1991). The model also accepts solar radiation in the form of beam (I_b) and diffuse (I_d) components, in which case I is computed from:

$$I = I_b \cos\theta + I_d \quad [6.21]$$

The angle of incidence (θ) of the sun's rays can be computed at each time step from correlations given by Spencer (1971), Duffie and Beckman (1991), and ASHRAE (1997).
The computation of the solar radiation was not required in the end and it was not considered in the modelling.

6.7.6 Thermal radiation heat flux

This heat transfer mechanism accounts for heat flux at the pavement's top surface due to thermal or long-wave radiation. This model uses a linearized radiation coefficient (h_r) defined as:

$$h_r = 4\varepsilon\sigma\left(\frac{T_{(x,z)} + T_2}{2}\right)^3 \quad [6.22]$$

where e is the emissivity coefficient of the pavement material, s is the Stefan-Boltzmann constant, $T_{(x,z)}$ is the surface node temperature in absolute units, and T_2 represents the sky temperature in absolute units. The thermal radiation heat flux at each node (q^nthermal) is then computed by:

$$q^n\text{thermal} = h_r(T_2 - T_{(x,z)}) \quad [6.23]$$

6.7.7 Convection heat flux at the pavement surfaces

This mechanism accounts for heat transfer at the pavement's top surface due to free and forced convection. The convection coefficient (h_c) is a function of the Nusselt Number (Nu). Several empirical formulations exist for determining the convection coefficient for different geometries. For a pavement surface, correlations for a horizontal flat plate are the most applicable. In free convection heat transfer, Nu is a function of the Rayleigh Number (Ra). In external free convection flows over a horizontal flat plate, the critical Rayleigh Number is about 10^7. Therefore, two empirical relations for the Nusselt number are used in the model, as described by Incropera and DeWitt (1996), for free convection from the upper surface of a heated or cooled plate:

$$Nu = 0.54Ra^{1/4} \ (10^4 < Ra < 10^7; \text{ laminar flow}) \quad [6.24a]$$

and

$$Nu = 0.15Ra^{1/3} \ (10^7 > Ra > 10^{11}; \text{ turbulent flow}) \quad [6.24b]$$

The convection coefficient (h_c) for free convection can then be determined from:

$$h_c = \frac{Nu\ k}{L} \quad [6.25]$$

where k is the thermal conductivity of air evaluated at the film temperature (as with the other thermal properties of air) and L is the characteristic length described for horizontal flat plates as the ratio of the area to the perimeter (Incropera and DeWitt, 1996).

In forced convection heat transfer, Nu is correlated to the Reynolds (Re) and Prandtl (Pr) Numbers. For external forced convection over a flat plate (i.e. the pavement surface), the critical Reynolds Number is approximately 105. Therefore, two empirical relations for the Nusselt number are used in the model, as described by Incropera and DeWitt (1996), for forced convection over a flat plate:

$$Nu = 0.664\ Re^{1/2}\ Pr^{1/3} \text{ (laminar flow regime)} \quad [6.26a]$$

$$Nu = 0.037\ Re^{4/5}\ Pr^{1/3} \text{ (mixed and turbulent flow)} \quad [6.26b]$$

The convection coefficient (h_c) for forced convection can then be determined by Equation 6.25 with the characteristic length value described as the ratio of the length (parallel to the wind direction) to the perimeter. Finally, the convection heat flux at each pavement surface node (q^nconvection) is computed by:

$$q^n\text{convection} = h_c\ (T_{air} - T_{(x,z)}) \quad [6.27]$$

where T_{air} is the enviromental temperature and h_c is taken as the maximum of the free convection coefficient and the forced convection coefficient. This practice of choosing the larger of the free and forced convection coefficients is recommended by Duffie and Beckman (1991) and McAdams (1954) and is used in the absence of additional experimental evidence regarding combined free and forced convection.

6.7.8 Introduction to the model program FEMMASSE HEAT-MLS

Firstly, to use this model, the structure of a pavement should be defined. The pavement structures used in this model consists of 400 mm BSM with an increasing percentage of RA. This is a normal structure of a South African pavement. Secondly, the properties of materials have to be defined. To simulate the heat diffusion process, the thermal properties of the materials including the heat capacity and thermal conductivity are required. Based on previous literature review and analysis, the thermal properties of some pavement materials and mixtures

are summarised in Table 6.1 (Wolfe *et al*., 1980; Tegeler and Dempseey, 1973; Corlew and Dickson, 1968; Turner *et al*., 1981; Luca and Mrawia, 2005; Wu *et al*., 2008 and Quantao, 2012).

Table 6.1: Heat capacity and thermal conductivity for different materials.

Mix type	**Heat Capacity (kJ/m^3K)**	**Thermal Conductivity (W/mK)**
Dense asphalt concrete	2254	1.3
Porous asphalt	1840	0.65
Bitumen	2000	0.17
Gravel base	1473	1.3

After a consistent number of computational trials in this research, the thermal capacity and the thermal conductivity of the three BSM-foam mixes were selected. Table 6.2 reports the data used in the MLS program for the simulation of the temperature distribution.

Table 6.2: Heat capacity and thermal conductivity for three BSM-foam mixes.

Mix type	**Heat Capacity (kJ/m3K)**	**Thermal Conductivity (W/mK)**
BSM-foam (2.3% bitumen content) with 100%G2 material	1800	0.60
BSM-foam (2.1% bitumen content) with 50%RA and 50%G2 material	1775	0.7
BSM-foam (2% bitumen content) with 100%RA material	1750	0.80

The data was initially compared with similar materials having density and mechanical properties similar to BSMs. The heat capacity of the BSM-foam mix with 100%RA lies between asphalt and porous asphalt. The trials for all three BSMs mixes are reported in the Appendix E. For BSMs materials there were no data available. In the following figures the temperature recorded in a BSM pavement section is compared with the temperature distribution values modelled through the FEMMASE HEAT-MLS program. The temperature recorded for every thermocouple matches the values obtained by the model. This study aimed to determine reasonable and representative values through extended research and a comparison to values determined in previous South African research for other materials.

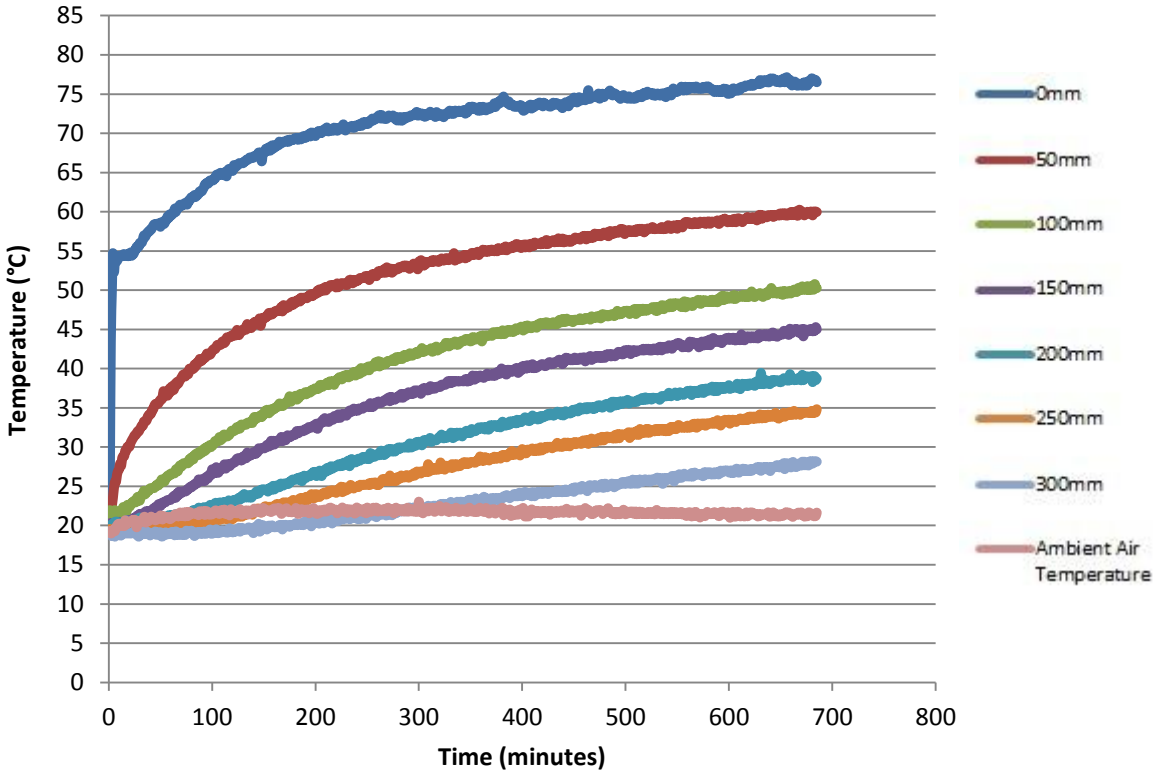

Figure 6.27: Real data measured in BSM-foam mix with 50%RA and 50%G2 (2.1% bitumen content) (measure).

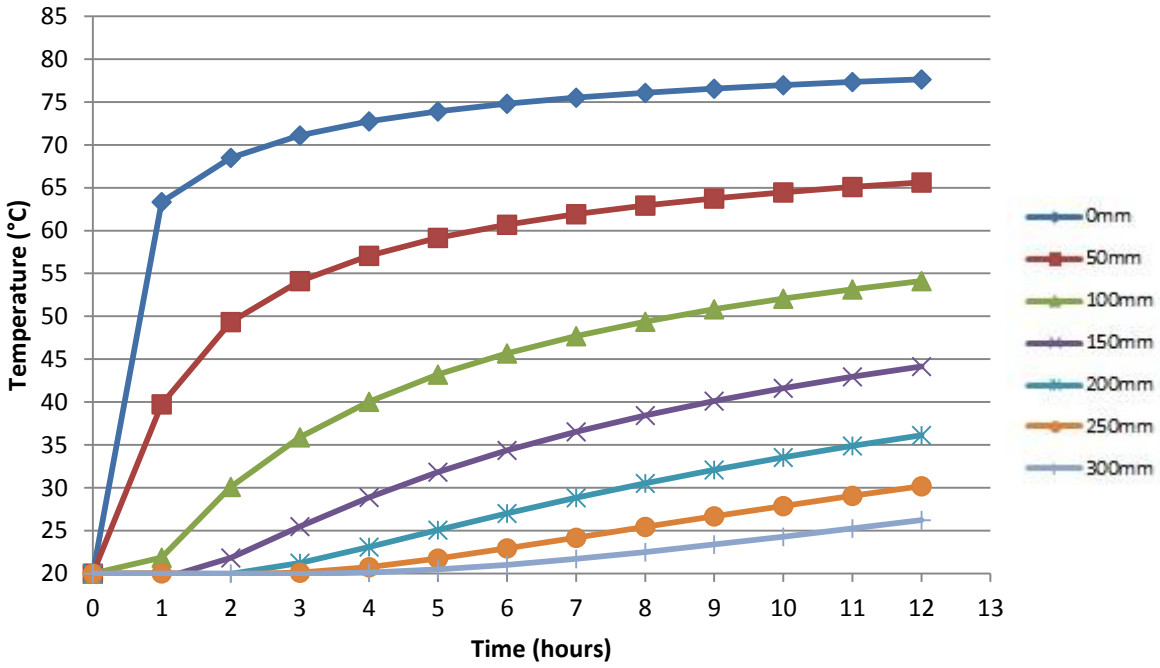

Figure 6.28: Temperature profiles at different layers predicted through the finite element program FEMMASSE HEAT-MLS (model).

The temperature boundaries for the pavement structure need to be defined. It is assumed that induction heating will be applied on the BSMs section. The initial temperature of all layers and the ambient air is assumed to be 20ºC (the mean air temperature in South Africa, South African Weather Service, 2007). Fourthly, the temperature of the heated BSM layer during induction heating should be defined. For simplicity, the BSM-foam layer is assumed to be heated completely. This 400mm layer is heated from 20ºC to 70ºC for a BSM-foam mix with 100%G2, and to 78 and 80 ºC for respectively a BSM-foam mix with 50%RA and 50%G2 material and a BSM-foam layer with 100%RA. It is also assumed that the conductive BSMs are heated homogeneously over their thickness. After setting the temperature boundaries, a mesh on the structure element was defined. The thermal transfer within the pavement during 18 hours was studied with this program. The time increment was changed to 0.1 hour. After setting the calculation parameters, the calculation of the thermal transfer process within the pavement was started. This temperature study was limited to the study of the temperature distribution in the pavement sections considering only the diurnal effects on the different layers. Further research should be carried out to analyse the nocturnal effects and the low temperatures in the pavement structures.

6.7.9 Results and analysis

To study the thermal transfer process in the pavement after induction heating, the temperature profiles at different layers of the pavement during 18 hours are plotted in Figure 6.29 for the three BSM-foam mixes. The three BSMs pavement sections are analysed using the data presented in the previous paragraph. Each section is divided into seven parts from the top surface with a distance of 50 mm from every single point. The points correspond at these different depths in the pavement: 0 mm, 50 mm, 100 mm, 150 mm, 200 mm, 250 mm, 300 mm. Figure 6.29 shows the points at which the temperature was measured.

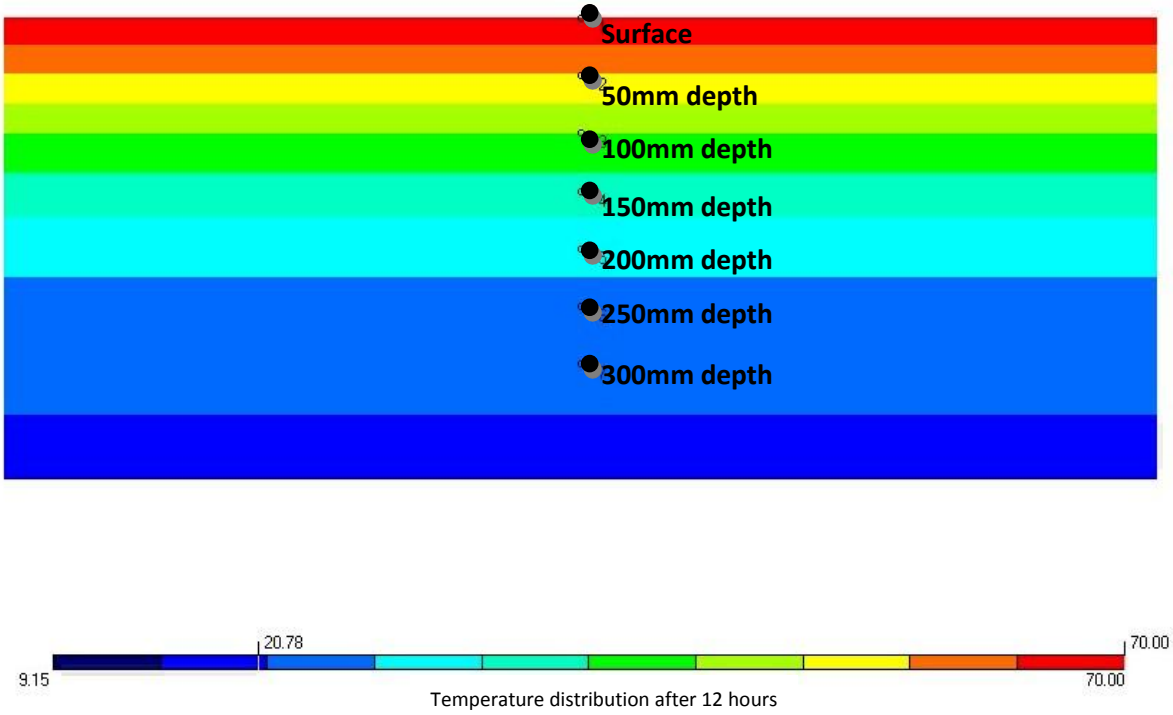

Figure 6.29: BSM section with the representation of the seven points at different depths.

Within the heated BSMs, the abilities of different layers to maintain the temperature are slightly different. The pavement surface is most susceptible to heating by means of convection and long wave radiation to the atmosphere: the temperature at the surface of the pavement increases more rapidly than in the deeper layers. Figures 6.30, 6.31 and 6.32 present the predicted temperature profiles at different layers obtained through the finite element program FEMMASSE HEAT-MLS for the three BSM-foam mixtures.

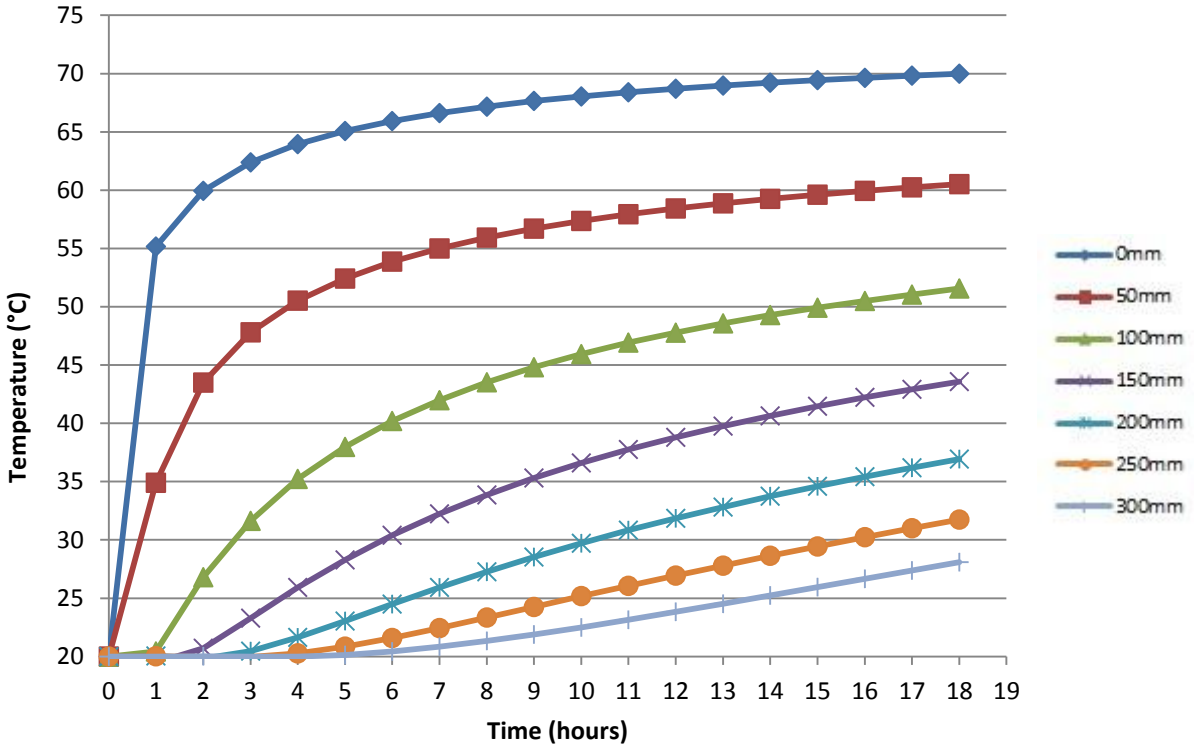

Figure 6.30: Predicted temperature profiles in a BSM-foam (2.3% bitumen content) with 100%G2 material, with thermal capacity of 1800(kJ/m^{3}K) and thermal conductivity of 0.60 (W/mK) (model).

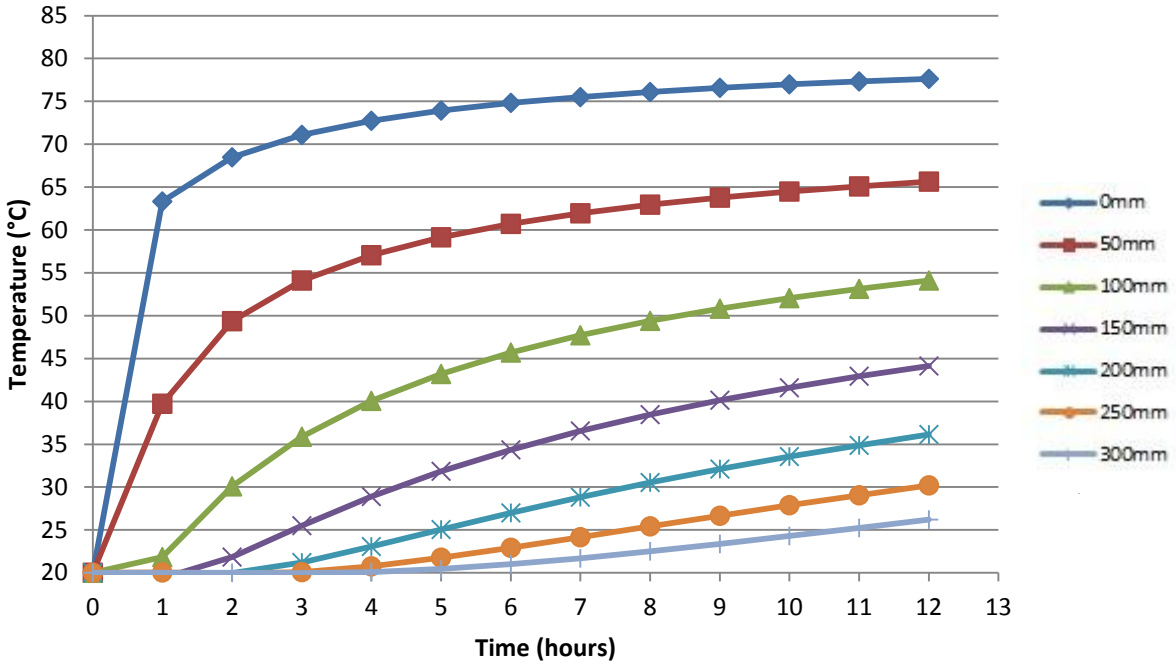

Figure 6.31: Predicted temperature profiles in a BSM-foam (2.1% bitumen content) with 50% RA and 50%G2 material, with thermal capacity of 1775 (kJ/m^{3}K) and thermal conductivity of 0.70 (W/mK) (model).

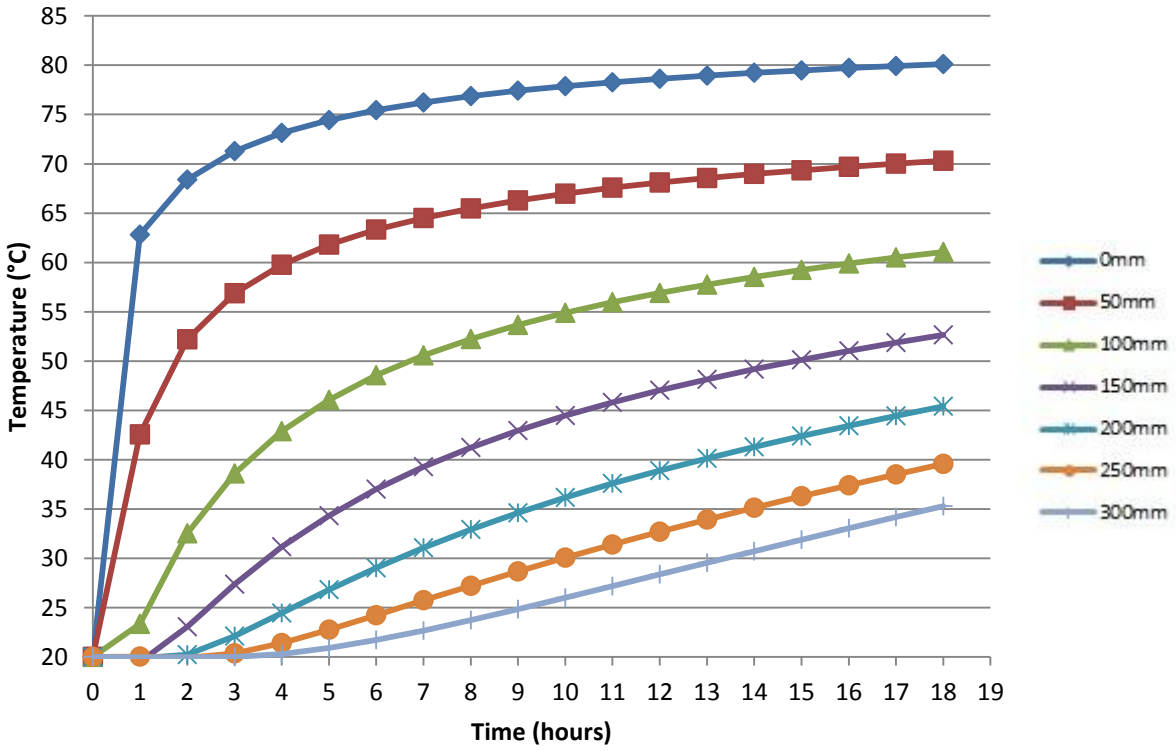

Figure 6.32: Predicted temperature profiles in a BSM-foam (2% bitumen content) with 100%RA material, with thermal capacity of 1750(kJ/m^{3}K) and thermal conductivity of 0.80(W/mK) (model).

It can be observed that the maximum temperatures decrease when the depths increase. The surface temperature of the pavement decreases when the thermal conductivity increases. The temperature in all three graphs increases rapidly especially at the surface. On the other hand, the temperature of the rest of the BSMs layers increases gradually. So, the temperature curve gradually turns into a parabolic curve in the second-third hour and after that time increases slowly with a low rate. The temperature on the top part of the pavement absorbs more energy than the deeper layers. The three graphs show values very close to the temperatures measured in the laboratory on a real BSM pavement (Figures 6.10, 6.11 and 6.12). The finite element model is able to reproduce the temperature distribution in the BSMs sections with good accuracy. Only a slight difference is identified in the BSM-foam with 100%G2 material and in the BSM-foam with 50%RA and 50%G2 material: the temperatures showed after the modelling have some degrees of difference from the real measurements. This could probably be due to the errors which can happen during the phase of temperature monitoring and recording. In fact the errors can be due to the possible circulation of air in the holes where the thermocouples are installed even if they are completely sealed on the top of the pavement surface and localised differences of densities in the pavement which can limit the heat transfer in the pavement section. The characteristics of the mix can always change marginally during the time of compaction and curing. The evaporation of the moisture inside the mix can always change the real temperature of the pavement section, especially if the percentage of air voids is not high.

6.7.10 Effect of the wind speed on the heating rate of the pavement sections

To study the factors influencing the heating rate of the conductive BSMs mixes, a moderate wind of 7m/s was varied with a strong wind of 14m/s in the modelling program to see its effect on the BSMs sections without surfacing. The wind chosen is normally present in South Africa throughout the year, especially in the coastal areas. The effects of the wind speed on the heating of the pavement sections are represented in the following graphs (Figures 6.33 to 6.38) for each of the BSM-foam mixes.

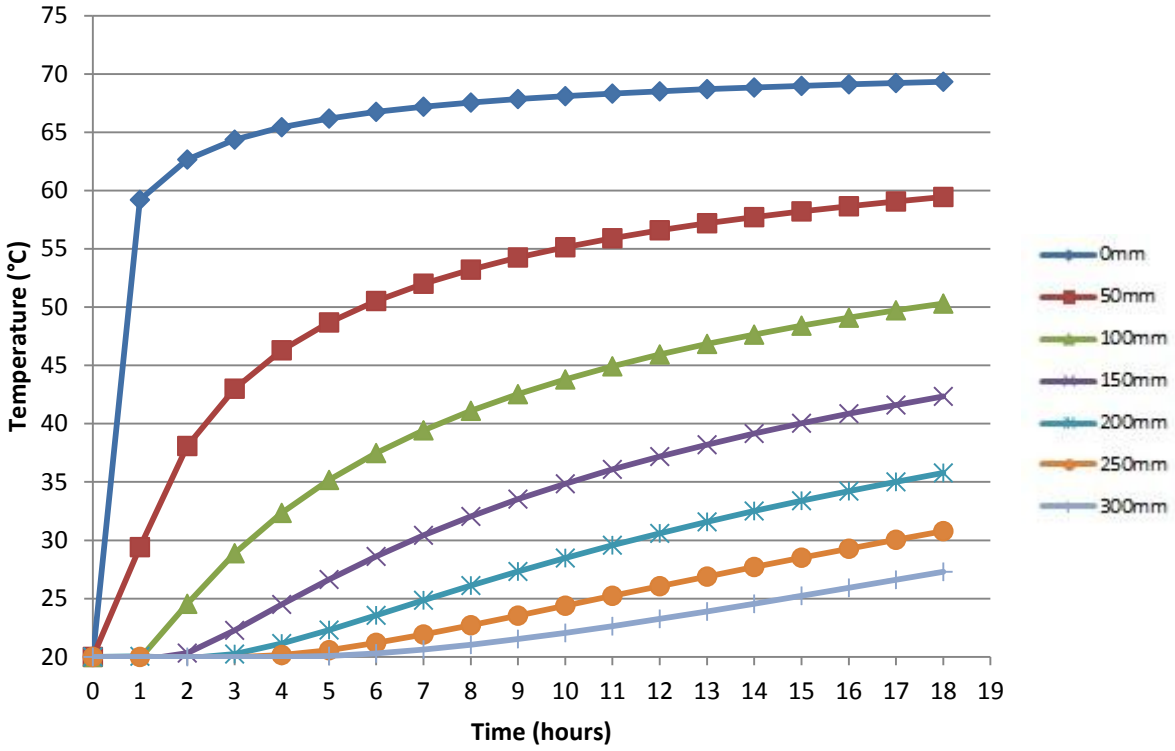

Figure 6.33: Predicted effect of the wind speed of 7m/s on the heating rate of the BSM-foam (2.3% bitumen content) with 100%G2 material (model).

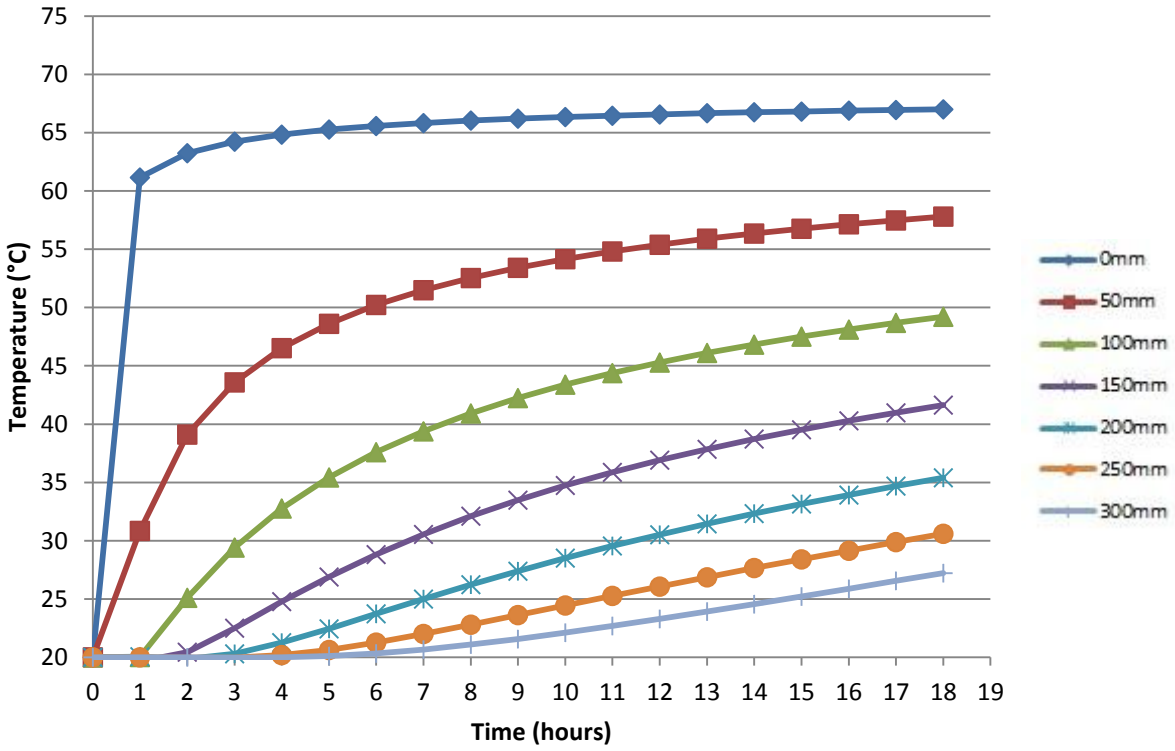

Figure 6.34: Predicted effect of the wind speed of 14m/s on the heating rate of the BSM-foam (2.3% bitumen content) with 100%G2 material (model).

The two graphs show a decrease in the temperature in the top layers of 2°C and 4°C for the BSM-foam section with 100%G2 material. As soon the wind increases, the capability of the pavement to transfer the heating through the deeper layers significantly decreases. In fact the initial parabolic slope in the deeper layers becomes markedly more linear as the wind increases especially during the first 3-4 hours.

This consequence becomes more visible with BSM-foam mixes with higher percentage of air voids and increasing quantity of RA. The following figures present the behaviour of the BSM-foam mixes with 50%RA and 50%G2 material and the BSM-foam mix with 100%RA. The slope in the deeper layers becomes more linear and with a heating rate lower than in the study case without the presence of wind on the surface. The final temperature measured after the 12 or 18 hours is significantly lower than in the initial situation without any wind speed. The temperature in the BSM-foam with 100%RA drops even with 10°C (wind speed 14m/s) for the top part of the pavement section.

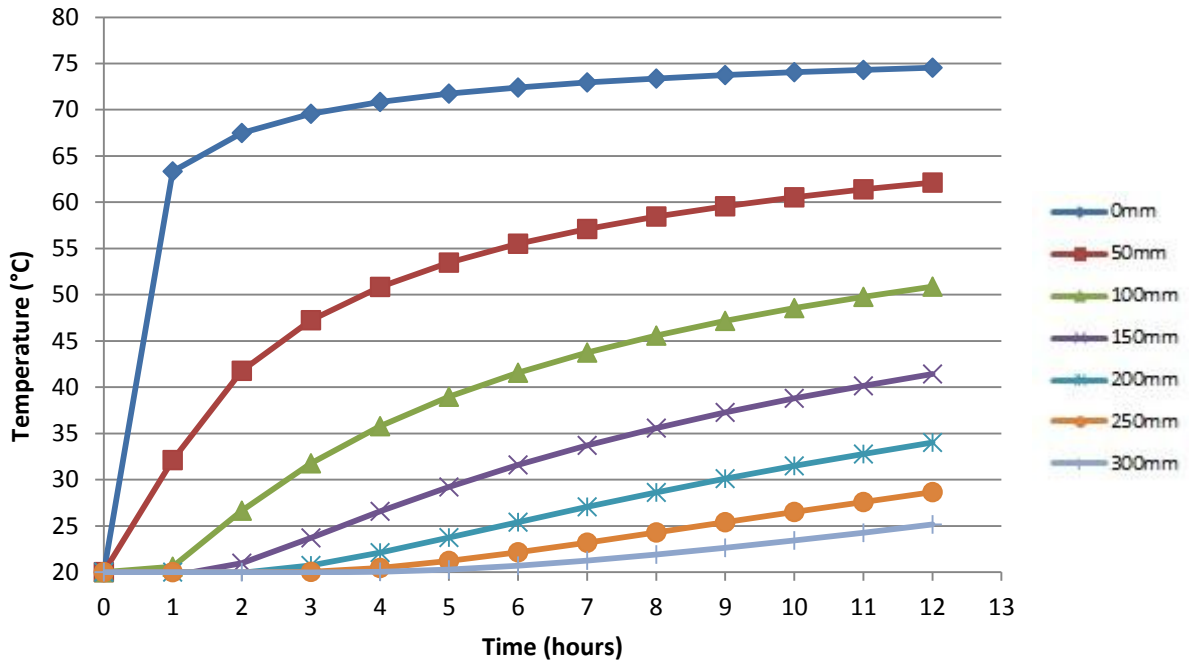

Figure 6.35: Effect of the wind speed of 7m/s on the heating rate of the BSM-foam (2.1% bitumen content) with 50%RA and 50%G2 material (model).

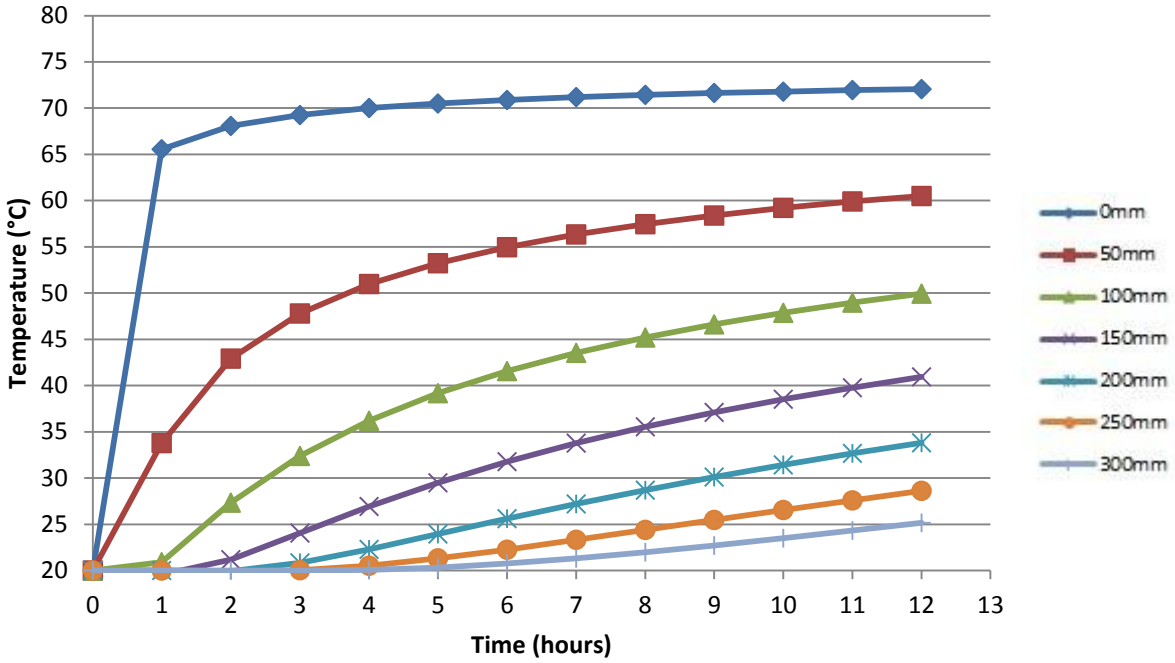

Figure 6.36: Effect of the wind speed of 14m/s on the heating rate of the BSM-foam (2.1% bitumen content) with 50%RA and 50%G2 material (model).

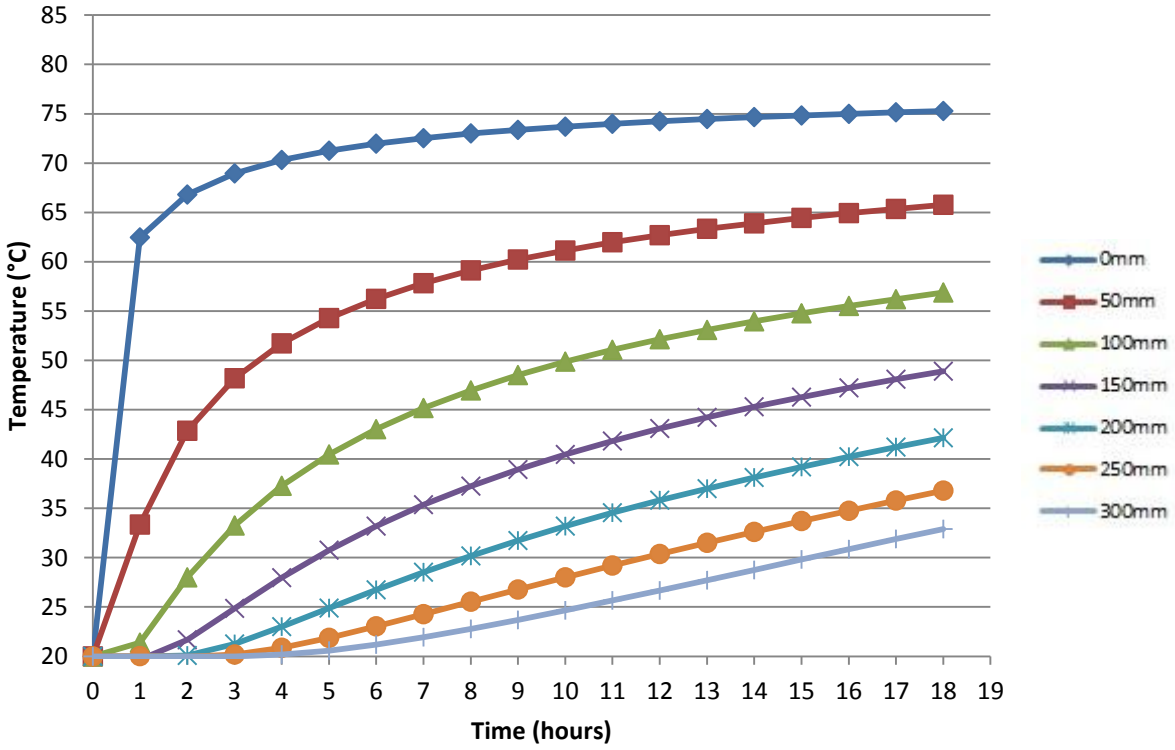

Figure 6.37: Effect of the wind speed of 7m/s on the heating rate of the BSM-foam (2% bitumen content) with 100%RA (model).

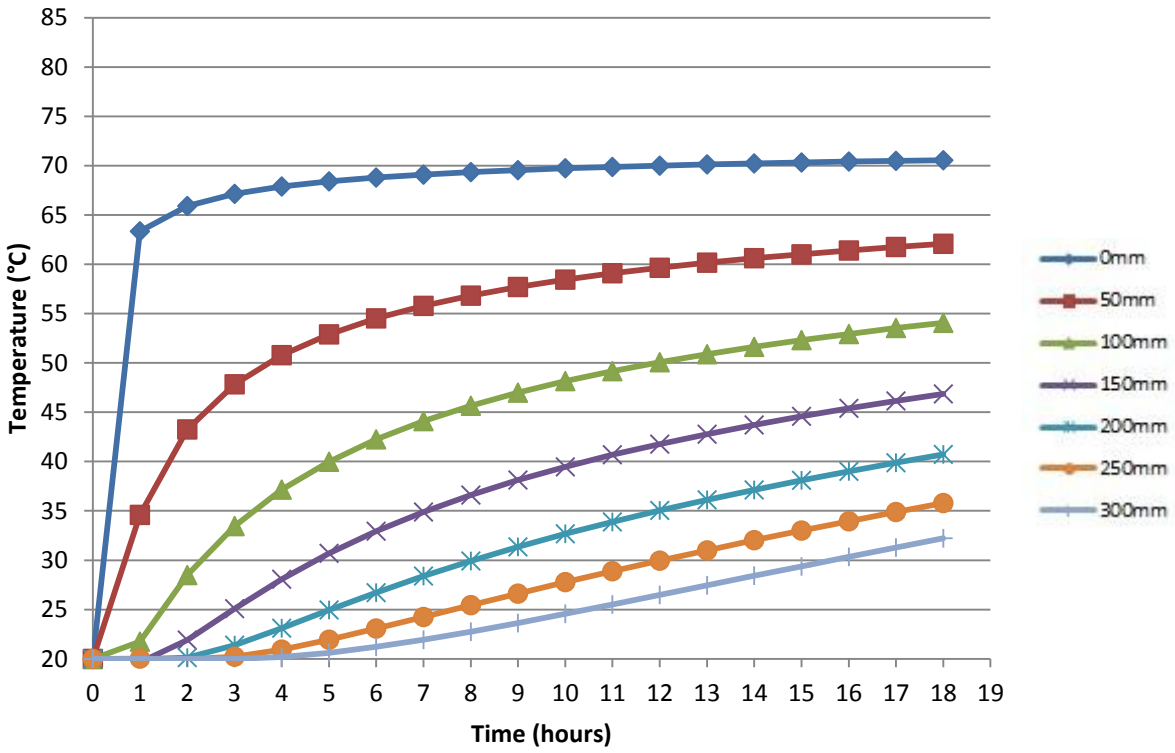

Figure 6.38: Effect of the wind speed of 14m/s on the heating rate of the BSM-foam (2% bitumen content) with 100%RA (model).

It's clear from these graphs that the wind speed significantly influences the heating rate of a pavement: the decrease of the wind speed greatly increases the ability of the pavement to keep the heat and maintain its temperature and the increase of the wind speed decreases this ability.

In windy conditions the temperature on the surface is always higher than in the deeper layers, but it is always less comparable to a situation without the presence of wind. An increase of the wind speed results in a higher convective thermal transfer coefficient, so the pavement loses heat more rapidly in higher wind speed conditions. The presence of air voids, a high quantity of RA and moisture in the mixture can strongly contribute in reducing the heating of BSMs pavements.

It is concluded that various improvements can be made at the design stage of transport infrastructure by understanding the implications of the interaction between pavement design, the thermophysical properties of the specified materials, and the environmental climatic conditions. Rutting is a particular problem in road pavements with bitumen, because they have a temperature-dependent viscous binder. The ability to reduce surface temperatures in climates with high peak temperatures and short-wave radiation gains might be highly beneficial. In general terms, a pavement surface with high conductivity and low absorptivity will be cooler, as confirmed by the predictions and data from the laboratory temperature tests and therefore, is less likely to suffer from rutting. As the studies above show, if the maximum surface temperature is reduced by around 10°C (i.e. BSM-foam with 100%G2 material and 2.3% of bitumen content) in hot climates, the pavement service life can potentially be extended for more years.

A numerical modelling tool of 2D transient thermal conduction has been presented for predicting temperature profile evolution on pavement structures. It has been well-validated in three contrasting BSM-foam mixtures using accepted experimental data from the laboratory. In the longer term, the influence of moisture transport and storage on the model accuracy and climate-dependent response should be investigated to determine the influence on prediction accuracy. In these scenarios the simple model is unlikely to fully reflect the actual thermal processes of convection, radiation, and evaporation at the pavement surface, or to accurately model heat and moisture movement inside the pavement. However, comparisons with models that do this suggest that there is no significant improvement in accuracy for the wide range of contrasting BSM-foam mixes tested in this study. A simple tool like this program FEMMASE MLS is easily used and applied by industry as part of pavement design protocol and material mix design specifications.

In cold climates, the ability to prevent the pavement materials from getting so cold would be likely to have a measurable effect on extending fatigue life. In very cold climates a thick, low-diffusivity pavement surface layer could provide a more stable temperature at shallower depths and improve the pavement stability beneath the surface (i.e. reducing intermittent thaw softening, a problem that is expected to increase significantly in many northern climates). Further research is needed to see how pavement design and material selection can be tailored to a specific location given the climatic variables of that region. The benefits of reduced rutting and extended fatigue life will only be realized for materials having the same temperature susceptibility to these damage mechanisms. The most important factor controlling rutting is mix design, which evaluates the binder content, aggregate properties and binder stiffness. Since BSMs with a low percentage of RA have lower surface temperatures, the pavement fatigue life can potentially be increased without greatly increasing the risk of rutting. The pavement with the highest absorptivity has the highest pavement temperatures, which makes it more prone to mix rutting. Decreasing the thermal capacity and conductivity in a BSM mixture, reduces the maximum temperature on the top of the pavement by up to 10°C, which can significantly decrease the risk of rutting. These results indicate that surface treatments with lower absorptivity may decrease the risk of rutting in BSMs mixes.

6.8 Conclusions

A two-dimensional finite difference model is presented that is capable of determining temperatures on an hour-by-hour basis at any arbitrary point in a BSM layer. The model considers thermal ambient conditions, such as the environmental temperature, global solar radiation intensity, pavement geometry, ambient wind conditions and pavement thermal properties. A numerical model was performed using actual pavement data from a series of tests performed in the laboratory at the University of Stellenbosch on the three different BSM-foam sections. To aid asphalt engineers in pavement design, temperature predictions at pavement surface and at different depths using temperature data recorded with thermocouples in a pavement section were compared to Superpave (1994) and Viljoen (2001) algorithms that are commonly used in the design of pavements. In addition, a series of sensitivity analyses were conducted to assess the influence of pertinent design variables such as BSM-foam material composition, thermal properties, wind speed, pavement geometry on temperature predictions of the numerical model.

The results of the analyses allow for the following conclusions:

- The proposed numerical model provides a useful understanding of behaviour that justifies further research and development using a wider range of materials and validation on actual projects with BSM layers. The model allows for an hour-by-hour calculation of the pavement thermal response in the form of pavement temperatures using primary temperature data for varying BSMs materials. The various BSM-foam mixes with an increased amount of RA materials can be entered into the model approximating layer geometry in 50mm grid increments in the direction normal to the BSM surface through specification of thermal properties of BSM materials (thermal conductivity, thermal heat capacity). This allows for the determination of temperature responses at different depths. In addition, the model allows for the specification of different temperatures on the surface of the pavement section and different wind speeds. Further field tests are necessary to validate the numerical model developed through the testing matrix.

- The numerical model predictions are strongly dependent on climatic data (external air temperature and wind speed) in addition to accurate knowledge of the thermal properties of pavement materials. An effort was made to calibrate possible realistic values for the thermal capacity and thermal conductivity indices. A comparison with previous South African research and other studies on asphalt material was used as a base for the calibration of these factors. Nevertheless, a comparison between actually measured and predicted pavement temperatures showed a high level of correlation for all three BSMs pavement sections.

- A comparison between real temperature data and the Superpave (1994) and Viljoen (2001) algorithms have shown some satisfactory results. The analysis conducted on the deeper layers pointed out completely different results between the temperature data recorded in the laboratory and the two previous algorithms (Appendix D). Further improvements can be considered in the pavement design after the temperature monitoring of the three BSM-foam mixes, especially for the study of the propagation of the heating in the deeper layers of a pavement section. In general the Superpave and the Viljoen algorithms underestimate or overestimate the BSM temperatures when compared to the real data measured on a real BSM-foam section.

- The volumetric heat capacity of the pavement thermal mass (the product of BSM density and specific heat capacity of the material) strongly influences thermal behaviour of the pavement where heat transfer is dominated by pure conduction. On the other hand, the minimum BSM temperature at the surface of the pavement primarily is dependent on ambient flow conditions (wind speed and direction), since convective cooling affects dominate the heat transfer at the surface. In fact, the higher the wind speed is, the higher the convection heat transfer coefficient at the BSM surface, resulting in lower surface temperatures.

- The impact of wind speed on the BSM surface is relatively high if the amount of air voids, percentage of moisture and quantity of RA are high. On the other hand, for BSM pavement segments when the wind speed increases considerably, the effects of convective cooling of the surface become more pronounced, yielding lower BSM surface temperatures. Nevertheless, it should be noted that the dependence of temperature predictions on wind speed is of more importance on pavement surfaces

exposed to light traffic conditions, where there might be the chance of encountering laminar flow regimes at suitably low wind speed. During typical traffic conditions, the wind speed near the pavement surface will be dominated by vehicle traffic. Thus, in practice, it is reasonable to expect a continuously turbulent flow regime near the pavement surface independent of the wind conditions. It has to be noted that pavements with BSM layers have to be completed with a top layer of HMA.

- The presence of air voids and RA can increase the temperature distribution in the pavement in time and magnitude, with the possibility to create mechanical problems and possible rutting during the summer period, when the environmental temperature is higher especially on the top of the surface of the pavement. This temperature differential is much larger during summer months where the asphalt pavement is heated considerably through solar radiation. The magnitude of this test temperature coupled with material properties can significantly influence the durability behaviour and long-term performance of BSM layers. The determined voids content varied from 13% for BSM-foam with 100%G2 material and 16% for BSMs-foam with 100%RA. These values are higher than typical voids for HMA, which can be typically between 4% and 6%. Therefore, understanding of temperature distribution and voids characteristics is vital in BSM mixes.

- The laboratory investigation of BSM-foam layers shows that the temperature across the pavement section is not uniformly distributed over the layer. The trend observed shows that the maximum temperature is higher closer to the top surface than deeper in the layer. Therefore, the temperature gradient in a layer may be used to determine the influence on moisture evaporation. That means, understanding of the temperature distribution in BSMs layer is important for judging the appropriate time (in hours or days) the constructed layer can be surfaced or opened to traffic.

- The key factors that have been indicated to influence temperature distribution and voids characteristics in BSMs are: heat transfer and voids structure. The heat transfer in the BSM-layer depends on local environmental factors such as solar radiation, wind speed and relative humidity as well as material composition. Therefore, modelling of these factors is required for proper prediction of evaporation and strength gain in the layer.

REFERENCES

Adams, E.E. and Curran, A.R. 1999. Proof of Concept for Prediction of Pavement Temperature: A Tactical Decision Aid for Highway Safety. FHWA/MT-99-003/8117-6: 17pp.

Andrew, R. D., Dehdezi,P.K. Matthew, R. H., Wang, J. and Isola,R 2012. Enhancing thermal properties of asphalt materials for heat storage and transfer applications. Road Materials and Pavement Design Journal, vol. 13, pp.784-803. Taylor & Francis Ltd.

ASHRAE. 1997, ASHRAE Handbook, Fundamentals, American Society of Heating, Refrigeration and Air-Conditioning Engineers, Inc., Atlanta, Ga.

Asphalt Academy. 2009. A guideline for the design and construction of bitumen emulsion and foamed bitumen stabilised materials. 2nd edition technical guideline. Pretoria, South Africa. (TG2).

Burger, M. 2005. Prediction of the temperature distribution in asphalt pavement samples. Master thesis, Department of mechanical engineering, Stellenbosch University, South Africa.

Cheng, D. 2002. Surface free energy of asphalt-aggregate system and performance analysis of asphalt concrete based on surface free energy. Ph.D. Dissertation, Texas A&M University, College Station, Texas.

Chiasson, A.D., Yavuzturk, C. and Ksaibati, K., 2008. Linearized approach for predicting thermal stresses in asphalt pavements due to environmental conditions. J. Master Civil Eng. ASCE., 20: 118-127.

Corlew, J.S. and Dickson, P.F. 1968. Methods for calculating temperature profiles of hot-mix asphalt concrete as related to the construction of asphalt pavements. Journal of Association of Asphalt Paving Technologists 37:101-140.

De la Roche, C. 1996. Module de Rigidité et Comportement en Fatigue des Enrobés Bitumineux – Expérimentations et Nouvelles Perspectives d'Analyse. Thèse de doctorat, École Centrale Paris [In French].

Duffie, J.A. and Beckman, W.A. 1991. Solar Engineering of Thermal Processes, 2nd Edition, John Wiley and Sons.

FEMMASSE-MLS8.5-User-Manual. 2006. Finite Element Modules for Material Science and Structural Engineering. The Netherlands.

Highter, W.H. and Wall, D.J. 1984. Thermal properties of some asphaltic concrete mixes. TRB no. 969 pg. 38-45.

Incropera, F.P. and De Witt, D.P. 1996. Introduction to Heat Transfer, 3rd Edition, John Wiley & Sons.

Jenkins, K.J. and Twagira, M.E. 2008. Failure mechanism of in-situ recycling with foamed bitumen stabilisation. Technical report on the investigation of distress on Shedgum Road in Saudi Arabia. Loudon International.

Jia, L. and Sun, L. 2007. Numerical prediction model and thermal properties for asphalt pavement. Journal of advanced characterisation of pavement and soil engineering materials. Taylor & Francis Group. London.

Kennedy, T.W., Huber, G.A., Harringan, E.T., Cominsky, R.J., Hughes, C.S., Von Quintis, H., Moultrop, J.S. 1994. Superior Performing Asphalt Pavements (SUPERPAVE): The product of the SHRP asphalt research program, Report no: SHRP-A-410, Strategic Highway Research Program, Washington.

Luca, J. and Mrawia, D. 2005. New measurement of thermal properties of Superpave asphalt concrete. Journal Materials in Civil Engineering 17:72-9.

Lukanen, E., Stad, R.S. and Briggs, R., 2000. Temperature prediction and adjustment factors of asphalt pavement. Office of Infrastructure Research and Development Federal Highway Administration. McLean, Virginia, pp. 5-10.

McAdams, W.H. 1954. Heat Transmission, 3rd Edition, McGraw-Hill Book Company.

Mrawira, D. and Luca, J. 2006. Effect of aggregate type, gradation, and compaction level on thermal properties of hot-mix asphalts. Canadian Journal of Civil Engineering, 33(11), 1410-1417.

Quantao, L. 2012. Induction Healing of Porous Asphalt Concrete. Master thesis. TUDelft, The Netherlands.

Solaimanian, M. and Kennedy, T.W. 1993. Predicting maximum pavement surface temperature using maximum air temperature and hourly solar radiation. TRB no. 1417 pp1-11.

South African Weather Service. 2007. The Mean Air Temperature in South Africa. Pretoria, South Africa.

Spencer, J.W. 1971, Fourier Series Representation of the Position of the Sun, Search, Vol 2, No. 5.

Tan, S.A., Fwa, T.F., Chuai, C.T. and Low, B.H. 1997. Determination of thermal properties of pavement materials and unbound aggregates by transient heat conduction. Journal of Testing and Evaluation, 25(1), 15–22.

Tegeler, P.A. and Dempsey, B.J. 1973. A method of predicting compaction time for hot-mix bituminous concrete. Asphalt Paving Technology 1973, Proceedings: Association of Asphalt Paving Technologists Technical Sessions 42:499-523.

Turner, W.C. and Malloy, J.F. 1981. Thermal insulation handbook, Robert E. Krieger Publishing Company, Malabar, Florida, p. 549.

Twagira, M.E. 2010. The influence of durability properties on the performance of Bitumen Stabilised Materials. PhD thesis. Stellenbosch University, South Africa

Viljoen, A. W., 2001, Estimating Asphalt temperatures from air temperatures and basic sky parameters. Internal report, Transportek, CSIR, Pretoria.

Wang, D. 2013. Prediction of Asphalt Pavement Temperature Profile During FWD Testing: Simplified Analytical Solution with Model Validation Based on LTPP Data. Journal of Transportation Engineering , January 2013, Vol. 139, No. 1 : pp. 109-113.

Wolfe, R.K., Heath, G.L.and Colony, D.C. 1980. University of Toledo time-temperature model laboratory field validation. Report No. FHWA/OH-80/006, Department of Industrial Engineering, University of Toledo, Toledo, Ohio.

CHAPTER 7

SYNTHESIS

7.1 Introduction

Structural design and modelling of pavements is a complex aspect of pavement engineering that in the past has been studied by many researchers and this will continue to be the case for a considerable time in the future. The modelling of pavements incorporating BSMs, and to be more precise, to estimate the stresses and strains at critical positions in the pavement structure and especially in the BSM layer, is studied in this chapter through different pavement structures.

This chapter aims to demonstrate how the experimentally determined material properties and behaviour of the BSM-foam mixes, as discussed in the previous chapters, link to pavement modelling. This objective is achieved by working out a limited number of practical examples using stress and strain analysis methods that are readily available to the practitioner.

It is noted that the material properties and behaviour as determined in this study are only valid for the test conditions that were adopted, i.e. temperature, loading frequency, thickness, etc. Care was taken to select typical and representative test conditions. The actual conditions in the pavement structure may however differ from these chosen laboratory conditions. The examples worked out in this chapter are therefore hypothetical and serve the purpose of illustrating how the material properties determined in this study may assist in pavement modelling. They are not intended to accurately estimate the structural capacity of the modelled pavement structure.

The linear-elastic multi-layer program BISAR 3.0 (Shell, 1998) is used in this case. Full friction between layers is considered in all the analyses conducted in this chapter. The use of multi-layer programs has certain limitations in the estimation of the pavement response. More advanced methods such as finite element methods are required to estimate the pavement response more accurately. The use of such advanced methods is however outside the scope of this study. Some of the limitations of multi-layer programs are discussed in this chapter.

The first section of this chapter evaluates the effect of using a uniform sub-grade or a dual sub-grade with a CTSB (Cemented Treated Sub Base) sub-base, compared with a pavement structure constituted by a uniform or dual sub-grade and a granular sub-base, in order to determine the response of the pavement structure with a BSM-foam layer in terms of stresses and strains. The influence of the different sub-base and sub-grade without temperature influences are analysed.

In the second part the better performing pavement structure presented in the first section incorporating a BSM-foam base layer is modelled with a low and high loading condition and two different HMA surface thicknesses.

After this part, a sensitivity analysis is carried out to determine the effect of changes to the typical pavement structure on the pavement response. These changes include varying the percentage of RA in the BSM-foam layer, the temperature on the top of the pavement sections and the Poisson's ratio BSM layer stiffness. At the end of this section, a possible link is drawn

between mechanical behaviour and thermal sensitivity of pavement with BSM materials . It is well known that BSM-foam mixtures are a visco-elasto-plastic material (Jenkins, 2000; Ebels, 2008) and, consequently, that thermal effects related, for example, to seasonal variations and solar heating have consequent influences on the mechanical behaviour. Modelling this time-dependent thermal mechanical behaviour is important for the assessment of the residual life-time for the pavement.

A method is proposed to determine the thermo-physical characteristics of a pavement with BSM-foam layers with an increasing amount of RA followed by the mechanical visco-elasto-plastic parameters. With these characteristics, it is then possible to model the mechanical behaviour of BSM-foam mixes. Very few values of intrinsic thermo-physical characteristics are available in the scientific literature. This method brings new considerations and can be used, for example, in the BSM layer design. BSMs as visco-elasto-plastic materials are characterised by mechanical characteristics depending on temperature and loading frequency.

Models developed with the FEMMASSE HEAT-MLS program are used to determine the temperature distribution in the pavement with a layer of BSM-foam. This simulation model is applied to different representative base layers incorporating three different BSM-foam mixes with an increased amount of RA. This section is devoted to the representation and comparison of the values obtained from the previous sections with the results coming from Chapters 4 and 6.

The fourth part of this chapter deals with the determination of the mechanical characteristic of the pavement sections based on the material characteristics analysed in the prevailing temperature conditions. This study results in the mechanical characterisation and performance analysis of the three different BSM-foam mixes linked to the temperature simulation.

The chapter ends with a brief illustration of how the experimentally determined material properties and temperature distribution can be used in the design of the pavement sections which include BSM-foam base layers with an increasing percentage of RA. This example can demonstrate that the different properties experimentally determined here for different mixes lead to significant differences in pavement design.

All the results not represented directly in these paragraphs are contained in the Appendix G at the end of this thesis.

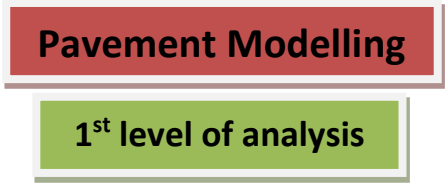

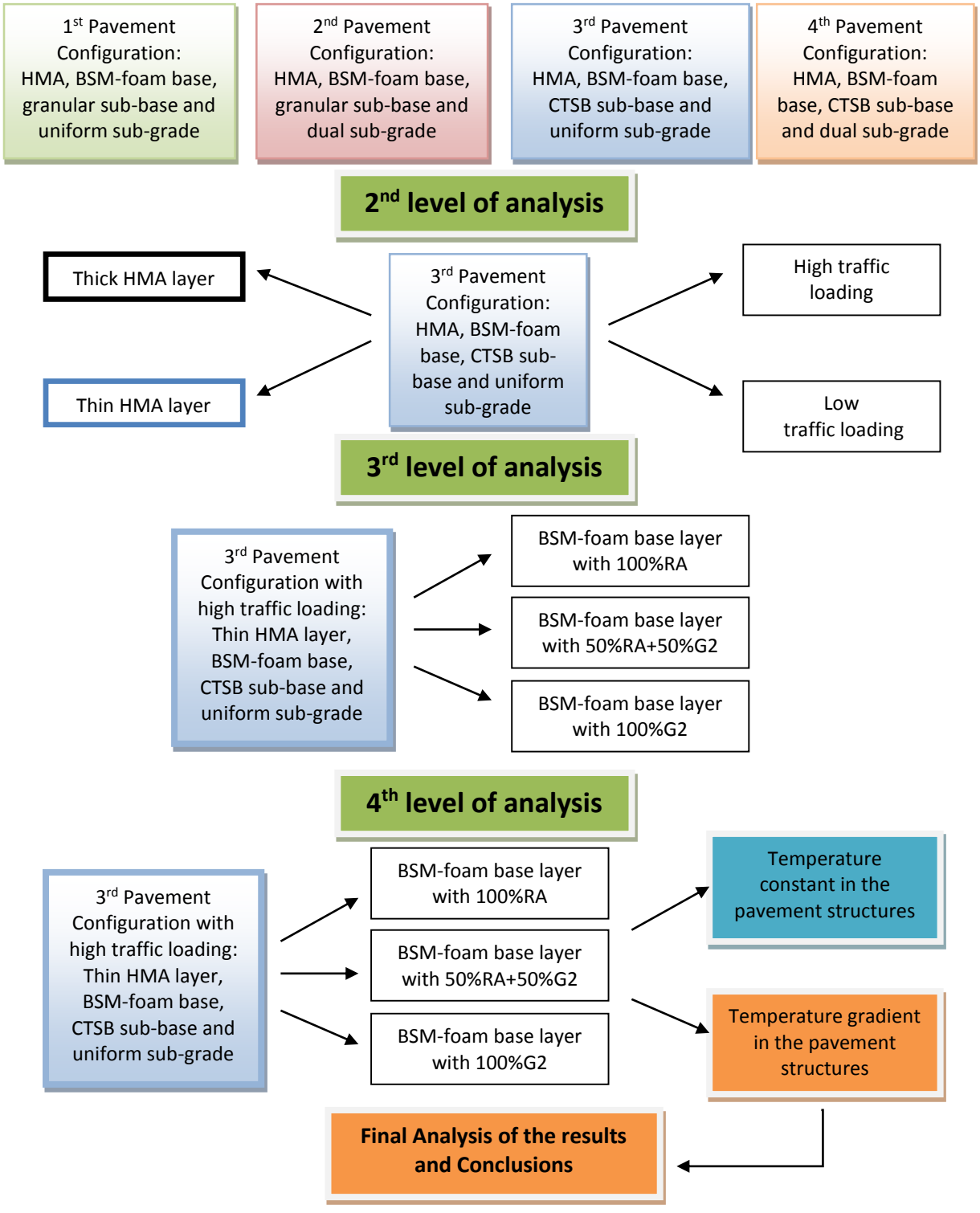

Figure 7.1 Flow diagram illustrating the pavement modelling explained in this chapter.

7.2 Comparison of BSM-foam pavement with CTSB sub-base and a uniform or dual sub-grade vs. BSM-foam pavement with granular sub-base and a uniform or dual sub-grade

Four pavement structures consisting of a constant thickness of BSM-foam layer and different sub-base and sub-grade layers are analysed. An axle load of 80 kN and tyre pressure of 800 kPa is applied on top of all the pavement structures. This load is modelled as a circular loading area with a radius of 143 mm and a uniform contact pressure equal to the tyre pressure. This is shown in Figure 7.2.

In view of the current traffic regime, this study's emphasis was focused on high traffic loading which is considered a major factor responsible for most pavement damage world-wide. The 2009 South African traffic statistics revealed that 35% of the 90 000 weighed heavy trucks were overloaded (De Beer, 2009). The decision to adopt a wheel load and a tyre pressure higher than the legal axle load in South Africa (45 kN) is well motivated by the latest research conducted by De Beer (2009) and Molenaar (2007).

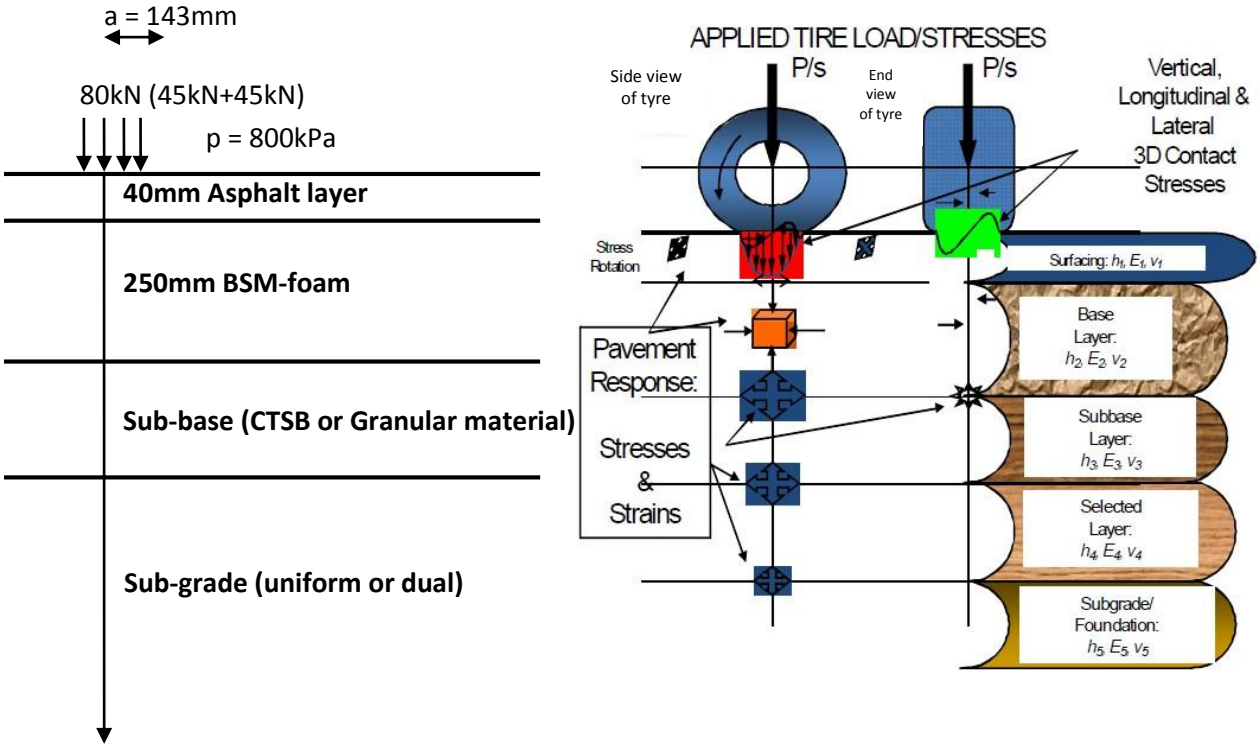

Figure 7.2: Loading configuration in the pavement section with a constant thickness of BSM-foam layer and different sub-base and sub-grade.

In terms of analysing the stresses in the two horizontal directions in the pavement structures, the analysis becomes symmetric by using a single wheel load instead of a dual wheel load. The dual wheel configuration is still widely in use in South Africa; however, modelling with a super single wheel load is easier because of the symmetry. When modelling with a dual wheel configuration one has to, for each layer, determine the critical horizontal position, i.e. under the centre of one wheel or in the middle between the two wheels. When using a super single the critical horizontal position is always under the centre of the wheel, which is to say when assuming a uniform contact pressure over the loading area. This assumption may also be made because non-uniform load distribution does not influence the stress condition deeper in the pavement, but only close to the surface. Using a super single wheel also leads to a slightly more

conservative estimate, because the stresses under single wheel loading are generally slightly higher than under dual wheel loading.

The asphalt thickness of 40 mm is typical for use in South Africa. The stiffness of 3000 MPa is taken from the range of values suggested by Jenkins (2000) in his research and presented in Appendix F. The thickness of 250 mm for the BSM-foam layer is a typical layer thickness often used *in situ* recycling operations in South Africa. The effect of varying the above assumed values is discussed further on in this chapter.

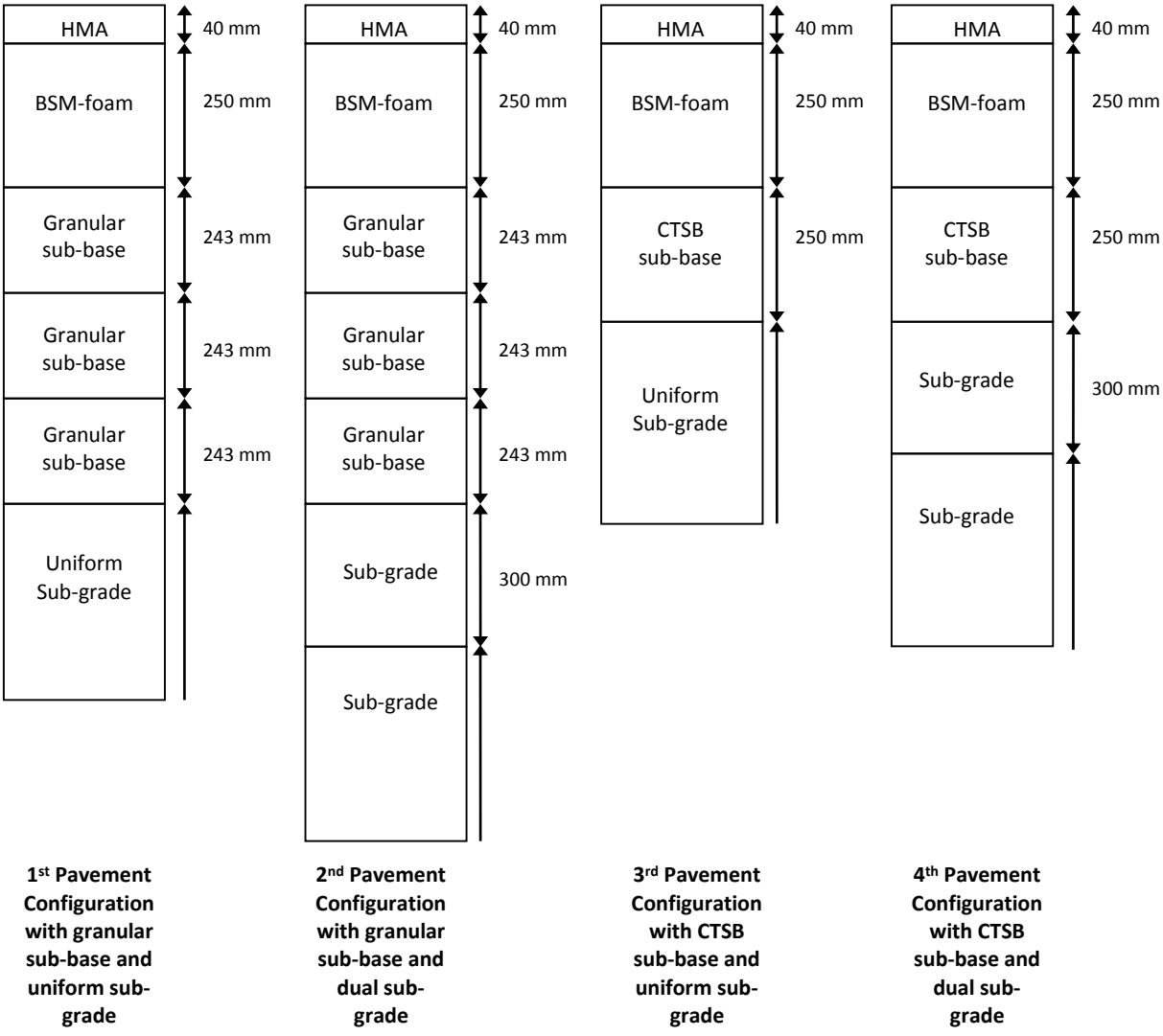

Figure 7.3: Comparative pavement structures comprising a BSM-foam layer, CTSB and granular sub-base and a uniform or dual sub-grade, used in BISAR analysis.

For reasons of simplicity it was chosen to model the BSM-foam layer with one stiffness value and to adopt a constant thickness and stiffness for the HMA top layer. The temperature distribution is assumed to be constant over all the pavement sections (25°C) as a reference system.

The pavement structures with their thickness and stiffness values assigned for each layer are compared in this part of the research and summarised in Figure 7.3 and Table 7.1.

Table 7.1: Material properties of layers analysed using BISAR 3.0 program.

1st Pavement Configuration

Layer	Material	Thickness (mm)	E (MPa)	Poisson's ratio (v)	Depth (mm)	Temperature (°C)
1	HMA	40	3000	0.35	0 to 40	25
2	BSM-foam	250	1000	0.35	40 to 290	25
3	Granular sub-base	243	350	0.35	290 to 533	25
4	Granular sub-base	243	225	0.35	533 to 776	25
5	Granular sub-base	243	150	0.35	776 to 1019	25
6	Uniform Sub-grade	∞	100	0.35	1019 to ∞	25

2nd Pavement Configuration

Layer	Material	Thickness (mm)	E (MPa)	Poisson's ratio (v)	Depth (mm)	Temperature (°C)
1	HMA	40	3000	0.35	0 to 40	25
2	BSM-foam	250	1000	0.35	40 to 290	25
3	Granular sub-base	243	350	0.35	290 to 533	25
4	Granular sub-base	243	225	0.35	533 to 776	25
5	Granular sub-base	243	150	0.35	776 to 1019	25
6	Dual Sub-grade	300	120	0.35	1019 to 1319	25
7		∞	50	0.35	1319 to ∞	25

3rd Pavement Configuration

Layer	Material	Thickness (mm)	E (MPa)	Poisson's ratio (v)	Depth (mm)	Temperature (°C)

1	HMA	40	3000	0.35	0 to 40	25
2	BSM-foam	250	1000	0.35	40 to 290	25
3	CTSB sub-base	250	1500	0.35	290 to 540	25
4	Uniform Sub-grade	∞	100	0.35	540 to ∞	25

4th Pavement Configuration

Layer	Material	Thickness (mm)	E (MPa)	Poisson's ratio (v)	Depth (mm)	Temperature (°C)
1	HMA	40	3000	0.35	0 to 40	25
2	BSM-foam	250	1000	0.35	40 to 290	25
3	CTSB sub-base	250	1500	0.35	290 to 540	25
4	Dual Sub-grade	300	120	0.35	540 to 840	25
5		∞	50	0.35	840 to ∞	25

7.2.1 Comparison of stress distribution and deviator stress with depth

The calculated stress distributions σ_1 and σ_3 in the first and second pavement structures with a granular sub-base and a uniform or dual sub-grade is represented in Figure 7.4.

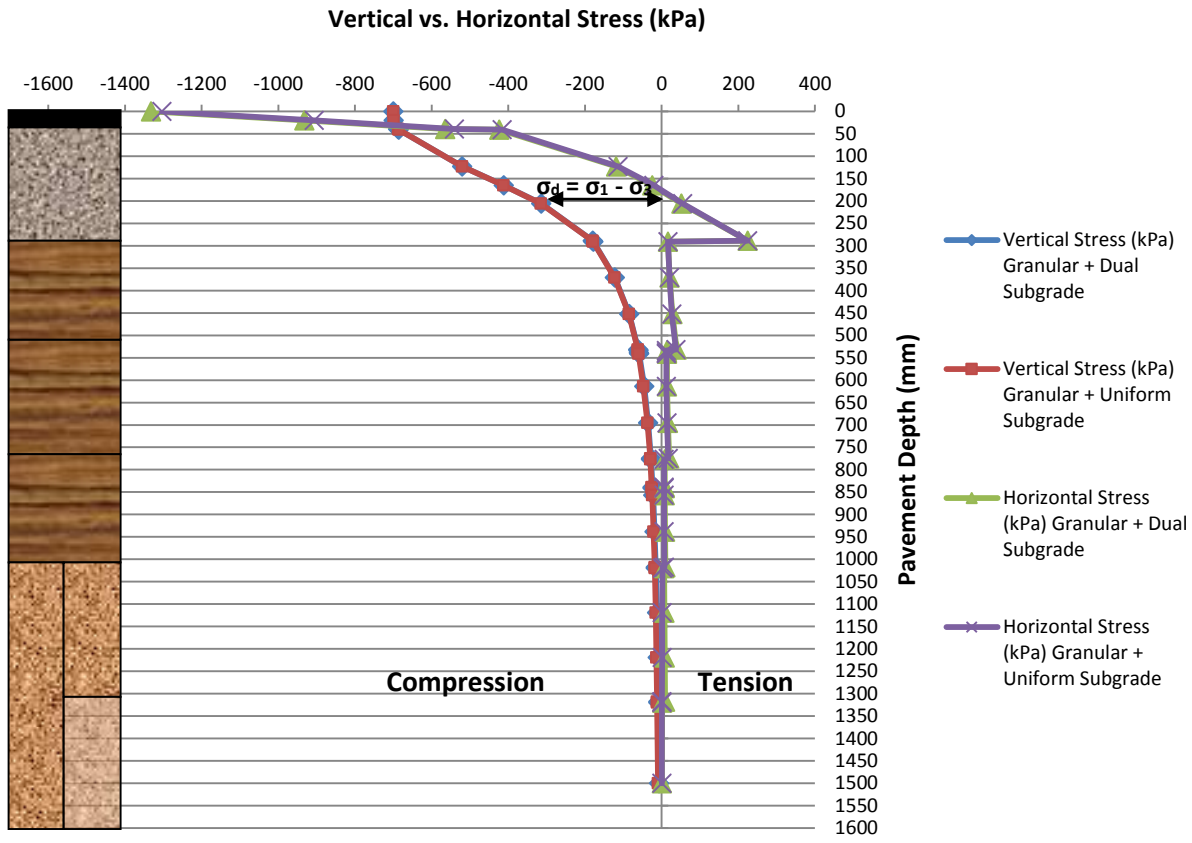

Figure 7.4: Comparison of vertical and horizontal stress distribution in BSM-foam pavement structure with granular sub-base and uniform or dual sub-grade.

The vertical stress σ_1 in Figure 7.4 shows no difference in distribution with a uniform or dual sub-grade. In addition, the influence of the vertical stress (wheel load) is minimal beyond the BSM-foam layer. This is an advantageous aspect of using BSMs as the load spreading layer. The uniform stress distributions between BSM-foam layer with a granular sub-base and a uniform or dual sub-grade indicates that the mix design of BSM-foam layer is beneficial for the durability behaviour and long-term performance of the pavement structure.

In Figure 7.4, the vertical and horizontal stresses are superimposed. The horizontal stress σ_3 distributions of the BSM-foam layer both with granular sub-base and uniform or dual sub-grade shift from compression (top) to tension (bottom). The two pavement configurations with a uniform and dual sub-grade show the same vertical and horizontal stress distribution. The horizontal stress maintains values close to zero in the granular sub-base layers and in the uniform and dual sub-grade layers.

The changes in horizontal stress from compression to tension (200 kPa) represent a significant shift compared with granular materials. Althought it can results in a minimum shift to tension if it is compared with HMA material. It should be noted that in any elastic multi-layer program, significant tensile stresses are calculated. The Mr - θ model used to predict the stiffness of a BSM-foam layer was developed from granular materials. Granular materials cannot take any

significant tension as coarse grained materials have very low cohesion. Therefore, in order to avoid a negative bulk stress θ and subsequently imaginary predicted Mr values, the stress as calculated by the elastic multi-layer program needs to be modified. That means that tensile horizontal stress σ_3 are set to 0 while maintaining the same deviator stress σ_d. In doing so, the major principal stress σ_1 can be shifted further into compression. This type of adjustment by shifting principal stress is also adopted in the SAMDM (Theyse *et al.*, 1996). Ebels (2008) comments that when shifting is not performed, the Mr - θ cannot be used because there is no solution for θ^{k2} when $\theta < 0$ and $k_2 < 1$. When a negative bulk stress exists, it means Mr < 0 at the bottom of the layer, which is highly improbable for these materials. Alternatively, when the bulk stress is very low and the horizontal stress is in tension (not shifted), this leads to unrealistically low Mr values, which are not expected to occur in the BSM-foam layer.

In Figure 7.5 the pavement structure with a CTSB sub-base (phase I) and a uniform and dual sub-grade is represented. The horizontal and vertical stress distributions with the two different sub-grades completely match one another. The horizontal stress in the CTSB layer shifts from compression (top) to tension (bottom), while the BSM-foam layer remains completely in the compression area.

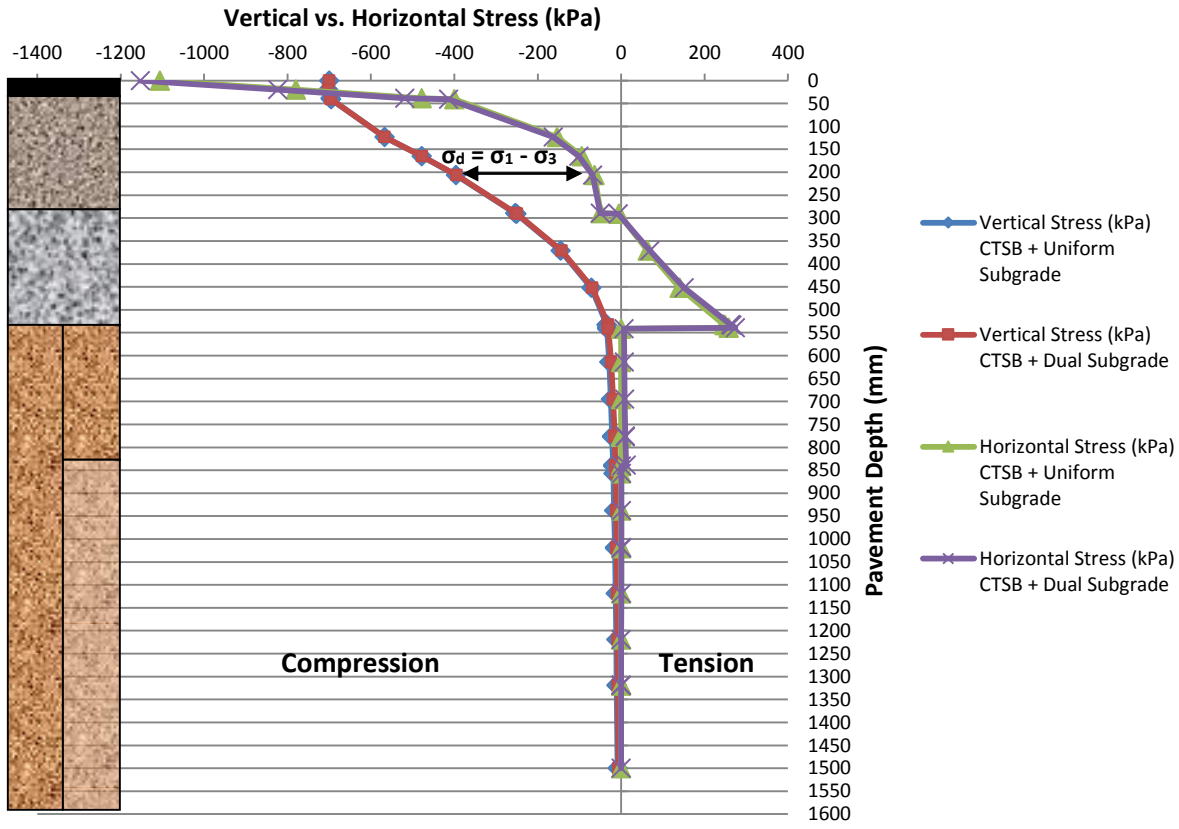

Figure 7.5: Comparison of vertical and horizontal stress distribution in BSM-foam pavement structure with CTSB sub-base and uniform or dual sub-grade.

A comparison of the two pavement structures with a different sub-base and sub-grade is placed in Figures 7.6 and 7.7. The deviator stress distribution ($\sigma_d = \sigma_1 - \sigma_3$) calculated for each

pavement section reveals a lower deviator stress distribution in the BSM-foam layer with a CTSB sub-base, while the CTSB shows higher values at the bottom of its layer. In the granular sub-base configuration the BSM-foam layer has a different vertical vs. horizontal stress distribution, the difference is small at the top and big deeper in the layer. This shows that the BSM-foam can experience possible higher permanent deformation at the bottom subsection compared to a similar BSM-foam layer with a CTSB sub-base. This is due to lower stress at the top layer compared to deeper in the layer, as indicated in Figure 7.6 as well as lower Mr values. Similar behaviour was observed during some testing conducted by Twagira (2010). The increased difference in the vertical vs. horizontal stress at the bottom of the BSM-foam layer indicates that the deviator stress distribution in the two pavement configurations is higher in the underlying layer.

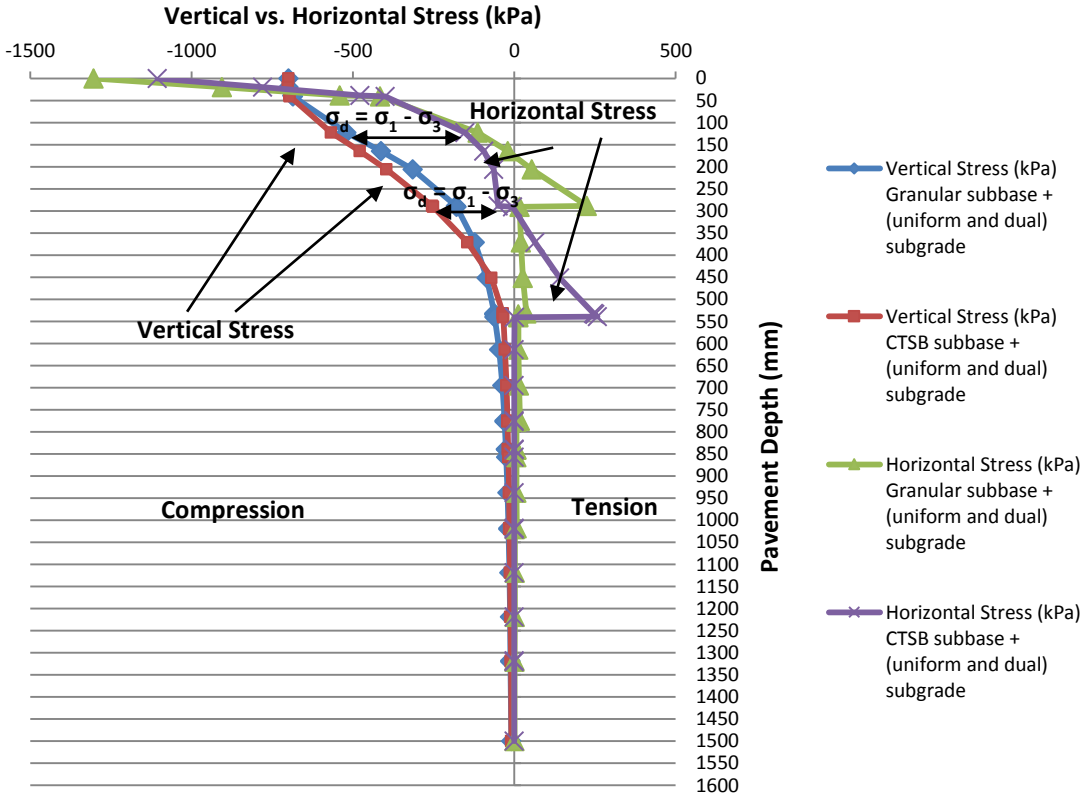

Figure 7.6: Comparison of vertical and horizontal stress distribution in BSM-foam pavement structure with CTSB sub-base, granular sub-base and uniform or dual sub-grade.

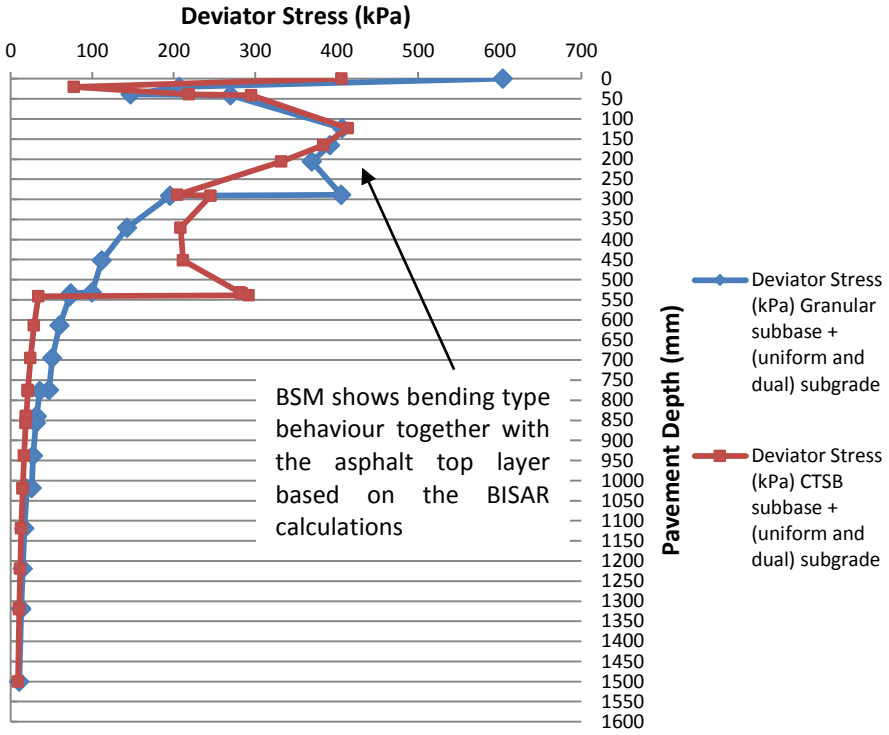

Figure 7.7: Comparison of the deviator stress distribution in the two pavement configurations with a CTSB sub-base and a granular sub-base and a uniform or dual sub-grade.

7.3 Comparison of BSM-foam pavement with CTSB sub-base under low and high loading conditions

Overloading is becoming a serious problem in almost every developing country. Two problems however are quite often overlooked, namely the very high wheel loads and very high tyre pressures that regularly occur. Axle load surveys that were performed in a country in West Africa in the early 1990's showed e.g. that especially the axle loads of timber trucks were very unequally divided over the wheels on either side of the axle (Kumapley and Molenaar, 1996). Of an axle load of 124kN in a dual wheel bogie, 32,5% was carried by the left of the axle and 67,5% by the right. Of the load on the right hand side of the dual wheel bogie, 95% was carried by the inner wheel and 5% by the outer wheel. This was caused by the fact that a tyre with a smaller diameter was placed on the outer wheel. All in all this meant that an axle load of 80 kN occurred. Given the fact that the legal axle load limit was 100 kN (so 25 kN per wheel assuming a dual wheel on either side of the axle), this 80 kN was producing approximately 105 times more damage than one would expect. Based on the axle loads however one would expect only 2.4 times more damage due to the 124 kN axle compared to the legal limit axle load of 100 kN. From this simple example it is clear that only axle load enforcement is not enough.

Another important issue is the tyre pressure. The contact pressure underneath a tyre is related to the tyre pressure and therefore tyre pressures should be limited to reasonable levels. The same study in West Africa revealed that the average pressure in the tyres of the wheels of the towed axles was approximately 850 kPa while the highest measured value was 980 kPa

(Kumapley and Molenaar 1996). The standard deviation was approximately 52 kPa. Pressures measured in the tyres of the wheels of the drive axle however showed an average value of approximately 780 kPa while the maximum values measured amounted 1015 kPa. In several studies, conducted by De Beer *et al*. (2004) and continued by De Beer in 2009, a detailed evaluation of the effects of the increasing loading conditions showed a shift of the vertical loading on the major South African highways from 80 kN to 100 kN.

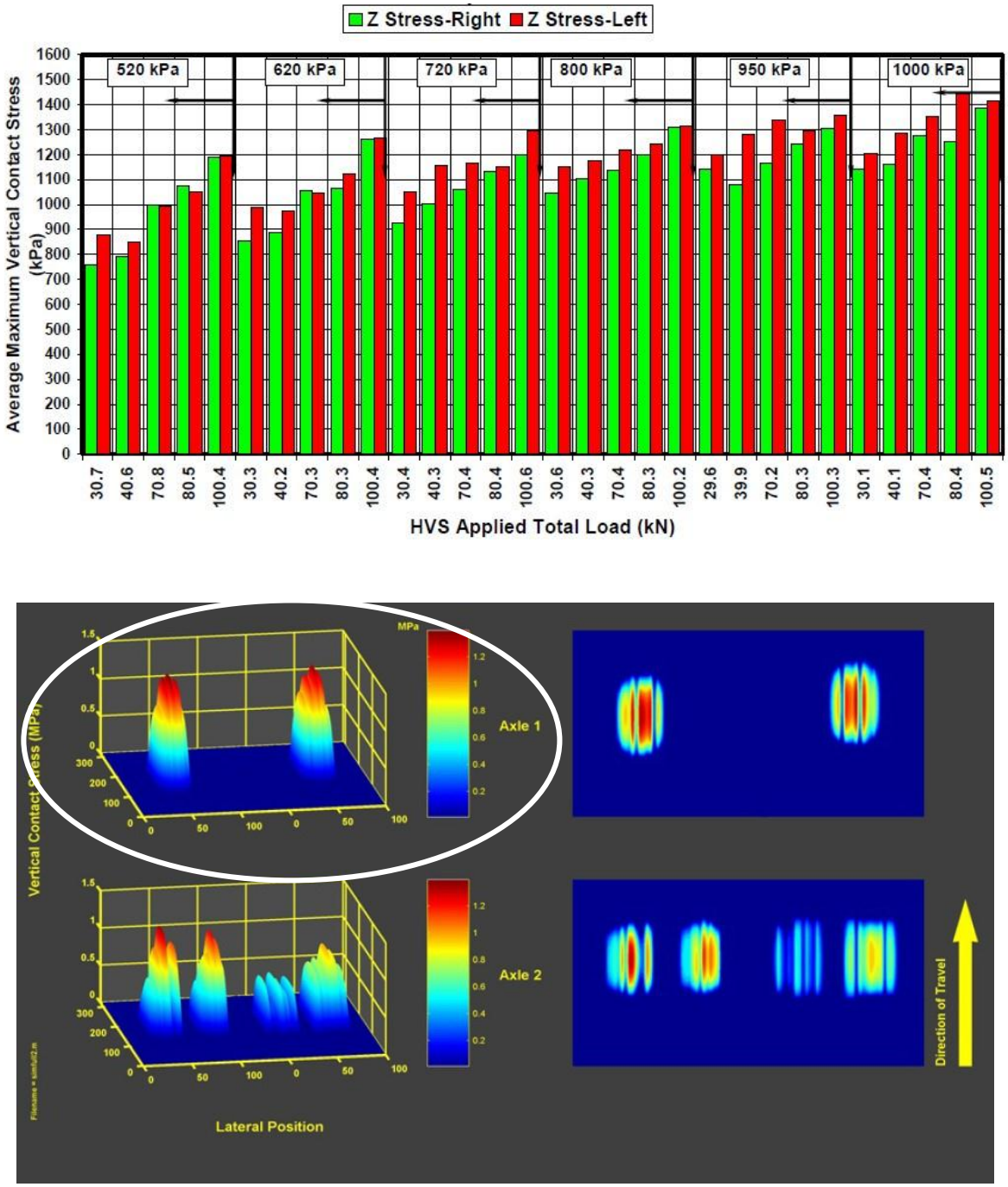

Figure 7.8: Typical tyre "fingerprint" of the vertical contact stress measured on the N3 in South Africa (De Beer, 2009).

The typical tyre inflation pressures of South African trucks travelling on this very important and heavily trafficked route (N3) found by De Beer (2009) are shown in Figure 7.9. The inflation pressures are normally distributed, and typically range between 400 kPa and 1 100 kPa. The inflation pressures of both tyres on the steering axles were approximately 100 kPa higher than those of the rest of the tyres measured.

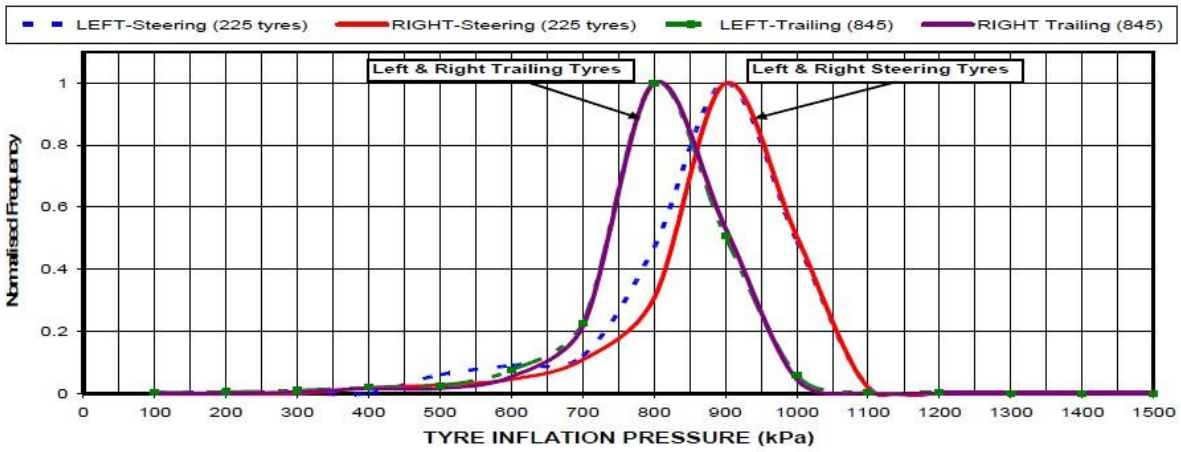

Figure 7.9: Tyre inflation pressures typically found on the N3 in South Africa (De Beer, 2009).

It will be no surprise that the combination of high wheel loads and high contact pressures is devastating for the surface layer as well as for the pavement structure as a whole.

Based on the increasing trend of truck tyre inflation pressures found in South Africa, two different combinations of loading conditions are applied on the top of the pavement structure:

- 80 kN, 700 kPa
- 100 kN, 1000 kPa

The pavement structure which is analysed with these loading combinations is represented in Figure 7.10. The mechanical properties of each layer are described in Table 7.2. The pavement structures are always analysed considering full friction between all the layers.

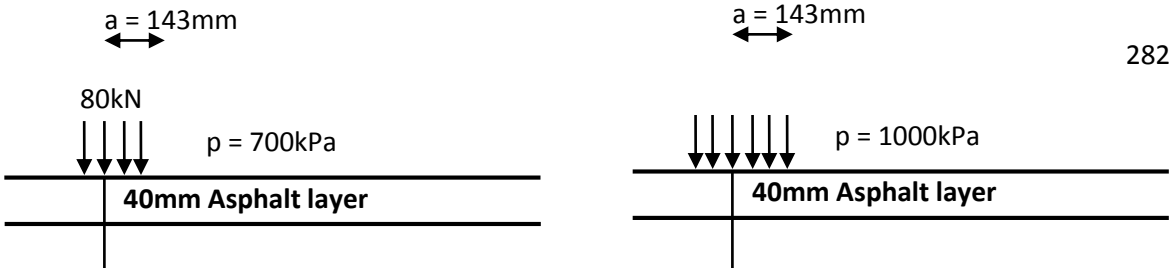

Figure 7.10: Comparative pavement structures with a different loading configuration, used in BISAR analysis.

Table 7.2: Material properties of layers analysed using BISAR 3.0 program.

Layer	Material	Thickness (mm)	E (MPa)	Poisson's ratio (ν)	Depth (mm)	Temperature (°C)
1	HMA	40	3000	0.35	0 to 40	25
2	BSM-foam	250	1000	0.35	40 to 290	25
3	CTSB sub-base	250	1500	0.35	290 to 540	25
4	Uniform Sub-grade	∞	100	0.35	540 to ∞	25

7.3.1 Comparison of stress distribution and deviator stress with depth

Figure 7.11 shows a simultaneous change in both axle loading and tyre pressure for a selected pavement with a BSM-foam base, a CTSB sub-base and a uniform sub-grade. As expected, horizontal and vertical stresses substantially increase as the traffic loading increases (Figure 7.11). This is the normal pavement response to loading, and implies more pavement damage as evident from the deviator stress analysis (Figure 7.12) and from the representation of the displacement in the pavement depth (Figure 7.13). The highest deviator stress values (Figure

7.12) are visible in the BSM-foam layer for 100 kN - 1000 kPa traffic loading compared to 80 kN – 700 kPa.

As the loading and pressure increase on the pavement, higher displacements are recorded in pavement structure, which could lead to higher permanent deformations.

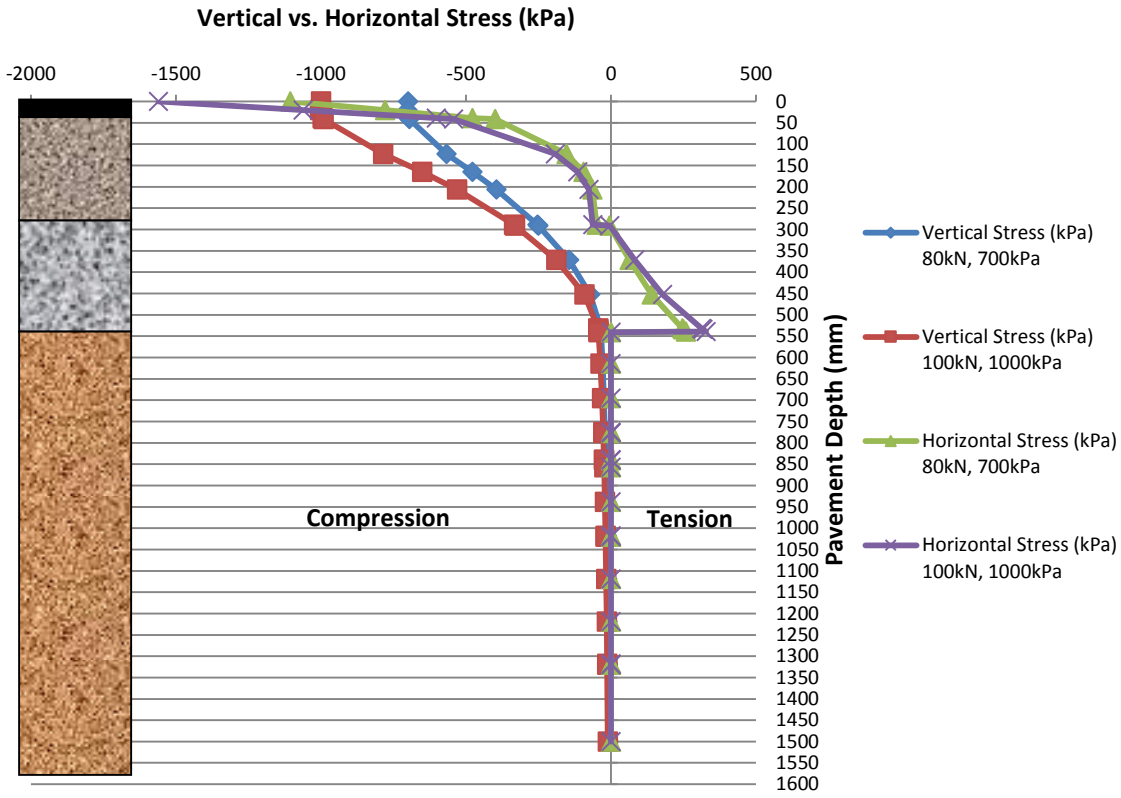

Figure 7.11: Comparison of vertical and horizontal stress distribution in BSM-foam pavement structure with two different loading configurations.

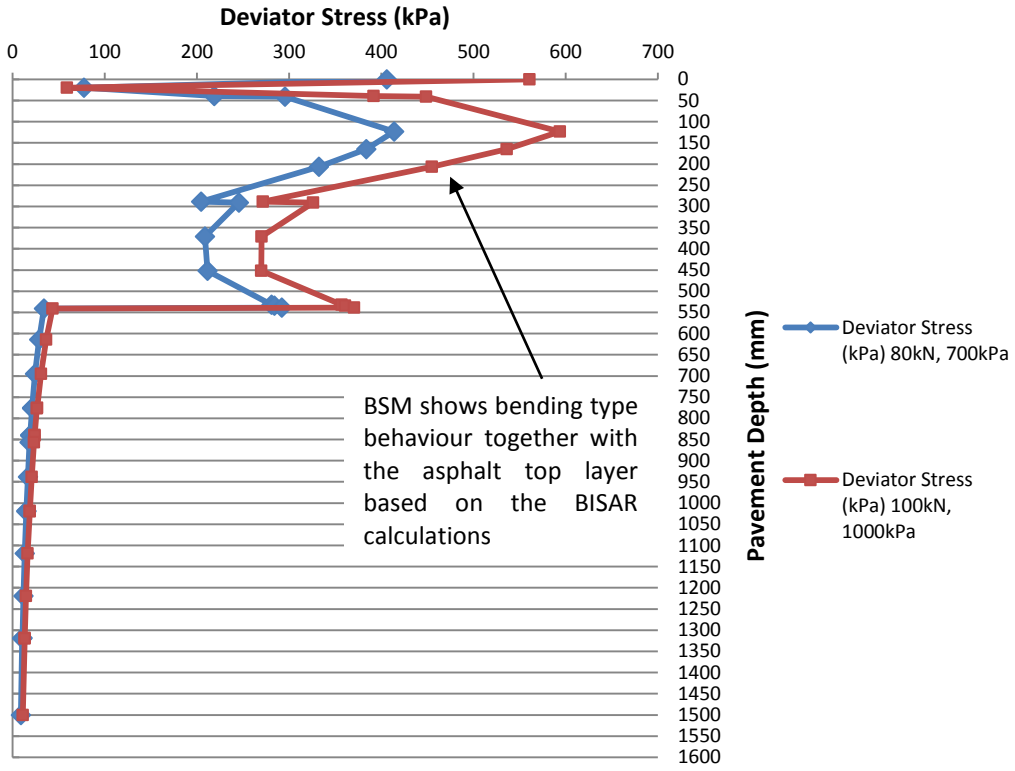

Figure 7.12: Comparison of the deviator stress distribution in the two loading configurations.

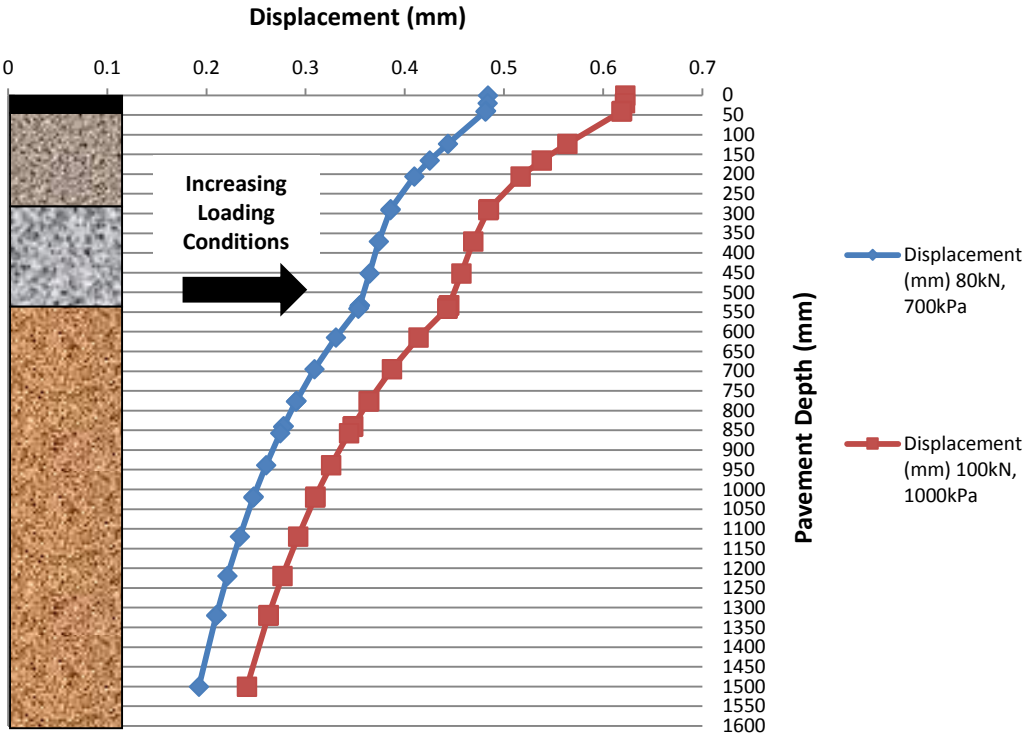

Figure 7.13: Comparison of the displacement distribution in the pavement sections in the two loading configurations.

7.4 Comparison of BSM-foam pavement with the variation of the asphalt-surfacing layer thickness

To better understand the possible mechanical influence of traffic loading on the BSM-foam layer, the surfacing layer of HMA is altered from 40 mm to 100 mm. The traffic loading remains constant at 80 kN and 700 kPa. The pavement structure analysed in this part of the research is represented in Figure 7.14 and Table 7.3.

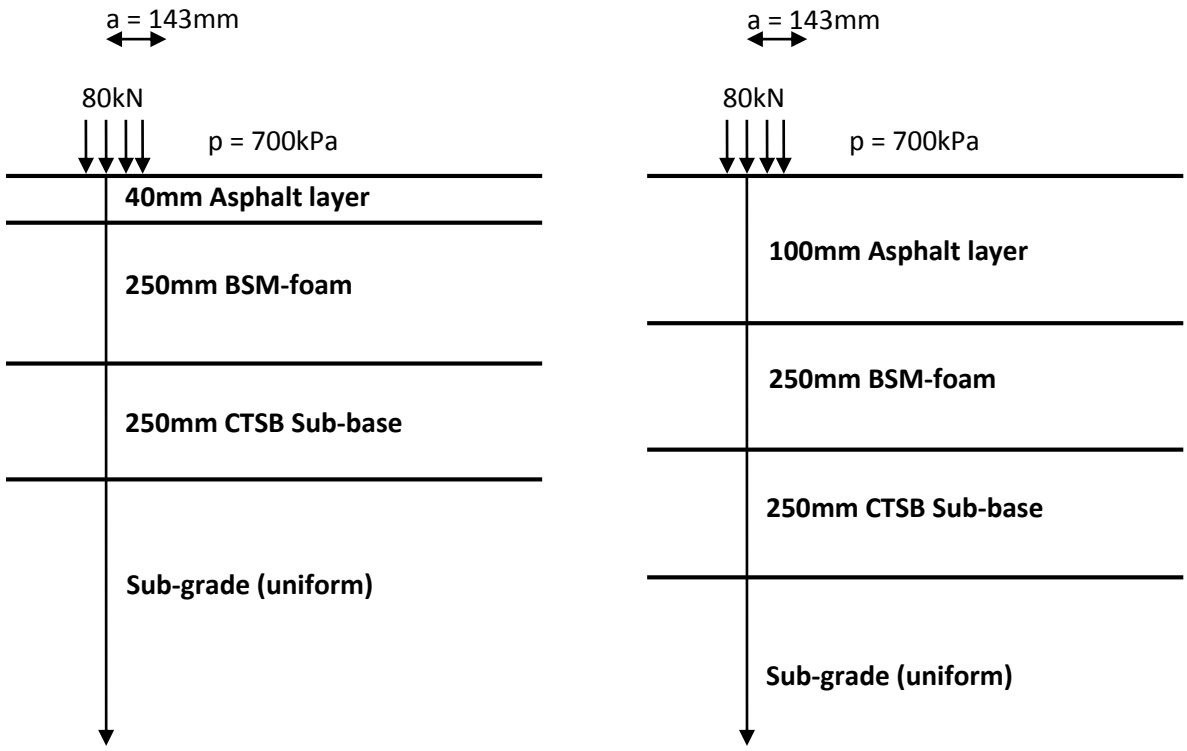

Figure 7.14: Comparative pavement structures with a different asphalt surfacing thickness, used in BISAR analysis.

Table 7.3: Material properties of layers analysed using BISAR 3.0 program.

1st Pavement Configuration

Layer	Material	Thickness (mm)	E (MPa)	Poisson's ratio (ν)	Depth (mm)	Temperature (°C)
1	HMA	40	3000	0.35	0 to 40	25
2	BSM-foam	250	1000	0.35	40 to 290	25
3	CTSB sub-base	250	1500	0.35	290 to 540	25
4	Uniform Sub-grade	∞	100	0.35	540 to ∞	25

2nd Pavement Configuration

Layer	Material	Thickness (mm)	E (MPa)	Poisson's ratio (ν)	Depth (mm)	Temperature (°C)
1	HMA	100	3000	0.35	0 to 100	25
2	BSM-foam	250	1000	0.35	100 to 350	25
3	CTSB sub-base	250	1500	0.35	350 to 600	25
4	Uniform Sub-grade	∞	100	0.35	600 to ∞	25

7.4.1 Comparison of stress distribution and deviator stress with depth

The calculated vertical and horizontal stress distribution are represented in Figure 7.15. The vertical stress σ_1 shows no particular difference in distribution with a different asphalt thickness. However, the horizontal stress changes drastically at the bottom of the HMA as the layer thickness increases. In fact the pavement section with 40 mm asphalt is completely in the compression area, while the 100 mm asphalt layer is in tension. This difference can probably create some problems of fatigue on the top of the pavement. In both the pavement configurations the BSM-foam layers show similar compression behaviour.

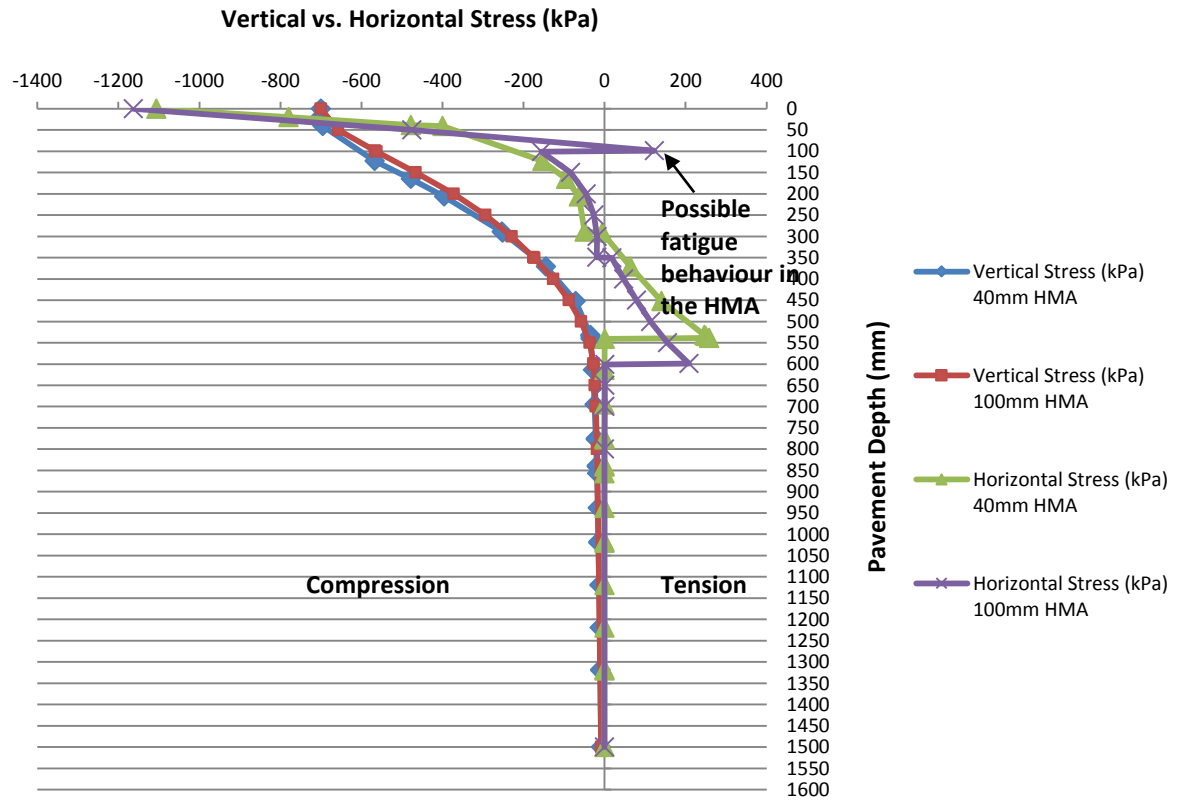

Figure 7.15: Comparison of vertical and horizontal stress distribution in BSM-foam pavement structure with two different asphalt layer thicknesses.

The horizontal stress in the CTSB in the two pavement sections differs. The horizontal stress value at the bottom of the layer in the pavement with the thicker asphalt is higher.

The deviator stress distribution calculated from linear elastic behaviour of BSM-foam layer is represented in Figure 7.16. The deviator stress calculated in the pavement section with the thicker layer of HMA is almost twice as big at the bottom of the HMA layer, while the BSM-foam shows a similar stress distribution compared to the first pavement configuration with a HMA layer of 40 mm.

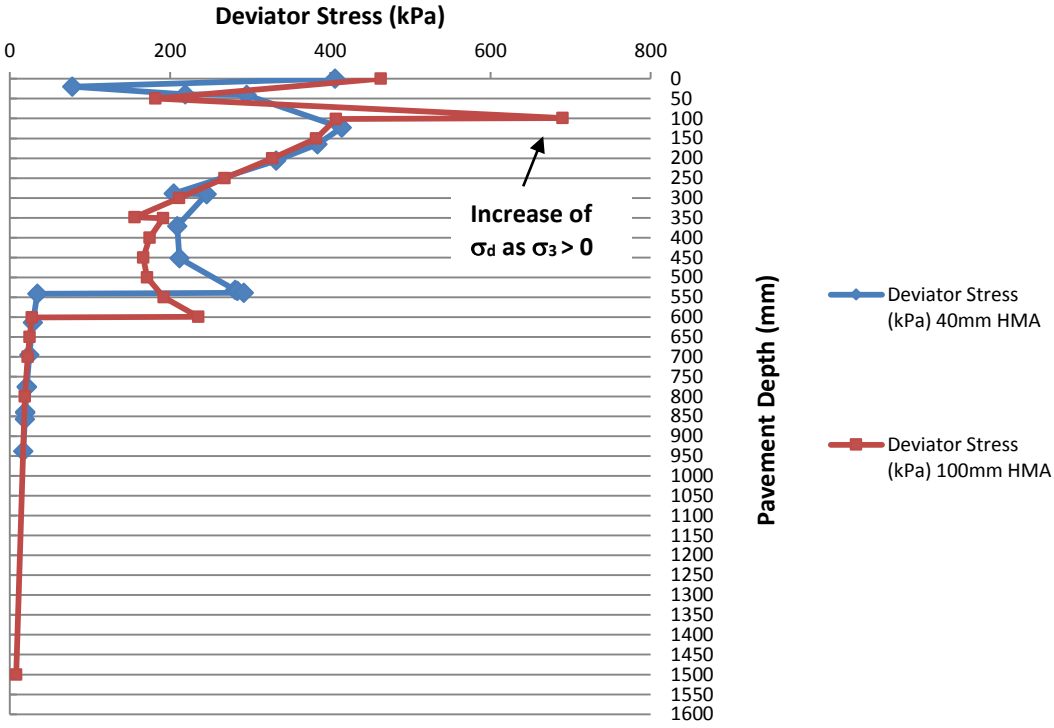

Figure 7.16: Comparison of the deviator stress distribution in the two pavement configurations with different HMA thickness.

7.5 Comparison of pavement sections with an increasing percentage of RA in the BSM-foam layer

The type of pavement structure selected for the analysis incorporates BSM-foam mixes with an increasing amount of RA as a base layer. The BSM-foam layers consist of:

- BSM-foam with 100%RA and with 2% of bitumen content;
- BSM-foam with 50%RA and 50%G2 material (Hornfels) and with 2.1% of bitumen content, and
- BSM-foam with 100%G2 (Hornfels) and with 2.3% of bitumen content.

The traffic loading consists of a super single of 100 kN and tyre pressure of 1000 kPa. The reason to adopt this kind of loading configuration is well described in numerous studies conducted by De Beer (2009) and De Beer *et al*. (2004).

The comparative pavement sections are represented in Figure 7.17 and the material properties in Table 7.4. The stiffness values selected for the BSM-foam layers come from the short dynamic tests described in Chapter 4. The stiffness of 3000 MPa for the HMA is taken from the range of values suggested by Jenkins (2000) in his research and presented in the Appendix F.

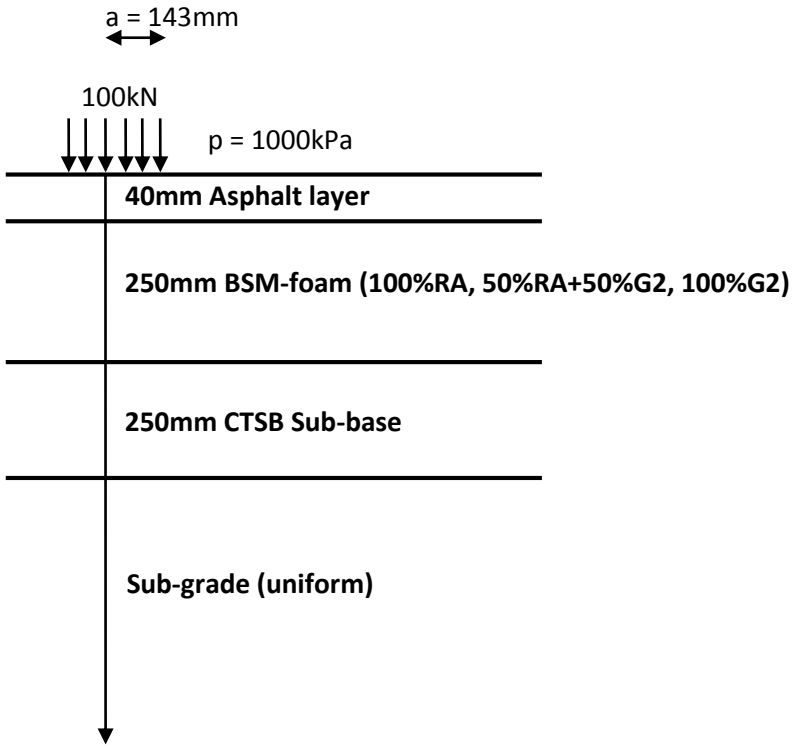

Figure 7.17: Comparative pavement structure with a BSM-foam layer with an increasing amount of RA, used in BISAR analysis.

Table 7.4: Material properties of layers analysed using BISAR 3.0 program.

1st Pavement Configuration

Layer	Material	Thickness (mm)	E (MPa)	Poisson's ratio (ν)	Depth (mm)	Temperature (°C)
1	HMA	40	3000	0.35	0 to 40	25
2	BSM-foam 100%RA	250	400	0.35	40 to 290	25
3	CTSB sub-base	250	1500	0.35	290 to 540	25
4	Uniform Sub-grade	∞	100	0.35	540 to ∞	25

2nd Pavement Configuration

Layer	Material	Thickness (mm)	E (MPa)	Poisson's ratio (v)	Depth (mm)	Temperature (°C)
1	HMA	40	3000	0.35	0 to 40	25
2	BSM-foam 50%RA+50%G2	250	600	0.35	40 to 290	25
3	CTSB sub-base	250	1500	0.35	290 to 540	25
4	Uniform Sub-grade	∞	100	0.35	540 to ∞	25

3rd Pavement Configuration

Layer	Material	Thickness (mm)	E (MPa)	Poisson's ratio (v)	Depth (mm)	Temperature (°C)
1	HMA	40	3000	0.35	0 to 40	25
2	BSM-foam 100%G2	250	1000	0.35	40 to 290	25
3	CTSB sub-base	250	1500	0.35	290 to 540	25
4	Uniform Sub-grade	∞	100	0.35	540 to ∞	25

7.5.1 Comparison of stress distribution with depth

The horizontal and vertical stress distributions are superimposed for all three pavement sections (Figure 7.18). The horizontal stress in the pavement configurations with an increasing amount of RA seems to shift from compression to tension at the bottom of the HMA layer. Similar behaviour is visible at the bottom of the BSM-foam layers; in fact a slight difference in the horizontal stress is calculated, almost moving the horizontal stress from compression to tension. The horizontal stress distribution in the CTSB layer seems to be equal in the middle and bottom part of the layer for all three pavement sections. The vertical stress shows no particular differences between the pavement configurations with an increasing percentage of RA.

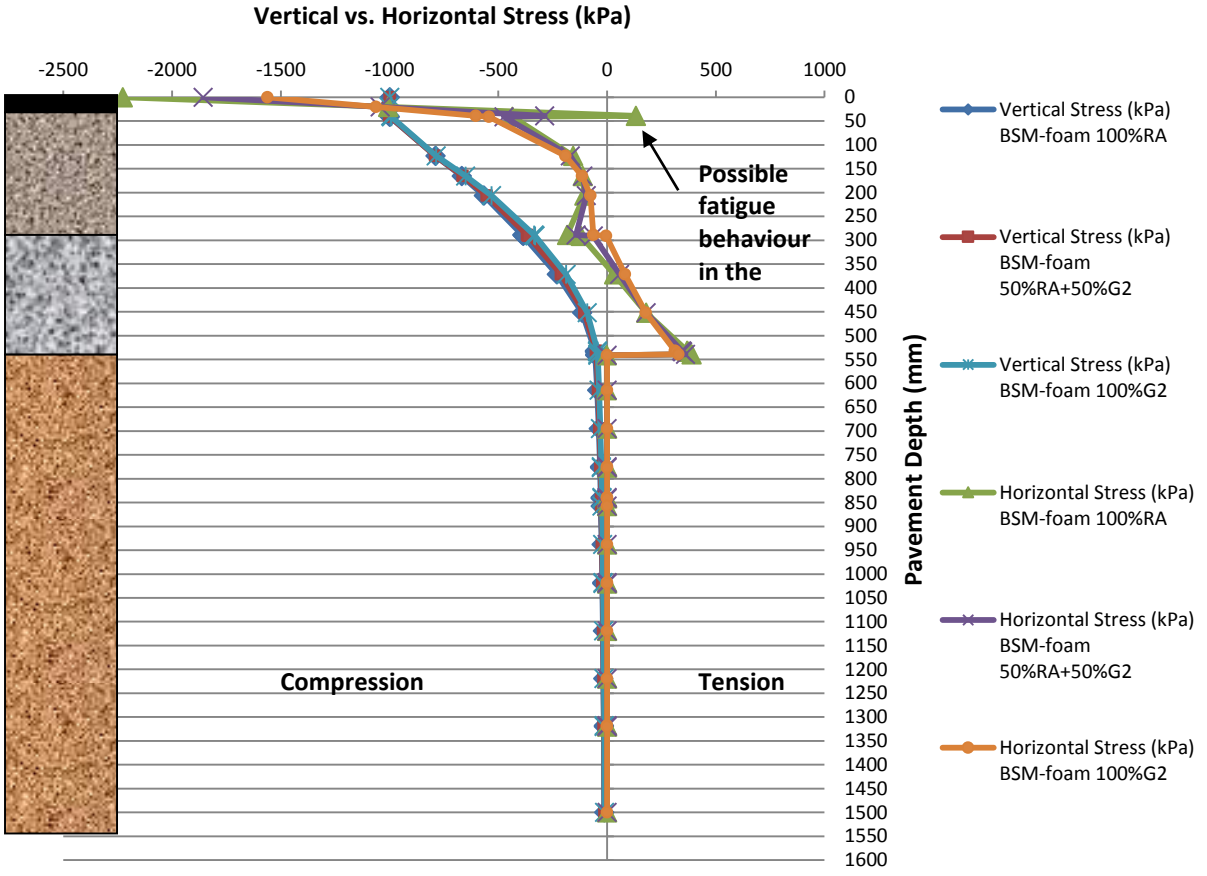

Figure 7.18: Comparison of vertical and horizontal stress distribution in pavement structures with BSM-foam base layer with an increasing percentage of RA.

7.5.2 Comparison of strain distribution with depth

From Figure 7.19 it can be seen that the vertical strain in BSM-foam layers is higher at the top than at the bottom. This strain distribution increases almost threefold at the top of the BSM layer if the percentage of RA reaches 100%. In addition, the vertical strain has a different distribution, namely big at the top and small deeper in the layer. This shows that BSM-foam with 100%RA can experience higher permanent deformation at the top subsection (1/3) compared to a similar material with 100%G2. This is due to higher stress at the top layer compared to deeper in the layer, as indicated in Figure 7.18. The decrease difference in the vertical strain at the bottom of the layer indicates that, either with a BSM-foam layer with 100%RA or 100%G2, there will be lower deformation of the underlying layer. Therefore, the selection of a lower percentage of RA (less than 50%) in the BSM layer can become important for the long-term performance of the pavement structure.

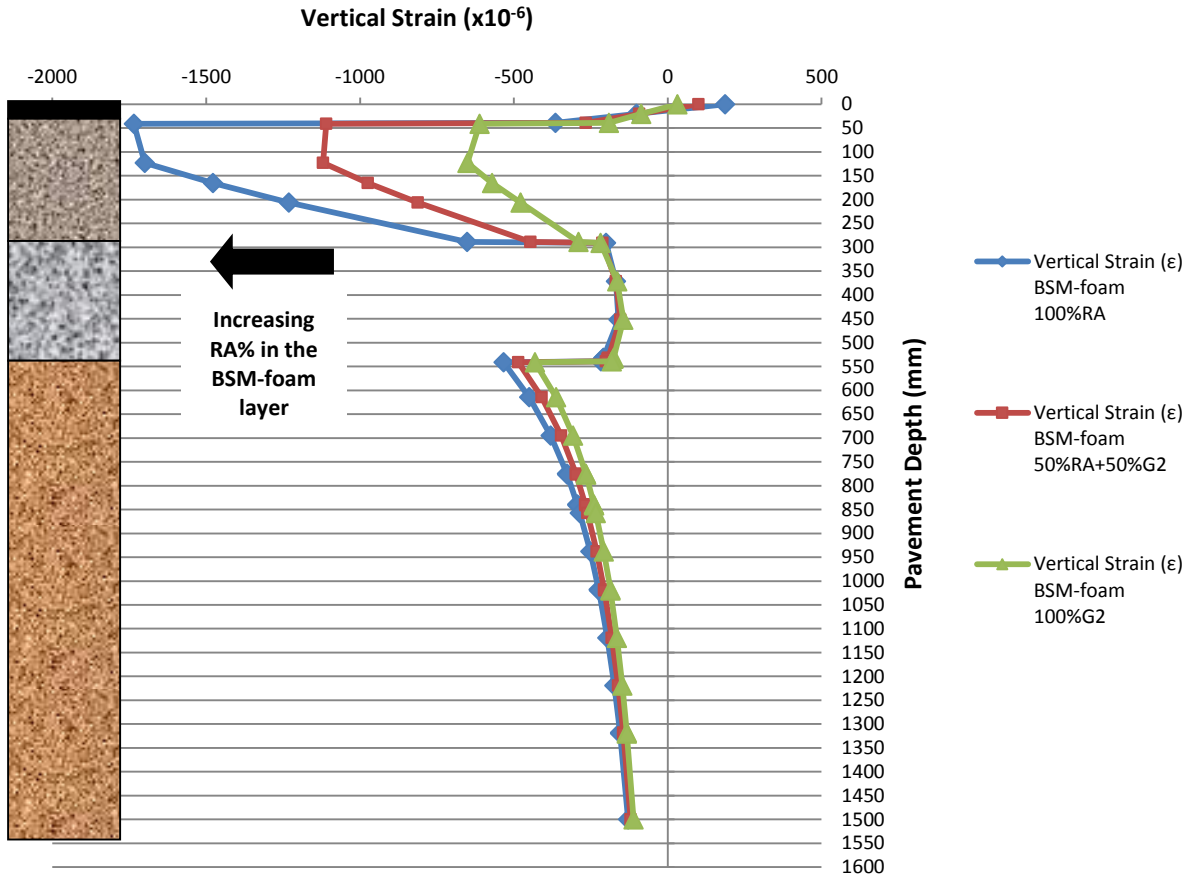

Figure 7.19: Comparison of vertical strain distribution in pavement structures with BSM-foam base layer with an increasing percentage of RA.

The horizontal strain distributions calculated from linear elastic behaviour of BSM-foam layer with an increasing amount of RA are represented in Figure 7.20. The horizontal strain varies from top to bottom, with the middle of the BSM-foam layer showing a higher strain level. It can also be seen that the horizontal strain of the BSM layer differs with the increasing amount of RA showing higher horizontal strain. Such magnitude of horizontal strain can result in fatigue failure in a long-term in-service condition, which is not a predominant failure mode for BSM-foam layers.

Figure 7.21 shows the displacement distribution in the pavement structures. As the percentage of RA increases, the displacement shifts to higher values at the top of the surface.

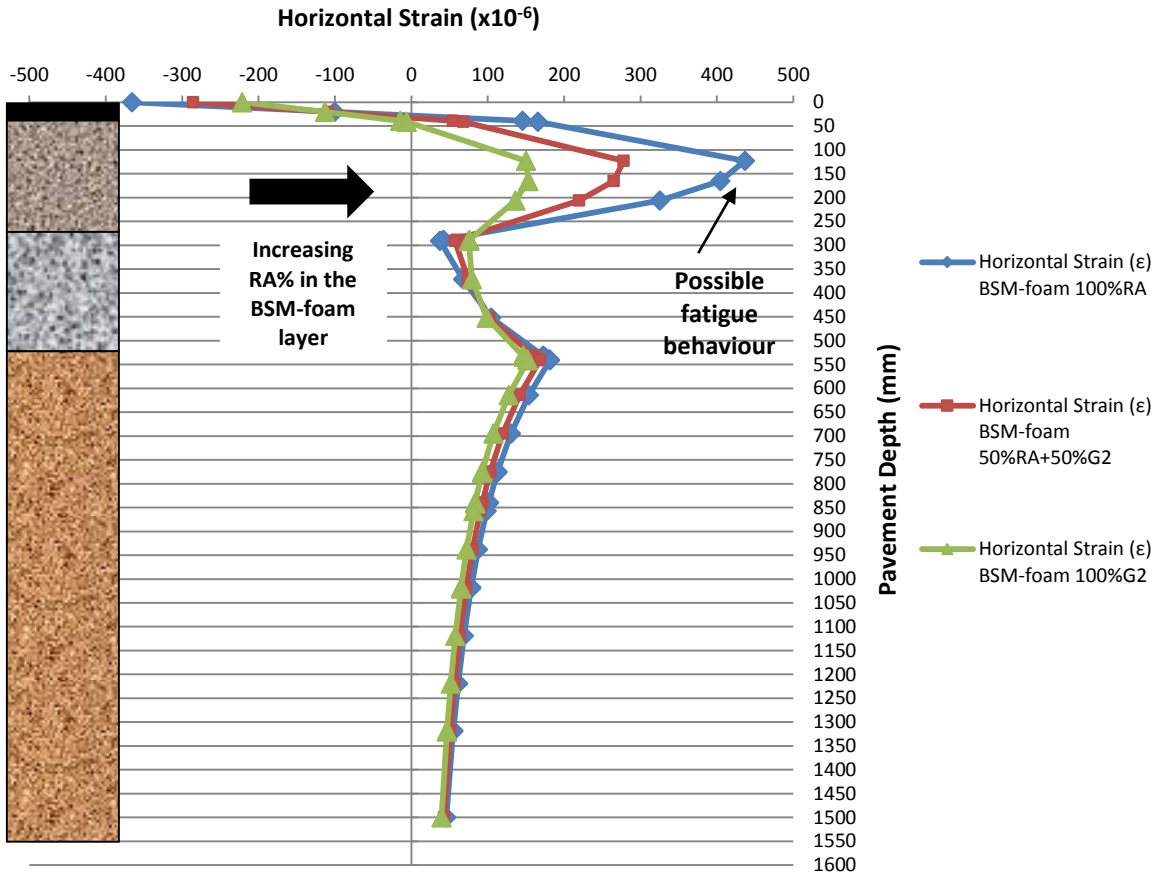

Figure 7.20: Comparison of horizontal strain distribution in pavement structures with BSM-foam base layer with an increasing percentage of RA.

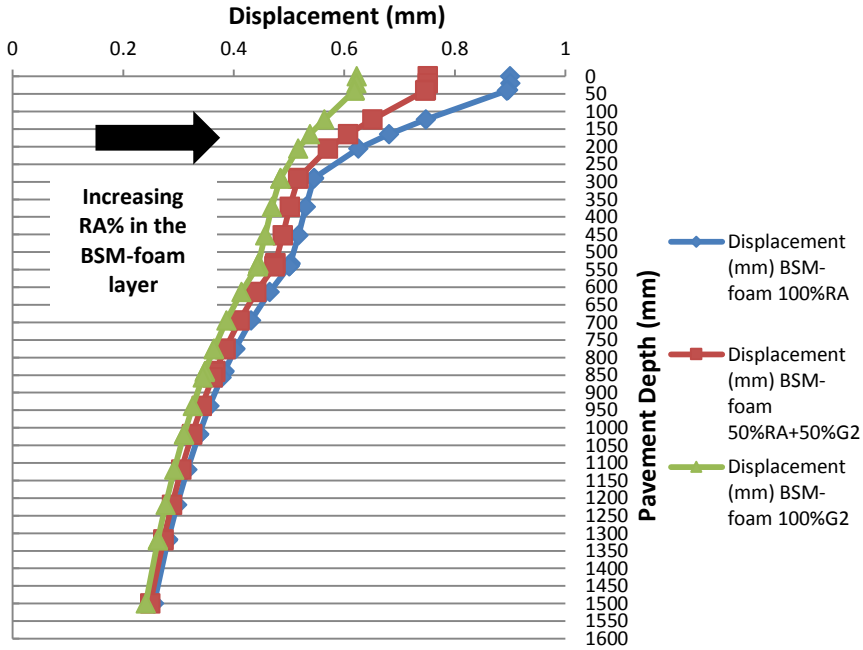

Figure 7.21: Comparison of displacement distribution in pavement structures with BSM-foam base layer with an increasing percentage of RA.

7.5.3 Comparison of deviator stress distribution with depth

BSM-foam with a high percentage of RA shows higher deviator stress at the top than in the BSM-foam layer with 100%G2 material. It can be seen from the deviator stress distribution that a critical deviator stress is calculated at the top where horizontal stress changed from compression to tension. The magnitude of the critical deviator stress for design purposes as well as the depth at which it occurs is therefore affected when the pavement is analysed using the linear elastic model. As the percentage of RA increases in the BSM-foam layer, the deviator stress at the top of the layer increases, while it decreases at the bottom.

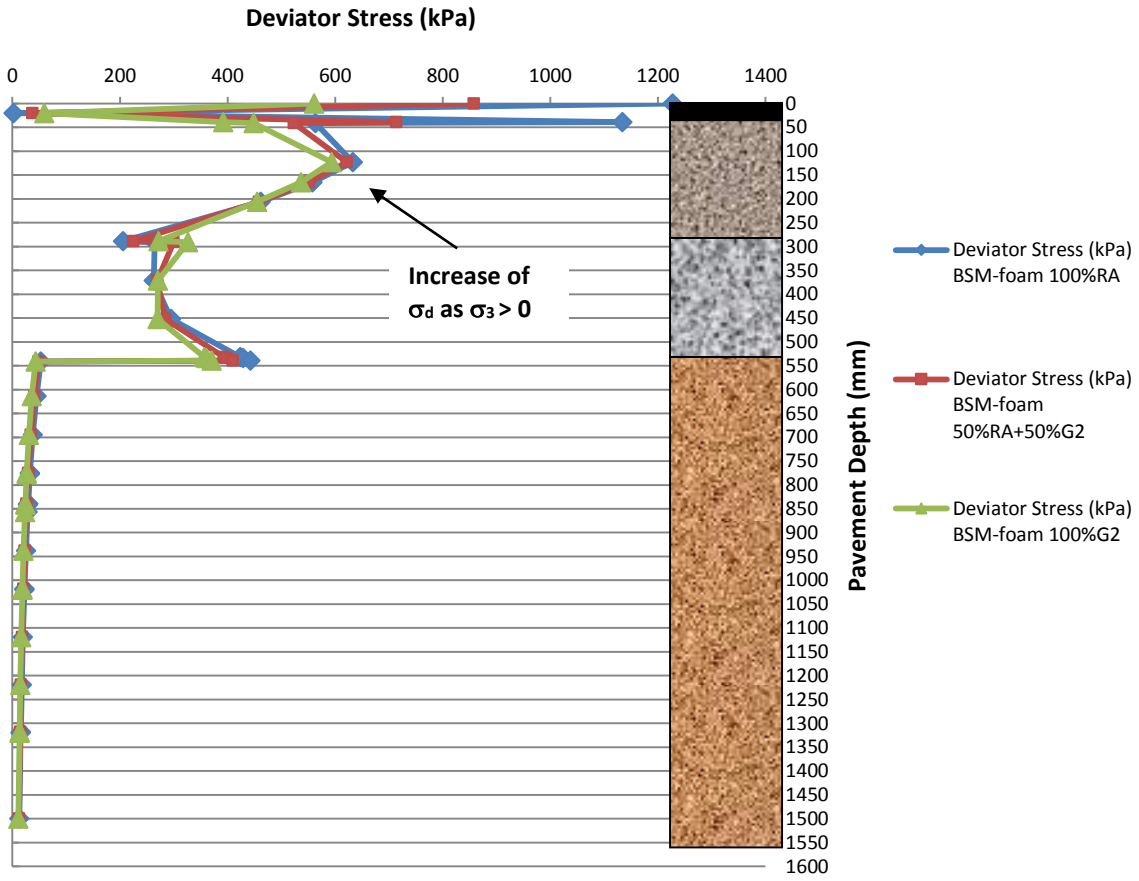

Figure 7.22: Comparison of deviator stress distribution in pavement structures with BSM-foam base layer with an increasing percentage of RA.

7.6 Intrinsic thermal characteristics of pavement sections with different BSM-foam mixes

A rise in temperature increases the viscous component of the visco-elasto-plastic behaviour, while a decrease in temperature increases the elastic component, increasing the material stiffness. The stiffness variation affects the stress, strains and displacements in BSMs pavements. This effect is even more important in regions with great temperature variations. In this case even the compression and tensile areas on the pavement can be changed. It is important to note that, in spite of the importance of the temperature effects in the behaviour of BSM mixes, there are still few research related to the thermo-visco-elasto-plastic analysis of pavements. A flexible pavement is analysed in order to assess the importance of temperature effects on the stress, strains and displacements in the structural behaviour of BSM-foam pavements.

The type of pavement structure selected for analysis incorporates BSM-foam mixes with an increasing amount of RA as a base layer. The BSM-foam layers consist of:

- BSM-foam with 100%RA and with 2% of bitumen content,
- BSM-foam with 50%RA and 50%G2 material (Hornfels) and with 2.1% of bitumen content, and
- BSM-foam with 100%G2 (Hornfels) and with 2.3% of bitumen content.

Three pavement structures, considering these three BSM-foam layers are analysed with a top layer of 40 mm of HMA. The full pavement structures are made with HMA, BSM-foam mixes, CTSB sub-base and a uniform sub-grade.

Temperature in the BSM-foam mixes is known to influence the following:
- evaporation of moisture present in the mixes;
- development of bonding between the binder and mineral aggregate surfaces;
- stiffening of the mastic, which in turn affects stiffness, shear properties, and ultimate strength of the mixes;
- equilibrium moisture content in the mixes and
- ultimate durability behaviour of the mixes and long-term performance.

BSMs are generally less susceptible to temperature variations (Jenkins, 2000; Loizos and Papavasiliou, 2007). However, depending on mix composition, e.g. higher binder content and RA content, temperature distribution in the layer may adversely influence the performance of BSMs. The heat transfer coefficient of the surface layer, i.e. thin HMA or seal, and its mix composition contribute to temperature distribution in BSMs. Jenkins and Twagira (2008) investigated the excess deformation that occurred in full-depth *in situ* recycled BSM-foam constructed in Saudi Arabia. The site inspection on the distressed area shows that during summer months the temperature distribution in the pavement layer ranged between 66°C on the top of the HMA (40 cm deep) and 47°C on the top of the BSM layer. Considering this study conducted directly in the field, the temperature simulated on the top of the pavement section is selected at 60°C.

To simulate the heat diffusion process, the thermal properties of the materials including the heat capacity and thermal conductivity are required. For dense asphalt mixtures (density of 2450 kg/m^3), the reported values of the heat capacity of 2254 kJ/m^{3}K and heat conductivity of

1.3 W/mK are used in this modelling (Turner and Malloy 1981, Luca and Mrawia 2005 and Wu *et al*. 2008).

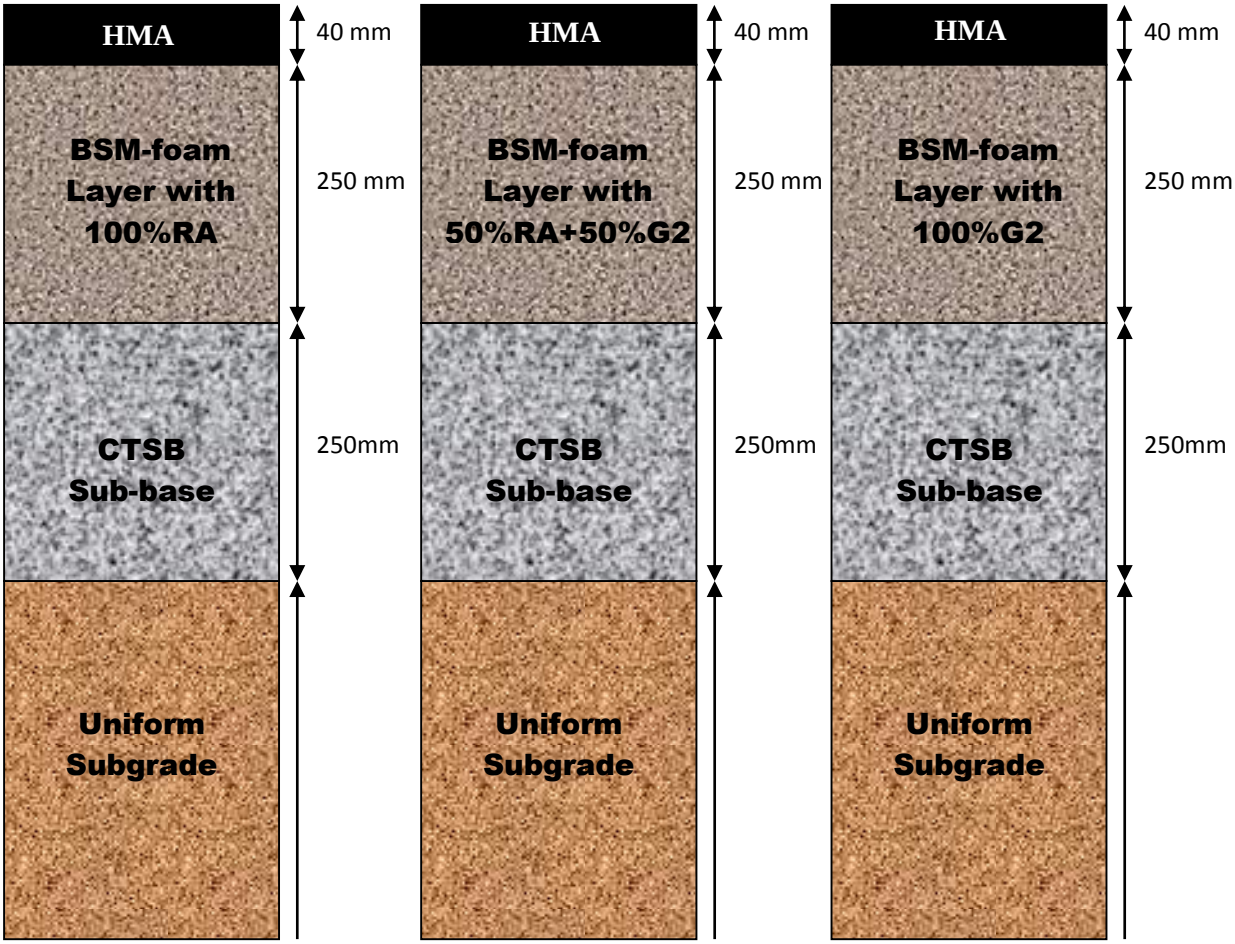

Figure 7.23: Thermal analysis of the three configurations of pavements.

For the three BSM-foam base layers, the thermal conductivity and the heat capacity are selected on the basis of the temperature distribution study presented in Chapter 6.

The thermal properties for the different layers of the three pavement configurations are summarized in Table 7.5.

Table 7.5: Heat capacity and thermal conductivity for the different layers of the pavement.

Layer	Heat Capacity (kJ/m^3K)	Thermal Conductivity (W/mK)
Hot Mix Asphalt	2254	1.3
BSM-foam with 100%RA (2% bitumen content)	1750	0.8
BSM-foam with 50%RA and 50%G2 material (2.1% bitumen content)	1775	0.7
BSM-foam with 100%G2 (2.3% bitumen content)	1800	0.6
CTSB Sub-base	1650	1.1
Gravel sub-grade	1473	0.5

7.6.1 Thermal transfer within the pavement

In order to predict the temperature distribution in the pavement, after induction heating, a numerical simulation of the thermal transfer in the two trial sections was carried out in this paragraph. To study the thermal transfer process in the pavements after induction heating, the temperature profiles at different layers of the pavement during the 12 hours are plotted in Figure 7.24, 7.25 and 7.26. The idea to extend the prediction of the temperature in a pavement constituted by a surface layer of HMA and a BSM-foam layer is referred to the 12 hours of daylight.

In Figures 7.24, 7.25 and 7.26 the temperature gradient in a pavement structure with a top layer of 40 mm of HMA for all three BSM-foam mixes is represented.

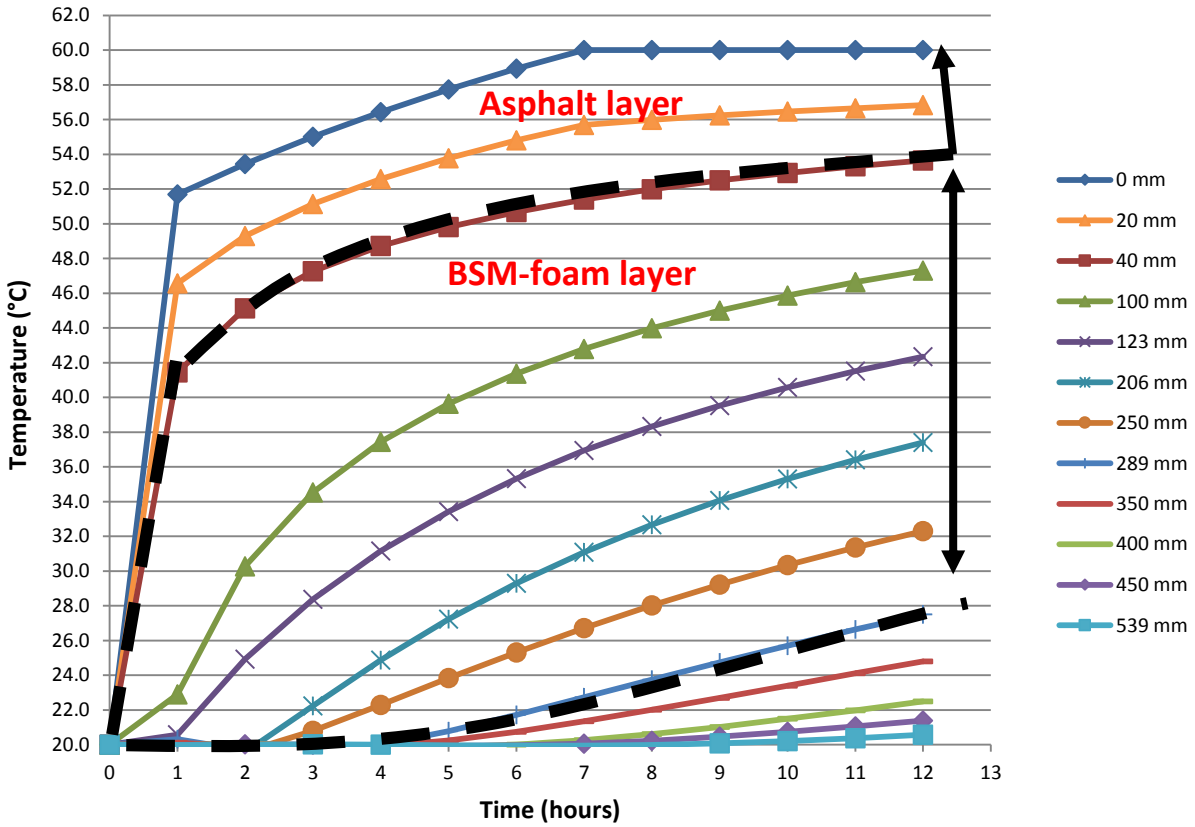

Figure 7.24: Temperature profile in 40 mm asphalt surfacing and BSM-foam with 100%RA base.

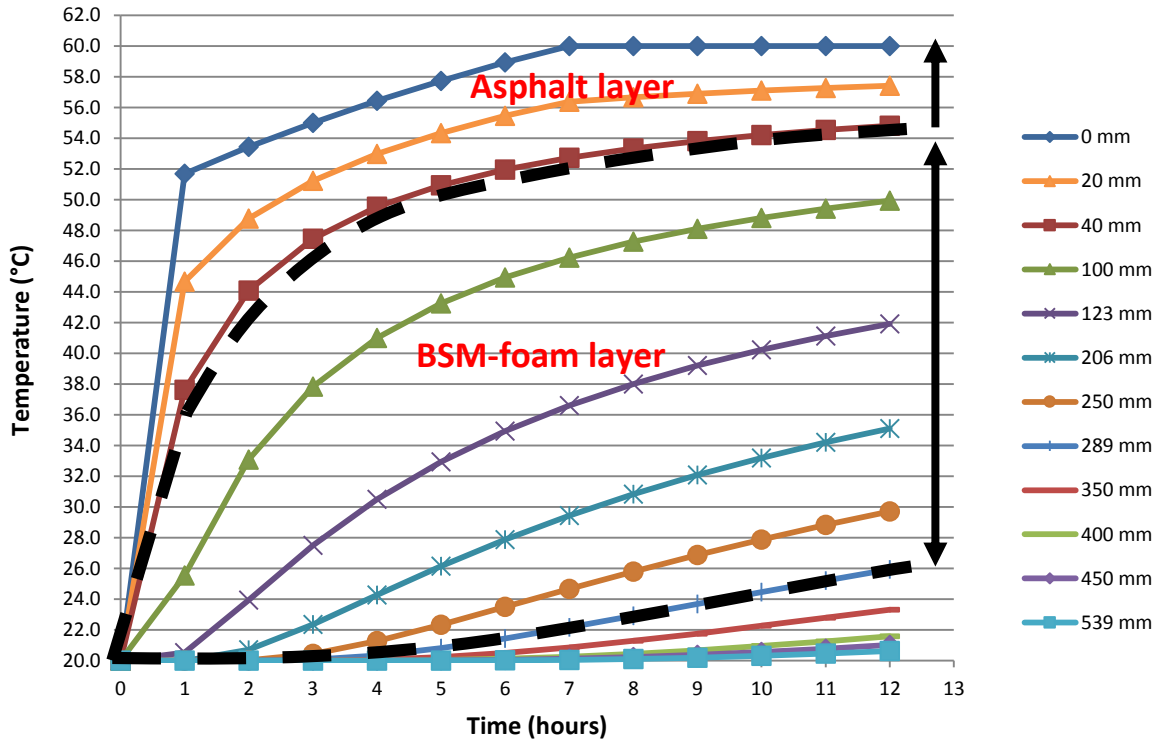

Figure 7.25: Temperature profile in 40 mm asphalt surfacing and BSM-foam with 50%RA +50%G2 (Hornfels-crushed stone) base.

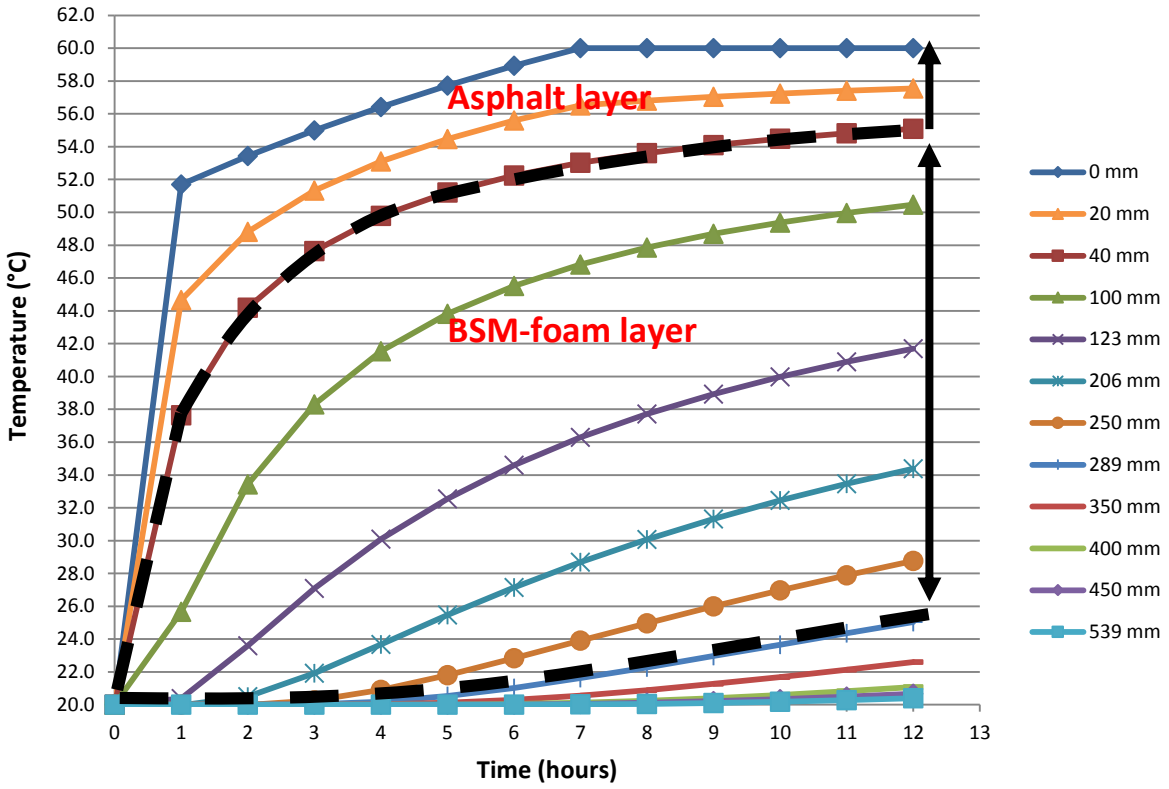

Figure 7.26: Temperature profile in 100mm asphalt surfacing and BSM-foam with 100%G2 (Hornfels-crushed stone) base.

From the analysis of the previous graph, the temperature in the BSMs layers ranges between 55 and 54°C and 27 and 25°C for the BSM-foam mixes. The 40 mm asphalt on the top of the pavement section in all the three cases absorbs a constant heat (almost 5°C). However, the thermal conductivity and heat capacity of every BSM-foam mix play a significant role in the distribution of temperature in the pavement, because the asphalt at the top absorbs only a small part of the heat.

Similar results were found in the pavement structure that Jenkins and Twagira (2008) analysed in the Shedgum Road project in Saudi Arabia. The temperature absorbed by that pavement section was higher than the previous case studied. In fact, the temperature in the BSMs layers ranged between 58°C and 47°C in the first 120 mm.

The evident difference in temperature on the interface between the asphalt layer and the BSM could create particular problems on the mechanical performance of the pavement. Most of the common tests that investigate the mechanical properties for BSMs (stiffness, fatigue,...) do not typically exceed 50°C. More analysis will be conducted in the following paragraphs and some values will be estimated due to the insufficient amount of data available for a mechanical analysis at these high temperatures.

The modelling of pavement material is an important aspect in order to predict long-term pavement performance accurately. However, modelling the temperature behaviour and mechanical properties of BSMs is a complex task due to the diversity of materials that are needed to be accounted for during pavement design. The material properties and behaviour determined in this study are valid for quality aggregates and the test conditions adopted accordingly.

The analysis of temperature vs. mechanical properties in this section uses the linear elastic theory to determine the influence in the changes of BSMs and the performance of pavement structures incorporating a BSM layer. The type of pavement structure selected for analysis is the same adopted in section 7.6.

7.6.2 Pavement structural analysis

The pavement analysed in this section represent the three configurations presented at the beginning of paragraph 7.6. The base layer of the structure is made of BSM-foam with three different percentages of RA. The material properties of BSMs have been already investigated in this study, in particular in Chapter 4.

The BSMs layers are divided in three different sub-layers: in every sub-layer the temperature is associated with the related stiffness value. Figures 7.27 to 7.29 summarise the stiffness values (Mr) according to the different temperatures tested in the laboratory at Stellenbosch University. Due to the lack of research in this area an extrapolation is indispensable to calculate the corresponding stiffness for all the BSM-foam mixes for the extreme temperatures over 40°C (from Figure 7.27 to 7.29). The Mr at high temperatures (over 40°C) and different percentages of RA were calculated through the formulas presented in Chapter 4, paragraph 4.5.1 of this research:

$$Mr = \left(k_2 870 e^{-\left(\frac{\%RA}{100}\right)} + \theta k_1\right) + (-4(T - T_{ref})) \text{ with a \%RA≤50\%}$$

where
Mr = Resilient modulus (MPa)
θ = Bulk stress = $\sigma_1 + \sigma_2 + \sigma_3$ (kPa)
T = temperature test (K)
T_{ref} = 298.15K (25°C)
k_1, k_2= model coefficients

$$Mr = \left(-\left(\frac{T-T_0}{10}\right)\left(\frac{\%RA}{100}\right) + \theta k_1\right) + \left(k_2 e^{\left(\left(\frac{\%RA-50}{100}\right)(-0.034)(T-T_{ref})\right)}\right) \text{ with a \%RA>50\%}$$

where
Mr = Resilient modulus (MPa)

θ = Bulk stress = $\sigma_1 + \sigma_2 + \sigma_3$(kPa)
T = temperature test (K)
T_0= 273.15K
T_{ref} = 298.15K (25°C)
k_1, k_2= model coefficients

Table 7.6 summarises the k_1 and k_2 coefficients for the two models and the R^2 values determined in this research.

Table 7.6: Summary of Mr model coefficients for BSM foam mixes with different percentages of RA.

Mix type	**K_1**	**K_2**	**R^2**
BSM foam mix with RA≤50%	0.073	0.950	0.98
BSM foam mix with R>50%	0.080	378.298	0.96

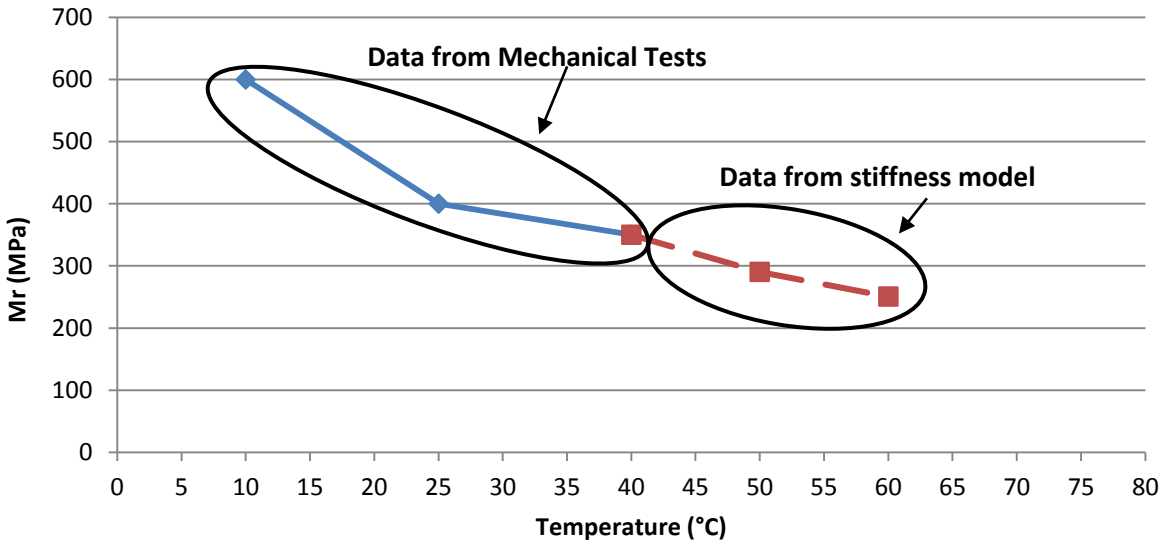

Figure 7.27: Stiffness values for BSM-foam with 100%RA at different temperatures.

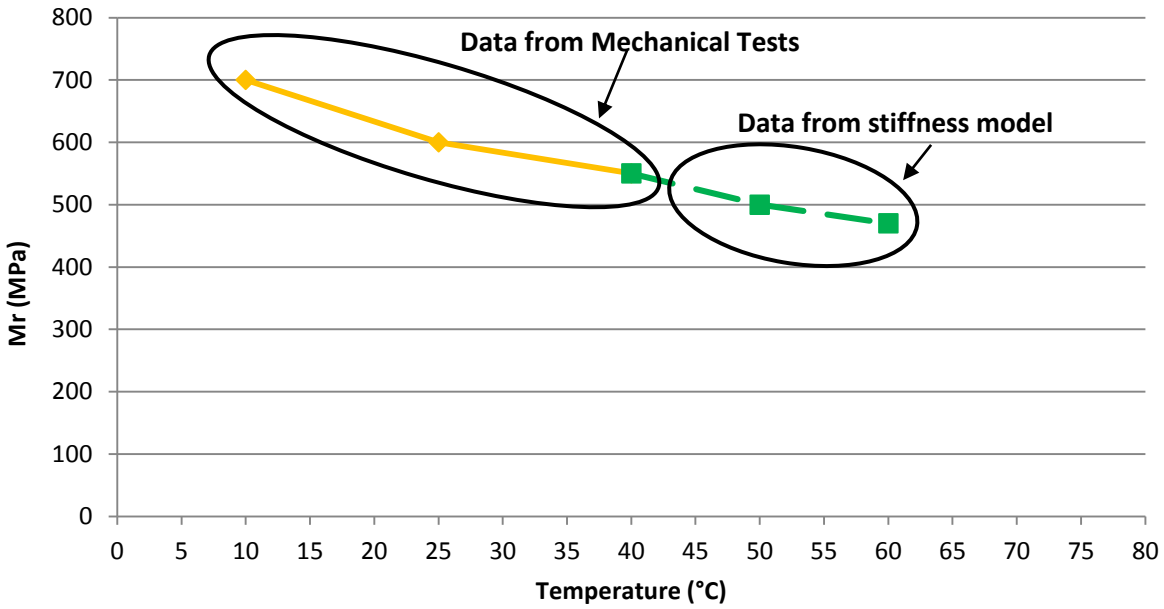

Figure 7.28: Stiffness values for BSM-foam with 50%RA+50%G2 (Hornfels crushed stone) at different temperatures.

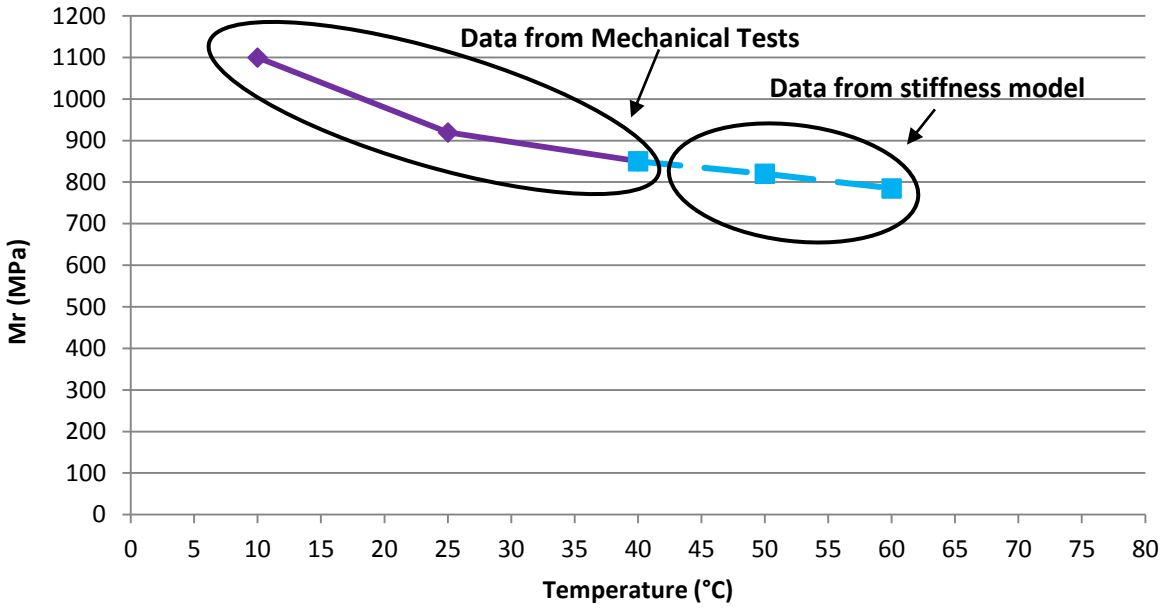

Figure 7.29: Stiffness values for BSM-foam with 100%G2 (Hornfels crushed stone) at different temperatures.

The stiffness strongly depends not only on the temperature but even on the frequency, the stress situation and softening point. The stiffness values presented in this research are calculated with the same frequency of 1 Hz (haversine wave form with 0.1 s loading and 0.9 s rest period) at different stress situations with σ_3 (confinement) varying from 50 kPa to 200 kPa. The

temperature above 50°C plays a key role. In fact the softening point is easily reached. The softening point is the temperature at which a material softens sufficiently to allow significant flow under a small stress. The BSM-foam mixes become less stiff because the softening point is almost reached, influencing the binder dispersion in the mix. Table 7.7 summarises all the stiffness values according to the temperature range for every single material which is used in the mechanical simulation.

It is necessary to calculate the stiffness for every single sub-layer in the BSM-foam base, because the temperature gradient ranges from high temperature (55-54°C) to lower temperature (27-26°C). The BSM-foam layers are divided into three parts to represent the stiffness behaviour of these materials with an increasing percentage of RA better. Stiffness values and Poisson's ratio are related to the corresponding range of temperature calculated through the FEMMASSE HEAT-MLS program, which found a reliable representation of the temperature distribution in the pavement in the study conducted by Twagira (2010) on the N7 expressway close to Cape Town and in the Shedgum Road Project in Saudi Arabia (Jenkins and Twagira, 2008).

The asphalt properties featured in the analysis are not investigated in this study; however, they are selected from a range of values suggested by Jenkins (2000) and presented in Appendix F and by Shell Bitumen (1998). The typical stiffness properties of the surface layer, BSMs, CTSB sub-base and natural gravel as a sub-grade layer and the corresponding Poisson's ratio are presented in Table 7.7. The absolute values (without stress dependency) are used in the BISAR calculation.

A comparison of the stiffness distribution in the pavement sections is drawn at the end of this section between pavement structure without sub-layering the BSM-foam bases and with no temperature gradient (paragraph 7.5) and the same pavement configuration with the influence of the temperature on the top of the HMA and the BSM-foam layers divided in sub-layer (Figure 7.30).

Table 7.7: BSM-foam layer material properties for BISAR analysis.

1st Pavement Configuration with BSM-foam 100%RA

Layer	Material	Thickness (mm)	E (MPa)	Poisson's ratio (ν)	Depth (mm)	Temperature (°C)
1	HMA	40	350	0.35	0 to 40	60 to 54
2.1	BSM-foam 100%RA	83	290	0.40	40 to 123	54 to 42
2.2	BSM-foam 100%RA	83	350	0.37	123 to 206	42 to 37
2.3	BSM-foam 100%RA	83	375	0.35	206 to 289	37 to 27
3	CTSB sub-base	250	1500	0.35	289 to 539	25
4	Uniform Sub-grade	∞	100	0.35	539 to ∞	20

2nd Pavement Configuration with BSM-foam 50%RA+50%G2

Layer	Material	Thickness (mm)	E (MPa)	Poisson's ratio (ν)	Depth (mm)	Temperature (°C)
1	HMA	40	350	0.35	0 to 40	60 to 55
2.1	BSM-foam 50%RA+50%G2	83	500	0.40	40 to 123	55 to 42
2.2	BSM-foam 50%RA+50%G2	83	550	0.37	123 to 206	42 to 35
2.3	BSM-foam 50%RA+50%G2	83	575	0.35	206 to 289	35 to 26
3	CTSB sub-base	250	1500	0.35	289 to 539	25
4	Uniform Sub-grade	∞	100	0.35	539 to ∞	20

3rd Pavement Configuration with BSM-foam 100%G2

Layer	Material	Thickness (mm)	E (MPa)	Poisson's ratio (ν)	Depth (mm)	Temperature (°C)
1	HMA	40	350	0.35	0 to 40	60 to 55
2.1	BSM-foam 100%G2	83	785	0.40	40 to 123	55 to 42
2.2	BSM-foam 100%G2	83	850	0.37	123 to 206	42 to 34
2.3	BSM-foam 100%G2	83	920	0.35	206 to 289	34 to 25
3	CTSB sub-base	250	1500	0.35	289 to 539	25
4	Uniform Sub-grade	∞	100	0.35	539 to ∞	20

Figure 7.30 shows a more reliable method to represent the stiffness distribution in the pavement, keeping into account the important effect of the temperature gradient in the pavement structures, where the BSM-foam base can be analysed in three different sub-layers.

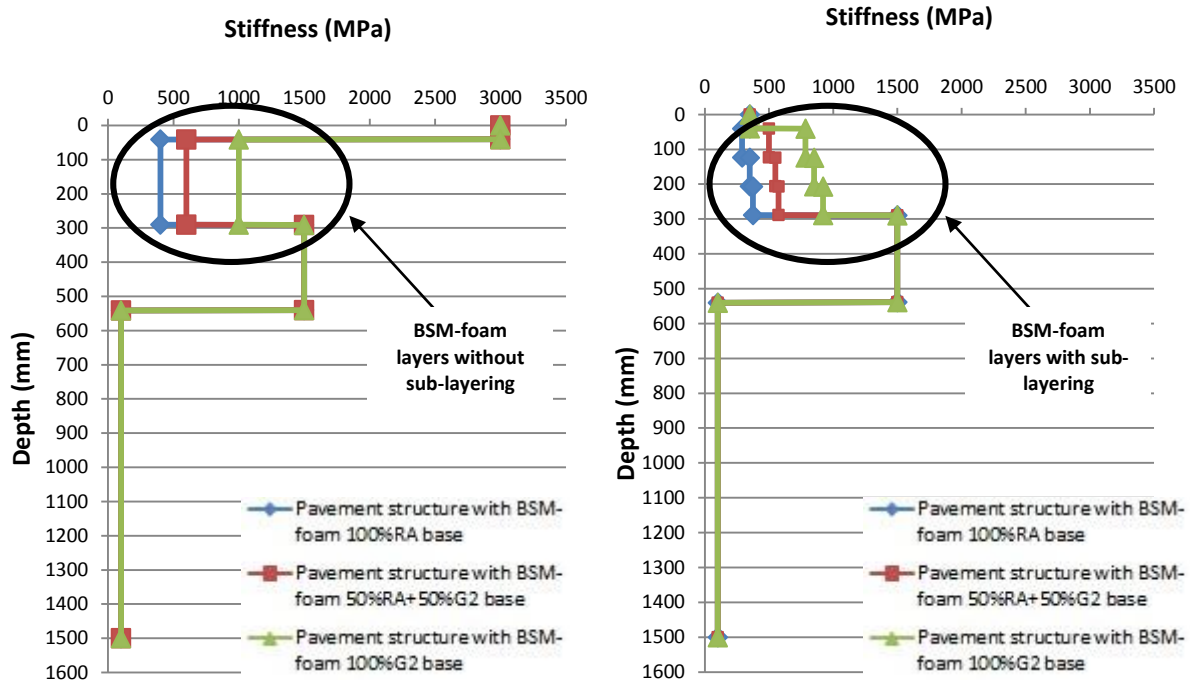

1) No temperature gradient and no BSM sub-layering 2) Temperature gradient and BSM sub-layering

Figure 7.30: Stiffness profiles in the pavement section with different BSM-foam bases.

7.6.3 BSM-foam analysis using BISAR 3.0 program

Three pavement structures consisting of a 40 mm of HMA top layer, a BSM-foam layer, a CTSB sub-base and a uniform sub-grade layer are analysed. The traffic loading conditions consist of a 100 kN single wheel load and a uniform contact pressure of 1000 kPa. The wheel load is modelled as a circular loading area with a radius of 143 mm and a uniform contact pressure equal to the tyre pressure. The comparative pavement structures with the same loading conditions are represented in Figure 7.31.

In terms of analysing the stress in the two horizontal directions in the pavement structures, the problem becomes symmetric by using a single wheel load instead of a dual wheel load. The dual wheel configuration is still widely in use in South Africa; however, modelling with a super single wheel load is easier because of the symmetry. When modelling with a dual wheel configuration one has to, for each layer, determine the critical horizontal position, i.e. under the centre of one wheel or in the middle between the two wheels. When using a super single the critical horizontal position is always under the centre of the wheel, which is to say when assuming a uniform contact pressure over the loading area. This assumption may also be made because a non-uniform load distribution does not influence the stress conditions deeper in the pavement, but only close to the surface. Using a super single wheel also leads to a slightly more conservative estimate, because the stressunder single wheel loading is generally slightly higher

than under dual wheel loading. For reasons of simplicity it was chosen to model the support of the layers underlying the BSM base layer by a single sub-grade layer.

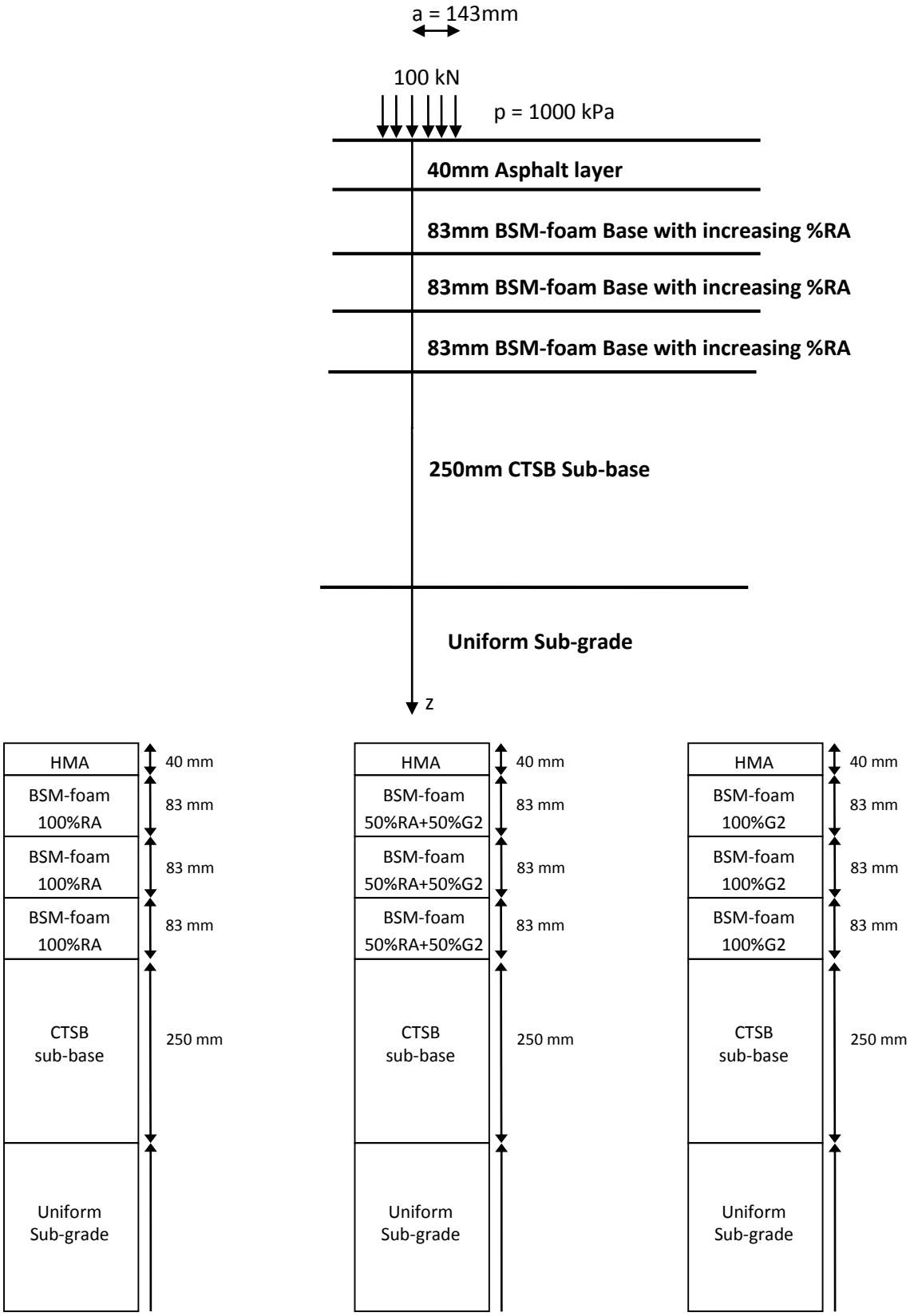

Figure 7.31: Comparative pavement structures comprising a BSM-foam layer, used in the BISAR analysis.

7.6.3.1 Comparison of stress distribution with depth

The calculated stress distribution σ_1 and σ_3 for the three different BSM-foam mixes with the same loading conditions is represented in Figure 7.32. All the calculations are made considering full friction between all the layers in the pavement structures.

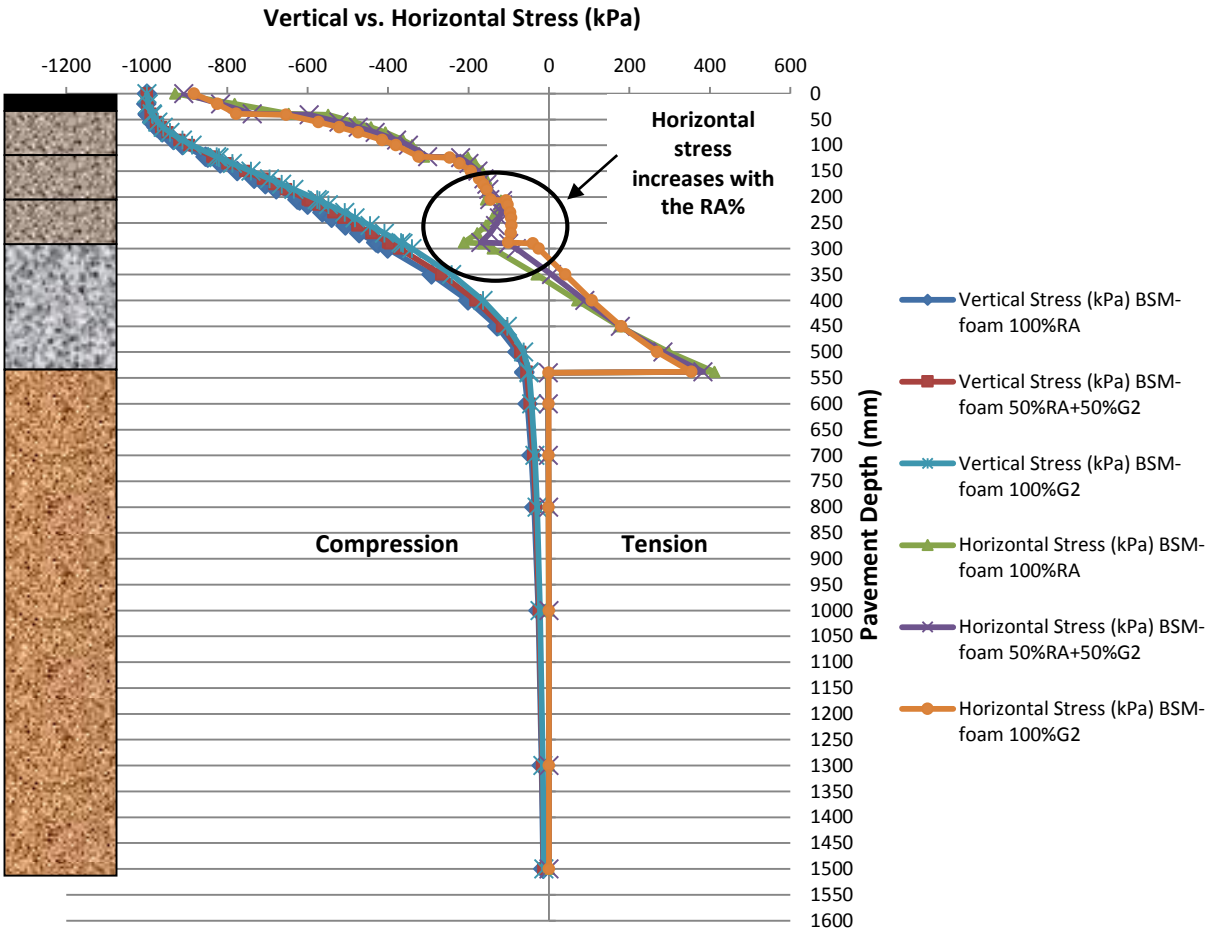

Figure 7.32: Comparison of vertical and horizontal stress distribution in the BSM-foam sub-layer with increasing percentages of RA with a loading of 100 kN and pressure of 1000 kPa.

The BSM-foam base with different percentage of RA takes into consideration the stiffness for every temperature change in the pavement section. Three different values of stiffness are used in the mechanical calculation of the BSM-foam layer due to the different temperature gradient between the top and the bottom of this layer.

From Figure 7.32 it can be seen that the vertical stress results are almost the same for all the pavement structures with different BSM-foam mixes. There is a slight shift from the BSM-foam base with 100%RA and 100%G2. The horizontal stress σ_3 changes throughout the depth of the pavement structure. The horizontal stress is superimposed for all the BSM-foam

structures. The uniform horizontal stress distributions in the top and middle part of the BSM-foam layers are almost completely equal in all three BSMs with increasing amounts of RA. At the bottom on the interface between the BSM-foam bases and the CTSB, the BSMs show a higher horizontal stress, which is higher for the BSM with higher percentages of RA. In fact, the pavement structure, which includes a BSM-foam layer with 100%G2 material, has a lower horizontal stress σ_3 than a BSM-foam with an increasing amount of RA. In the CTSB layer there is a shift in the horizontal stress from compression (top part) to tension (bottom part). This is due to higher stress at the top layer compared to deeper in the layer.

7.6.3.2 Comparison of strain distribution with depth

From Figure 7.33 it can be seen that the vertical strain in BSM layers is higher at the top (first 1/3 of the total thickness of the BSM-foam layers) than at the bottom. In addition, BSM-foam with different amounts of RA has a different vertical strain distribution: the difference is big at the top and small deeper in the layer as the percentage of RA increases in the BSM-foam. This shows that BSM-foam with higher percentages of RA experiences higher permanent deformation at the top subsection (1/3) compared to a similar material with 100%G2. This is due to higher stress at the top layer compared to deeper in the layers well as lower Mr values. Similar behaviour was observed in the studies conducted by Twagira (2010). The difference in the decrease in vertical strain at the bottom of the layer indicates that there will be minimal deformation of the underlying layer. Therefore, the selection of a BSM layer with a low percentage of RA is vital for the long-term performance of the pavement structure.

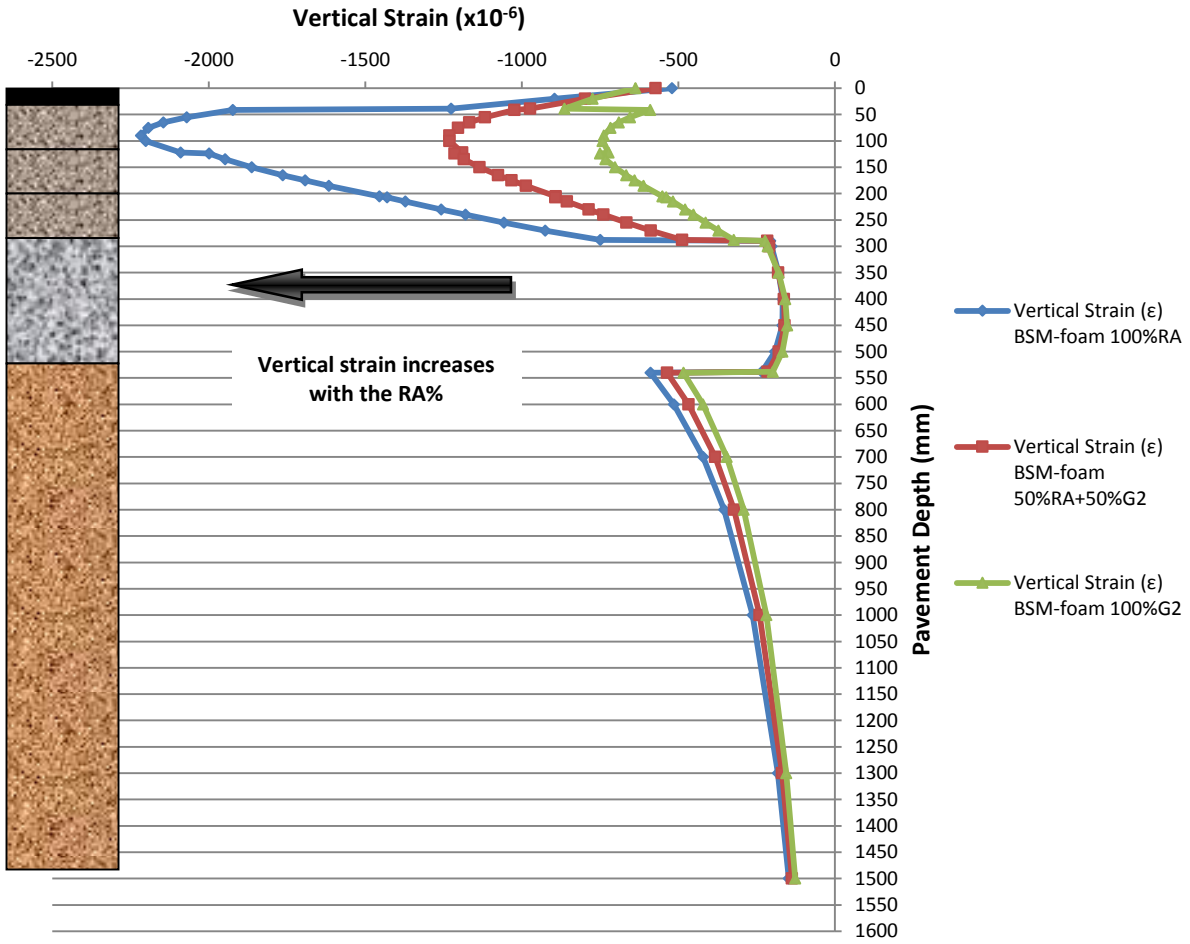

Figure 7.33: Comparison of vertical strain distribution in the BSM-foam sub-layer with increasing percentages of RA.

The horizontal strain distribution calculated from the linear elastic behaviour of BSM-foam layers are represented in Figure 7.34. The horizontal strain varies from top to bottom, with the middle part of the BSMs showing higher strain level. It can also be seen that the horizontal strain of the BSM layer differs as the percentage of RA increases, with the BSM-foam layer with 100%RA showing higher horizontal strain. The horizontal strain level at the bottom of the BSM-foam layer averages between 33 and 68 micro strains. Depending on the support conditions of a BSM layer and the amount of cement content, such magnitude of horizontal strain can be measured at the bottom of layer Brown *et al*. (2000). The maximum horizontal stress measured in the middle of the BSM layer can result in fatigue in a long-term in-service situation (rutting).

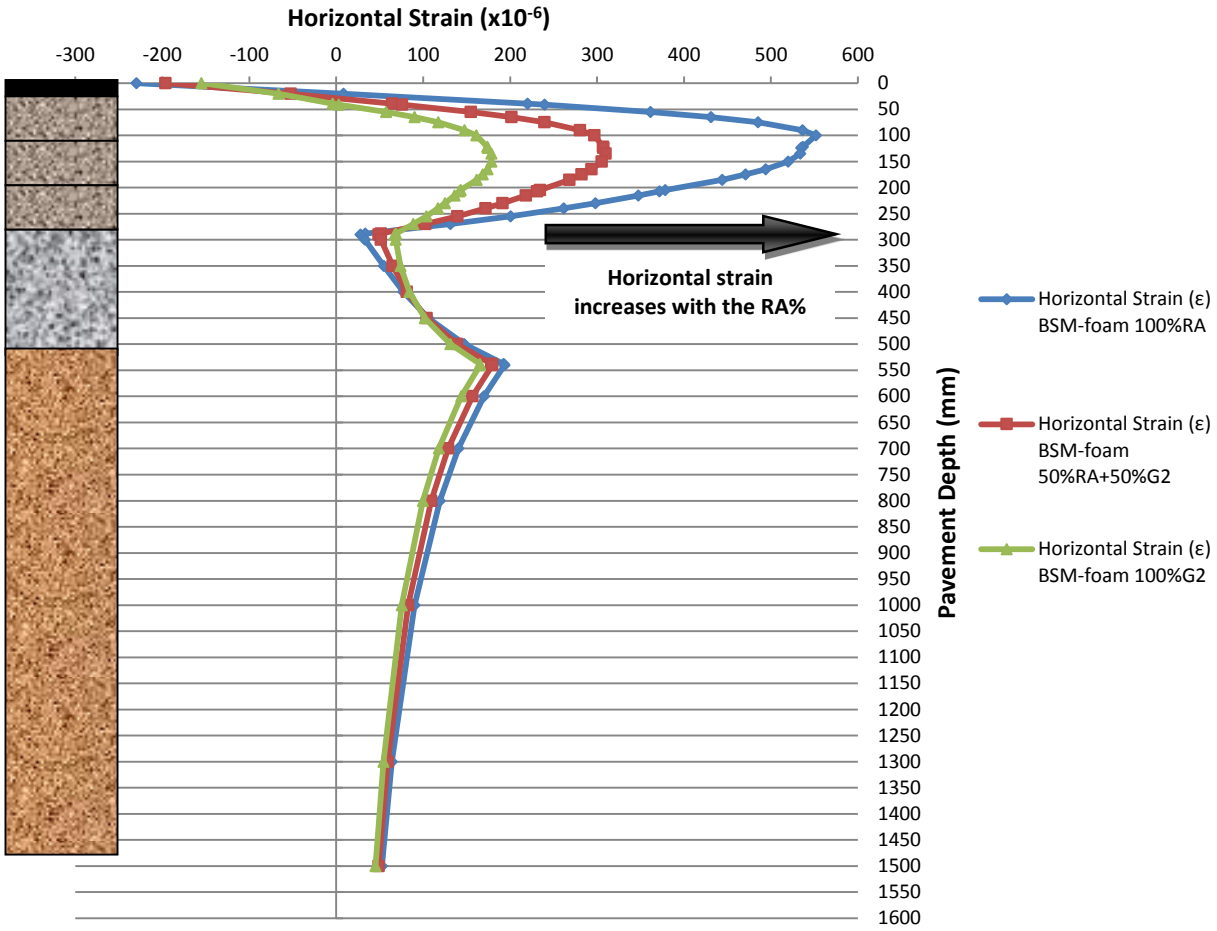

Figure 7.34: Comparison of horizontal strain distribution in the BSM-foam sub-layer with increasing percentages of RA.

Figure 7.35 represents the displacement distribution in pavement sections with different BSM-foam bases with an increasing percentage of RA. The displacement from the top of the layers shifts to higher values when the structure consists of a BSM-foam base with a larger amount of RA. This could lead to possible damage and fatigue problems on the top of the pavement section.

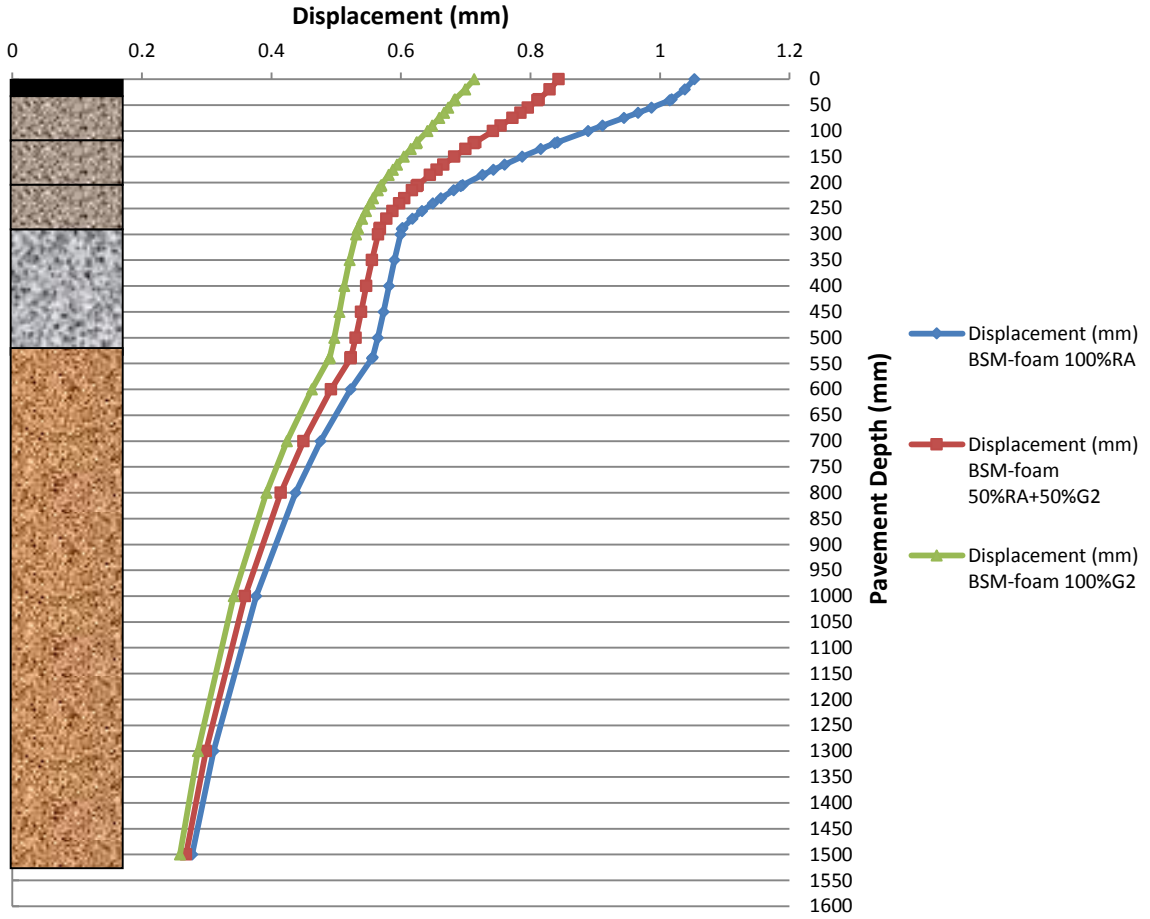

Figure 7.35: Comparison of displacement distribution in the BSM-foam sub-layer with increasing percentages of RA.

The vertical strain in the BSM layer results in horizontal strain; that means from the applied stressand resultant strain, Poisson's ratio, ν, and the modulus can be determined. Jenkins (2000) indicates that a model for the change in Poisson's ratio with a variation in stress conditions has been established for granular materials (Niekerk *et al.*, 2000). The same model was found to be applicable to BSMs. The model indicates that Poisson's ratio is a function of principal stress ratio σ_1/σ_3. This shows that increasing the percentage of RA leads to an increase in the deformation results and an increase in Poisson's ratio. Therefore the change in Poisson's ratio is not only a function of axial deformation but also of the critical stress ratio $\sigma_d/\sigma_{d,f}$. The application of ν in the linear elastic analysis is therefore necessary for closer representation of field behaviour to determine the critical design stress ratio. The critical stress ratio determined using the linear elastic behaviour of BSMs is represented in Figure 7.36 and Figure 7.37.

The effect of dividing the BSM-foam base layer into sub-layers can clearly be seen in the horizontal stress and vertical strain. This is the result of differential stiffness of the sub-layers. Caution is required when analysing the stressand strains throughout the depth of the layer when it is divided in sub-layers. If the analysis points do not include the top and bottom of each of the sub-layers, it is possible to not identify the step-wise shape of the horizontal stress and

vertical strain curves. One needs to understand though, that these steps are the result of mathematical modelling and that in the real pavement structure these steps do not occur.

7.6.3.3 Comparison of deviator stress distribution with depth

The principal stress at various points in a BSM layer is used to calculate the critical deviator stress and deviator stress ratio. In that light, a large number of points were evaluated throughout the depth in order to compare deviator stress at different points in the BSMs sufficiently.

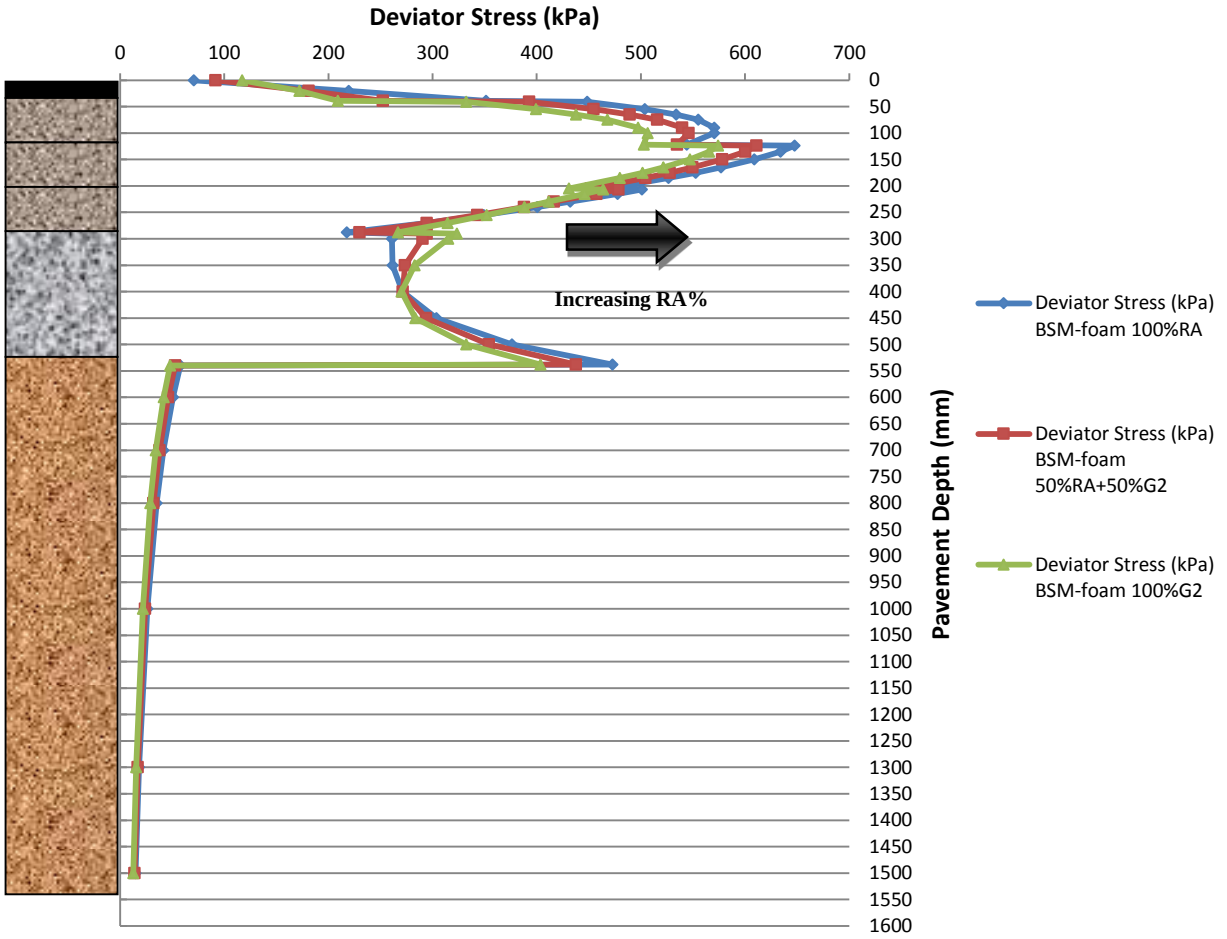

Figure 7.36: Comparison of deviator stress distribution in the BSM-foam sub-layer with increasing percentages of RA.

In Figure 7.36, the deviator stress results are higher for a BSM-foam mix with a high percentage of RA than in the mix with a smaller amount of RA. At the bottom part of the BSM, next to the CTSB, the deviator stress is significantly lower than in the middle of the BSM layer.

7.6.3.4 Comparison of deviator stress ratio between BSM-foam bases with the influence of the temperature and without a temperature gradient

The deviator stress ratio is represented in Figure 7.37. A comparison is drawn between the pavement structures with different percentages of RA, already analysed in section 7.5, and the pavement configurations with increasing percentages of RA, a temperature gradient and different stiffness values for each sub-layer.

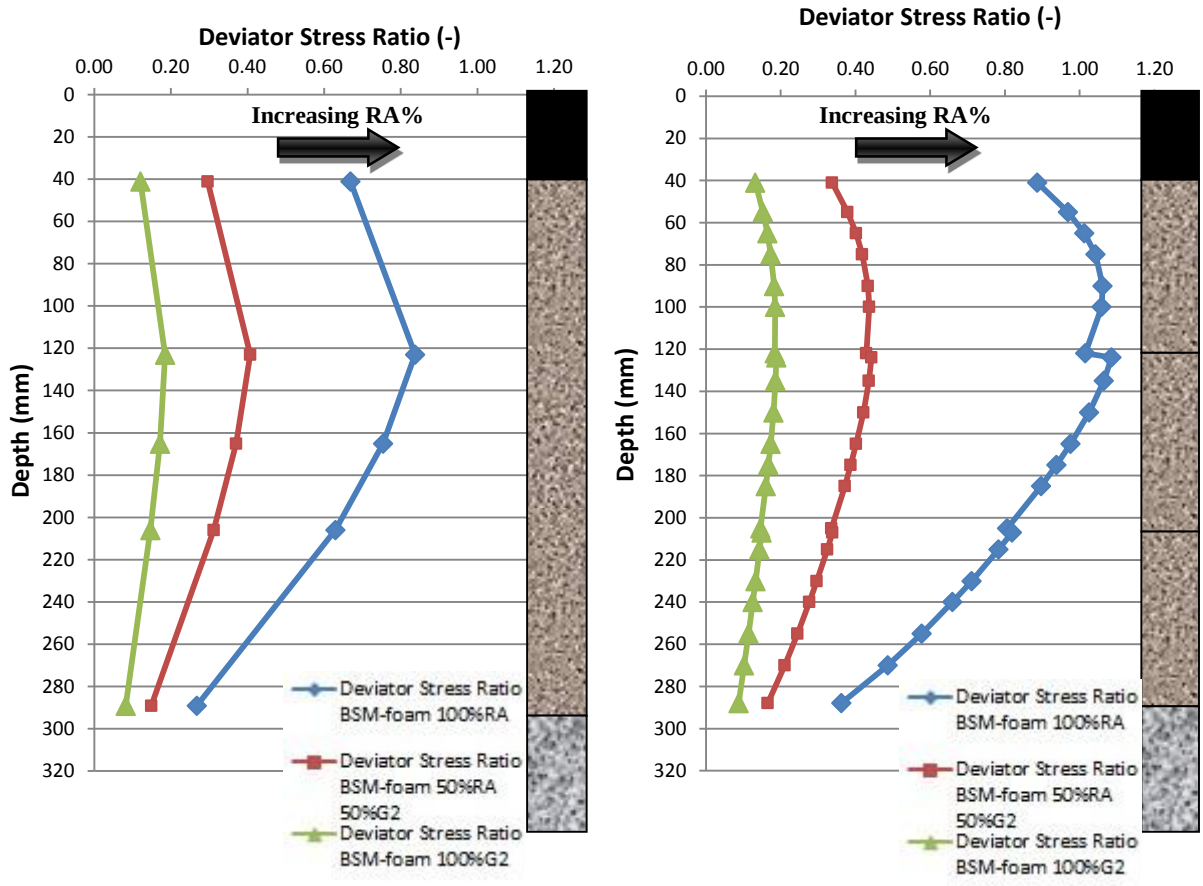

1) No temperature gradient and no BSM sub-layering 2) Temperature gradient and BSM sub-layering

Figure 7.37: Comparison of deviator stress ratio distribution in the BSM-foam bases with increasing percentages of RA.

The deviator stress ratio in both the graphs in Figure 7.37 shows higher values for the BSM-foam base with a higher percentage of RA. In the first graph the stress ratio in the BSM-foam base with 100%RA material increases almost 4 times more than in BSM-foam base with 100%G2. In the second graph this difference is almost 5 times bigger than in the case without temperature gradient and no sub-layering.

BSM-foam bases without the influence of temperature and sub-layering show lower deviator stress at the middle of the BSM-foam layer compared to the scenario in which the temperature gradient affects the stiffness distribution in the layers.

It can be seen from the deviator stress distributions that a critical deviator stress is calculated at the middle where the horizontal stress is higher than in the rest of the layer. The effect is twofold: firstly, when $\sigma_3 \leq 0$ it causes an increase in deviator stress: secondly, the calculated major principal stress at failure $\sigma_{1,f} = A\sigma_3 + B$ and subsequently the deviator stress at failure $\sigma_{d,f}$ reduces because of the diminishing first term ($A\sigma_3$). However, once $\sigma_3 > 0$, deviator stress increases and deviator stress at failure also increases. Deviator stress ratio is calculated from deviator stress σ_d and deviator stress at failure $\sigma_{d,f}$. Deviator stress at failure is calculated based on the shear parameters of BSM materials. In a tri-axial test, σ_3 is always in compression, therefore $\sigma_{d,f}$ increases as σ_3 increases. In a linear elastic analysis, σ_3 changes from compression at the top to almost tension at the bottom.

The effect of the change in horizontal stress from the top to the bottom of the BSM layer indicates that the critical stress ratio therefore occurs at the middle of the BSM-foam layer. The magnitude of the critical deviator stress ratio for design purposes as well as the depth at which it occurs is therefore affected when the pavement is analysed using the linear elastic model.

The temperature distribution changes the mechanical properties of the pavement section. In fact the deviator stress in the BSM-foam layers shifts towards higher values (second graph in Figure 7.37), preserving almost the same deviator stress on the bottom part of the BSM layers. All three BSM-foam mixes shows a consistant increase in the deviator stress as soon the temperature influences the pavement sections. The BSM-foam mix with 100%RA shows a deviator stress higher than all the other mixes.

According to the results presented in Chapter 4, mixes with a high percentage of RA have less resistance to permanent deformation as the temperature and the amount of reclaimed asphalt increase. Chapter 4 showed that the critical temperature of BSM mixes with a high percentage of RA lies between 40°C and 50°C and that a deviator stress higher than 40% can quickly lead to an accelerated deformation.

Figure 7.37 shows a high deviator stress ratio in the middle of the BSM layer in both the graphs. This probably leads to possible effects of fatigue, which is more evident in the second graph where the BSM-foam with 100%RA reaches very high values.

The analysis using BISAR 3.0 has shown that it is possible to model the influence of temperature and different loading conditions in a pavement structure using stress-strain material characteristics. However, the magnitude of stress and strain states (σ-ε) calculated using BISAR are likely to be an estimation of the actual stress states expected in the field. This is because the stress dependence behaviour of BSMs is to a certain extent not accurately modelled in the linear elastic model calculations. Therefore, one needs to take note of this shortfall when selecting design critical deviator stress ratios observed in the BSMs layers.

7.6.3.5 Comparison of number of load repetitions between BSM-foam bases with the influence of temperature and without a temperature gradient

The response of pavements incorporating BSMs would improve when the density of the BSMs increases. Vertical deflections would reduce significantly due to better load spreading ability and shear failure would occur only at higher load levels. This would improve the load carrying capacity of the pavement and therefore impact on the structural design. This is illustrated by the transfer functions for permanent deformation provided in the Wirtgen Manual (2010) for foamed BSMs, in which the deviator stress is the most important variable (Figure 7.38).

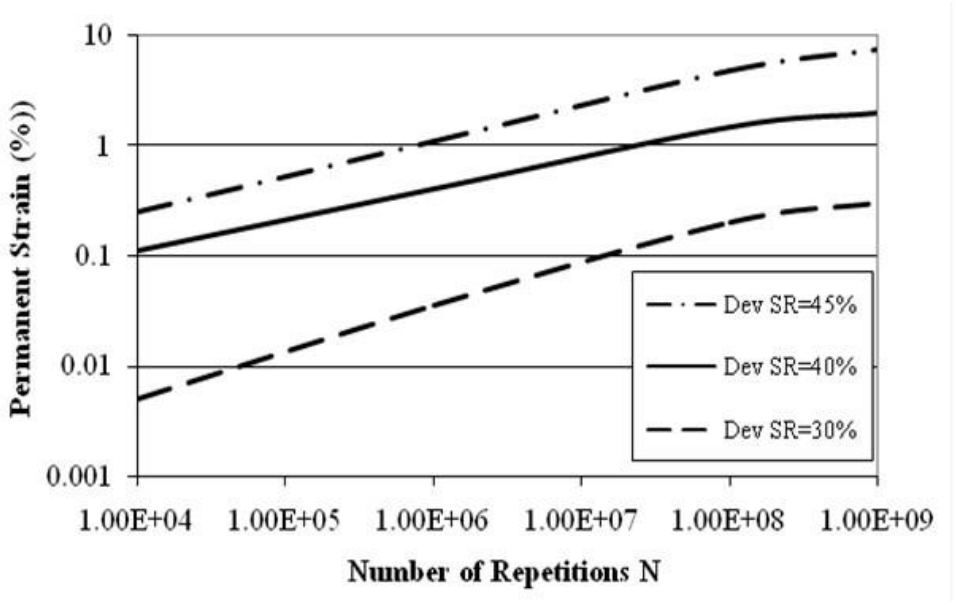

Figure 7.38: Recommended deviator stress ratio limits, based on the Wirtgen manual (2010).

The deviator stressalready represented in Figure 7.37 for the two pavement configurations with and without sub-layering is used for the calculation of the number of load repetitions (N_{pd}) to reach 10 mm rut (Figure 7.39).

A comparison between the number of load repetitions is represented in Figure 7.39, taking into account the different scenarios with and without temperature gradient and sub-layering in the pavement structures with BSM-foam mixes with an increasing percentage of RA. As the amount of RA increases in the BSM-foam base layer, the number of load repetitions becomes lower compared to the BSM-foam base with 100%G2 material. This probably means that the pavement structure with a BSM-foam layer with 100%RA is going to reach 10 mm rut before the BSM-foam with 100%G2. The BSM-foam with virgin aggregates performs better in terms of possible permanent deformations compared to the BSM-foam with an increased percentage of RA.

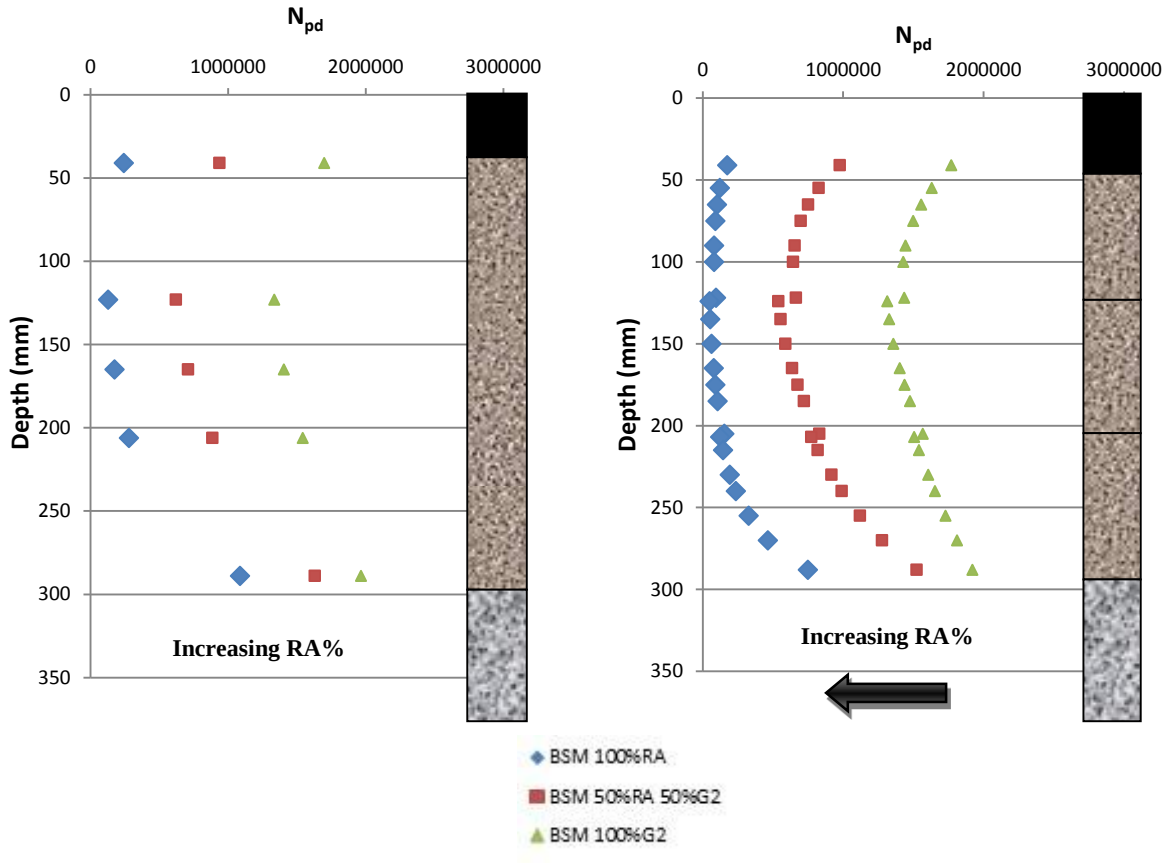

1) No temperature gradient and no BSM sub-layering 2) Temperature gradient and BSM sub-layering

Figure 7.39: Comparison of number of load repetitions in the BSM-foam bases with increasing percentages of RA.

The influence of the stress ratios on the number of load repetitions to reach a certain strain level (10 mm rut) is summarised in Figure 7.40 for 4 % plastic strain respectively for the two scenarios (with and without temperature gradient). For a 250 mm thick pavement layer 4 % strain means 10 mm at the top of the layer.

At lower deviator stress ratios the BSM-foam with 100%G2 performs better than the BSM-foam with a higher percentage of RA.

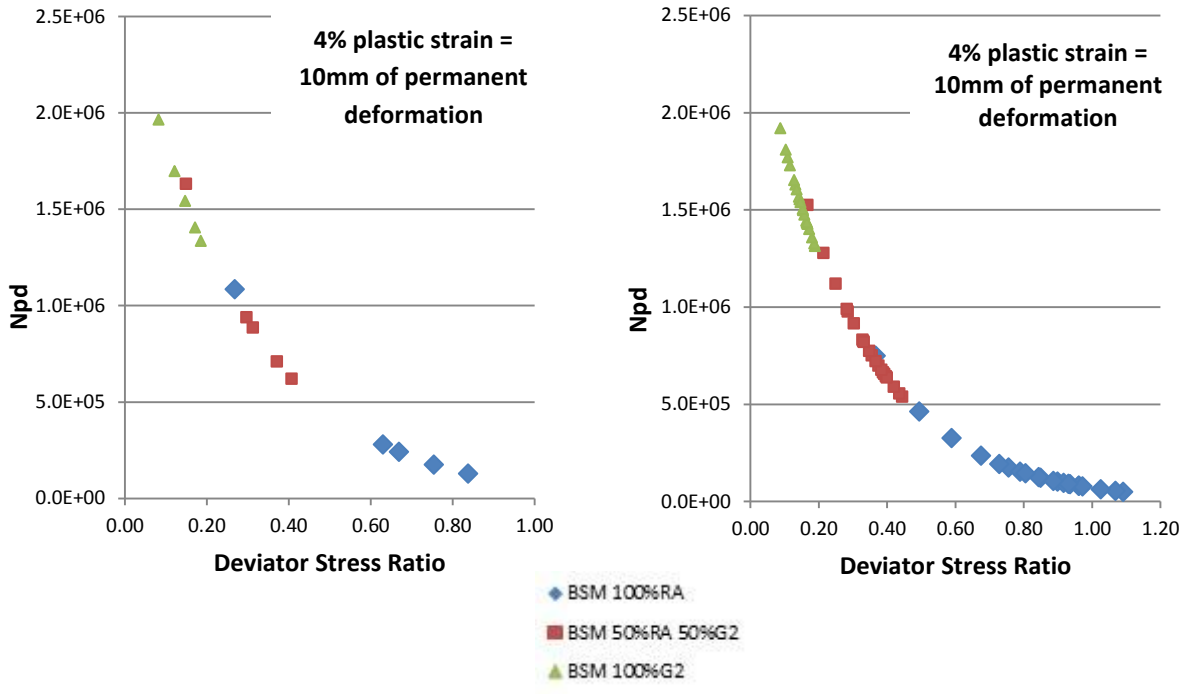

1) No temperature gradient and no BSM sub-layering 2) Temperature gradient and BSM sub-layering

Figure 7.40: Influence of deviator stress ratio on permanent deformation to achieve 4% plastic strain in the BSM-foam bases with increasing percentages of RA.

7.7 Conclusions

The most important findings after the modelling of different pavement structures with the BISAR multi-layer program are summarised here.

Different sub-base and sub-grade layers
In the first part of Chapter 7 four different pavement structures were evaluated. The pavement structure with a uniform or dual sub-grade showed the same horizontal and vertical stress in both configurations. Using a CTSB sub-base, instead of a granular multilayer sub-base, it is possible to reduce the horizontal stress in the BSM-foam base, reducing the risk of fatigue damage on the top of the HMA.

Different loading
Using high traffic loading conditions on the pavement creates a higher possibility to create permanent deformation and damage to the top of the pavement. The deviator stress becomes bigger in the BSM-foam layer as well as on the interface between the BSM and the CTSB sub-base.

Different HMA thickness
Increasing the HMA thickness from 40 mm to 100 mm can easily lead to possible fatigue problems at the top of the pavement. In fact the horizontal stress at the bottom of the HMA layer changes from compression to tension, increasing the deviator stress to very high values (700 kPa). The deviator stress remains almost uniform in both scenarios with a thin and a thick HMA layer. This means that the BSM-foam layer has the capability to spread the loading deeper into the pavement, without creating serious fatigue problems.

Different BSM-foam base layers with an increasing percentage of RA
The stiffness of the BSM layer has a considerable effect on the horizontal strain at the bottom of the asphalt surface and the horizontal strain at the bottom of the BSM layer itself. An increased stiffness and a smaller amount of RA reduce these strains. The stiffness of a BSM-foam base with 100%G2 material has a small effect on the deviator stress in the BSM layer and the vertical strain on top of the sub-grade. Increasing the BSM layer stiffness, which means a lower percentage of RA in the mix, reduces these pavement responses. When designing by means of pavement modelling it is very important to work with correct input data. As concluded above the sub-grade stiffness has a significant effect on design criterions used for the performance prediction of the BSM layer.

Temperature gradient in the pavement structure
The influence of the temperature and stress-strain (σ-ε) relationship on the mechanical behaviour of BSMs was analysed at the end of this chapter. The temperature distribution was investigated in the pavement sections with three different BSM-foam layers. The stress-strain analysis of the BSM foam mixes incorporated into a pavement structure was done using a linear elastic model in the BISAR program.

The findings in this part of the study lead to the following conclusions:

- The asphalt layer at the top of the pavement was able to absorb the same amount of heat even with different BSM-foam layers at the bottom.
- The sub-base and sub-grade layers always recorded values close to 20°C independently from the specific heat capacity of the material (CTSB or natural gravel).
- The analysis indicates that the BSM has a key role in distributing the loading in the pavement.
- High deviator stress in the BSM layer with 100%RA can possibly lead to permanent deformation, especially when the stress ratio is higher than 40% and the temperature is increasing.
- Care should be taken when critical design values are determined from these stress state calculations, as they are likely to be an overestimation.
- The results obtained in the stress analysis of a pavement considering different temperatures for the asphalt layer demonstrated the importance of the consideration of this parameter in pavement design. Higher temperatures lead to higher displacements and greatly affect the horizontal stress.
- High percentages of RA in the BSM-foam base layer could lead to early fatigue in the pavement as well as permanent deformation.

Pavement stress-strain analyses have been demonstrated as a tool for analytical modelling of pavement behaviour in terms of traffic load-response and performance evaluation. Stress strain modelling thus constitutes an integral part of pavement design.

The temperature distribution in the pavement sections was always representing the diurnal effects of the heat on the pavement surface. Major work should have to be done to analyse the effects of the temperature gradient in the pavement section during the night-time period.

REFERENCES

Brown, S. and Needham, A. 2000. A study of cement modified bitumen emulsion mixtures.Proceeding of the association of asphalt paving technologists.AAPT, vol. 69, Reno.

De Beer, M., Fisher. C. and Kannemeyer, L. 2004. Tyre-Pavement Interface Contact Stresses on Flexible Pavements - quo Vadis? Roads - The Arteries of Africa, Eighth Conference on Asphalt Pavements for Southern Africa, Sun City, North West Province, South Africa.

De Beer, M. 2009. Improved Performance Improved Evaluation of Road Pavements by Using Measured Tyre Loading. CSIR, Pretoria, South Africa.

Ebels, L.J. 2008. Characterisation of materials properties and rehabilitation of cold bituminous mixture for road pavements. PhD dissertation, published at the University of Stellenbosch, South Africa.

Luca, J. and Mrawia, D. 2005. New measurement of thermal properties of Superpave asphalt concrete. Journal Materials in Civil Engineering 17:72-9.

Jenkins, K.J. 2000. Mix design consideration for the cold and half-warm bituminous mixes with emphasis on famed bitumen. PhD dissertation, published at the University of Stellenbosch, South Africa.

Jenkins, K.J. and Twagira, M.E. 2008. Failure mechanism of in-situ recycling with foamed bitumen stabilisation. Technical report on the investigation of distress on Shedgum Road in Saudi Arabia. Loudon International.

Kumapley, N.K. and Molenaar, A.A.A. 1996. Axle Load Survey Report. Report to the Commission of the European Communities. Accra, Ghana.

Loizos, A. and Papavasiliou, V. 2007. Assessment of in-situ cold in-place recycling performance using the foam asphalt technique. Workshop on pavement recycling. Athens, Greece.

Molenaar, A.A.A. 2007. Lecture notes CT4860 Structural Pavement Design; Design of Flexible Pavements. Delft, the Netherlands; Delft University of Technology.

Shell Bitumen U.K., 1998. The Shell Bitumen Handbook, United Kingdom.

Shell Global Solutions. 1998. BISAR 3.0 Software and user manual, CD_ROM, Shell International oil products, Amsterdam, the Netherlands.

Theyse, H.L., De Beer, M. and Rust, F.C. 1996. Overview of the South African mechanisticpavement design method. Transportation research record no. 1539. USA. pg 6-32.

Turner, W.C. and Malloy, J.F. 1981. Thermal insulation handbook, Robert E. Krieger Publishing Company, Malabar, Florida, p. 549.

Twagira, E.M. 2010. Influence of durability properties on performance of bitumen stabilised materials, PhD Dissertation, Department of Civil Engineering, Faculty of Engineering, University of Stellenbosch, South Africa.

Van Niekerk, A.A. van Sheers, J. and Galjaard, P.J. 2000. Resilient deformation behaviour of coarse grained mix granulate base course materials from testing scaled gradings at smaller specimen sizes. UNBAR 5 Conference, University of Nottingham.

Wirtgen GmbH. 2010. Cold Recycling Manual, 3rd edition published by Wirtgen GmbH, Windhagen, Germany, 2004.

Wu, S. Li, B., Wang, H. and Qiu, J. 2008.Numerical simulation of temperature distribution in conductive asphalt solar collector due to pavement material parameters. Materials Science Forum Vols. 575-578:1314-1319.

CHAPTER 8

CONCLUSIONS AND RECOMMENDATIONS

8.1 Introduction

Throughout this dissertation, and especially in Chapter 4 (mechanical properties of BSM-foam mixes), Chapter 5 (durability properties of BSM-foam mixes), Chapter 6 (influence of temperature distribution on BSMs) and Chapter 7 (synthesis), the main issues, conclusions and recommendations based on this research are provided. This chapter aims to summarise these findings in general terms, synthesizing the key conclusions. For more details on a specific conclusion or recommendation reference is made to the relevant mentioned chapters.

8.2 Conclusions

8.2.1 Mechanical properties of BSM-foam mixes

Strength
The Indirect Tensile Strength test (ITS) is used as a BSM shear / tensile strength evaluation indicator. The ITS shows higher values at decreasing temperatures. A trend of curvilinear behaviour can be established for all the tests, similar to HMA. The three BSM-foam mixes with an increasing amount of RA range on values markably higher than the boundary value for BSM 1 at 25°C (TG2, Asphalt Academy, 2009). The results indicate the importance of the temperature factor during all the tests.

The shear properties of BSM-foam mixes evaluated using monotonic tri-axial tests yielded a consistent increase of the friction angle as the percentage of RA decreases. According to the results obtained in this research, the friction angle φ decreases whilst the cohesion of the mix increases with the inclusion of more reclaimed asphalt (RA) in a cold mix. This shift in the failure envelope leads to an increase in the maximum principal stress $\sigma_{1,f}$ at low confining stress σ_3 through the addition of reclaimed asphalt. Depending on the confining stress, $\sigma_{1,f}$ can increase through the incorporation of a higher percentage of reclaimed asphalt. The cohesion value increases with a higher RA content. From the results reported in this thesis it is possible to conclude that increased density (improved compaction) reduces the risk of shear failure at different load levels. Improved compaction thus increases the pavement life. It is important to control the quality and quantity of RA to prevent a lower angle of friction and a consequent shear failure. The following general trends in shear strength were observed:

- The amount of fines in the mix is an important factor when using BSMs;
- The angle of internal friction is more dependent on the aggregate properties, but also on the level of cohesion;

– Increasing the percentage of RA and temperature in the BSM generally results in a reduction of the shear strength.

Testing demonstrated that the temperature gradient influences the reduction of the $\sigma_{d,f}$ for BSM-foam mixes with an increasing percentage of RA. This is more pronounced for mixes with a higher percentage of RA.

Table 8.1: Summary of cohesion and angle of internal friction.

BSM-foam mix	Cohesion C (MPa)	Angle of internal friction Φ (°)	Correlation Coefficient (R^2)	Temperature (°C)
100% RA	0.432	8.2	0.98	25
50%RA 50%G2	0.374	36	0.94	25
100%G2	0.516	45.5	0.89	25
100% RA	0.341	5.3	0.99	40
50%RA 50%G2	0.355	24	0.96	40
100%G2	0.494	39.2	0.88	40

Table 8.2: Summary $\sigma_{d,f}$ for BSM-foam mixes with increasing percentages of RA at different temperatures.

BSM-foam mix	$\sigma_{d,f}$ (kPa)	Temperature (°C)
100% RA	1043.3	25
100% RA	773.3	40
100% RA	593.3*	50
50%RA 50%G2	1670	25
50%RA 50%G2	1493	40
50%RA 50%G2	1375	50
100%G2	3196	25
100%G2	3098.02	40
100%G2	3032.7*	50

Extrapolation of $\sigma_{d,f}$ for BSM-foam mixes with increasing percentages of RA.

Stiffness

The resilient modulus of BSMs evaluated in the tri-axial test ranges from 600 MPa to 1200 MPa. This ranks BSM in between granular material and HMA in terms of their typical resilient modulus values. Higher values have been recorded for BSM-foam mixes subjected to a period of six months of curing at environmental temperature. The resilient modulus can easily reach values similar to HMA after this long period, but these values have to be critically compared with the real values from the field. More research needs to be carry out to describe better the mechanical performance of the BSM-foam layer in the long period of curing. The resilient modulus of BSMs is stress dependent. The Mr-θ model is able to describe this stress dependent behaviour accurately. For high percentages of RA in the mix (100% in this study) the resilient modulus is fairly independent of the bulk stress, but decreases significantly with increasing deviator stress levels at a constant confining pressure. The resilient modulus and the stress dependent behaviour of BSM are not sensitive to the type of binders tested. The stiffness of BSMs is dependent on the loading time and temperature.

Deformation resistance

Permanent deformation behaviour of BSMs consists of three phases, i.e. a primary bedding-in phase, a secondary stable phase and a tertiary phase with accelerating flow to failure. The occurrence of tertiary flow depends on the applied deviator stress ratio. Critical deviator stress ratios have been determined only for a BSM-foam mix with 50%RA and 50%G2 Hornfels crushed stone materials. According to this research, a ratio of $\sigma_d/\sigma_{d,f}$ = 42.5% defines this critical boundary for BSM-foam with 50%RA and 50%G2. BSM-foam mixes with high percentage of RA are very sensitive to the increasing of the stress ratio. After 40% stress ratio the material is not able to support a continuous level of stress. Temperature plays a key role in the permanent deformation test, especially with BSMs with a higher percentage of RA. BSM-foam mixes with a high percentage of RA have less resistance to permanent deformation as the temperature and the amount of reclaimed asphalt increase. It is evident from the results in Chapter 4 that the critical temperature of BSM mixes with a high percentage of RA lies between 40°C and 50°C. However, the critical temperature is influence by binder content and percentage of RA.

8.2.2 Durability properties BSM-foam mixes

The quantification of the mechanical properties of BSMs has been widely used to determine durability and long-term performance. BSMs have been successfully applied in a wide range of mineral aggregates with significant differences in physico-chemical and mechanical properties. In this light, analysis of the durability behaviour of binder and mineral aggregates in BSMs is vital. Understanding this behaviour provides confidence in determining the failure mechanisms and the ability to characterise the durability properties with a higher percentage of certainty during all phases of application of BSMs, which is mix design, construction and in-service condition.

The brush test does not simulate the mechanism of moisture damage but has the potential to evaluate the adhesion loss of the bitumen and the cohesion loss of the mix. Although the Brush test gives an insight into the physical disintegration of adhesion and cohesion of the BSMs mixes in a wet state and a reduction in strength, understanding the physico-chemical properties

of the surface of mineral aggregates is vital in exploring the long-term durability of BSMs under different adverse conditions.

The wet-dry brushing test is considered to have the potential of providing improved durability evaluations of BSMs to ITS_{wet} versus ITS_{dry}. The cumulative percentage of material loss in the brush test increases with the percentage of reclaimed asphalt. This is influenced by the percentage of air voids of the mix, which is increasing at the same time. The BSM-foam mix with a high percentage of RA has higher air voids than a BSM-foam mix with 100%G2 crushed stone. During the research it was found that the biggest percentage of loss of material occurs during the first four cycles; after the fifth cycle the percentage of loss remains almost constant. Soaking leads to a plateau in the cumulative percentage of loss for the specimens tested. In fact the standard deviation is relatively low for the specimens tested in the same conditions.

The behaviour of the material is conditioned from the amount of air voids present in the mix. As the percentage of air voids increases, the cumulative percentage of loss measured during the 12 cycles of wet and dry brushing test increases. At the same time the MIST apparatus preconditions the BSMs specimen, and reduces the angle of friction and cohesion during the monotonic tri-axial tests. The same situation was in part presented by Twagira (2010) in his research focusing on the possible relationship between the MIST device and the ITS test. The study of moisture damage characterisation presented in this thesis indicates that BSM-foam mixes with a higher percentage of RA are more susceptible to moisture damage than similar BSM stabilised with only good quality crushed stone (Hornfels).

The use of tri-axial testing before and after moisture conditioning of a specimen can identify mechanical property changes in BSMs due to infiltration of excess moisture. In this way, it is possible to screen BSMs mixes in terms of moisture susceptibility. The σ-ε properties determined under monotonic tri-axial testing demonstrated that the excess moisture in BSMs influences the reduction of cohesion and adhesion of the mix matrices. This is more pronounced for BSM-foam mixes with a high percentage of RA. The dominant mode of failure in MIST/tri-axial testing is shear failure and in ITS testing is tensile cracking. In pavement structure, tensile cracks are not a dominant failure of BSMs. Therefore, tensile cracking in the ITS test do not simulate the failure mechanism of BSMs accurately compared to MIST/tri-axial testing. The reason for this is that crack formation and development due to tensile stress in the centre of BSM specimens, as well as the unconfined nature of the test are not typical representations of the failure mechanisms occurring in BSMs during in-service condition.

The wet-dry brushing test has some limits due to the possible effects caused by the changing of the weight on the mechanical shaft that controls the brush as well as the rate of revolutions. These variables could lead to different results, increasing the percentage of loss during the first four cycles. More tests are needed in this direction.

8.2.3 Influence of temperature distribution on BSMs

Currently, the temperature distribution of BSM-foam layers is neither modelled nor used in performance analyses. The study of the temperature gradient of three different BSM-foam mixes can help to predict the temperature and heat transfer at different depths in a pavement section. The model developed in Chapter 4 can be considered useful to predict the temperature in a BSM-foam pavement with a high percentage of RA. These factors can be used to predict

the heat transfer in a BSM layer and related moisture evaporation accurately. In addition, the temperature data presented in this study indicates that BSM layers experience significant temperature variation as the depth and the percentage of RA increase. The temperature algorithms developed in this research provide an acceptable prediction of temperature gradient in BSM-foam mixes with a high percentage of RA at different depths.

Temperature influences full strength bonding, equilibrium moisture content, age hardening potential, physico-chemical and mechanical properties in BSMs. It is apparent from temperature distribution that the proposed models (heat transfer) need further research into their applicability to different BSM layers. However, heat transfer and thermal conductivity of BSMs is a multidisciplinary topic, therefore input of specialised experts is required.

Laboratory investigations of BSM-foam layers show that the temperature across the pavement section is not uniformly distributed over the layer. The trend observed shows that the maximum temperature is relatively higher in the upper BSM layers than in the granular base layers. Therefore, the temperature gradient in a layer may be used to determine its influence on moisture evaporation. This implies that an understanding of the temperature distribution in BSM-layer is important for preparing the appropriate mix design of a pavement avoiding the future problem of permanent deformation. The key factors that have been indicated to influence temperature distribution and voids characteristics in BSMs are: heat transfer, thermal conductivity and voids structure. The heat transfer in the BSM-layer depends on local environmental factors such as solar radiation, wind speed and relative humidity as well as the materials' properties. Therefore, modelling of these factors is required for proper prediction of evaporation and strength gain in the layer.

In the longer term, the influence of moisture transport and storage on the model and climate-dependent response should be investigated to determine the influence on the accuracy of prediction on different geographical areas, especially in high rainfall regions.

This temperature study was limited to the study of the temperature distribution in the pavement sections considering only the diurnal effects on the different layers. Further research should be carried out to analyse the nocturnal effects and the low temperatures in the pavement structures.

8.2.4 Synthesis

In this research, deflections of a flexible pavement, composed by three different BSM-foam mixes with a high percentage of RA, CTSB or granular sub-bases and uniform or dual subgrades, have been tested. Measurements have been carried out at pavement structures and different loading configurations.

The uniform or dual subgrades don't create any particular effects on the horizontal and vertical stress distributions. However, considering a different sub-base, CTSB (phase I) or granular material, a shift in the deviator stress distribution is present in the pavement structure. In fact the deviator stress in the BSM-foam base layer increases as soon as the sub-base passes from CTSB to granular material.

Different thicknesses of the HMA contribute to create horizontal stress tensions on the edge between the asphalt layer and the BSM-foam base. A thinner HMA layer represents the best method to reduce tension effects in the pavement. High traffic loading which can occur on the top of the pavement can easily lead to possible fatigue behaviour and permanent deformation in the HMA.

The influence of the temperature gradient on the mechanical properties of the BSMs gave the possibility to study the pavement section with more precision: every single layer of BSM has a different temperature and different resilient modulus as the depth increases. This can lead to a better representation of the road package as well as to a more effective pavement design.

- It is concluded that various improvements can be made at the design stage of transport infrastructure by understanding the implications of the interaction between pavement design, the thermo-physical properties of the BSM-foam materials with a high percentage of RA, and the ambient climatic conditions.
- The stress-strain analysis of a BSM-foam incorporated into a pavement structure was done using a linear elastic model in the BISAR 3.0 program. The analysis indicates that tensile stress occurs in the BSM-foam layer. Care should be taken when critical design values are determined from these stress state calculations, as they are likely to be an overestimation.
- The results obtained in the stress analysis of a pavement considering different temperatures for the asphalt layer demonstrated the importance of the consideration of this parameter in pavement design. Higher temperatures lead to higher displacements and greatly affect the horizontal stresses. An understanding of all mechanical and thermal properties is essential for the comprehension of other performances of BSMs, such as fatigue and damage behaviour.
- High deviator stress ratio in the BSMs could lead to possible fatigue effects, especially when the temperature in a pavement rises. The magnitude of the critical deviator stress ratio for design purposes as well as the depth at which it occurs is therefore affected when the pavement is analysed using the linear elastic model.
- The critical stress ratio has to be evaluated together with the stiffness and ultimate strength of the material. Two materials with similar performances in terms of stress ratio can perform substantially different from each other in the pavement structure under similar absolute levels of loading.
- The deviator stress ratio increases in the middle of the BSM-layers as the temperature rises in the pavement structure. This difference is more outlined in the BSM-foam mix with 100%RA than in the mix with a low percentage of RA.
- Vertical deformations increase in the BSM layer as the temperature and the loading configuration increase. The deformations in the BSM-foam layer with 100%RA are higher than the other two mixes.
- The temperature gradient should be studied in the pavement section even during the night period, focusing more on the possible effects of the lower temperatures on the BSM-foam layers.

8.3 Recommendations

- This research confirms the importance of the cyclic tri-axial test, for determining the mechanical properties of BSM-foam mix with different percentages of reclaimed asphalt. The sensitivity to temperature and percentage of RA are important, and should be studied in more detail. The work should be continued on the same material, to study in particular the influence of a greater range of temperatures and different percentages of reclaimed asphalt on the response models and laboratory performance BSM-foam mixes.
- The complex nature of the mechanical dynamic tests suggests further tests in this direction, focusing more on a possible link between temperatures, different deviator stress ratios and percentage of RA. When performing permanent deformation tests in a research environment it is recommended to adopt a minimum test duration of 1 million load repetitions (unless failure occurs prior to this).
- It is recommended that the structural design of BSM pavements focuses on shear strength and permanent deformation behaviour.
- More research is needed to expand the understanding of the performance and durability properties of BSM-foam mixes with different percentages of reclaimed asphalt. Further tests are necessary to explain possible relationships between mechanical tests and the durability brushing test. A greater range of BSM-foam mixes needs to be evaluated using the brushing test. The understanding of this behaviour will provide confidence in determining the failure mechanisms and the ability to characterise the durability properties with a higher percentage of certainty during all phases of application of BSMs, which is mix design, construction and in-service condition.
- One of the weak points of the research conducted on the BSM-foam mixes is that no field trial was conducted due to time constraints and availability of material. Similarly, only artificial RA was used in the study. The variability of RA in the stockpiles did not help. The results presented therefore are essentially from laboratory investigations and would require field trials for the validation of the laboratory results. Future laboratory studies should similarly be extended to RA obtained from the field.
- Further research is needed to see how pavement design and material selection can be tailored to a specific location given the climatic variables of that region. Much more work is required to balance mechanical properties and thermal properties— a balance that will need to be determined in a climate-specific framework.
- It is recommended that the laboratory behaviour established in this study should be validated by linking it to known performances in the field. This should be combined with efforts focussing on developing reliable transfer functions between laboratory performance and known behaviour in the field.
- More field research needs to be done in order to evaluate more deeply the laboratory results conducted in this research.
- Laboratory test results unfortunately don’t take fully into consideration all the possible aspects that are presented in the field as weather conditions, real traffic, temperature,long term effect of curing, fatigue and rutting behaviour, etc. More efforts has to be considered in the future to validate and compare more closely all the laboratory results to the field tests.
- It is recommended to gather accurate information on temperature regimes in BSM base layers. The development of the moisture content and the stiffness of BSM’s over time should also be investigated further. This should include a range of mixes in different climatic areas (temperature and rainfall).

APPENDIX A

NEW WET – DRY DURABILITY TEST PROCEDURE FOR BITUMEN STABILISED MATERIALS (BSMs), USING THE MECHANICAL BRUSHING APPARATUS

BACKGROUND

The study for investigating the wet-dry durability of BSMs highlighted the need for the development of a laboratory test procedure. The aim was to determine the moisture resistance and durability of BSMs with a wet-dry durability test.

The test method developed in this study has been adopted at the laboratory of the University of Stellenbosch.

SCOPE

This method covers the procedure for determining the percentage of loss material obtained by repeated wetting, drying and brushing of BSMs mixtures.

APPARATUS

1. A suitable water bath with thermostatic control capable of maintaining a temperature of 25°C ± 1°C.

2. A scale to weight up to 10 kg, accurate to 0.5 g

3. A brushing apparatus of the type shown in the Figure A.1 with the following characteristics:

   - capable of rigidly holding a specimen or core (150mm diameter and 150mm height) and rotating it, under the prescribed load, at the rate of 60 ± 5 revolutions per minute around its longitudinal axis;
   - incorporating an electronic device for setting and controlling the number of revolutions (50) and the rate of the revolutions (60 ± 5);
   - having a wire brush that can be brought into contact with the specimen and loaded with 2.25 kg ± 0.05 kg. The brush should be made of 40mm x 1.8mm x 0.5mm spring steel bristles randomly assembled in 180 groups of 6 bristles and mounted on a 200mm x 60mm wooden block.

Figure A.1: Wet-Dry Brushing apparatus.

Figure A.2: Details of the wire brush.

METHOD

1. Preparation of the specimens

   Prepare the specimens in accordance with the procedure described in the TG2 technical guideline (Asphalt Academy 2009). Enough material should be mixed to produce at least three specimens on the recommended binder.

2. Curing of Specimens

   Cure the specimens in accordance with the procedure described in the TG2 (Asphalt Academy, 2009).

3. Evaluation and grouping of specimens

   After curing, remove the wet bag and let the specimens cool at ambient temperature (25°C) for about one hour. Cover the specimens immediately if delay occurs for conditioning.

   After cooling, the following measurements of each specimen must be carried out:

   - the average height;
   - average diameter;
   - the initial weight of the specimen after curing.

4. Wetting, drying and brushing

   a) Submerge the specimens in a water bath at the controlled temperature of 25°C for a period of four hours.

      a. Remove the specimens from the water and measure the weight of the specimen in a controlled temperature environment at 25°C.

      b. Clamp the specimens securely between the pads of the brushing apparatus.

      c. Lower the brush onto the specimen and switch on the machine (brush load = 2.25 kg ± 0.05 kg; revolutions = 50).

      d. After the test, measure the weight of the specimen again, determining afterwards the difference in weight and the consequent percentage loss (see calculations below).

      e. Leave the specimen unsealed to dry in a controlled temperature environment at 25°C for one hour.

      f. Return the specimen in the thermostatically controlled water bath for other four hours.

g. Repeat the procedure described in the points numbered a, b, c and d.

h. After the test, place the specimen sealed in a plastic bag overnight in a temperature controlled environment (25°C) .

The procedure described so far in this section constitutes two cycles (almost 6 hours) of the wet-dry durability test. The specimens are again submerged in water the following day and the procedure repeated for 12 cycles.

DETERMINATION OF THE PERCENTAGE LOSS

After 12 cycles, the percentage loss measured for each cycle has to be added to the other values to obtain the cumulative percentage loss. The data collected will permit the calculation of the BSMs loss of the specimens after the prescribed 12 cycle test.

CALCULATION

Calculate the single percentage loss for every BSMs specimen after one cycle as follows:

$$L = \frac{W - M}{W} \text{ x } 100$$

where

L = percentage loss per cycle (%);
W = original mass of the specimen before the brushing test (g);
M = final mass of the specimen after the wet-dry brush test (g).

The mass determination of the specimens before and after brushing must be recorded at the end of each cycle. The cumulative percentage loss is carried out adding the single percentage loss measured during every cycle.

The percentage loss shall be calculated and reported to the nearest 0.1 per cent.

These results are required for designing a mix and are normally reported graphically against the bitumen binder content.

REFERENCES

ASTM Designation D558-57 (AASHTO Designation T134-61)
ASTM Designation D559-57 (AASHTO Designation T135-57)
TMH1 Method A19

APPENDIX B

WET – DRY DURABILITY TEST RESULTS FOR BITUMEN STABILISED MATERIALS (BSMs), USING THE MECHANICAL BRUSHING MACHINE – 4 HOURS SOAKING

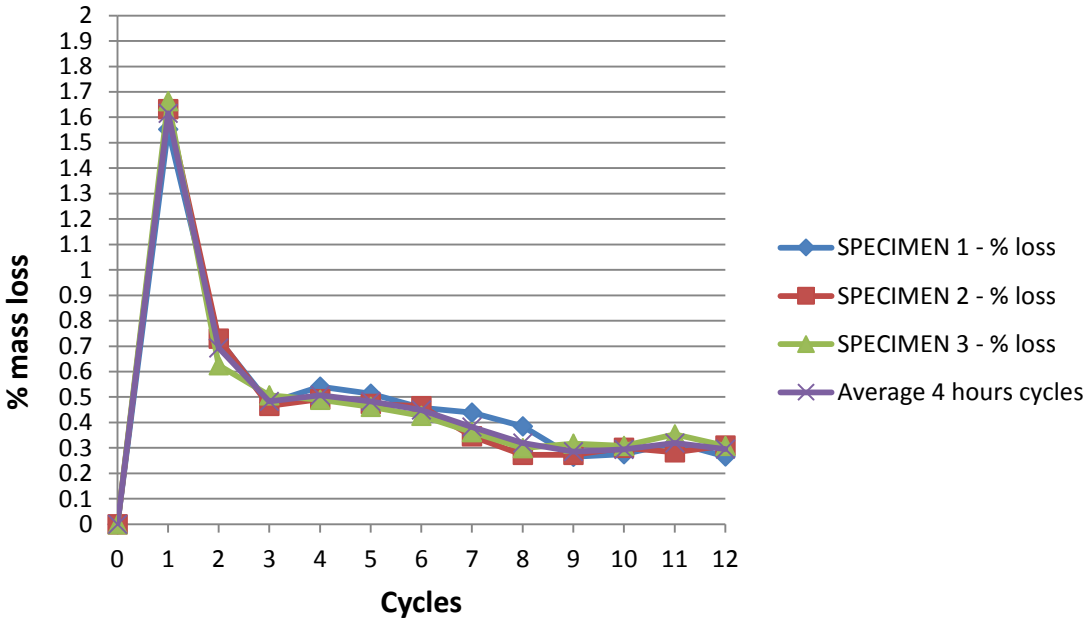

Figure B.1: Percentage loss on BSM-foam (2% bitumen content) with 100%RA.

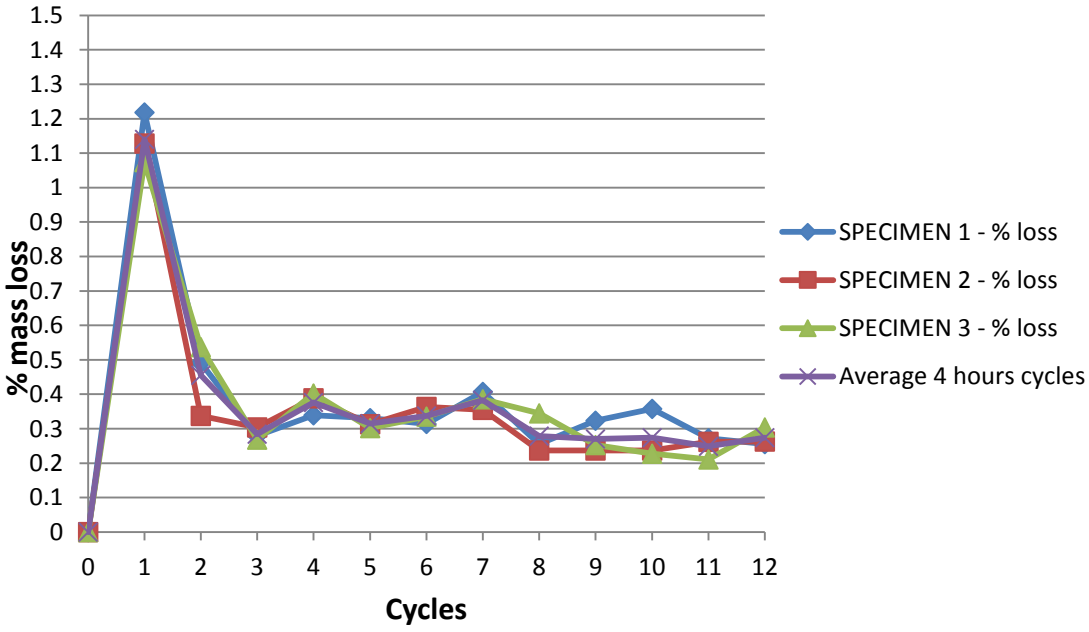

Figure B.2: Percentage loss on BSM-foam (2.1% bitumen content) with 50%RA and 50%G2 (Hornfels) crushed stone.

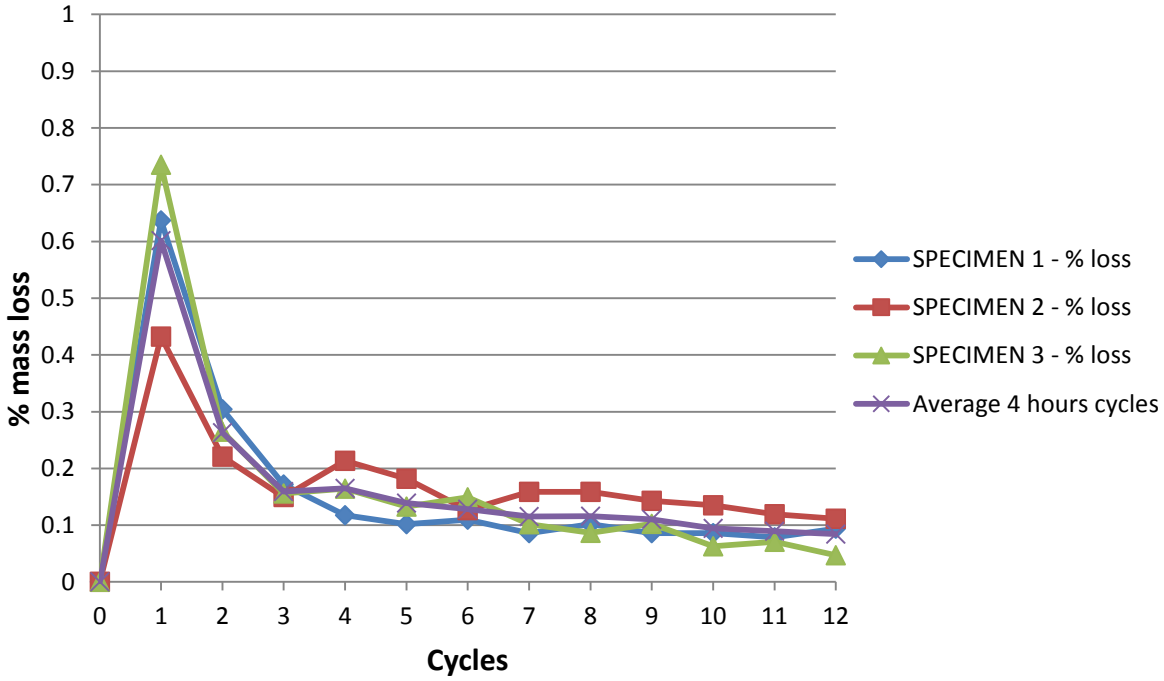

Figure B.3: Percentage loss on BSM-foam (2.3% bitumen content) with 100%G2 (Hornfels) crushed stone.

Table B.1: Summary of the cumulative average mass loss for the three BSM-foam mixes with an increasing percentage of RA.

BSM-foam mix	**Cumulative average loss (%)**	**Standard Deviation**	**Cov**
100% RA	6.13	0.09	1.45
50%RA 50%G2	4.64	0.21	4.53
100%G2	2.07	0.09	4.26

APPENDIX C

DYNAMIC TEST SET-UP AND PROCEDURE USING A TRI-AXIAL CELL

BACKGROUND

Dynamic tri-axial testing was carried out using a testing system comprising an actuator, a reaction frame, a control panel and a data acquisition system. The Material Testing System (MTS 810), which is a closed loop servo-hydraulic testing press system was used in this experiment for short and long dynamic tri-axial tests. The system uses a MTS model 506.03 hydraulic power unit with a high pressure supply of approximately 70,000 kPa. It has a 98.1 kN actuator with 80 mm stroke (up and down). The University's MTS was upgraded in March 2012 with an external laptop which was able to control and configure the dynamic tests.

SCOPE

This method covers the procedure to set-up a 150mm diameter x 300mm height specimen for a dynamic (short and long) tri-axial test.

APPARATUS

1. MTS (Material Testing System) machine with a closed loop servo-hydraulic testing press system.
2. Tri-axial cell with a maximum rating pressure of 1700kPa.
3. Load cell with a capability of 98.1kN.
4. Three deformation transducers (LVDTs) with a range of ± 5mm.
5. Two circumferential LVDTs with a range of ± 5mm.
6. Two brackets to accommodate the three external LVDTs around the specimen.
7. Two o-rings for circumferential measurements.

METHOD

The tri-axial specimen set-up for the short and long duration dynamic testing (resilient modulus and permanent deformation test) is more complicated than a monotonic tri-axial test and

requires the installation of three on-specimen LVDTs and two circumferential LVDTs. The installation of these LVDTs shall be done according to the following protocol:

The specimen is placed on the top of the base of the tri-axial cell.

The membrane is placed over the specimen and the seating plates.

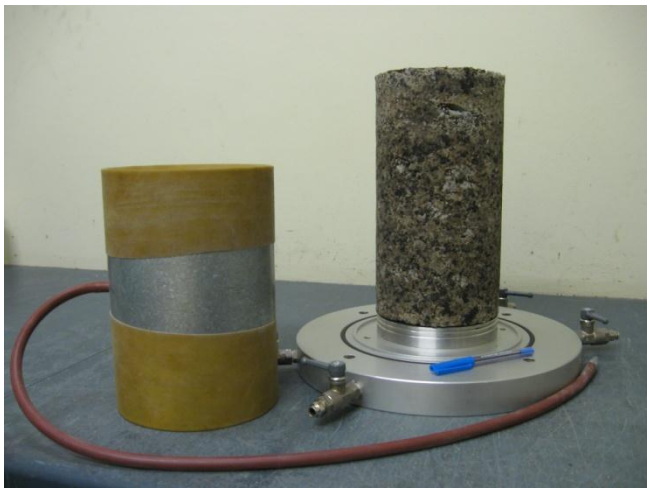

The two o-rings for the measurement of the circumferential displacement are placed in the middle third area of the specimen.

The two clamps are fitted around the specimen exactly on the middle third.

The three vertical LVDTs (range ±5.0mm with an output of ± 10V) are placed in the clamps and are fastened;

The two clip gauges (range ±5.0mm) are attached to the two circumferential o-rings.

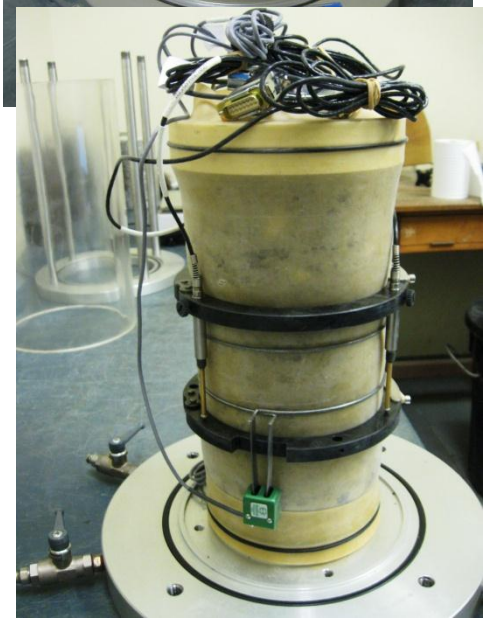

The tri-axial shall be closed accurately, avoiding air leaks and connecting all the LVDTs and clip gauges through the top plate to the data acquisition system (Spider® 8).

The test is controlled through a laptop with a MATLAB® program designed at the University of Stellenbosch. The program can assist the operator to configure the set-up of the loading sequence of the dynamic tests. The spider 8 shall acquire all the data coming from the clip gauges at the frequency of 200Hz.

At the end of the tests all the data shall be processed through an Excel folder.
The testing system was operated in loading control mode. The cell pressures for a series of dynamic tri-axial tests performed are 50kPa, 100 kPa and 200 kPa. The loading consists of a continuous haversine load with a pre-load of 20% of the confining pressure with frequency of 1 Hz. Using a haversine shaped load pulse consisting of 0.1 second followed by 0.9 second rest period, 1000 conditioning repetitions were applied.

The selection of stress levels for the resilient modulus test is related to the type of material tested in the Monotonic tri-axial tests. The cyclic stress has to be specified as a ratio to the average failure deviator stress ($\sigma_{d,f}$) obtained from a monotonic tri-axial test, performed on replica specimens at a similar confining pressure and prepared in the same way as those for the resilient modulus test, i.e $\sigma_{cyclic} = 0.3\sigma_{d,f}$.

For the subsequent loading stages after the conditioning, 100 cycles of loading and unloading are applied to the specimens, using a haversine shaped load pulse consisting of 0.1s followed by 0.9s rest period. The data was sampled at a rate of 200Hz.

APPENDIX D

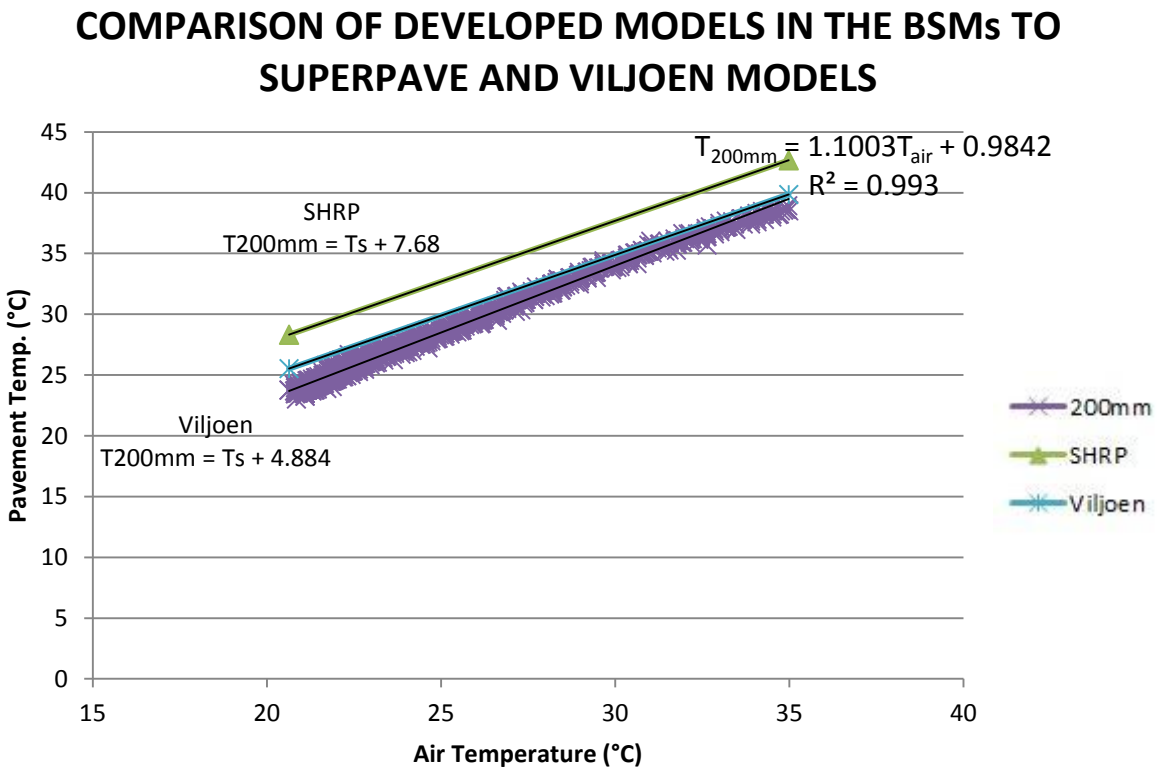

Figure D.1: Comparison between temperature prediction models at 200mm depth for BSM-Foam (2.3% bitumen content) with 100%G2.

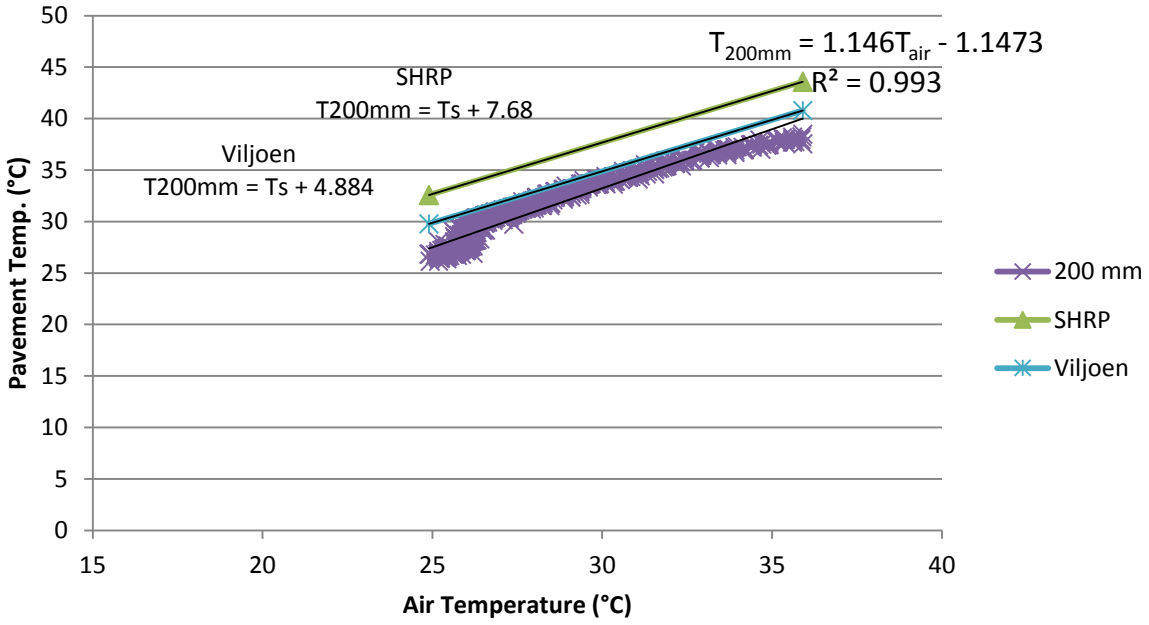

Figure D.2: Comparison between temperature prediction models at 200mm depth for BSM-Foam (2.1% bitumen content) with 50%RA+50%G2.

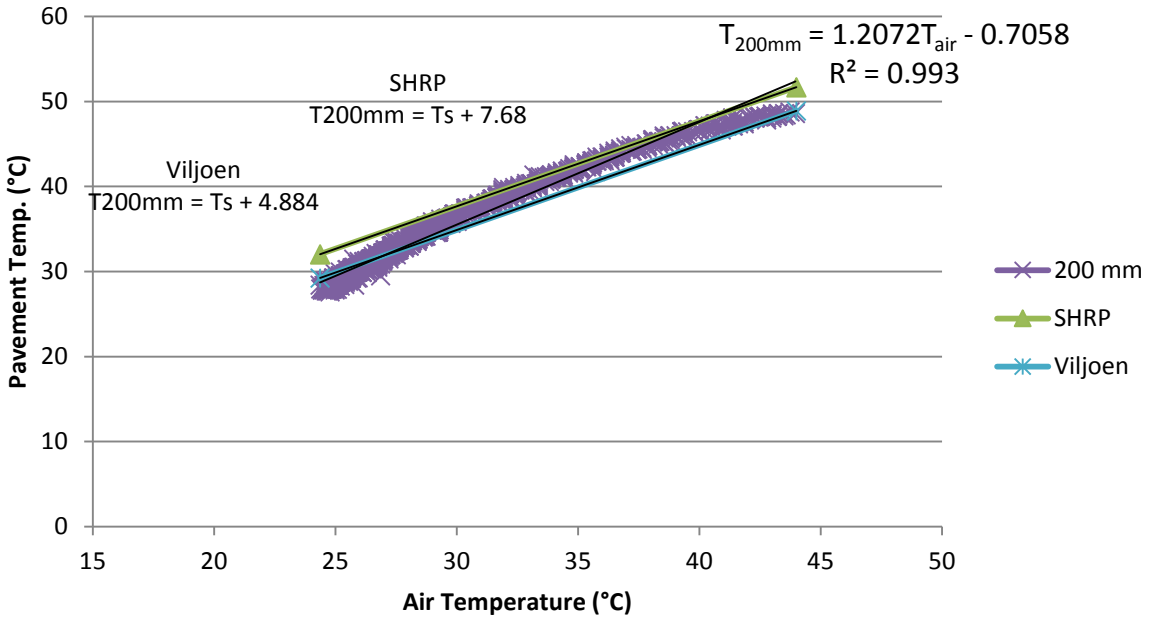

Figure D.3: Comparison between temperature prediction models at 200mm depth for BSM-Foam (2% bitumen content) with 100%RA.

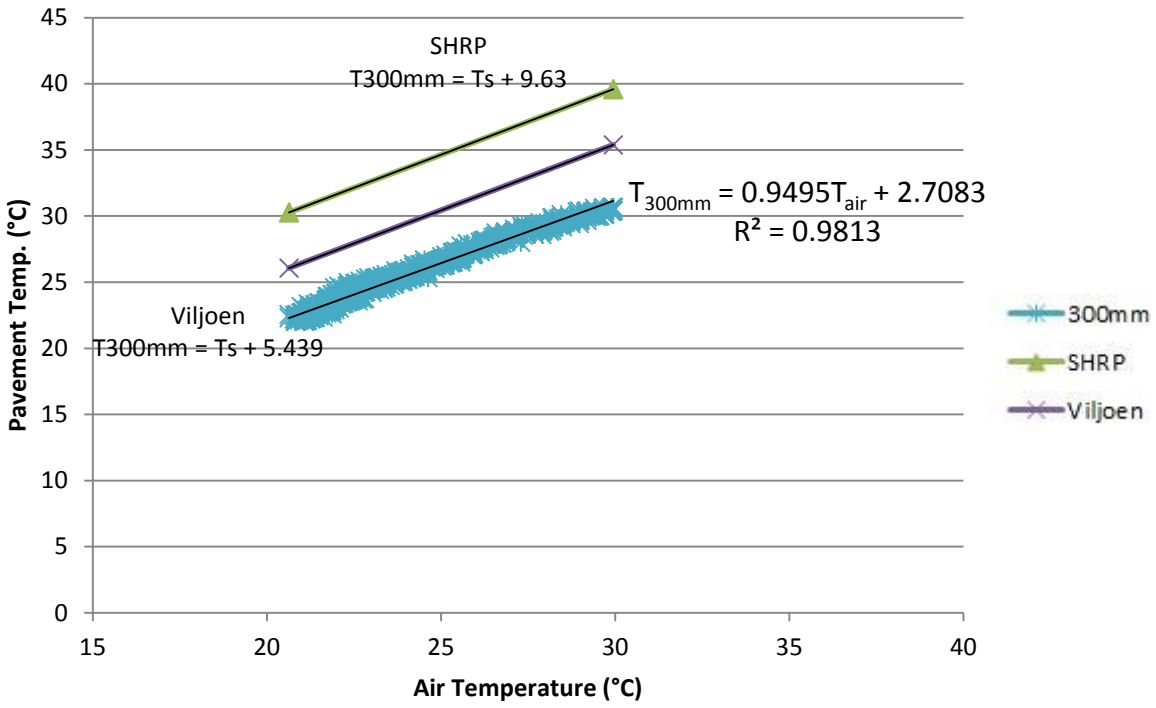

Figure D.4: Comparison between temperature prediction models at 300mm depth for BSM-Foam (2.3% bitumen content) with 100%G2.

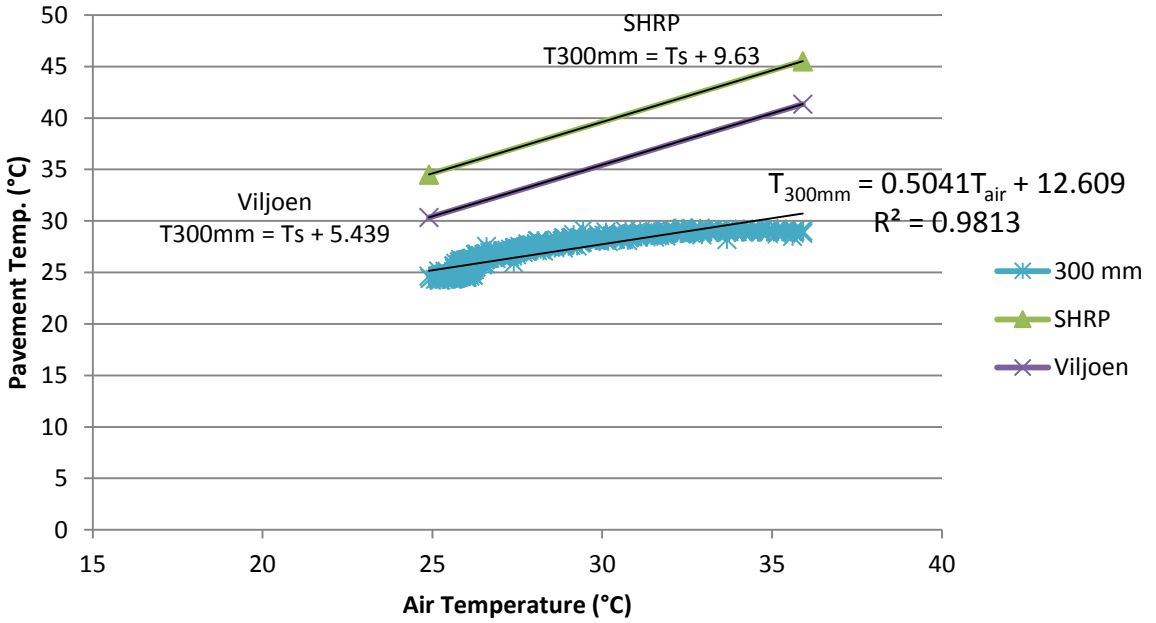

Figure D.5: Comparison between temperature prediction models at 300mm depth for BSM-Foam (2.1% bitumen content) with 50%RA+50%G2.

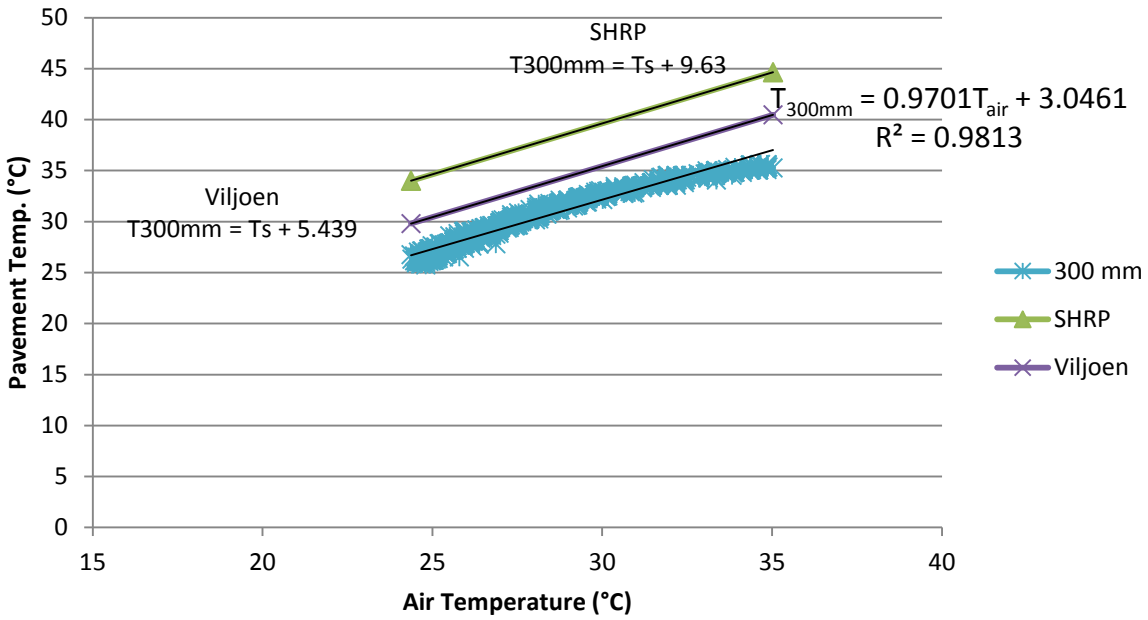

Figure D.6: Comparison between temperature prediction models at 300mm depth for BSM-Foam (2% bitumen content) with 100%RA.

APPENDIX E

COMPARISON OF THE THERMAL CAPACITY AND THERMAL CONDUCTIVITY OF THREE BSMs MIXTURES

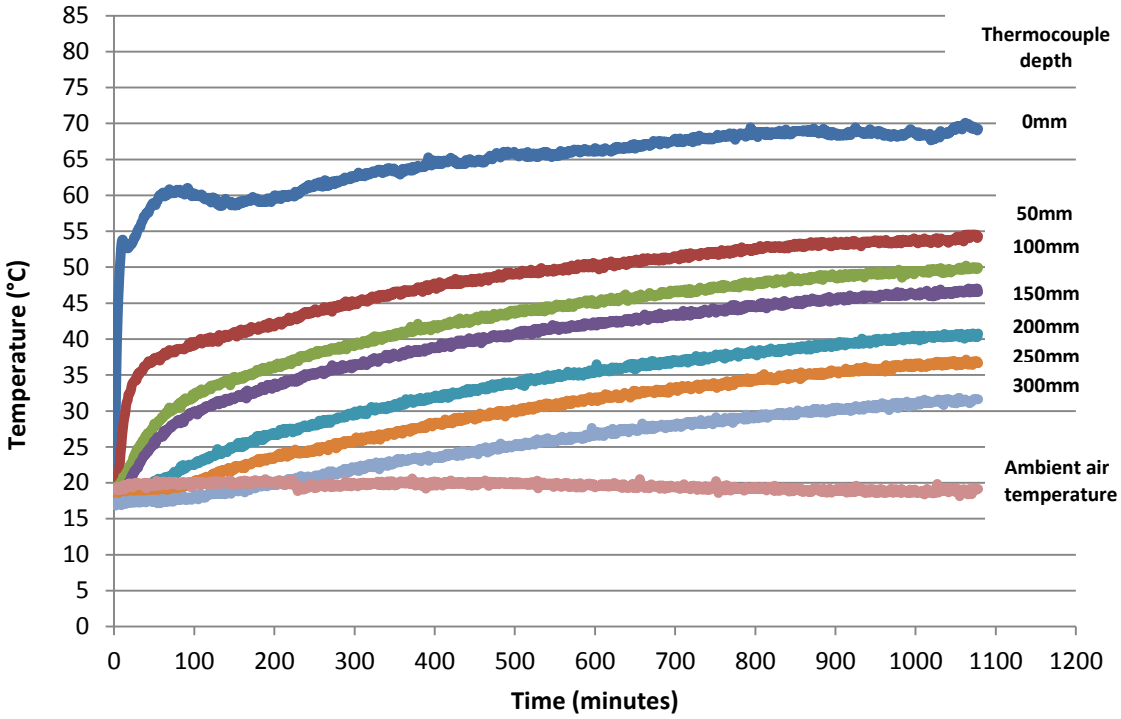

Figure E.1: Temperature distribution recorded in a BSM-foam section with 100%G2 Hornfels crushed stone (2.3% bitumen content), sustained IR heating.

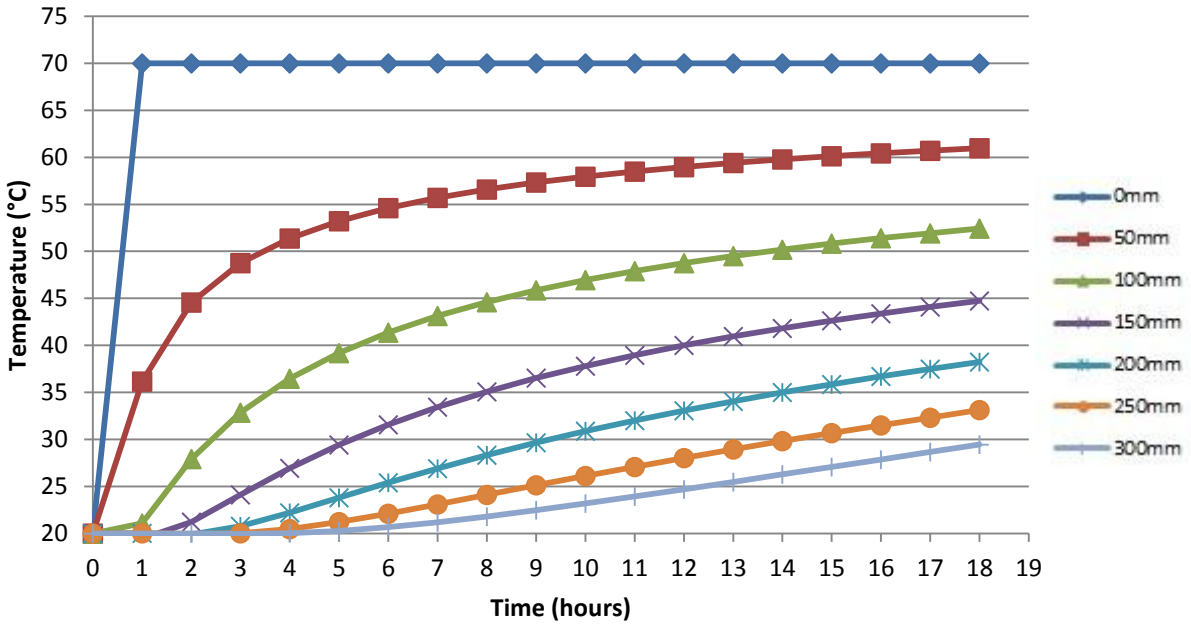

Figure E.2: Predicted temperature profiles in a BSM-foam (2.3% bitumen content) with 100%G2 material, with thermal capacity of 1900(kJ/m^{3}K) and thermal conductivity of 0.70(W/mK).

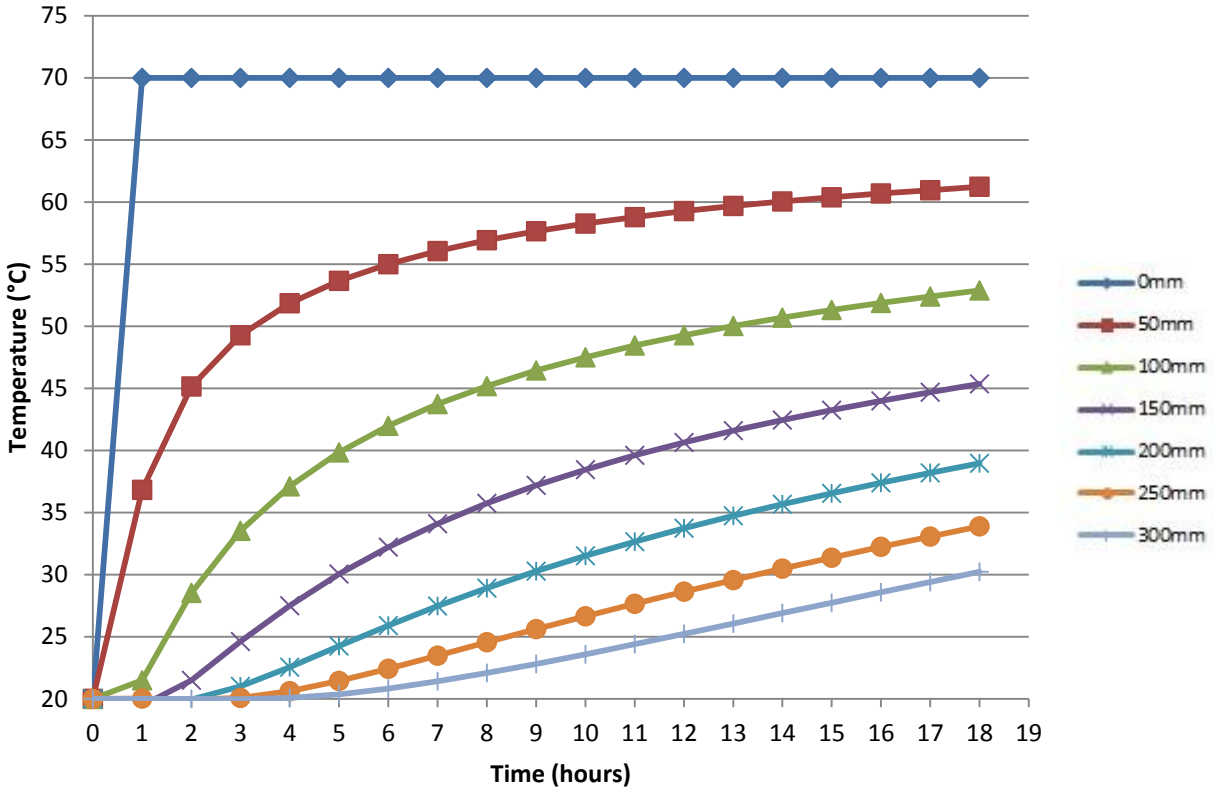

Figure E.3: Predicted temperature profiles in a BSM-foam (2.3% bitumen content) with 100%G2 material, with thermal capacity of 1800(kJ/m^{3}K) and thermal conductivity of 0.70(W/mK).

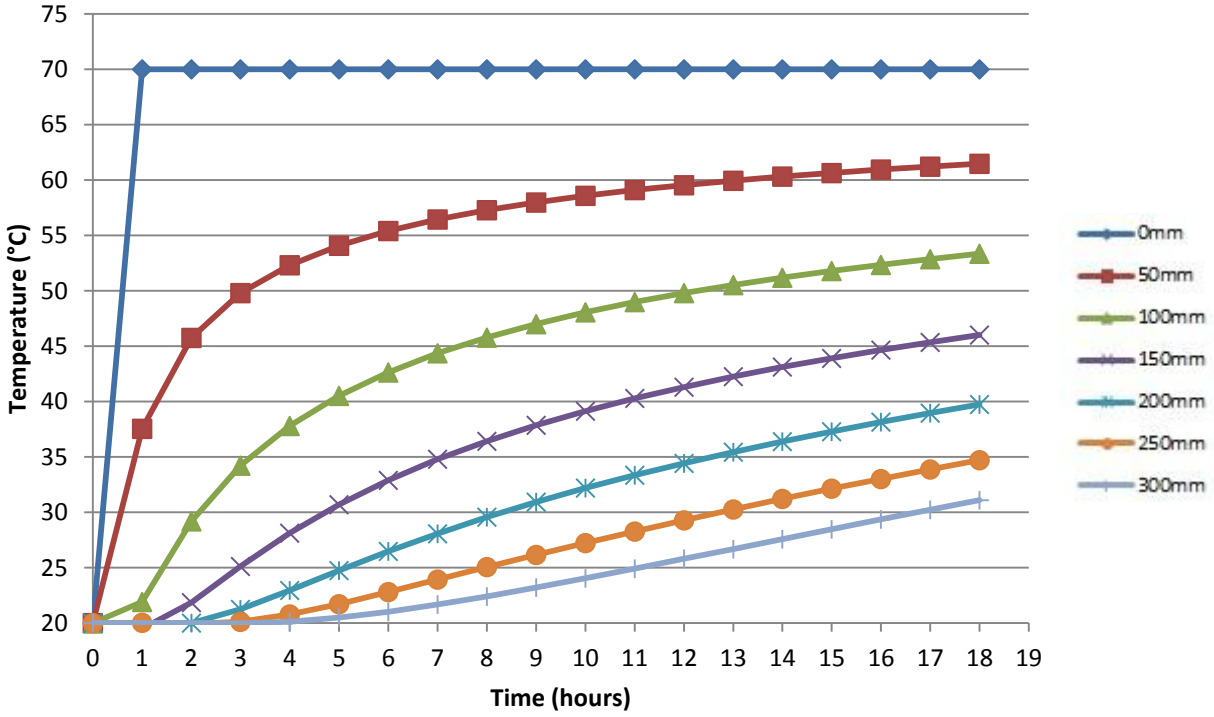

Figure E.4: Predicted temperature profiles in a BSM-foam (2.3% bitumen content) with 100%G2 material, with thermal capacity of 1700(kJ/m^{3}K) and thermal conductivity of 0.70(W/mK).

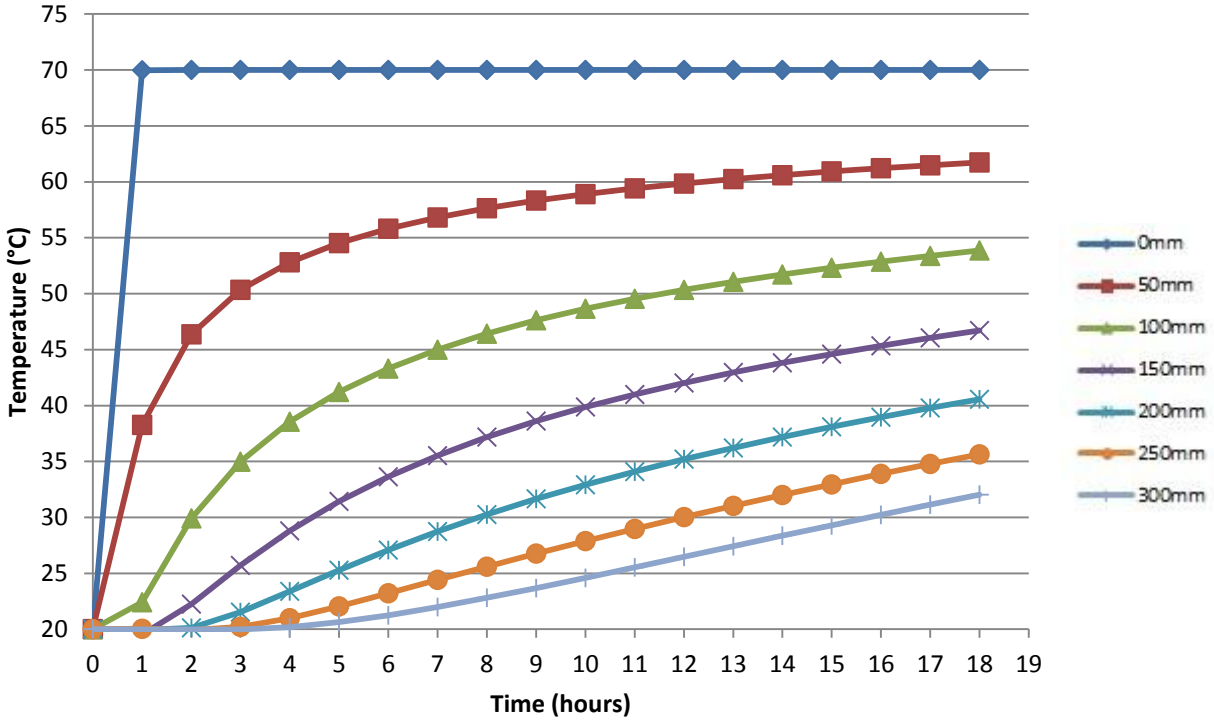

Figure E.5: Predicted temperature profiles in a BSM-foam (2.3% bitumen content) with 100%G2 material, with thermal capacity of 1600(kJ/m^{3}K) and thermal conductivity of 0.70(W/mK).

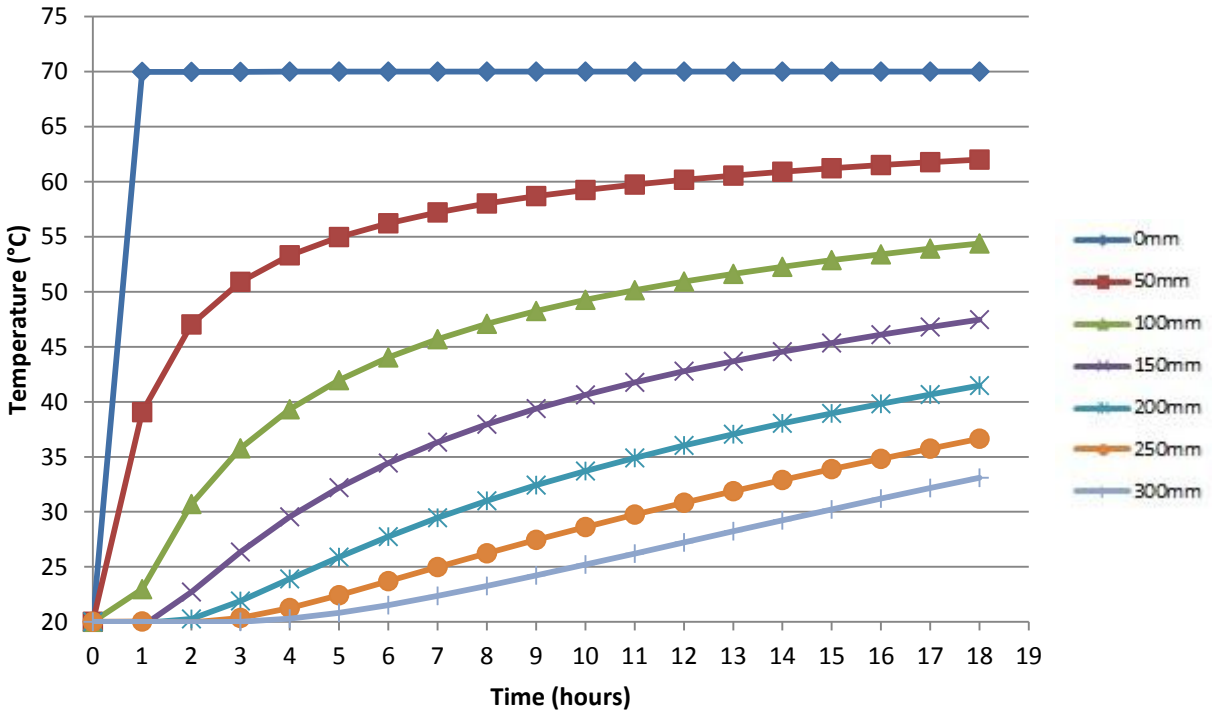

Figure E.6: Predicted temperature profiles in a BSM-foam (2.3% bitumen content) with 100%G2 material, with thermal capacity of 1500(kJ/m^{3}K) and thermal conductivity of 0.70(W/mK).

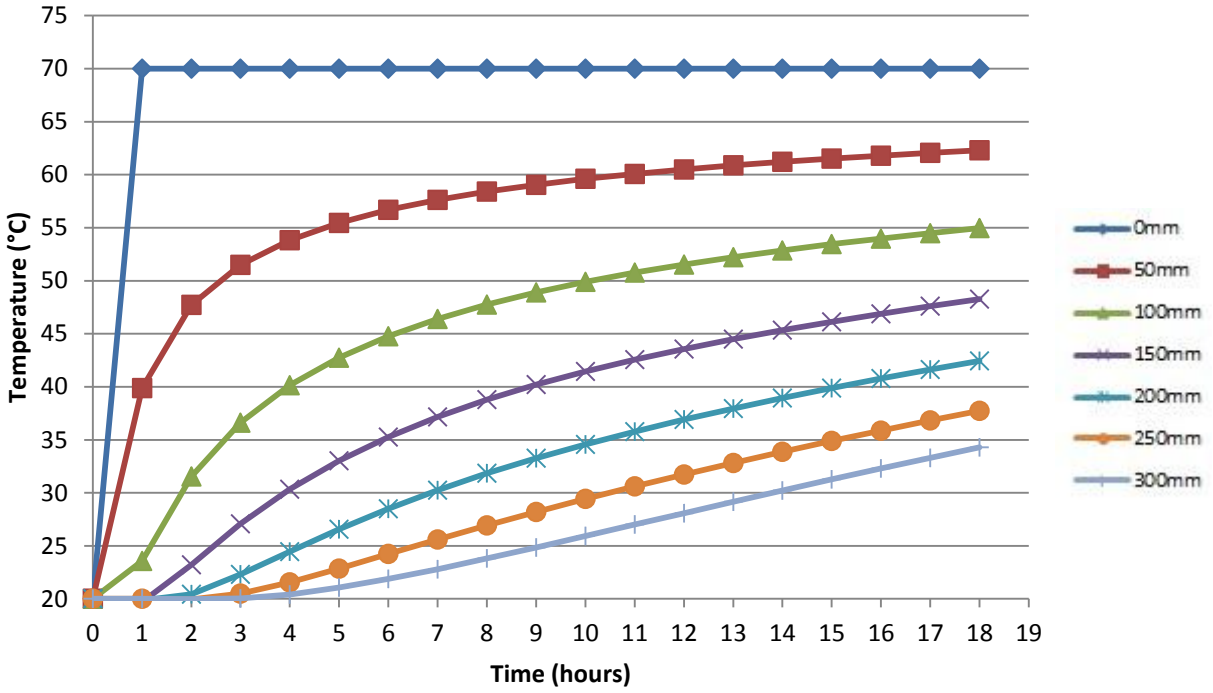

Figure E.7: Predicted temperature profiles in a BSM-foam (2.3% bitumen content) with 100%G2 material, with thermal capacity of 1800(kJ/m^{3}K) and thermal conductivity of 0.90(W/mK).

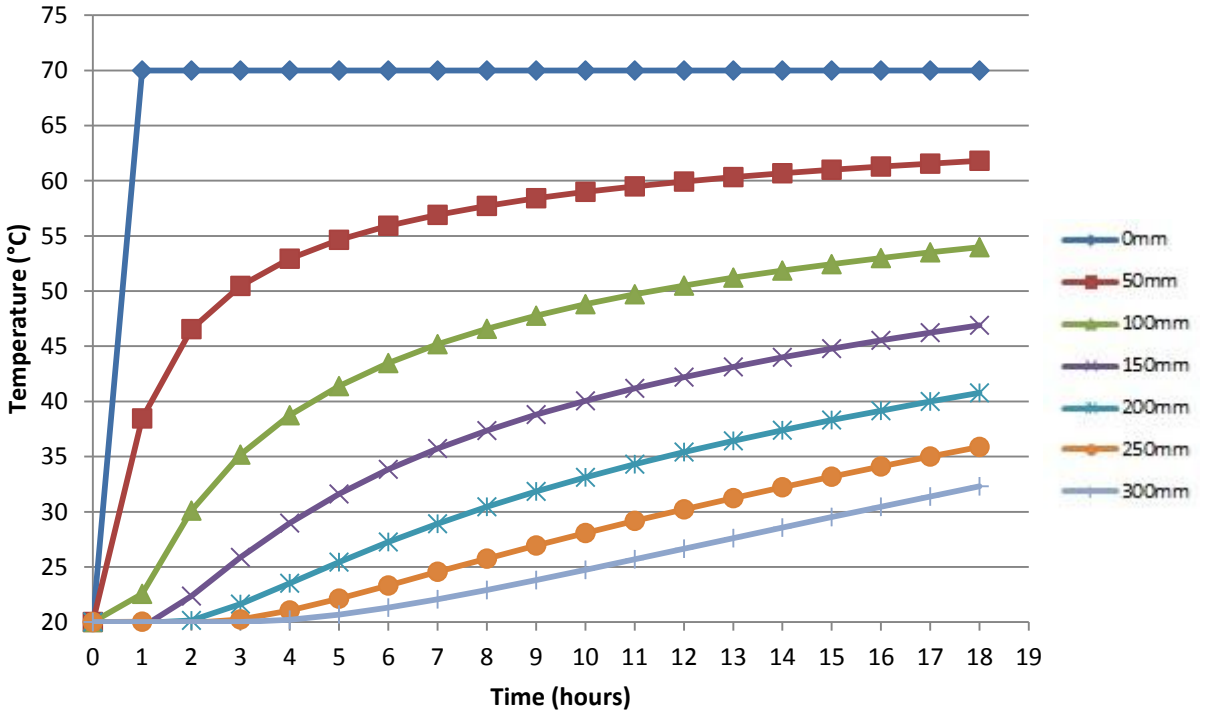

Figure E.8: Predicted temperature profiles in a BSM-foam (2.3% bitumen content) with 100%G2 material, with thermal capacity of 1800(kJ/m^{3}K) and thermal conductivity of 0.80(W/mK).

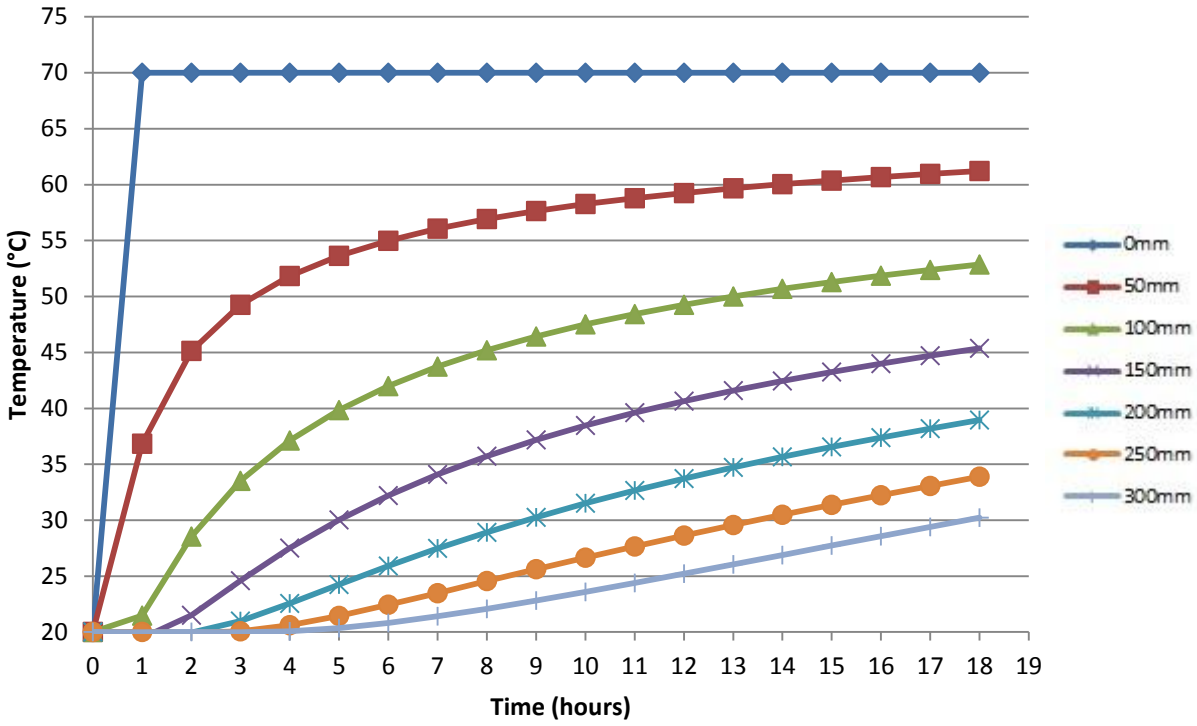

Figure E.9: Predicted temperature profiles in a BSM-foam (2.3% bitumen content) with 100%G2 material, with thermal capacity of 1800(kJ/m^{3}K) and thermal conductivity of 0.70(W/mK).

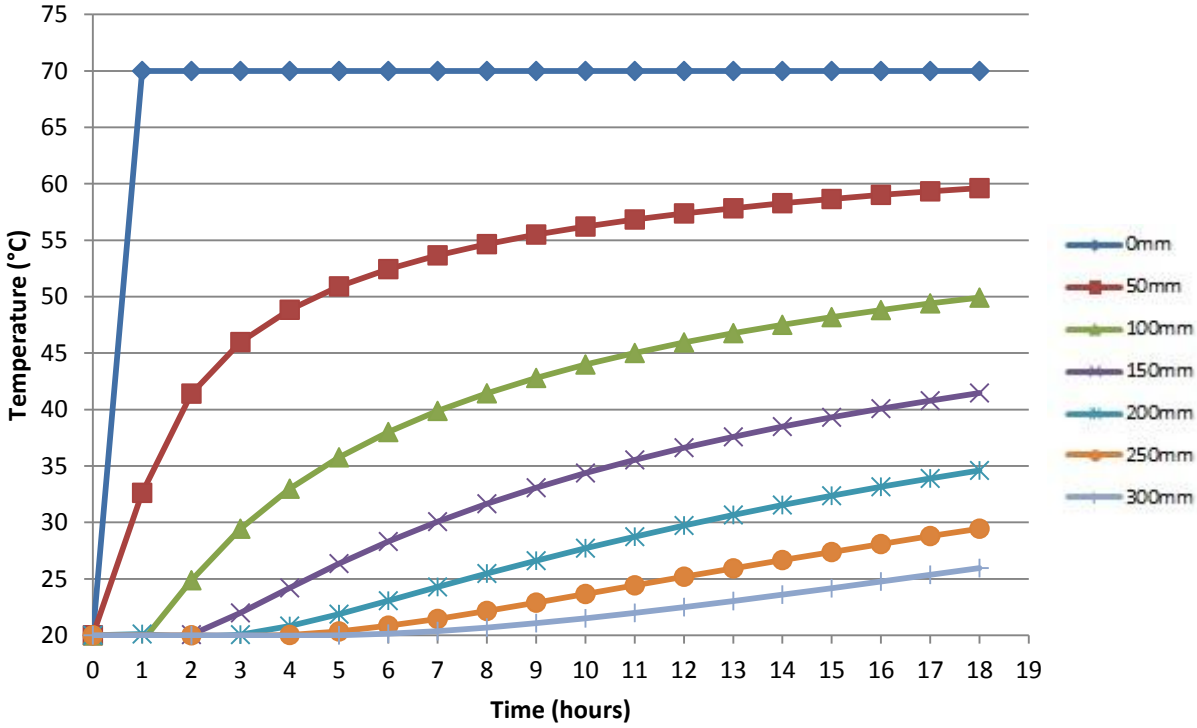

Figure E.10: Predicted temperature profiles in a BSM-foam (2.3% bitumen content) with 100%G2 material, with thermal capacity of 1800(kJ/m^{3}K) and thermal conductivity of 0.50(W/mK).

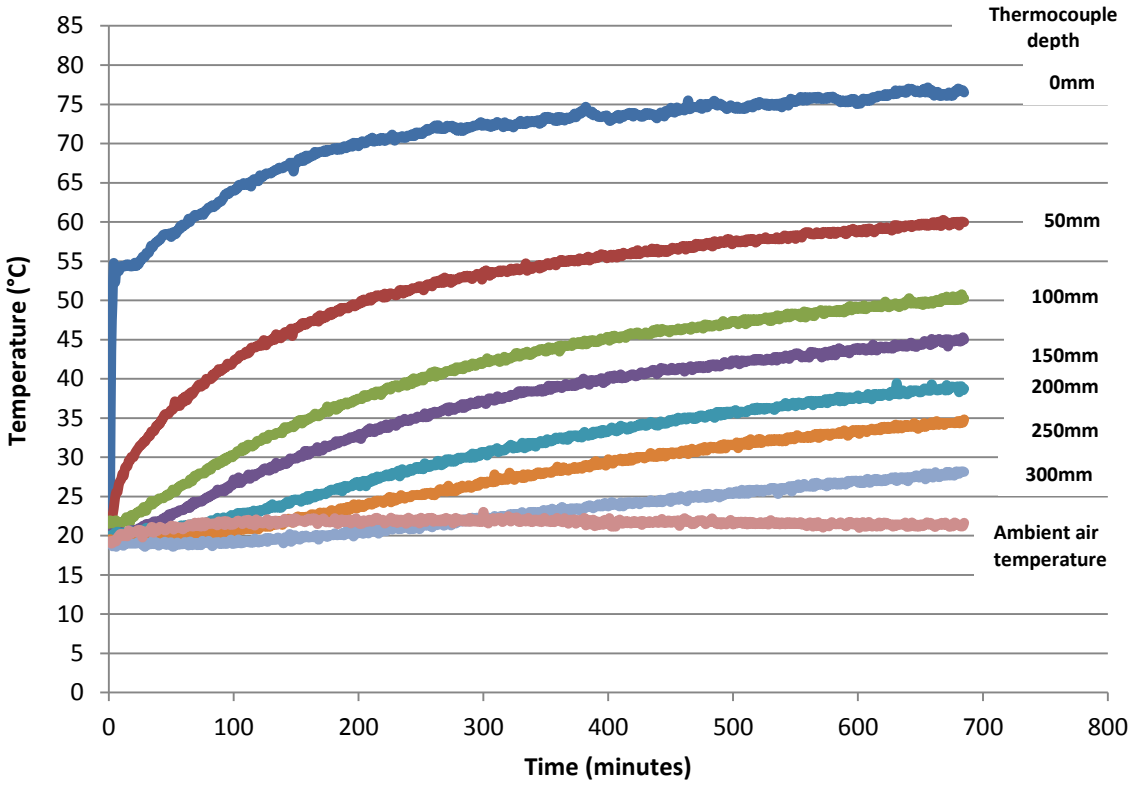

Figure E.11: Temperature distribution recorded in a BSM-foam section with 50%RA and 50%G2 Hornfels crushed stone (2.1% bitumen content), sustained IR heating.

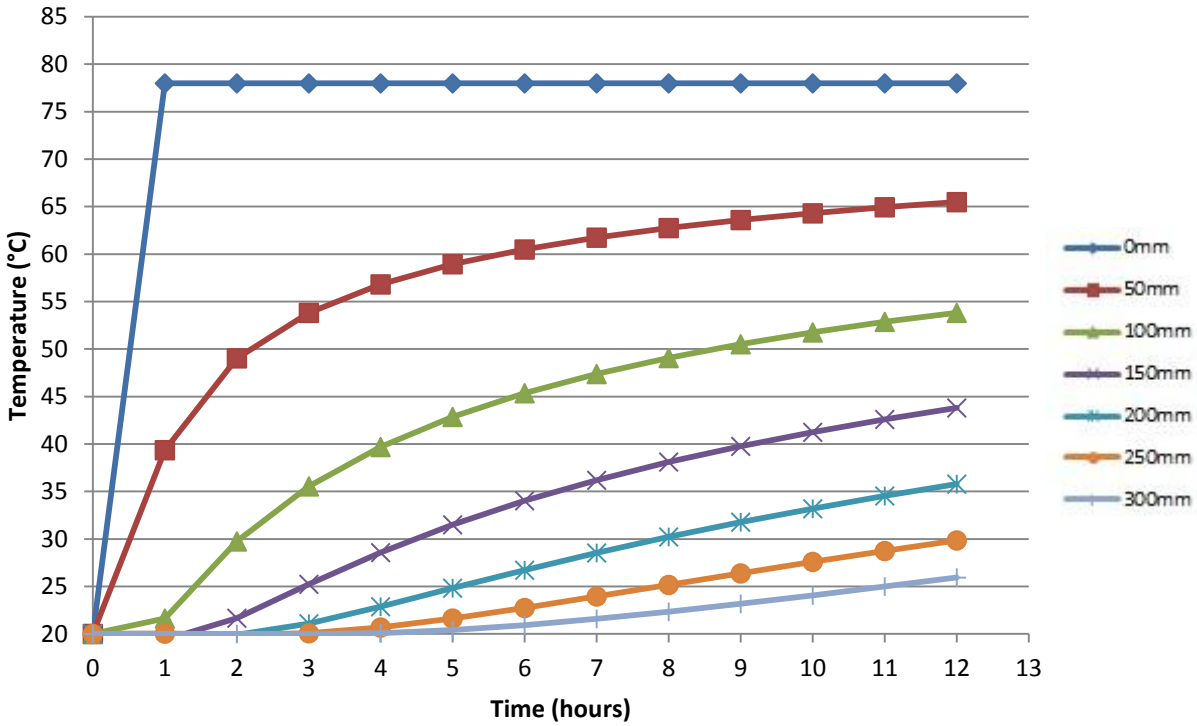

Figure E.12: Predicted temperature profiles in a BSM-foam (2.1% bitumen content) with 50%RA+50%G2 material, with thermal capacity of 1950(kJ/m^{3}K) and thermal conductivity of 0.75(W/mK).

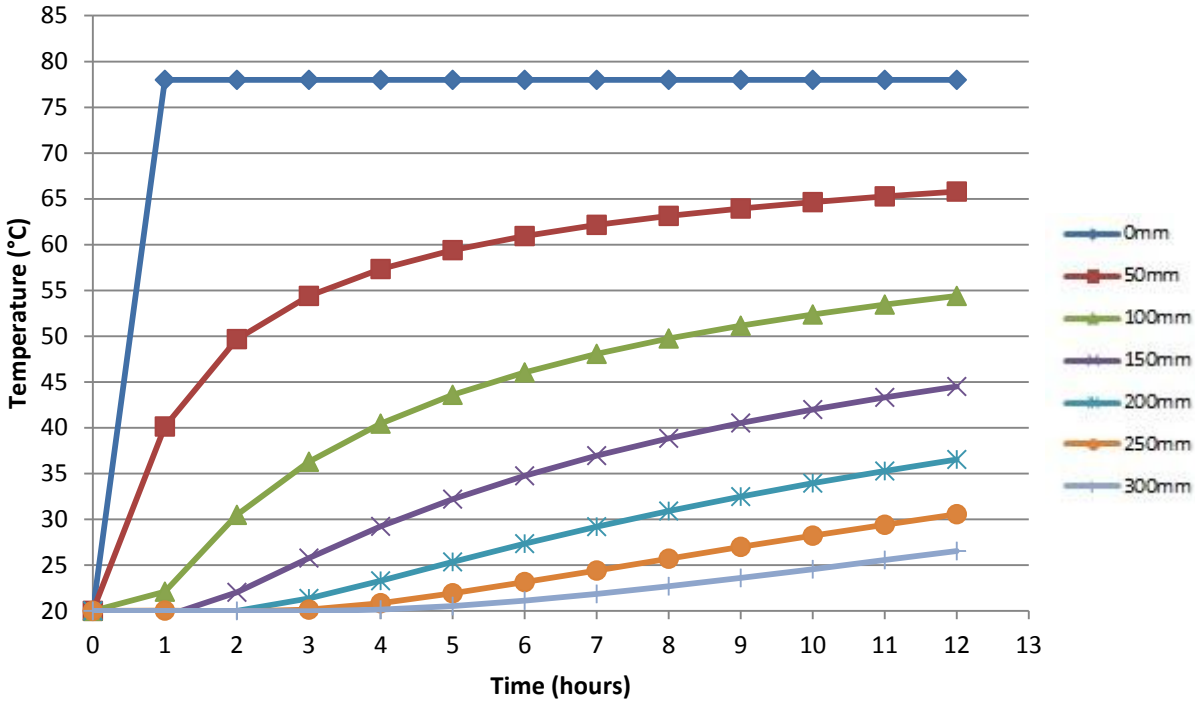

Figure E.13: Predicted temperature profiles in a BSM-foam (2.1% bitumen content) with 50%RA+50%G2 material, with thermal capacity of 1850(kJ/m^{3}K) and thermal conductivity of 0.75(W/mK).

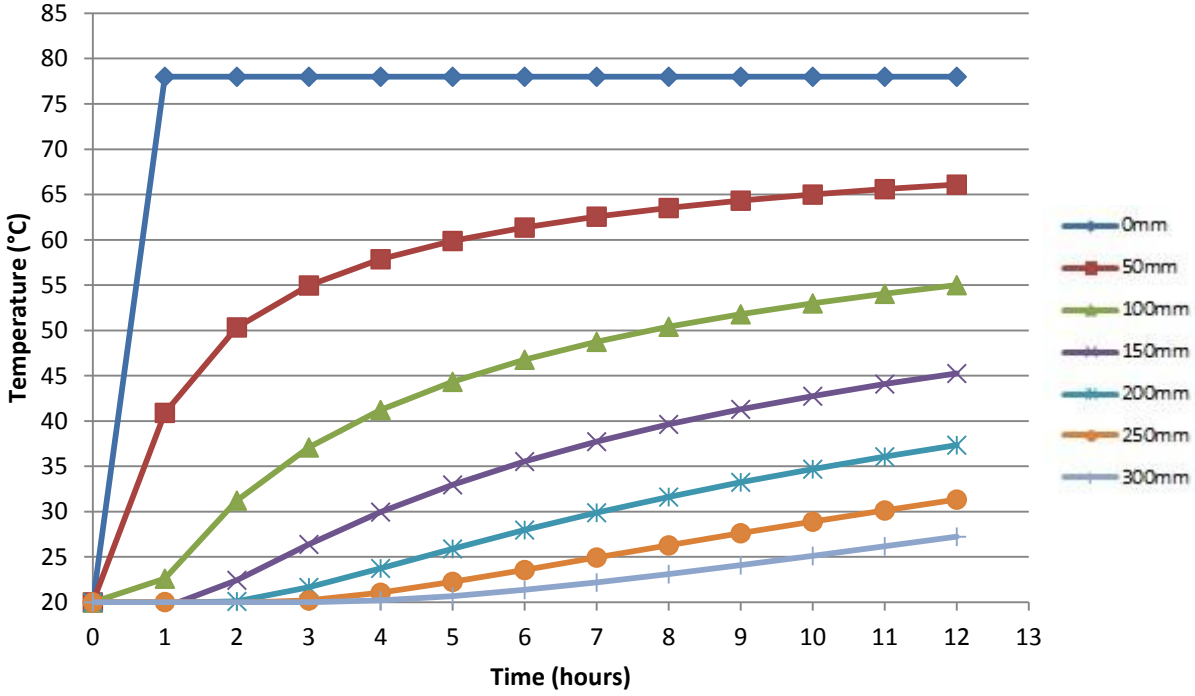

Figure E.14: Predicted temperature profiles in a BSM-foam (2.1% bitumen content) with 50%RA+50%G2 material, with thermal capacity of 1750(kJ/m^{3}K) and thermal conductivity of 0.75(W/mK).

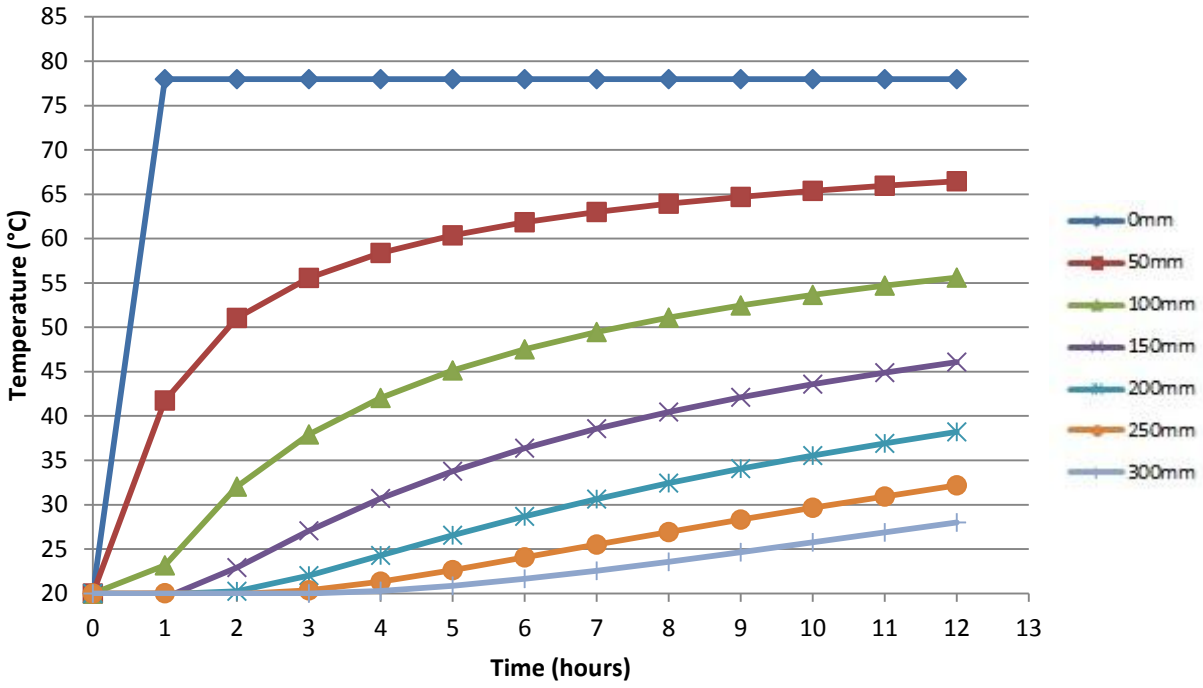

Figure E.15: Predicted temperature profiles in a BSM-foam (2.1% bitumen content) with 50%RA+50%G2 material, with thermal capacity of 1650(kJ/m^{3}K) and thermal conductivity of 0.75(W/mK).

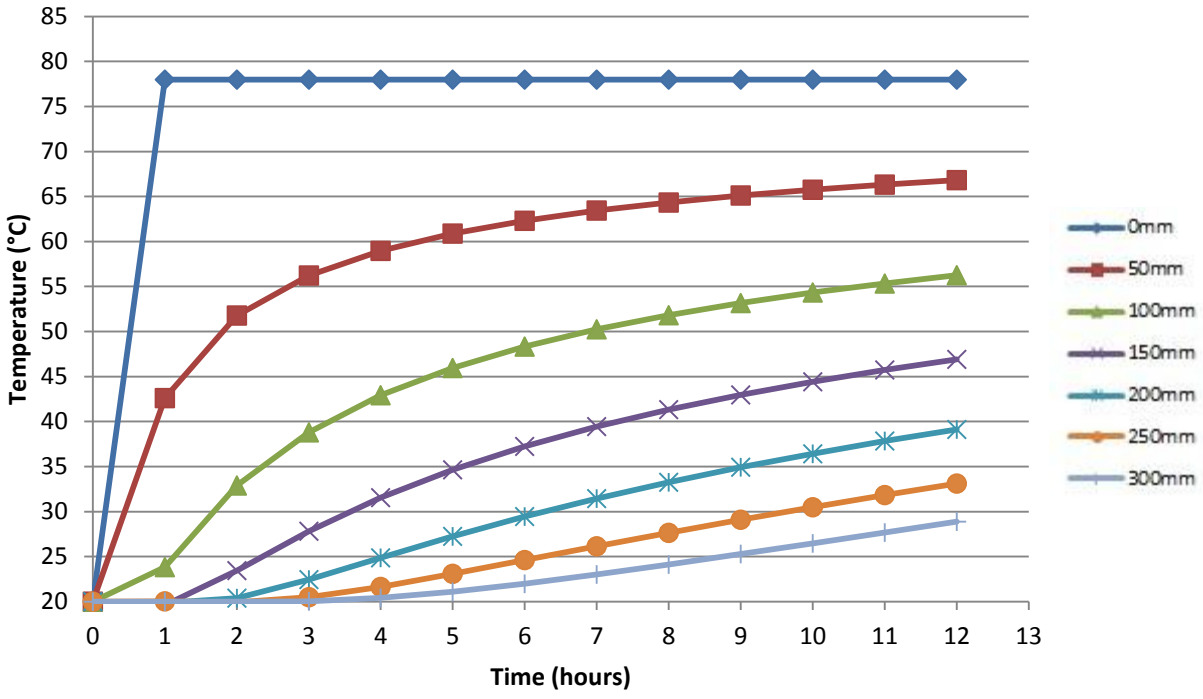

Figure E.16: Predicted temperature profiles in a BSM-foam (2.1% bitumen content) with 50%RA+50%G2 material, with thermal capacity of 1550(kJ/m^{3}K) and thermal conductivity of 0.75(W/mK).

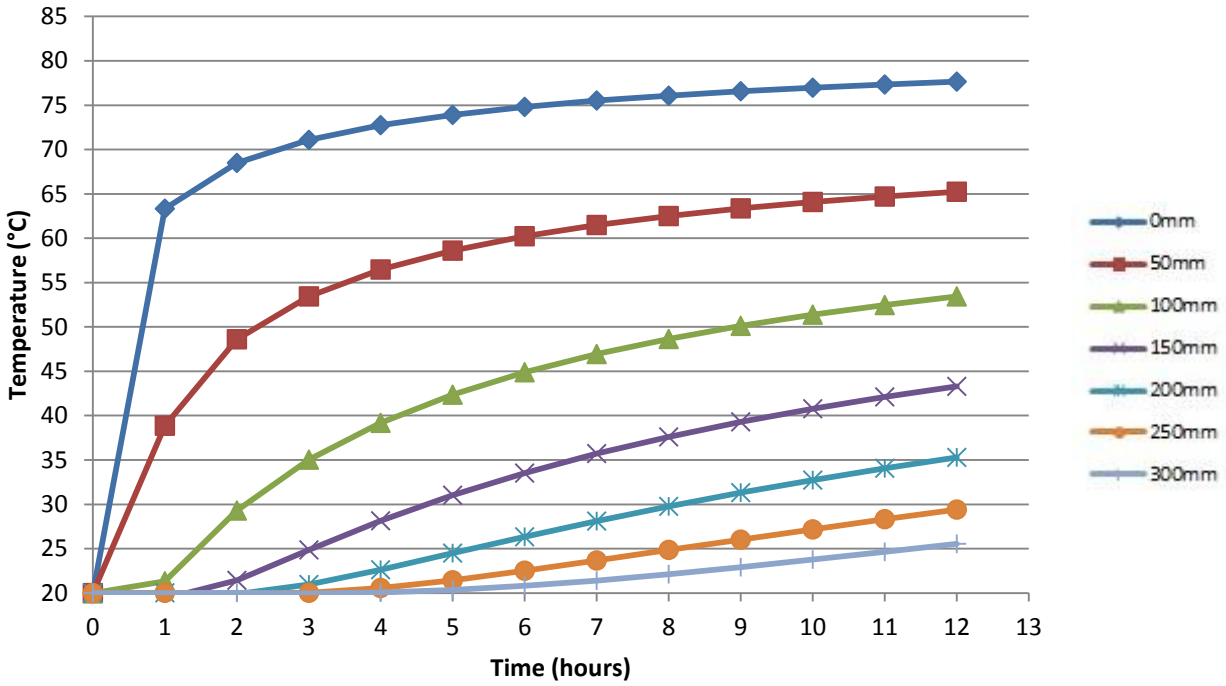

Figure E.17: Predicted temperature profiles in a BSM-foam (2.1% bitumen content) with 50%RA+50%G2 material, with thermal capacity of 1750(kJ/m^{3}K) and thermal conductivity of 0.65(W/mK).

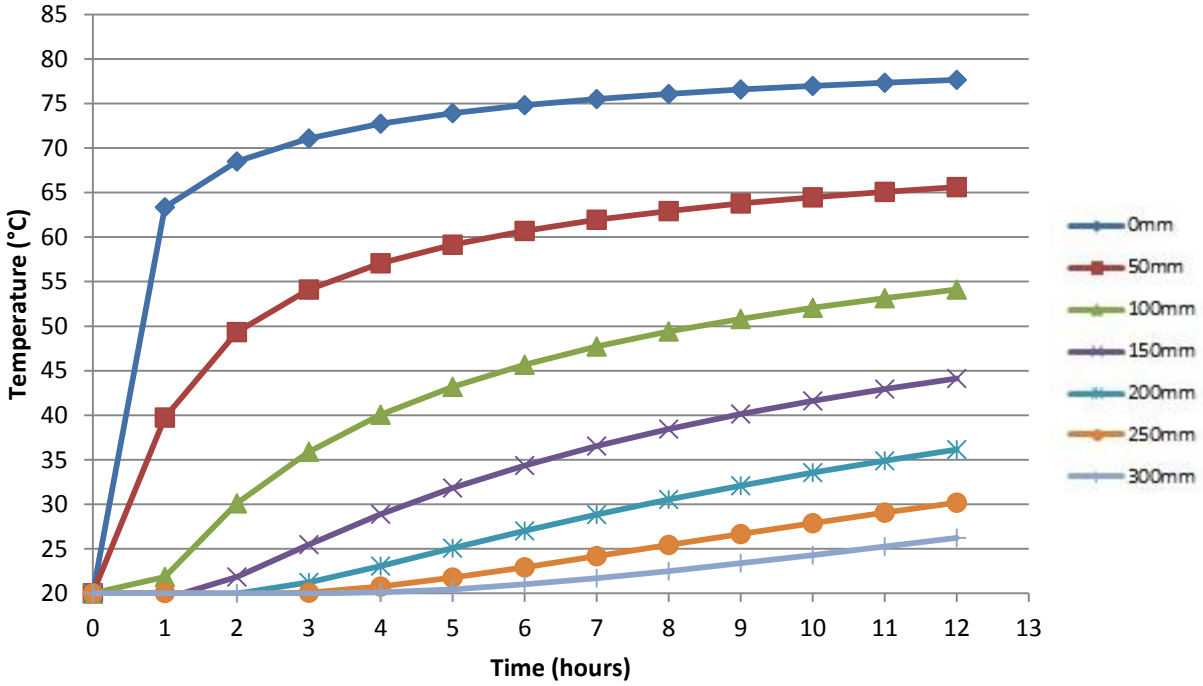

Figure E.18: Predicted temperature profiles in a BSM-foam (2.1% bitumen content) with 50%RA+50%G2 material, with thermal capacity of 1775(kJ/m^{3}K) and thermal conductivity of 0.70(W/mK).

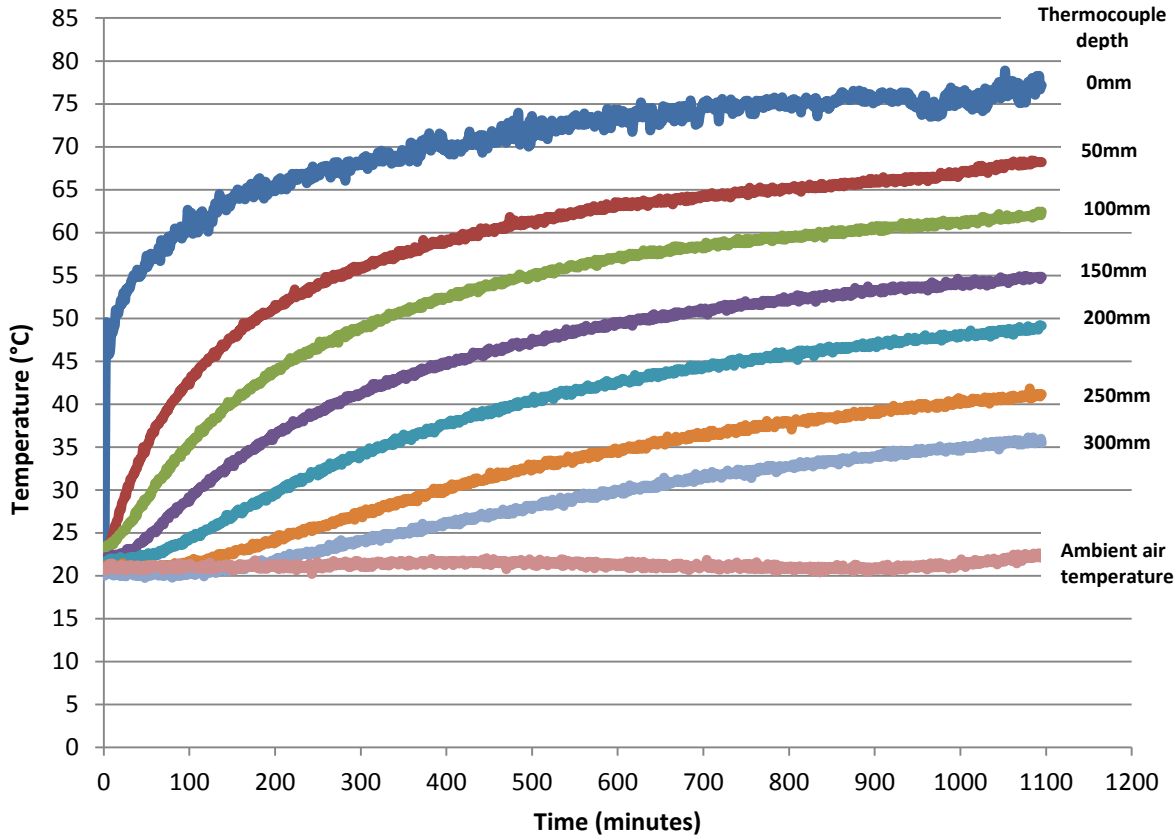

Figure E.19: Temperature distribution recorded in a BSM-foam section with 100%RA (2% bitumen content), sustained IR heating.

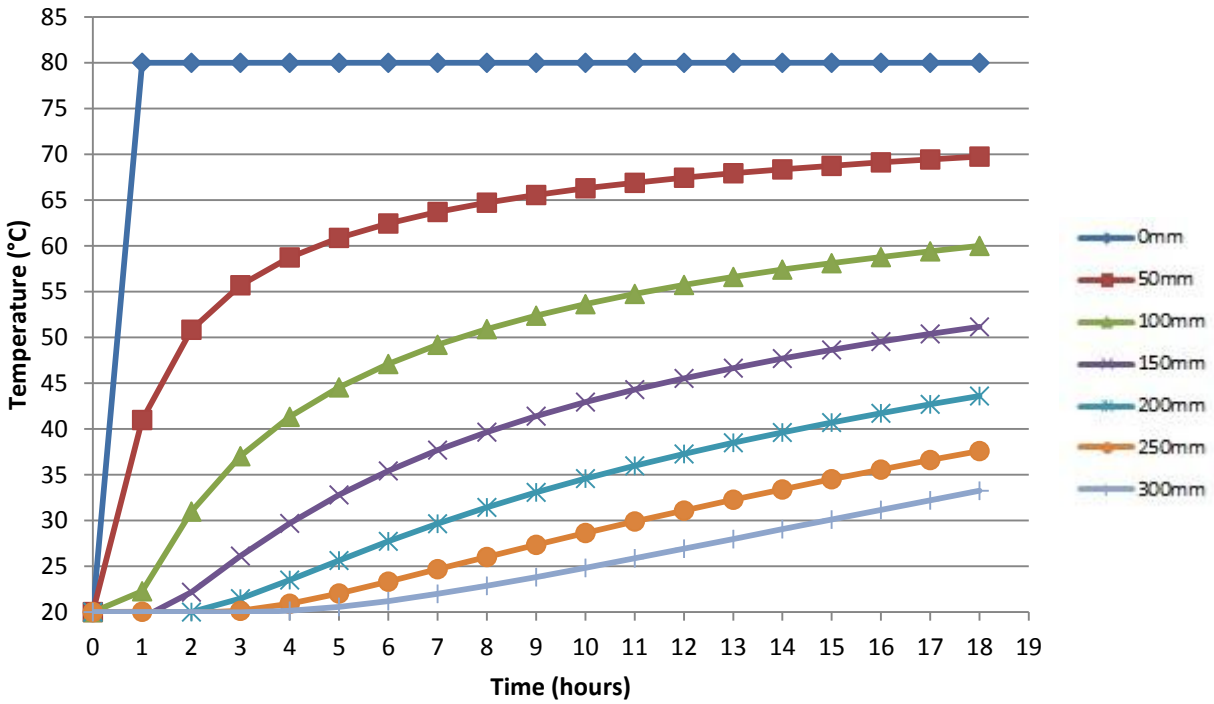

Figure E.20: Predicted temperature profiles in a BSM-foam (2% bitumen content) with 100%RA material, with thermal capacity of 1950(kJ/m^{3}K) and thermal conductivity of 0.80(W/mK).

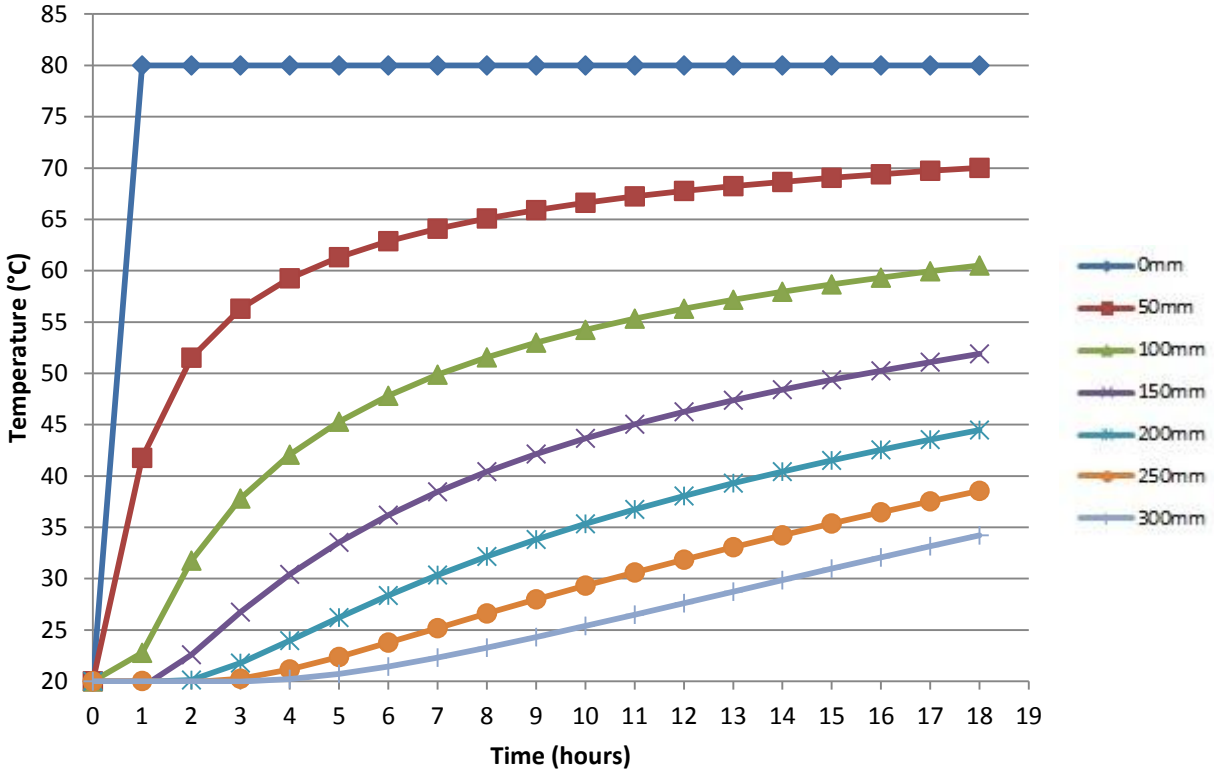

Figure E.21: Predicted temperature profiles in a BSM-foam (2% bitumen content) with 100%RA material, with thermal capacity of 1850(kJ/m^{3}K) and thermal conductivity of 0.80(W/mK).

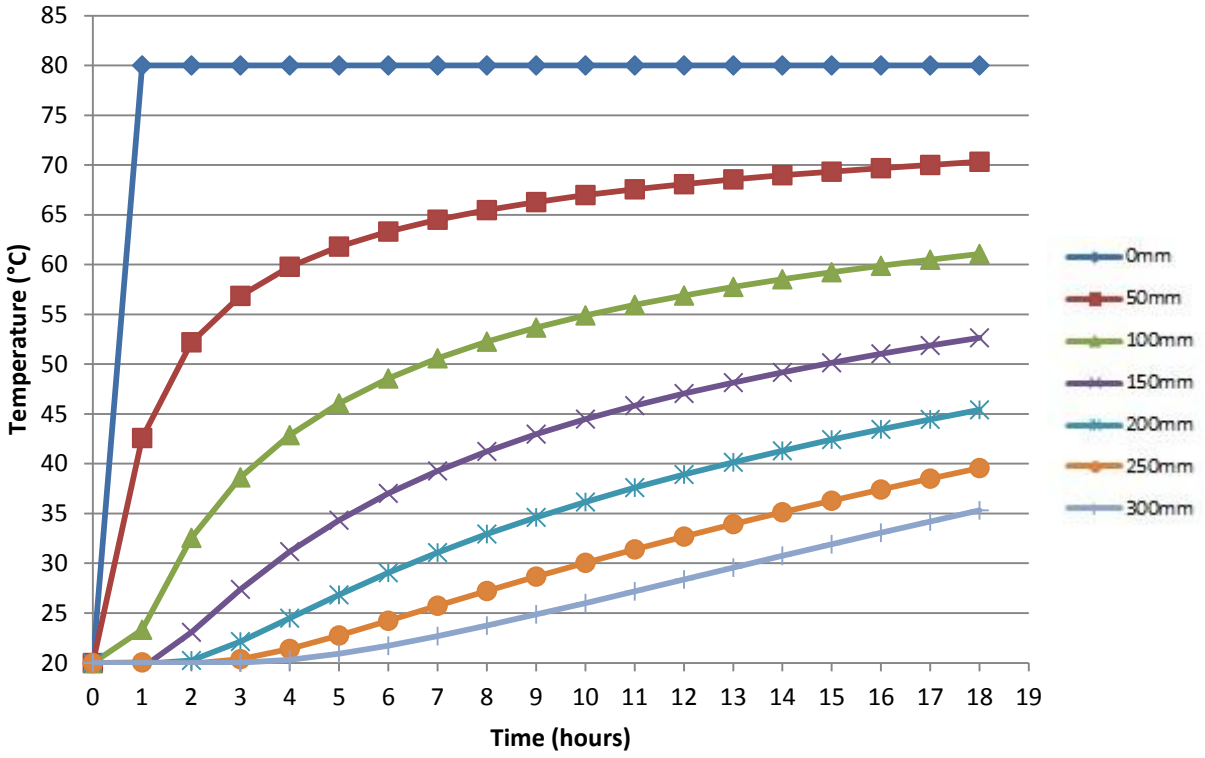

Figure E.22: Predicted temperature profiles in a BSM-foam (2% bitumen content) with 100%RA material, with thermal capacity of 1750(kJ/m^{3}K) and thermal conductivity of 0.80(W/mK).

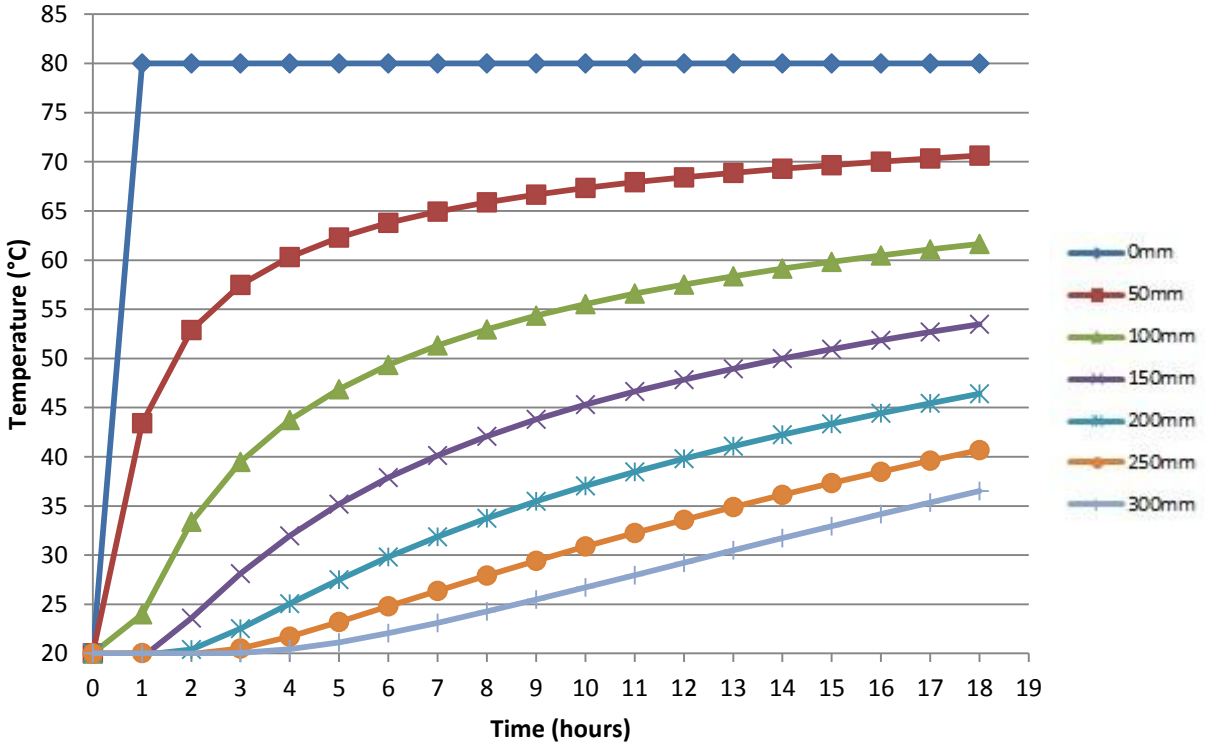

Figure E.23: Predicted temperature profiles in a BSM-foam (2% bitumen content) with 100%RA material, with thermal capacity of 1650(kJ/m^{3}K) and thermal conductivity of 0.80(W/mK).

APPENDIX F

MASTER CURVES OF HOT MIX ASPHALT DEVELOPED BY JENKINS (2000)

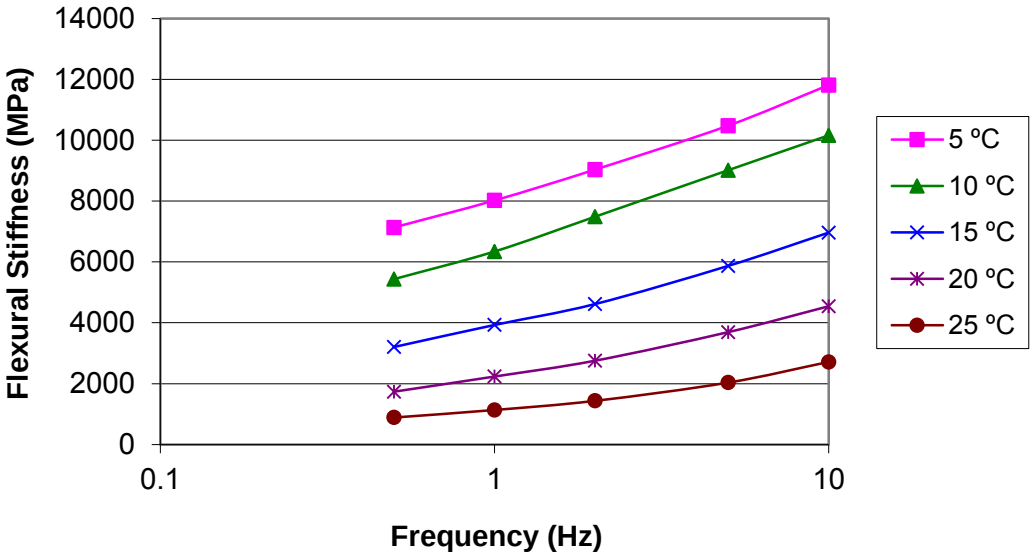

Figure F.1: Flexural stiffness determined for load frequency at given temperatures for a HMA by Jenkins (2000).

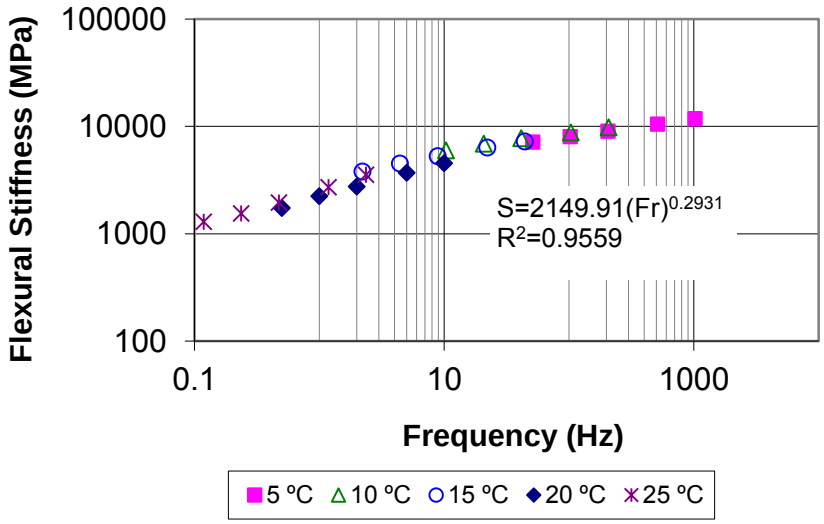

Figure F.2: Master Curve of HMA determined by Jenkins in his thesis (2000).

APPENDIX G

MULTI-LAYER ANALYSIS CONDUCTED ON DIFFERENT PAVEMENT STRUCTURES WITH BISAR 3.0

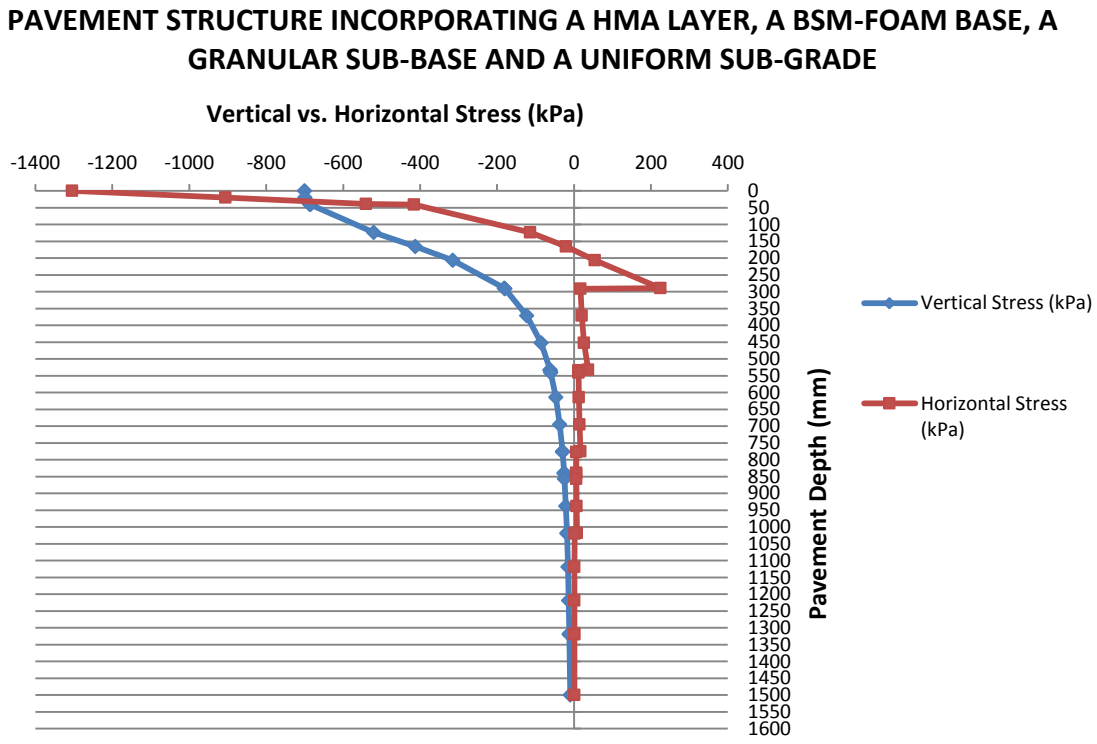

Figure G.1: Vertical and horizontal stress distribution in a pavement structure incorporating a HMA layer, a BSM-foam base, a granular sub-base and a uniform sub-grade (Loading condition = 80 kN, 700 kPa).

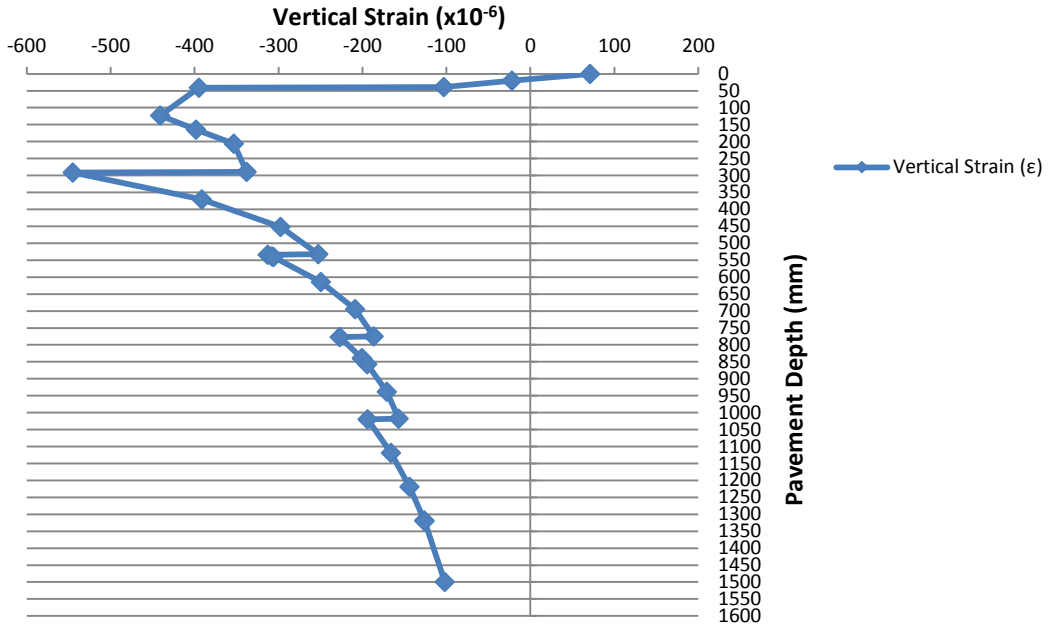

Figure G.2: Vertical strain distribution in a pavement structure incorporating a HMA layer, a BSM-foam base, a granular sub-base and a uniform sub-grade (Loading condition = 80 kN, 700 kPa).

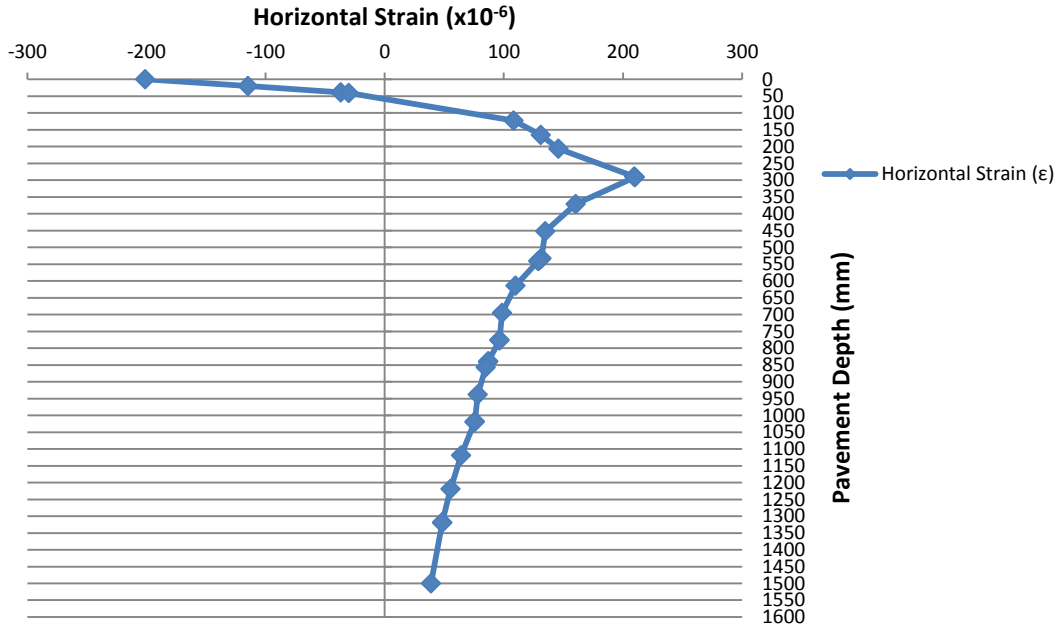

Figure G.3: Horizontal strain distribution in a pavement structure incorporating a HMA layer, a BSM-foam base, a granular sub-base and a uniform sub-grade (Loading condition = 80 kN, 700 kPa).

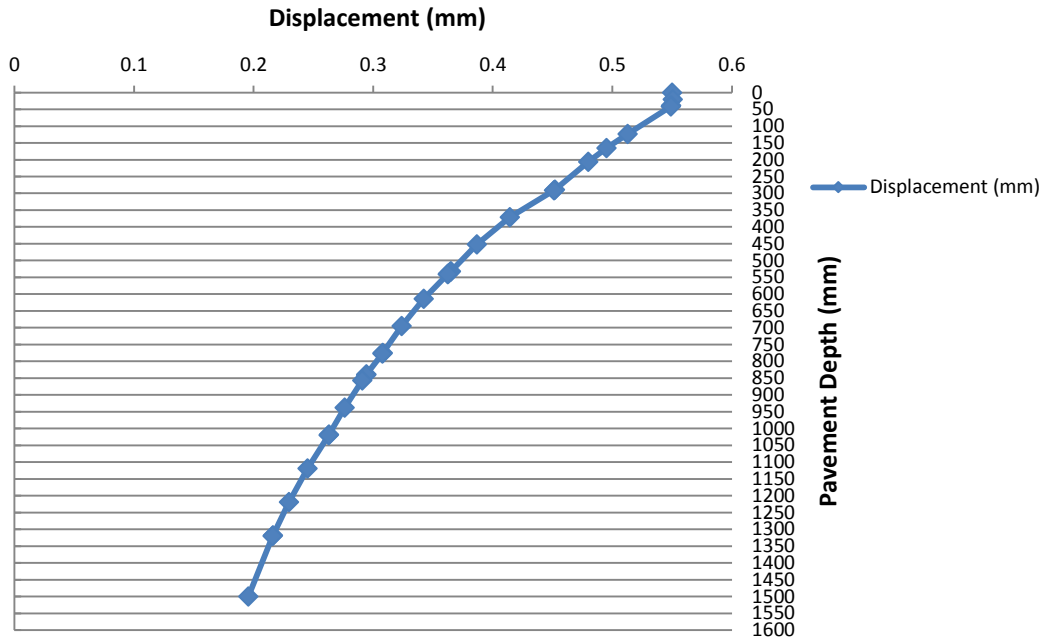

Figure G.4: Displacement distribution in a pavement structure incorporating a HMA layer, a BSM-foam base, a granular sub-base and a uniform sub-grade (Loading condition = 80 kN, 700 kPa).

PAVEMENT STRUCTURE INCORPORATING A HMA LAYER, A BSM-FOAM BASE, A GRANULAR SUB-BASE AND A DUAL SUB-GRADE

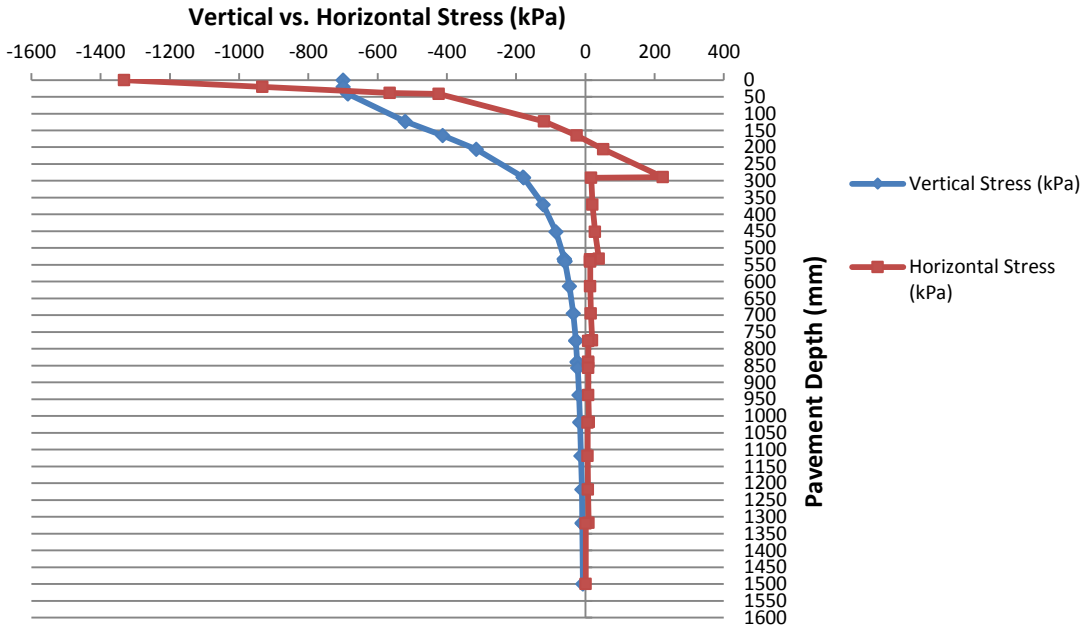

Figure G.5: Vertical and horizontal stress distribution in a pavement structure incorporating a HMA layer, a BSM-foam base, a granular sub-base and a dual sub-grade (Loading condition = 80 kN, 700 kPa).

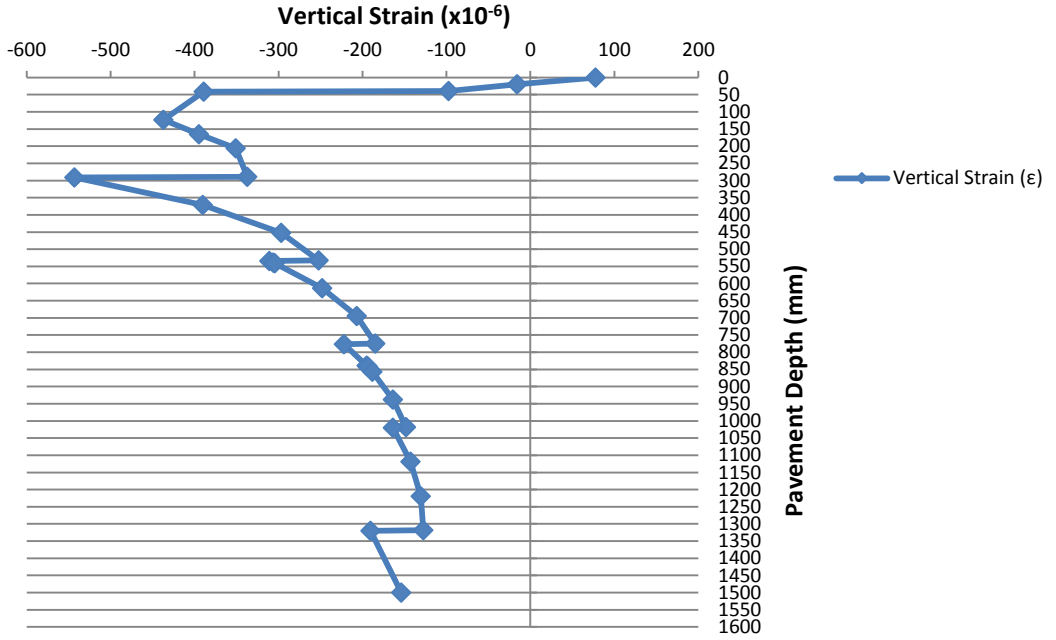

Figure G.6: Vertical strain distribution in a pavement structure incorporating a HMA layer, a BSM-foam base, a granular sub-base and a dual sub-grade (Loading condition = 80 kN, 700 kPa).

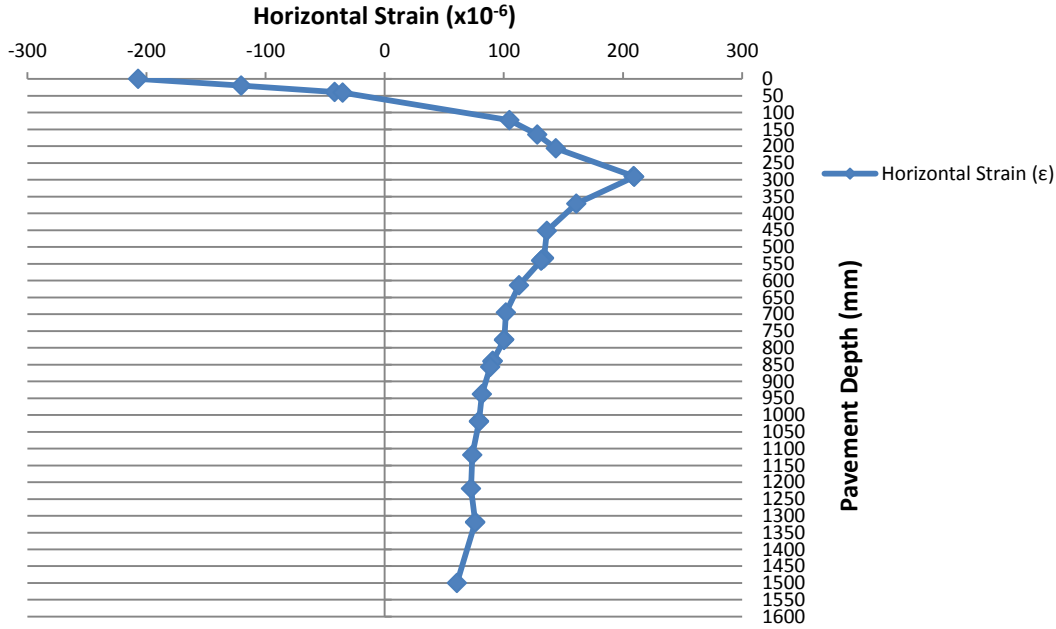

Figure G.7: Horizontal strain distribution in a pavement structure incorporating a HMA layer, a BSM-foam base, a granular sub-base and a dual sub-grade (Loading condition = 80 kN, 700 kPa).

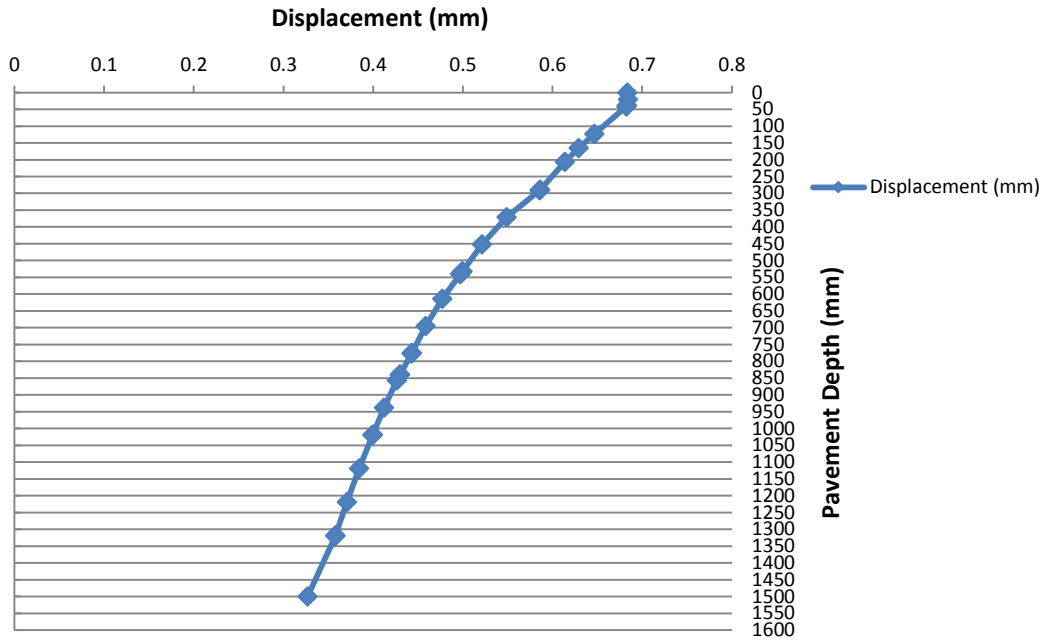

Figure G.8: Displacement distribution in a pavement structure incorporating a HMA layer, a BSM-foam base, a granular sub-base and a dual sub-grade (Loading condition = 80 kN, 700 kPa).

PAVEMENT STRUCTURE INCORPORATING A HMA LAYERS, A BSM-FOAM BASE, A CTSB SUB-BASE AND A UNIFORM SUB-GRADE

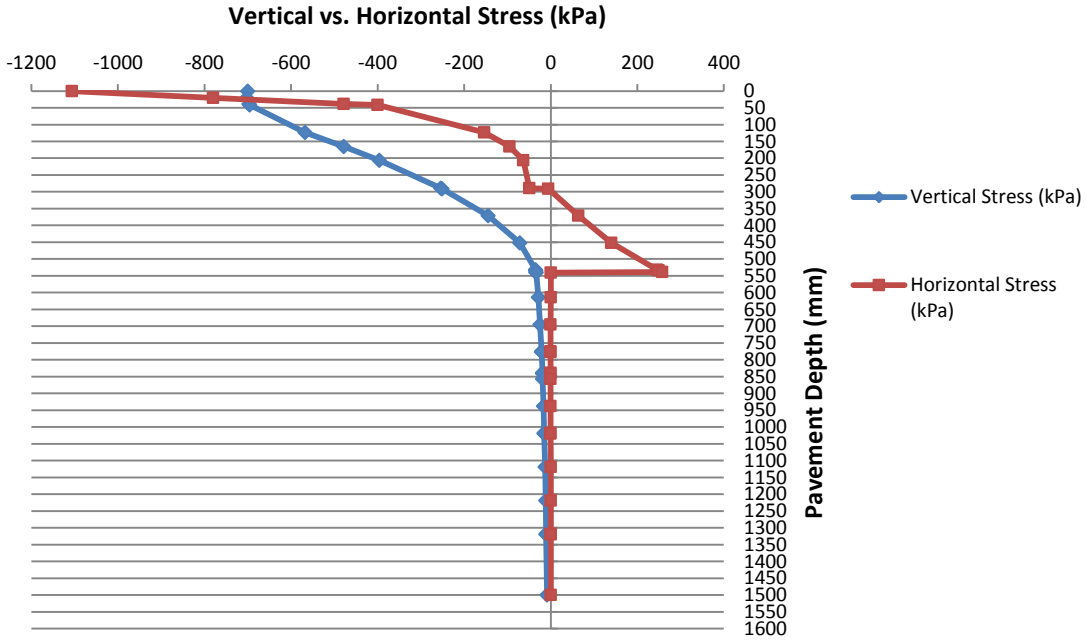

Figure G.9: Vertical and horizontal stress distribution in a pavement structure incorporating a HMA layer, a BSM-foam base, a CTSB sub-base and a uniform sub-grade (Loading condition = 80 kN, 700 kPa).

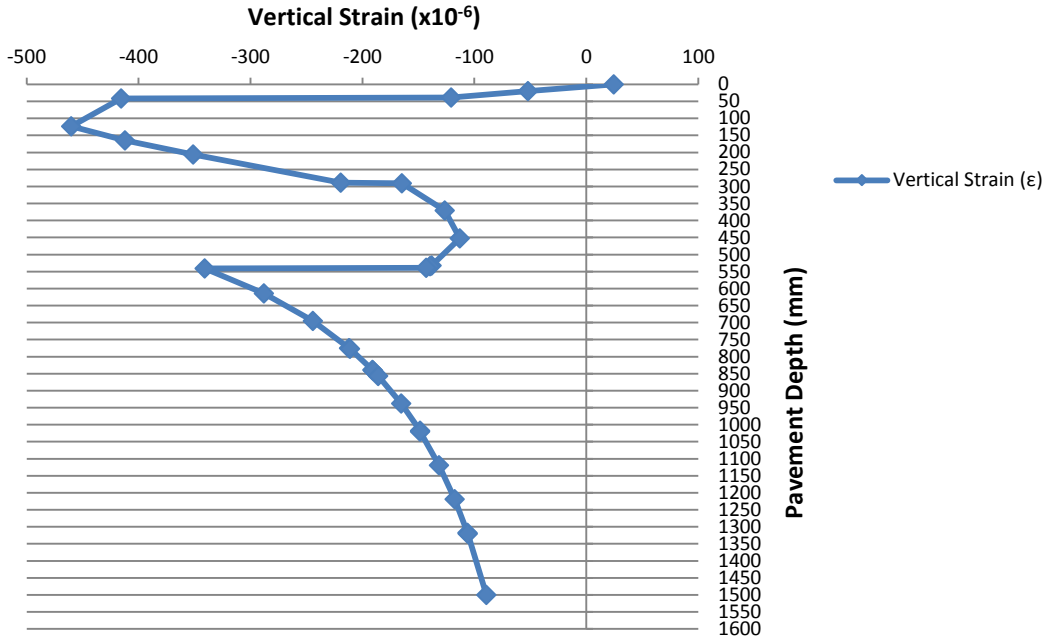

Figure G.10: Vertical strain distribution in a pavement structure incorporating a HMA layer, a BSM-foam base, a CTSB sub-base and a uniform sub-grade (Loading condition = 80 kN, 700 kPa).

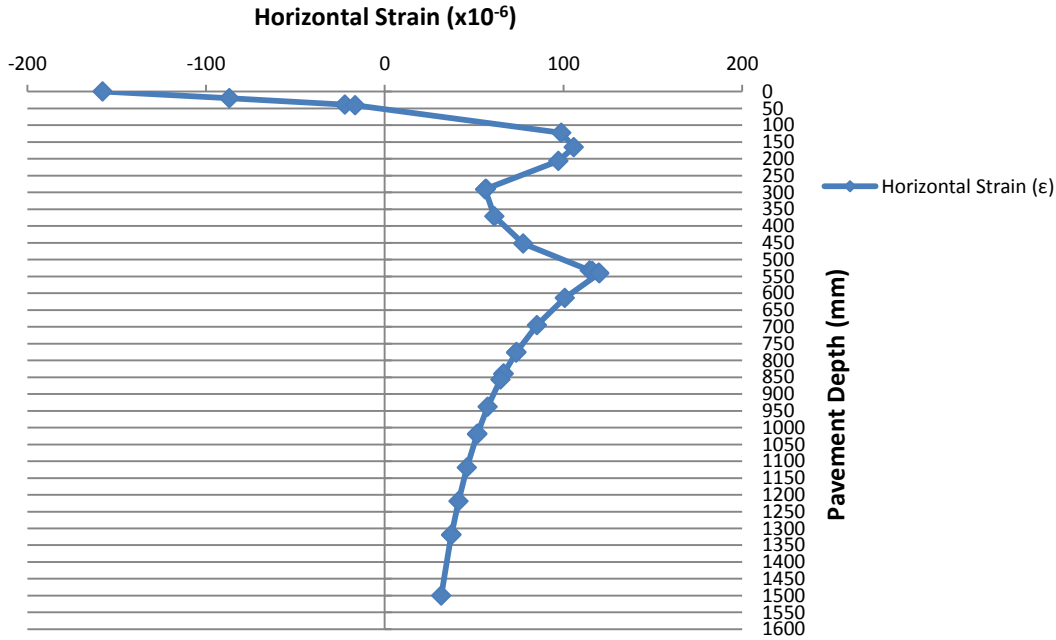

Figure G.11: Horizontal strain distribution in a pavement structure incorporating a HMA layer, a BSM-foam base, a CTSB sub-base and a uniform sub-grade (Loading condition = 80 kN, 700 kPa).

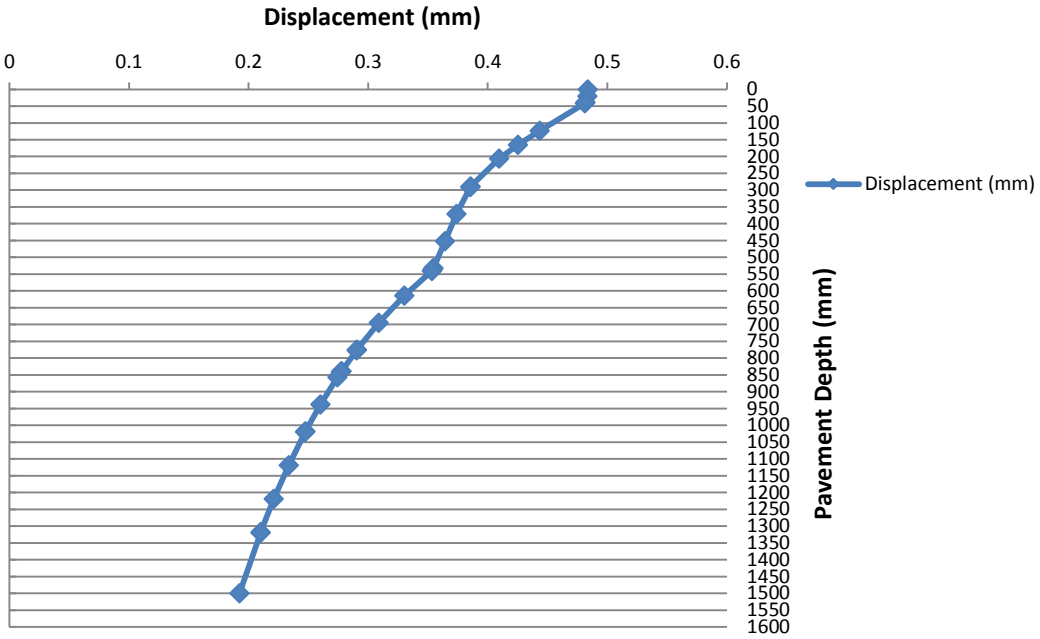

Figure G.12: Displacement distribution in a pavement structure incorporating a HMA layer, a BSM-foam base, a CTSB sub-base and a uniform sub-grade (Loading condition = 80 kN, 700 kPa).

PAVEMENT STRUCTURE INCORPORATING A HMA LAYER, A BSM-FOAM BASE, A CTSB SUB-BASE AND A DUAL SUB-GRADE

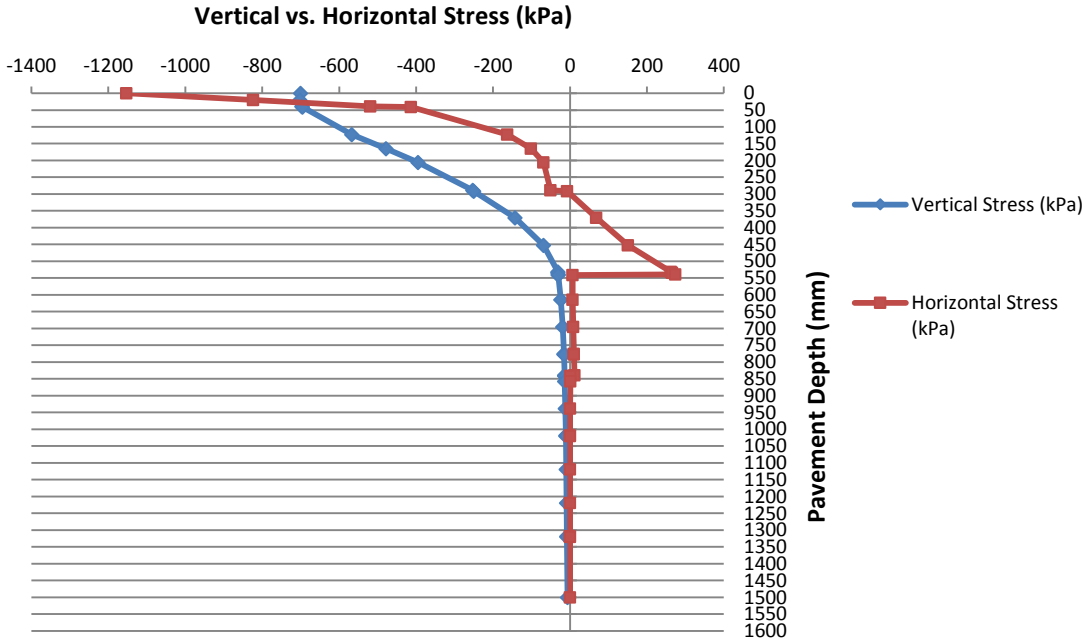

Figure G.13: Vertical and horizontal stress distribution in a pavement structure incorporating a HMA layer, a BSM-foam base, a CTSB sub-base and a dual sub-grade (Loading condition = 80 kN, 700 kPa).

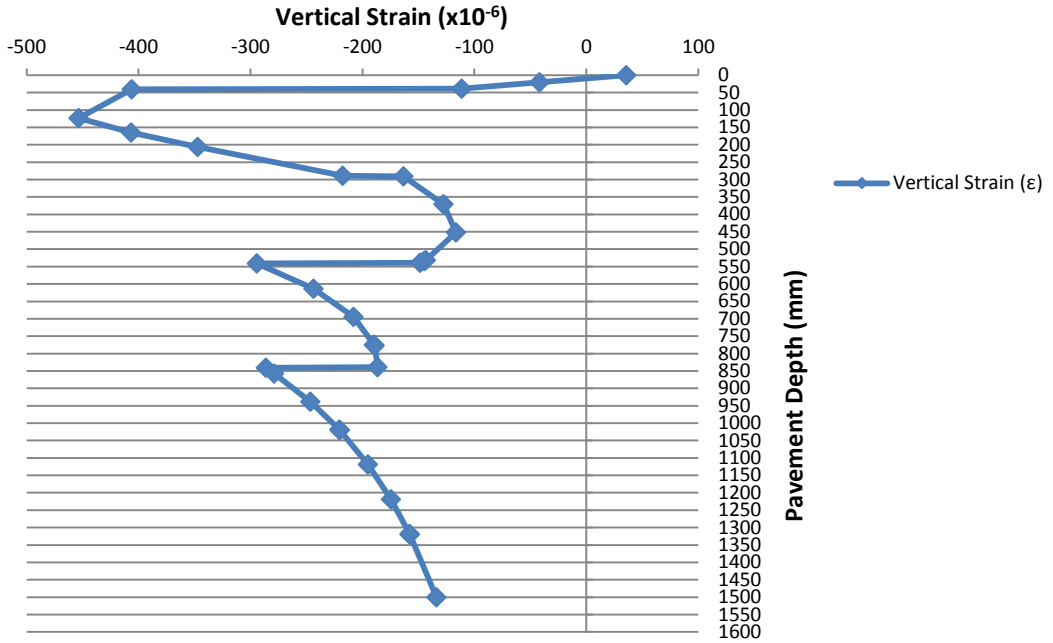

Figure G.14: Vertical strain distribution in a pavement structure incorporating a HMA layer, a BSM-foam base, a CTSB sub-base and a dual sub-grade (Loading condition = 80 kN, 700 kPa).

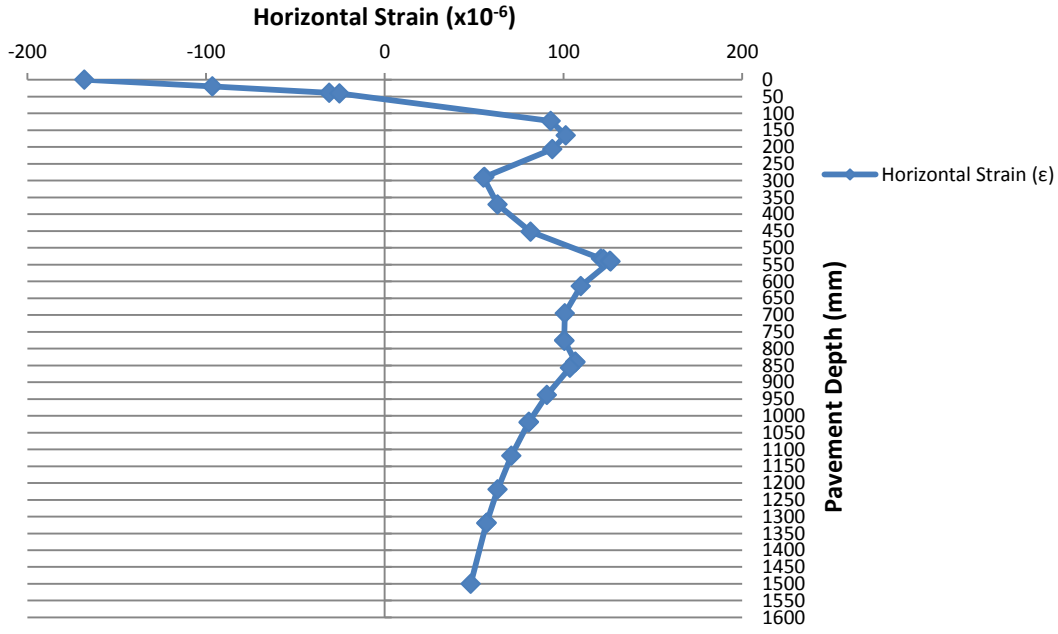

Figure G.15: Horizontal strain distribution in a pavement structure incorporating a HMA layer, a BSM-foam base, a CTSB sub-base and a dual sub-grade (Loading condition = 80 kN, 700 kPa).

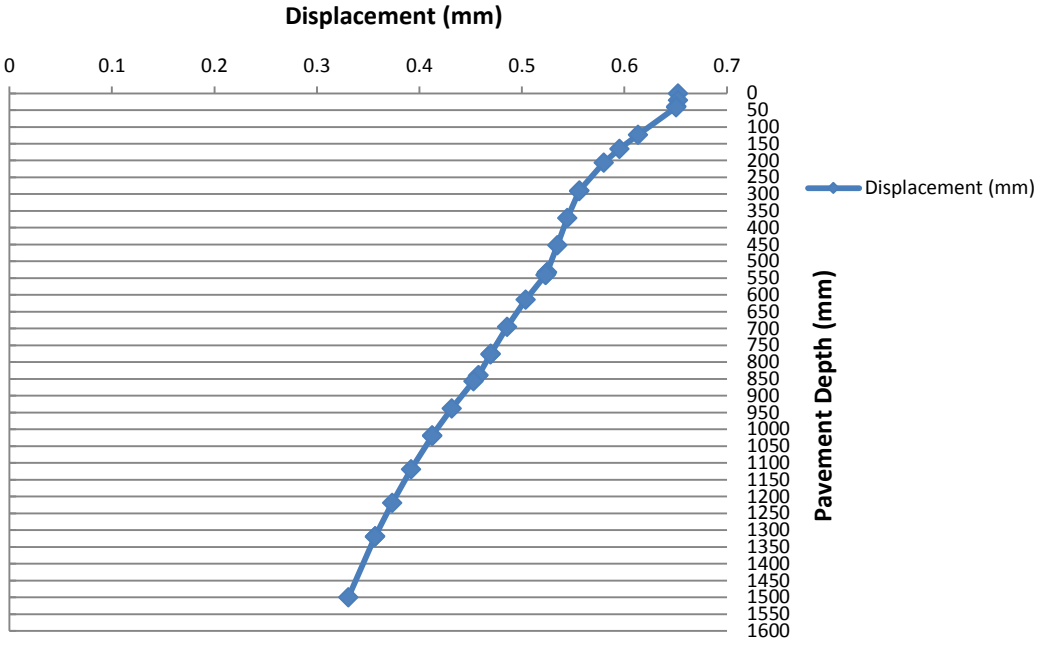

Figure G.16: Displacement distribution in a pavement structure incorporating a HMA layer, a BSM-foam base, a CTSB sub-base and a dual sub-grade (Loading condition = 80 kN, 700 kPa).

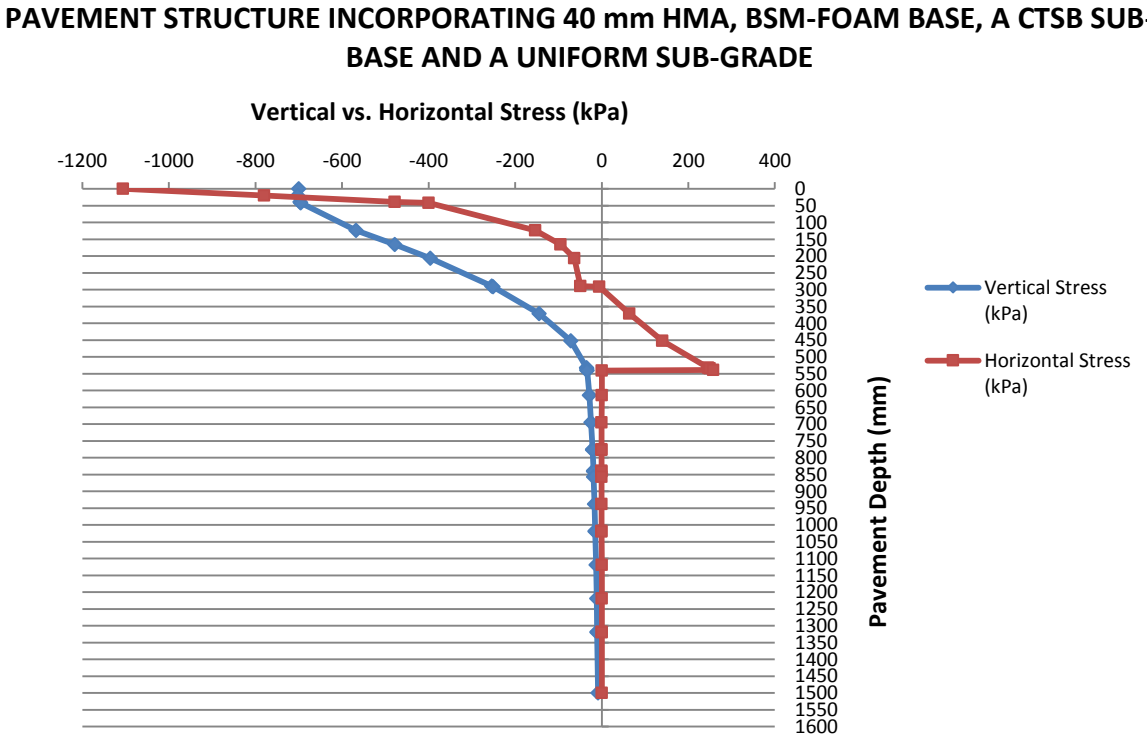

Figure G.17: Vertical and horizontal stress distribution in a pavement structure incorporating 40 mm HMA, a BSM-foam base, a CTSB sub-base and a uniform sub-grade (Loading condition = 80 kN, 700 kPa).

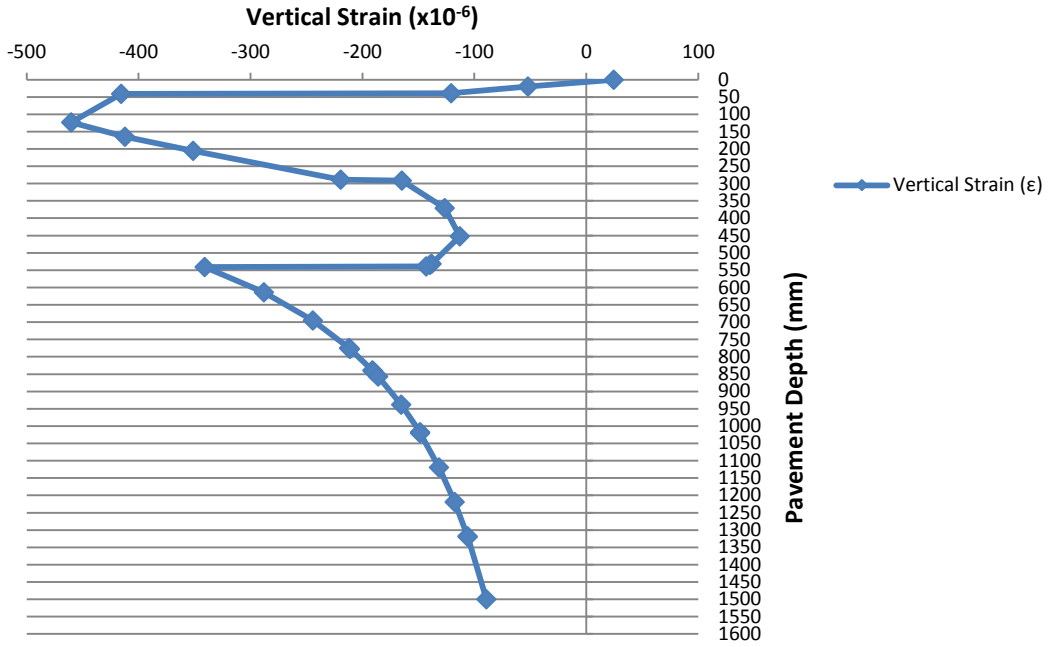

Figure G.18: Vertical strain distribution in a pavement structure incorporating 40 mm HMA, a BSM-foam base, a CTSB sub-base and a uniform sub-grade (Loading condition = 80 kN, 700 kPa).

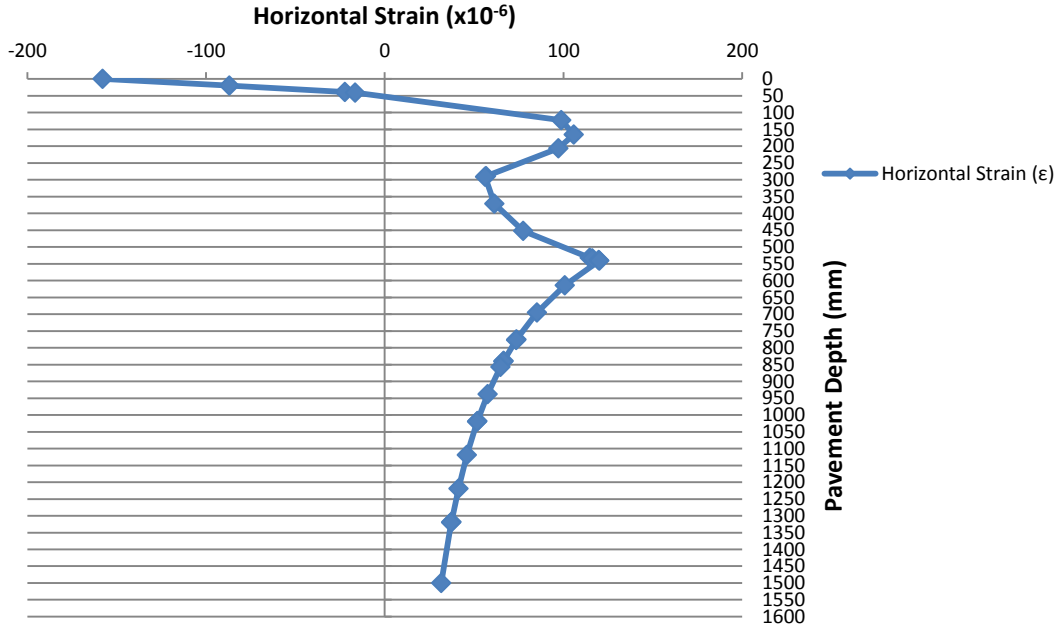

Figure G.19: Horizontal strain distribution in a pavement structure incorporating 40 mm HMA, a BSM-foam base, a CTSB sub-base and a uniform sub-grade (Loading condition = 80 kN, 700 kPa).

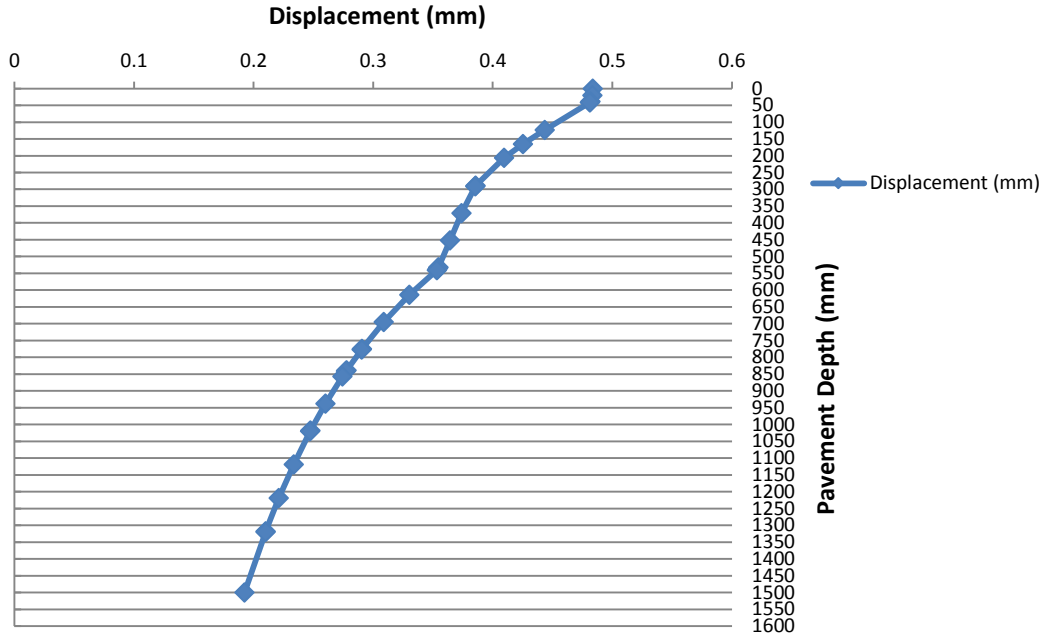

Figure G.20: Displacement distribution in a pavement structure incorporating 40 mm HMA, a BSM-foam base, a CTSB sub-base and a uniform sub-grade (Loading condition = 80 kN, 700 kPa).

PAVEMENT STRUCTURE INCORPORATING 100 mm HMA, BSM-FOAM BASE, A CTSB SUB-BASE AND A UNIFORM SUB-GRADE

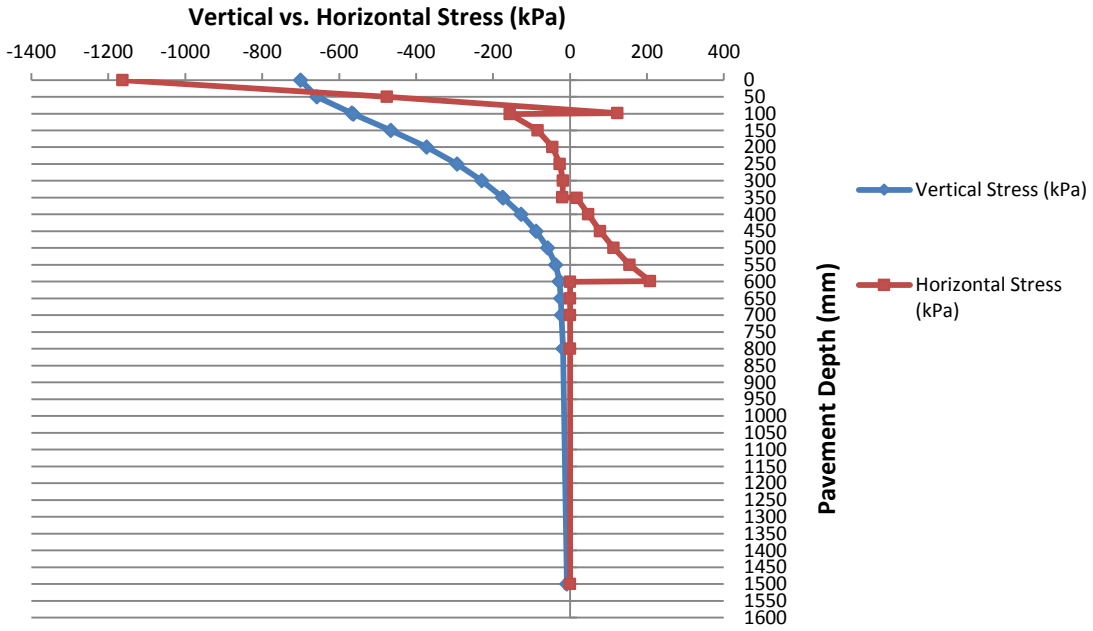

Figure G.21: Vertical and horizontal stress distribution in a pavement structure incorporating 100 mm HMA, a BSM-foam base, a CTSB sub-base and a uniform sub-grade (Loading condition = 80 kN, 700 kPa).

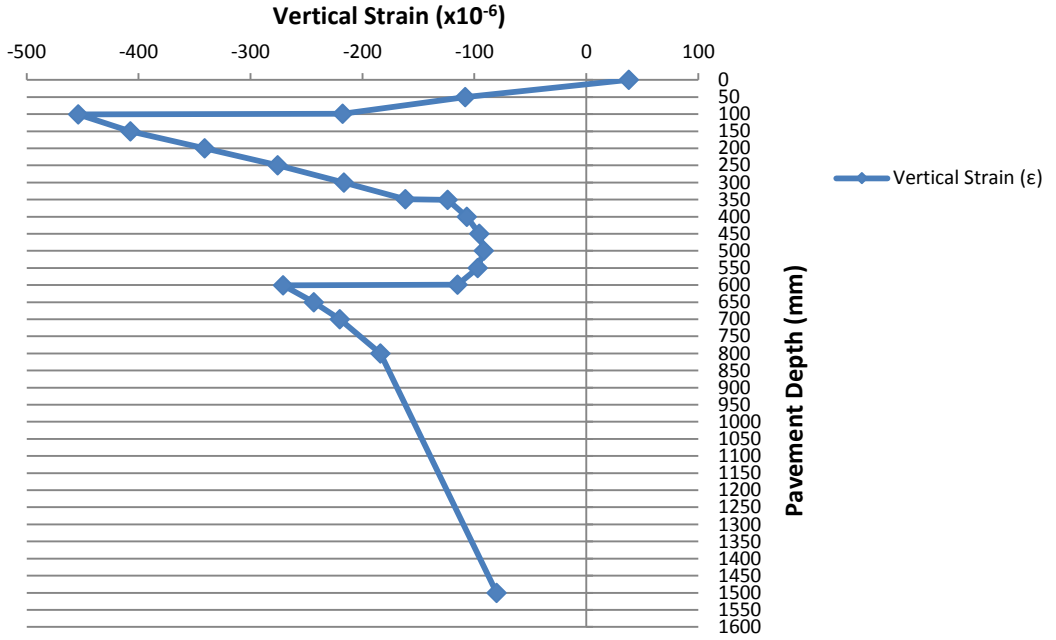

Figure G.22: Vertical strain distribution in a pavement structure incorporating 100 mm HMA, a BSM-foam base, a CTSB sub-base and a uniform sub-grade (Loading condition = 80 kN, 700 kPa).

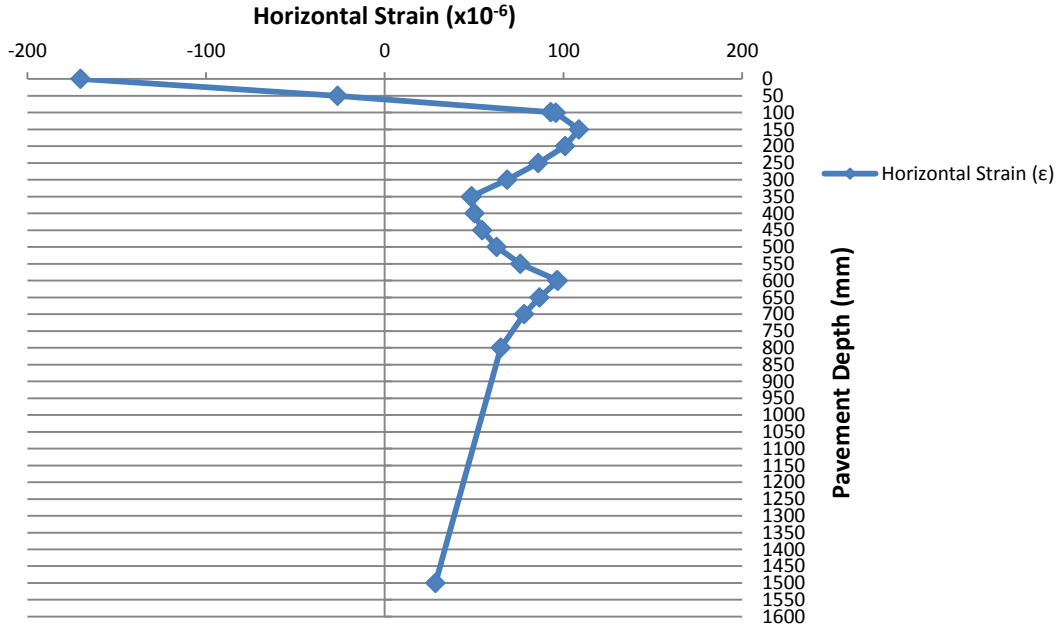

Figure G.23: Horizontal strain distribution in a pavement structure incorporating 100 mm HMA, a BSM-foam base, a CTSB sub-base and a uniform sub-grade (Loading condition = 80 kN, 700 kPa).

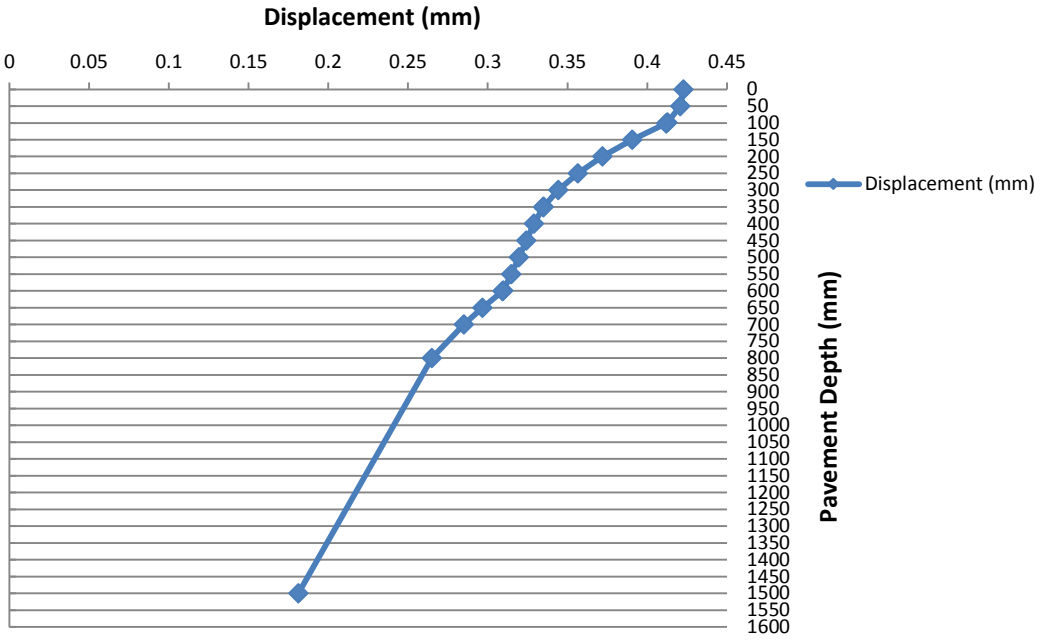

Figure G.24: Displacement distribution in a pavement structure incorporating 100 mm HMA, a BSM-foam base, a CTSB sub-base and a uniform sub-grade (Loading condition = 80 kN, 700 kPa).

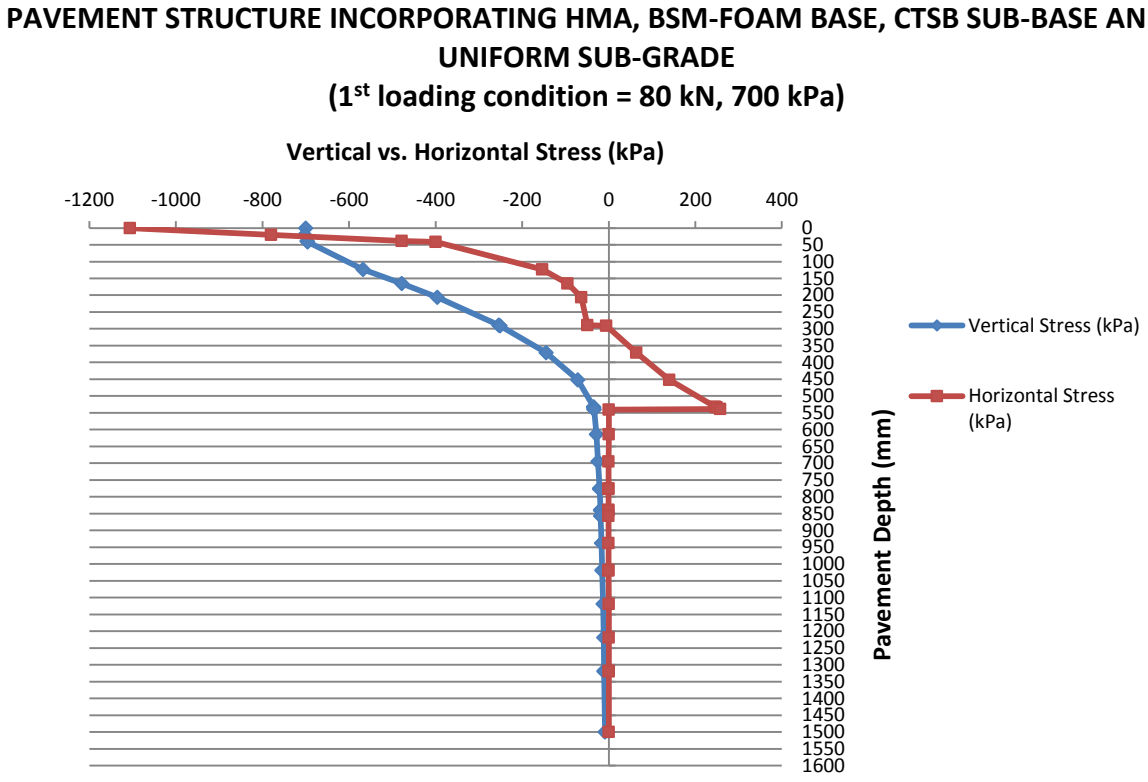

Figure G.25: Vertical and horizontal stress distribution in a pavement structure incorporating a HMA layer, a BSM-foam base, a CTSB sub-base and a uniform sub-grade (Loading condition = 80 kN, 700 kPa).

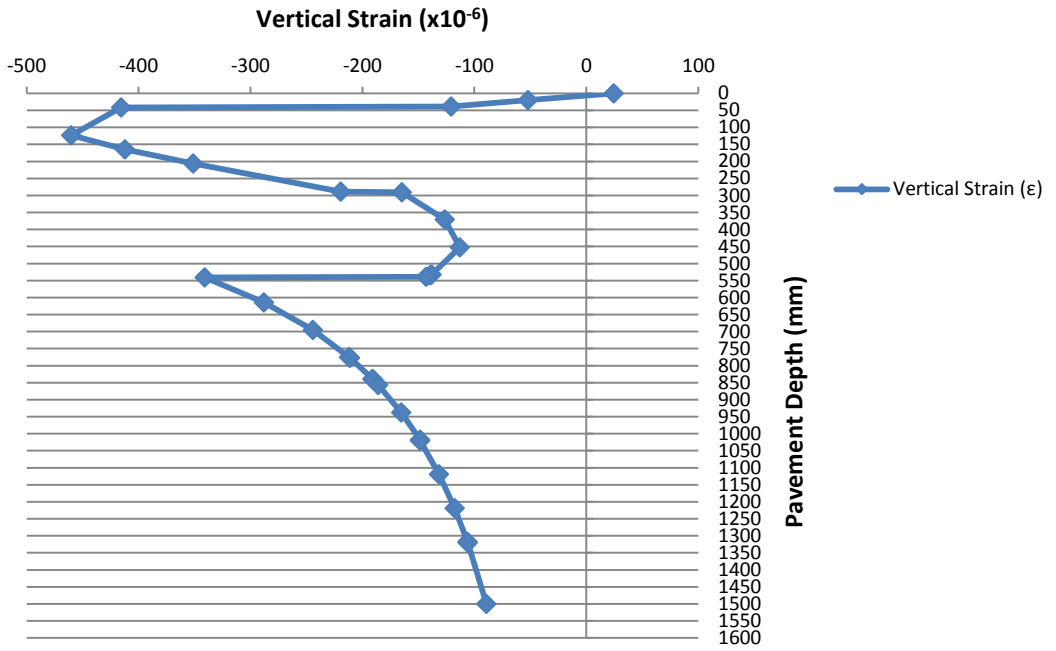

Figure G.26: Vertical strain distribution in a pavement structure incorporating a HMA layer, a BSM-foam base, a CTSB sub-base and a uniform sub-grade (Loading condition = 80 kN, 700 kPa).

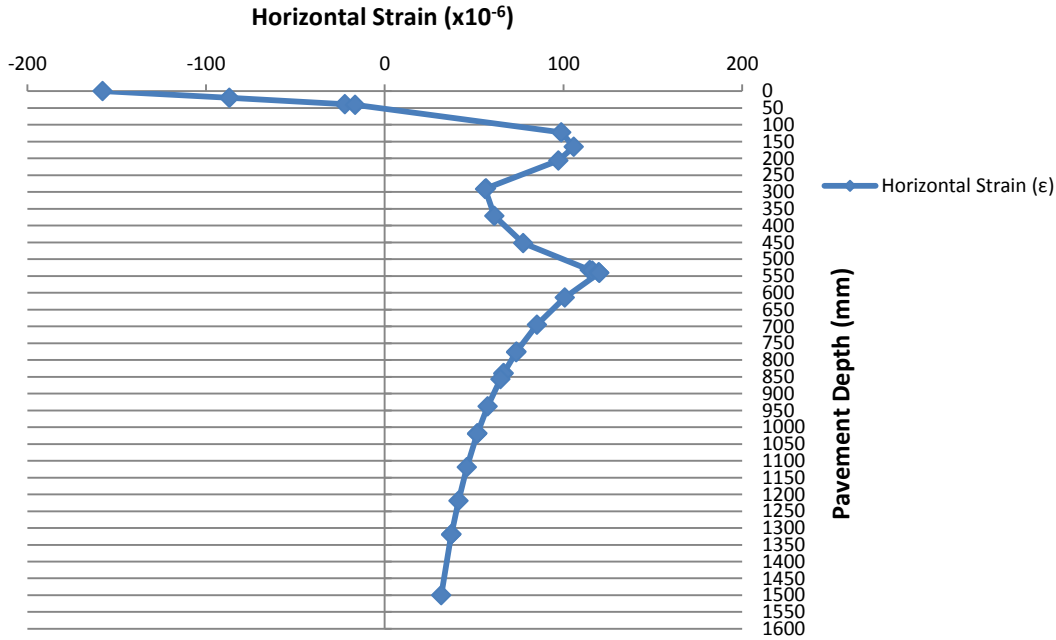

Figure G.27: Horizontal strain distribution in a pavement structure incorporating a HMA layer, a BSM-foam base, a CTSB sub-base and a uniform sub-grade (Loading condition = 80 kN, 700 kPa).

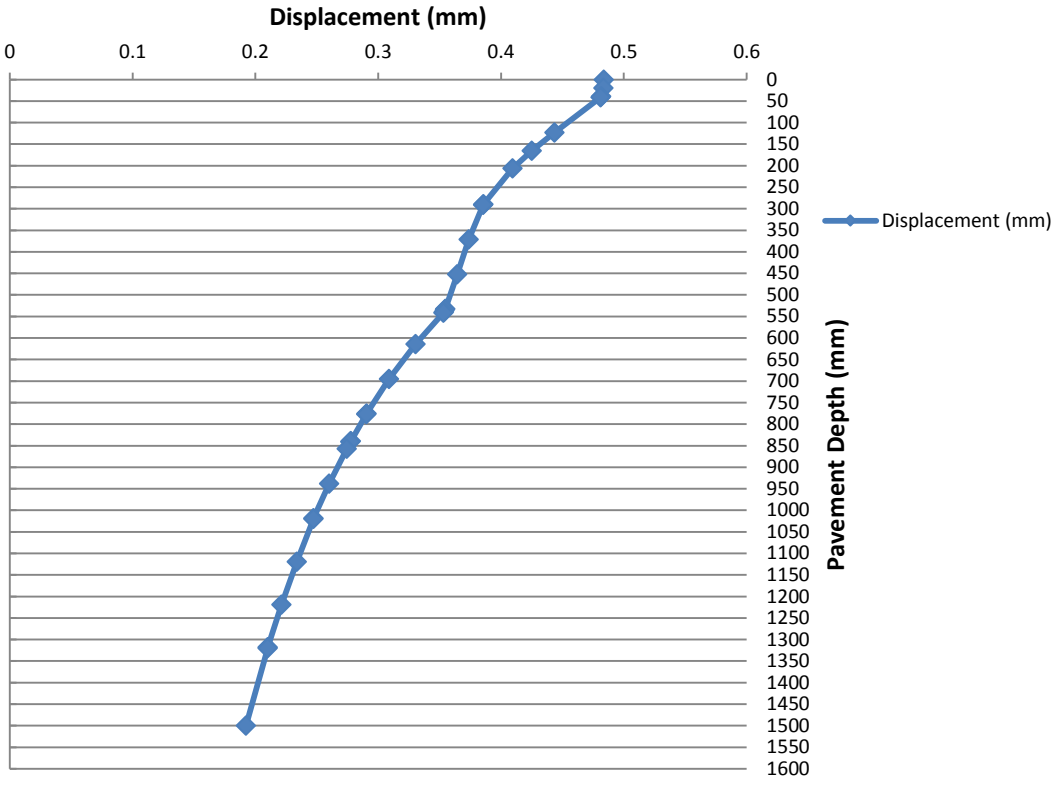

Figure G.28: Displacement distribution in a pavement structure incorporating a HMA layer, a BSM-foam base, a CTSB sub-base and a uniform sub-grade (Loading condition = 80 kN, 700 kPa).

PAVEMENT STRUCTURE INCORPORATING HMA, BSM-FOAM BASE, CTSB SUB-BASE AND UNIFORM SUB-GRADE
(2nd loading condition = 100 kN, 1000 kPa)

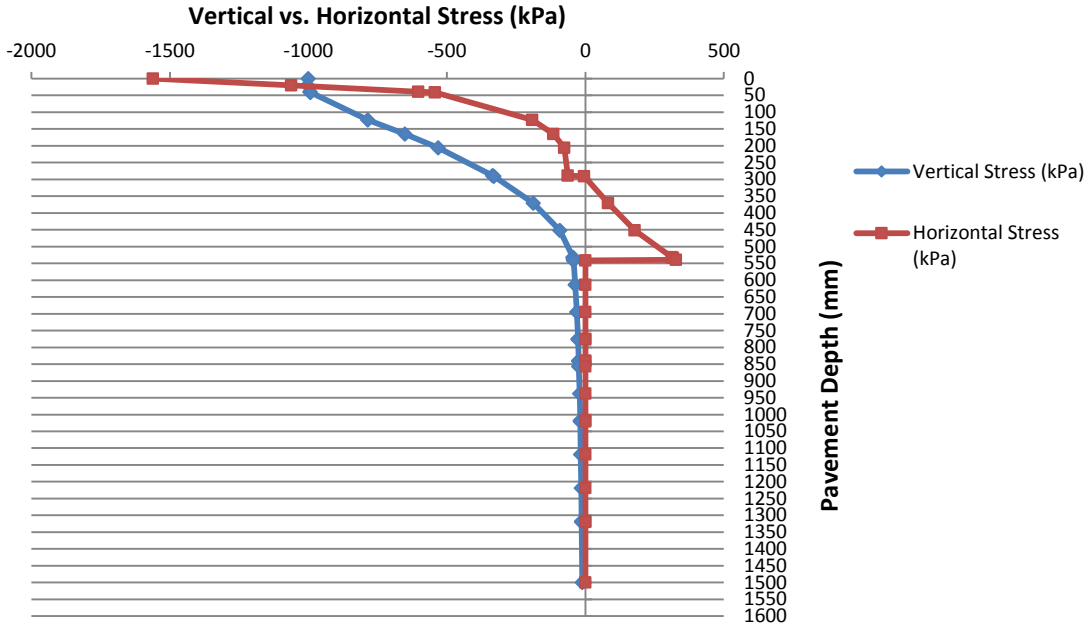

Figure G.29: Vertical and horizontal stress distribution in a pavement structure incorporating a HMA layer, a BSM-foam base, a CTSB sub-base and a uniform sub-grade (Loading condition = 100 kN, 1000 kPa).

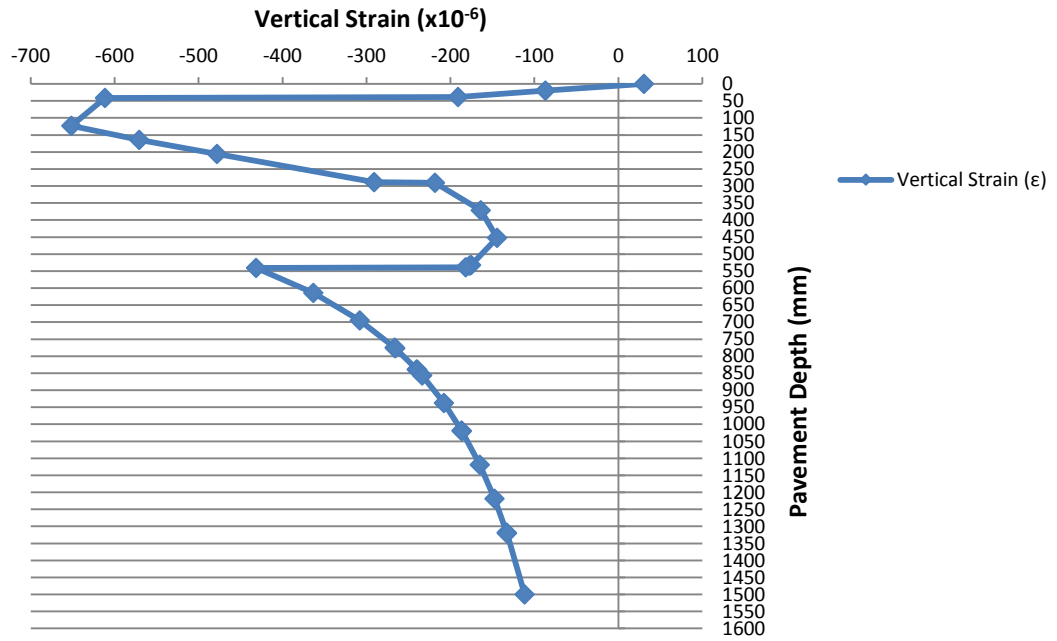

Figure G.30: Vertical strain distribution in a pavement structure incorporating a HMA layer, a BSM-foam base, a CTSB sub-base and a uniform sub-grade (Loading condition = 100 kN, 1000 kPa).

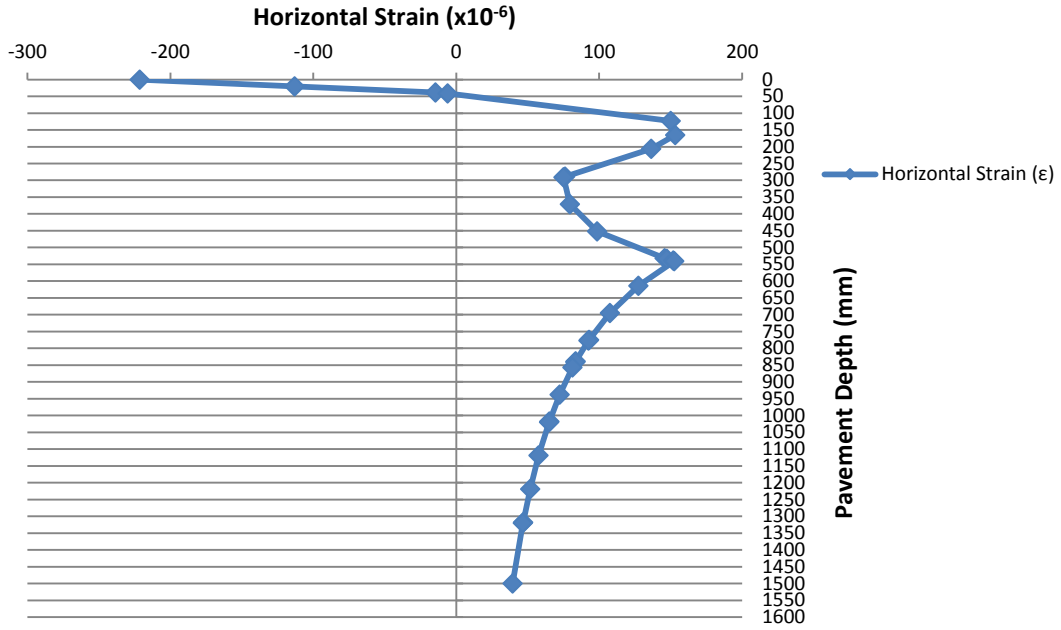

Figure G.31: Horizontal strain distribution in a pavement structure incorporating a HMA layer, a BSM-foam base, a CTSB sub-base and a uniform sub-grade (Loading condition = 100 kN, 1000 kPa).

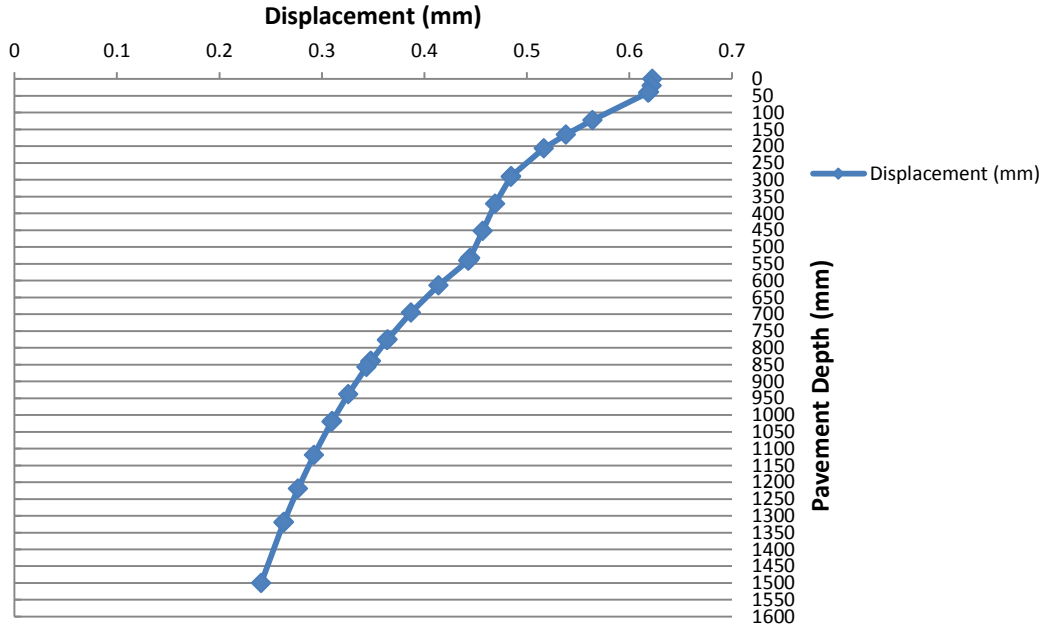

Figure G.32: Displacement distribution in a pavement structure incorporating a HMA layer, a BSM-foam base, a CTSB sub-base and a uniform sub-grade (Loading condition = 100 kN, 1000 kPa).

APPENDIX H

MOD AASHTO COMPACTION TEST RESULTS

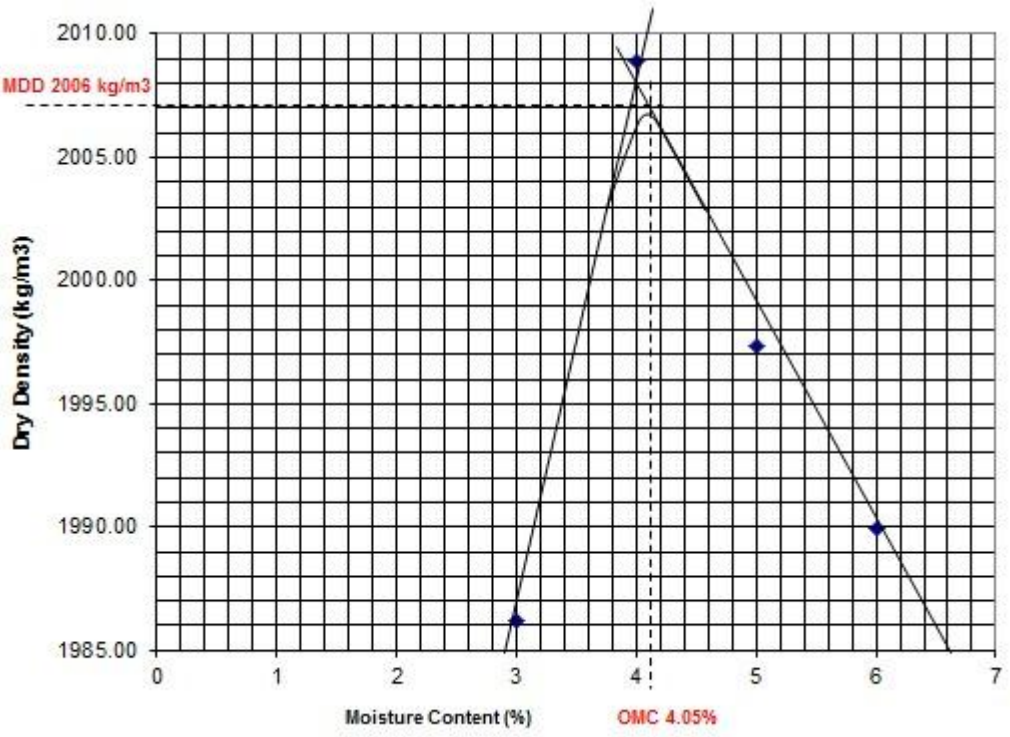

Figure H.1: MDD and OMC results for a mix with 100%RA.

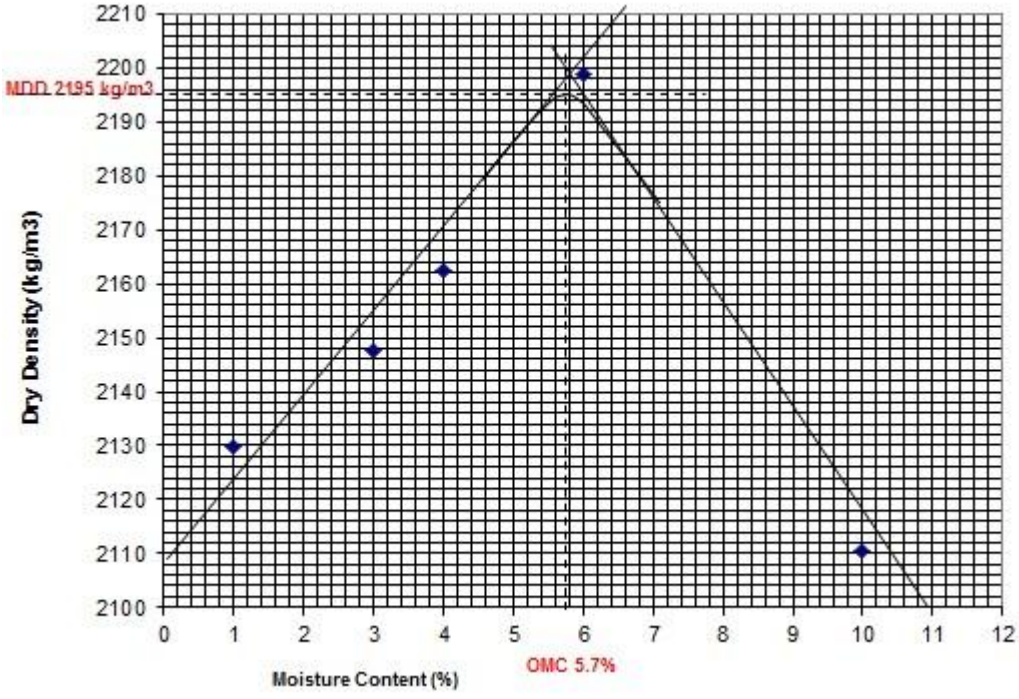

Figure H.2: MDD and OMC results for a mix with 50%RA+50%G2.

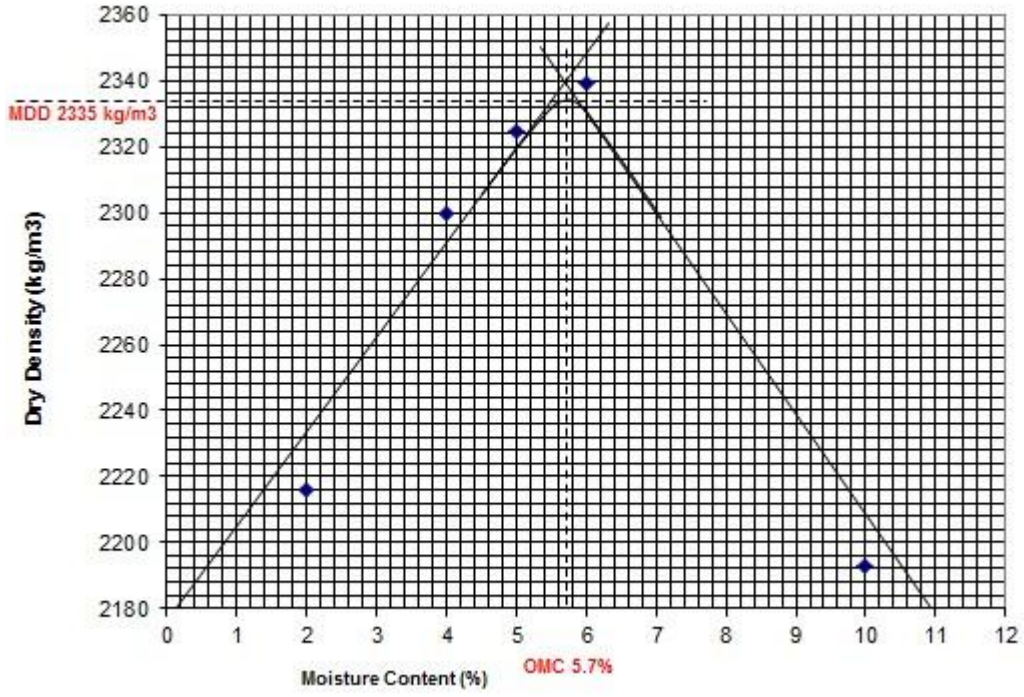

Figure H.3: MDD and OMC results for a mix with 100%G2 material.

APPENDIX I

EXAMPLE OF RESILIENT MODULUS SIGNAL

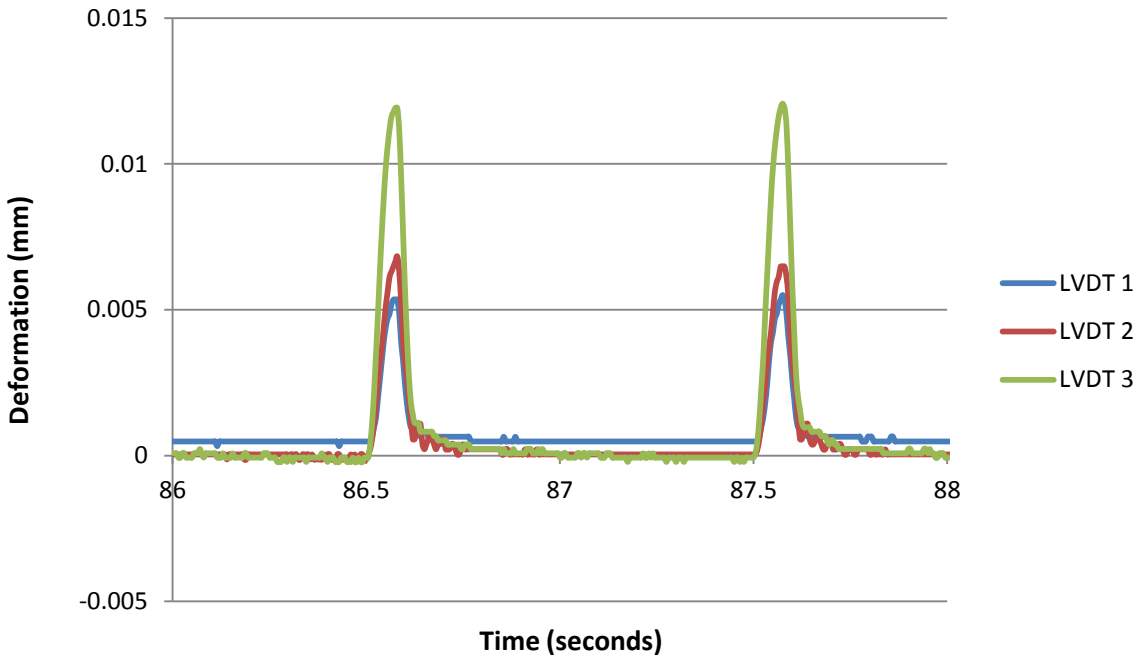

Figure I.1: Typical resilient modulus test at the temperature of 25°C.

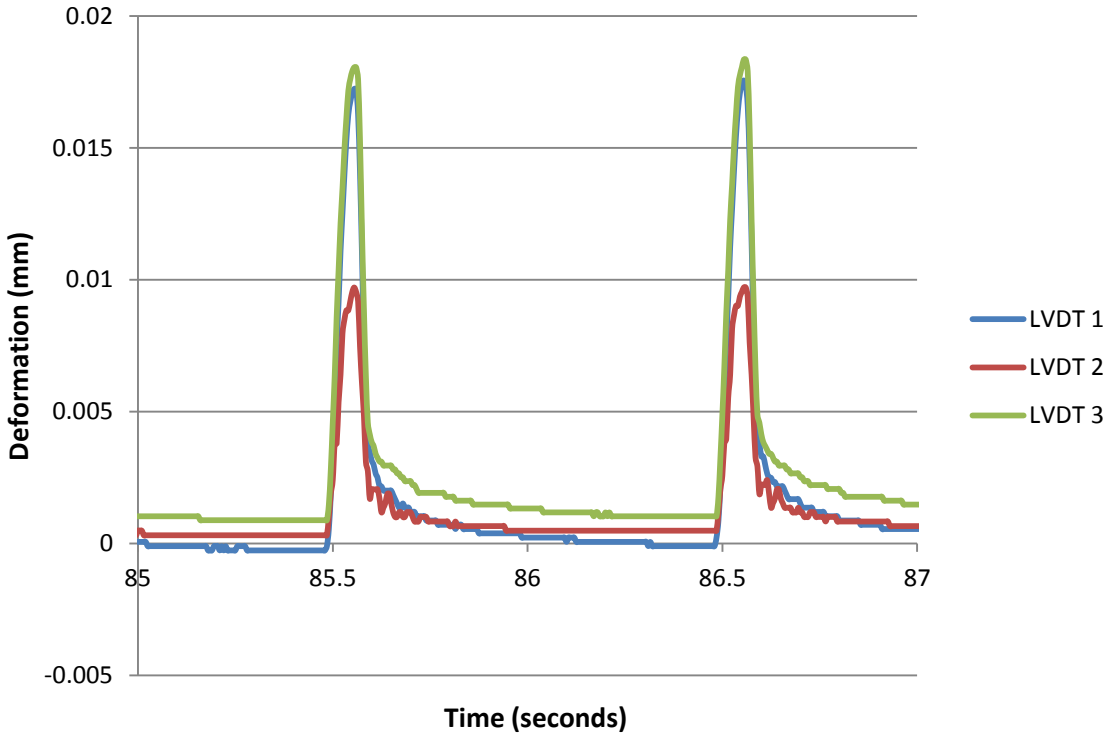

Figure I.2: Typical resilient modulus test at the temperature of 40°C.